SECONDARY METABOLITES OF SELECTED HELICOSPOROUS TUBEUFIACEAE

LIJUAN ZHANG

DOCTOR OF PHILOSOPHY
IN
BIOLOGICAL SCIENCE

SCHOOL OF SCIENCE
MAE FAH LUANG UNIVERSITY
2025

SECONDARY METABOLITES OF SELECTED HELICOSPOROUS TUBEUFIACEAE

LIJUAN ZHANG

THIS DISSERTATION IS A PARTIAL FULFILLMENT OF THE REQUIREMENTS FOR THE DEGREE OF DOCTOR OF PHILOSOPHY IN BIOLOGICAL SCIENCE

SCHOOL OF SCIENCE
MAE FAH LUANG UNIVERSITY
2025

DISSERTATION APPROVAL

MAE FAH LUANG UNIVERSITY

FOR

DOCTOR OF PHILOSOPHY IN BIOLOGICAL SCIENCE

Dissertation Title: Secondary Metabolites of Selected Helicosporous Tubeufiaceae

Author: Lijuan Zhang

Examination Committee:

Dan-Feng Bao, Ph. D.	Chairperson
Assistant Professor Mahamarakkalage Mary Ruvishika Shehali Jayawardena, Ph. D.	Member
Professor Yong-Zhong Lu, Ph. D.	Member
Assistant Professor Pattana Kakumyan, Ph. D.	Member
Associate Professor Tianming Zhao, Ph. D.	Member

Advisors:

.....Advisor

(Assistant Professor Mahamarakkalage Mary Ruvishika Shehali Jayawardena, Ph. D.)

.....Co-Advisor

(Professor Yong-Zhong Lu, Ph. D.)

Dean:

.....

(Professor Surat Laphookhieo, Ph. D.)

ACKNOWLEDGEMENTS

Over the past four and a half years, my doctoral journey has been both arduous and enriching. I have had moments of strong resolve as well as periods of self-doubt. I am deeply grateful to everyone whose steadfast care and support accompanied me to this milestone.

I am profoundly grateful to Professor Kevin David Hyde, my academic advisor, for inviting me into his group and for cultivating the excellent research environment that enabled this PhD. His broad expertise and uncompromising academic standards have shaped how I think about science. Thanks to his trust, I was able to devote myself fully to research; thanks to his original ideas and steady guidance, I learned to ask better questions and pursue them rigorously. This dissertation carries his imprint in countless ways, and I extend my sincere thanks and best wishes to Prof. Kevin David Hyde.

I am especially grateful to my co-advisor, Professor Yongzhong Lu, whose farsighted vision and personal warmth opened the path that led me to study in Thailand. In China, he built an excellent experimental platform and a supportive group culture; throughout every stage of this projects he offered professional guidance, tangible resources, and hands-on help. When progress slowed or problems arose, his calm encouragement and strategic perspective helped me regain direction. His rigorous standards, deep knowledge, and incisive advice consistently raised the bar, while his generosity—including financial support—made steady work possible. Above all, his integrity, humane leadership, and quiet charisma have profoundly shaped how I work and think. I extend my heartfelt thanks and best wishes to Prof. Yongzhong Lu.

I am deeply grateful to Assistant Prof. Dr. Ruvi for guidance and support with the administrative and organizational aspects of my degree—particularly arranging the proposal and defense, coordinating progress, and facilitating communication with the group leader and the university. These efforts were instrumental in the timely completion of my thesis. I also thank Dr. Mapook Ausana and Dr. Jingzu Sun for their insightful comments and for guidance on scientific writing and revisions to my papers and research topic. Special thanks to Dr. Fandong Kong and Mr. Wenwen He for their help with natural-product structure elucidation, and to Dr. Xiaoyan Ma and Dr.

Tianming Zhao for assistance with compound bioactivity assays. I am also very grateful to Assistant Prof. Dr. Patana and Dr. Danfeng Bao for their valuable advice. I am likewise grateful to the staff of CEFR—especially P′. Pooh—for their assistance. I look forward to continued, rewarding collaboration as we take on new challenges and achieve even greater success together.

I also would like to express my heartfelt gratitude to my friends and colleagues for their unwavering care and support throughout my PhD journey. Their encouragement made it possible for me to persevere during challenging times, and they brought joy and energy to my daily life. Special thanks to Jian Ma, Meiyan Han, Dege Zheng, Jingyi Zhang, Xing-Juan Xiao, Xia Tang, Yu Yang, Zheng Zhang, Shuliang Zou, Qing Wu, Shuqiong Xie, Lirong Huang, Ningguo Liu, Nvdan Hu, Xiaohui Liu, Yuanping Xiao, Xingguo Tian, Xiaojie Wang, Na Wu, Le Luo, Hua Li, Xixi Han, Arttapon Walker, Songqing Wang, Fei Zhang, Xiangdong Li and other friends for their invaluable advice, kind support, collaboration, and sincere friendships.

I would like thank the National Natural Science Foundation of China (NSFC 31900020, 32360011) and Youth Science and Technology Talent Development Project from Guizhou Provincial Department of Education (QJHKYZ[2022]345), the China Postdoctoral Science Foundation Project (2020M683657XB), the Guizhou Province high-level talent innovation and entrepreneurship merit funding project (No. 202104), the Thesis/Dissertation Support Grant from Mae Fah Luang University (Grant number: 0382), the Research Presentation Support Grant from Mae Fah Luang University (Grant number: 0331), and the tuition scholarship for my Ph.D. studies (scholarship number: 029) for their financial support.

Finally, I want to express my heartfelt gratitude to my family and friends for their understanding and unwavering support. Their constant encouragement has been a source of strength during challenging and stressful times. I would like to express my deepest gratitude to my husband for his boundless patience and support, and to my daughter, who has been a guiding light on my path. Their love sustained me and made this dream possible.

Lijuan Zhang

Dissertation Title	Secondary Metabolites of Selected Helicosporous Tubeufiaceae
Author	Lijuan Zhang
Degree	Doctor of Philosophy (Biological Science)
Advisor	Assistant Professor Mahamarakkalage Mary Ruvishika Shehali Jayawardena, Ph. D.
Co-Advisor	Professor Yong-Zhong Lu, Ph. D.

ABSTRACT

Helicosporous hyphomycetes is a group of saprophytic fungi, with occasional endophytic forms. Its characteristic feature is the presence of helicoid conidia, which can coil at least 180° on a two-dimensional or three-dimensional plane. Despite their distinctive morphology and strong biosynthetic potential—yielding alkaloids, glycolipids, polyketides, and terpenoids with antibacterial, antitumor, and antidiabetic activities—chemical studies remain limited. In our prior work, we accumulated an extensive Tubeufiaceae strain collection and, via small-scale solid-state fermentations, generated crude extracts for chemical and cytotoxicity screening. Five strains—*Neohelicosporium guangxiense* (SLGY-5), *N. griseum* (GYSLGY-1, SLGY-15), *Tubeufia longihelicospora* (WZS71), and *Helicosporium sexuale* (LZ15)—were prioritized for detailed metabolite and bioactivity studies.

From *Neohelicosporium guangxiense* SLGY-5, three α-tetralone derivatives (**C1**–**C3**) and one isocoumarin (**C4**) were isolated; notably, **C1** was obtained from natural sources for the first time. From *N. griseum* GYSLGY-1, two new polyketides—neogrisphenol A (**C5**) and neogrisphenol B (**C6**)—one new isochroman-1-one, (*S*)-6-hydroxy-7-methoxy-3,5-dimethylisochroman-1-one (**C7**), and four known compounds (**C8**–**C11**) were characterized. From *N. griseum* SLGY-15, seven polyketides (**C12**–**C18**) and one steroid (**C19**) were obtained. From *Tubeufia longihelicospor*a WZS71, two dimeric naphtho-γ-pyrones (**C20**–**C21**), two dimeric coumarins (**C22**–**C23**), and one alkaloid (**C24**) were isolated. From *Helicosporium sexuale* LZ15, seven new dibenzo-α-pyrone derivatives—Helicolide A (**C25**), Helicohydrins B–D (**C26**–**C28**), and Helicochlorins E–G (**C29**–**C31**)—together with eight known congeners (**C32**–**C39**) were obtained. Structures were elucidated by 1D/2D NMR,

mass spectrometry, NOE analysis, single-crystal X-ray diffraction, and ECD, supported by quantum-chemical calculations.

Cytotoxicity testing revealed that neogrisphenol A (**C5**) showed potent activity against A2780, PC-3, and MDA-MB-231 cells (IC_{50} = 3.20, 10.68, and 16.30 μM, respectively), exceeding the potency of cisplatin (CDDP) in A2780 under the same conditions. Neogrisphenol B (**C6**) was also active against A2780 (IC_{50} = 10.13 μM). *In vitro* mechanistic assays indicated that **C5** suppressed A2780 proliferation, induced apoptosis, and caused S-phase cell-cycle arrest in a concentration-dependent manner. Compounds **C12**, **C14**, and **C15** exhibited cytotoxicity toward HeLa cells (IC_{50} = 30.8, 13.7, and 14.1 μM) and A549 cells (IC_{50} = 24.7, 7.4, and 10.3 μM), respectively. Compound **C36** exhibited potent activity in HepG2/HeLa (IC_{50} both < 20 μM), indicating selectivity toward these two cell lines; compound **C38** showed moderate activity in A549/HeLa (16.55–26.49 μM), also displaying selectivity; compound **C37** was moderate and selective toward A2780 (25.73 μM); and compound **C30** showed moderate activity only in A549 (38.81 μM). Compound **C32** exhibited inhibitory activity across multiple cell lines with IC_{50} values of 22.49–85.14 μM, indicating broad-spectrum activity.

Antimicrobial testing showed that compounds **C5–C6** and **C10** were active against *Bacillus subtilis*, *Clostridium perfringens*, and *Staphylococcus aureus* (MIC 16–31 μg/mL). Compounds **C12–C15** displayed moderate activity against *Pseudomonas aeruginosa*, with **C13** also showing weak activity against *S. aureus*. Compounds **C20** and **C21** were active against *P. aeruginosa*, with MIC 62.0 μg/mL and MBC 248 μg/mL. In addition, compound **C9** showed antifungal activity against *Sclerotinia sclerotiorum* and *Phytophthora nicotianae* var. nicotianae, with respective IC_{50} values of 88.14 ± 2.21 μg/mL and 52.36 ± 1.38 μg/mL.

Overall, this work expands the chemical space of helicosporous hyphomycetes and yields promising lead scaffolds; coupling genome mining and metabolomics with SAR/MoA studies around **C5**, and leveraging scale-up fermentation and semisynthesis for supply and derivatization, will accelerate the discovery of antibacterial and anticancer candidates.

Keywords: Helicosporous Hyphomycetes, Tubeufiaceae, *Neohelicosporium*, *Tubeufia*, *Helicosporium*, Secondary Metabolites, Polyketides, *A*-Tetralone, Dibenzo-*A*-Pyrone, Antifungal, Antibacterial, Cytotoxicity

TABLE OF CONTENTS

TABLE OF CONTENTS

TABLE OF CONTENTS

LIST OF TABLES

LIST OF FIGURES

LIST OF FIGURES

CHAPTER 1

INTRODUCTION

1.1 Fungal Natural Products: An Important Source of Antibacterial and Anticancer Drugs

Fungi, by virtue of their rich and distinctive secondary metabolites, occupy a central place in natural products chemistry and drug discovery, and show particular promise for addressing antibacterial resistance and the bottlenecks of cancer therapy (Charria-Girón et al., 2025; Newman & Cragg, 2020; Vijayalakshmi et al., 2020). Compared with other sources, fungal metabolites offer advantages in scaffold diversity, functional-group combinations, and downstream derivatizability; they not only yield directly active molecules but also frequently serve as starting points for semisynthetic optimization (Bills & Gloer, 2016; Newman & Cragg, 2020). Both historical experience and current clinical practice bear this out: penicillins, cephalosporins (Bush & Bradford, 2016), pleuromutilin derivatives (File et al., 2019), and fusidic acid (Fernandes, 2016) have established multiple pillars of modern antibacterial therapy. In oncology, fungal small-molecule secondary metabolites have furnished distinctive cytotoxic scaffolds and mechanism-diverse leads—several advancing into clinical evaluation—including the illudin-derived agent irofulven (Poindessous et al., 2003); the fumagillin analog TNP-470 (AGM-1470) (Zhang et al., 2000), an anti-angiogenic compound tested in phase I/II; and plinabulin (Han et al., 2024), a derivative of the Aspergillus metabolite phenylahistin, which improved overall survival when combined with docetaxel in a phase 3 trial in EGFR-wild-type NSCLC.

Taken together, both historical experience and current clinical needs underscore the central role of fungal natural products in the discovery of antibacterial and

anticancer agents. Compared with other sources, their chemical space offers greater novelty and amenability to derivatization, enabling differentiated mechanisms of action and facilitating clinical translation. Accordingly, the exploration of fungal secondary metabolites with anticancer or antibacterial activity remains—and will continue to be—a priority for current and future research.

1.2 Current Status of Research on Secondary Metabolites of Helicosporous Hyphomycetes

Helicosporous hyphomycetes are asexual fungi whose conidia coil more than 180° in two or three dimensions (Lu et al., 2018; Ma et al., 2024; Lu & Kang, 2020). Existing studies indicate that they are chiefly isolated from lignicolous substrates on land or from submerged wood, predominantly saprobic with occasional endophytic records (Lu et al., 2018; Ma et al., 2024; Lu & Kang, 2020). As a distinctive saprobe-dominated group, they combine unique morphological traits with notable metabolic potential. Guizhou's typical karst landforms—with their mountainous gorges and stream habitats—harbor diverse decaying-wood microenvironments. In recent years, multiple new helicosporous taxa have been discovered from this region, providing key material for exploring species and chemical diversity in this lineage (Lu et al., 2018; Ma et al., 2024; Lu & Kang, 2020). Reported metabolites from helicosporous hyphomycetes include alkaloids, glycolipids, polyketides, and terpenoids, exhibiting antibacterial, anticancer, and antidiabetic activities (Lu & Kang, 2020). Early work can be traced to Itazaki et al. (1990), who isolated two new cyclic peptides from *Helicoma ambiens* RF-1023; these natural histone deacetylase inhibitors suppressed the proliferation of NIH3T3 cells transformed by the v-sis oncogene. Subsequently, Zenkoh et al. (2004) obtained two new cyclic tripeptides from *Helicomyces* sp. No. 19353 as inhibitors of gluconeogenesis. Hu et al. (2006) purified six polyketides from

Helicoma viridis, four of which were new and all active against drug-resistant *Pseudomonas aeruginosa*. Mudur et al. (2006) isolated three new hemiketal compounds from cultures of *Helicodendron giganteum*; among them, heliconol A exhibited both antifungal and antibacterial activities. Choi et al. (2012) reported that the fermentation products of *Helicosporium* sp. displayed multiple bioactivities—including antibacterial, antifungal, and cytotoxic effects—with 2-methylresorcinol identified as the major active component. Lee et al. (2013) showed that *Helicosporium* sp. 0635BP had strong antagonistic activity against turfgrass pathogens (e.g., *Fusarium* spp., *Rhizoctonia solani*, and *Pythium* spp.), highlighting its potential as a biocontrol agent. Shan et al. (2014) and Tian et al. (2016) isolated nine new helical binaphthalene derivatives from the endophytic fungus *Berkleasmium* sp.; some exhibited pronounced antibacterial, anticancer, and insecticidal activities, indicating promising medicinal potential. Qian et al. (2023), Li et al. (2024), and Zeng et al. (2022) isolated 32 compounds from T*ubeufia rubra* PF02-2, including one new and uncommon symmetric 16-membered-ring scaffold, three new nitrogen-containing glycerides, two new glyceroglycolipids, and one new ergosterol-type compound. Among them, the nitrogenous glyceride Rubracin A markedly lowered the IC_{50} of doxorubicin when co-administered, demonstrating multidrug-resistance (MDR)–reversing activity (Zeng et al., 2022). The glyceroglycolipids Rubracin D (2) and Rubracin E (3) also showed pronounced MDR-reversal effects, restoring drug sensitivity in resistant cancer cell lines (MCF-7/ADM, K562/ADM, A549/ADM) by suppressing P-glycoprotein overexpression; under certain conditions their activity even surpassed that of the positive control verapamil (Qian et al., 2023; Kang et al., 2022, 2023). Zheng et al. (2024a), Zheng et al. (2023), and Zheng (2024) obtained one new alkaloid, one new ergosterol derivative, and 15 known compounds from *Neohelicomyces hyalosporus* PF11-1. The ergosterol Citrostadienol exhibited strong cytotoxicity against HepG2 cells (Zheng et al., 2023). The macrolide Paecilomycin F targets TAK1, modulates the MAPK and mTOR pathways, inhibits

cisplatin-induced autophagy, and thereby enhances cisplatin's inhibitory effect on ovarian cancer cells (Zheng, 2024). Zheng (2024) and Zheng et al. (2024b) also isolated four new sesquiterpene dimers and two new nucleoside derivatives from *Helicoma septoconstrictum* TW03-2; among them, the sesquiterpene dimer Helicoside C displayed potent cytotoxicity toward A2780 cells, elevated intracellular ROS levels, and induced mitochondria-dependent apoptosis by suppressing STAT3 phosphorylation.

Collectively, helicosporous hyphomycetes constitute an ecologically diverse yet conspicuously under-studied fungal group with substantial chemical promise. Their characteristic helicoid conidia are associated with rich, differentiated repertoires of secondary metabolites; published members already include molecules with antibacterial and cytotoxic activities, indicating strong potential to deliver new scaffolds and modes of action. Therefore, we prioritized this group as a focal subject of investigation to discover lead molecules with anticancer and/or antibacterial activities.

1.3 Practical Routes to Enhancing the Diversity of Fungal Secondary Metabolites

However, the biosynthesis of fungal secondary metabolites is regulated by multiple factors. To promote the production of more secondary metabolites, two main approaches are commonly employed: (i) strain-level molecular (genetic) regulation and (ii) culture-based metabolic regulation (Atanasov et al., 2021). The former typically involves higher development costs, longer timelines, and greater technical difficulty, and is more suitable for strains with available genome information and well-characterized biosynthetic pathways (Lyu et al., 2020). By contrast, the OSMAC strategy (one strain–many compounds) uses a series of simple, practical measures—such as altering medium composition and cultivation conditions, or introducing perturbations like enzyme

inhibitors—to stimulate microorganisms to activate different biosynthetic gene clusters, thereby yielding structurally novel and highly active compounds (Hu et al., 2021). Given that genomic information for helicosporous hyphomycetes remains incomplete, this study prioritizes culture-based approaches to mine their bioactive secondary metabolites.

1.4 Research Gaps

Insufficient Mining of Chemical Novelty and Diversity in Helicosporous Hyphomycetes

1.5 Objectives

1.5.1 To expand the chemical diversity of Selected Helicosporous Tubeufiaceae and explore its metabolic potential.

1.5.2 To expand the chemical novelty of Selected Helicosporous Tubeufiaceae and definitively elucidate the structures of new compounds.

1.5.3 To clarify the pharmacological active substance basis and to discover lead compounds.

1.5.4 To summarize strategies for mining new fungal secondary metabolites.

1.6 Expected Outcome

1.6.1 Obtain 4~6 active target fungal strains and 30~50 monomer compounds.

1.6.2 Obtain 1-3 lead compounds and to preliminarily elucidate its mechanism of action.

1.6.3 Provide a review on strategies for mining new secondary metabolites from fungi.

CHAPTER 2

SELECTION OF TARGET ACTIVE STRAINS

2.1 Introduction

This chapter aims to obtain Tubeufiaceae fungi with antitumor potential through systematic screening based on bioactivity assays and metabolite profiling. The fermentation conditions of the active strains will then be optimized, followed by large-scale fermentation. The fermentation products will be systematically isolated and purified to obtain monomeric compounds. These compounds will subsequently undergo antitumor activity assays to identify promising lead compounds, which will be subjected to preliminary studies on their antitumor mechanisms. Ultimately, the goal is to elucidate the bioactive basis underlying their antitumor pharmacological effects.

2.2 Materials and Methods

2.2.1 Materials

2.2.1.1 Preparation of culture medium

PDA medium: A total of 39 g of commercial PDA powder (Oxoid, UK) was dissolved in distilled water to a final volume of 1 L. The solution was kept at its natural pH and sterilized at 121°C for 20 min.

PDB medium: Two hundred grams of peeled potatoes were cut into small pieces and boiled in 1 L of distilled water for 30 min. The decoction was filtered through four layers of cheesecloth, the filtrate was made up to 1 L with distilled water, and 20 g of glucose was added. The pH was not adjusted, and the medium was sterilized at 121°C for 20 min.

Fungal medium No. 2: Maltose (20 g), sodium glutamate (10 g), KH_2PO_4 (0.5 g), $MgSO_4$ (0.3 g), glucose (10 g), yeast powder (3 g), and mannitol (20 g) were

dissolved in tap water and adjusted to 1 L. The pH was left unchanged, and sterilization was performed at 121°C for 20 min.

Sabouraud Dextrose Broth (SDB): Peptone (10 g) and glucose (40 g) were dissolved in distilled water and brought up to 1 L. The natural pH was maintained, and the solution was sterilized at 121°C for 30 min.

Modified Martin's liquid medium: Glucose (10 g), peptone (5 g), KH_2PO_4 (1 g), and $MgSO_4 \cdot 7H_2O$ (0.5 g) were dissolved in distilled water and diluted to 1 L. Without adjusting the pH, the medium was autoclaved at 121°C for 20 min.

Rice solid medium: Fifty grams of rice were placed in a 200 mL autoclavable bag with 50 mL of distilled water. The mixture was gently shaken to ensure the rice was moistened, the pH remained natural, and sterilization was carried out at 121°C for 30 min.

Oat solid medium: Fifty grams of raw oatmeal were weighed into a 200 mL autoclavable bag, followed by the addition of 35 mL of distilled water. After gentle shaking until the oatmeal was wetted, the pH was kept unadjusted, and the medium was sterilized at 121°C for 30 min.

2.2.1.2 Preparation of chromogenic reagent

10% sulfuric acid–ethanol chromogenic reagent: 50 mL of concentrated sulfuric acid was slowly added to 500 mL of ethanol with continuous stirring, and the solution was mixed thoroughly.

2.2.1.3 HPLC conditions

Chromatographic analyses were performed on an Agilent 1260 system using a ZORBAX C18 column (250 × 4.6 mm, 5 μm). Elution employed water (A) and methanol (B) with a linear increase of B from 10% to 100% over 0–50 min, followed by a 15-min hold at 100% B. The flow rate was 1.0 mL/min, the column temperature was kept at 40°C, and detection was acquired by a photodiode-array detector at 220, 254, 280, 310, and 330 nm.

2.2.2 Methods

2.2.2.1 Small-scale fermentation of strains

The fungal strains were first activated and inoculated onto PDA medium, then incubated at 28°C in a thermostatic incubator until the colony diameter reached 2 cm. The mycelia were subsequently transferred to liquid medium and and cultured in

a rotary shaker (28°C, 180 rpm) for approximately one week to prepare seed inocula. The seed culture was then inoculated onto solid medium for small-scale fermentation, which was maintained for 2–5 months until the substrate was fully colonized by mycelia. The fermented materials were extracted with ethyl acetate–methanol (10:1) by soaking and stirring, and the extracts were concentrated to dryness using a rotary evaporator for further use.

2.2.2.2 Preliminary screening of antitumor activity of crude extracts

The antitumor activity was evaluated using the MTT assay to examine the effects of crude extracts from small-scale fermentation on the proliferation of human ovarian cancer cells (A2780), breast cancer cells (MCF-7), non-small cell lung cancer cells (A549), prostate cancer cells (PC-3), and other tumor cell lines.

Cytotoxicity assay (MTT or CCK-8)

Log-phase cells were seeded in 96-well plates (5×10^3 cells/well) and incubated overnight for attachment. Cells were then treated with graded concentrations of crude extracts, with 0.1% DMSO as the control (n = 5 per group). After 24 h, cytotoxicity was assessed using either the MTT assay (20 μL of 5 mg/mL MTT, 4 h incubation, formazan dissolved in 150 μL DMSO, absorbance at 570 nm) or the CCK-8 assay (10 μL reagent, 2 h incubation, absorbance at 450 nm). IC_{50} values were calculated from dose–response curves.

2.2.2.3 Evaluation of extract abundance

Fermentation products obtained from small-scale fermentation using rice medium were extracted with ethyl acetate–methanol (10:1) by soaking and stirring. The extracts were analyzed by thin-layer chromatography (TLC), and the chromatograms were observed under UV light at 254 nm and 365 nm. Plates were then developed using visualization reagents, including 10% sulfuric acid–ethanol, modified potassium iodide, and 5% vanillin–sulfuric acid, and the resulting spots were recorded. In addition, the crude extracts were concentrated to dryness, dissolved in methanol, and analyzed by high-performance liquid chromatography (HPLC) to establish chromatographic fingerprints.

Based on the combined results of preliminary antitumor activity screening and metabolite abundance profiling, the target active strains were selected for further investigation.

2.3 Results and Discussion

2.3.1 Selection of Liquid Medium for Seed Culture

Activated strains were inoculated into five different liquid media (PDB, SDB, Fungal medium No. 2, and Modified Martin's liquid medium), and after one week of cultivation, the results indicated that the majority of strains grew more rapidly in Modified Martin's medium (Figure 2.1).

Figure 2.1 Growth status of seed cultures in different liquid media

2.3.2 Cytotoxicity of Crude Extracts from Small-scale Fermentation

The MTT assay revealed that crude extracts of secondary metabolites from strains SLGF-5, GYSLGY-1, SLGF-15, WZS71, and LZ15 significantly inhibited the proliferation of A2780 cells, with IC_{50} values of 0.0067, 0.0042, 0.0046, 0.0072, and 0.0083 mg/mL, respectively (Figure 2.2).

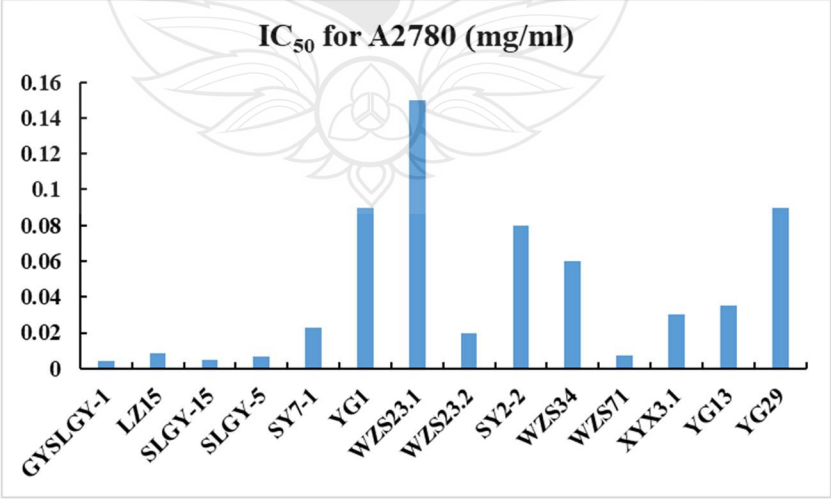

Figure 2.2 Cytotoxicity of crude extracts from small-scale fermentation

2.3.3 Metabolite Profiling of Crude Extracts from Representative Strains

The small-scale fermentation products of the strains were extracted three times with ethyl acetate–methanol (10:1, v/v) under repeated stirring. The combined extracts were evaporated to dryness, and the residues were dissolved in methanol to obtain samples at a concentration of 1 mg/mL. After filtration through a 0.22 μm microporous membrane, 20 μL of each sample was injected for fingerprint analysis. The results revealed that strain LZ15 produced the most abundant secondary metabolites, with the fermentation on raw oatmeal yielding a richer metabolite profile than that on rice (Figure. 2.7). Among the other strains, the abundance of secondary metabolites followed the order: GYSLGY-1 > WZS71 > SLGY-15 > SLGF-5 (Figures 2.3–2.6).

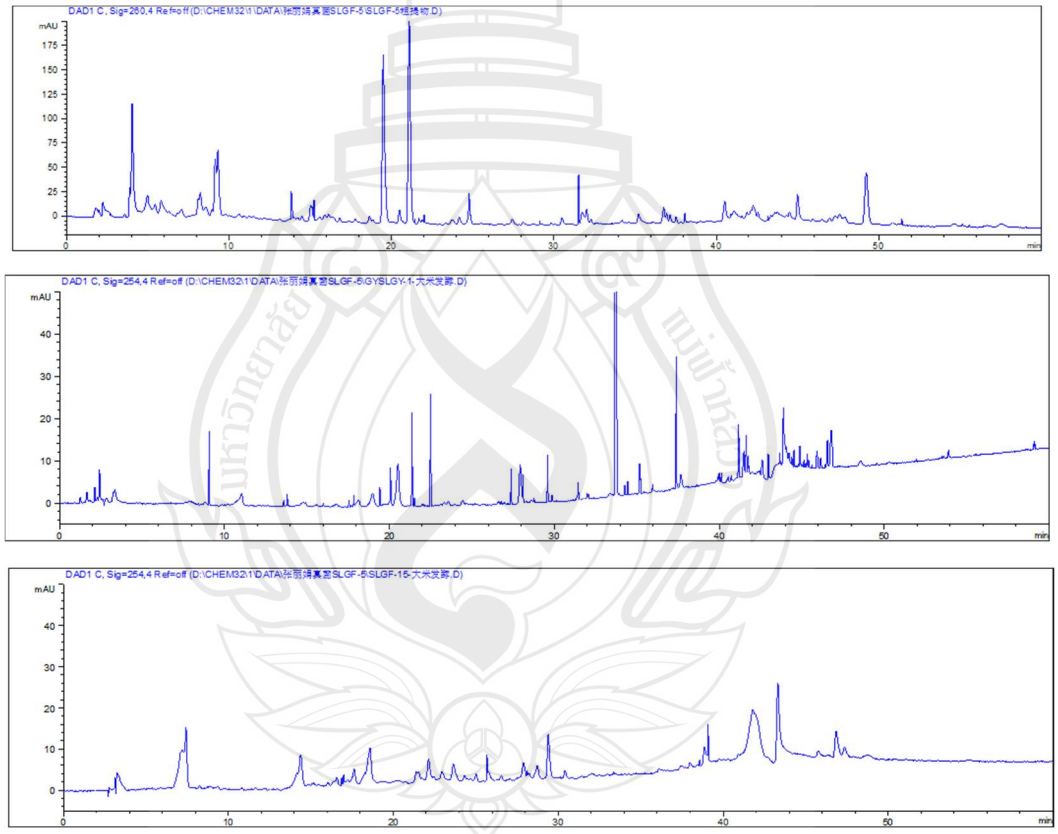

Figure 2.3 HPLC profiles of the fermentation products of strain *Neohelicosporium guangxiense* SLGY-5

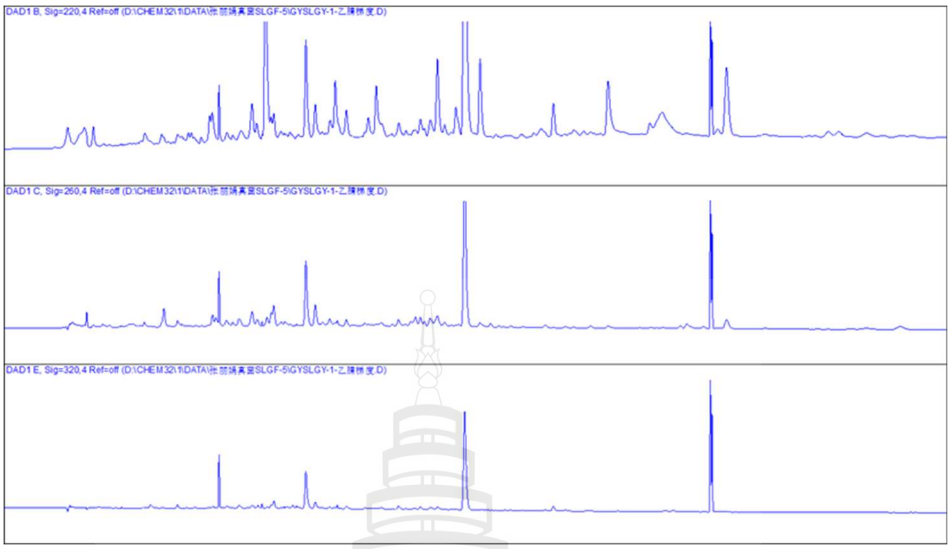

Figure 2.4 HPLC profiles of the fermentation products of strain *N. griseum* GYSLGY-1

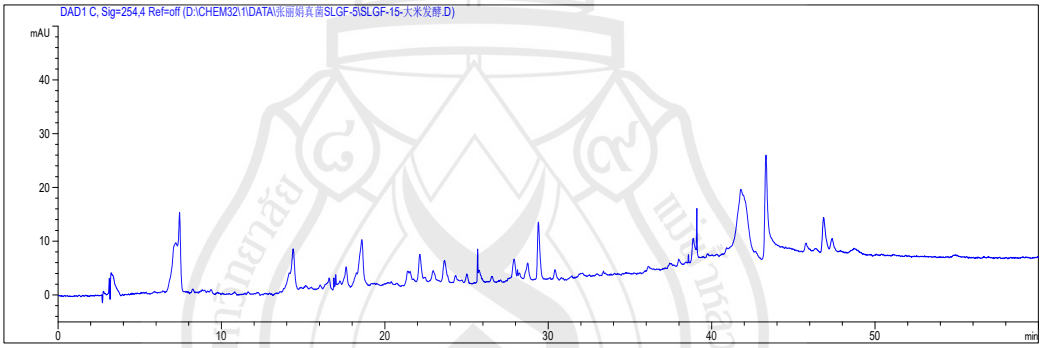

Figure 2.5 HPLC profiles of the fermentation products of strain *N. griseum* SLGY-15

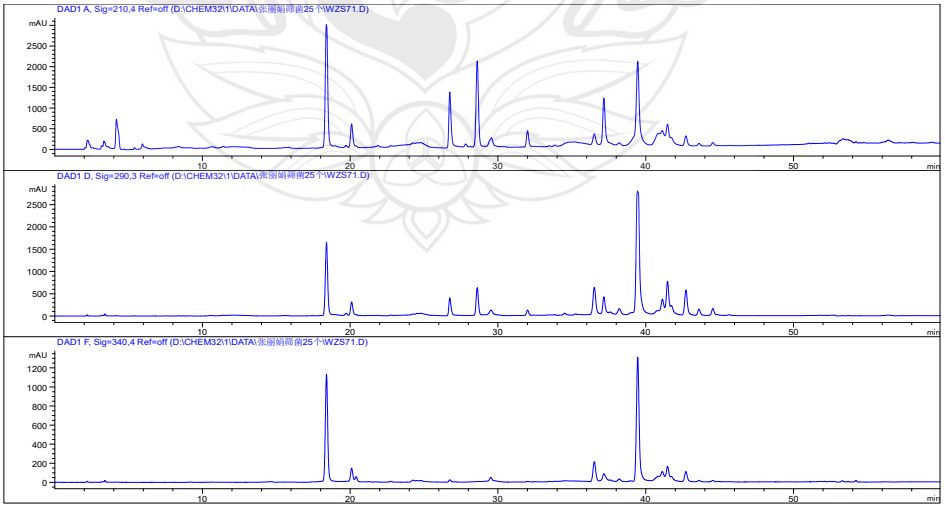

Figure 2.6 HPLC profiles of the fermentation products of strain *Tubeufia longihelicospora* WZS71

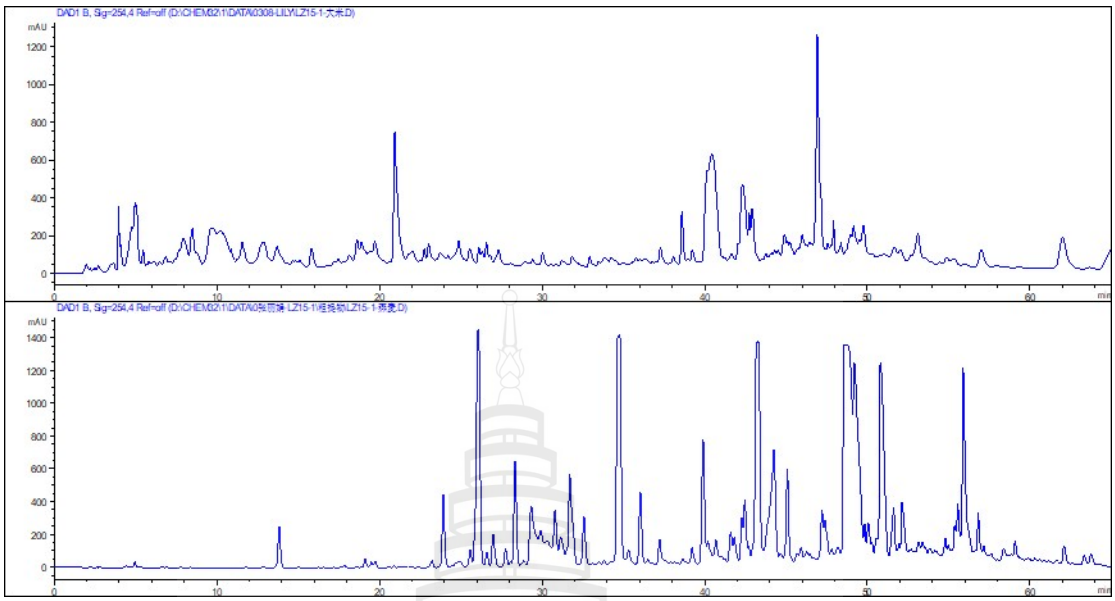

Figure 2.7 HPLC profiles of the fermentation products of strain *H. sexuale* LZ15-1 [rice (top) vs. raw oatmeal (bottom)], detected at λ = 254 nm.

2.4 Conclusion

Based on chemical screening and cytotoxicity evaluation, five Tubeufiaceae strains were ultimately selected as the focus of this study, namely *Neohelicosporium guangxiense* SLGY-5, *N. griseum* GYSLGY-1, *N. griseum* SLGY-15, *Tubeufia longihelicospora* WZS71, and *Helicosporium sexuale* LZ15, for which a systematic investigation of their secondary metabolites is planned.

CHAPTER 3

RESEARCH ON THE SECONDARY METABOLITES OF *NEOHELICOSPORIUM GUANGXIENSE* SLGY-5

3.1 Introduction

Helicosporous hyphomycetes as asexual fungi with their specific conidia coiled at least 180 in a two-dimensional plane or three-dimensional space are widely distributed in terrestrial and aquatic environments, especially in tropical and subtropical regions (Boonmee et al., 2014; Lu, Boonmee, et al., 2018; Lu, Liu, et al., 2018; Tsui & Berbee, 2006). Researches on helicosporous hyphomycetes have been mainly focused on morphological and phylogenetic studies (Boonmee et al., 2014; Lu, Boonmee, Bhat, et al., 2017; Lu, Boonmee, Liu, et al., 2017; Lu, Boonmee, et al., 2018; Lu, Liu, et al., 2018; Luo et al., 2017; Tian et al., 2022; Tsui & Berbee, 2006). Until now only a few species were studied for their secondary metabolites with several novel structures, which had various biological activities including anti-tumor, anti-bacterial, anti-diabetes, etc (Baker & Alvi, 2004; Hu et al., 2006; Itazaki et al., 1990; Nakai et al., 1991; Ohtsu et al., 2003; Zeng et al., 2022). All the above studies indicated that the metabolites of helicosporous hyphomycetes were abundant and had a potentially wide range of biological activities. These studies prompted us to study this kind of fungi to further discover novel active metabolites.

In this study, Activity-guided fractionation of the EtOAc extract of solid fermentation product of Neohelicosporium guangxiense yielded four compounds (**C1**–**C4**) by various chromatographic separation and purification techniques. Their isolation, structure determination and biological activity are described.

3.2 Materials and Methods

3.2.1 Materials

NMR spectra were recorded on Bruker 600 MHz, and tetramethylsilane (TMS) was used as an internal standard. Electro-spray ionization mass spectrometry (ESIMS) and high-resolution electrospray ionization mass spectrometry (HRESIMS) analyses were measured on Waters Xevo TQS and A Waters Xevo G2S Q-TOF LC/MS, respectively. Optical rotations were recorded in methanol (MeOH) solution on an AUTOPOL1 polarimeter at 25°C (Rudolph, American). CD spectra were obtained on a J-810 circular dichroism spectropolarimeter (JASCO Corp., J-810, Japan). Column chromatography was performed on silica gel (200−300 mesh, Qingdao Marine Chemical Co., Ltd., China) and Sephadex LH-20 (Amersham Biosciences, Uppsala, Sweden), respectively. HPLC analysis was performed on Agilent 1260 with a C18 column (Agilent Extend-C18, 4.6 ×250 mm, 5 μm, 1 mL/min). HPLC separation was performed on Shimadzu Soviet production LC-16P with an ODS column (MC-pack ODS-A, 10 × 250 mm, 5 μm, 3 mL/min).

Fungal materials: The producing strain N. guangxienseSLGY-5 was isolated from decaying wood in a terrestrial montane habitat (Guiyang Forest Park, Guiyang City, Guizhou Province, China; 14 September 2020; collector: Jian Ma). The strain is deposited as GZAAS 22-2001 (voucher) and maintained as a living culture GZCC 22-2001. Identification was supported by DNA sequences deposited in GenBank: OQ073569 (ITS), OQ073570 (LSU), OQ091255 (RPB2), OQ091256 (TEF1-α).

3.2.2 Methods

3.2.2.1 Cultivation and fermentation of crude extracts

The strain of N. guangxiense was cultured on PDA at 28°C for 10 days and then was inoculated into 20 × 250 mL Erlenmeyer flasks, each containing a 125 mL liquid medium (maltose 20 g, sodium glutamate 10 g, potassium dihydrogen phosphate 0.5 g, magnesium sulfate 0.3 g, glucose 10 g, yeast powder 3 g, mannitol 20 g, tap water 1 L). These flasks were incubated on a shaking table at 28°C and 180 RPM for 7 days. About 5 mL of the seed liquid was transferred to a 200 mL plastic bag prepared from 50 g rice and 55 mL distilled water. These bags were incubated at 28 °C under static conditions for 2 months. A total of 400 bags were fermented.

3.2.2.2 Extraction and isolation of metabolites from *Neohelicosporium guangxiense*

The rice fermentation product was extracted three times with EtOAc/ methanol (10:1) (each 50 L), and the combined EtOAc /methanol (10:1) solutions were dried in vacuo to yield 72.3 g crude extract. The 72.3 g of crude extract was subjected to column chromatography (CC) over silica gel (PE/EtOAc, v/v, 100:0→0:100) to give 15 fractions (Fr.1–15). Fr.7 was separated with Sephadex LH-20 in MeOH to yield 4 subfractions (Fr.7.1–7.4). Fr.7.4 was chromatographed again with silica gel (PE/EtOAc, v/v, 7:3) to afford 5 subfractions (Fr.7.4.1–7.4.5). Fr.7.4.4 was further purified by Sephadex LH-20 in MeOH to afford compound **C2** (100.0 mg). Fr.7.4.3 was further purified by semi-preparative HPLC eluted with MeOH/H2O (50:50, 3 mL/min) to afford compound **C3** (t_R =15 min, 8.5 mg). Fr.7.4.5 was further purified by semi-preparative HPLC eluted with MeOH/H2O (40:60, 3 mL/min) to afford compound **C1** (t_R = 18 min, 3.0 mg). Fr.10 was chromatographed again with silica gel (PE/EtOAc, v/v, 6:4) to afford 4 subfractions (Fr.10.1–10.4). Fr.10.3 was separated with Sephadex LH-20 in MeOH to afford compound **C4** (210.0 mg).

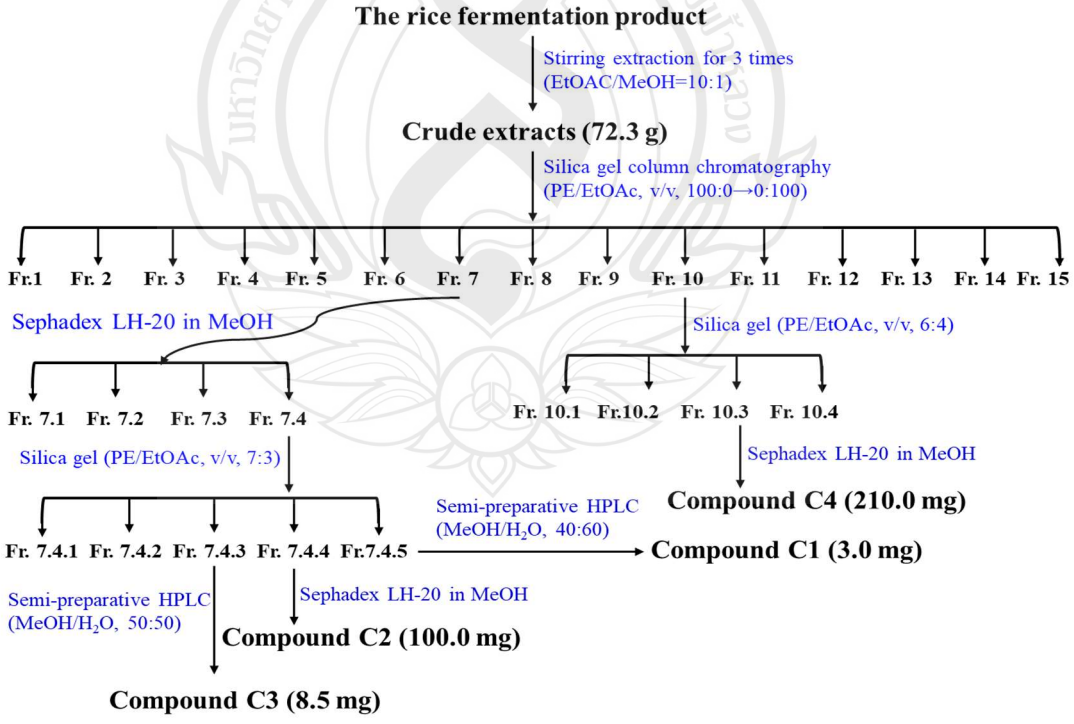

Figure 3.1 Flowchart of extraction and separation of metabolites from *Neohelicosporium guangxiense*

3.2.2.3 Biological assays

Compounds **C1** to **C4** were tested for their antimicrobial activity against two fungi (*Candida albicans* and *C. glabrata*), three agricultural pathogenic fungi (*Fusarium graminearum*, *Phytophthora nicotianae* var. nicotianae, *Sclerotinia sclerotiorum*), five Gram-positive bacteria (*Bacillus subtilis*, *Clostridium perfringens*, *Ralstonia solanacearum*, *Staphylococcus aureus*, MRSA strain *Staphylococcus aureus*), and three Gram-negative bacteria (*Escherichia coli*, *Paratyphoid fever*, *Pseudomonas aeruginosa*), using ciprofloxacin as a positive control against Gram-positive and Gram-negative bacteria, while ketoconazole was used as an antifungal positive control. Besides, cytotoxicities of the compounds against three mammalian cell lines (human ovarian cancer cell A2780, human prostate cancer cell PC-3, and human breast cancer cell MBA-MD-231) were determined by the microculture tetrazolium test (MTT) method, using cis-platinum as the positive control against A2780 and PC-3, while adriamycin was used as a positive control against MBA-MD-231. All bioactivity assays were performed following the standard protocols (Shao et al., 2020; Wang et al., 2019)

3.3 Results and Discussion

Identification of the major metabolite from Neohelicosporium guangxiense

Three α-tetralon derivatives (**C1**-**C3**) and one isocoumarin derivative (**C4**) were isolated from rice fermentation products of *Neohelicosporium guangxiense*. Their structures are shown in Figure 3.2.

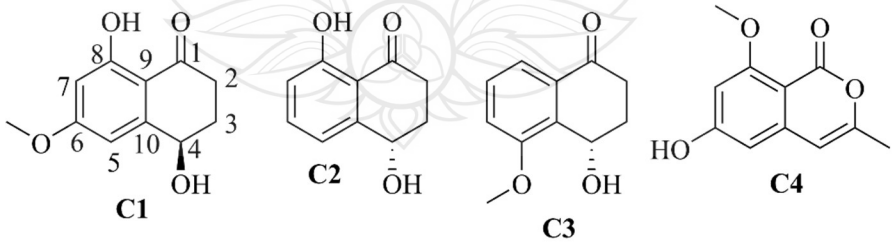

Figure 3.2 Chemical structures of compound **C1**–**C4** isolated from *Neohelicosporium guangxiense*

(*R*)-4,8-dihydroxy-6-methoxy-3,4-dihydronaphthalen-1(2*H*)-one (**C1**) Yield 3.0 mg, light brown solid; $[\alpha]_D^{25}$ +100 (c 0.2, MeOH). ^1H and ^{13}C NMR data (Table 3.1). Its molecular formula was determined as $C_{11}H_{12}O_4$, according to the ESI-MS (*m/z* 208.9 $[M+H]^+$, 207.0 $[M-H]^-$), HR-ESI-MS (*m/z* 209.26057 $[M+H]^+$, 207.0696 $[M-H]^-$), indicating 6 degrees of unsaturation. The ^1H NMR spectrum, recorded at 600 Hz in DMSO, exhibited 12 protons (including two active hydrogens, three hydrogens on methoxy groups, two aromatic hydrogen, five alkyl hydrogen, Table 3.1), and two aromatic hydrogens on the benzene ring are meta-coupled [6.63 (d, J = 2.5 Hz, 1H), 6.37 (d, J = 2.5 Hz, 1H)]. Furthermore, the ^{13}C NMR spectrum revealed the presence of 11 carbons (including one carbonyl carbon, Table 3.1). Combining with the 1H NMR spectrum and the unsaturation (6) of the molecular formula, compound **C1** belongs to a benzo-cyclohexanones derivative. According to the molecular formula and the ^1H, ^{13}C HSQC spectrum, the carbon signals could be classified into 3 groups showing seven signals (including an sp3-methoxy carbon, two sp3-methines carbons, one sp3 oxygen-bearing carbon, 2 sp2 aromatic carbons), and 5-nonprotonated carbons including three oxygenated ones. The HSQC spectrum also shows that both H-3 (δ_H 1.91 ppm) and H-4 (δ_H 2.15 ppm) are correlated with C-3, which indicates that H-3 and H-4 are connected to the same carbon (C-3). Moreover, the ^1H-^1H -COSY spectrum (Figure 3.3) indicates that H-3 (δ_H 1.91 ppm) and H-4 (δ_H 2.15 ppm) coupled with each other, H-3 (δ_H 1.91 ppm) and H-1/H-2 (δ_H 2.67 ppm) coupled with each other, H-4 (δ_H 2.15 ppm) and H-1/H-2 (δ_H 2.67 ppm) coupled with each other, H-3 (δ_H 1.91 ppm) and H-5 (δ_H 4.68 ppm) coupled with each other, H-5 (δ_H 4.68 ppm) and H-6 (δ_H 5.64 ppm) coupled with each other, the above signals shows that C-2 (δ_C 35.0 ppm) and C-3(δ_C 31.5 ppm) are connected, C-3 (δ_C 31.5 ppm) and C-4(δ_C 66.2 ppm) are connected, H-5 (δ_H 4.68 ppm) and H-6 (δ_H 5.64 ppm) are connected to the same carbon (C-4). Due to the ^1H, ^{13}C HMBC correlation (Figure 3.3) from H-1/H-2 (δ_H 2.67 ppm) to C-1 (δ_C 202.9 ppm), C-3 (δ_C 31.5 ppm), C-4 (δ_C 66.2 ppm), combined with COSY signal, the connection mode of C-1 to C-4 are determined. According to the ^1H, ^{13}C HMBC correlation from C-8-OH (δ_H 12.87 ppm) to C-7 (δ_C 99.3 ppm), C-8 (δ_C 164.6 ppm), C-8a (δ_C 109.4 ppm), the ^1H, ^{13}C HMBC correlation from H-9 (δ_H 3.82 ppm) to C-6 (δ_C 165.9 ppm), the 1H, 13C HMBC correlation from H-7 (δ_H 6.37 ppm) to C-5 (δ_C 104.9ppm), C-8 (δ_C 164.6 ppm), C-8a (δ_C 109.4 ppm), the ^1H, ^{13}C HMBC correlation from H-5 (δ_H 6.63 ppm) to C-4 (δ_C 66.2 ppm), C-7 (δ_C 99.3 ppm), C-8a (δ_C 109.4 ppm), the connecting position of substituents on benzene

ring and the way of union between the benzene ring and cyclohexanone were determined. Based on the above analysis, compound **C1** was identified as 4,8-dihydroxy-6-methoxy-3,4-dihydronaphthalen-**C1** (2*H*)-one (for detailed data see APPENDIX A). In order to determine the absolute configuration of C-4, the ECD curves (Figure 3.4) for the two possible isomers (4*R*) and (4*S*)-**C1** were calculated and compared with the experimental one. As shown in Figure 3.3, the calculated ECD curve for (4*R*)-**C1** matched well with the experimental curve, assigning (4*R*) absolute configuration for compound **C1**.

Table 3.1 1D-NMR spectroscopic data for compounds **C1** in DMSO-d6

No.	δC	δH (mult., J)
1	202.9, C	-
2	35.0, CH2	2.67 (overlap)
3	31.5, CH2	1.91 (overlap), 2.15 (overlap)
4	66.2, CH	4.68 (dt, 9.4, 5.2)
5	104.9, CH	6.63 (dd, 2.5, 1.1)
6	165.9, C	-
7	99.3, CH	6.37 (d, 2.5)
8	164.6, C	-
9	109.4, C	-
10	150.7, C	-
OCH3	55.7, CH3	3.82 (s)
4-OH	-	5.64 (d, 5.2)
8-OH	-	12.87 (s)

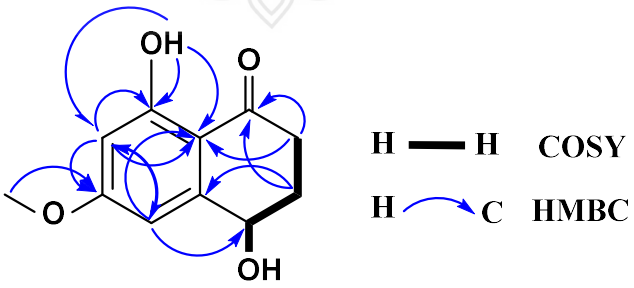

Figure 3.3 ^{1}H, ^{1}H COSY, ^{1}H, ^{13}C HMBC correlations for compound **C1**

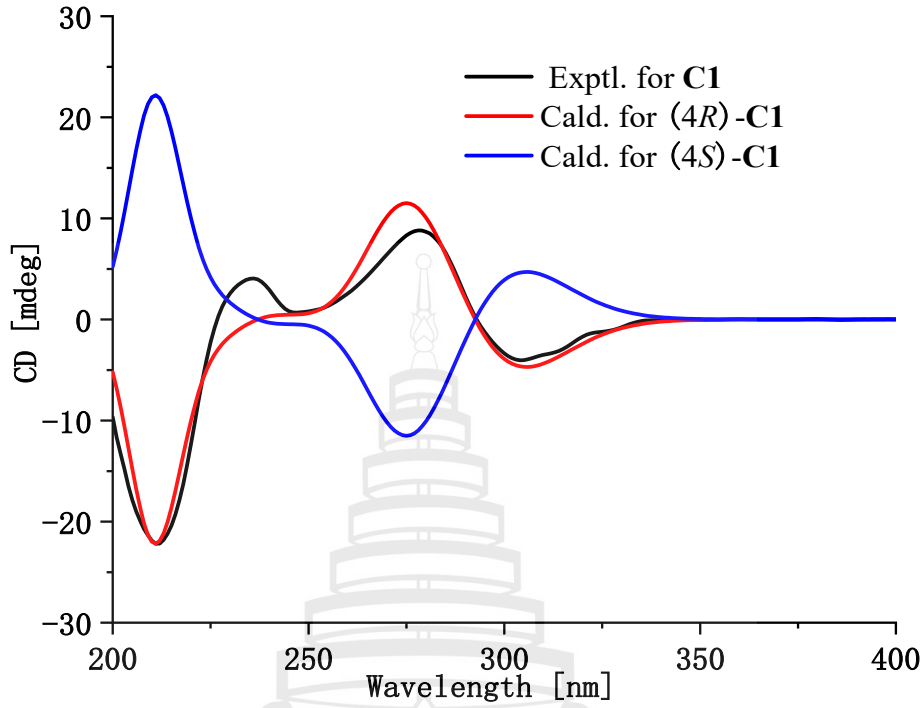

Figure 3.4 The experimental and calculated ECD curves for compound **C1**

(*S*)-3,4-dihydro-4, 8-dihydroxy-2H-naphthalen-1-one (**C2**) Yield 100.0 mg, white needle crystal; $[\alpha]_D^{25}$ -67.4 (c 0.27, MeOH). Its molecular formula was determined as $C_{10}H_{10}O_3$, according to the ESI-MS m/z 177.1 $[M-H]^-$ and ^1H and ^{13}C NMR data (for detailed data see APPENDIX A). Based on the above data, the compound **C2** was identified as (*S*)-3,4-dihydro-4, 8-dihydroxy-2H-naphthalen-1-one (Lu et al., 2014; Talapatra et al., 1988).

(*S*)-naphthalenone-3,4-dihydro-4-hydroxy-5-methosy (**C3**) Yield 8.5 mg, light yellow solid; $[\alpha]_D^{25}$ -28.9 (c 0.1, MeOH). Its molecular formula was determined as $C_{11}H_{12}O_3$, according to the ESI-MS *m/z* 215.1 $[M+Na]^+$, 191.1 $[M-H]^-$ and ^1H and ^{13}C NMR data (for detailed data see APPENDIX A). Based on the above data, the compound **C3** was identified as (*S*)-naphthalenone-3,4-dihydro-4-hydroxy-5-methosy (Wang et al., 2022; Yamamoto et al., 2003).

6-hydroxy-8-methoxy-3-methyl-isochromen-1-one (**C4**) Yield 210.0 mg, white needle crystal; Its molecular formula was determined as $C_{11}H_{10}O_4$, according to the ESI-MS m/z 229.1 $[M+Na]^+$, 435.0 $[2M+Na]^+$, and ^1H and ^{13}C NMR data (for detailed data see APPENDIX A). Based on the above data, the compound **C4** was identified as

6-hydroxy-8-methoxy-3-methyl-isochromen-1-one (Wu et al., 2019).

The biological activity

The cytotoxicity of the ethyl acetate (EtOAc) extracts of the solid fermentation broth from *Neohelicosporium guangxiense* was preliminarily evaluated. All compounds were tested for their antimicrobial activity and cytotoxicities. Although the EtOAc extract of the fermentation broth exhibited significant cytotoxicity against PC3 cell lines with IC_{50} value of 6.7 μg/mL, compounds **C1** to **C4** did not show significant antimicrobial and cytotoxic activity. A list of test microorganisms and cell lines used is in Supplementary Information.

3.4 Conclusion

Compounds **C1** to **C4** are firstly reported from helicosporous hyphomycetes. They are composed of only carbon, hydrogen, and oxygen, and contain a carbonyl and phenolic hydroxyl functional groups, suggesting that the biosynthetic pathway of these compounds might be polyketides (Chen et al., 2018).

The structure type of compounds **C1** to **C3** belongs to α-tetralon. Compounds with similar skeletons have previously been found in Tubeufiaceae (Hu et al., 2006); α-tetralon may serve as chemical markers for this kind of fungi. Meanwhile, α-tetralon is a kind of crucial pharmaceutical intermediate, which can be used in the synthesis of a variety of chemical drugs. It plays a vital role in drug design and functional group modification, and its derivatives have a wide range of biological activities. If this fungus can be used as a raw material to obtain α-tetralon intermediates, it may be possible to develop a green chemical synthesis process route than traditional ones. To the best overall knowledge, compound **C1** was isolated for the first time as a natural product from helicosporous hyphomycetes, and additionally, the absolute configuration of compound **C1** was revealed for the first time. The synthesized compound **C1** (Bös et al., 1997) is commercially available, but no report regarding its original natural sources has been confirmed. Nevertheless, it is reported from a fungal source (and as a natural product) for the first time. Meanwhile, the NMR spectra of compound **C1** were described in detail in this paper. The structure type of compound **C4** belongs to

dihydroisocoumarin, and the quantity is relatively large (210.0 mg), so dihydroisocoumarin may also serve as a chemical marker for this fungus. However additional strains, as well as related species, need to be further studied to assess whether this compound is species-specific.

Kokubun et al. (2003) reported that compound **C2** was mildly antibacterial towards Bacillus subtilis. The mixture of fermentation products had cytotoxic activity in this study, whereas compounds **C1**–**C4** did not. It is possible that the mixture had a synergistic effect or that the amount of active substances was so small that we were unable to isolate them.

CHAPTER 4

THE SECONDARY METABOLITES OF NEOHELICOSPORIUM GRISEUM GYSLGY-1

4.1 Introduction

Secondary metabolites of fungi have enormous potential, particularly for drug discovery (Keller, 2019). More than half of the compounds isolated from fungi were antibacterial, antifungal, or antitumor (Keller, 2019). Research on secondary metabolites of fungi concentrated primarily on endophytic fungi of medicinal plants, whereas research on secondary metabolites of saprophytic fungi was relatively uncommon (Meena et al., 2019).

Helicosporous hyphomycetes, such as the species of *Helicosporium*, *Helicoma*, *Helicomyces,* and *Tubeufia,* are capable of producing a variety of bioactive compounds (Hu et al., 2006; Itazaki et al., 1990; Nakai et al., 1991; Ohtsu et al., 2003; Qian et al., 2023; Zeng et al., 2022; Zheng et al., 2024). The vast majority of helicosporous hyphomycetes are members of the family *Tubeufiaceae* (Tubeufiales, Dothideomycetes) (Lu et al., 2018). However, this family study focuses primarily on morphology and phylogeny (Lu et al., 2018; Tian et al., 2022), and reports on secondary metabolites are scarce.

In this study, bioassay-guided isolation led to the discovery of three new compounds [two new polyketide derivatives, neogrisphenol A (**C5**) and neogrisphenol B (**C6**), and a new isochroman-1-one derivative named (*S*)-6-hydroxy-7-methoxy-3,5-dimethylisochroman-1-one (**C7**)] and four known compounds from the EtOAc extracts of the rice fermentation product of a new record fungus, *Neohelicosporium griseum* (Figure 4.1). Compounds **C5** and **C6** have a rare C-3~C-2′ linkage between the cyclohexanone ring of one *α*-naphthalone derivative and the cyclohexanone ring of another *α*-naphthalone derivative, which has not been reported in natural or synthetic products. The antimicrobial and cytotoxic activities of compounds **C5**–**C11** were

evaluated. Compound **C5** exhibited significant cytotoxicity against the A2780 cell line with IC_{50} values of 3.20 μM, higher than that of cisplatin (CDDP). The results showed that this compound might serve as a potential inhibitor of ovarian cancer.

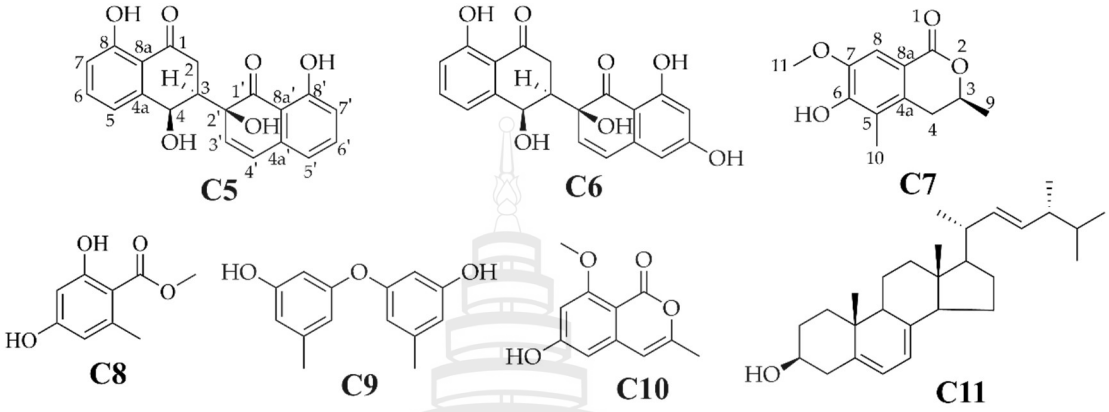

Figure 4.1 Chemical structures of compounds **C5–C11** isolated from *N. griseum*

4.2 Materials and Methods

4.2.1 General Experimental Procedure

Ultraviolet-visible (UV/Vis) spectra were acquired using a UV-Vis spectrophotometer, the UV-5300 (Hitachi, Tokyo, Japan). Infrared (IR) spectra were measured on a Bruke Vertex 80 (KBr disks) infrared spectrometer. Optical rotations were recorded in methanol (MeOH) solution on an AUTOPOL1 polarimeter at 28℃ (Rudolph, Wilmington, Massachusetts, USA). CD spectra were obtained on a J-810 circular dichroism spectropolarimeter (JASCO Corp., J-810, Tokyo, Japan). Electro-spray ionization mass spectrometry (ESIMS) and high-resolution electrospray ionization mass spectrometry (HRESIMS) analyses were measured on a Waters Xevo TQS and a Waters Xevo G2S Q-TOF LC/MS, respectively. NMR spectra were recorded on a Bruker 600 MHz instrument, and tetramethylsilane (TMS) was used as an internal standard. Column chromatography was performed on silica gel (200−300 mesh, Qingdao Marine Chemical Co., Ltd., Qingdao., China) and Sephadex LH-20 (Amersham Biosciences, Uppsala, Sweden), respectively. HPLC analysis was performed on an Agilent 1260 with a C18 column (Agilent Extend-C18, 4.6 × 250 mm, 5 μm, 1 mL/min). HPLC separation was performed on Shimadzu Soviet production LC-

16P with an ODS column (Silgreen C18AB, 10 × 250 mm, 5 μm, 180 Å, 3 mL/min). Cell apoptosis and cycle kits were purchased from BD Biosciences (San Jose, CA, USA).

4.2.2 Fungal Taxonomy and Identification

Decaying wood samples were collected randomly from sites in Guiyang Forest Park, China. The specimen examination, micromorphological study, DNA extraction, PCR amplification, sequencing, and phylogenetic analysis were conducted using the method described in Lu et al. (2022).

4.2.3 Fermentation, Extraction, and Isolation

The strain of *Neohelicosporium griseum* was cultured on PDA at 28℃ for 10 days and then was inoculated into 20 × 250 mL Erlenmeyer flasks, each containing a 125 mL liquid medium (maltose 20 g, sodium glutamate 10 g, potassium dihydrogen phosphate 0.5 g, magnesium sulfate 0.3 g, glucose 10 g, yeast powder 3 g, mannitol 20 g, tap water 1 L). These flasks were incubated on a shaking table at 28℃ and 180 RPM for 7 days. About 5 mL of the seed liquid was transferred to a 200-mL plastic bag prepared from 50 g rice and 55 mL of distilled water. These bags were incubated at 28℃ under static conditions for 3 months. A total of 400 bags were fermented.

The fermented product was extracted three times with ethyl acetate (EtOAc)/methanol (10:1) (each 50 L), and the combined EtOAc/methanol (10:1) solutions were dried in vacuo to yield 99.4 g of crude extract. The 99.4 g of crude extract was subjected to column chromatography (CC) over silica gel (PE/EtOAc, *v/v*, 100:0→0:100) to give 20 fractions (Fr.1–20). Of these, Fr.12 was separated with Sephadex LH-20 in MeOH to yield 4 subfractions (Fr.12.1–12.4). Sephadex LH-20 was used to separate Fr.12.4 into two subfractions (Fr.12.4.1–12.4.2) in MeOH. Fr.12.4.2 was further purified by RP-HPLC with MeOH/H_2O (50:50, 3 mL/min) to afford 4 (t_R = 18.5 min, 3.0 mg). Fr.12.3 was chromatographed again with silica gel (PE/EtOAc, *v/v*, 7:3) to afford 4 subfractions (Fr.12.3.1–12.3.4). Fr.12.3.2 was further purified by RP-HPLC with MeOH (3 mL/min) to afford 7 (t_R = 13.0 min, 6.3 mg). Fr.15 was divided into 4 subfractions (Fr.15.1–15.4) using Sephadex LH-20 in MeOH. Fr15.3 was further purified by RP-HPLC with MeOH/H_2O (60:40, 3 mL/min) to afford 1 (t_R = 10.3 min, 140.0 mg) and 5 (t_R = 13.4 min, 12.4 mg). Seven subfractions (Fr.18.1–18.7) of Fr.18 were obtained after separation using Sephadex LH-20 in MeOH. Fr18.2 was

further purified by RP-HPLC with MeOH/H_2O (35:65, 3 mL/min) to afford 3 (t_R = 16.6 min, 16.5 mg). Fr.18.4 was further separated with Sephadex LH-20 in $CHCl_2$/MeOH (1:1) to yield 3 subfractions (Fr.18.4.1–18.4.3). Fr.18.4.3 was further purified by RP-HPLC with MeOH/H_2O (40:60, 3 mL/min) to afford 6 (t_R = 18.2 min, 91.0 mg). Fr18.7 was further purified by RP-HPLC with MeOH/H_2O (40:60, 3 mL/min) to afford 2 (t_R = 22.0 min, 6.0 mg).

4.2.4 Biological Assays

4.2.4.1 Antimicrobial and Cytotoxic Activities of Compounds **C5**–**C11**

Compounds were evaluated for their antimicrobial activity against two fungi (*Candida albicans* and *C. glabrata*), three agricultural pathogenic fungi (*Fusarium graminearum*, *Phytophthora nicotianae var. nicotianae*, *Sclerotinia sclerotiorum*), five Gram-positive bacteria (*Bacillus subtilis*, *Clostridium perfringens*, *Ralstonia solanacearum*, *Staphylococcus aureus*, MRSA strain *Staphylococcus aureus*), and three Gram-negative bacteria (*Escherichia coli, Paratyphoid fever, Pseudomonas aeruginosa*), using ciprofloxacin as a positive control against Gram-positive and Gram-negative bacteria, while ketoconazole was used as an antifungal positive control. In addition, the compounds' cytotoxicities against three mammalian cell lines (human ovarian cancer A2780, human prostate cancer PC-3, and human breast cancer MBA-MD-231 cell lines) were examined by the MTT method, using cisplatin (CDDP) as the positive control against A2780 and PC-3, while adriamycin was used as a positive control against MBA-MD-231. The A2780 cell line was purchased from Xiamen Immocell Biotechnology Co.,Ltd (Xiamen, China). The PC-3 cell line was purchased from Shanghai Zhongqiao Xinzhou Biological Technology Co., Ltd. (Shanghai, China). The MBA-MD-231 cell line was purchased from Cell bank of Chinese Academy of Sciences (Shanghai, China). Following our standard protocols, all bioactivity assays were carried out (Shao et al., 2020; Wang et al., 2019).

4.2.4.2 Effect of Neogrisphenol A on the Growth of A2780 Cells

1. Cell Culture and Compound Treatment

The A2780 cells were maintained in Roswell Park Memorial Institute (RPMI) 1640 medium with 10% fetal bovine serum (FBS) and 1% Penicillin-Streptomycin Solution (100 mg/L streptomycin and 1×10^5 U/L penicillin) in a 37°C

incubator chamber with 5% CO_2. A stock solution of 2×10^4 μmol/L was prepared by dissolving neogrisphenol A (abbreviated as NeoA) in DMSO.

2. Cell Proliferation Assay

A2780 cells were plated in a 96-well plate with 5×10^3 cells/well, and various NeoA (1.25, 2.5, 5, 10, and 20 μmol/L) concentrations were added and incubated for 24, 48, and 72 h. Each concentration consisted of five multiple pores. The number of cells and morphological changes in the cells were observed under an inverted fluorescence microscope. An amount of 20 μL of MTT (5 mg/mL) reagent was added, and the plates were incubated for 4 h in the incubator chamber. The supernatant was discarded by centrifugation, and 150 μL of DMSO was added. The absorbance was measured at 490 nm, and the inhibition rate of cell proliferation was calculated: the inhibition rate = 1 (OD processing/OD control) × 100%.

3. Cell Apoptosis Assay

In order to detect the effect of NeoA on the apoptosis of A2780 cells, we selected to use the apoptosis detection kit. The A2780 cells were seeded into 6-well plates with 3×10^5 cells/well and incubated with NeoA (3.0, 6.0, and 12.0 μmol/L) and 0.1% DMSO for 24 h. Cells were digested and collected with trypsin without ethylenediaminetetraacetic acid (EDTA), washed twice with phosphate-buffered saline (PBS), and mixed with 500 μL of PBS to form a cell suspension. We added 5.0 μL of annexin V-FITC and 5.0 μL of PI to the cell suspension and incubated it for 30 min in the dark. Finally, the apoptosis rate of each concentration group was assessed by flow cytometry.

4. Cell Cycle Assay

RNase A and PI staining kit used the effects of NeoA in the cell cycle of A2780. The process of inoculating and treating cells is described in “Cell Apoptosis Assay”. The cells were digested and collected with trypsin-containing EDTA and fixed in 70% pre-cooled ethanol at 4°C for more than 12 h. The cells were then washed twice with PBS, bathed in 5μL RNase A at 37℃ for 30 min, followed by 25μL PI solution at room temperature, and stained in the dark for 15 min. The changes in the cell cycle were analyzed by flow cytometry.

4.3 Results and Discussion

4.3.1 Structural Analysis of Compounds

Compound **C1** was obtained as an earthy yellow powder, and its molecular formula was established as $C_{20}H_{16}O_6$ based on HRESIMS data at 375.08386 $[M+Na]^+$ (calcd. for $C_{20}H_{16}O_6N_a$, 375.083909), indicating 13 degrees of unsaturation. The 1D NMR data (Table 4.2) of **C1** and HSQC correlations showed signals for two 1,2,3-trisubstituted benzene rings, two carbonyls, a methylene, a methine, and two olefinic protons [6.74 (d, J = 10.0 Hz, 1H), 6.35 (d, J = 10.0 Hz, 1H)], as well as four exchangeable protons [12.19 (s, 1H), 12.17 (s, 1H), 6.10 (s, 1H), 5.52 (d, J = 4.2 Hz, 1H)]. The COSY correlations of H-3 with H-2a and H-4 along with the HMBC correlations of H-2a/C-1, C-3, C-4, H-2b/C-1, C-3, C-4, H-3/C-1, and H-4/C-2, C-3, C-4a, C-5, and C-8a indicated the presence of a substituted tetralone moiety (Figure 4.2). The observed HMBC correlations from 2′-OH- to C-2′, C-3′, from H-3′ to C-1′, C-4a', and from H-4′ to C-2′, C-4a', C-5′, and C-8a′ implied the presence of another substituted α-(*2H*)-naphthalenone moiety (Figure 4.2). The observed HMBC correlations from 2′-OH to C-3, from H3′ to C-3, from H-2a to C-2′, and from H-3 to C-1′ and C-3′ suggested that there is a C-3~C-2′ linkage between the two α-naphthalenone moieties. The observed HMBC correlations from 8-OH to C-7, C-8, and C-8a and from 8′-OH to C-7′, C-8′, and C-8a' indicated that 8-OH attached to C-8 and 8′-OH attached to C-8′, respectively. Thus, the planar structure of compound **C5** was determined (Figure 4.1). The relative configuration of compound **C5** was confirmed by analysis of the coupling constants, NOESY correlations (Figure 4.2), and ^{13}C-NMR calculations (Figure 4.3). The large coupling constant of Hax-2a with Hax-3 (J = 13.3 Hz) indicated a Jaa coupling between Hax-2a and Hax-3, and a Jae coupling between Hax-3 and Heq-2b (J = 3.9 Hz). The very small coupling constant of Hax-3 with H-4 (J = 2.0 Hz) indicated a Jae coupling between them. Thus, H-3 and 4-OH were in the opposite orientations of the substituted tetralone moiety plane. The NOESY correlation of H-2a with 4-OH further confirmed this deduction. However, since the C-3~C-2′ bond can rotate, the relative configuration of the right part of compound **C5** cannot be determined. Thus, we performed theoretical NMR chemical shift calculations for the two diastereomers **C5**a and **C5**b of **C5** using the gauge-independent atomic orbital (GIAO) ^{13}C NMR calculations (Grimblat et al.,

2015). The calculated ^{13}C NMR chemical shifts of **C5**b showed the best agreement with the experimental values (Figure 4.3). Furthermore, DP4^{+} analysis predicted that **C5**b was the most likely candidate with 100% probability (Table S2). ECD calculations were used to determine the absolute configuration of **C5**, and they revealed that the experimental and calculated ECDs for (3*R*,4*R*,2′*S*)-**C5** are in agreement (Figure 4.4). Thus, compound **C5** was identified as (3*R*,4*R*,2′*S*)-**C5** and named neogrisphenol A.

Table 4.1 The ^{1}H (600 MHz) and ^{13}C NMR (150 MHz) Data of Compounds **C5** and **C6** in DMSO-*d*6

	C5		C6	
No	**δ_C, Type**	**δ_H (*J* in Hz)**	**δ_C, Type**	**δ_H (*J* in Hz)**
1	205.1, C		205.0, C	
2	32.8, CH_2	3.14, dd (17.7, 13.3), Ha	33.2, CH_2	3.03, dd (17.6, 13.4), Ha
		2.49, dd (17.7, 3.9), Hb		2.25, dd (17.6, 3.8), Hb
3	49.2, CH	2.61, ddd (13.3, 3.9, 2.0)	48.8, CH	2.57, ddd (13.4, 3.8, 2.0)
4	65.9, CH	4.87, d (4.2)	65.7, CH	4.98, d (4.9)
4a	145.7, C		146.0, C	
5	119.7, CH	6.88, overlap	119.5, CH	6.89, overlap
6	137.1, CH	7.51, dd (8.4, 7.4)	137.2, CH	7.53, dd (7.9, 7.9)
7	117.1, CH	6.88, overlap	117.0, CH	6.89, overlap
8	161.4, C		161.4, C	
8a	114.7, C		114.7, C	
1′	206.4, C		203.4, C	
2′	73.5, C		73.6, C	
3′	136.3, CH	6.35, d (10.0)	136.8, CH	6.43, d (10.0)
4′	125.7, CH	6.74, d (10.0)	125.3, CH	6.61, d (10.0)
4a’	137.6, C		139.6, C	
5′	118.9, CH	6.88, overlap	107.9, CH	6.31, d (2.2)
6′	137.8, CH	7.56, dd (8.4, 7.4)	166.2, C	
7′	117.1, CH	6.88, overlap	101.5, CH	6.17, d (2.2)
8′	161.5, C		164.8, C	
8a’	113.2, C		106.7, C	
4-OH		5.52, br d (4.2)		5.50, br d (4.9)
8-OH		12.17, s		12.12, s
2′-OH		6.10, br s		6.03, br s
6′-OH				10.94, s
8′-OH		12.19, s		12.68, s

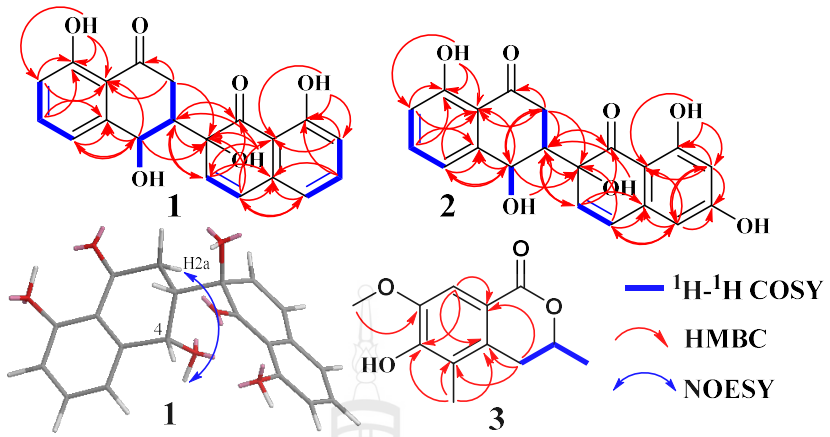

Figure 4.2 Key COSY, Key NOSEY, and HMBC correlations of compounds **C5**–**C7**

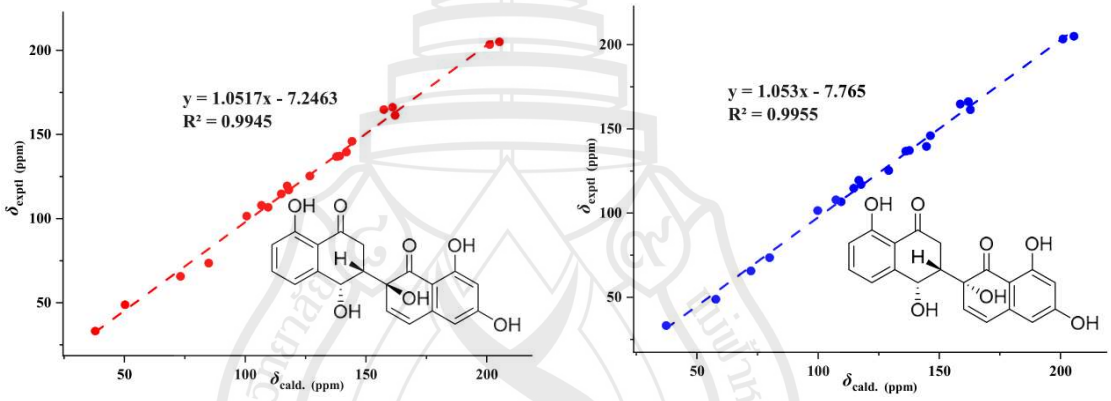

Figure 4.3 Linear regression analysis between experimental and calculated ^{13}C NMR chemical shift of isomers of **C6**

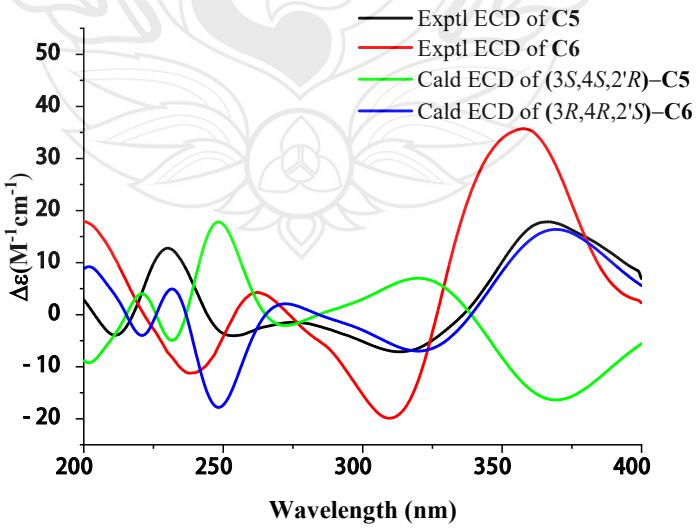

Figure 4.4 Calculated and experimental ECD spectra of compounds **C5** and **C6**

Compound **2** was obtained as a brownish-black solid, and its molecular formula was established as $C_{20}H_{16}O_7$ based on HRESIMS data at 391.07761 $[M+Na]^+$ (calcd. for $C_{20}H_{16}O_7N_a$, 391. 078824), indicating 13 degrees of unsaturation. The molecular formula of compound **C6** has only one more oxygen atom than compound **C5**, and the ^{1}H-NMR spectrum is very similar, except for one less aromatic proton and one more exchangeable proton, suggesting that compound **C6** has only one more phenolic hydroxyl group (10.94, s, 1H) than compound **C5**. The 1D and 2D NMR data of the left part of compound 2 are almost identical to those of compound **C5,** indicating they share the same planar structure and relative configuration of the left part. The ^{1}H-NMR data of compound **C6** showed the two protons [6.31, (d, J = 2.2 Hz, 1H), 6.17, (d, J = 2.2 Hz, 1H)] were meta-coupling on the right benzene ring. The HSQC correlations of H-5′/C-5′, H-7′/C-7′, along with the HMBC correlations of H-5′/C-4′, C-7′, C-8a', H-7′/ C-5, C-6, C-8, 6′-OH/C-5′, C-7′, 8′-OH/ C-7′, C-8′, C-8a', and H-4/C-2, C-3, C-4a, C-5, and C-8a, indicated that 6′-OH was connected to C-6′ and 8′-OH connected to C-8′, respectively. The position of the carbon-carbon double bond (C3′~4′) in the right cyclohexanone ring is also the same as in compound **C5**, based on similar HMBC correlations. In addition, the HMBC correlations, similar to compound **C5**, proved the connection position is also a C-3~C-2′ linkage between the two naphthalenone derivative moieties. Thus, the planar structure of compound **C6** was determined (Figure 4.1). In the same way, the relative configuration of compound **C6** is defined as **C6**b (Figure 4.2). The relative configurations of compound **C5** and compound **C6** were assigned the same by ^{13}C NMR calculation (Figure 4.3), and their experimental ECD curves were similar (Figure 4.4). The sign of the specific rotation is also positive, so the absolute configuration of compound C6 was defined as (3R,4R,2′S)-**C6** and named neogrisphenol B.

Compound **C7** was obtained as a rufous solid, and its molecular formula was established as $C_{20}H_{16}O_7$ based on the HRESIMS data at 245.07921 $[M+Na]^+$ (calcd. for $C_{12}H_{14}O_4N_a$, 245.078430), indicating 6 degrees of unsaturation. The 1D-NMR data and HSQC correlation showed signals for an aromatic proton, an exchangeable proton, a methoxyl, two methyls, one methylene, and an oxygenated methine. These data were close to those of the isochroman-1-one skeleton (Xiao et al., 2022), with the exception that an aromatic proton signal was absent and one sp^3-methoxyl signal ($\delta_{H/C}$ 1.98/10.6)

and one oxygen-bearing sp^3-methoxyl signal ($\delta_{H/C}$ 3.71/55.4) were present. The structure of the right part was confirmed by the COSY and HMBC correlations (Figure 4.2). The connection positions of the phenolic hydroxyl, methoxyl, and methyl groups on the benzene ring were determined by the key HMBC correlation from H-4a to C-5, H-8 to C-4a, C-6, C-8a, H-11 to C-7, and H-10 to C-6 (Figure 4.2). Thus, the planar structure of compound 3 was determined. The relative configuration of compound **3** was confirmed by coupling constants. The large coupling constant of Hax-4a with Hax-3 (J = 12.4 Hz) indicated a *J*aa coupling between Hax-4a and Hax-3, and a Jae coupling between Hax-3 and Heq-4b (J = 2.8 Hz). ECD calculations were used to determine compound **C7′**s absolute configuration, and the results showed that the experimental and computed ECDs for (3*S*)-**C7** are consistent (Figure 4.5). Thus, compound **C7** was identified as (*S*)-6-hydroxy-7-methoxy-3,5-dimethylisochroman-1-one.

Table 4.2 The ^{1}H (600 MHz) and ^{13}C NMR (150 MHz) data for compound **C7** in DMSO-d_6

	C7	
No	**δ_C, Type**	**δ_H (*J* in Hz)**
1	161.8, C	
2		
3	72.3, CH	4.36, dqd (12.0, 6.2, 2.8)
4	32.8, CH_2	2.54, dd (16.5, 12.0), Ha 2.93, dd (16.5, 2.8), Hb
4a	112.6, C	
5	142.0, C	
6	160.7, C	
7	160.5, C	
8	97.8, CH	6.47, s
8a	104.8, C	
9	20.5, CH_3	1.35, d (6.2)
10	10.6, CH_3	1.98, s
11	55.4, OCH_3	3.71, s
6-OH		10.41, br s

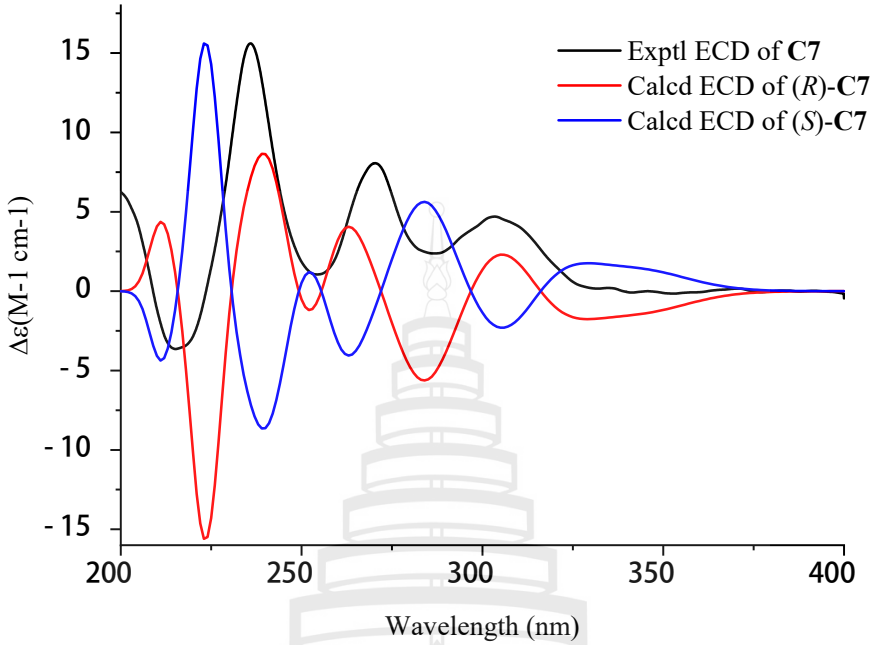

Figure 4.5 Calculated and experimental ECD spectra of compound **C7**

Neogrisphenol A (**C5**): earthy yellow powder; $[\alpha]_D^{28}$ +510 (c 4.0, MeOH); UV (MeOH) λmax log ε) 221 (4.42), 280 (3.13), 339 (3.66) nm; ECD (c 5.7 × 10^{-4}M, MeOH) λmax (Δε) 200 (+1.53), 211 (−2.09), 230 (+6.80), 254 (−2.16), 276 (−0.77), 314 (−3.79), 367 (+9.47) nm; IR (KBr) Vmax 3429, 3051, 2923, 2855, 1635, 1454, 1338, 1241, 1210, 1128 cm^{-1} ; ^1H and ^{13}C NMR, Table 2; HRESIMS at *m/z* 375.08386 $[M+Na]^+$ (calcd. for $C_{20}H_{16}O_6Na$, 375.083909).

Neogrisphenol B (**C6**): brownish black solid; $[\alpha]_D^{28}$ +160 (c 0.5, MeOH); UV (MeOH) λmax (log ε) 223 (3.33), 286 (2.59), 336 (2.92) nm; ECD (c 5.4 × 10^{-4} M, MeOH) λmax (Δε) 200 (+10.07), 238 (–6.31), 262 (+2.39), 309 (–11.16), 358 (+20.04) nm; IR (KBr) Vmax 3403, 2924, 2855, 1614, 1458, 1383, 1245, 1169 cm^{-1}; ^1H and ^{13}C NMR, Table 2; HRESIMS at *m/z* 391.07761 $[M+Na]^+$ (calcd. for $C_{20}H_{16}O_7Na$, 391. 078824).

(*S*)-6-hydroxy-7-methoxy-3,5-dimethylisochroman-1-one (**C7**): rufous solid; $[\alpha]_D^{28}$ +52 (c 0.4, MeOH); UV (MeOH) λmax (logε) 213 (3.11), 243 (2.45), 266 (2.84), 285 (2.41), 305 (2.63) nm; ECD (c 9.0 × 10–4 M, MeOH) λmax (Δε) 200 (+2.10), 215

(−1.23), 236 (+5.25), 254 (+0.53), 270 (+2.71), 286 (+0.80), 303 (+1.58) nm; IR (KBr) Vmax 3418, 2932, 1690, 1596, 1260, 1122, 1084 cm−1; ^{1}H and ^{13}C NMR, Table 4.2; HRESIMS at m/z 245.07921 $[M+Na]^{+}$ (calcd. for $C_{12}H_{14}O_4Na$, 245.078430).

Compound **C8** (Figure 4.1), $C_9H_{10}O_4$, was a white solid, ESIMS at *m/z* 181.2 [M-H]- (calcd. for $C_9H_{10}O_4$, 182.1), 363.1 $[2M - H]^{-}$, 183.1 $[M+H]^{+}$, 205.1 $[M + Na]^{+}$ (calcd. for $C_9H_{10}O_4Na$, 205.1); ^{1}H NMR (600 MHz, DMSO-d_6) δ 10.69 (s, 1H), 6.16 (t, J = 2.1 Hz, 2H), 3.79 (s, 3H), 2.27 (s, 3H); ^{13}C NMR (150 MHz, DMSO) δ 170.2, 161.4, 161.0, 140.7, 110.2, 107.6, 100.5, 51.8, 22.1. Compound **4** was identified as methyl orsellinate.

Compound **C9** (Figure 4.1), $C_{14}H_{14}O_3$, was a brown oil; ^{1}H NMR (600 MHz, DMSO-d_6) δ 9.44 (s, 2H), 6.34 (ddd, J = 2.2, 1.5, 0.8 Hz, 2H), 6.24 (ddd, J = 2.2, 1.4, 0.7 Hz, 2H), 6.15 (td, J = 2.2, 2.2, 0.6 Hz 2H), 2.18 (s, 6H); ^{13}C NMR (150 MHz, DMSO) δ 158.5, 157.6, 140.1, 111.2, 110.1, 103.0, 21.1; ESIMS at *m/z* 229.1 $[M-H]^{-}$, 459.1 $[2M-H]^{-}$ (calcd. for $C_{14}H_{14}O_3$, 230.1). Compound **5** was identified as diorcinol (Tian et al., 2015; Yurchenko et al., 2010).

Compound **C10** (Figure 4.1), $C_{11}H_{10}O_4$, was a white needle crystal; ^{1}H NMR (600 MHz, DMSO-d_6) δ 10.67 (s, 1H), 6.42 (d, J = 2.2 Hz, 1H), 6.32 (d, J = 2.2 Hz, 1H), 6.26 (d, J = 1.1 Hz, 1H), 3.80 (s, 3H), 2.12 (d, J = 1.0 Hz, 3H); ^{13}C NMR (150 MHz, DMSO) δ 164.2, 163.2, 157.9, 154.7, 141.8, 103.1, 102.4, 100.3, 98.6, 55.8, 18.9; ESIMS at *m/z* 205.1 $[M-H]^{-}$ (calcd. for $C_{11}H_{10}O_4$, 206.1), 229.1 $[M+Na]^{+}$ (calcd. for $C_{11}H_{10}O_4Na$, 229.1), 435.0 $[2M+Na]^{+}$ (calcd. for $C_{22}H_{20}O_8Na$, 435.0). Compound **C10** was identified as 6-hydroxy-8-methoxy-3-methyl-isocoumarin (Wu et al., 2019).

Compound **C11** (Figure 1), $C_{28}H_{44}O$, was a white needle crystal; ^{1}H NMR (600 MHz, $CDCl_3$-d) δ 5.57 (dd, J = 5.7, 2.6 Hz, 1H), 5.39 (dt, J = 5.6, 2.8 Hz, 1H), 5.20 (qd, J = 15.3, 7.6 Hz, 2H), 3.64 (tt, J = 11.2, 4.2 Hz, 1H), 2.48 (dd, J = 4.7, 2.4 Hz, 1H), 2.28 (ddd, J = 14.0, 11.7, 2.3 Hz, 1H), 2.05 (dddd, J = 14.4, 13.2, 7.1, 4.7 Hz, 2H), 2.00–1.94 (m, 1H), 1.93–1.86 (m, 3H), 1.85 (dd, J = 7.0, 5.8 Hz, 1H), 1.81–1.56 (m, 4H), 1.54–1.43 (m, 2H), 1.38 (qd, J = 11.0, 10.6, 5.1 Hz, 1H), 1.34–1.31 (m, 1H), 1.31–1.29 (m, 1H), 1.29–1.22 (m, 3H), 1.04 (d, J = 6.7 Hz, 3H), 0.96–0.89 (m, 6H), 0.83 (dd, J = 9.1, 6.8 Hz, 6H), 0.63 (s, 3H); ^{13}C NMR (150 MHz, $CDCl_3$) δ 141.5, 139.9, 135.7, 132.1, 119.7, 116.4, 70.6, 55.9, 54.7, 46.4, 43.0, 43.0, 41.0, 40.6, 39.2, 38.5, 37.2, 33.2,

32.2, 28.4, 23.2, 21.3, 21.2, 20.1, 19.8, 17.8, 16.4, 12.2. Compound **C11** was identified as ergosterin (Wang et al., 2004).

4.3.2 Antimicrobial and Cytotoxic Activities of Compounds C5–C11

The ethyl acetate (EtOAc) extracts from the rice fermentation product of *Neohelicosporium griseum* showed cytotoxicity against PC3 cell lines, with IC_{50} values of 0.4 mg/mL, as part of our ongoing research into the medical applications of helicosporous hyphomycetes. To investigate the bioactivities of compounds **C5**–**C11**, their antimicrobial and cytotoxic properties were evaluated. Compounds **C5**–**C6** and **C11** exhibited moderate antibacterial activity against *Bacillus subtilis*, *Clostridium perfringens*, *Staphylococcus aureus*, and *Staphylococcus aureus* with MIC values between 16 and 31 µg/mL (Table 4.3). Only compound **5** exhibited antifungal activity against *Sclerotinia sclerotiorum* and *Phytophthora nicotianae var. nicotianae*, with respective IC_{50} values of 88.14 ± 2.21 µg/mL and 52.36 ± 1.38 µg/mL (Table 4.4). Compound **C5** showed significant cytotoxicity against the A2780, PC-3, and MBA-MD-231 cell lines, with respective IC_{50} values of 3.20, 10.68, and 16.30 µM (Table 4.5). Compound **2** showed significant cytotoxicity against A2780 cell lines, with an IC_{50} value of 10.13 µM (Table 4.3).

Table 4.3 Minimum inhibitory concentrations (MIC, µg/mL) of **C5**–**C6** and **C10** against bacterial test organisms

Compound	*B. subtilis*	*C. perfringens*	*R. solanacarum*	*MRSA Stain ATCC43300*	*S. aureus*
C5	15.63	31.25	15.63	31.25	31.25
C6	-	-	-	31.25	-
C10	-	250.00	-	-	-
ciprofloxacin	0.63	0.08	0.32	0.32	0.08

Table 4.4 Antifungal activity of compound **C10** against plant pathogenic fungi

Compound	*P. nicotianae var. nicotianae*	*S. asclerotiorum*
	IC_{50} (µg/mL)	
C10	52.36 ± 1.38	88.14 ± 2.21

Table 4.5 Cytotoxicity of **C5–C11** against mammalian cell lines [half maximal inhibitory concentration (IC_{50}): μM]

Compound	A2780	PC-3	MBA-MD-231
C5	3.20	10.68	16.30
C6	10.13	>20	>20
C7	>20	>20	>20
C8	>20	>20	>20
C9	>20	>20	>20
C10	>20	>20	>20
C11	>20	>20	>20
cis-platinum	9.34	7.53	-
adriamycin	-	-	12.71

4.3.3 Effect of Neogrisphenol A on the Growth of A2780 Cells

4.3.3.1 Effect of Neogrisphenol A on the Cell Viability of A2780 Cells

The cytotoxicity of NeoA toward cancer cells was evaluated using the MTT technique. According to Figure 9B, the growth inhibition rate of the A2780 cells increased dose-dependently with rising NeoA concentrations and peaked by 80% at 10 mol/L. As Figure 9C shows, the quantitative analysis of the IC_{50} values at 24 h (4.78 ± 1.57 mol/L), 48 h (3.46 ± 1.19 mol/L), and 72 h (4.74 ± 0.39 mol/L) demonstrates that the inhibitory effect of NeoA on the A2780 cells was not time-dependent. Hence, it was decided to treat A2780 cells with NeoA for 24 hours in order to conduct further research. After 24 h of A2780 cell culture, dose-dependent inhibition of cell proliferation and stimulation of cell division by NeoA were observed (Figure 4.6D). This study suggests that NeoA may inhibit the proliferation of A2780 cells and cause apoptosis.

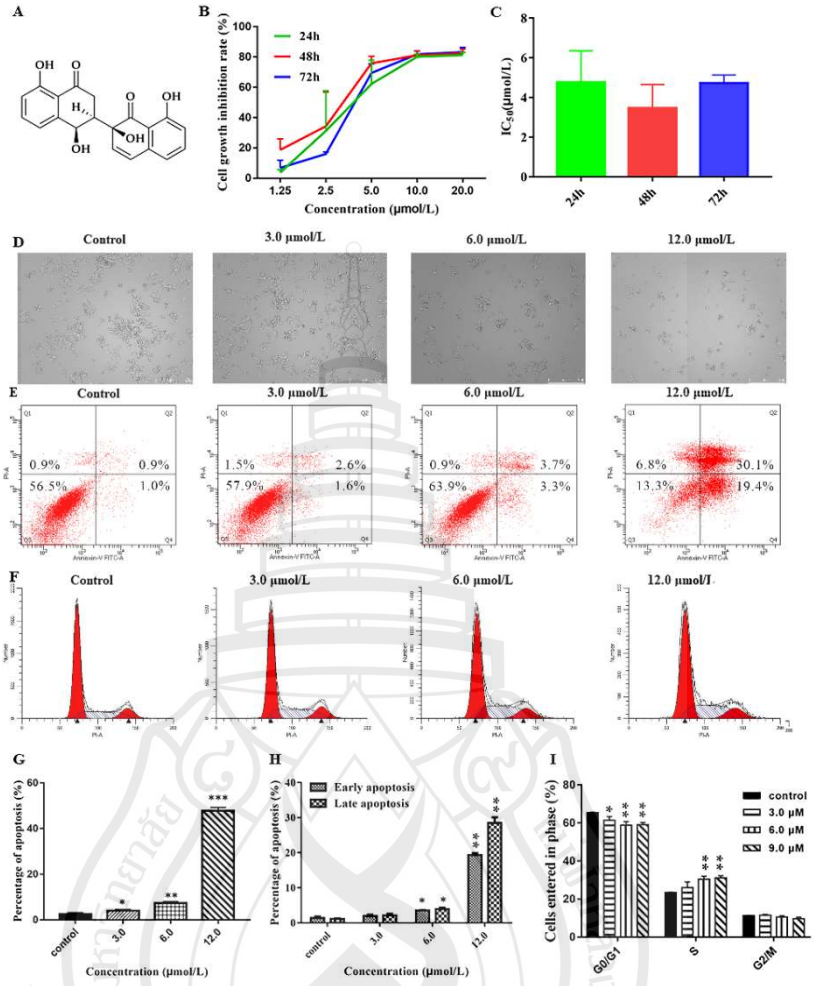

Figure 4.6 The effect of Neogrisphenol A on A2780 cell growth at various doses

Note: (A) The chemical structure of NeoA; (B) The MTT test was used to detect the inhibitory impact of NeoA on the proliferation of A2780 cells; (C) The semi-inhibitory concentration (IC_{50}) values of NeoA at various periods (24, 48, and 72 h); (D) Using an inverted microscope (magnification = 100x), morphological alterations in A2780 cells treated with various doses of NeoA for 24 h were detected; (E) Flow cytometry was used to assess the apoptosis of A2780 cells; (F) Flow cytometry was used to detect cell cycle alterations in the A2780 cell line in the control (DMSO) and NeoA groups at various doses; (G) The total rate of apoptosis in A2780 cells that were treated with various concentrations of NeoA; (H) A comparison of the effects of various concentrations of NeoA on the early and late apoptosis rates in A2780 cells; (I) The proportion of A2780 cells in each of the three cell-cycle stages altered following

treatment with NeoA. The data is presented as the mean ± SD (n = 3). * $p < 0.05$, ** $p < 0.01$, *** $p < 0.001$ vs. the control (DMSO) group; n.s, non-significant. For statistical analysis, one-way ANOVA and multiple t tests were both performed.

4.3.3.2 Effect of Neogrisphenol A on Apoptosis of A2780 Cells

Flow cytometry analysis showed that the number of apoptotic cells increased with the increase in NeoA concentration (Figure 4.6E). As shown in Figure 4.6G, the A2780 cells apoptosis rate increased with the increase of NeoA concentration in a concentration-dependent manner; the early and late apoptosis rates of all concentration groups differed significantly from those in the control group (DMSO), except for the low concentration group. The late apoptosis rate reached 47.80 ± 1.49% at 12 μmol/L, indicating that apoptosis induction mainly occurred in late apoptosis. This suggested that NeoA could prevent A2780 cells from proliferating by triggering early and late apoptosis.

4.3.3.3 Effects of Different Concentrations of Neogrisphenol A on the Cycle of A2780 Cells

The percentage of cells in the G0/G1 phase dramatically dropped as NeoA concentration increased, whereas the number of cells in the S-phase sharply increased (Figure 4.6F). The results of the quantitative study (Figure 4.6I) showed that NeoA interfered with the regulation of components that control cell cycle progression and prevented the entry of the cell cycle into the S-phase. This was shown by the increase in the number of S-phase cells with rising NeoA concentrations in comparison to the control cells (DMSO). The reduction in G0/G1 phase cells indicates that NeoA probably prevented the A2780 cells from replicating their DNA. NeoA was shown to regulate the G0/G1 and S-phases of the cell cycle to inhibit the malignant proliferation of A2780 cells.

4.3.4 Discussion

Derivatives of the *α*-naphthalenone dimer are primarily derived from microbial metabolites. Most of them were isolated from the fungal genus *Cladosporium*, named cladosporols (Sakagami et al., 1995), and to a lesser extent from plants, named naphthoquinones (Lall et al., 2006; Weigenand et al., 2004), through the carbon-carbon bond polymerization of two *α*-naphthalenone derivatives into a dimer. Typically, they are connected through the polymerization of the benzene ring of one *α*-naphthalone

derivative with the benzene ring of another α-naphthalone derivative or the benzene ring of one α-naphthalone derivative with the cyclohexanone ring of another *α*-naphthalone derivative. The biological activities of *α*-naphthalenone dimer derivatives include anticancer, antimicrobial, and so on (Bai et al., 2019; Blacutt et al., 2020; Li et al., 2017; Nasini et al., 2004; Rapuano et al., 2021; Yamazaki et al., 2018; Zhang et al., 2020). Two novel *α*-naphthalenone dimer derivatives were isolated and identified during the study of secondary metabolites of *Neohelicosporium griseum*. They have a rare 3~2′ polymerization mode between the cyclohexanone ring of one α-naphthalone derivative and the cyclohexanone ring of another α-naphthalone derivative. This study demonstrated that helicosporous hyphomycetes are worthy of study, and future research may uncover additional active secondary metabolites with novel structures. Neogrisphenol A is anticipated to be a new anticancer drug with a bright future in both development and application.

4.4 Conclusions

Neogrisphenol A-B (**C5**–**C6**) and (*R*)-6-hydroxy-7-methoxy-3,5-dimethylisochroman-1-one (**C7**) are three new polyketone derivatives isolated from the rice fermentation product of a new record fungus for China viz *Neohelicosporium griseum*, which is a new record for China. NOE and ^{13}C-NMR calculations determined the relative configurations of compounds **C5**–**C6**. The absolute configurations of compounds **C5**–**C6** were determined through ECD calculations. Neogrisphenol A showed extensive antibacterial activity against *Bacillus subtilis*, *Clostridium perfringens*, *Staphylococcus aureus*, MRSA-strain *Staphylococcus aureus*, and *Ralstonia solanacearum*. Meanwhile, neogrisphenol B exhibited antibacterial activity against the MRSA-strain *Staphylococcus aureus*. Diorcinol showed antifungal and antibacterial activity against *Phytophthora nicotianae* var. *nicotianae* and *Sclerotinia sclerotiorum* and weak antibacterial activity against *Clostridium perfringens*. Neogrisphenol A also showed potent inhibition on A2780, PC-3, and MBA-MD-231 cell lines, particularly A2780 cell lines, with more potency than the positive drug cis-platinum. Neogrisphenol B also exhibited cytotoxicity against A2780. Neogrisphenol A dramatically reduced the rate

of proliferation of A2780 cells, induced apoptosis, and prevented the S-phase of the cell cycle in a concentration-dependent manner. It is anticipated that neogrisphenol A will be further developed and utilized as a novel anticancer chemical entity.

CHAPTER 5

RESEARCH ON THE SECONDARY METABOLITES OF *N. GRISEUM* SLGY-15

5.1 Introduction

Cancer incidence and mortality are rising worldwide. By 2020, roughly 19.3 million new cancer cases and nearly 10 million cancer-related deaths were documented, with an estimated 28.4 million new cancer cases projected for 2040 (Sung et al., 2021). Concurrently, antimicrobial resistance (AMR) is emerging as a profound global public health challenge, with a predicted 10 million deaths annually worldwide by 2050 (Tang, Millar et al., 2023). Given these trends, there is a pressing need to expedite the discovery of effective anti-tumor and new antimicrobial drugs. As science and technology advance, the approach to drug discovery has evolved from random screening to more rational design (Zhang & Meng, 2020). Nevertheless, natural products remain a vital source for discovering and developing drugs or lead compounds (Zhang & Meng, 2020). As the possibilities of obtaining natural products with novel structures and potent activity from traditional resources diminish, the exploration of microorganisms, particularly underutilized fungal resources, has gained considerable attention from researchers (Conrado et al., 2022).

Helicosporous hyphomycetes are a group of saprophytic fungi characterized by helicoid conidia. In the past, researchers have paid more attention to their morphology and phylogeny (Lu et al., 2018; Xiao et al., 2023). However, these fungi can also produce secondary metabolites with novel structures and significant biological activity, especially in terms of anti-tumour activity (Qian et al., 2023; Zhang et al., 2023). For instance, Neogrisphenol A, which is isolated from *Neohelicosporium griseum* (GZCC 23-0142), exhibits considerable inhibitory activity against the ovarian cancer cell line (A2780), and its effect is superior to that of cisplatin (Zhang et al., 2023). Rubracin D and E, isolated from *Tubeufia rubra*, have demonstrated the ability to reverse the multidrug resistance of human breast cancer cells (MCF-7), showing superior

effectiveness compared with verapamil (Qian et al., 2023). Further studies of these compounds are underway, and they are expected to be developed as new anti-tumor lead compounds.

In our search for fungal metabolites with promising bioactivities, we conducted a chemical investigation of the rice fermentation process involving the saprophytic fungus *Neohelicosporium griseum* GZCC 23-0142, which yielded eight polyketides (**C12**–**C19**) (Figure 5.1). This study examines the biological activities of these fungal metabolites, including their antimicrobial properties and *in vitro* cytotoxicity.

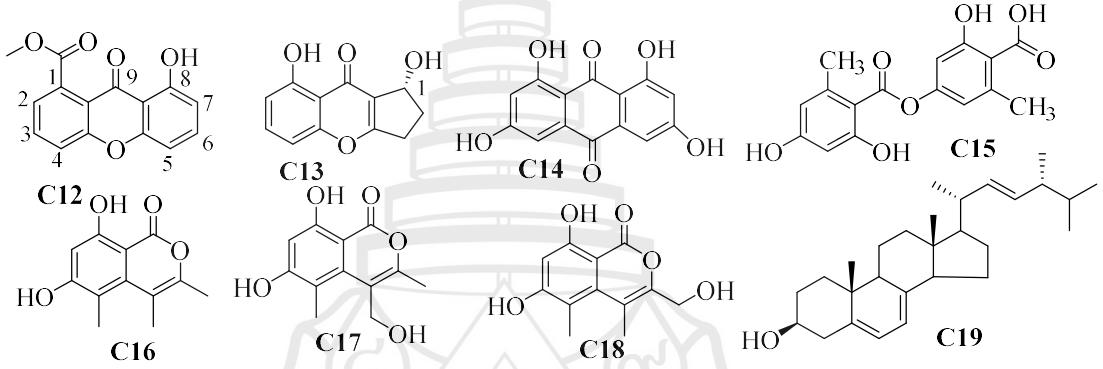

Figure 5.1 Chemical structures of compounds **C12**–**C19** isolated from *Neohelicosporium griseum* GZCC 23-0142

5.2 Materials and Methods

5.2.1 General

Tetramethylsilane (TMS) was used as an internal standard for recording NMR spectra on a Bruker 400 MHz or 600 MHz. ESIMS data and HR-ESIMS data were measured on a Waters Xevo G2S Q-TOF LC/MS and a Waters Xevo TQS, respectively. Optical rotations were captured on an AUTOPOL1 polarimeter (Rudolph, American) operating at 25℃. Both silica gel (200~300 mesh, Qingdao Marine Chemical Co., Ltd., China) and Sephadex LH-20 (GE Healthcare, Uppsala, Sweden) were used for column chromatography. The HPLC system (Agilent 1260, USA) was equipped with a C18 column (Agilent ZORBAX SB-C18, 4.6 × 250 mm, 5 μm, 1 mL/min, USA) as stationary phase. Shimadzu Soviet-produced LC-16P was used for HPLC separation, and an 18 column (MC-pack ODS-A, 10 × 250 mm, 5 μm, 3 mL/min) was used.

5.2.2 Fungal Material

Random samples of decaying wood were taken from Guiyang Forest Park, Guiyang, China, on October 25, 2020, marked as SLGY-15, and were identified based on morphological characters and phylogenetic analyses (Lu et al., 2018). The specimen is preserved in the Guizhou Academy of Agriculture Sciences Herbarium (Herb. GZAAS 23-0144), in Guiyang, China. Living cultures are deposited at Guizhou Culture Collection (GZCC 23-0142). The sequences (ITS OR412363, LSU OR412360, TEF1α OR420657) produced in this research were added to GenBank.

5.2.3 Cultivation and Fermentation of *N. griseum*

Fermentation had been carried out in Fungal medium No. 2 as described recently by Zhang et al (2023).

5.2.4 Extraction and Isolation of Metabolites from *N. griseum*

The fermented rice was stirred and extracted three times (each 50L) with ethyl acetate. The ethyl acetate extract was evaporated by rotation to obtain a crude extract of 150.3 g. The extract was separated by silica gel using a gradient elution of PE–EtOAc, yielding nine fractions (Fr.1–9). Crystallization occurred while sample Fr.4 was being placed in methylene chloride-methanol, yielding compound **C12** (36.0 mg). Fr.5 was further separated with Sephadex LH-20 in MeOH, producing five subfractions (Fr.5.1–5.5). The methanol-dissolved portion of Fr.5.3 was purified by Semi-preparative HPLC eluting with MeOH–H_2O (55:45), affording compound **C16** (t_R = 29.4 min, 43.3 mg). The insoluble methanol portion of Fr.5.3 was dissolved with a small amount of methylene chloride and subsequently purified using Semi-preparative HPLC with MeOH, affording compound **C19** (t_R = 13.0 min, 26.3 mg). Fr.6 was separated by Sephadex LH-20 eluting with MeOH to produce five subfractions (Fr.6.1–6.5). Compound **C14** (103.0 mg) was obtained by recrystallizing Fr.6.5 in methanol. Fr.6.2 was chromatographed with Sephadex LH-20 to yield four subfractions (Fr.6.2.1–6.2.4). Four subfractions (Fr.6.2.2.1–6.2.2.4) were obtained by further purifying Fr.6.2.2 with silica gel (PE–EtOAc, v/v, 7:3). Fr.6.2.2.3 was then further purified by Semi-preparative HPLC with MeOH/H_2O (50:50) to yield compound **C13** (t_R = 10.6 min, 160.0 mg). Silica gel (PE–EtOAc, v/v, 4:6) was used to further purify Fr.6.2.3 to produce three subfractions (Fr.6.2.3.1–6.2.3.3). Fr.6.2.3.3 was then further purified by Semi-preparative HPLC with MeOH–H_2O (37.5:62.5) to yield compounds **C17** (t_R =

25.8 min, 18.1 mg) and **C18** (t_R = 33.7 min, 33.7 mg). Fr.6.3 was further purified by RP-HPLC with ACN–H_2O (contains 0.1% HCOOH) (40:60) to yield compound **C15** (t_R =9.1 min, 11.8 mg).

5.2.5 Biological Assays

Compounds C12–C19 were tested for their antibacterial efficacy against two Gram-negative bacteria (Escherichia coli and Pseudomonas aeruginosa), one fungus (Candida albicans), and one gram-positive bacteria (Staphylococcus aureus). As a positive control for an antifungal, amphotericin B was used, while gentamicin was employed as a positive control for both Gram-positive and Gram-negative bacteria. Additionally, four mammalian cell lines (human ovarian cancer cell A2780, human non-small cell lung cancer cell A549, human liver cancer cell HePG2, and human cervical cancer cell HELA) were used to test the cytotoxicity of the compounds, with DOX serving as the positive control. All bioactivity assays were conducted with conventional methods (Shao et al., 2020; Wang et al., 2019).

5.3 Results and Discussion

5.3.1 Structural Analysis of Compounds

Eight polyketides were isolated from rice fermentation products of *Neohelicosporium griseum* GZCC 23-0142.

Vertixanthone (**C12**) was obtained as a yellow crystal; ESI-MS at *m/z* 293.0 $[M+Na]^+$, 563.1 $[2M+Na]^+$, 269.0 $[M-H]^-$, HR-ESI-MS at *m/z* 293.04229 $[M+Na]^+$, 563.09495 $[2M+Na]^+$, 269.04675 $[M-H]^-$ (calcd for $C_{15}H_{10}O_5$, 270.05266). ^1H NMR and ^{13}C NMR data are shown in APPENDIX A. The data above closely parallels 1-hydroxy-10-methoxy-dibenz[*b*,*e*]oxepin-6,11-dione (**a**) (Yamazaki et al., 2012) and vertixanthone (Yamazaki et al., 2012), making it challenging to establish whether its structure is compound **a** or vertixanthone (Figure 5.2). Consequently, we performed additional tests on the compound's HSQC and HMBC spectra. The molecular formula, 1D-NMR, and HSQC correlation indicated signals for an exchangeable proton, six aromatic protons, a methoxyl, and eight non-protonated carbons, five of which are oxygenated. The key HMBC correlation from H-3 (δ_H 7.95 ppm) to C-1 (δ_C 133.2 ppm)

revealed that C-1 (δ_C 133.2 ppm) is not an oxygenated carbon (Figure 5.2), thus establishing the structure of compound **C12** as vertixanthone rather than compound **a**.

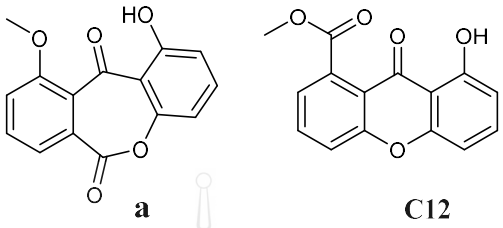

Figure 5.2 Chemical structures of 1-hydroxy-10-methoxy-dibenz[*b*,*e*]oxepin-6,11-dione (**a**) and vertixanthone (**C12**)

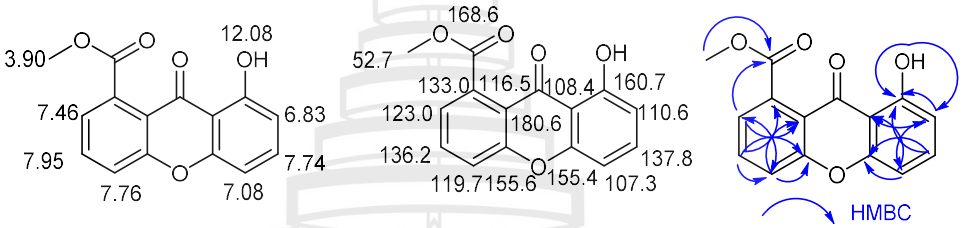

Figure 5.3 NMR signals assignment and key HMBC correlations of compound **C12**

Diaportheone A (**C13**) was obtained as a light-yellow crystal; $[a]_D^{25}$ -58.9 (*c* 0.1, $CHCl_3$). ESI-MS at *m/z* 241.0 $[M+Na]^+$, HR-ESI-MS at *m/z* 241.04749 $[M+Na]^+$, 217.05118$[M-H]^-$(calcd for $C_{12}H_{10}O_4$, 218.05771). 1D-NMR data are shown in APPENDIX A. These data are consistent with those reported in reference (Bungihan et al., 2011; Tan et al., 2019), so the structure of compound **C13** was identified as Diaportheone A.

1,3,6,8-tetrahydroxyanthraquinone (**C14**) was obtained as a red crystal; ESI-MS at *m/z* 271.0 $[M-H]^-$, HR-ESI-MS at *m/z* 271.02578 $[M-H]^-$ (calcd for $C_{14}H_8O_6$, 272.02578). 1D-NMR data are shown in APPENDIX A. These data are consistent with the reference (Cheng et al., 2022; Lum et al., 2020), so compound **C14** was identified as 1,3,6,8-tetrahydroxyanthraquinone.

Lecanoric acid (**C15**) was obtained as a colorless amorphous powder; ESI-MS at *m/z* 317.3 $[M-H]^-$, HR-ESI-MS at *m/z* 317.06809 $[M-H]^-$ (calcd for $C_{16}H_{14}O_7$, 318.06809). 1D-NMR data are shown in APPENDIX A. These data are consistent with the reference (Pavan Kumar et al., 2020), so compound **C15** was identified as lecanoric acid.

Decarboxycitrinone (**C16**) was obtained as a colorless solid. ESI-MS at *m/z* 221.1 $[M+H]^+$, 463.1 $[2M+Na]^+$, HR-ESI-MS at *m/z* 221.08128 $[M+H]^+$, 243.06303 $[M+Na]^+$, 219.06724$[M-H]^-$, (calcd for $C_{12}H_{12}O_4$, 220.07426). 1D-NMR data are shown in APPENDIX A. These data are consistent with the reference (Jia, 2020; Liu et al., 2021), so compound **C16** was identified as decarboxycitrinone.

6,8-Dihydroxy-4-hydroxymethyl-3,5-dimethyl-isochromen-1-one (**C17**) was obtained as a colorless oil. ESI-MS at *m/z* 235.1 $[M-H]^-$, HR-ESI-MS at *m/z* 235.06223 $[M-H]^-$ (calcd for $C_{12}H_{12}O_5$, 236.06223). 1D-NMR data are shown in APPENDIX A. These data are consistent with the reference (Jia, 2020), so compound **C17** was identified as 6,8-dihydroxy-4-hydroxymethyl-3,5-dimethyl-isochromen-1-one.

Decarboxyhydroxycitrinone (**C18**) was obtained as colorless needles. ESI-MS at *m/z* 235.1 $[M-H]^-$, HR-ESI-MS at *m/z* 237.07927 $[M+H]^+$, 259.05806 $[M+Na]^+$, 235.06211 $[M-H]^-$ (calcd for $C_{12}H_{12}O_5$, 236.07069). 1D-NMR data are shown in APPENDIX A. These data are consistent with the reference (Cai et al., 2021; Liu et al., 2021), so compound **7** was identified as decarboxyhydroxycitrinone.

Ergosterin (**C19**) was obtained as a colorless needle crystal; 1D-NMR data are shown in APPENDIX A. The above data are consistent with the reference (Jia, 2020; Tang, Xu et al., 2023), so the structure of compound **C19** was identified as ergosterin.

5.3.2 Biological Activity

Compounds **C12**–**C19** were tested for their antimicrobial activity against *Candida albicans*, Gram-positive bacteria *Staphylococcus aureus*, and Gram-negative bacteria *Escherichia coli* and *Pseudomonas aeruginosa*. They were also tested for cytotoxicity against four mammalian cell lines: human ovarian cancer cell A2780, human non-small cell lung cancer cell A549, human liver cancer cell HePG2, and human cervical cancer cell HELA. Compounds **C12**–**C15** exhibited moderate activity against *Pseudomonas aeruginosa*, with an MIC of 62.5 μg mL^{-1} and an MMC of 250 μg mL^{-1}. Compound **C14** showed weak activity against *Staphylococcus aureus*, displaying an MIC of 125.0 μg mL^{-1} and an MMC of 500.0 μg mL^{-1} (Table 5.1). *In-vitro* cytotoxic testing revealed that compounds **C12**, **C14**, and **C15** possessed cytotoxic activity against the HELA cell line, with corresponding IC_{50} values of 30.8, 13.7, and 14.1 μM. Compounds **C12**, **C14**, and **C15** also showed considerable cytotoxicity

against the A549 cell line, with IC_{50} values of 24.7, 7.4, and 10.3 μM, respectively (Table 5.2).

Table 5.1 Minimum inhibitory concentrations (MIC, μg mL^{-1}) and minimum microbicidal concentrations (MMC, μg mL^{-1}) of **C12**–**C15** against microorganisms

Compound	*P. aeruginosa*		*S. aureus*		*E. coli*		*C. albicans*	
	MIC	MMC	MIC	MMC	MIC	MMC	MIC	MMC
C12	62.5	250.0	-	-	-	-	-	-
C13	62.5	250.0	-	-	-	-	-	-
C14	62.5	250.0	125.0	500.0	-	-	-	-
C15	62.5	250.0	-	-	-	-	-	-
C16	-	-	-	-	-	-	-	-
C17	-	-	-	-	-	-	-	-
C18	-	-	-	-	-	-	-	-
C19	-	-	-	-	-	-	-	-
Gentamicin	0.2	0.78	0.05	0.1	-	-	-	-
Amphotericin B	-	-	-	-	-	-	3.13	6.25

Note (–) = no activity investigated

Table 5.2 Cytotoxicity of **C12**–**C19** against mammalian cell lines [48 hrs half maximal inhibitory concentration (IC_{50}): μM]

Compound	HELA	A549	A2780	HePG2
C12	30.8	24.7	-	-
C13	NT	NT	NT	NT
C14	13.7	7.4	-	-
C15	14.1	10.3	-	-
C16	NT	NT	NT	NT
C17	NT	NT	NT	NT
C18	NT	NT	NT	NT
C19	NT	NT	-	NT
Adriamycin	3.2	7.1	1.1	4.3

Note (–) = no activity investigated, NT= not tested

The synthesis of fungal secondary metabolites is modulated by various factors. From the *N. griseum* strain GZCC 23-0142, eight polyketones were isolated. Compounds **C12** and **C13** are classified as oxanthrone, compound **C14** as an

anthraquinones, compound **C15** as a methylbenzoate derivative, compounds **C16**–**C18** as isocoumarins, and compound **C19** as a steroid. Contrastingly, a previous study on *N. griseum* strain GZCC 22-2002 yielded seven polyketones (Zhang et al., 2023). This variation underscores that even genetically similar fungal species can produce unique secondary metabolites, likely attributed to strain-specific genomic differences, even under identical fermentation conditions. Interestingly, ergosterol, a vital component of the fungal cell membrane, was the sole metabolite consistently found in both strains (Guo et al., 2023; Rangsinth et al., 2023) and is prevalent in various other fungal strains (Guo et al., 2023; Rangsinth et al., 2023). The simultaneous production of polyketones by both strain points to an inherent genetic framework in *N. griseum* conducive for polyketone biosynthesis, signaling a promising avenue for future research in this domain.

5.4 Conclusions

In this study, eight compounds were isolated from *Neohelicosporium griseum* (GZCC 23-0142), they exhibited noteworthy biological activities. Notably, compounds **C12**, **C14**, and **C15** showed significant cytotoxic effects on human tumour cells HELA and A549. The IC_{50} value of compound **C14** (1,3,6,8-tetrahydroxyanthraquinone) against the A549 cell line was comparable to that of the positive control drug, adriamycin. While the promising potential of compound **C14** as an anti-tumor agent is evident, a more in-depth study is crucial to fully understand its influence on A549 cell growth. Additionally, compounds **C12**–**C15** demonstrated moderate antibacterial prowess against *P. aeruginosa*. Moving forward, our research will also focus on discovering secondary metabolites with enhanced antimicrobial capacities.

CHAPTER 6

RESEARCH ON THE SECONDARY METABOLITES OF TUBEUFIA LONGIHELICOSPORA WZS71

6.1 Introduction

Since the advent of penicillin, fungal secondary metabolism has become a focal point in drug discovery (Keller, 2019; Quinn, 2013). Over the last 40 years, approximately 300 compounds have been isolated from freshwater fungi, including polyketones, quinones, alkaloids, and peptides (El-Elimat et al., 2021). These compounds have exhibited significant biological activities, such as inhibiting tumor cell proliferation, antibacterial, and insecticidal properties (El-Elimat et al., 2021). Many have been developed into anti-tumor drugs and antibiotics, with widespread applications in agriculture and the pharmaceutical industry (El-Elimat et al., 2021; Wang et al., 2023).

Helicosporous Tubeufiaceae are found in both terrestrial and aquatic environments. However, research on their secondary metabolites remains sparse, with even fewer studies focusing on aquatic species (Lu et al., 2018). It's worth noting that unexplored natural sources often yield novel active secondary metabolites (Conrado et al., 2022). Recent discoveries affirm this, with several unique active compounds identified from aquatic fungi (Qian et al., 2023; Zeng et al., 2022; Zheng et al., 2024). Lu et al. discovered a novel fungal species, *Tubeufia rubra*, from decaying wood in freshwater (Lu et al., 2018). Subsequent research by Qian et al. and Zeng et al. led to the isolation of four new and 22 known compounds from this species. Notably, Rubracin A, D, and E have shown potential in reducing Multi-Drug Resistance (MDR) in the MCF-7/ADM cancer cell line by targeting P-glycoprotein overexpression (Qian et al., 2023; Zeng et al., 2022). Similarly, Zheng et al. identified three alkaloids from the fungal strain *Neohelicomyces hyalosporus*, which exhibited cytotoxic activity against specific human cancer cells.

Our ongoing research into helicosporous Tubeufiaceae has uncovered a freshwater fungus, *Tubeufia longihelicospora* WZS71. From this strain, we have isolated five compounds (Figure 6.1) including two dimeric naphtha-*γ*-pyrones (**C20**–**C21**), two dimeric coumarins (**C22**–**C23**), and an alkaloid (**C24**). This study details their extraction, isolation, structure elucidation, and antimicrobial properties.

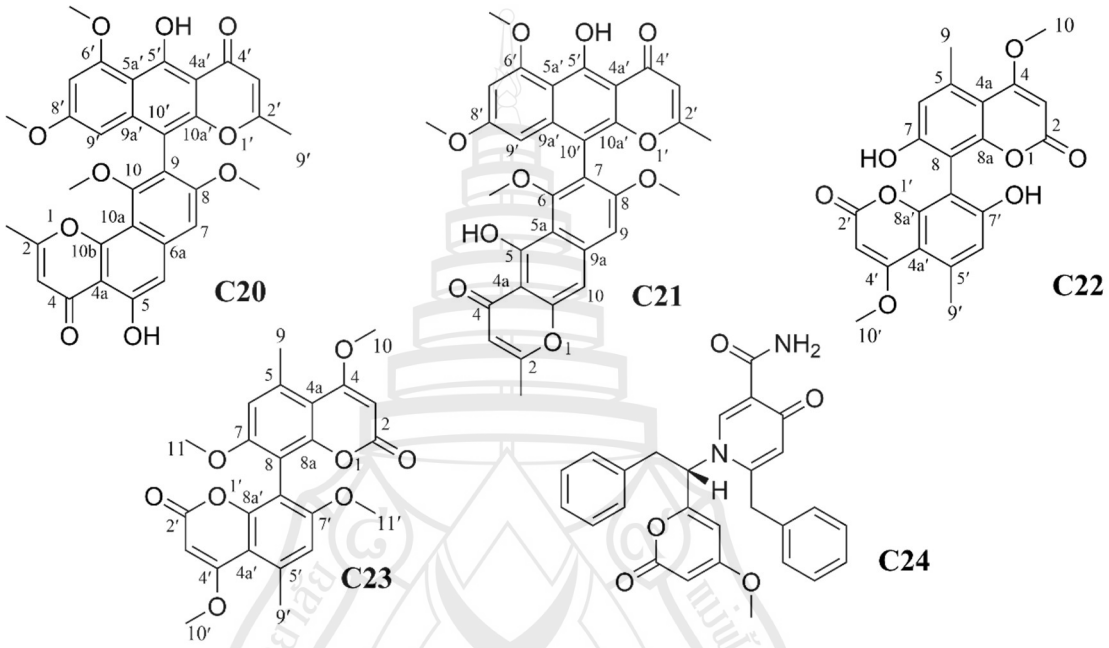

Figure 6.1 Chemical structures of compounds **C20**–**C24** isolated from *Tubeufia longihelicospora*. Fonsecinone A (**C20**), Aurasperone A (**C21**), Orlandin (**C22**), Kotanin (**C23**), and Aspernigrin B (**C24**)

6.2 Materials and Methods

6.2.1 General Experimental Procedures

The chemical shifts (δ) were referenced to the solvent peaks of $CDCl_3$ (δ_H 7.26/δ_C 77.16) and DMSO-d_6 (δ_H 2.50/δ_C 39.52) in the NMR spectra acquired on a Bruker AM-400. The specific rotation was determined using an AUTOPOL1 polarimeter. Electro-spray ionization mass spectrometry (ESIMS) data were obtained on a WATERS XEVO TQ-S. Sephadex LH-20 (Amersham Biosciences, Uppsala, Sweden) and ODS (50 μm, Merck, Germany) were employed for column chromatography. HPLC analysis was performed on an UltiMate 3000 (Thermo Fisher

Scientific, Waltham, America) using an Agilent Extend C18 column (4.6 × 100 mm, 5 μm, 1mL/min) and a DAD-30000 detector. Rapid purification by ODS column was carried out on a Biotage Isolera One (Biotage Sweden AB, Uppsala, Sweden) equipped with a dual-wavelength variable UV detector and an ODS column (35 ×250 mm, 50 μm, 30 mL/min). Semipreparative HPLC purification was performed on an Essentia Prep LC-16P (Shimadzu Instrument (Suzhou) Co., LTD, Suzhou, China) equipped with a SPD-16 UV-VIS dual-wavelength detector, utilizing an MC-pack ODS-A column (20 × 250 mm, 5 μm, 15 mL/min).

6.2.2 Fungal Material

On August 15, 2021, *Tubeufia longihelicospora* (WZS71) was isolated from a submerged woody substrate collected at the Shuiman River Tropical Rainforest Scenic Area in Wuzhishan City, Hainan Island, China. This fungus was identified based on morphological and phylogenetic evidence by Ma, Xiao et al. (2023), Ma, Zhang et al. (2023). The type materials (Herb. GZAAS 23-0409) have been deposited at the Guizhou Academy of Agriculture Sciences Herbarium, and the living cultures (GZCC 23-0405) are deposited at the Guizhou Culture Collection. Sequences generated in this study were uploaded to GenBank (ITS OR650832, LSU OR650833, TEF1α OR670527).

6.2.3 Fermentation

Fermentation and extraction processes were carried out based on the recent description by Zhang et al. (Zhang et al., 2023).

The mycelia of *T. longihelicospora* WZS71 on the grown plate culture were transferred in liquid medium (maltose 20 g, mannitol 20 g, glucose 10 g, sodium glutamate 10 g, yeast powder 3 g, potassium dihydrogen phosphate 0.5 g, magnesium sulfate 0.3 g, tap water 1 L) and inoculated in a rotary shaker at 28℃ and 180 rpm/min for 10 days to prepare the seed culture. The fermentation was conducted in 50 × 200 mL plastic bags. Each bag contained 50 g of rice and 55 mL of distilled water, which was then autoclaved at 121℃ for 30 min. Subsequently, the seed culture (5 mL) was inoculated into each bag and they were incubated in a temperature incubator at 28℃ for 120 days.

6.2.4 Compounds Extraction and Isolation Procedure

The fermentation cultures of *T. longihelicospora* WZS71 were extracted three times with ethyl acetate/MeOH (10:1), and 25.3 g of crude extract was obtained by rotary evaporation of the combined extracts. This crude extract was dissolved in methanol and filtered through a 0.22 μm nylon membrane to obtain the solution. The filtered solution was then subjected to separation using a Sephadex LH-20 column, yielding 5 fractions (Fr.1–Fr.5). All fractions and subfractions were monitored by TLC (GF254) and spots were visualized by an Ultraviolet analyzer (254 nm). Fr.4 (6.3 g) was further separated using rapid purification chromatography on an ODS column with 70% methanol, resulting in 2 subfractions (Fr.4-1–Fr.4-2). Fr.4-1 (1.1 g) was purified by semipreparative HPLC using 60% ACN, yielding compound **C20** (t_R = 17.0 min). Fr.4-2 (0.9 g) was processed with semipreparative -HPLC using 45% ACN to yield compound **C21** (t_R = 24.0 min). Fr.3 (4.5 g) underwent another round of separation on a Sephadex LH-20 column, resulting in 5 subfractions (Fr.3-1–Fr.3-5). Fr.3-4 (2.8 g) was purified using semipreparative HPLC with 40% ACN, producing 3 subfractions (Fr.3-4-1–Fr.3-4-3). Fr.3-4-2 (0.7 g) was refined with semipreparative HPLC using 35% ACN, affording compound **C22** (t_R = 19.0 min). Both Fr.3-4-3 (0.6 g) and Fr.3-4-1 (0.5 g) were separately processed with semipreparative HPLC using 40% ACN to afford compounds **C23** (t_R = 20.0 min) and **C24** (t_R = 16.7 min) respectively. The flowchart detailing the extraction and separation processes can be seen in Figure 6.2.

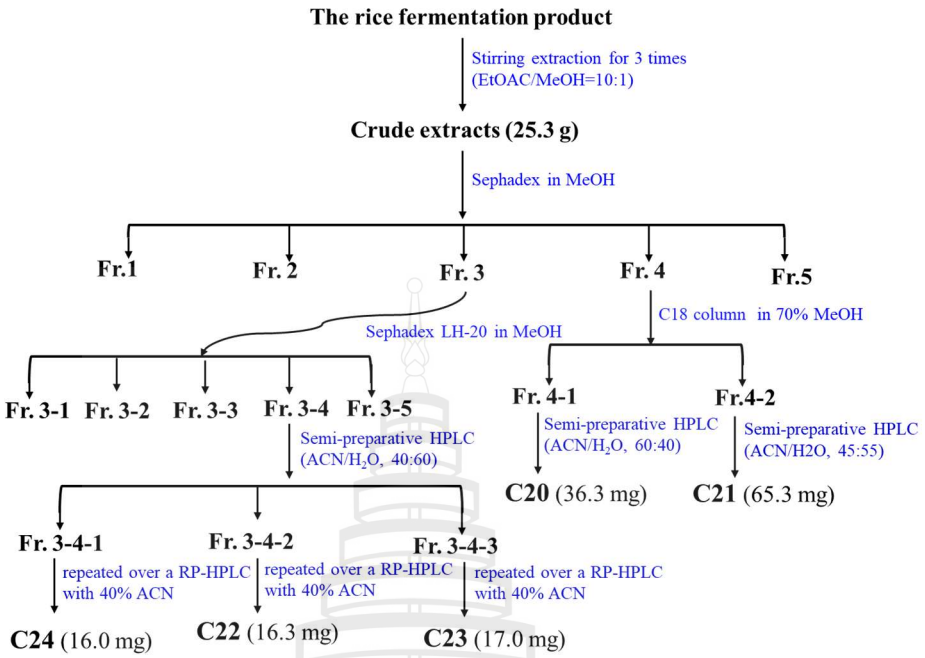

Figure 6.2 Flowchart of extraction and separation of metabolites from *Tubeufia longihelicospora*

6.2.5 Biological Assays

Compounds **C20**–**C24** were tested for antimicrobial activity against several microorganisms, including *Pseudomonas aeruginosa* (ATCC 15442), *Staphylococcus aureus* (ATCC 6538), *Escherichia coli* (BNCC 185254), and *Candida albicans*. The specific test method was 96-well plate method, referring to the previous publication by Zhao et al. (2021).

6.3 Results and Discussion

6.3.1 Structure Elucidation

The rice fermentation products of *Tubeufia longihelicospora* yielded five compounds. Their structures are shown in Figure 6.1.

Fonsecinone A (**C20**) Yield 36.3 mg, yellow powder. ^{1}H and ^{13}C NMR are shown in Table 6.1. ESIMS at *m/z* 569.1 $[M-H]^-$, 593.1 $[M+Na]^+$, 1163.3 $[2M+Na]^+$, (calcd for $C_{32}H_{26}O_{10}$, 570.1). The above data are matched with the literature data (Campos et al., 2005), compound **C20** was identified as Fonsecinone A.

Aurasperone A (**C21**) Yield 65.3 mg, yellow powder. ^{1}H and ^{13}C NMR are shown in Table 6.1. ESIMS at *m/z* 569.1 $[M-H]^-$, 593.1 $[M+Na]^+$, 1163.3 $[2M+Na]^+$, (calcd for $C_{32}H_{26}O_{10}$, 570.1). A comparison of the data with those reported in the literature (Zhao et al., 2021) showed that compound **C21** was determined as Aurasperone A.

Table 6.1 ^{1}H (400 MHz) and ^{13}C NMR (100 MHz) data for Fnsecinone A (**C20**) and Aurasperone A (**C21**) in $CDCl_3$

No	1		2	
	δ_C, Type	**δ_H (*J* in Hz)**	**δ_C, Type**	**δ_H (*J* in Hz)**
2	167.6		167.7	
2-CH_3	20.6	2.48 (s, 3H)	20.8	2.41 (s, 3H)
3	110.7	6.33 (s, 1H)	107.5	6.05 (s, 1H)
4	183.0		184.5	
4a	109.5		104.8	
5-OH	156.8	12.83 (s, 1H)	162.0	14.83 (s, 1H)
5a	/		111.5	
6	106.1	7.05 (s, 1H)	158.6	
6-OCH_3	/		62.1	3.46 (s, 3H)
6a	140.9		/	
7	101.6	6.97 (s, 1H)	117.7	
8	160.1		160.2	
8-OCH_3	56.1	3.78 (s, 3H)	56.1	3.78 (s, 3H)
9	117.2		101.4	6.97 (s, 1H)
9a	/		140.8	
10	157.1		101.3	7.15 (s, 1H)
10-OCH_3	61.3	3.43 (s, 3H)	/	
10a	108.1		153.4	
10b	155.2		/	
2′	167.1		167.7	
2′-CH_3	20.8	2.12 (s, 3H)	20.8	2.12 (s, 3H)
3′	107.4	6.00 (s, 1H)	107.3	5.98 (s, 1H)
4′	184.6		184.7	
4a′	104.3		104.3	
5′-OH	162.9	15.24 (s, 1H)	162.8	15.24 (s, 1H)
5a′	108.7		108.5	
6′	161.2		161.1	
6′-OCH_3	56.3	4.03 (s, 3H)	56.3	4.02 (s, 3H)
7′	97.1	6.42 (d, *J* = 2.2 Hz, 1H)	97.0	6.41 (d, J = 2.2 Hz, 1H)
8′	161.6		161.5	
8′-OCH_3	55.3	3.61 (s, 3H)	55.2	3.61 (s, 3H)
9′	96.4	6.19 (d, *J* = 2.2 Hz, 1H)	96.6	6.21 (d, J = 2.2 Hz, 1H)
9a′	140.7		140.6	
10′	105.1		105.2	
10a′	150.9		150.9	

Orlandin (**C22**) Yield 16.3 mg, colorless solid. ^{1}H and ^{13}C NMR are shown in Table 6.2. ESIMS at *m/z* 409.1 $[M-H]^-$, 433.1 $[M+Na]^+$, 843.2 $[2M+Na]^+$, (calcd for $C_{22}H_{18}O_8$, 410.1). A comparison of the data with the literature (Campos et al., 2005) revealed that compound **C22** is Orlandin.

Kotanin (**C23**) Yield 17.0 mg, yellow solid. ^{1}H and ^{13}C NMR are shown in Table 6.2. ESIMS at *m/z* 339.2 $[M-H]^-$, 461.1 $[M+Na]^+$, 899.2 $[2M+Na]^+$, (calcd for $C_{22}H_{18}O_8$, 438.1). These data are very similar to the reference (Cutler et al., 1979; Nozawa et al., 1994), so compound **C23** was identified as Kotanin.

Table 6.2 ^{1}H (400 MHz) and ^{13}C NMR (100 MHz) data for Orlandin (**C22**) in DMSO-*d6* and Kotanin (**C23**) in $CDCl_3$

No	C22		C23	
	δ_C, Type	**δ_H (*J* in Hz)**	**δ_C, Type**	**δ_H (*J* in Hz)**
2/2′	169.8		169.9	
3/3′	86.4	5.55 (s, 1H)	87.8	5.50 (s, 1H)
4/4′	154.1		153.5	
4a/4a	105.9		107.5	
5/5	137.0		138.6	
6/6′	116.1	6.70 (s, 1H)	111.5	6.72 (s, 1H)
7/7′	159.4	10.46 (brs, 1H)	159.6	
8/8′	106.2		108.5	
8a/8a′	161.9		163.2	
9/9′	23.3	2.59 (s, 3H)	24.2	2.70 (s, 3H)
10/10′	56.6	3.93 (s, 3H)	56.2	3.92 (s, 3H)
11/11′	/		56.0	3.79 (s, 3H)

Aspernigrin B (**C24**) Yield 16.0 mg, colorless oil. $[a]_D^{25}$ +38.9 (*c* 0.1, $CHCl_3$). ^{1}H NMR (400 MHz, $CDCl_3$) δ 9.83 (d, *J* = 4.9 Hz, 1H), 8.73 (s, 1H), 7.28 (m, 7H), 7.01 (dd, *J* = 7.4, 2.0 Hz, 2H), 6.85 (m, 2H), 6.28 (s, 1H), 5.66 (d, *J* = 2.2 Hz, 1H), 5.47 (d, *J* = 2.1 Hz, 1H), 5.30 (dd, *J* = 10.0, 5.5 Hz, 1H), 3.80 (s, 3H), 3.64 (s, 2H), 3.57 (dd, *J* = 14.3, 5.5 Hz, 1H), 3.22 (dd, *J* = 14.3, 10.0 Hz, 1H). ^{13}C NMR (100 MHz, $CDCl_3$) δ 177.1, 169.8, 165.7, 162.4, 158.6, 150.6, 142.8, 134.2, 134.0, 129.3, 129.3, 129.1, 129.1, 128.8, 128.7, 128.6,128.5, 127.7, 127.7, 122.8, 119.3, 101.8, 89.4, 61.8, 56.2, 38.5, 37.7. ^{1}H NMR (400 MHz, DMSO-*d6*) δ 9.36 (d, *J* = 4.9 Hz, 1H), 8.62 (s, 1H), 7.61 (d, *J* = 4.8 Hz, 1H), 7.28 (m, 5H), 7.05 (m, 5H), 6.23 (d, *J* = 2.3 Hz, 1H), 5.99 (s, 1H), 5.65 (d, *J* =2.3 Hz, 1H), 5.63 (dd, *J* = 9.2, 6.5 Hz, 1H), 3.93 (d, *J* = 16.6 Hz, 1H), 3.79 (s, 3H),

3.74 (d, J = 16.6 Hz, 1H), 3.57 (m, 1H), 3.29 (dd, J = 14.0, 9.2 Hz, 1H). ^{13}C NMR (100 MHz, DMSO) δ 176.3, 170.2, 164.8, 162.2, 158.5, 151.9, 142.8, 135.5, 135.1, 129.3, 129.3, 129.0, 129.0, 129.0, 129.0, 128.8, 128.8, 127.4, 127.4, 121.3, 119.3, 102.5, 89.4, 61.8, 56.8, 37.1, 36.9. ESIMS at *m/z* 455.2 $[M-H]^-$, 479.2 $[M+Na]^+$, 935.3 $[2M+Na]^+$, (calcd for $C_{27}H_{24}N_2O_5$, 456.1). The above data are consistent with the reference (Hiort et al., 2004; Zhou et al., 2016), so the structure of the compound was determined to be Aspernigrin B.

6.3.2 Biological Activity

The results of the antimicrobial activity assay for the five compounds derived from *Tubeufia longihelicospora* are presented in Table 6.3. Compounds **C20**–**C24** exhibited inhibitory activities against *P. aeruginosa* (ATCC 15442). The MICs for compounds **C20** and **C24** against *P. aeruginosa* (ATCC 15442) were 62.0 μg mL^{-1}, while their MBCs were 248.0 μg mL^{-1}.

Table 6.3 Antimicrobial activity of compounds **C20**–**C24**

Compounds	Antimicrobial activity (μg mL^{-1})							
	P. aeruginosa		***S. aureus***		***E. coli***		***C. albicans***	
	MIC	**MBC**	**MIC**	**MBC**	**MIC**	**MBC**	**MIC**	**MMC**
C20	62.0	248.0	-	-	-	-	-	-
C21	62.0	248.0	-	-	-	-	-	-
C22	ND	ND	ND	ND	ND	ND	ND	ND
C23	ND	ND	ND	ND	ND	ND	ND	ND
C24	ND	ND	ND	ND	ND	ND	ND	ND
Gentamicin	0.2	0.78	0.05	0.1	-	-	-	-
Amphotericin B	ND	ND	ND	ND	ND	ND	3.13	6.25

Note (–) = no activity investigated, ND= not detected

6.4 Conclusion

Five compounds (**C20**–**C24**) were isolated from the rice fermentation of *Tubeufia longihelicospora* (WZS71). These include two dimeric naphtha-*γ*-pyrones (**C20**–**C21**), two dimeric coumarins (**C22**–**C23**), and an alkaloid (**C24**). Notably, these compounds were isolated from helicosporous hyphomycetes for the first time. Due to

the high energy barrier preventing the rotation of the bond connecting different aromatic systems, compounds (**C20**–**C24**) typically exhibit axial chirality (He et al., 2016; Magdy et al., 2017; Zhou et al., 2016).

These compounds are known to possess a broad spectrum of biological activities (He et al., 2016; Hiort et al., 2004; Kim et al., 2020; Magdy et al., 2017; Zhao et al., 2022). Fonsecinone A (**C20**) and Aurasperone A (**C21**) have demonstrated potent antimicrobial activity, irrespective of their (*S*)-configuration or (*R*)-configuration (He et al., 2016; Magdy et al., 2017; Shaaban et al., 2012; Xiao et al., 2014). However, to date, there has not been a comparative analysis of the biological activity between two compounds with differing configurations, mainly because enantiomers of these compounds have not been obtained simultaneously. Previous studies have shown that compounds (**C20–C21**) exhibit strong anti-phytopathogenic fungal activities (Xiao et al., 2014) and effective antibacterial activity against multiple bacteria strains (He et al., 2016; Magdy et al., 2017). Moreover, compound (**C20**) has also displayed notable anti-inflammatory effects (Kim et al., 2020). While this study found moderate antibacterial efficacy of compounds (**C20**–**C21**) against *P. aeruginosa* (ATCC 15442). Wang et al. (Cutler et al., 1979) reported that Kotanin (**C23**) showed inhibitory activity against *Listeria monocytogene* and *Bacillus subtilis*. Additionally, Aspernigrin B (**C24**) offered significant neuroprotective effects against glutamic acid-induced toxicity (Hiort et al., 2004). *Tubeufia longihelicospora* can produce a large number of secondary metabolites with antibacterial activity and anti-phytopathogenic fungal activities, indicating that this fungal strain has great application potential in biological control. Helicosporous Tubeufiaceae represent a promising group, however, many of its species remain unexplored. There is significant potential awaiting in-depth research and discovery.

CHAPTER 7

RESEARCH ON THE SECONDARY METABOLITES OF HELICOSPORIUM SEXUALE LZ15

7.1 Introduction

Dibenzo-*α*-pyrone (DAP) derivatives are widely distributed in plant and fungal secondary metabolism, and display a broad spectrum of bioactivities, including antibacterial, antifungal, anticancer, anti-inflammatory, antidiabetic, antioxidant, and insecticidal effects (Küpeli Akkol et al., 2020; Lai et al., 2016; Liu et al., 2021; Mao et al., 2017; Tian et al., 2017; Zhang et al., 2022; Zhao et al., 2020).

Reported DAP derivatives are dominated by C6–C3 skeletons and C6–C3–C6 frameworks; in the latter, the terminal C6 units are typically benzene rings (Aichinger, 2021; Mao et al., 2014). In most cases, structural variation localizes to the C ring (Figure 7.1), which shifts from saturation to varying degrees of unsaturation (Mao et al., 2014). Zhao et al. reported novel C6–C5–C5 tricyclic scaffolds, occurring either as C5–C5 spiro or C5–C5 fused architectures (Zhao et al., 2020). Lai et al. described a novel C6–C3–C6–C5 tetracyclic scaffold bearing a C5–C5 spiro junction (Lai et al., 2016). Most DAP congeners contain only C, H, and O; however, chlorinated, thio-substituted, and amino-substituted congeners have been reported (Aly et al., 2008; Lai et al., 2016). Notably, all chlorinations reported to date are confined to C-2. Herein, we isolated compounds **C25**–**C39** from *H. sexuale* LZ15 and elucidated their structures by 1D/2D NMR and HRMS, with the configurations of new compounds **C25**–**C31** secured by X-ray diffraction, NOE, TD-DFT ECD. We delineate a new C6–C3–C6 series featuring C-1–C-4 sp^3 hydroxylation and site-selective chlorination at C-2/-3/-4 (Figure 7.1), and propose biosynthetic pathway covering **C25**–**C32** (Figure 7.12). Herein, we report the discovery and structural characterization of a dibenzo-α-pyrone scaffold and its cytotoxicity profile across five human cancer cell lines, supporting its consideration as a promising scaffold for SAR–guided optimization and subsequent mechanistic studies.

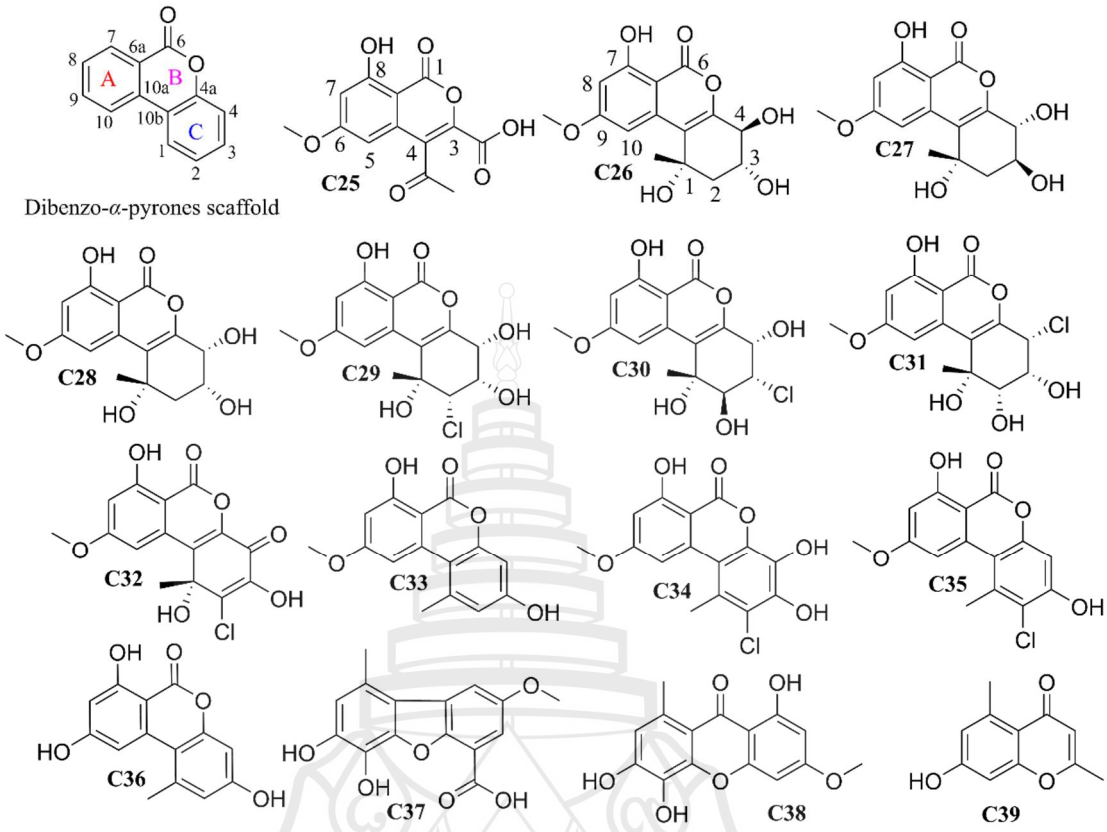

Figure 7.1 Structures of compounds **C25**–**C39** from *Helicosporium sexuale*

7.2 Materials and Methods

7.2.1 General Experimental Procedures

Optical rotations were measured on a JASCO P-2000 polarimeter. Electronic circular dichroism (ECD) spectra were recorded at room temperature on a JASCO J-815 CD spectrometer. Ultraviolet–visible (UV/Vis) spectra were obtained on a UV-5300 spectrophotometer (Hitachi, Tokyo, Japan). Single-crystal X-ray diffraction data were collected on an XtaLAB AFC12 (RINC) Kappa diffractometer equipped with Cu-Kα radiation and a graphite monochromator. Infrared (IR) spectra were recorded on a JASCO FT/IR-4600 spectrometer (JASCO, Gross-Umstadt, Germany). Tetramethylsilane (TMS) was used as an internal standard for recording NMR spectra on Bruker 400 MHz and 600 MHz spectrometers. Electrospray ionization mass spectrometry (ESIMS) and high-resolution ESIMS (HR-ESIMS) data were acquired on Waters Xevo G2-S Q-TOF LC/MS and Waters Xevo TQ-S instruments, respectively. High-performance liquid chromatography

(HPLC) was carried out on an Agilent 1260 system (Agilent, USA) equipped with a Eclipse Plus C18 column (4.6 × 250 mm, 5 μm; flow rate 1 mL/min). A Shimadzu LC-16P system was also employed for HPLC separation using an MC-pack ODS-A column (10 × 250 mm, 5 μm; flow rate 15 mL/min). Column chromatography was performed on silica gel (200–300 mesh, Qingdao Marine Chemical Co., Ltd., Qingdao, China), Sephadex LH-20 (Amersham Biosciences, Uppsala, Sweden), AB-8 macroporous adsorption resin (Tianjin Nankai Hecheng S&T Co., Ltd., Tianjin, China), and Sepax C18 preparative silica (20–30 μm, Sepax Technologies, Newark, DE, USA).

7.2.2 Fungal Material

The saprophytic fungus H. sexuale (strain LZ15) was isolated on May 4, 2021, from submerged decaying wood in a freshwater stream in Luzhai County, Liuzhou City, Guangxi Zhuang Autonomous Region, China. The fungus was identified by Yong-zhong Lu using morphological characteristics and phylogenetic analyses (Lu et al., 2022). GenBank accession numbers are OP508731 (ITS), OP508771 (LSU), OP698071 (RPB2), and OP698082 (TEF1α). The type specimen (GZAAS 22-2007 = HKAS 125866) has been deposited in the Herbarium of the Guizhou Academy of Agricultural Sciences, and the living cultures (GZCC 22-2007/CGMCC 3.29103) are maintained in the Guizhou Culture Collection and the China General Microbiological Culture Collection Center.

7.2.3 Fermentation Condition

H. sexuale was grown on PDA at 28°C for 20 days and then inoculated into twenty 250 mL Erlenmeyer flasks, each containing 125 mL Modified Martin medium (per L: peptone 5 g; KH_2PO_4 1 g; $MgSO_4 \cdot 7H_2O$ 0.5 g; yeast extract 2 g; glucose 20 g; tap water to 1 L). Flasks were incubated on an orbital shaker at 28°C and 180 rpm for 7 days. Approximately 5 mL of the seed culture was transferred to 200 mL plastic cultivation bags (each containing 50 g raw rolled oats and 35 mL distilled water). Bags were incubated statically at 28°C for 4 months. In total, 400 bags were fermented.

7.2.4 Extraction and Isolation

The fermentated raw rolled oats culture of H. sexuale was extracted three times with EtOAc/MeOH (10:1) to afford a crude extract (529.6 g). After salting out with hot saturated aqueous NaCl, the mixture was partitioned with EtOAc to give the EtOAc-soluble fraction (206.2 g). This fraction was subjected to AB-8 macroporous resin and eluted with an EtOH/H_2O gradient to yield six fractions (L1–L6). L2 (13.82 g) was chromatographed

on a silica gel column, eluting with CH_2Cl_2/EtOAc/HCOOH (5:5:0.1, v/v/v), to afford seven subfractions (L2-1–L2-7). L2-3 was chromatographed on Sephadex LH-20 to afford two subfractions (L2-3-1–L2-3-2). L2-3-2 was purified by HPLC on a semipreparative RP18 column (MeOH/H_2O = 40:60, v/v) to give **C25** (256.1 mg, t_R = 16.3 min). L2-4 was chromatographed on Sephadex LH-20 to afford two subfractions (L2-4-1–L2-4-2). L2-4-2 was purified by HPLC on a semipreparative RP18 column, eluting with ACN/H_2O = 25:75 (v/v) to give **C29** (58.0 mg, tR = 22.3 min) and with ACN/H_2O = 20:80 (v/v) to give **C30** (10.0 mg, t_R = 40.3 min). L2-7 was chromatographed on Sephadex LH-20 to give subfraction L2-7-3; subsequent purification by HPLC on a semipreparative C18 column (ACN/H_2O = 20:80, v/v) afforded **C26** (890.3 mg, t_R = 16.3 min), **C27** (171.8 mg, t_R = 24.3 min), and **C28** (18.1 mg, t_R = 32.5 min). L3 (50.0 g) was chromatographed on silica gel, eluting with PE/EtOAc (7:3→5:5, v/v), to furnish seven subfractions (L3-1–L3-7). L3-1 was chromatographed on Sephadex LH-20 to afford three subfractions (L3-1-1–L3-1-3). L3-1-2 was purified by HPLC on a semipreparative RP18 column (MeOH/H_2O = 60:40, v/v) to give **C32** (442.2 mg, t_R = 14.625 min). L3-1-3 was purified by HPLC on a semipreparative RP18 column (MeOH/H_2O = 70:30, v/v) to afford **C33** (71.6 mg, t_R = 11.979 min) and **C34** (33.6 mg, t_R = 23.169 min). L3-2 was chromatographed on Sephadex LH-20 to afford three subfractions (L3-2-1–L3-2-3). L3-2-3 was further purified on a C18 (RP-18) column with a 50% MeOH → 100% MeOH gradient to give L3-2-3-5, which was then purified by HPLC on a semipreparative C18 column (ACN/H_2O = 15:85, v/v) to afford **C39** (28.6 mg, t_R = 33.5 min) and **C31** (6.0 mg, t_R = 25.1 min). L4 (47.0 g) was chromatographed on silica gel, eluting with PE/EtOAc (9:1→6:4, v/v), to give seven subfractions (L4-1–L4-7). L4-3 was subjected to RP18 chromatography (60% MeOH→MeOH) followed by Sephadex LH-20 to afford seven subfractions (L4-3-1–L4-3-7). L4-3-2 was subjected to Sephadex LH-20 and then purified by HPLC on a semipreparative C18 column (ACN/H_2O = 35:65, v/v) to give **C36** (22.5 mg, t_R = 33.5 min). L4-3-3 was treated similarly (Sephadex LH-20) and purified by HPLC on a semipreparative C18 column (MeOH/H_2O = 75:25, v/v) to afford **C35** (12.5 mg, t_R = 23.5 min). L4-5 was chromatographed on an RP-18 column with a 70% MeOH → 100% MeOH gradient and then on Sephadex LH-20 to give five subfractions (L4-5-1–L4-5-5). L4-5-2 was first chromatographed on Sephadex LH-20 and then purified by HPLC on a

semipreparative C18 column (ACN/H_2O = 35:65, v/v) to give **C37** (132.3 mg, t_R = 26.5 min) and **C38** (28.1 mg, t_R = 38.1 min).

1. Helicolide A (**C25**)

Colorless crystals; UV (MeOH) λmax (log ε) 248 (3.90), 307 (3.73) nm; IR (film) νmax 3600, 3061, 1695, 1614, 1577, 1353, 1249, 1206, 1147, 1097, 1036, 957 cm^{-1}; ^1H and ^{13}C NMR data, Table 7.1; HR-ESIMS *m/z* 277.03548 [M+H]+ (calcd for $C_{13}H_9O_7$, 277.035376).

2. Helicohydrin B (**C26**)

Colorless crystals; $[\alpha]_D^{25}$ +15.6 (c 0.25, MeOH); UV (MeOH) λmax (log ε) 243 (3.21), 331(2.77) nm; ECD (c 0.49, MeOH) λmax (Δε) 246 (8.11), 332 (2.94) nm; IR (film) νmax 3499, 3461, 1660, 1604, 1583, 1500, 1197, 1188, 1116, 1077, 1013, 837 cm^{-1}; ^1H and ^{13}C NMR data, Table 7.2; HR-ESIMS *m/z* 331.07840 $[M+H]^+$ (calcd for $C_{15}H_{16}O_7Na$, 331.07882).

3. Helicohydrin C (**C27**)

Colorless crystals; $[\alpha]_D^{25}$ -7 (c 0.20, MeOH); UV (MeOH) λmax (log ε) 244 (4.48), 330 (3.86) nm; ECD (c 0.81, MeOH) λmax (Δε) 243 (8.77), 324 (-0.43) nm; IR (film) νmax 3398, 2323, 2311, 1696, 1604, 1578, 1500, 1351, 1250, 1196, 1147, 1103, 1066 cm^{-1}; ^1H and ^{13}C NMR data, Table 7.1; HR-ESIMS *m/z* 331.07822 $[M+Na]^+$ (calcd for $C_{15}H_{16}O_7Na$, 331.07882).

4. Helicohydrin D (**C28**)

Colorless crystals; $[\alpha]_D^{25}$ +7.6 (c 0.25, MeOH); UV (MeOH) λmax (log ε) 243 (4.41), 332 (3.82) nm; ECD (c 1.62, MeOH) λmax (Δε) 246 (3.51), 332 (0.17) nm; IR (film) νmax 3400, 2301, 1693, 1604, 1587, 1501, 1483, 1267, 1203, 1157, 1102, 1051 cm^{-1}; ^1H and ^{13}C NMR data, Table 7.2; HR-ESIMS *m/z* 331.07884 $[M+Na]^+$ (calcd for $C_{15}H_{16}O_7Na$, 331.078824).

5. Helicochlorin F (**C29**)

Brown, hygroscopic powder; $[\alpha]_D^{25}$ -29.2 (c 0.13, MeOH); UV (MeOH) λmax (log ε) 243 (4.06), 331 (3.61) nm; ECD (c 1.46, MeOH) λmax (Δε) 243 (5.22), 326 (-0.16) nm; IR (film) νmax 3401, 2361, 2354, 1693, 1654, 1583, 1493, 1487, 1349, 1326, 1037, 853, 757, 496 cm^{-1}; ^1H and ^{13}C NMR data, Table 7.3; HR-ESIMS *m/z* 365.03972 $[M+Na]^+$ (calcd for $C_{15}H_{15}O_7ClNa$, 365.039852).

6. Helicochlorin E (**C30**)

Brown, hygroscopic powder; $[\alpha]_D^{25}$ +19.0 (c 0.10, MeOH); UV (MeOH) λmax (log ε) 243 (4.19), 331 (3.76) nm; ECD (c 1.46, MeOH) λmax (Δε) 242 (4.88), 332 (0.96) nm; IR (film) νmax 3490, 2461, 2454, 1667, 1494, 1177, 1353, 1249, 1206, 1147, 907, 836, 757 cm^{-1}; ^1H and ^{13}C NMR data, Table 7.3; HR-ESIMS m/z 343.05763 $[M+H]^+$ (calcd for $C_{15}H_{16}O_7Cl$, 343.057907).

7. Helicochlorin G (**C31**)

Brown, hygroscopic powder; [α]25 D -7.0 (c 0.10, MeOH); UV (MeOH) λmax (log ε) 248 (3.79), 331 (4.41) nm; ECD (c 0.73, MeOH) λmax (Δε) 244 (9.89), 331 (2.39) nm; IR (film) νmax 3498, 2961, 2387, 2375, 1700, 1666, 1583, 1507, 1417, 1253, 1249, 1201, 1167, 1083, 1041, 833 cm^{-1}; ^1H and ^{13}C NMR data, Table 7-3; HR-ESIMS *m/z* 365.0388 $[M+Na]^+$ (calcd for $C_{15}H_{15}O_7ClNa$, 365.0399).

7.2.5 ECD Calculations

The conformational ensembles of the isomers were generated using the iMTD-GC procedure implemented in the CREST program (Pracht et al., 2020). Conformers showing both a root-mean-square deviation below 0.5 Å and an energy difference smaller than 0.25 kcal/mol were regarded as duplicates, and only one representative was retained. All subsequent DFT computations were carried out with Gaussian 09. Electronic circular dichroism (ECD) spectra were obtained via TDDFT calculations at the B3LYP/def2-TZVP level, applying the IEFPCM solvent model for methanol. The final spectra were produced by Boltzmann-weighted averaging of the lowest-energy conformers according to their relative Gibbs free energies (ΔG).

7.2.6 X-ray Crystallographic Analyses of Compounds C25, C26 and C32

Single crystals of C25 and C32 were obtained from a MeOH/C_5D_5N mixed solvent (v/v = 1:1) at room temperature (RT) after 3–7 days of slow solvent evaporation. Single crystals of C26 were obtained from a MeOH/CH_2Cl_2 mixed solvent (v/v = 1:1) at RT after 3 days of solvent evaporation. Single-crystal X-ray diffraction data were collected on a Bruker D8 Quest diffractometer (Mo Kα radiation, λ = 0.71073 Å). Crystallographic data for all of these compounds have been deposited with the Cambridge Crystallographic Data Centre (CCDC).

Crystal data of C25: C18H15NO7 (M =357.31 g/mol): monoclinic, space group P21/n (no. 14), a = 7.3371 (3) Å, b = 17.2387 (7) Å, c = 12.4539(5) Å, β = 92.373 (4), V =

1573.83 (11) Å3, Z = 4, T = 149.98 (10) K, μ (Cu Kα) = 0.999 mm-1, Dcalc = 1.508 g/cm3, 7956 reflections measured (8.764° ≤ 2Θ ≤ 149.154°), 3005 unique (Rint = 0.0580, Rsigma = 0.0439) which were used in all calculations. The final R1 was 0.0746 [I > 2σ (I)] and wR2 was 0.2071 (all data). CCDC number: 2487694.

Crystal data of C26: Crystal Data for C15.5H18O7.5 (M =324.30 g/mol): monoclinic, space group P21 (no. 4), a = 10.14651 (7) Å, b = 7.33583 (5) Å, c = 19.59379 (13) Å, β = 101.9844 (7)°, V = 1426.637 (17) Å3, Z = 4, T = 100.00 (10) K, μ (Cu Kα) = 1.033 mm-1, Dcalc = 1.510 g/cm3, 18330 reflections measured (4.61° ≤ 2Θ ≤ 149.734°), 5448 unique (Rint = 0.0180, Rsigma = 0.0122) which were used in all calculations. The final R1 was 0.0271 [I > 2σ (I)] and wR2 was 0.0757 (all data). CCDC number: 2487695.

Crystal data of C32: Crystal Data for C25H21ClN2O7 (M =496.89 g/mol): monoclinic, space group P21 (no. 4), a = 9.65935 (13) Å, b = 27.1918(2) Å, c = 10.02497 (14) Å, β = 118.6450 (18)°, V = 2310.84 (6) Å3, Z = 4, T = 100.00 (10) K, μ (Cu Kα) = 1.900 mm-1, Dcalc = 1.428 g/cm3, 21917 reflections measured (10.054° ≤ 2Θ ≤ 149.828°), 7408 unique (Rint = 0.0153, Rsigma = 0.0126) which were used in all calculations. The final R1 was 0.0209 [I > 2σ (I)] and wR2 was 0.0557 (all data). CCDC number: 2487696.

7.2.7 Cytotoxicity Assay

Compounds C25−C39 were assayed for their cytotoxicities against tumor cell lines HepG2, A2780, A549, Hela, and MDA-MB231 as previously described (Zhang et al., 2023).

7.3 Results and Discussion

7.3.1 Compounds Identification

A total of fifteen dibenzo-*α*-pyrones derivatives (**C25**−**C39**) (Figure 7.1) were isolated from the cultures of the fungus *Helicosporium sexuale* LZ15, including seven previously unreported ones **C25**–**C31** (Figure 7.1). Their structures were identified below.

Compound **C25** was obtained as colorless crystals (MeOH-C_5D_5N). HRESIMS exhibited a prominent ion at *m/z* 277.03548 $[M-H]^-$, consistent with the molecular formula $C_{13}H_{10}O_7$ and indicating nine degrees of unsaturation. The 1D NMR and HSQC

spectram of **C25** revealed seven quaternary and two methine carbons; two meta-coupled aromatic protons at δ_H 6.66 (d, J = 2.3 Hz, H-5) and 6.85 (d, J = 2.3 Hz, H-7); a methyl group at δ_H 2.77 (s, 3H; δ_C 32.0; 4-Ac-CH_3); a methoxy group at δ_H 3.76 (s, 3H; δ_C 56.3; 6-OCH_3); and two exchangeable protons at δ_H 11.16 (br s, 2H). One carbon resonance was not visible in the ^{13}C NMR spectrum but was clearly detected in the HMBC experiment at δ_C 191.0, assignable to the acetyl carbonyl. Key HMBC correlations (Figure 7.2) — from H-5 to C-4/C-6/C-7, from H-7 to C-5/C-8/C-8a, from 6-OCH_3 to C-6, and from 4-Ac-CH_3 to the acetyl carbonyl (C-4) — defined the substitution pattern and thus secured the planar structure of **C25.** The carbon framework closely resembles that of methyl 4-acetyl-6,8-dimethoxy-1-oxo-1*H*-isochromene-3-carboxylate (Arlt & Koert, 2010), except that **C25** bears 8-OH (instead of 8-OCH_3) and a free 3-carboxylic acid (instead of the methyl ester). The structure of **C25** (Figure 7.1) was unequivocally confirmed by single-crystal X-ray diffraction (Figure 7.3).

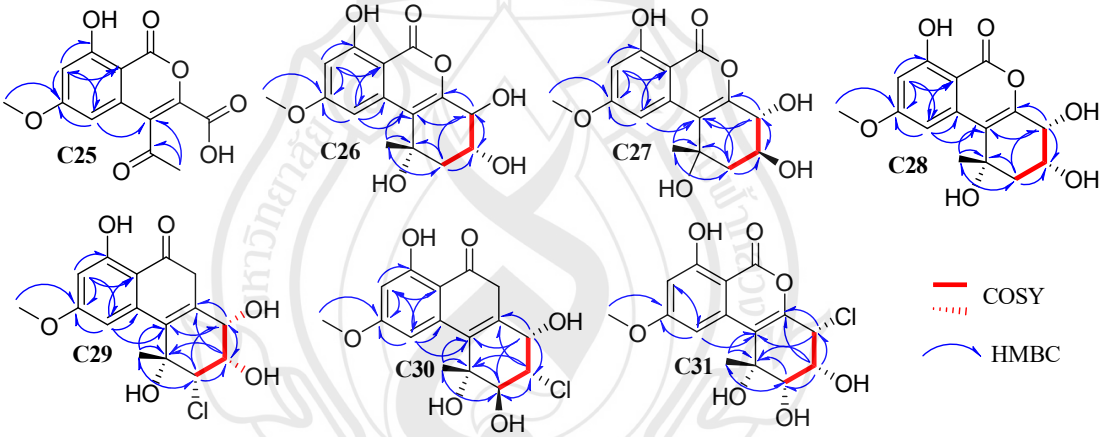

Figure 7.2 Key HMBC and ^1H-^1H COSY correlations and HMBC correlations of compounds **C25**–**C31**

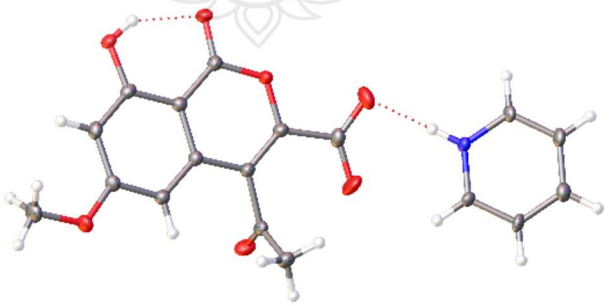

Figure 7.3 X-ray crystal structure of **C25**

Table 7.1 ^{1}H (400 MHz) and ^{13}C (100 MHz) NMR Data of **C25**

position	C25 (C_5D_5N-d_5)	
	δ_C, type	δ_H, mult. (*J* in Hz)
1	164.0, C	
3	142.2, C	
4	127.0, C	
4a	136.0, C	
5	103.0, CH	6.66 (d, *J* = 2.3)
6	167.6, C	
7	103.2, CH	6.85 (d, *J* = 2.3)
8	165.4, C	
8a	101.8, C	
3-COOH	165.1, C	11.16 (br s)
4-$COCH_3$	C, 191.0	
4-$COCH_3$	CH_3, 32.1	2.77 (s)
6-OCH3	CH_3, 56.3	3.76 (s)
8-OH		11.16 (br s)

Compound **C26** was obtained as colorless crystals (MeOH–CH_2Cl_2). HRESIMS showed a prominent pseudomolecular ion at *m/z* 331.07840 $[M+Na]^+$, consistent with the molecular formula $C_{15}H_{16}O_7$ and corresponding to eight degrees of unsaturation. The 1D NMR data (Table 7.2), together with HSQC correlations, revealed a 1,3-disubstituted (meta) benzene ring at δ_H 6.78 (d, *J* = 2.4 Hz, 1H, H-8)/δ_C 100.9 (C-8) and δ_H 8.07 (d, *J* = 2.4 Hz, 1H, H-10)/δ_C 105.3 (C-10), a methyl group at δ_H 1.91 (s, 3H, 1-CH_3)/δ_C 29.0; a methoxy at δ_H 3.76 (s, 3H, 9-OCH_3)/δ_C 56.0; one methylene unit (CH_2); two methines (CH); a lactone carbonyl at δ_C 167.0 (C-6), a chelated phenolic hydroxy at δ_H 12.12 (br s, 1H; 7-OH), and three exchangeable alcoholic OH protons at δ_H 5.03 (br s, 3H, 1-OH, 3-OH, 4-OH). Sequential COSY correlations (Figure 7.2) H-2/H-3 and H-3/H-4 defined a contiguous CH_2–CH–CH spin system. Key HMBC (Figure 7.2) cross-peaks — from H-8 to C-6a/C-7/C-9/C-10; from H-10 to C-10b/C-9/C-10a; from 9-OCH_3 to C-9; from 1-CH_3 to C-10b/C-1/C-2; from H-2 to C-1/

C-10b/C-3/C-4 and the methyl carbon (C-1-CH_3); from H-3 to C-4; and from H-4 to C-10b/C-3/C-4a — established the planar structure (constitution) of compound **C26**. The relative configuration of compound **C26** was established by analysis of the ^{1}H-^{1}H coupling constants (Table 7.2) and NOESY correlations (Figure 7.4). A large vicinal coupling ($^3J_{\text{H-2a, H-3}}$ = 10.8 Hz) between H-2a (δ_H 2.70, dd) and H-3 (δ_H 4.60, ddd) indicated a diaxial relationship (both axial), whereas the smaller coupling ($^3J_{\text{H-2b, H-3}}$ = 3.5 Hz) between H-2b (δ_H 2.82, dd) and H-3 (δ_H 4.60, ddd) supported an equatorial orientation for H-2b. Moreover, the relatively large vicinal coupling (^3J = 7.0 Hz) between H-3 (δ_H 4.60, ddd) and H-4 (δ_H 4.97, d) suggested an axial–axial arrangement. In the NOESY spectrum cross-peaks observed between 1-CH_3 (δ_H 1.91), and H-2b/ H-3, indicated that these protons are co-facial, while the correlation between H-2a and H-4 placed them on the opposite face. Taken together, these results unambiguously established the relative configuration of compound **C26**. In addition, single-crystal X-ray diffraction analysis of compound **C26** (Figure 7.5) further confirmed the relative configuration and unambiguously determined the absolute configuration as 1*S*, 3*R*, 4*S* (Figure 7.1).

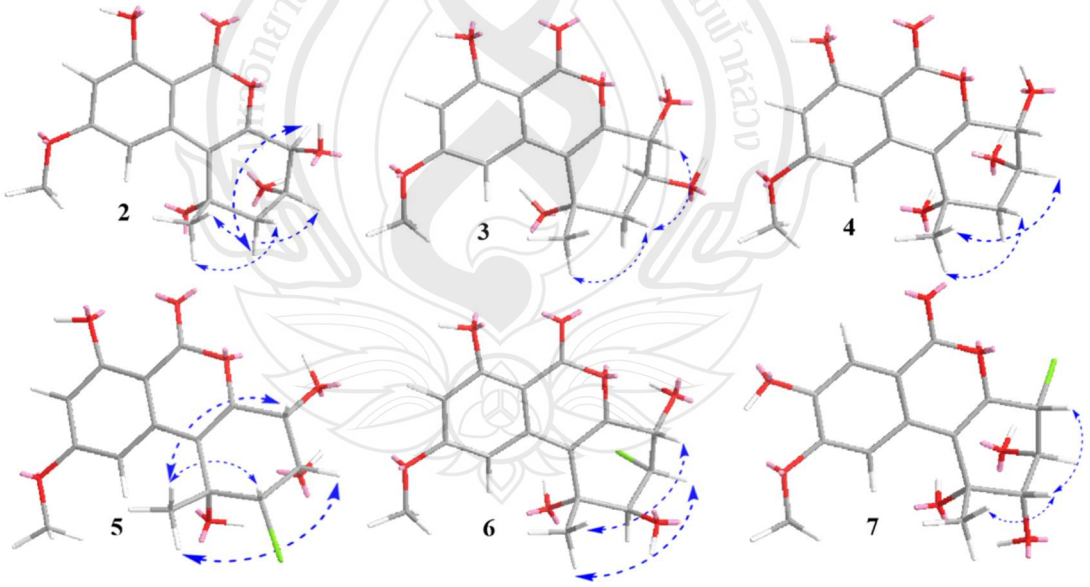

Figure 7.4 Key NOESY correlations of compounds **C26**–**C31**

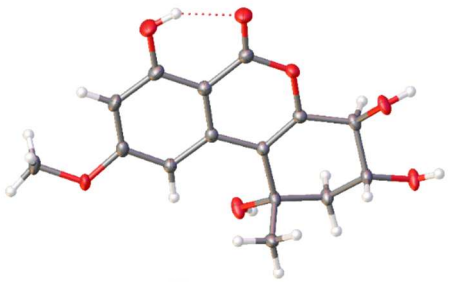

Figure 7.5 X-ray crystal structure of **C26**

Compound **C27** was obtained as colorless crystals (MeOH-CH_2Cl_2). Its HRESIMS spectrum displayed a prominent pseudomolecular ion peak at *m/z* 331.07822 $[M+Na]^+$, corresponding to the molecular formula $C_{15}H_{16}O_7$ and indicating eight degrees of unsaturation. Compound **C27** exhibits 1D NMR (Table 7.2) chemical shifts very similar to those of compound **C25**, whereas the ^1H NMR coupling constants differ (Table 7.2), indicating that the two compounds share the same planar (constitutional) structure with different stereochemistry; this conclusion is corroborated by diagnostic COSY, HSQC, and HMBC correlations (Figure 7.2). The relative configuration was elucidated from ^1H-^1H coupling constants (Table 7.2) in combination with NOESY data (Figure 7.4). A large vicinal coupling constant ($^3J_{H\text{-}2a,\,H\text{-}3}$ = 7.8 Hz) between H-2a (δ_H 2.57, dd) and H-3 (δ_H 4.83, ddd) indicated a diaxial relationship, consistent with both protons being axial. In contrast, the smaller coupling constant between H-2b (δ_H 3.06, dd) and H-3 ($^3J_{H\text{-}2b,\,H\text{-}3}$ = 3.0 Hz) supported an equatorial orientation for H-2b. Furthermore, the relatively small vicinal coupling between H-3 and H-4 (^3J = 4.9 Hz) suggested an axial–equatorial arrangement. In the NOESY spectrum, cross-peaks were observed between 1-CH_3 (δ_H 2.20) and H-2a/H-4, indicating that these protons are co-facial. Conversely, correlations between H-2b and H-3 revealed that they are positioned on the opposite face. Taken together, these data unambiguously established the relative configuration of compound **C27**. The experimental ECD spectrum of compound **C27** (Figure 7.6) matched well with the TDDFT-calculated spectrum of (1*S*, 3*S*, 4*R*)-**C27** (B3LYP/def2TZVP, IEFPCM/MeOH), which was obtained from Boltzmann-weighted averaging of the lowest-energy conformers generated by the CREST/iMTD-GC procedure (Pracht et al., 2020). This good agreement confirmed the absolute configuration of **C27** as 1*S*, 3*S*, 4*R* (Figure 7.1).

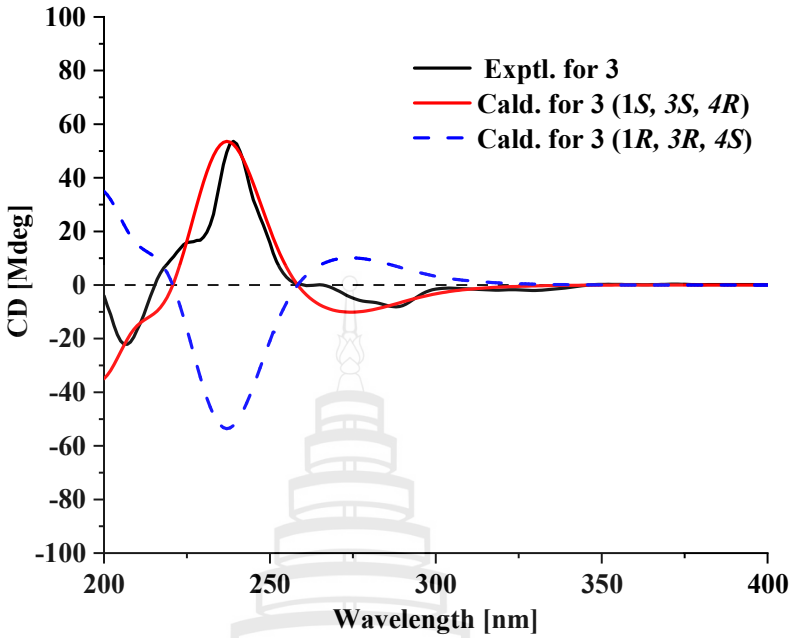

Figure 7.6 Calculated ECD spectra and experimental spectra of compound **C27**

Compound **C28** was obtained as colorless crystals (MeOH–CH_2Cl_2). HRESIMS displayed a prominent pseudomolecular ion peak at *m/z* 331.07884 $[M+Na]^+$, consistent with the formula $C_{15}H_{16}O_7$ and indicating eight degrees of unsaturation. The 1D NMR chemical shifts of **C28** (Table 7.2) closely resemble those of compound **C28**, whereas distinct ^1H-^1H coupling constants indicate stereochemical rather than constitutional differences. An identical planar structure for **C28** and **C26** is further supported by diagnostic COSY, HSQC and HMBC cross-peaks (Figure 7.2). The relative configuration was deduced from ^1H-^1H coupling constants (Table 7.2) and NOESY data (Figure 7.4). Both vicinal couplings of H-3 to the C-2 methylene are small — $^3J_{H\text{-}2a,\,H\text{-}3}$ = 3.5 Hz for H-2a (δ_H 2.55, dd) and $^3J_{H\text{-}2b,\,H\text{-}3}$ = 3.9 Hz for H-2b (δ_H 3.15, dd) —which rules out a diaxial arrangement and is consistent with H-3 occupying an equatorial position in a chair-like ring. The small coupling between H-3 (δ_H 4.35, ddd) and H-4 (J = 3.9 Hz) likewise supports an equatorial–equatorial (gauche) relationship. In the NOESY spectrum, cross-peaks between 1-CH_3 (δ_H 1.91) and H-2a/H-3 indicate that these protons are co-facial; in conjunction with the coupling analysis, this assigns H-2a as equatorial (and hence H-2b as axial). Collectively, these data establish the relative configuration of **C28**. The experimental ECD spectrum (Figure 7.7) of **C28** matched well with the TDDFT-calculated spectrum of (1*S*, 3*R*, 4*R*)-**C28** (B3LYP/def2TZVP, IEFPCM/MeOH), obtained as the Boltzmann-weighted

average of the lowest-energy conformers generated by the CREST/iMTD-GC procedure (Pracht et al., 2020). This agreement confirms the absolute configuration of **C28** as 1*S*, 3*R*, 4*R* (Figure 7.1).

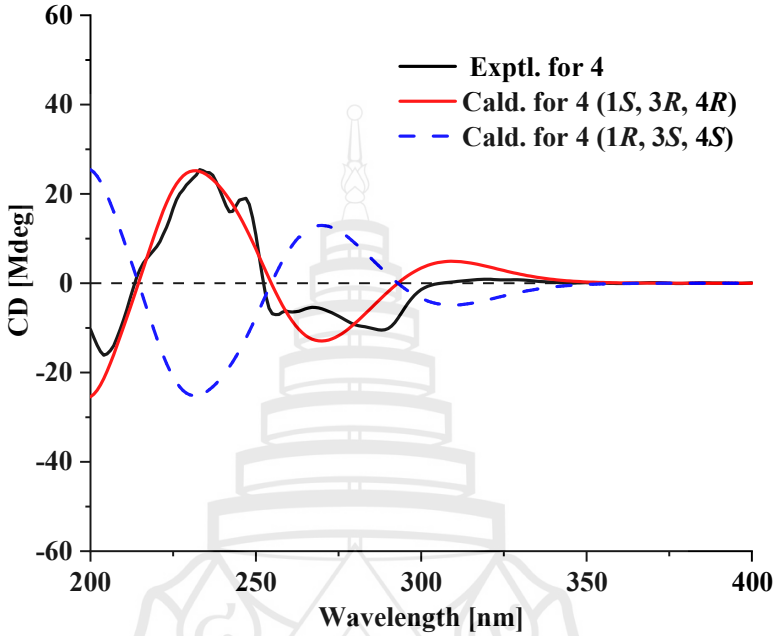

Figure 7.7 Calculated ECD spectra and experimental spectra of compound **C28**

Table 7.2 ^{1}H (400 MHz) and ^{13}C (100 MHz) NMR Data of **C25~C28**

position	C25 (C_5D_5N-d_5)		C26 (C_5D_5N-d_5)		C27 (C_5D_5N-d_5)	
	δ_C, type	δ_H, mult. (*J* in Hz)	δ_C, type	δ_H, mult. (*J* in Hz)	δ_C, type	δ_H, mult. (*J* in Hz)
1	71.3, C		71.0, C		71.5, C	
2	48.6, CH_2	2.70, (dd, *J* = 12.9, 10.8) 2.82, (dd, *J* = 12.9, 3.5)	46.2, CH_2	2.57, (dd, *J* = 13.7, 7.8) 3.06, (dd, *J* = 13.7, 3.0)	46.0, CH_2	2.55, (dd, *J* = 12.0, 3.5) 3.15, (dd, *J* = 12.0, 3.9)
3	70.8, CH	4.60, (ddd, *J* = 10.8, 7.0, 3.5)	69.9, CH	4.83, (ddd, *J* = 7.8, 4.9, 3.0)	67.0, CH	4.35, (ddd, *J* = 3.9, 3.9, 3.5)
4	73.8, CH	4.97, (d, *J* = 7.0)	72.5, CH	4.90, (d, *J* = 4.9)	69.0, CH	4.91, (d, *J* = 3.9)
4a	152.3, C		153.1, C		152.5, C	
6	167.0, C		167.0, C		166.9, C	
6a	101.7, C		102.0, C		101.7, C	
7	164.9, C		164.8, C		164.9, C	
8	100.9, CH	6.78, (d, *J* = 2.4)	100.8, CH	6.75, (d, *J* = 2.4)	101.1, CH	6.76, (d, *J* = 2.4)
9	166.9, C		166.9, C		166.9, C	
10	105.3, CH	8.07, (d, *J* = 2.4)	105.6, CH	8.09, (d, *J* = 2.4)	105.9, CH	8.18, (d, *J* = 2.4)
10a	138.8, C		139.1, C		138.7, C	
10b	119.0, C		118.7, C	2.20, (s)	120.0, C	1.91, (s)
1-CH_3	29.0, CH_3	1.91, (s)	30.9, CH_3	5.03, (br s)	28.5, CH_3	5.04, (br s)
1-OH		5.03, (br s)		5.03, (br s)		5.04, (br s)
3-OH		5.03, (br s)		5.03, (br s)		5.04, (br s)
4-OH		5.03, (br s)		12.08, (br s)		12.14, (br s)
7-OH		12.12, (br s)		3.76, (s)		3.77, (s)
9-OCH_3	56.0, CH_3	3.76, (s)	56.0, CH_3		56.0, CH_3	

Compound **C29** was obtained as brown, hygroscopic powder. HRESIMS showed a prominent pseudomolecular ion at *m/z* 365.03792 $[M+Na]^+$, consistent with $C_{15}H_{15}ClO_7$ and eight degrees of unsaturation; a 3:1 isotope cluster confirmed the presence of one chlorine atom. The 1D NMR (Table 7.3) and HSQC spectra of **C29** displayed a 1,3-disubstituted (meta) benzene ring at δ_H 6.66 (d, *J* = 2.4 Hz, 1H, H-8)/δ_C 100.3 (C-8) and δ_H 7.53 (d, *J* = 2.4 Hz, 1H, H-10)/δ_C 105.1 (C-10), a methyl at δ_H 1.68 (s, 3H, 1-CH_3)/δ_C 23.9; a methoxy at δ_H 3.86 (s, 3H, 9-OCH_3)/δ_C 55.9; three methines (CH); a lactone carbonyl at δ_C 165.1 (C-6), and three exchangeable alcoholic OH protons at δ_H 5.72 (br s, 1H), δ_H 5.83 (br s, 1H), δ_H 6.35 (br s, 1H), and a chelated phenolic hydroxy at δ_H 11.46 (br s, 1H; 7-OH). These data indicate that compound **C29**

and compound **C25** share the same 7-hydroxy-9-methoxycoumarin nucleus. Sequential COSY correlations H-2/H-3, H-3/3-OH, H-3/H-4, H-4/4-OH not only defined a contiguous CH–CH–CH spin system, but also located the chlorine at C-2. The upfield ^{13}C shift of C-2 (δ_C = 68.4) compared with the adjacent oxymethines (C-3/C-4, δ_C = 73.7/70.3) provides additional support for the chlorine being located at C-2 (de Oliveira et al., 2006; Nakanishi et al., 2025). Key HMBC cross-peaks — from 1-CH_3 to C-10b/C-1/C-2; from H-2 to C-1/C-3/C-4 and the methyl carbon (C-1-CH_3); from H-3 to C-1/C-4/C-4a; and from H-4 to C-10b/C-3/C-4a — established the planar structure (constitution) of compound **5**. The relative configuration of compound **5** was elucidated from ^{1}H-^{1}H coupling constants (Table 7.3) and NOESY correlations (Figure 7.4). The small vicinal couplings, $^{3}J_{H\text{-}2,\ H\text{-}3}$ = 2.3 Hz and $^{3}J_{H3,\ H\text{-}4}$ = 3.0 Hz, indicate gauche relationships (≈60° dihedrals) that are consistent with an all-equatorial arrangement of H-2/H-3/H-4 in the predominant half-chair conformation. In the NOESY spectrum, cross-peaks between 1-CH_3 (δ_H 1.68) and H-2/H-3/H-4 show that these protons are co-facial. Aken together, these observations define the relative configuration of **C29**. Moreover, the experimental ECD spectrum (Figure 7.8) agrees well with the TDDFT-calculated spectrum for (1*R*, 2*S*, 3*S*, 4*R*)-**5** (B3LYP/def2-TZVP, IEFPCM/MeOH), obtained as the Boltzmann-weighted average of the lowest-energy conformers generated by the CREST/iMTD-GC protocol (Pracht et al., 2020). This match assigns the absolute configuration of **C29** as 1*R*, 2*S*, 3*S*, 4*R* (Figure 7.1).

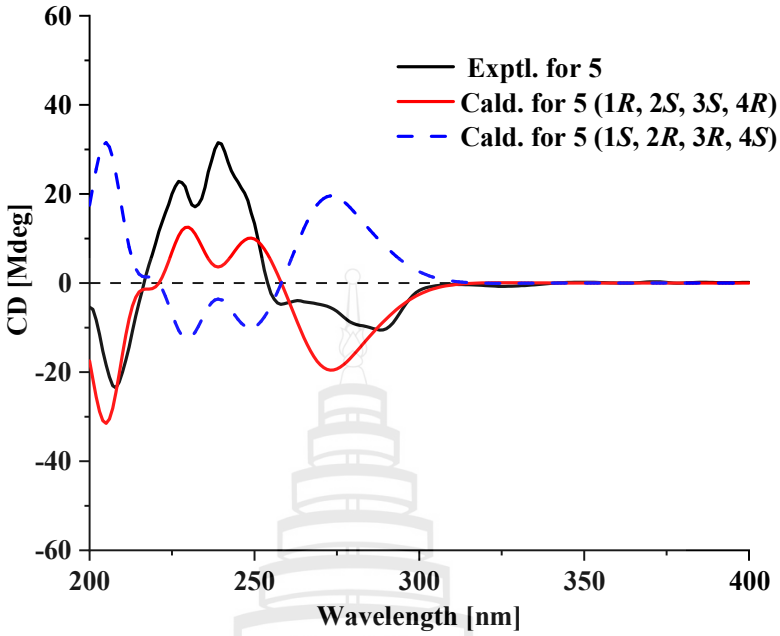

Figure 7.8 Calculated ECD spectra and experimental spectra of compound **C29**

Compound **C30** was obtained as brown, hygroscopic powder. HRESIMS showed a protonated molecule at *m/z* 343.05763 $[M+H]^+$, consistent with the formula $C_{15}H_{15}ClO_7$ and eight degrees of unsaturation, a characteristic 3:1 isotope cluster confirmed the presence of a single chlorine atom. Except for differences in coupling constants and NOESY correlations, the NMR features (Table 7.3, Figure 7.2) of **C30** closely match those of **C30**. Guided by the diagnostic chemical-shift pattern for CH-OH versus CH–Cl established in **C29**, the chlorine substituent in **C30** is assigned to C-3 (δ_C 67.4) (de Oliveira et al., 2006; Nakanishi et al., 2025). The relative configuration was elucidated through analysis of ^{1}H-^{1}H coupling constants (Table 7.3) in combination with NOESY data (Figure 7.4). A large vicinal coupling constant ($^3J_{H\text{-}2,\ H\text{-}3}$ = 11.6 Hz) between H-2 (δ_H 4.40, d) and H-3 (δ_H 3.68, dd) indicates a diaxial relationship (both protons axial), whereas the smaller coupling constant ($^3J_{H\text{-}3,\ H\text{-}4}$ = 4.3 Hz) between H-3 (δ_H 3.68, dd) and H-4 (δ_H 4.37, d) supports an equatorial orientation for H-4. In the NOESY spectrum, cross-peaks between 1-CH_3 (δ_H 1.51) and H-3/H-4 show that these protons are co-facial, with H-2 located on the opposite face. Collectively, these observations unambiguously establish the relative configuration of **C30**. Moreover, the experimental ECD spectrum (Figure 7.9) agrees well with the TDDFT-calculated

spectrum for (1*R*, 2*S*, 3*R*, 4*S*)-**C30** (B3LYP/def2-TZVP, IEFPCM/MeOH), obtained as the Boltzmann-weighted average of the lowest-energy conformers generated by the CREST/Imtd-GC protocol (Pracht et al., 2020). This agreement assigns the absolute configuration of **C30** as 1*R*, 2*S*, 3*R*, 4*S* (Figure 7.1).

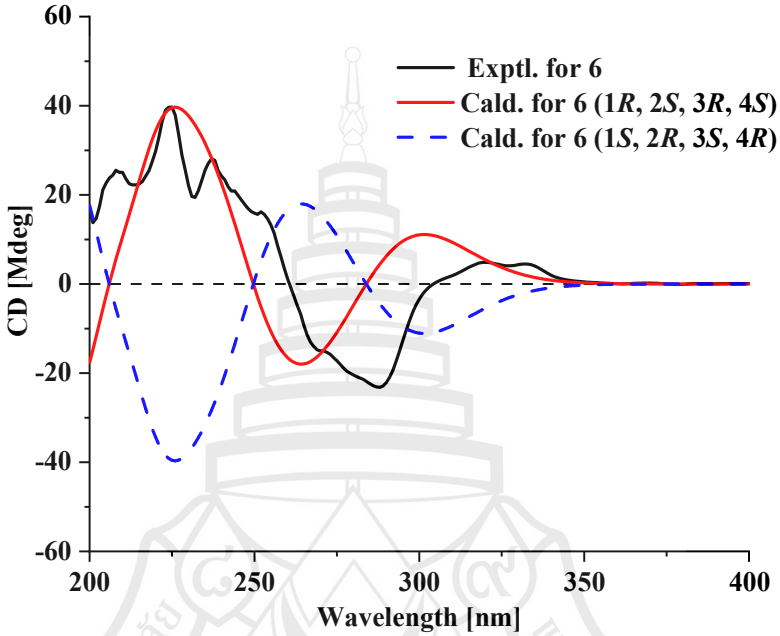

Figure 7.9 Calculated ECD spectra and experimental spectra of compound **C30**

Compound **C31** was obtained as a brown, hygroscopic powder. HRESIMS showed a prominent $[M+Na]^+$ ion at m/z 365.0388, consistent with $C_{15}H_{15}ClO_7$ and eight degrees of unsaturation; a diagnostic 3:1 isotope cluster confirmed the presence of one chlorine atom. The 1D NMR and HSQC spectra revealed two aromatic proton signals at δ_H 6.66 (1H, H-8)/δ_C 100.0 (C-8) and δ_H 7.48 (1H, H-10)/δ_C 104.9 (C-10), a methyl at δ_H 1.72 (3H, 1-CH_3)/δ_C 23.4, a methoxy at δ_H 3.85 (3H, 9-OCH_3)/δ_C 55.9, three oxymethines, a lactone carbonyl at δ_C 165.1 (C-6), three exchangeable alcoholic OH signals at δ_H 5.60 (br s, 3H; 1-OH, 2-OH, 3-OH), and a chelated phenolic OH at δ_H 11.39 (br s, 1H; 7-OH). Even though H-8 and H-10 show little or no discernible splitting in the ^{1}H NMR (appearing nearly as singlets), the aromatic proton and carbon chemical shifts closely match those of compounds **C29** and **C30**. In addition, H-8 and H-10 display clear COSY cross-peaks, and diagnostic HMBC correlations (H-10 → C-10b/C-8; H-8 → C-10) are observed. We therefore conclude that compound **C31** shares

the same core framework as compounds **C29** and **C31**, namely 7-hydroxy-9-methoxycoumarin. Guided by the established trend that CH–OH resonates downfield relative to CH–Cl (de Oliveira et al., 2006; Nakanishi et al., 2025), the most upfield oxymethine carbon at δ_C 66.9 (C-4) is assigned as CH–Cl, whereas C-2/C-3 at δ_C 68.9/71.8, are assigned as CH–OH. Additional HMBC cross-peaks (1-CH_3 → C-10b/C-1/C-2; H-2 → C-1 and the methyl carbon; H-3 → C-1/C-2/C-4/C-4a; H-4 → C-10b/C-4a) establish the planar constitution of **C31** (Figure 7.2). The relative configuration follows from small vicinal couplings ($^3J_{H2,\ H3}$ = 2.0 Hz; $^3J_{H3,\ H4}$ = 4.3 Hz), consistent with gauche relationships (≈60°) and an all-equatorial arrangement of H-2/H-3/H-4 in a predominant half-chair, and from NOESY cross-peaks (1-CH_3 ↔ H-2; H-2 ↔ H-4) showing these protons are co-facial (Table 7.3, Figure 7.4). Finally, the experimental ECD spectrum (Figure 7.10) matches the TDDFT simulation (B3LYP/def2-TZVP, IEFPCM/MeOH) obtained as a Boltzmann-weighted average of CREST/iMTD-GC conformers (Pracht et al., 2020), assigning the absolute configuration of **C31** as 1*R*, 2*S*, 3*R*, 4*R* (Figure 7.1).

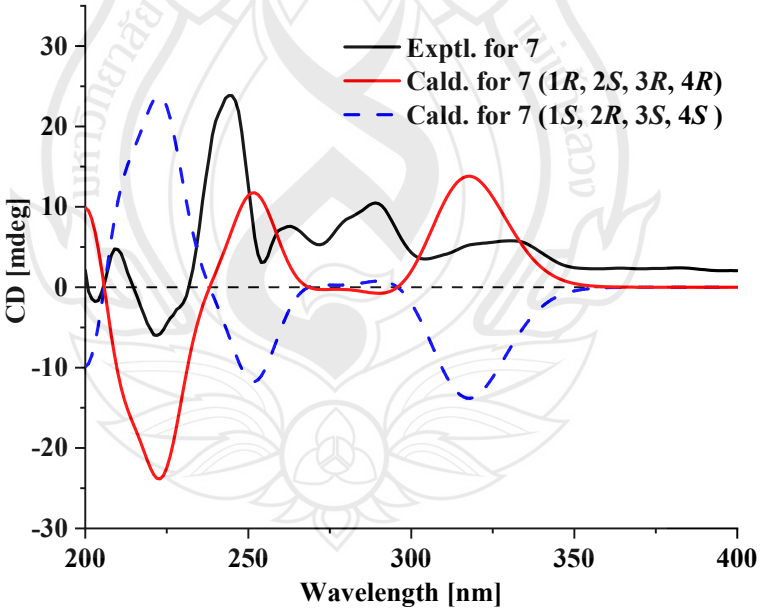

Figure 7.10 Calculated ECD spectra and experimental spectra of compound **C31**

In addition to seven previously unreported compounds, eight known compounds (Figure 7.1) were identified: rhizopycnin C (Figure 7.11) (**C32**) (Lai et al., 2016), djalonensone (**C33**) (Zhou et al.), 2-chloro-3,4,7-trihydroxy-9-methoxy-1-methyl-6*H*-

benzo[c]chromen-6-one (**C34**) (Darsih et al., 2017), palmariol B (**C35**) (Meng et al., 2012), alternariol (**C36**) (Xiao et al., 2014), porric acid D(**C37**) (Xu et al., 2012), 3,4,8-trihydroxy-6-methoxy-1-methylxanthone (**C38**) (Zhuang et al., 2015; 荣先国 et al., 2024), and altechromone A (**C39**) (Li et al., 2024) based on single-crystal X-ray diffraction and comparison of their spectroscopic data with those reported in the literature.

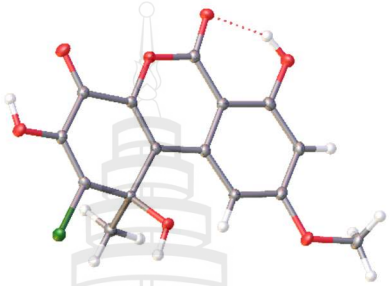

Figure 7.11 X-ray crystal structure of **C32**

We propose a hypothetical biosynthetic pathway for compounds **C25**–**C32** (Figure 7.12). A fungal non-reducing polyketide synthase (nrPKS) assembles an acetyl-starter heptaketide from six malonyl-CoA extender units and, under Product-Template (PT) domain control, programs cyclization to the benzopyranone (dibenzo-*α*-pyrone) precursor S*(Lai et al., 2016; Zhao et al., 2020). A SAM-dependent O-methyltransferase together with a site-specific oxidation furnishes S2; from S2, stereoselective reductions by SDR-type enzymes deliver the non-halogenated congeners **C26**–**C28**. In the halogenation manifold, S* first converts to S1: a flavin-dependent halogenase effects 2-chlorination to give **C32**, which upon reduction affords **C29**; alternatively, S1 → S3 → S4 followed by 3-chlorination yields **C30**, or S1 → S3 → S4 → S5 followed by 4-chlorination furnishes **C31**. In a parallel deep-oxidation branch, successive oxidations (S6 → S7), anhydride-like opening to S8 (Zhang et al., 2008), decarboxylation to S9, and keto–enol isomerization produce **C25**.

Table 7.3 ^{1}H and ^{13}C NMR Data of **C29~C31**

position	C29 (400MHz, DMSO-d_6)		C30 (400 MHz, DMSO-d_6)		C31 (600 MHz, DMSO-d_6)	
	δ_C, type	δ_H, mult. (*J* in Hz)	δ_C, type	δ_H, mult. (*J* in Hz)	δ_C, type	δ_H, mult. (*J* in Hz)
1	72.2, C		73.0, C		73.0, C	
2	68.4, CH	4.59, (d, *J* = 3.0)	70.9, CH	4.40, (d, *J* = 11.6)	68.9, CH	4.39, (d, *J* = 2.0)
3	73.7, CH	4.00, (dd, *J* = 2.3, 3.0)	67.4, CH	3.68, (dd, *J* = 11.6, 4.3)	71.8, CH	4.15, (dd, *J* = 4.3, 2.0)
4	70.3, CH	4.24, (d, *J* = 2.3)	68.0, CH	4.37, (d, *J* = 4.3)	66.9, CH	4.65, (d, *J* = 4.3)
4a	149.8, C		149.6, C		150.1, C	
6	165.1, C		165.1, C		165.1, C	
6a	100.1, C		100.1, C		103.9, C	
7	163.4, C		163.5, C		163.5, C	
8	100.3, CH	6.66, (d, *J* = 2.3)	100.4, CH	6.64, (d, *J* = 2.3)	100.0, CH	6.60, (d, *J* =1.3)
9	165.9, C		166.0, C		165.9, C	
10	105.1, CH	7.53, (d, *J* = 2.3)	105.0, CH	7.58, (d, *J* = 2.3)	104.9, CH	7.48, (br s)
BR	137.0, C		137.0, C		137.3, C	
10b	117.5, C		117.8, C		116.1, C	
1-CH_3	23.9, CH_3	1.68, (s)	22.3, CH_3	1.51, (s)	23.4, CH_3	1.72, (s)
1-OH		5.72, (br s)		5.84, (br s)		5.60, (br s)
2-OH				5.84, (br s)		5.60, (br s)
3-OH		5.83, (br s)				5.60, (br s)
4-OH		6.35, (br s)		5.84, (br s)		
7-OH		11.46, (br s)		11.47, (br s)		11.39, (br s)
9-OCH_3	55.9, CH_3	3.86, (s)	56.0, CH_3	3.85, (s)	55.9, CH_3	3.85, (s)

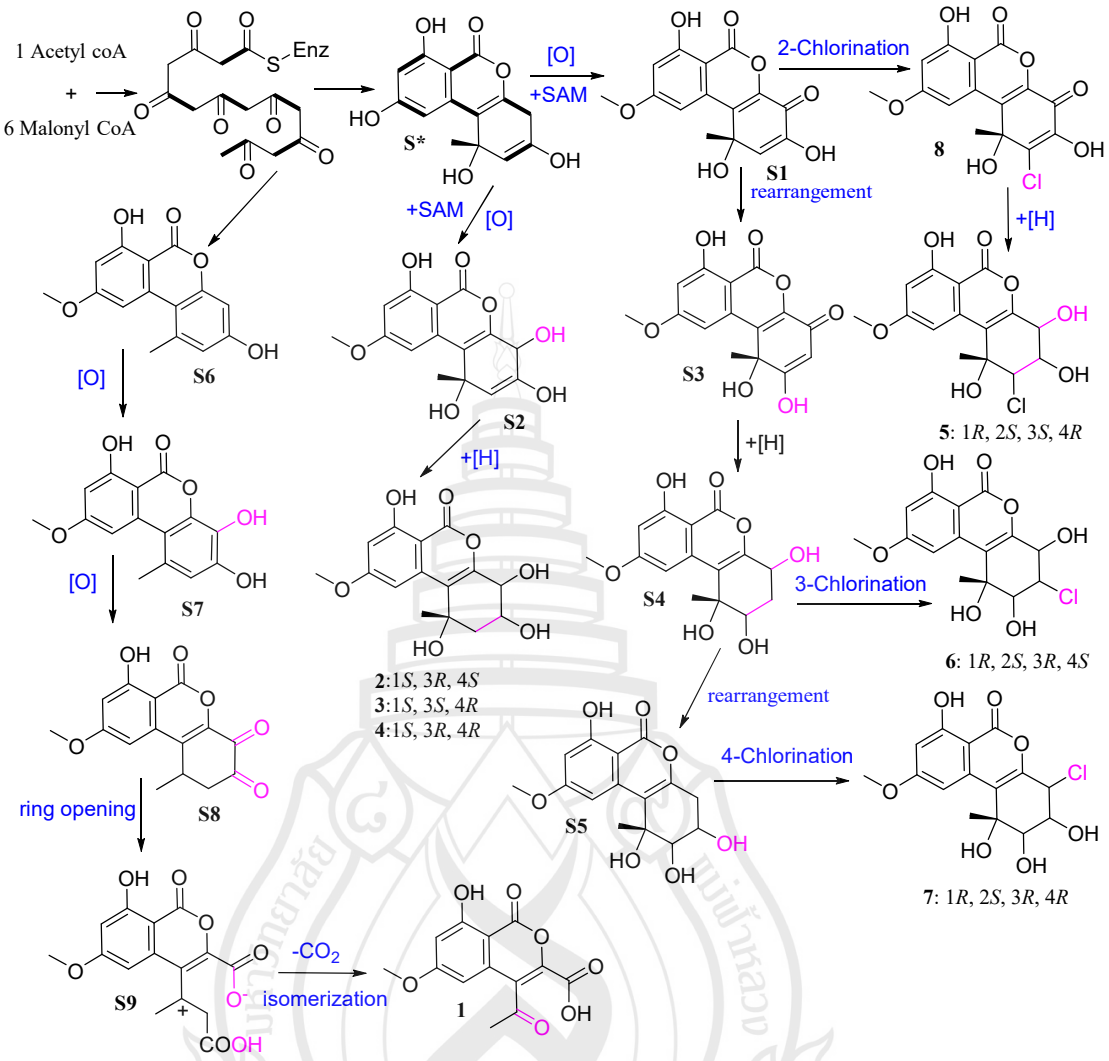

Figure 7.12 Proposed Biosynthetic Pathway for **C25–C32**

7.3.2 Cytotoxic Activity

All compounds were assessed for their cytotoxicity against HepG2, A2780, A549, Hela, and MDA-MB231 cell lines. Doxorubicin was used as a positive control. As a result, Compound **C36** exhibited potent activity in HepG2/HeLa (IC_{50} both < 20 μM), indicating selectivity toward these two cell lines; compound **C39** showed moderate activity in A549/HeLa (16.55–26.49 μM), also displaying selectivity; compound **13** was moderate and selective toward A2780 (25.73 μM); and compound **C30** showed moderate activity only in A549 (38.81 μM). Compound **C32** exhibited inhibitory activity across multiple cell lines with IC_{50} values of 22.49–85.14 μM, indicating broad-spectrum activity (Table 7.4).

Table 7.4 Cytotoxicity of **C25**–**C39** against mammalian cell lines [half maximal inhibitory concentra-tion (IC_{50}): μM]

Compound	A2780	A549	HepG2	Hela	MDA-MB231
C25	>100	>100	>100	>100	>100
C26	>100	>100	>100	>100	>100
C27	>100	>100	>100	>100	>100
C28	>100	>100	>100	>100	>100
C29	>100	>100	>100	>100	>100
C30	>100	38.81	>100	>100	>100
C31	>100	>100	>100	>100	>100
C32	85.14	22.49	27.24	54.67	49.50
C33	>100	54.62	>100	19.22	68.12
C34	>100	>100	24.07	>100	>100
C35	>100	>100	>100	>100	>100
C36	74.02	>100	13.43	15.77	72.39
C37	25.73	26.21	>100	>100	98.74
C38	45.90	16.55	>100	26.49	50.51
C39	>100	>100	>100	>100	>100
cis-platinum	9.34	-	-	-	-
adriamycin	-	7.12	4.35	3.22	12.71

7.4 Conclusion

In summary, a total of fifteen dibenzo-*α*-pyrone derivatives including three previously undescribed ones have been characterized from the rolled oats fermentation of the fungus *H. sexuale* LZ15. Their structures were established by means of spectroscopic and computational methods. Bioactivity assays revealed a clear potency–selectivity pattern across five cell lines: compound **C36** was potent and selective in HepG2 and HeLa; compound **C38** showed moderate, selective activity in A549 and HeLa; compound **C37** was moderate and selective toward A2780; compound **C30** showed moderate activity only in A549; and compound **C32** exhibited broad-spectrum activity (including MDA-MB-231). These findings support consideration of compounds **C36**−**C38** for follow-up optimization and mechanism studies, while compound **C32** may serve as an initial scaffold for SAR exploration.

CHAPTER 8

CONCLUSION

8.1 Overall Conclusion

Taken together, this dissertation centers on helicosporous hyphomycetes (Tubeufiaceae) and, through small-scale solid-state fermentation, chemistry/bioactivity-guided screening, and comprehensive characterization (compounds numbered **C1–C39** throughout, see Figure 8.1), reveals substantial chemical diversity and pharmacological potential. From *Neohelicosporium guangxiense* SLGY-5, we obtained α-tetralone derivatives **C1–C3** and an isocoumarin **C4** (with **C1** isolated from natural sources for the first time). *N. griseum* GYSLGY-1 produced the new polyketides neogrisphenols A (**C5**) and B (**C6**) together with congeners (**C7–C11**), while *N. griseum* SLGY-15 yielded seven polyketides (**C12–C18**) and one steroid (**C19**). *Tubeufia longihelicospora* WZS71 afforded dimeric naphtho-*γ*-pyrones (**C20–C23**) and one alkaloid (**C24**), and *Helicosporium sexuale* LZ15 provided a suite of unprecedented polyhydroxy-chlorinated fused-coumarins (**C25–C31**) plus known analogues (**C32–C39**). In terms of activity, **C5** exhibited pronounced cytotoxicity against A2780, PC-3, and MDA-MB-231 cells—surpassing cisplatin in A2780—and inhibited proliferation, induced apoptosis, and caused S-phase arrest; **C6** was also active against A2780. **C12**, **C14**, and **C15** showed cytotoxicity toward HeLa and A549 cells. Antimicrobial assays identified **C5–C6** and **C10** as active against *Bacillus subtilis*, *Clostridium perfringens*, and *Staphylococcus aureus* (MIC 16–31 μg/mL), and **C20–C21** as active against *Pseudomonas aeruginosa* (MIC 62.0 μg/mL; MBC 248 μg/mL). Overall, this work broadens the metabolic landscape of helicosporous fungi and furnishes promising lead scaffolds. These findings support consideration of compounds **C5**, **C6**, **C12**, **C14**, and **C15** for follow-up optimization and mechanism studies, while compound **C31** may serve as an initial scaffold for SAR exploration.

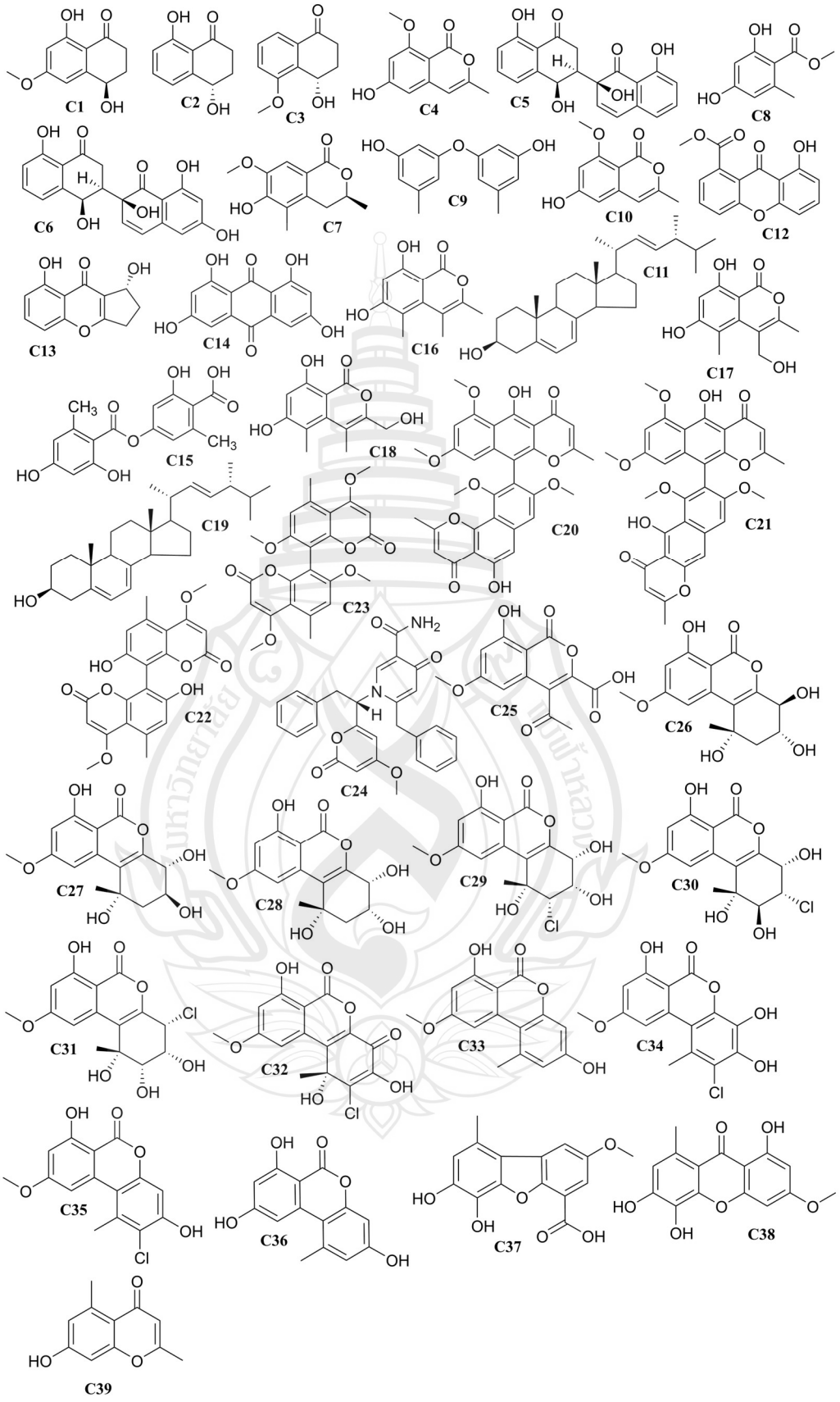

Figure 8.1 Structures of compounds **C1**-**C39** from helicosporous Tubeufiaceae

8.2 Highlights

8.2.1 Enriched the Chemical Diversity and Novelty of Helicosporous Hyphomycetes

From five bioactive strains of helicosporous hyphomycetes, 39 metabolites (**C1**–**C39**) were obtained, spanning α-tetralones, isocoumarins, naphtho-γ-pyrones, dimeric coumarins, alkaloids, and dibenzo-α-pyrones. Ten molecules were new—**C5**–C6 (polyketides), **C7** (an isochroman-1-one), and **C25**–**C31** (seven dibenzo-α-pyrones)—and **C1** was isolated from natural sources for the first time.

8.2.2 Discovery of Important Anticancer Lead Compounds

Led by neogrisphenol A (**C5**), which showed IC_{50} values of 3.20, 10.68, and 16.30 μM against A2780, PC-3, and MDA-MB-231, respectively, and outperformed cisplatin in A2780. Mechanistic studies indicated suppressed proliferation, induction of apoptosis, and S-phase arrest. Neogrisphenol B (**C6**) was also active against A2780 (IC_{50} = 10.13 μM). Compounds **C12**, **C14**, and **C15** exhibited micromolar activity in HeLa and A549 cells (lowest 7.4 μM), and **C36**, **C38**, **C37**, and **C30** showed cell-line selectivity, collectively supporting their potential as anticancer lead scaffolds.

8.2.3 New Findings in Antibacterial Activity

C5–**C6** and **C10** exhibited activity against *Bacillus subtilis*, *Clostridium perfringens*, and *Staphylococcus aureus* (MICs 16–31 μg/mL). **C12**–**C15** showed moderate activity against *Pseudomonas aeruginosa*, with **C13** additionally displaying weak activity against *S. aureus*. **C20**–**C21** were active against *P. aeruginosa* (MIC 62.0 μg/mL; MBC 248 μg/mL).

8.2.4 Established an Experimental Platform Tailored to Helicosporous Hyphomycetes, Spanning from Bioactive Strain Screening to Lead Compound Discovery

Established an experimental platform tailored to helicosporous hyphomycetes, linking bioactive-strain screening, small-scale solid-state fermentation, and MS/NMR-guided isolation to MoA assays and SAR. Crucially, we resolved the contamination issue during fermentation of helicosporous hyphomycete strains with long growth cycles.

8.3 Future Work

8.3.1 To elucidate the Anticancer Mechanism of C5

In sensitive cell models such as A2780, systematically validate the causal chain "proliferation inhibition → apoptosis induction → S-phase arrest," define direct/indirect molecular targets and key pathways, and build concentration–time–effect and selectivity profiles.

8.3.2 To Identify the Biosynthetic Gene Cluster (BGC) for C5 and Elucidate its Biosynthetic Pathway

To identify and functionally validate the biosynthetic gene cluster (BGC) for **C5**, and to elucidate its biosynthetic pathway by integrating genome mining with gene disruption/heterologous expression and isotopic labeling.

8.3.3 To Systematically Optimize Fermentation of *N. griseum* GYSLGY-1 to Raise C5 Titer and Broaden Product Novelty/Chemical Diversity

Optimize medium and process parameters (e.g., cultivation time, temperature, pH), coupled with metabolite profiling and induction strategies, to activate and expand the accessible secondary-metabolite spectrum.

8.3.4 To modify the Structure of C30 and Investigate its Structure–Activity Relationships (SAR).

Design and synthesize a series of homologues/derivatives of **C30** and conduct structure–activity relationship (SAR) studies to identify more potent candidate compounds.

8.3.5 Chemical Taxonomy Based on Secondary Metabolite Profiles

Chemical fingerprints of representative helicosporous hyphomycetes in Tubeufiaceae will be compared based on the available secondary metabolite data to identify chemical markers with taxonomic significance. These chemical characteristics will be integrated with multi-gene phylogenetic frameworks to further improve and refine the chemical taxonomy of this group.

8.4 Publications

List of publications

8.4.1 First Author

Zhang, L. J., Yang, M. F., Ma, J., Xiao, X. J., Ma, X. Y., Zheng, D. G., . . . Lu, Y. Z. (2023). Neogrisphenol A, a potential ovarian cancer inhibitor from a new record fungus *Neohelicosporium griseum*. *Metabolites*, 13(3), 435. https://doi.org/10.3390/metabo13030435

Zhang, L. J., Ma, J., Ma, X., Feng, X., Bai, X., Huang, Y., . . . Lu, Y. Z. (2023). A new record of *Neohelicosporium guangxiense* and its secondary metabolites. *Chiang Mai Journal of Science, 50*(2), 1–12. https://doi.org/10.12982/CMJS.2023.010

Zhang, L., Ma, J., Yang, M., Zhao, T., Han, M. Y., Zheng, D., . . . Lu, Y. (2024). Polyketides from *Neohelicosporium griseum*: Structure assignment and bioactivity investigation. *Medicinal Chemistry Research, 33*(2), 308–313. https://doi.org/10.1007/s00044-023-03172-1

Zhang, L., Ma, J., Zhao, T., Han, M., Zheng, D., Jayawardena, R. S., . . . Lu, Y. (2024). Antimicrobial metabolites from the freshwater fungus *Tubeufia longihelicospora* strain GZCC 23-0405. *Chiang Mai Journal of Science, 51*(4), e2024053. https://doi.org/10.12982/CMJS.2024.053

Zhang, L.-J., Jayawardena, R. S., Ausana, M., Liu, N.-G., Ma, J., Xiao, X.-J., . . . Sun, J.-Z. (2025). Strategies for mining new secondary metabolites from fungi: From classical approaches to genomics-based mining. *Fungal Biology Reviews*. (in press)

Zhang, L. J., Ma, X., Han, M., Zheng, D., Ma, J., Xiao, X., . . . Lu, Y. (2025). Novel polyhydroxy-chlorinated dibenzo-α-pyrones derivatives with fused six-membered rings from the saprophytic fungus Helicosporium sexuale LZ15. *Phytochemistry*. (in press)

8.4.2 Co-author

Lu, Y. Z., Ma, J., Xiao, X. J., Zhang, L. J., Xiao, Y. P., & Kang, J. C. (2022). Four new species and three new records of helicosporous hyphomycetes from China and their multi-gene phylogenies. *Frontiers in Microbiology, 13*, 1053849. https://doi.org/10.3389/fmicb.2022.1053849

Wang, X., Wanasinghe, D. N., Zhang, J., Ma, J., Zhou, P., Zhang, L., . . . Zhang, Z. (2023). Insights from the endophytic fungi in Amphisphaeria (Sordariomycetes): A. orixae sp. nov. from Orixa japonica and its secondary metabolites. *Microorganisms, 11*(5), 1268. https://doi.org/10.3390/microorganisms11051268

Xiao, X. J., Ma, J., Zhang, L. J., Liu, N. G., Xiao, Y. P., Tian, X. G., . . . Lu, Y. Z. (2023). Additions to the genus Helicosporium (Tubeufiaceae, Tubeufiales) from China with an identification key for Helicosporium taxa. *Journal of Fungi, 9*(7), 775. https://doi.org/10.3390/jof9070775

Ma, J., Zhang, L. J., Boonmee, S., Xiao, X. J., Liu, N. G., Xiao, Y. P., . . . Lu, Y. Z. (2023). Morphological and phylogenetic analyses reveal three new species and one new record of Tubeufia (Tubeufiales, Tubeufiaceae) from southern China. *MycoKeys, 99*, 87–116. https://doi.org/10.3897/mycokeys.99.107606

Ma, J., Gomdola, D., Boonmee, S., Shen, H. W., Tang, X., Zhang, L. J., . . . Lu, Y. Z. (2024). Three new species of Neohelicomyces (Tubeufiales, Tubeufiaceae) from freshwater and terrestrial habitats in China. *MycoKeys, 105*, 317–340. https://doi.org/10.3897/mycokeys.105.124129

Zhang, J. Y., Hyde, K. D., Zhang, L. J., Bai, S., Bao, D. F., Al-Otibi, F., . . . Lu, Y. Z. (2025). Two novel hyphomycetes associated with ferns from China. *MycoKeys, 113*, 101–122. https://doi.org/10.3897/mycokeys.113.137678

Zhang, J. Y., Hyde, K. D., Ma, J., Wu, N., Al-Otibi, F., Zhang, L. J., . . . Lu, Y. Z. (2025). Morpho-phylogenetic evidence reveals Pseudolomaanthathailandica gen. et sp. nov. and Submultiguttulisporamultiseptata gen. et sp. nov. in Chaetosphaeriaceae. *MycoKeys, 113*, 123–146. https://doi.org/10.3897/mycokeys.113.142643

Xiao, X. J., Liu, N. G., Ma, J., Zhang, L. J., Bao, D. F., Bai, S., . . . Lu, Y. Z. (2025). Three new asexual Kirschsteiniothelia species from Guizhou Province, China. *MycoKeys, 113*, 147–170. https://doi.org/10.3897/mycokeys.113.139427

Han, M. Y., Karunarathna, S. C., Lu, L., Zheng, D. G., Suwannarach, N., Elgorban, A. M., . . . Tibpromma, S. (2025). Three new species of Camporesiomyces (Tubeufiaceae, Tubeufiales, Dothideomycetes) associated with coffee in Yunnan, China. *MycoKeys, 117*, 315–348. https://doi.org/10.3897/mycokeys.117.154573

Zheng, D., Lu, W., Han, M., Dai, D. Q., Zhang, L. J., Elgorban, A. M., . . . Karunarathna, S. C. (2025). Volvopluteus yunnanensis (Pluteaceae, Agaricales), a novel species from Yunnan Province, China. *Phytotaxa, 706*(3), 269–280. https://doi.org/10.11646/phytotaxa.706.3.5

Han, M., Karunarathna, S. C., Lu, L., Zheng, D., Dai, D., Suwannarach, N., . . . Hyde, K. D. (2025). Pseudodictyosporium yunnanensis sp. nov. (Dictyosporiaceae, Pleosporales) from dead twigs of Coffea arabica in China. *Phytotaxa, 711*(1), 28–42. https://doi.org/10.11646/phytotaxa.711.1.2

Zheng, D., Voto, P., Tibpromma, S., Lu, W., Han, M., Kumla, J., . . . Karunarathna, S. C. (2025). Candolleomyces yunnanensis (Psathyrellaceae, Agaricales), a novel species from Yunnan Province, China. *Phytotaxa, 711*(3), 281–292. https://doi.org/10.11646/phytotaxa.711.3.3

REFERENCES

Aichinger, G. (2021). Natural dibenzo-α-pyrones: Friends or foes?. *International Journal of Molecular Sciences, 22*(23), 13063.

Aly, A. H., Edrada-Ebel, R., Indriani, I. D., Wray, V., Müller, W. E. G., Totzke, F., . . . Ebel, R. (2008). Cytotoxic metabolites from the fungal endophyte *Alternaria* sp. and their subsequent detection in its host plant *Polygonum senegalense*. *Journal of Natural Products, 71*(6), 972–980.

Arlt, A., & Koert, U. (2010). Total synthesis of (±)-cephalosol via silyl enol ether acylation. *Synthesis, 2010*(6), 917–922.

Atanasov, A. G., Zotchev, S. B., Dirsch, V. M., & Supuran, C. T. (2021). Natural products in drug discovery: Advances and opportunities. *Nature Reviews Drug Discovery, 20*(3), 200–216.

Bai, M., Zheng, C.-J., Tang, D.-Q., Zhang, F., Wang, H.-Y., & Chen, G.-Y. (2019). Two new secondary metabolites from a mangrove-derived fungus *Cladosporium* sp. JS1-2. *The Journal of Antibiotics, 72*(10), 779–782.

Baker, D. D., & Alvi, K. A. (2004). Small-molecule natural products: New structures, new activities. *Current Opinion in Biotechnology, 15*(6), 576–583.

Bills, G. F., & Gloer, J. B. (2016). Biologically active secondary metabolites from the fungi. *Microbiology Spectrum, 4*(6), Funk-0009-2016.

Blacutt, A., Ginnan, N., Dang, T., Bodaghi, S., Vidalakis, G., Ruegger, P., . . . Drozd, C. (2020). An in vitro pipeline for screening and selection of citrus-associated microbiota with potential anti-*Candidatus Liberibacter asiaticus* properties. *Applied and Environmental Microbiology, 86*(8), e02883-19.

Boonmee, S., Rossman, A. Y., Liu, J.-K., Li, W.-J., Dai, D.-Q., Bhat, J. D., . . . Hyde, K. D. (2014). Tubeufiales *ord. nov.,* integrating sexual and asexual generic names. *Fungal* Diversity, 68*(1), 239–298.*

Bös, M., Canesso, R., Inoue-Ohga, N., Nakano, A., Takehana, Y., & Sleight, A. J. (1997). O-methylasparvenone, a nitrogen-free serotonin antagonist. *Bioorganic & Medicinal Chemistry, 5*(12), 2165–2171.

Bungihan, M. E., Tan, M. A., Kitajima, M., Kogure, N., Franzblau, S. G., dela Cruz, T. E. E., . . . Nonato, M. G. (2011). Bioactive metabolites of *Diaporthe* sp. P133, an endophytic fungus isolated from *Pandanus amaryllifolius*. *Journal of Natural Medicines, 65*(3), 606–609.

Bush, K., & Bradford, P. A. (2016). β-lactams and β-lactamase inhibitors: An overview. *Cold Spring Harbor Perspectives in Medicine, 6*(8), a025247.

Cai, Y., Rao, L., & Zou, Y. (2021). Genome mining discovery of a C4-alkylated dihydroisocoumarin pathway in fungi. *Organic Letters, 23*(6), 2337–2341.

Campos, F., Barison, A., Daolio, C., Ferreira, A., & Rodrigues-Fo, E. (2005). Spectral assignments and reference data—Complete ^{1}H and ^{13}C NMR assignments of aurasperone A and fonsecinone A, two bis-naphthopyrones produced by *Aspergillus aculeatus*. *Magnetic Resonance in Chemistry, 43*(11), 962–965.

Charria-Girón, E., Tchamgoue, J., Stadler, M., & Marin-Felix, Y. (2025). Coprophilous fungi in the search for new antimicrobials and other beneficial natural products. *Natural Product Reports, 42,* 1835-1848. https://doi.org/10.1039/D5NP00015G

Chen, X.-W., Xu, M., Feng, C., & Hu, C.-H. (2018). Advances in the biosynthesis of fungal polyketides. *Chinese Journal of Biotechnology, 34*(2), 151–164.

Cheng, M.-J., Wu, M.-D., Chang, H.-S., Chen, J.-J., & Tseng, M. (2022). Secondary metabolites from the actinobacterium *Amycolatopsis taiwanensis*. *Chemistry of Natural Compounds, 58*(1), 175–177.

Choi, H. J., Lee, S. M., Kim, S.-H., Kim, D. W., Choi, Y. W., & Joo, W. H. (2012). A novel *Helicosporium* isolate and its antimicrobial and cytotoxic pigment. *Journal of Microbiology and Biotechnology, 22*(9), 1214–1217.

Conrado, R., Gomes, T. C., Roque, G. S. C., & de Souza, A. O. (2022). Overview of bioactive fungal secondary metabolites: Cytotoxic and antimicrobial compounds. *Antibiotics, 11*(11), 1604.

Cutler, H. G., Crumley, F. G., Cox, R. H., Hernandez, O., Cole, R. J., & Dorner, J. W. (1979). Orlandin: A nontoxic fungal metabolite with plant growth inhibiting properties. *Journal of Agricultural and Food Chemistry, 27*(3), 592–595.

Darsih, C., Prachyawarakorn, V., Mahidol, C., Ruchirawat, S., & Kittakoop, P. (2017). A new polyketide from the endophytic fungus *Penicillium chermesinum*. *Indonesian Journal of Chemistry, 17*(3), 360–364.

de Oliveira, P. R., Tasic, L., Rocco, S. A., & Rittner, R. (2006). Stereoelectronic and inductive effects on ^{1}H and ^{13}C NMR chemical shifts of some cis-1,3-disubstituted cyclohexanes. *Magnetic Resonance in Chemistry, 44*(8), 790–796.

El-Elimat, T., Raja, H. A., Figueroa, M., Al Sharie, A. H., Bunch, R. L., & Oberlies, N. H. (2021). Freshwater fungi as a source of chemical diversity: A review. *Journal of Natural Products, 84*(3), 898–916.

Fernandes, P. (2016). Fusidic acid: A bacterial elongation factor inhibitor for the oral treatment of acute and chronic staphylococcal infections. *Cold Spring Harbor Perspectives in Medicine, 6*(1), a025437.

File, T. M., Jr., Goldberg, L., Das, A., Sweeney, C., Saviski, J., Gelone, S. P., . . . Talbot, G. H. (2019). Efficacy and safety of intravenous-to-oral lefamulin, a pleuromutilin antibiotic, for the treatment of community-acquired bacterial pneumonia: The Phase III LEAP 1 trial. *Clinical Infectious Diseases, 69*(11), 1856–1867.

Grimblat, N., Zanardi, M. M., & Sarotti, A. M. (2015). Beyond DP4: An improved probability for the stereochemical assignment of isomeric compounds using quantum chemical calculations of NMR shifts. *The Journal of Organic Chemistry, 80*(24), 12526–12536. https://doi.org/10.1021/acs.joc.5b02396

Guo, Z., Liu, X., Wang, N., Mo, P., Shen, J., Liu, M., . . . Zhang, Z. (2023). Membrane component ergosterol builds a platform for promoting effector secretion and virulence in *Magnaporthe oryzae*. *New Phytologist, 237*(3), 930–943.

Han, B., Feinstein, T., Shi, Y., Chen, G., Yao, Y., Hu, C., . . . Cheng, Y. (2024). Plinabulin plus docetaxel versus docetaxel in patients with non–small-cell lung cancer after disease progression on platinum-based regimen (DUBLIN-3): A phase 3, international, multicentre, single-blind, parallel-group, randomised controlled trial. *The Lancet Respiratory Medicine, 12*(10), 775–786.

He, Y., Tian, J., Chen, X., Sun, W., Zhu, H., Li, Q., . . . Wang, J. (2016). Fungal naphtho-γ-pyrones: Potent antibiotics for drug-resistant microbial pathogens. *Scientific Reports, 6*, 24291.

Hiort, J., Maksimenka, K., Reichert, M., Perović-Ottstadt, S., Lin, W., Wray, V., . . . Proksch, P. (2004). New natural products from the sponge-derived fungus *Aspergillus niger*. *Journal of Natural Products, 67*(9), 1532–1543.

Hu, H., Guo, H., Li, E., Liu, X., Zhou, Y., & Che, Y. (2006). Decaspirones F–I, bioactive secondary metabolites from the saprophytic fungus *Helicoma viridis*. *Journal of Natural Products, 69*(12), 1672–1675.

Hu, Z., Ye, Y., & Zhang, Y. (2021). Large-scale culture as a complementary and practical method for discovering natural products with novel skeletons. *Natural Product Reports, 38*(10), 1775–1793.

Itazaki, H., Nagashima, K., Sugita, K., Yoshida, H., Kawamura, Y., Yasuda, Y., . . . Nakai, H. (1990). Solation and structural elucidation of new cyclotetrapeptides, trapoxins A and B, having detransformation activities as antitumor agents. *The Journal of Antibiotics, 43*(12), 1524–1532.

Itazaki, H., Nagashima, K., Sugita, K., Yoshida, H., Kawamura, Y., Yasuda, Y., . . . Nakai, H. (1991). Structure of a new cyclotetrapeptide trapoxin A. *Crystal Structure Communications, 47*(7), 1496–1499.

Jia, L.-C. (2020). A new benzofuran from *Penicillium oxalicum*, an endophytic fungus isolated from *Pseudostellaria heterophylla*. *Zhongcaoyao*, 5681–5686.

Kang, J., Qian, S., Zeng, X., Qian, Y., Lu, Y., Chen, L., . . . He, Z. (2022). *A long-chain fatty acid glycerol compound, Rubracin D: Preparation method and applications* [Chinese patent]. China National Intellectual Property Administration.

Kang, J., Qian, S., Zeng, X., Qian, Y, Lu, Y., Chen, L., . . . He, Z. (2023). *A long-chain fatty acid glycerol compound, Rubracin E: Preparation method and applications* [Chinese patent]. China National Intellectual Property Administration.

Keller, N. P. (2019). Fungal secondary metabolism: Regulation, function and drug discovery. *Nature Reviews Microbiology, 17*(3), 167–180.

Kim, M. J., Kim, D.-C., Kwon, J., Ryu, S. M., Kwon, H., Guo, Y., . . . Lee, D. (2020). Anti-inflammatory metabolites from *Chaetomium nigricolor*. *Journal of Natural Products, 83*(4), 881–887.

Kokubun, T., Veitch, N. C., Bridge, P. D., & Simmonds, M. S. (2003). Dihydroisocoumarins and a tetralone from *Cytospora eucalypticola*. *Phytochemistry, 62*(5), 779–782.

Küpeli Akkol, E., Genç, Y., Karpuz, B., Sobarzo-Sánchez, E., & Capasso, R. (2020). Coumarins and coumarin-related compounds in pharmacotherapy of cancer. *Cancers*, *12*(7), 1959.

Lai, D., Wang, A., Cao, Y., Zhou, K., Mao, Z., Dong, X., . . . Peng, Y. (2016). Bioactive dibenzo-α-pyrone derivatives from the endophytic fungus *Rhizopycnis vagum* Nitaf22. *Journal of Natural Products, 79*(8), 2022–2031.

Lall, N., Weiganand, O., Hussein, A., & Meyer, J. (2006). Antifungal activity of naphthoquinones and triterpenes isolated from the root bark of *Euclea natalensis*. *South African Journal of Botany, 72*(4), 579–583.

Lee, S. M., Kim, D. S., Lee, K.-S., Lee, C.-K., & Lee, D. (2013). Antibiotic properties of *Helicosporium* sp. KCTC 0635BP to *Rhizoctonia solani* AG2-2 IV. *Weed and Turfgrass Science, 2*(2), 202-206. https://doi.org/10.5660/WTS.2013.2.2.202

Li, H.-L., Li, X.-M., Mándi, A., Antus, S., Li, X., Zhang, P., . . . Wang, B.-G. (2017). Characterization of cladosporols from the marine algal-derived endophytic fungus *Cladosporium cladosporioides* EN-399 and configurational revision of previously reported derivatives. *Journal of Organic Chemistry, 82*(19), 9946–9954.

Li, L., Huang, J., Feng, L., Xu, L., Lin, H., Liu, K., . . . Wang, R. (2024). Altechromone A ameliorates inflammatory bowel disease by inhibiting NF-κB and NLRP3 pathways. *Marine Drugs, 22*(9), 410.

Li, X., Zheng, W., Han, L., He, Z.-J., & Kang, J.-C. (2024). A new aglycone derivative from the saprophytic fungus *Tubeufia rubra*. *Natural Product Research*, 1–7. https://doi.org/10.1080/14786419.2024.2424391

Liu, Y., Wang, W., & Miao, J. (2021). New antiproliferative dibenzo-α-pyrone from whole plants of *Centella asiatica*. *Natural Product Communications, 16*(3), 1934578X211003019.

Liu, T.-T., Liao, X.-J., Xu, S.-H., & Zhao, B.-X. (2021). Solieritide A, a new polyketide from the red alga *Solieria* sp. *Natural Product Research, 35*(21), 3780–3786.

Lu, C. H., Liu, S. S., Wang, J. Y., Wang, M. Z., & Shen, Y. M. (2014). Characterization of eight new secondary metabolites from the mutant strain G-444 of *Tubercularia* sp. TF5. *Helvetica Chimica Acta, 97*(3), 334–344.

Lu, Y., & Kang, J. (2020). Advances in helicosporous hyphomycetes research [In Chinese]. *Mycosystema, 18*(4), 304–314.

Lu, Y.-Z., Liu, J.-K., Hyde, K. D., Jeewon, R., Kang, J.-C., Fan, C., . . . Lin, C.-G. (2018). A taxonomic reassessment of Tubeufiales based on multi-locus phylogeny and morphology. *Fungal Diversity, 92*(1), 131–344.

Lu, Y.-Z., Ma, J., Xiao, X.-J., Zhang, L.-J., Xiao, Y.-P., & Kang, J.-C. (2022). Four new species and three new records of helicosporous hyphomycetes from China and their multi-gene phylogenies. *Frontiers in Microbiology, 13*, 1053849.

Lu, Y.-Z., Boonmee, S., Bhat, D. J., Hyde, K. D., & Kang, J.-C. (2017). *Helicosporium luteosporum* sp. nov. and *Acanthohelicospora aurea* from terrestrial habitats. *Phytotaxa, 319*(3), 241–253.

Lu, Y.-Z., Boonmee, S., Liu, J.-K., Hyde, K. D., McKenzie, E. H., Eungwanichayapant, P. D., . . . Kang, J.-C. (2018). Neohelicosporium gen. nov. and five new species of helicosporous hyphomycetes from aquatic habitats. *Mycological Progress, 17*(5), 631–646. https://doi.org/10.1007/s11557-017-1366-1

Lum, K. Y., Taki, A. C., Gasser, R. B., Tietjen, I., Ekins, M. G., & Davis, R. A. (2020). Comatulins A–E, taurine-conjugated anthraquinones from the Australian crinoid *Comatula rotalaria*. *Journal of Natural Products, 83*(6), 1971–1979.

Luo, Z.-L., Bhat, D. J., Jeewon, R., Boonmee, S., Bao, D.-F., Zhao, Y. C., . . . Hyde, K. D. (2017). Molecular phylogeny and morphological characterization of asexual fungi (Tubeufiaceae) from freshwater habitats in Yunnan, China. *Cryptogamie, Mycologie, 38*(1), 27–53. https://doi.org/10.7872/crym/v38.iss1.2017.27

Lyu, H.-N., Liu, H.-W., Keller, N. P., & Yin, W.-B. (2020). Harnessing diverse transcriptional regulators for natural product discovery in fungi. *Natural Product Reports, 37*(1), 6–16.

Ma, J., Hyde, K. D., Tibpromma, S., Gomdola, D., Liu, N.-G., Norphanphoun, C., . . . Lu, Y. Z. (2024). Taxonomy and systematics of lignicolous helicosporous hyphomycetes. *Fungal Diversity, 129*(1), 365–653. https://doi.org/10.1007/s13225-024-00544-9

Ma, J., Xiao, X.-J., Liu, N.-G., Boonmee, S., Xiao, Y.-P., … Lu, Y.-Z. (2023). *Pseudotubeufia* gen. nov. and two new species in Tubeufiaceae. *Journal of Fungi, 9*(7), 742.

Ma, J., Zhang, L.-J., Boonmee, S., Xiao, X.-J., Liu, N.-G., . . . Lu, Y.-Z. (2023). Three new species and one new record of *Tubeufia* from southern China. *MycoKeys, 99*, 87.

Magdy, W., Abdel-Motaal, F. F., El-Zayat, S. A., El-Sayed, M. A., & Helaly, S. E. (2017). Nigragillin, Nigerazine B and five naphtho-γ-pyrones from *Aspergillus japonicus*. *Natural Products Journal, 7*(3), 216–223.

Mao, Z., Lai, D., Liu, X., Fu, X., Meng, J., Wang, A., . . . Liu, Y. (2017). Dibenzo-α-pyrones: A new class of larvicidal metabolites against Aedes aegypti from the endophytic fungus Hyalodendriella sp. Ponipodef12. *Pest Management Science, 73*(7), 1478–1485. https://doi.org/10.1002/ps.4481

Mao, Z., Sun, W., Fu, L., Luo, H., Lai, D., & Zhou, L. (2014). Natural dibenzo-α-pyrones and their bioactivities. *Molecules, 19*(4), 5088–5108.

Meena, H., Hnamte, S., & Siddhardha, B. (2019). Secondary metabolites from endophytic fungi. In B. P. Singh (Ed.), *Advances in endophytic fungal research* (pp. 145–169). Springer.

Meng, X., Mao, Z., Lou, J., Xu, L., Zhong, L., Peng, Y., . . . Wang, M. (2012). Benzopyranones from endophytic *Hyalodendriella* sp. Ponipodef12. *Molecules, 17*(10), 11303–11314. https://doi.org/10.3390/molecules171011303

Mudur, S. V., Swenson, D. C., Gloer, J. B., Campbell, J., & Shearer, C. A. (2006). Heliconols A–C from *Helicodendron giganteum*. *Organic Letters, 8*(15), 3191–3194.

Nakanishi, W., Hayashi, S., & Matsuzaki, K. (2025). Origin of 13C NMR chemical shifts elucidated based on molecular orbital theory: Paramagnetic contributions for pre-α, α, β, α-X, β-X and ipso-X effects. *RSC Advances, 15*(3), 1924–1940.

Nakai, H., Nagashima, K., & Itazaki, H. (1991). Structure of a new cyclotetrapeptide trapoxin A. *Crystal Structure Communications, 47*(7), 1496–1499.

Nasini, G., Arnone, A., Assante, G., Bava, A., Moricca, S., & Ragazzi, A. (2004). Secondary mould metabolites of *Cladosporium tenuissimum*, a hyperparasite of rust fungi. *Phytochemistry, 65*(14), 2107–2111.

Newman, D. J., & Cragg, G. M. (2020). Natural products as sources of new drugs from 1981 to 2019. *Journal of Natural Products, 83*(3), 770–803.

Nozawa, K., Nakajima, S., Kawai, K.-I., Udagawa, S.-I., & Miyaji, M. (1994). Bicoumarins from ascostromata of *Petromyces alliaceus*. *Phytochemistry, 35*(4), 1049–1051.

Ohtsu, Y., Sasamura, H., Shibata, T., Nakajima, H., Hino, M., & Fujii, T. (2003). Novel gluconeogenesis inhibitors FR225659 and related compounds from *Helicomyces* sp. No.19353 II: Biological profiles. *The Journal of Antibiotics, 56*(8), 689–693.

Pavan Kumar, P., Siva, B., Anand, A., Tiwari, A. K., Vekata Rao, C., Boustie, J., . . . Suresh Babu, K. (2020). Isolation, semi-synthesis, free-radicals scavenging, and advanced glycation end products formation inhibitory constituents from *Parmotrema tinctorum*. *Journal of Asian Natural Products Research, 22*(10), 976–988.

Poindessous, V., Koeppel, F., Raymond, E., Comisso, M., Waters, S. J., & Larsen, A. K. (2003). Marked activity of irofulven toward human carcinoma cells: Comparison with cisplatin and ecteinascidin. *Clinical Cancer Research, 9*(7), 2817–2825.

Pracht, P., Bohle, F., & Grimme, S. (2020). Automated exploration of the low-energy chemical space with fast quantum chemical methods. *Physical Chemistry Chemical Physics, 22*(14), 7169–7192.

Qian, S., Zeng, X., Qian, Y., Lu, Y., He, Z., & Kang, J. (2023). A saprophytic fungus *Tubeufia rubra* produces novel rubracin D and E reversing multidrug resistance in cancer cells. *Journal of Fungi, 9*(3), 309.

Quinn, R. (2013). Rethinking antibiotic research and development: World War II and the penicillin collaborative. *American Journal of Public Health, 103*(3), 426–434.

Rangsinth, P., Sharika, R., Pattarachotanant, N., Duangjan, C., Wongwan, C., Sillapachaiyaporn, C., . . . Tencomnao, T. (2023). Potential beneficial effects and pharmacological properties of ergosterol, a common bioactive compound in edible mushrooms. *Foods, 12*(13), 2529.

Rapuano, R., Ziccardi, P., Cioffi, V., Dallavalle, S., Moricca, S., & Lupo, A. (2021). Cladosporols A and B, two natural peroxisome proliferator-activated receptor gamma (PPARγ) agonists, inhibit adipogenesis in 3T3-L1 preadipocytes and cause a conditioned-culture-medium-dependent arrest of HT-29 cell proliferation. *Biochimica et Biophysica Acta (BBA) – General Subjects, 1865*(11), 129973.

Rong, X., Ma, L., Liu, W., & Liu, D. (2024). A new naphthoquinone compound from *Penicillium resedanum*. *Chinese Journal of Marine Drugs, 43*(1), 10–16.

Sakagami, Y., Sano, A., Hara, O., Mikawa, T., & Marumo, S. (1995). Cladosporol, a β-1,3-glucan biosynthesis inhibitor isolated from the fungus *Cladosporium cladosporioides*. *Tetrahedron Letters, 36*(9), 1469–1472.

Shaaban, M., Shaaban, K. A., & Abdel-Aziz, M. S. (2012). Seven naphtho-γ-pyrones from the marine-derived fungus *Alternaria alternata*: Structure elucidation and biological properties. *Organic and Medicinal Chemistry Letters, 2*(1), 6.

Shan, T., Tian, J., Wang, X., Mou, Y., Mao, Z., Lai, D., . . . Wang, M. (2014). Bioactive spirobisnaphthalenes from the endophytic fungus *Berkleasmium* sp. *Journal of Natural Products, 77*(10), 2151–2160.

Shao, L., Marin-Felix, Y., Surup, F., Stchigel, A. M., & Stadler, M. (2020). Seven new cytotoxic and antimicrobial xanthoquinodins from *Jugulospora vestita*. *Journal of Fungi, 6*(4), 188.

Sung, H., Ferlay, J., Siegel, R. L., Laversanne, M., Soerjomataram, I., Jemal, A., . . . Bray, F. (2021). Global cancer statistics 2020: GLOBOCAN estimates of incidence and mortality worldwide for 36 cancers in 185 countries. *CA: A Cancer Journal for Clinicians, 71*(3), 209–249.

Talapatra, S. K., Karmacharya, B., De, S. C., & Talapatra, B. (1988). (−)-Regiolone, an α-tetralone from *Juglans regia*: Structure, stereochemistry and conformation. *Phytochemistry, 27*(12), 3929–3932.

Tan, M. A., Züger, P. P., & Roggo, S. (2019). Total synthesis of diaportheone A. *Tetrahedron Letters, 60*(1), 52–54.

Tang, J., Xu, R., Zhao, X., Wang, Y.-T., Tan, H.-Y., Shan, J.-J., . . . Cui, C.-B. (2023). Chemical constituents and their biological activities of *Lanmaoa asiatica*. *Mycosystema, 42*(6), 1345-1359. https://doi.org/10.13346/j.mycosystema.220246

Tang, K. W. K., Millar, B. C., & Moore, J. E. (2023). Antimicrobial resistance (AMR). *British Journal of Biomedical Science, 80*, 11387.

Tian, J., Fu, L., Zhang, Z., Dong, X., Xu, D., Mao, Z., . . . Zhou, L. (2017). Dibenzo-α-pyrones from the endophytic fungus *Alternaria* sp. Samif01: Isolation, structure elucidation, and their antibacterial and antioxidant activities. *Natural Product Research, 31*(4), 387–396.

Tian, J., Liu, X. C., Liu, Z. L., Lai, D., & Zhou, L. (2016). Larvicidal spirobisnaphthalenes from the endophytic fungus *Berkleasmium* sp. against *Aedes albopictus*. *Pest Management Science, 72*(5), 961–965.

Tian, X., Karunarathna, S. C., Xu, R., Lu, Y., Suwannarach, N., Mapook, A., . . . Tibpromma, S. (2022). Three new species, two new records and four new collections of Tubeufiaceae from Thailand and China. *Journal of Fungi, 8*(2), 206.

Tian, Y.-Q., Lin, X.-P., Liu, J., Kaliyaperumal, K., Ai, W., Ju, Z.-R., . . . Liu, Y. (2015). Ascomycotin A, a new citromycetin analogue produced by *Ascomycota* sp. Ind19F07 isolated from deep sea sediment. *Natural Product Research, 29*(9), 820–826.

Tsui, C., & Berbee, M. (2006). Phylogenetic relationships and convergence of helicosporous fungi inferred from ribosomal DNA sequences. *Molecular Phylogenetics and Evolution, 39*(3), 587–597.

Vijayalakshmi, S., Karthik, K., Crossia, A. W. F., Subashini, G., Bhuvaneswari, S., Panneerselvam, A., . . . Park, M.-K. (2020). Fungal secondary metabolites: A potential source of anticancer compounds. In J. Singh & P. Gehlot (Eds.), *New and future developments in microbial biotechnology and bioengineering* (pp. 81–93). Elsevier.

Wang, F., Tan, J. W., & Liu, J. K. (2004). Vibratilicin: A novel compound from the basidiomycete *Cortinarius vibratilis*. *Helvetica Chimica Acta, 87*(7), 1912–1915.

Wang, G., Yin, Z., Wang, S., Yuan, Y., Chen, Y., & Kang, W. (2022). Diversified polyketides with anti-inflammatory activities from mangrove endophytic fungus *Daldinia eschscholtzii* KBJYZ-1. *Frontiers in Microbiology, 13*, 900227.

Wang, K., Jiang, S., Pu, T., Fan, L., Su, F., & Ye, M. (2019). Antifungal activity of phenolic monoterpenes and structure-related compounds against plant pathogenic fungi. *Natural Product Research, 33*(10), 1423–1430.

Wang, L., Zong, S., & Zhu, M. (2023). Chemical and biological diversity of secondary metabolites from freshwater fungi. *Chinese Journal of Biochemistry and Molecular Biology, 39*, 385–399.

Weigenand, O., Hussein, A. A., Lall, N., & Meyer, J. J. (2004). Antibacterial activity of naphthoquinones and triterpenoids from *Euclea natalensis* root bark. *Journal of Natural Products, 67*(11), 1936–1938.

Wu, J.-S., Shi, X.-H., Zhang, Y.-H., Yu, J.-Y., Fu, X.-M., Li, X., . . . Wang, C.-Y. (2019). Co-cultivation with 5-azacytidine induced new metabolites from the zoanthid-derived fungus *Cochliobolus lunatus*. *Frontiers in Chemistry, 7*, 763.

Xiao, Y., Liang, W., Zhang, Z., Wang, Y., Zhang, S., Liu, J., . . . Zhu, D. (2022). Polyketide derivatives from the endophytic fungus *Phaeosphaeria* sp. LF5 isolated from *Huperzia serrata* and their acetylcholinesterase inhibitory activities. *Journal of Fungi*, *8*(3), 232.

Xiao, X.-J., Ma, J., Zhang, L.-J., Liu, N.-G., Xiao, Y.-P., Tian, X.-G., . . . Lu, Y.-Z. (2023). Additions to the genus *Helicosporium* (Tubeufiaceae, Tubeufiales) from China with an identification key for *Helicosporium* taxa. *Journal of Fungi*, *9*(7), 775.

Xiao, J., Zhang, Q., Gao, Y.-Q., Shi, X.-W., & Gao, J.-M. (2014). Antifungal and antibacterial metabolites from an endophytic *Aspergillus* sp. associated with *Melia azedarach*. *Natural Product Research*, *28*(17), 1388–1392.

Xiao, J., Zhang, Q., Gao, Y.-Q., Tang, J.-J., Zhang, A.-L., & Gao, J.-M. (2014). Secondary metabolites from the endophytic *Botryosphaeria dothidea* of *Melia azedarach* and their antifungal, antibacterial, antioxidant, and cytotoxic activities. *Journal of Agricultural and Food Chemistry*, *62*(16), 3584–3590.

Xu, X., Zhao, S., Wei, J., Fang, N., Yin, L., & Sun, J. (2012). Porric acid D from marine-derived fungus *Alternaria* sp. isolated from Bohai Sea. *Chemistry of Natural Compounds*, *47*(6), 893–895.

Yamamoto, K., Hatano, H., Arai, M., Shiomi, K., Tomoda, H., & Ōmura, S. (2003). Structure elucidation of new monordens produced by *Humicola* sp. FO-2942. *The Journal of Antibiotics*, *56*(6), 533–538.

Yamazaki, H., Yagi, A., Akaishi, M., Kirikoshi, R., Takahashi, O., Abe, T., . . . Namikoshi, M. (2018). Halogenated cladosporols produced by sodium-halide-supplemented fermentation of the plant-associated fungus *Cladosporium* sp. TMPU1621. *Tetrahedron Letters*, *59*(20), 1913–1915.

Yamazaki, H., Rotinsulu, H., Kaneko, T., Murakami, K., Fujiwara, H., Ukai, K., . . . Namikoshi, M. (2012). A new dibenz[b,e]oxepine derivative from the marine-derived fungus *Beauveria bassiana* TPU942. *Marine Drugs*, *10*(12), 2691–2697.

Yurchenko, A., Smetanina, O., Kalinovsky, A., Pivkin, M., Dmitrenok, P., & Kuznetsova, T. (2010). A new meroterpenoid from the marine fungus *Aspergillus versicolor*. *Russian Chemical Bulletin*, *59*(4), 852–856.

Yamamoto, K., Hatano, H., Arai, M., Shiomi, K., Tomoda, H., & Ōmura, S. (2003). Structure elucidation of new monordens produced by *Humicola* sp. FO-2942. *The Journal of Antibiotics*, *56*, 533–538.

Zeng, X., Qian, S., Lu, Y., Li, Y., Chen, L., Qian, Y., . . . Kang, J. (2022). A novel nitrogen-containing glyceride from fungal saprobe *Tubeufia rubra* reverses MDR of tumor cell lines to doxorubicin. *Records of Natural Products*, *16*(6), 622–632.

Zeng, X., Qian, S., Lu, Y., Li, Y., Chen, L., Qian, Y., . . . Kang, J. (2022). A novel nitrogen-containing glyceride from fungal saprobe *Tubeufia rubra* reverses MDR of tumor cell lines to doxorubicin. *Records of Natural Products*, *16*(6), 622-632.

Zenkoh, T., Ohtsu, Y., Yoshimura, S., Shigematsu, N., Takase, S., & Hino, M. (2004). The novel gluconeogenesis inhibitors FR225659 and FR225656 from *Helicomyces* sp. No. 19353. Part 3. Structure determination. *ChemInform*, *35*(5), e200402142.

Zhang, F., Zhou, L., Kong, F., Ma, Q., Xie, Q., Li, J., . . . Zhao, Y. (2020). Altertoxins with quorum-sensing inhibitory activities from the marine-derived fungus *Cladosporium* sp. KFD33. *Marine Drugs*, *18*(1), 67.

Zhang, H.-W., Huang, W.-Y., Chen, J.-R., Yan, W.-Z., Xie, D.-Q., & Tan, R.-X. (2008). Cephalosol: An antimicrobial metabolite with an unprecedented skeleton from endophytic *Cephalosporium acremonium* IFB-E007. *Chemistry – A European Journal*, *14*(34), 10670–10674.

Zhang, J., Zhang, B., Cai, L., & Liu, L. (2022). New dibenzo-α-pyrone derivatives with α-glucosidase inhibitory activities from the marine-derived fungus *Alternaria alternata*. *Marine Drugs*, *20*(12), 778.

Zhang, L.-J., Yang, M.-F., Ma, J., Xiao, X.-J., Ma, X.-Y., Zheng, D.-G., . . . Mapook, A. (2023). Neogrisphenol A, a potential ovarian cancer inhibitor from a new record fungus *Neohelicosporium griseum*. *Metabolites*, *13*(3), 435.

Zhang, Y., Griffith, E. C., Sage, J., Jacks, T., & Liu, J. O. (2000). Cell cycle inhibition by the anti-angiogenic agent TNP-470 is mediated by p53 and p21WAF1/CIP1. *Proceedings of the National Academy of Sciences*, *97*(12), 6427–6432.

Zhao, J., Fan, X., Zou, X., Yang, P., Tang, S., Li, M., . . . Ding, J. (2022). Chemical constituents and antioxidant activity of solid-state fermentation products of the soil fungus *Aspergillus fumigatus*. *Natural Product Research and Development*, *34*(1), 70.

Zhao, S., Tian, K., Li, Y., Ji, W., Liu, F., Khan, B., . . . Ye, Y. (2020). Enantiomeric dibenzo-α-pyrone derivatives from *Alternaria alternata* ZHJG5 and their potential as agrochemicals. *Journal of Agricultural and Food Chemistry*, *68*(51), 15115–15122.

Zhao, T., Ma, C., & Zhu, G. (2021). Chemical composition and biological activities of essential oils from the leaves, stems, and roots of *Kadsura coccinea*. *Molecules*, *26*(20), 6259.

Zheng, C.-J., Bai, M., Tang, D.-Q., Zhang, F., Wang, H.-Y., & Chen, G.-Y. (2019). Two new secondary metabolites from a mangrove-derived fungus *Cladosporium* sp. JS1-2. *The Journal of Antibiotics*, *72*(10), 779–782.

Zheng, W. (2024). Antitumor substances produced by two *Amphisphaeriaceae* fungi and their mechanisms of action (Doctoral dissertation, Guizhou University). (in Chinese)

Zheng, W., Han, L., He, Z.-J., & Kang, J.-C. (2023). New spirostane from a fungus *Neohelicomyces hyalosporus* and its bioactivity. *Chemistry & Biodiversity*, *20*(5), e202300313.

Zheng, W., Han, L., He, Z.-J., & Kang, J.-C. (2024a). A new alkaloid derivative from the saprophytic fungus *Neohelicomyces hyalosporus* PF11-1. *Natural Product Research*, *38*(13), 2215–2219.

Zheng, W., Han, L., He, Z.-J., & Kang, J.-C. (2024b). Novel drimane-type sesquiterpenoids and nucleosides from *Helicoma septoconstrictum* suppress the growth of ovarian cancer cells. *Bioorganic Chemistry*, *145*, 107214.

Zhou, M., Lin, M., Qi, X., Peng, S., Xiao, J., Gao, C., . . . Luo, X. (2024). Secondary metabolites of coral-associated fungus *Alternaria* sp. GXIMD 02516 from Weizhou Island. *Chinese Herbal Medicines*, *55*(21), 7208–7216.

Zhou, X., Fang, W., Tan, S., Lin, X., Xun, T., Yang, B., . . . Liu, Y. (2016). Aspernigrins with anti-HIV-1 activities from the marine-derived fungus *Aspergillus niger* SCSIO Jcsw6F30. *Bioorganic & Medicinal Chemistry Letters*, *26*(2), 361–365.

Zhuang, Y.-B., Yin, H., Zhang, X.-W., Zhou, W., & Liu, T. (2015). Three new xanthones from the fungus *Penicillium* sp. NH-7-1. *Helvetica Chimica Acta*, *98*(5), 699–703.

APPENDIX A

COMPOUND STRUCTURE CHARACTERIZATION SPECTRA

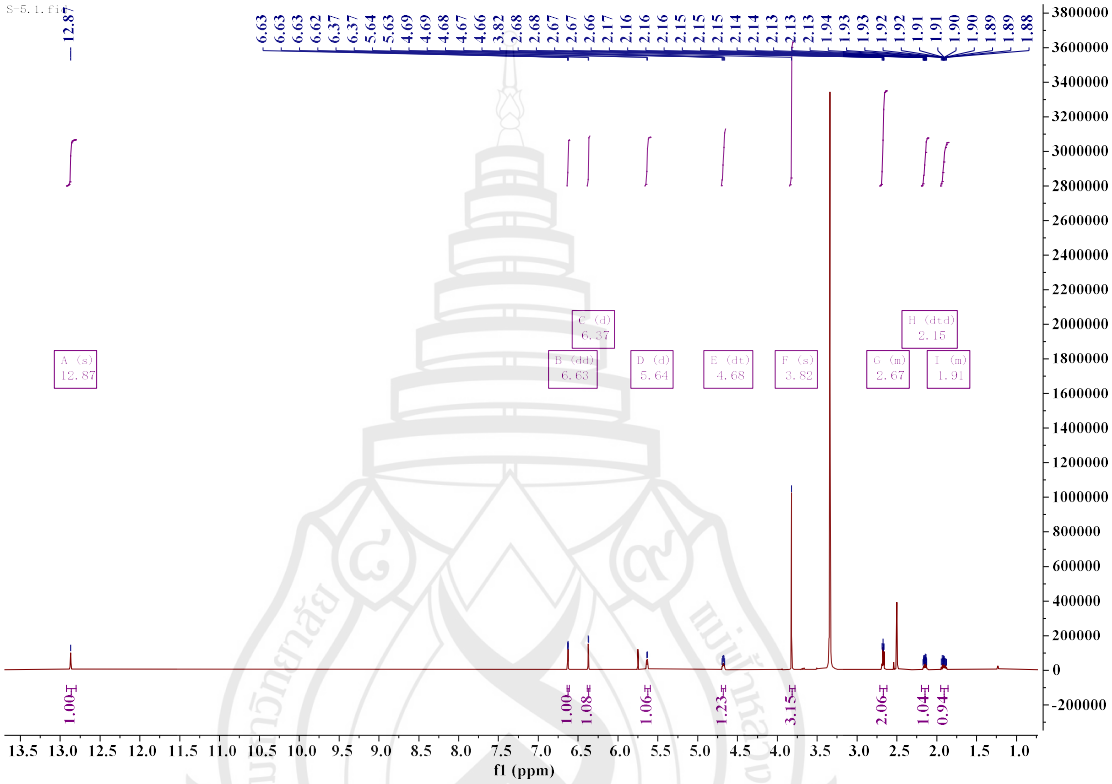

Figure A1 ^{1}H NMR spectrum of compound **C1** (600 MHz, DMSO)

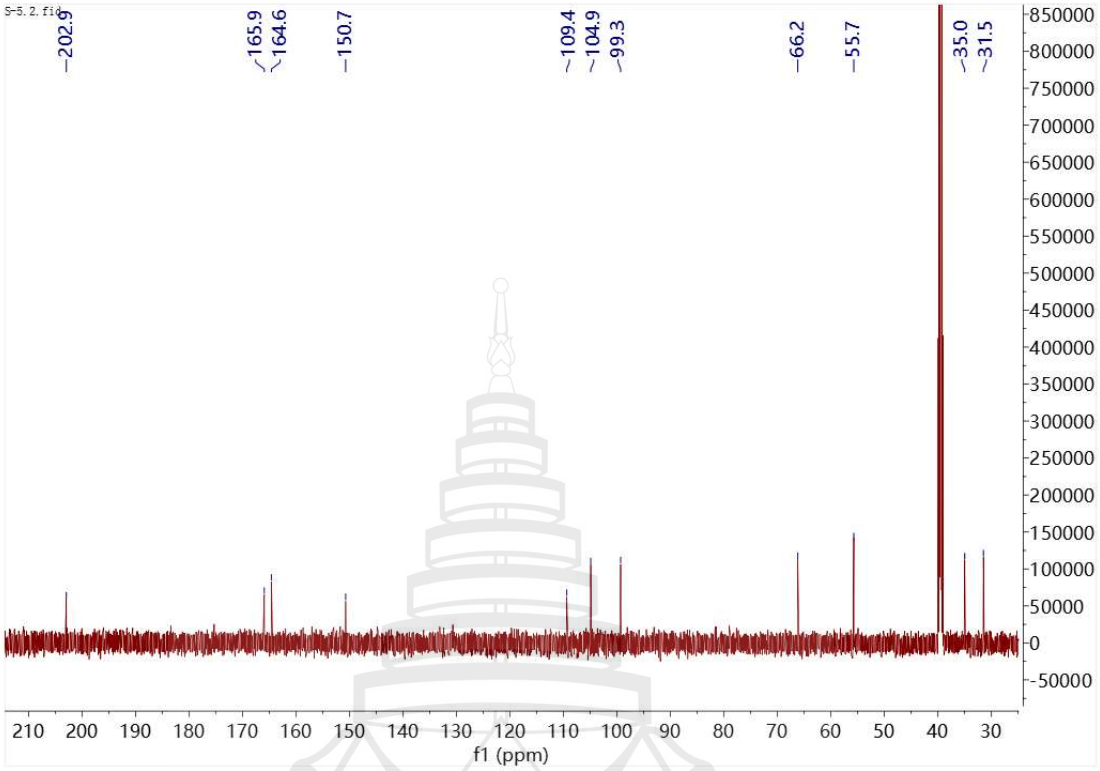

Figure A2 ^{13}C NMR spectrum of compound **C1** (150 MHz, DMSO)

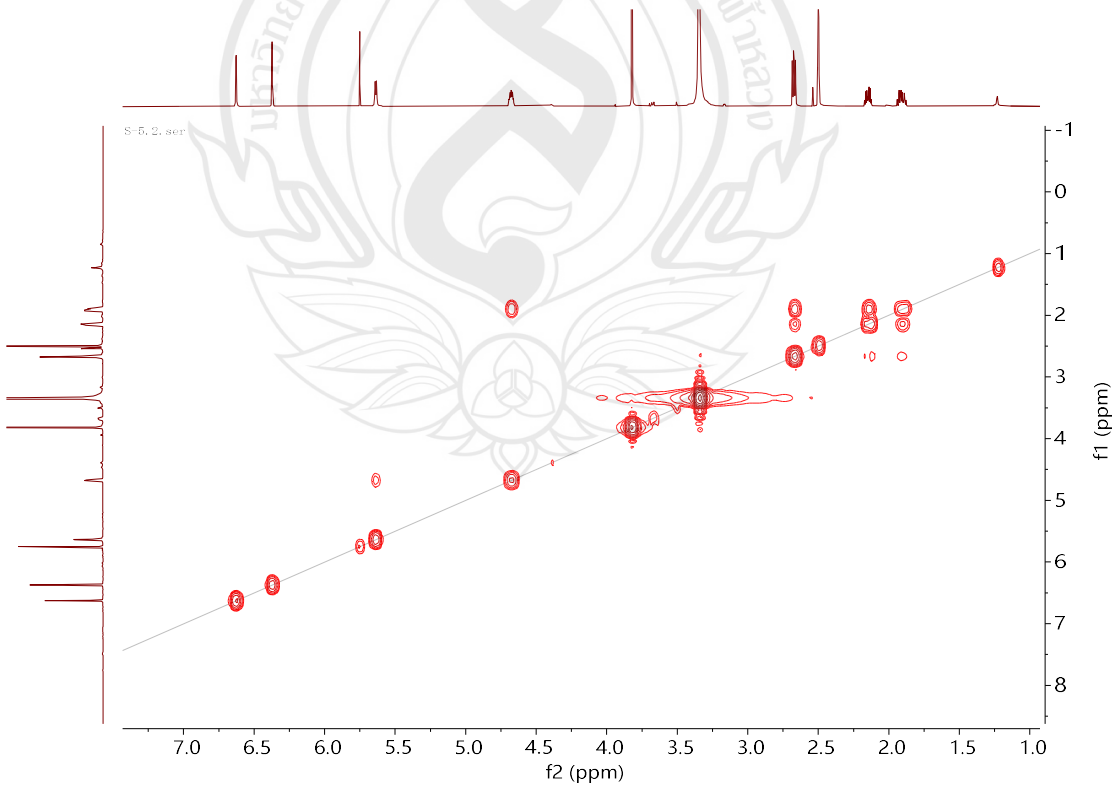

Figure A3 ^{1}H-^{1}H COSY spectrum of compound **C1** (600 MHz, DMSO)

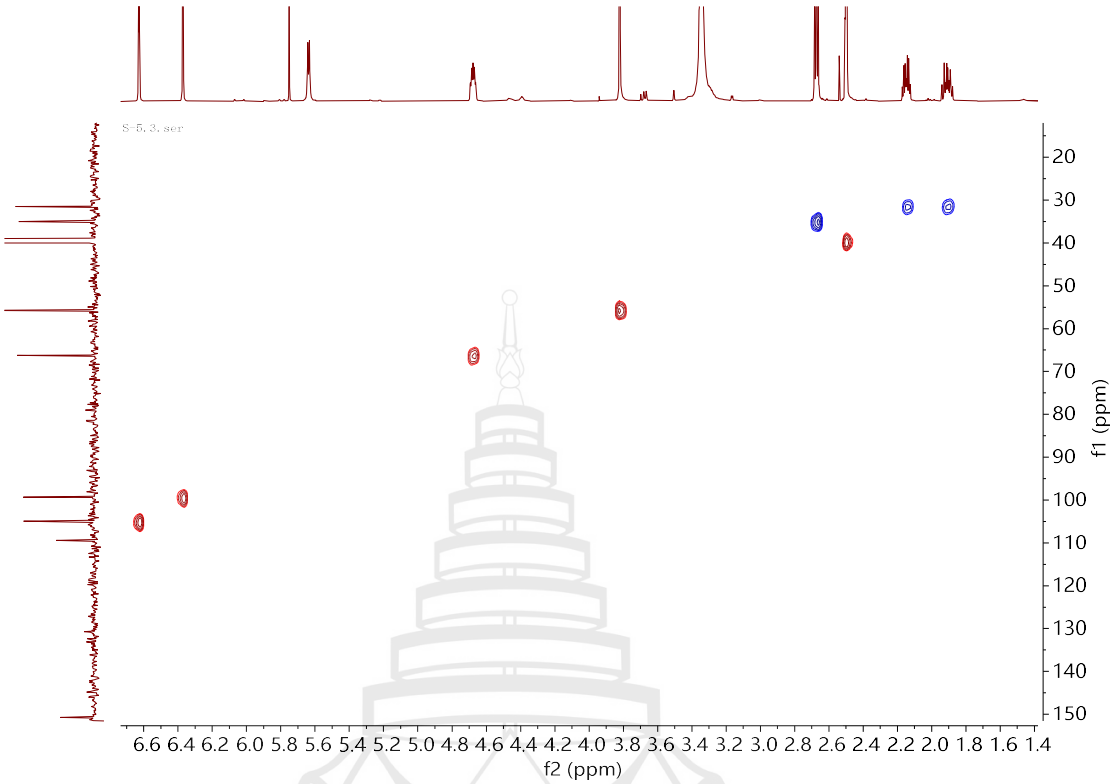

Figure A4 HSQC spectrum of compound **C1** (150 MHz, DMSO)

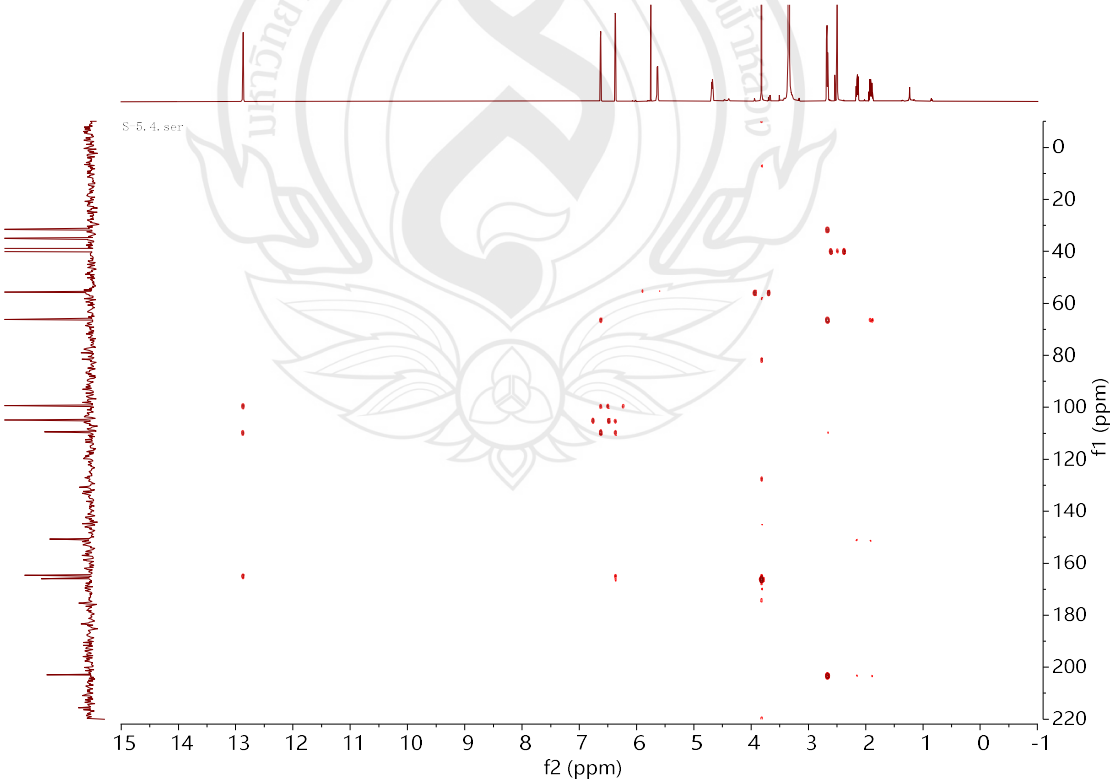

Figure A5 HMBC spectrum of compound **C1** (150 MHz, DMSO)

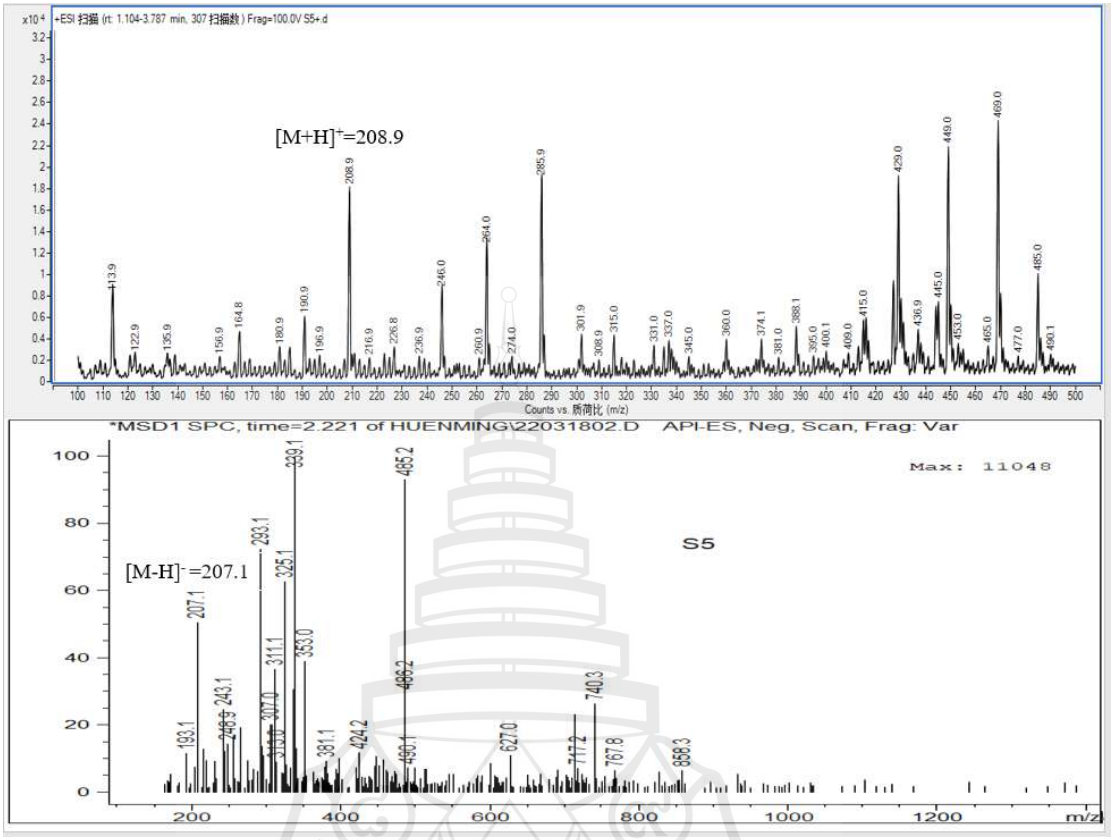

Figure A6 ESIMS of compound **C1**

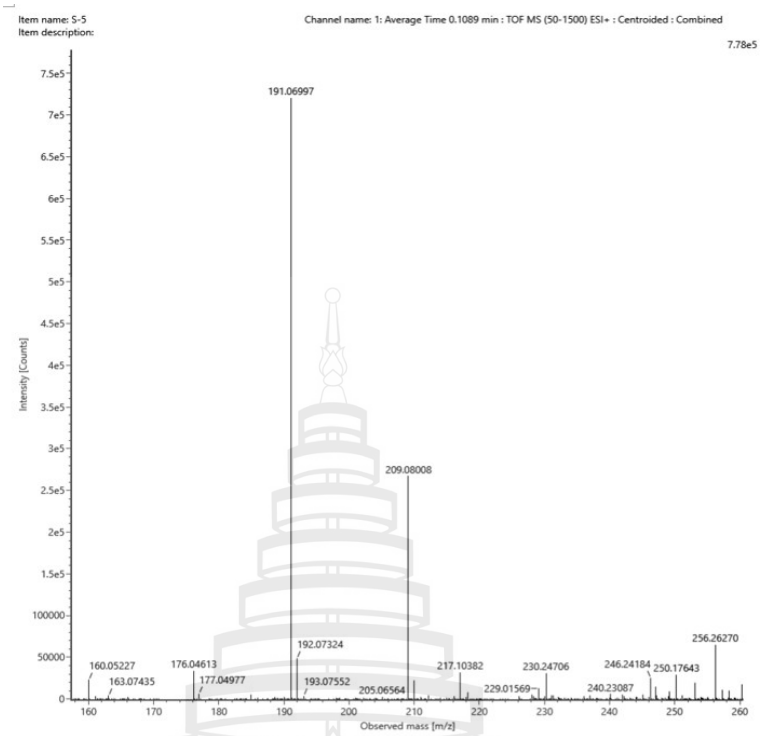

Composition	i-FIT Confidence (%)	Predicted m/z	m/z error (PPM)
$C_{11}H_{12}O_4+H$	100.000000	209.080835	-3.630095

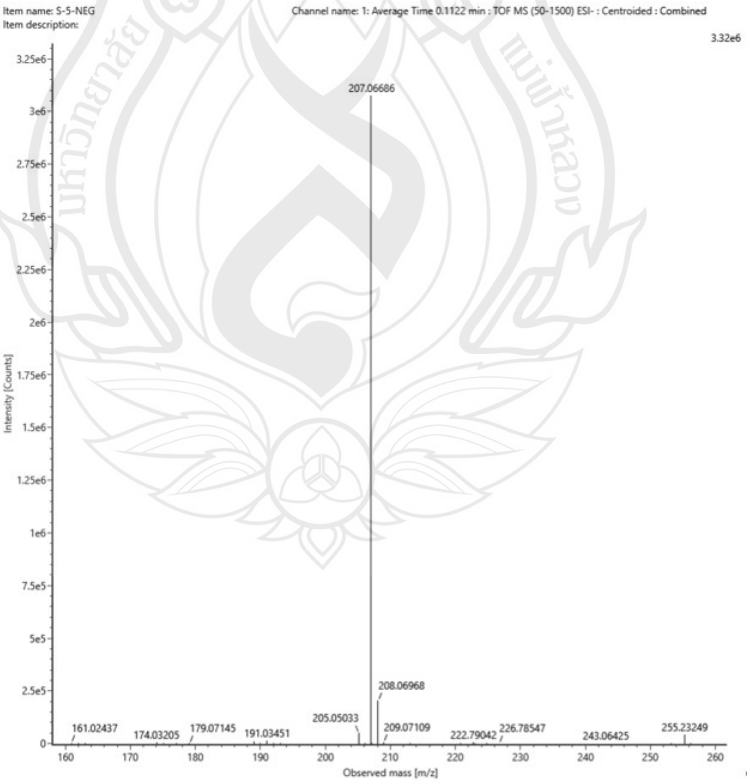

Composition	i-FIT Confidence (%)	Predicted m/z	m/z error (PPM)
$C_{11}H_{12}O_4-H$	100.000000	207.066282	2.775837

Figure A7 HR-ESIMS of compound **C1**

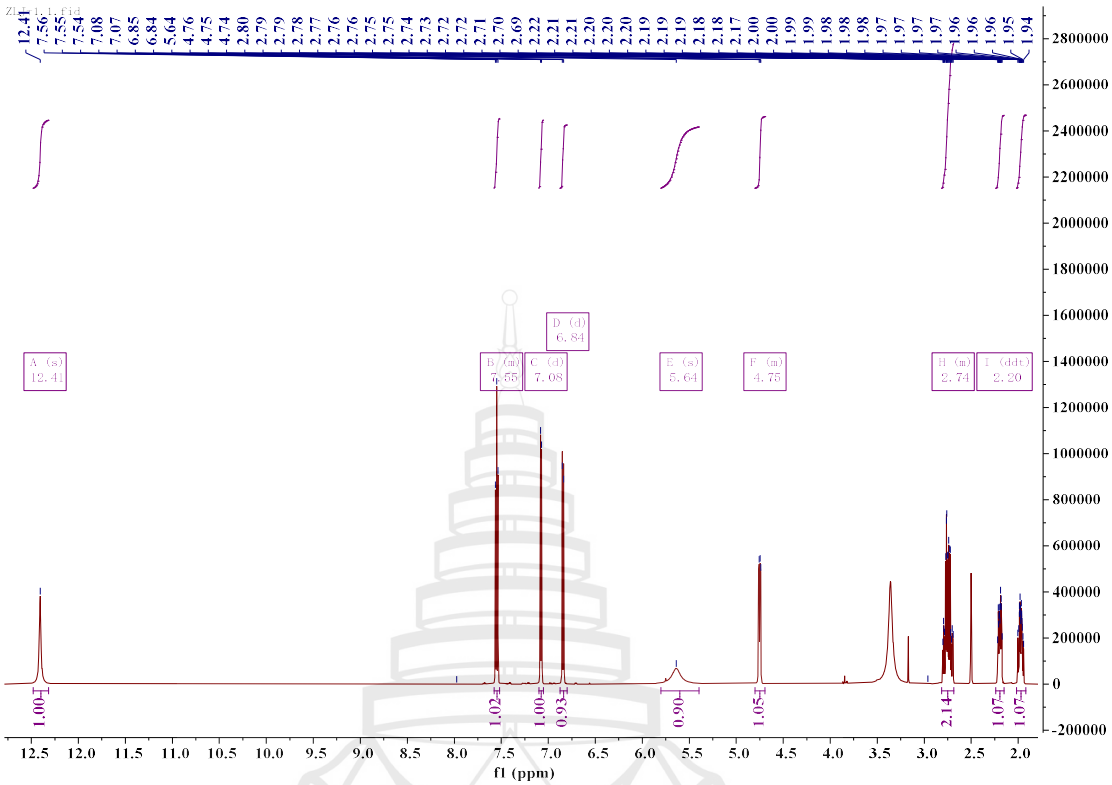

Figure A8 ^{1}H NMR spectrum of compound **C2** (600 MHz, DMSO)

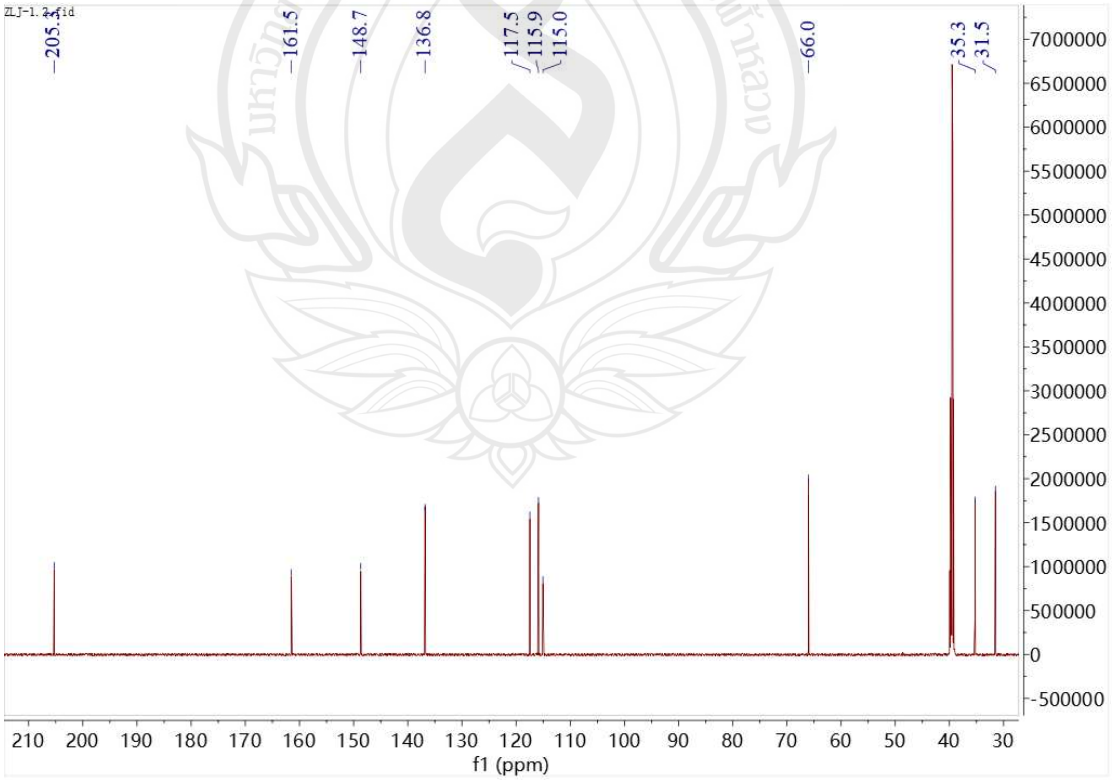

Figure A9 ^{13}C NMR spectrum of compound **C2** (150 MHz, DMSO)

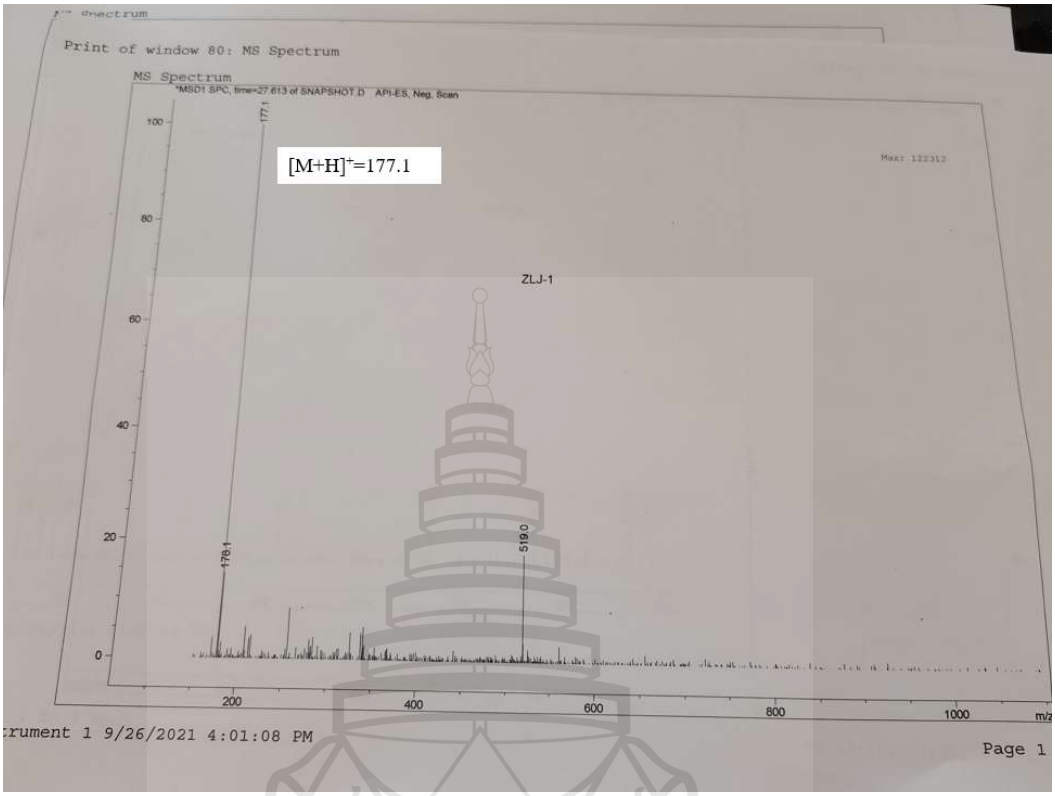

Figure A10 ESIMS of compound **C2**

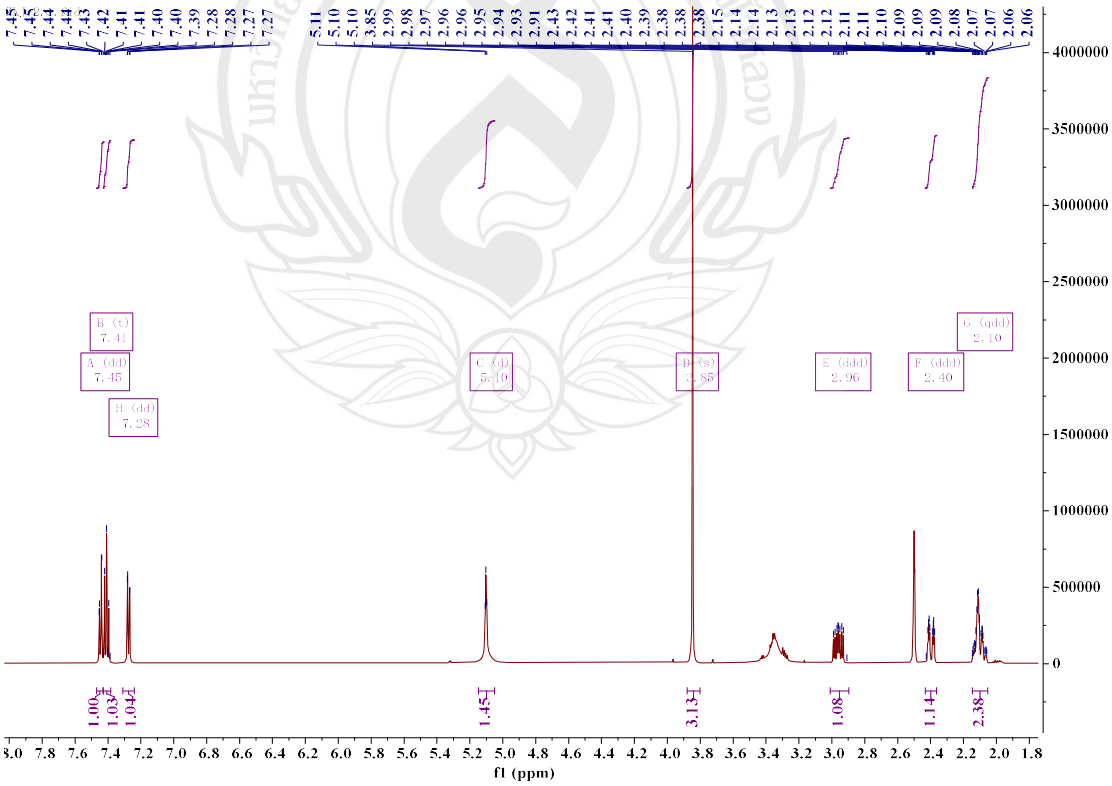

Figure A11 ^{1}H NMR spectrum of compound **C3** (600 MHz, DMSO)

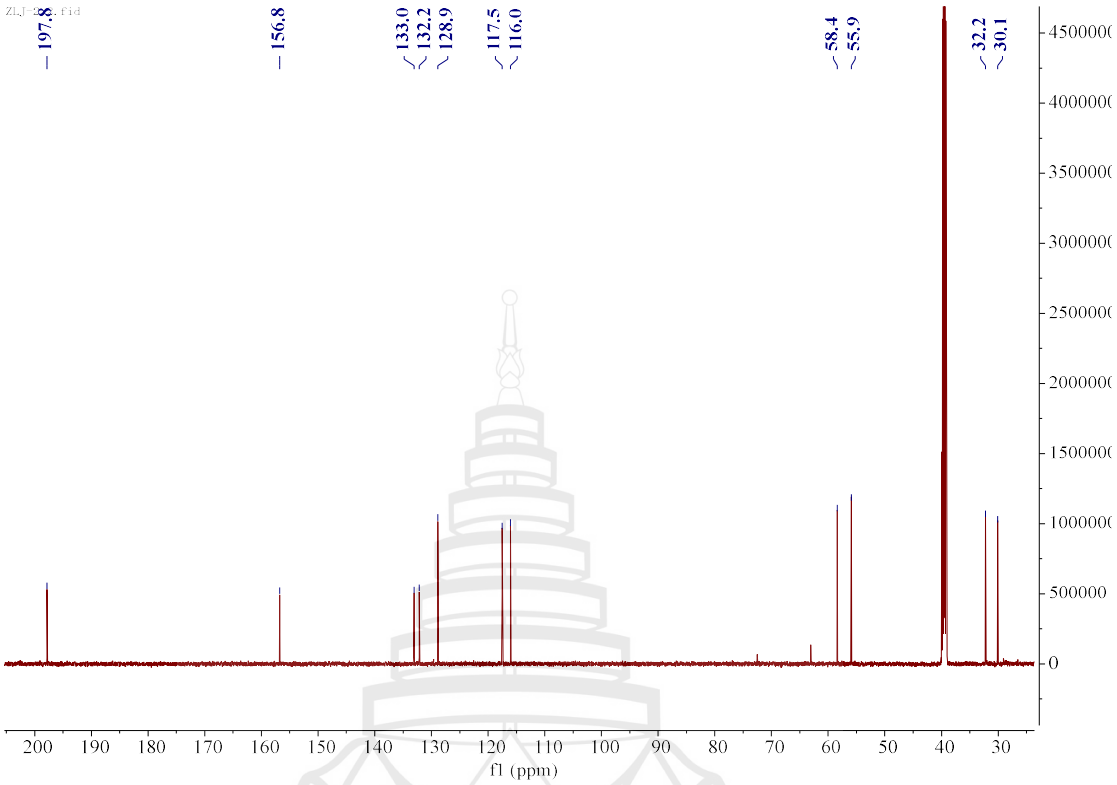

Figure A12 ^{13}C NMR spectrum of compound **C3** (150 MHz, DMSO)

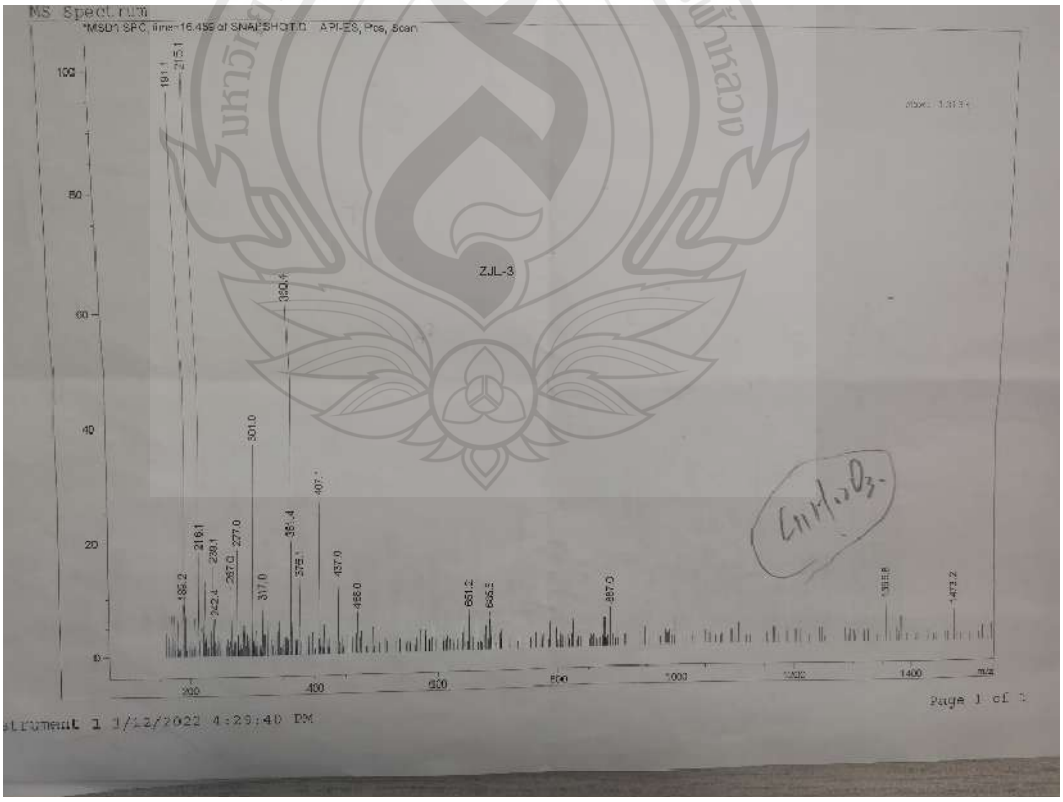

Figure A13 ESIMS of compound **C3**

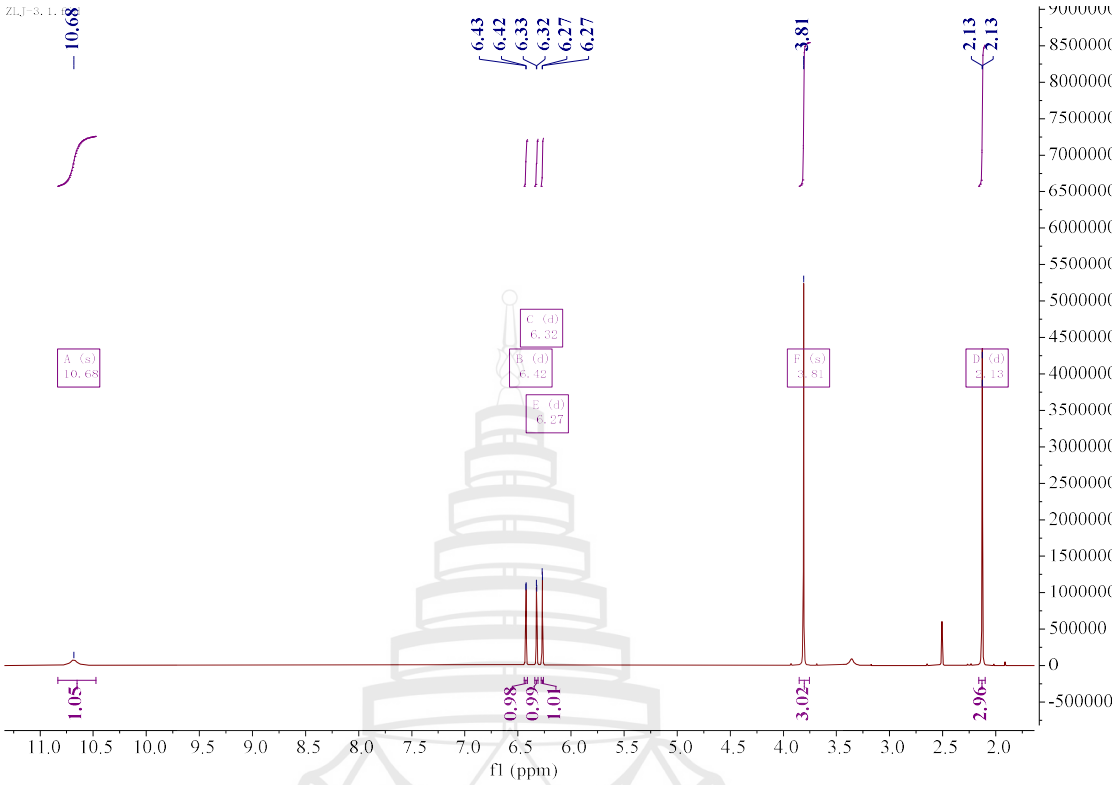

Figure A14 ^{1}H NMR spectrum of compound **C4** (600 MHz, DMSO)

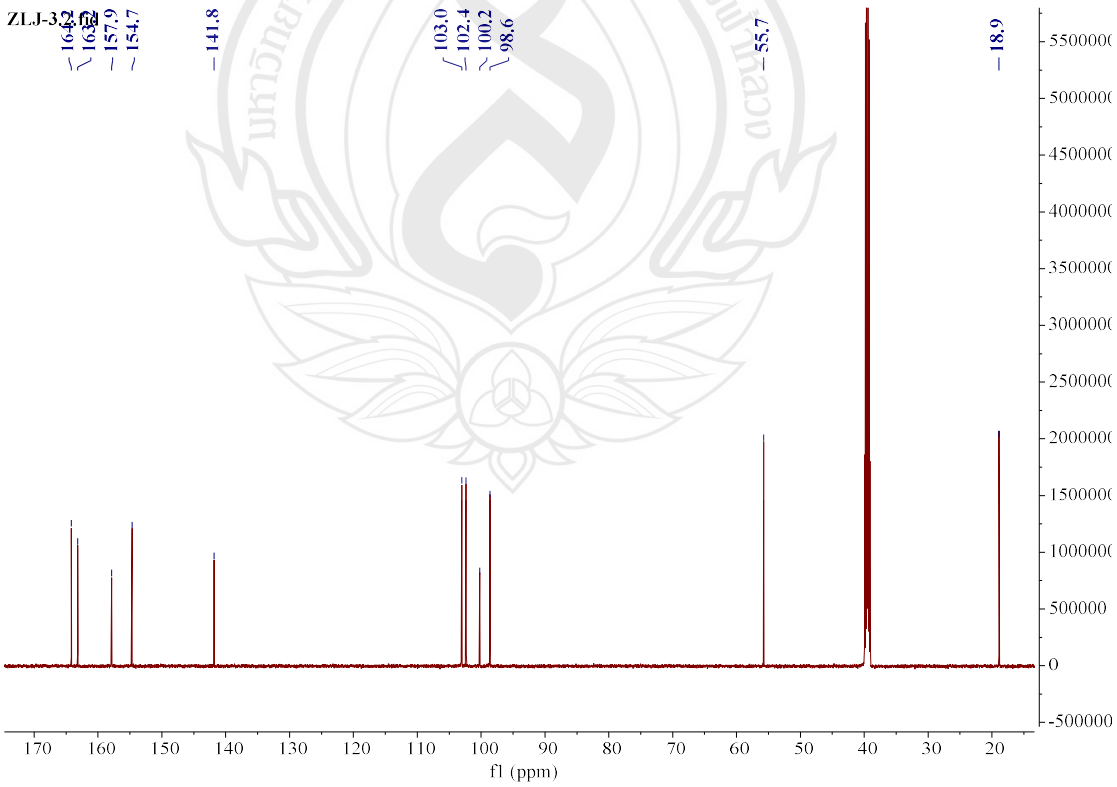

Figure A15 ^{13}C NMR spectrum of compound **C4** (150 MHz, DMSO)

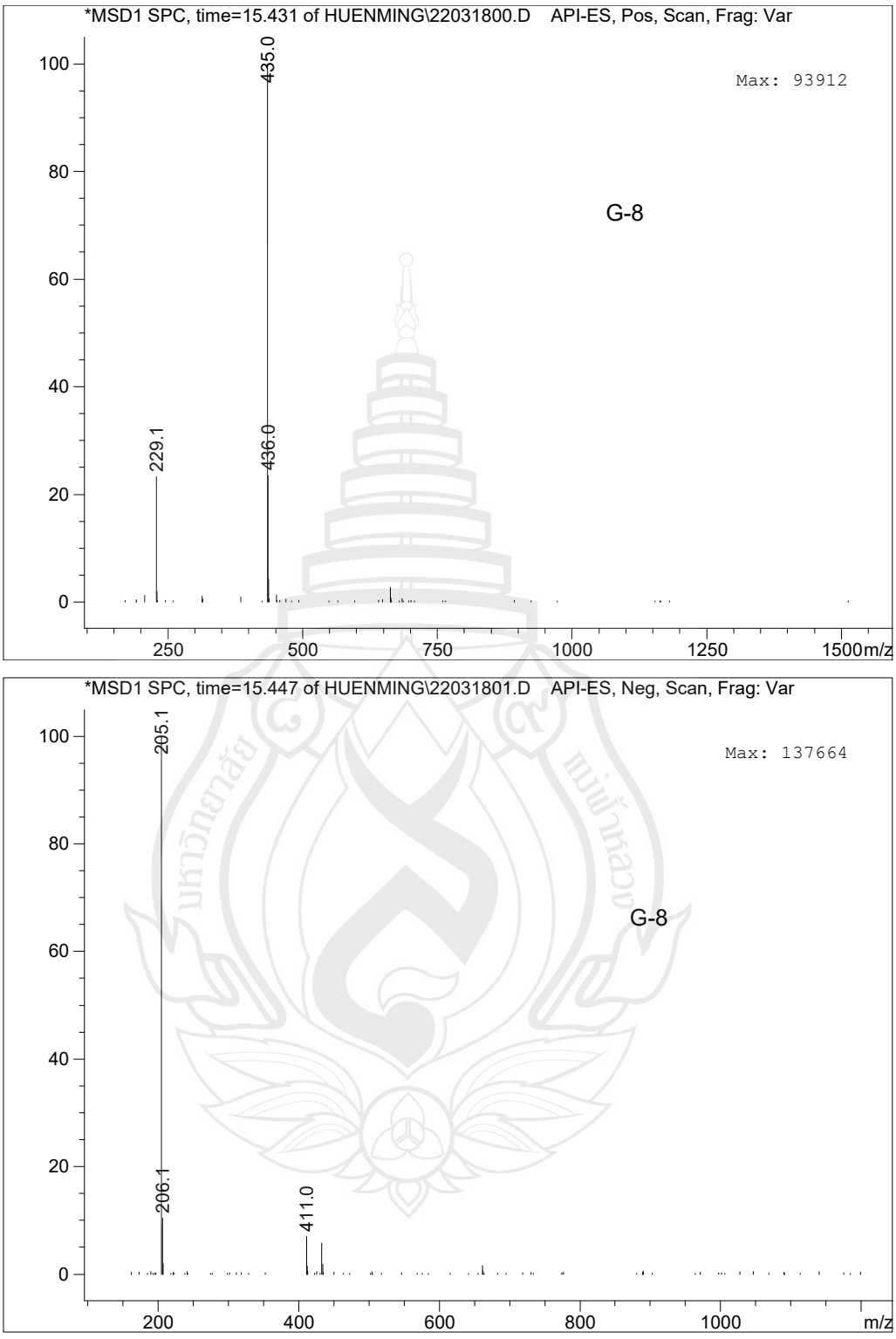

Figure A16 ESIMS of compound **C4**

The conformations of the isomers of compounds were generated by iMTD-GC method embedded in Crest program (Pracht et al., 2020). Two conformations with the root-mean-square (RMS) distance and energy deviation of 0.5 Å and 0.25 kcal/mol, respectively, were considered as duplicates and one of them was removed. Density functional theory calculations were performed with the Gaussian 09 package. ECD spectra were calculated by the TDDFT methodology at the B3LYP/def2TZVP utilizing IEFPCM in methanol. The final ECD spectra were simulated by averaging the spectra of lowest energy conformers according to the Boltzmann distribution theory and their relative Gibbs free energy (*ΔG*).

Reference

Pracht P., Bohle F., & Grimme S. (2020) Automated exploration of the low-energy chemical space with fast quantum chemical methods. *Phys. Chem. Chem. Phys.* 22, 7169–7192.

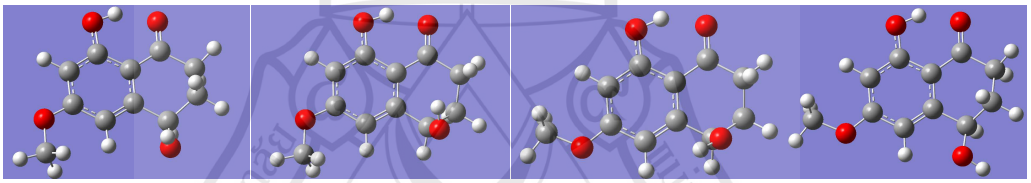

39.60% **2.90%** **19.41%** **38.08%**

Figure A17 The optimized geometries for **C1**

Table A1 Results of the antimicrobial activity assessment of compounds (**C1-C4**)

test organism	strain number	MIC [µg/mL]			
		C1	**C2**	**C3**	**C4**
Bacillus subtilis	ATCC 6051	–	–	–	–
Escherichia coli	ATCC 11775	–	–	–	–
Pseudomonas aeruginosa	ATCC 10145	–	–	–	–
Staphylococcus aureus	ATCC 43300	–	–	–	–
Staphylococcus aureus	ATCC 6538	–	–	–	–
Clostridium perfringens	ATCC 13124	–	–	–	–
Paratyphoidfever		–	–	–	–
Ralstonia solanacarum		–	–	–	–
Canidia albicans	ATCC 10231	–	–	–	–
Candida glabrata	ATCC 2001	–	–	–	–

Note Bacterial positive control: ciprofloxacin (Initial concentration before serial dilution is 5 µg/ml)

Fungal positive control: ketoconazole (Initial concentration before serial dilution is 0.1 mg/ml)

Table A2 Results of the antifungal activity assessment of compounds (**C1-C4**)

test organism	IC_{50} [µg/mL]			
	C1	**C2**	**C3**	**C4**
Sclerotinia sclerotiorum	–	–	–	–
FusaHum graminearum	–	–	–	–
Phytophthora nicotianae	–	–	–	–

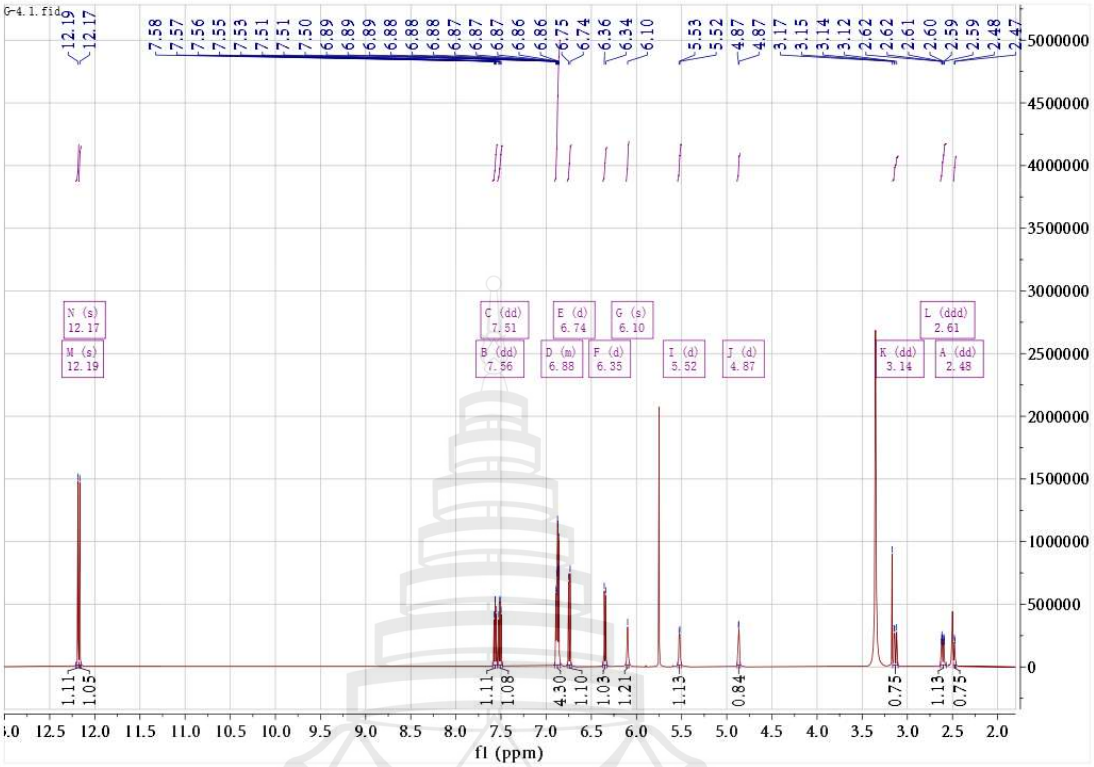

Figure A18 ^{1}H NMR spectrum of compound **C5** (600 MHz, DMSO)

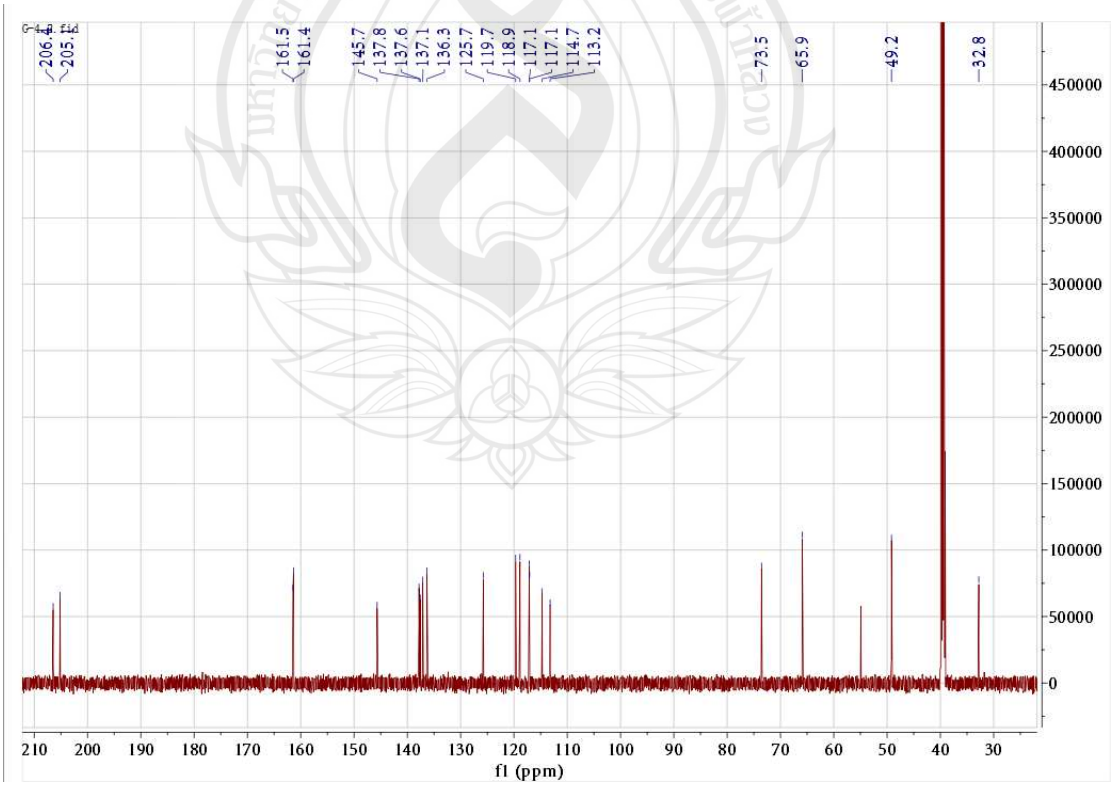

Figure A19 ^{13}C NMR spectrum of compound **C5** (150 MHz, DMSO)

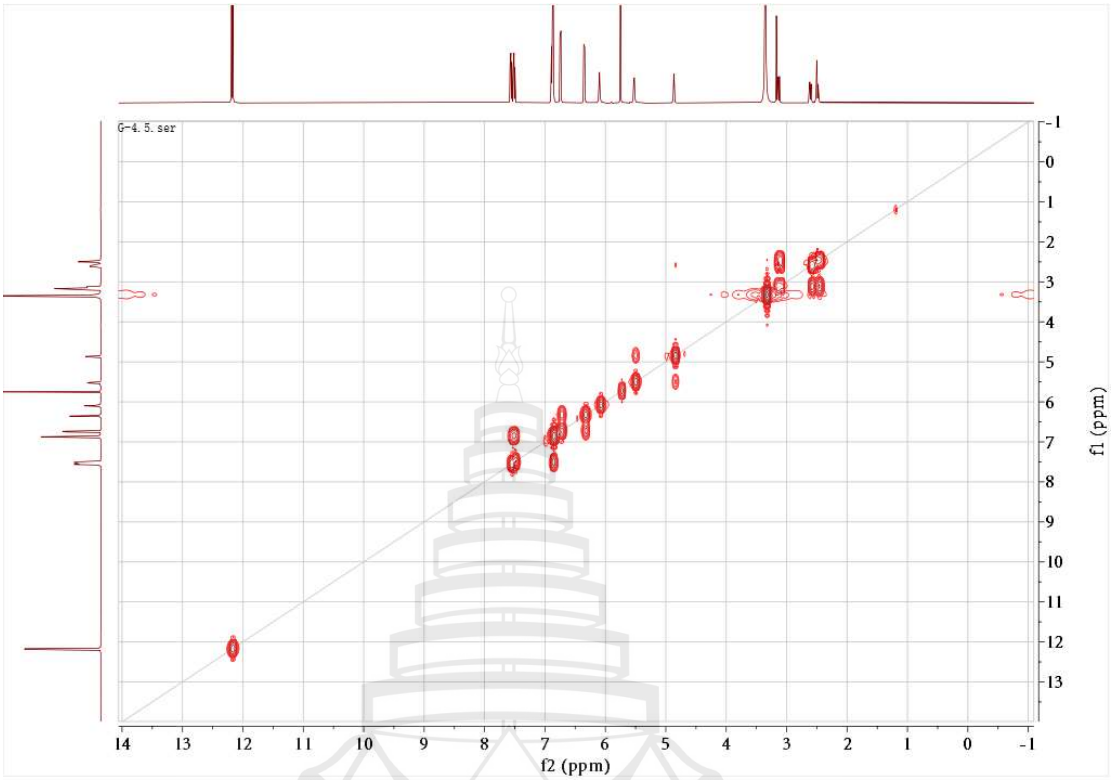

Figure A20 ^{1}H-^{1}H COSY spectrum of compound **C5** (DMSO)

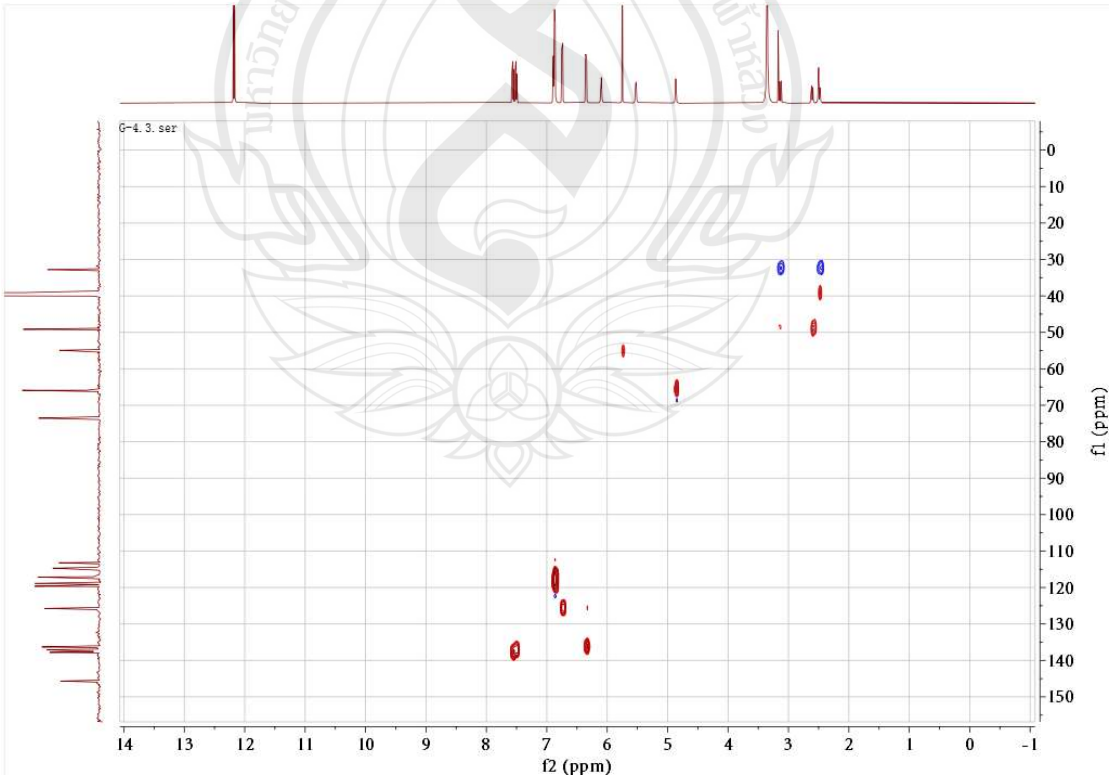

Figure A21 HSQC spectrum of compound **C5** (DMSO)

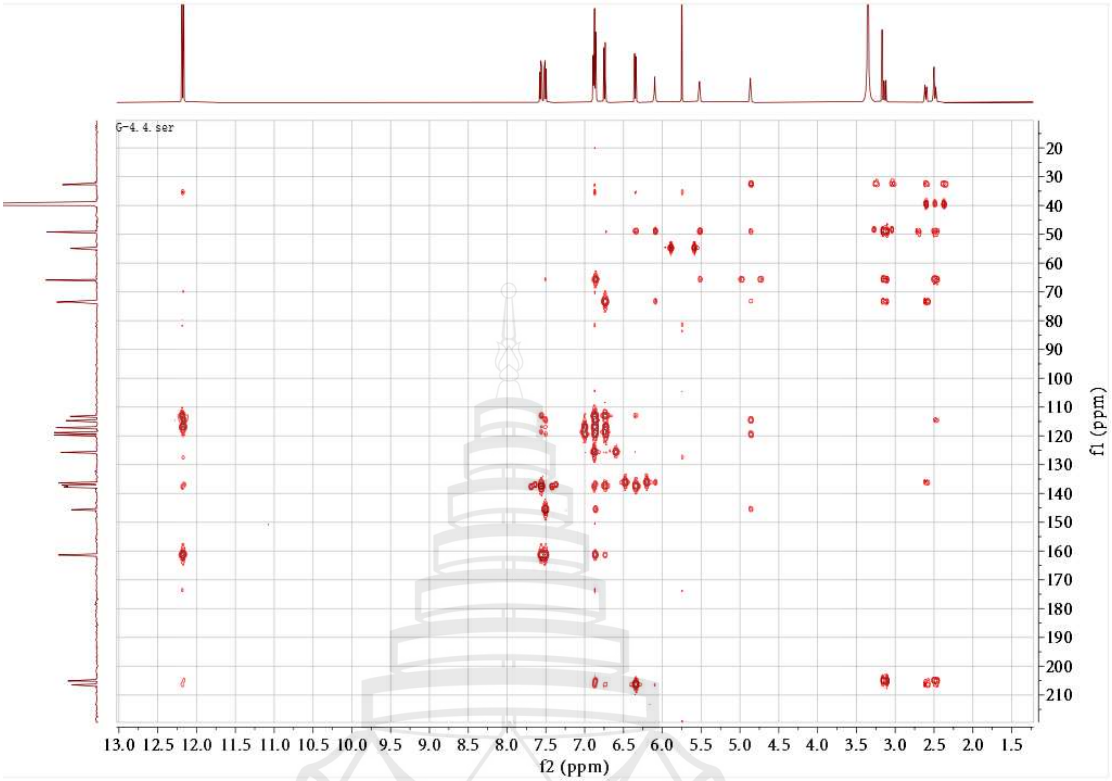

Figure A22 HMBC spectrum of compound **C5** (DMSO)

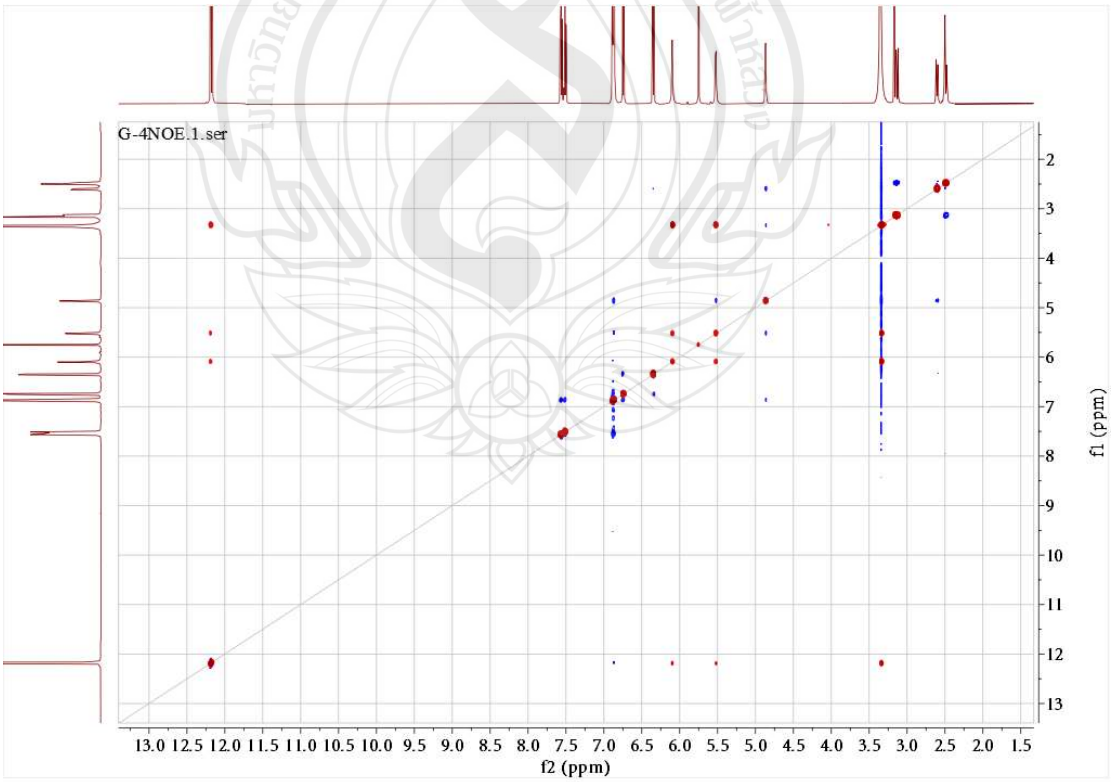

Figure A23 NOESY spectrum of compound **C5** (DMSO)

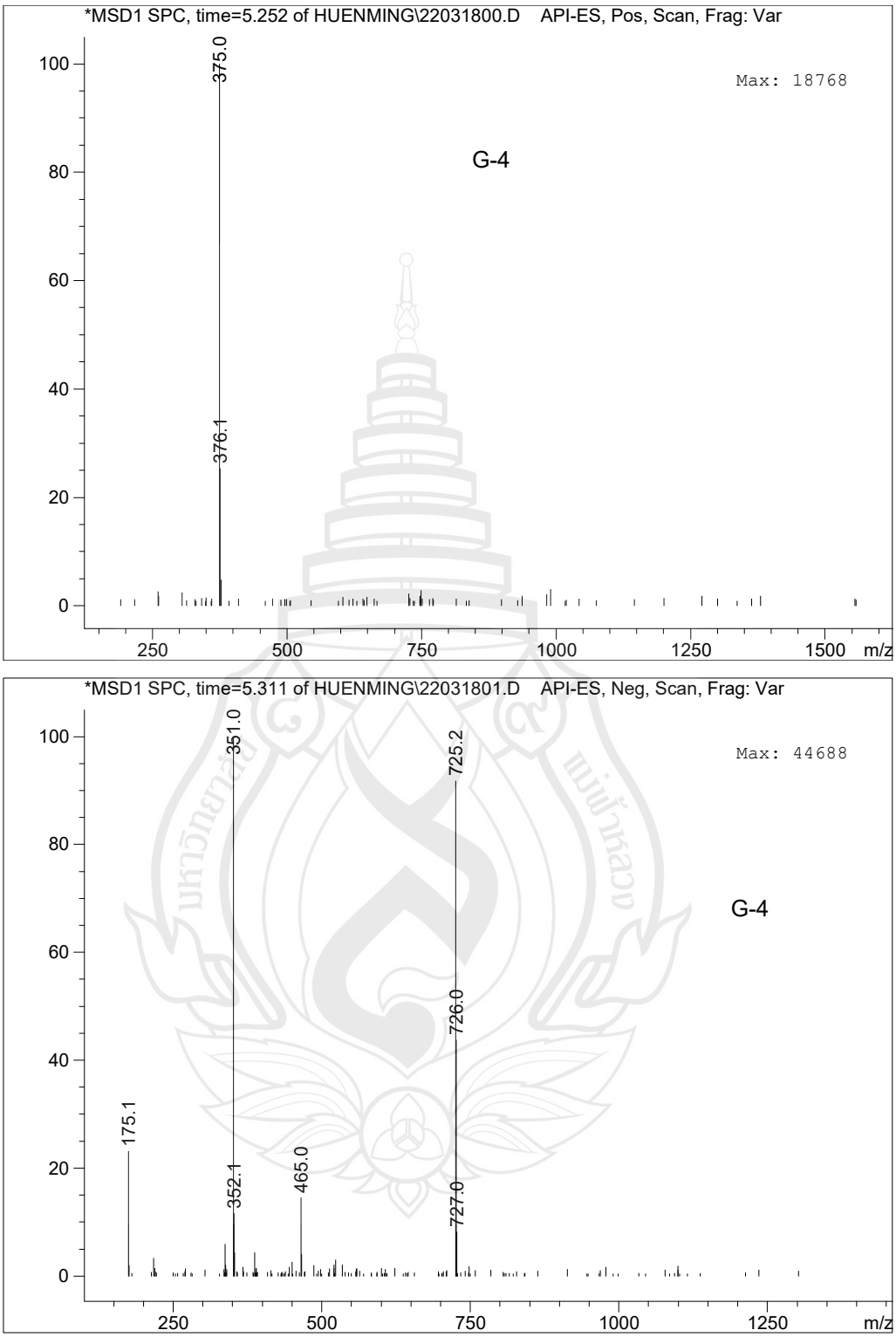

Figure A24 ESIMS of compound **C5**

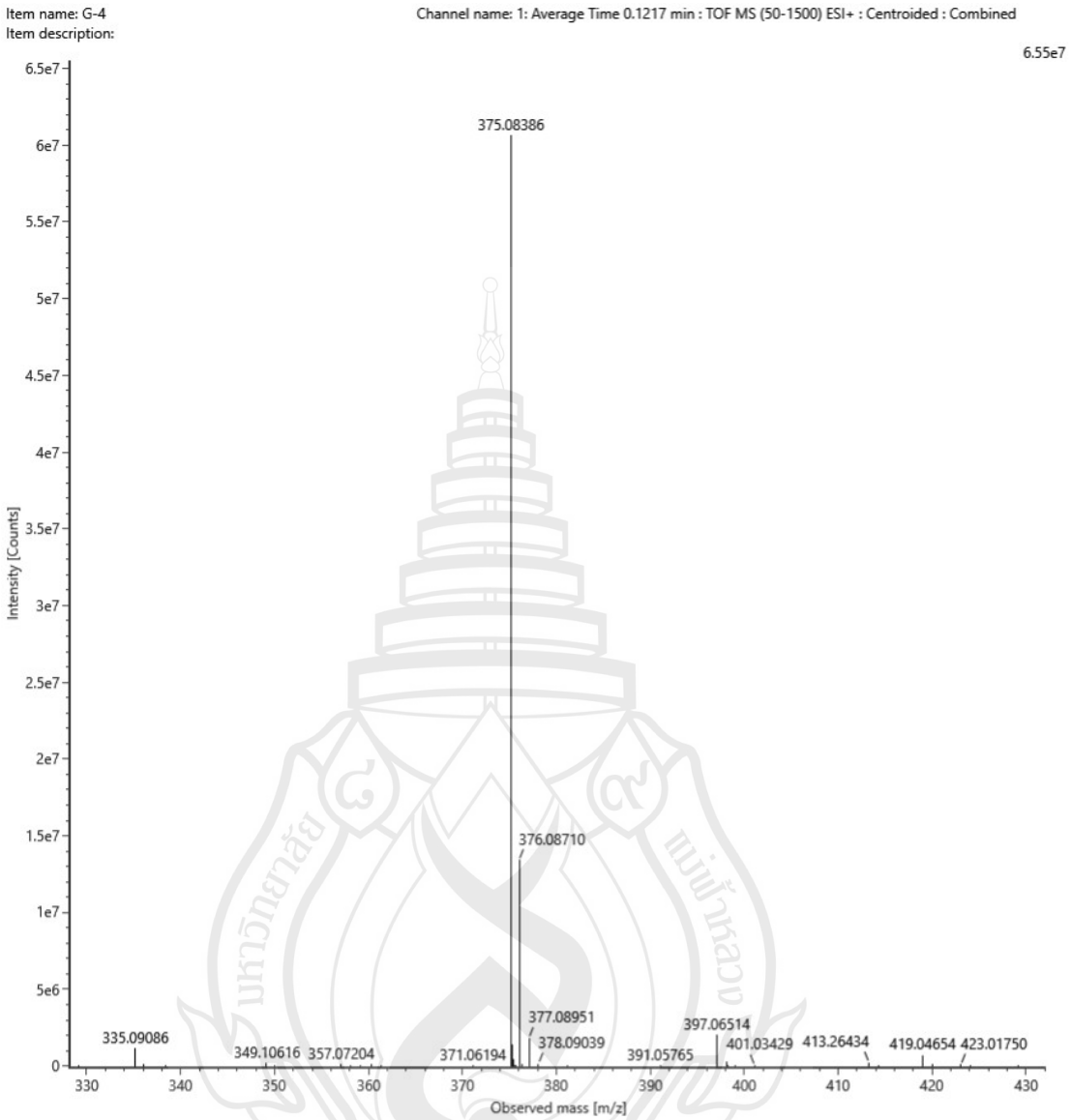

Note Add:Na+

Composition	$C_{20}H_{16}O_6Na$
i-FIT Confidence (%)	100.000000
Predicted m/z	375.083909
m/z error (PPM)	-0.131856

Figure A25 HR-ESIMS of compound **C5**

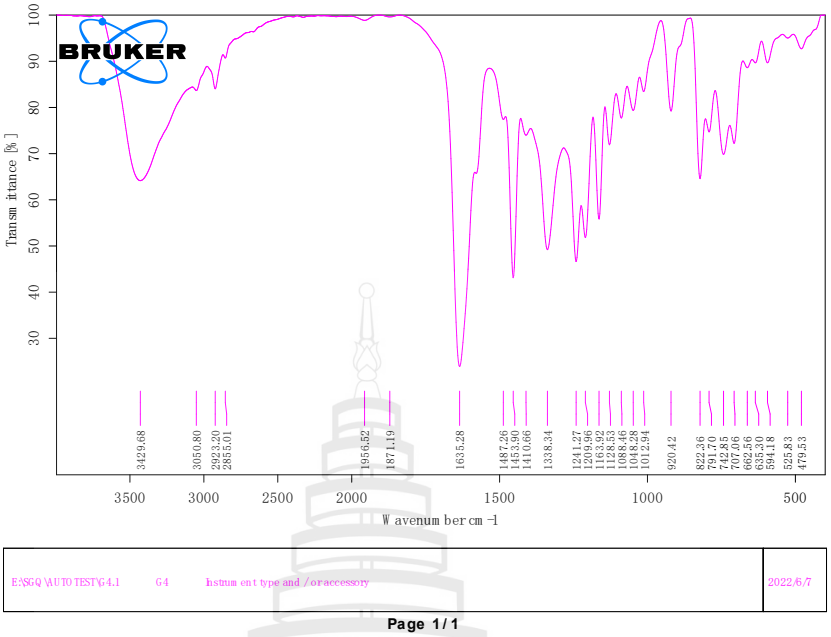

Figure A26 IR (KBr) spectrum of compound **C5**

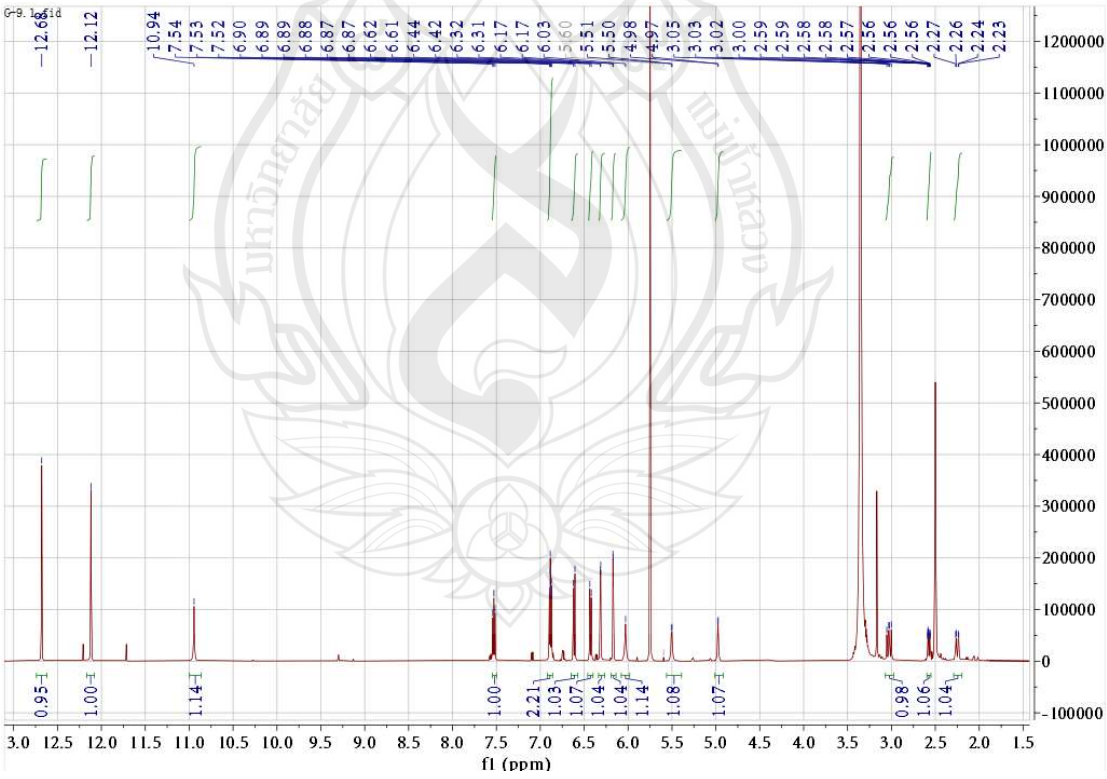

Figure A27 ^{1}H NMR spectrum of compound **C6** (600 MHz, DMSO)

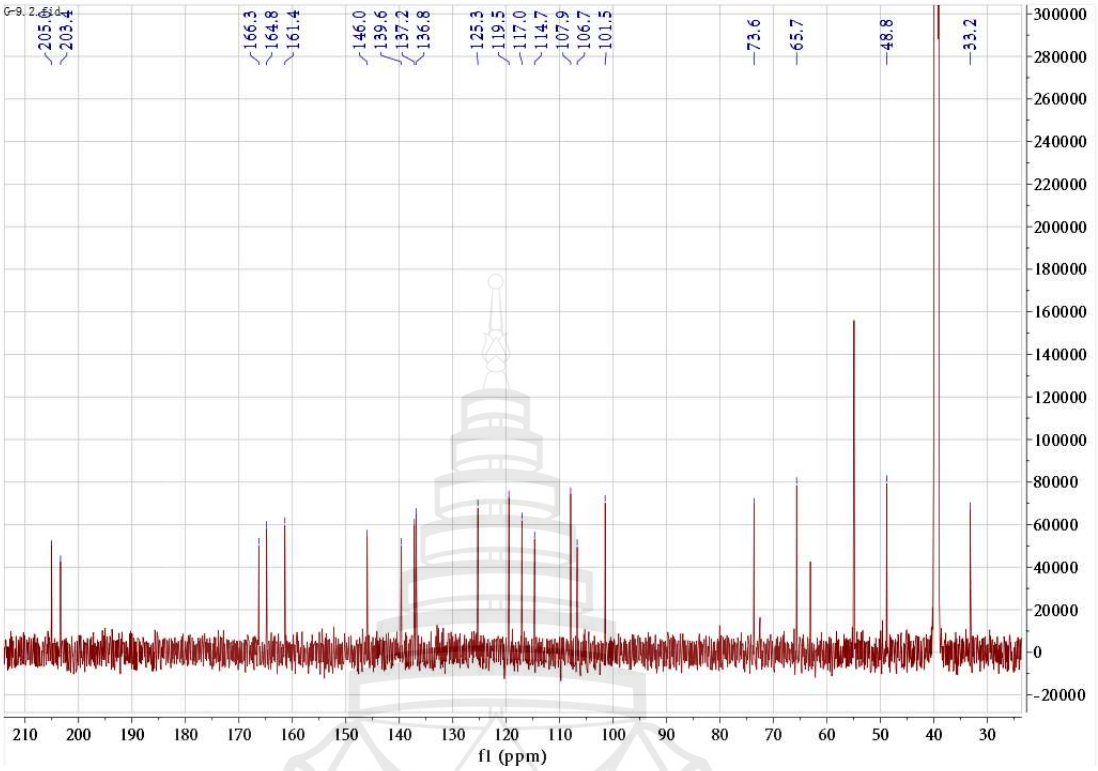

Figure A28 ^{13}C NMR spectrum of compound **C6** (150 MHz, DMSO)

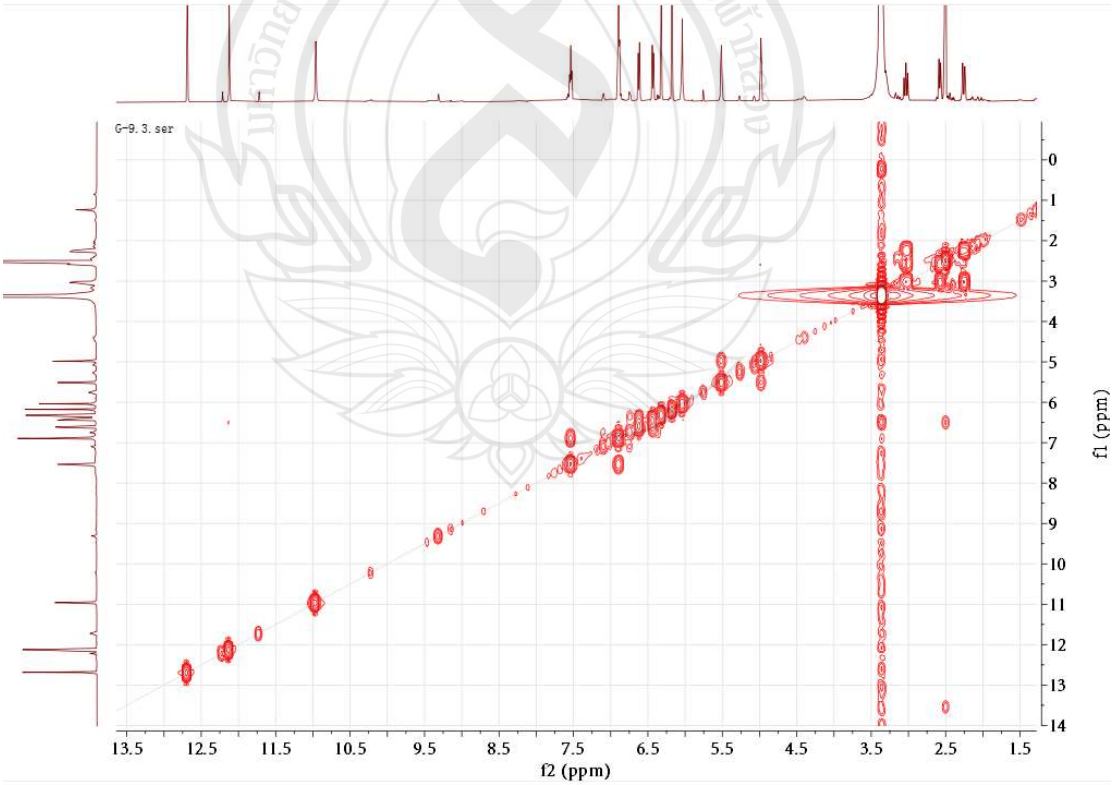

Figure A29 ^{1}H-^{1}H COSY spectrum of compound **C6** (DMSO)

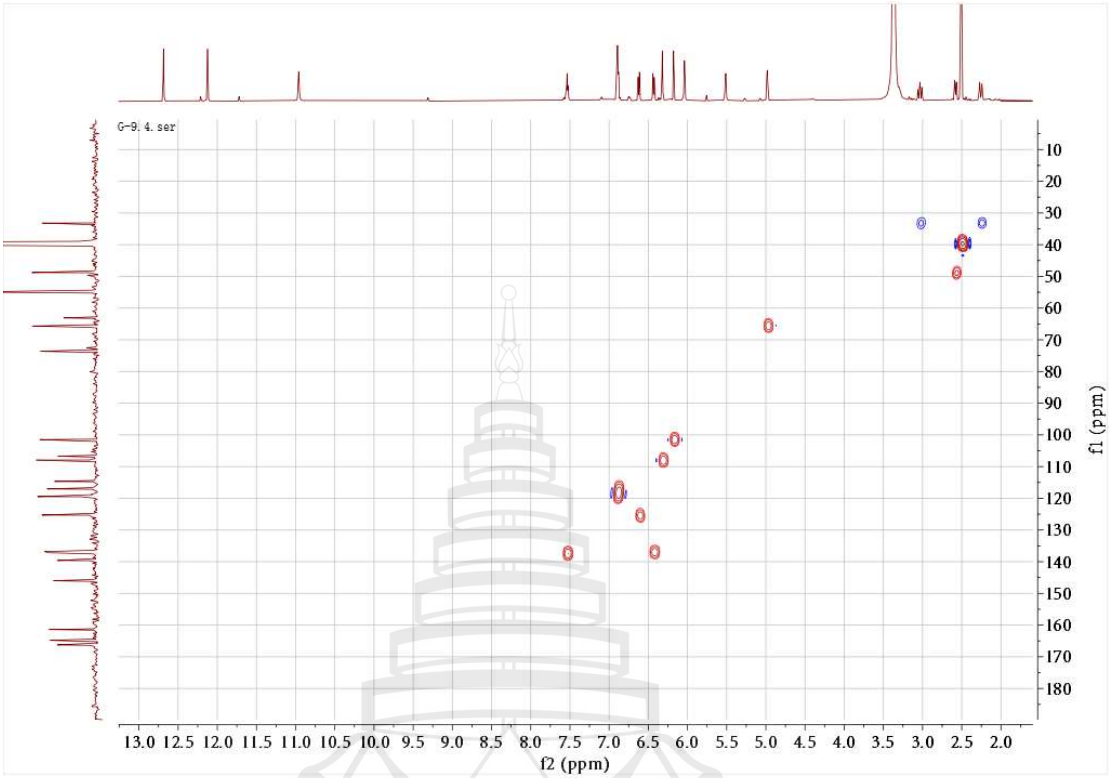

Figure A30 HSQC spectrum of compound **C6** (DMSO)

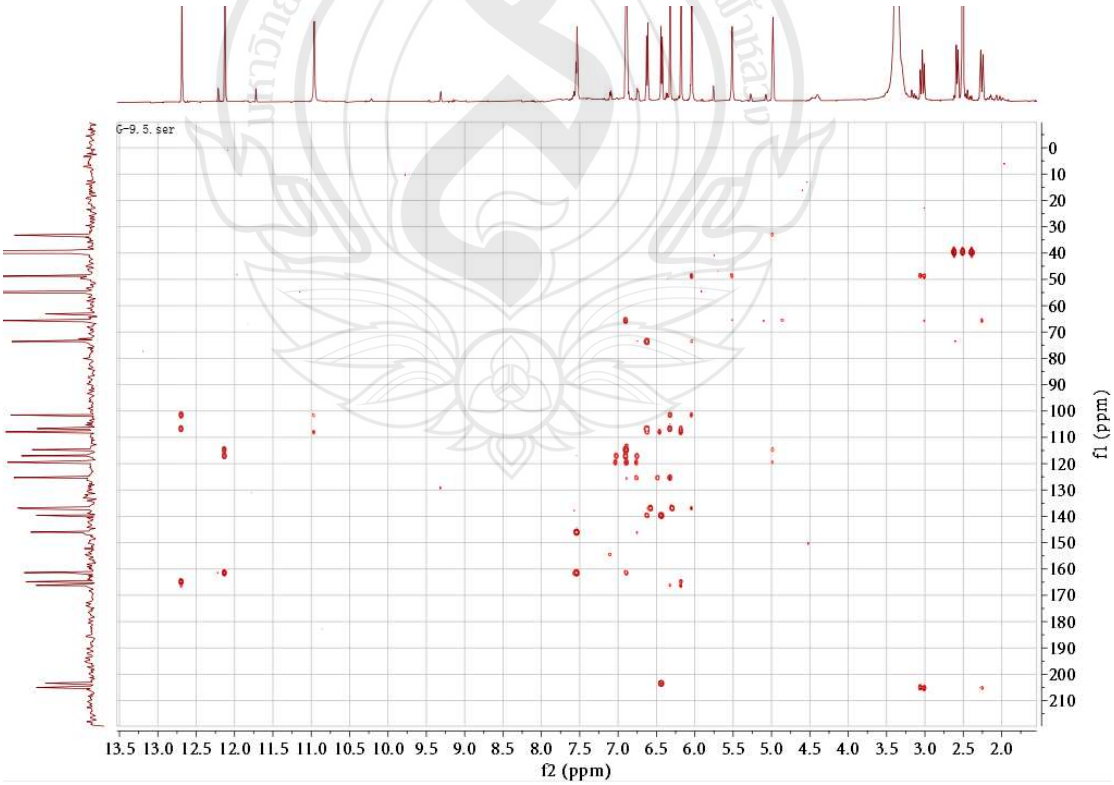

Figure A31 HMBC spectrum of compound **C6** (DMSO)

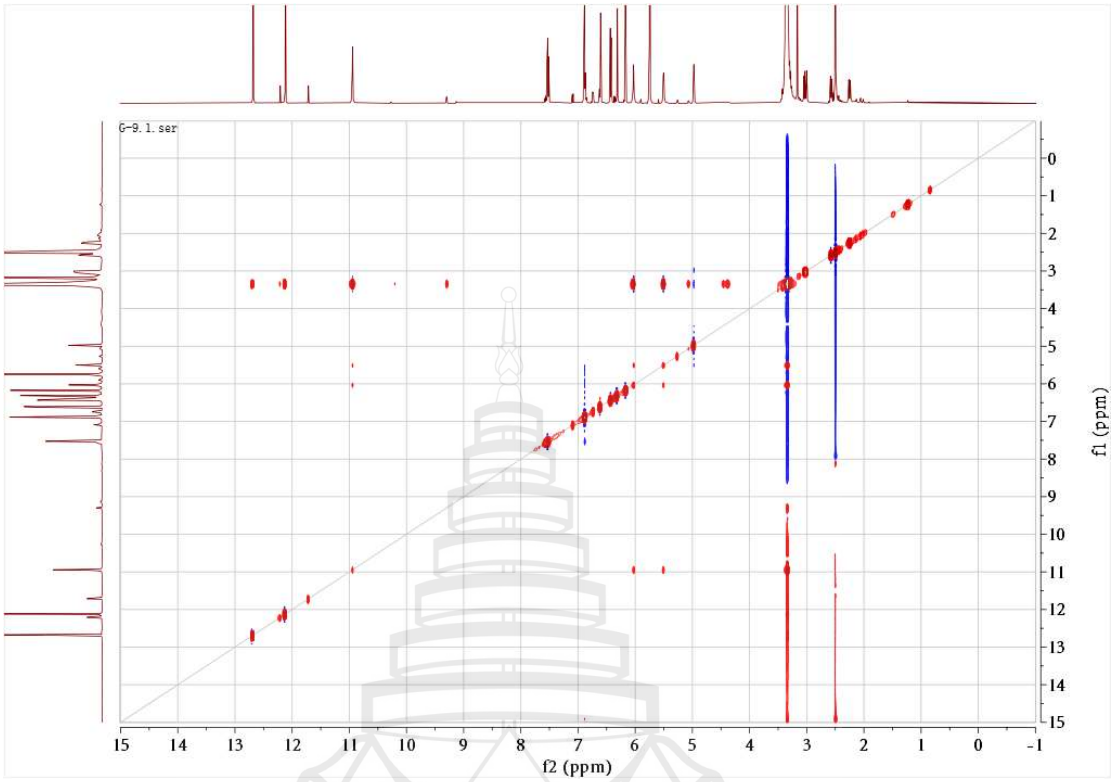

Figure A32 NOESY spectrum of compound **C6** (DMSO)

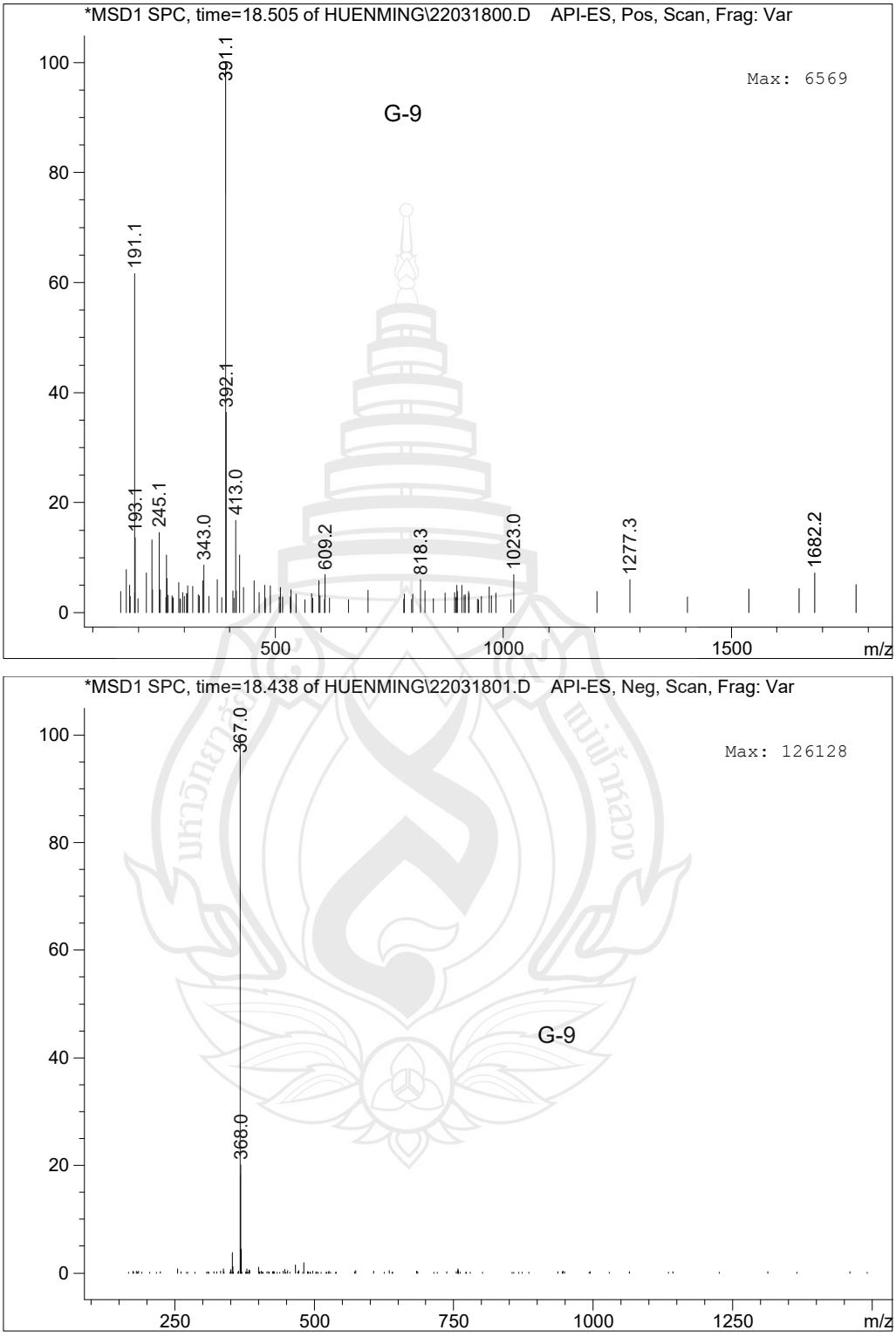

Figure A33 ESIMS of compound **C6**

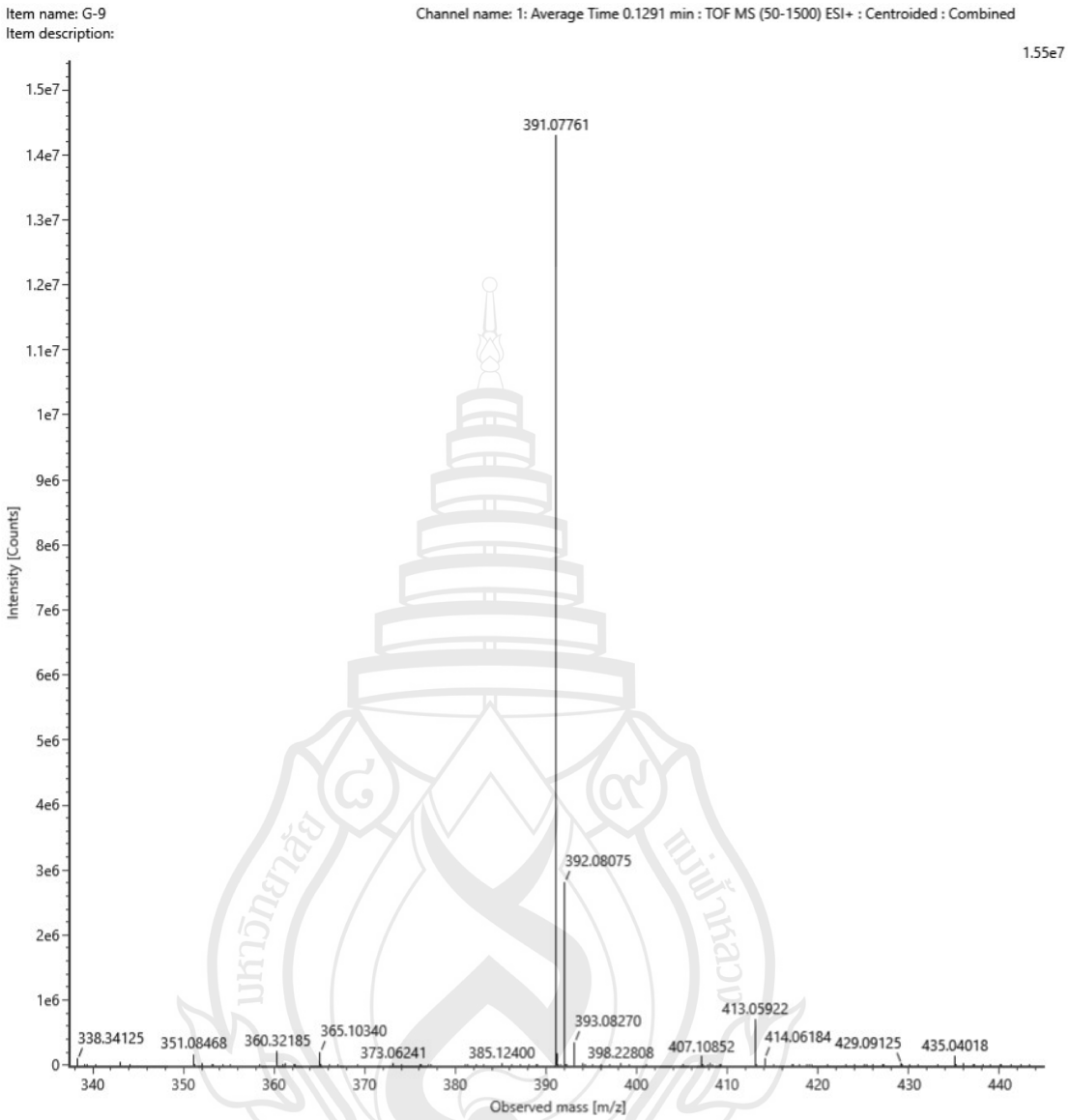

Note Add:Na+

Composition	$C_{20}H_{16}O_7Na$
i-FIT Confidence (%)	100.000000
Predicted m/z	391.078824
m/z error (PPM)	-3.112122

Figure A34 HR-ESIMS of compound **C6**

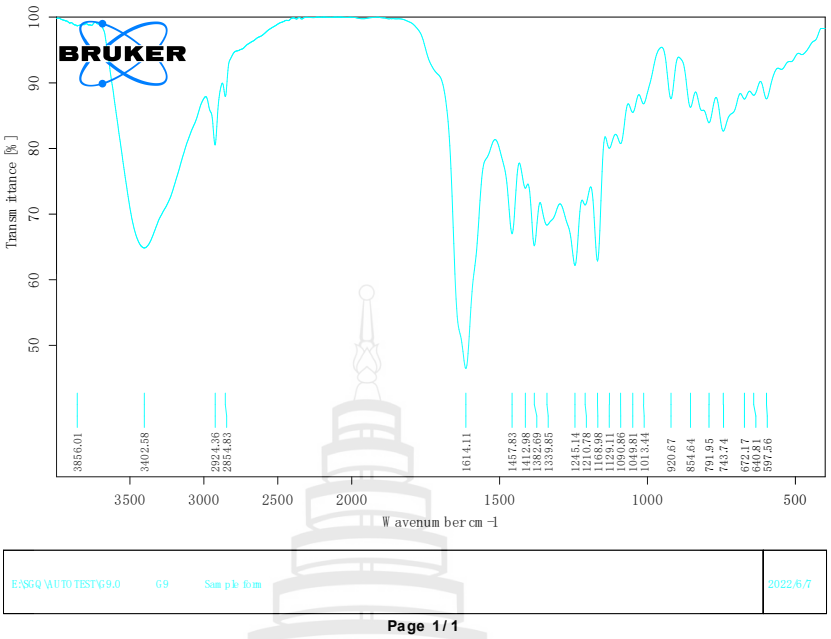

Figure A35 IR (KBr) spectrum of compound **C6**

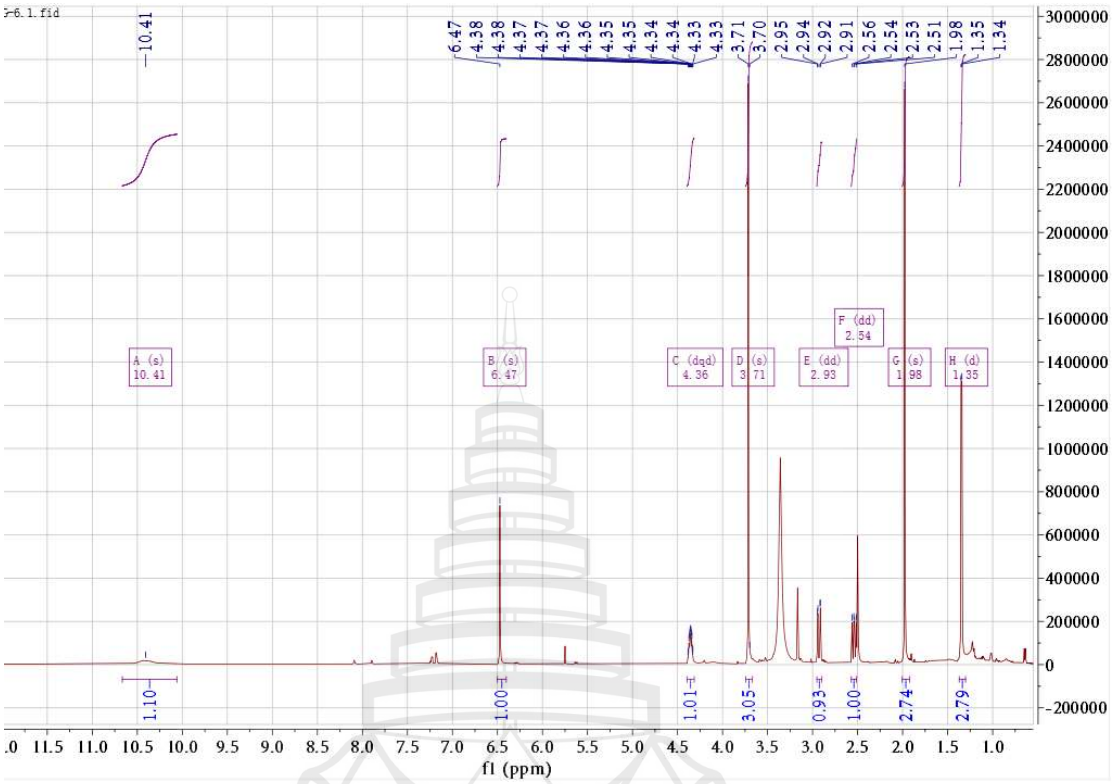

Figure A36 ^{1}H NMR spectrum of compound **C7** (600 MHz, DMSO)

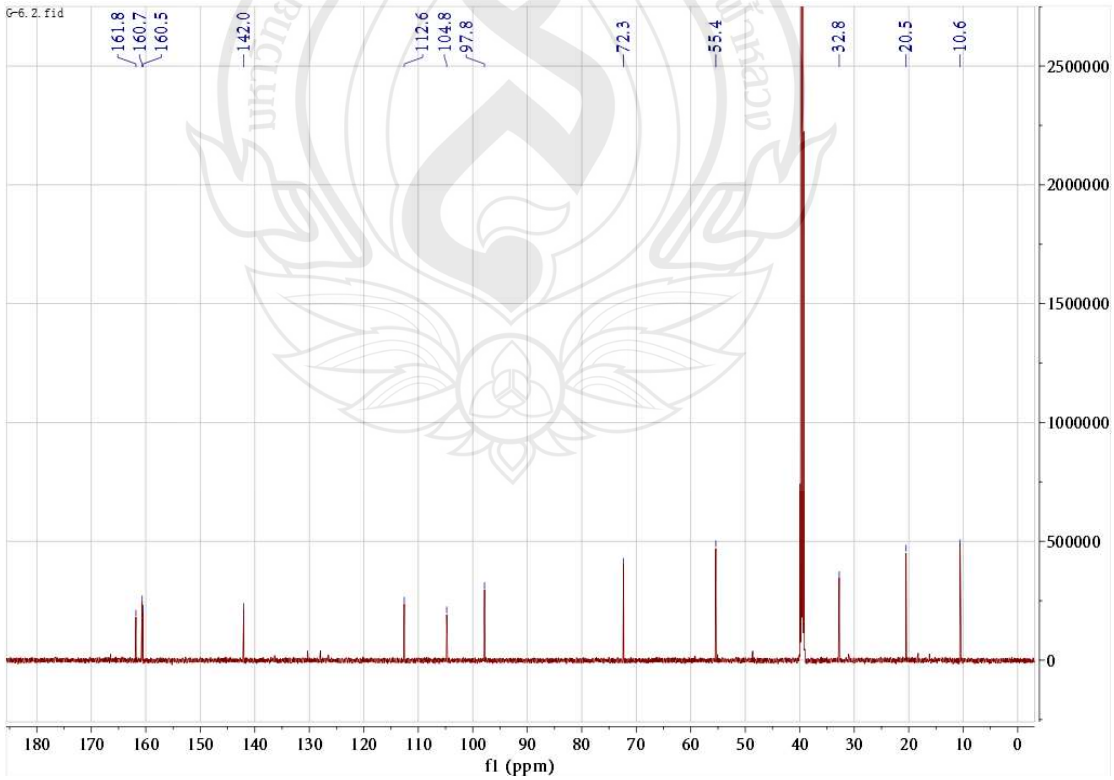

Figure A37 ^{13}C NMR spectrum of compound **C7** (150 MHz, DMSO)

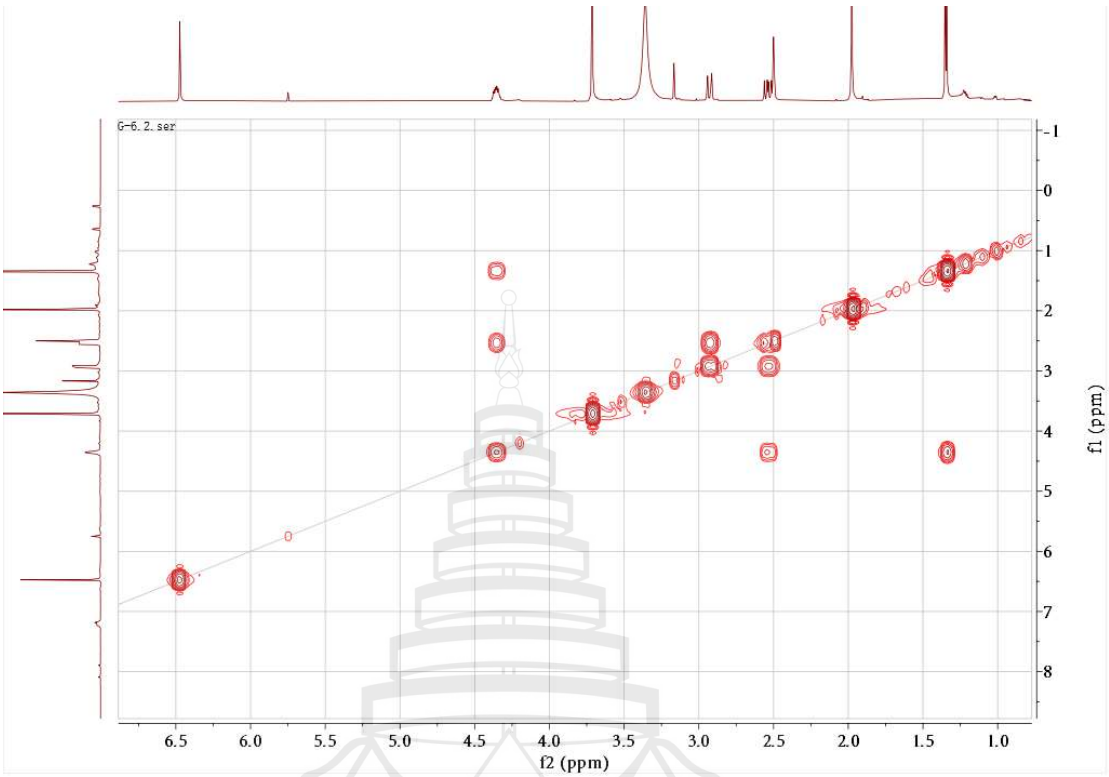

Figure A38 ^{1}H-^{1}H COSY spectrum of compound **C7** (DMSO)

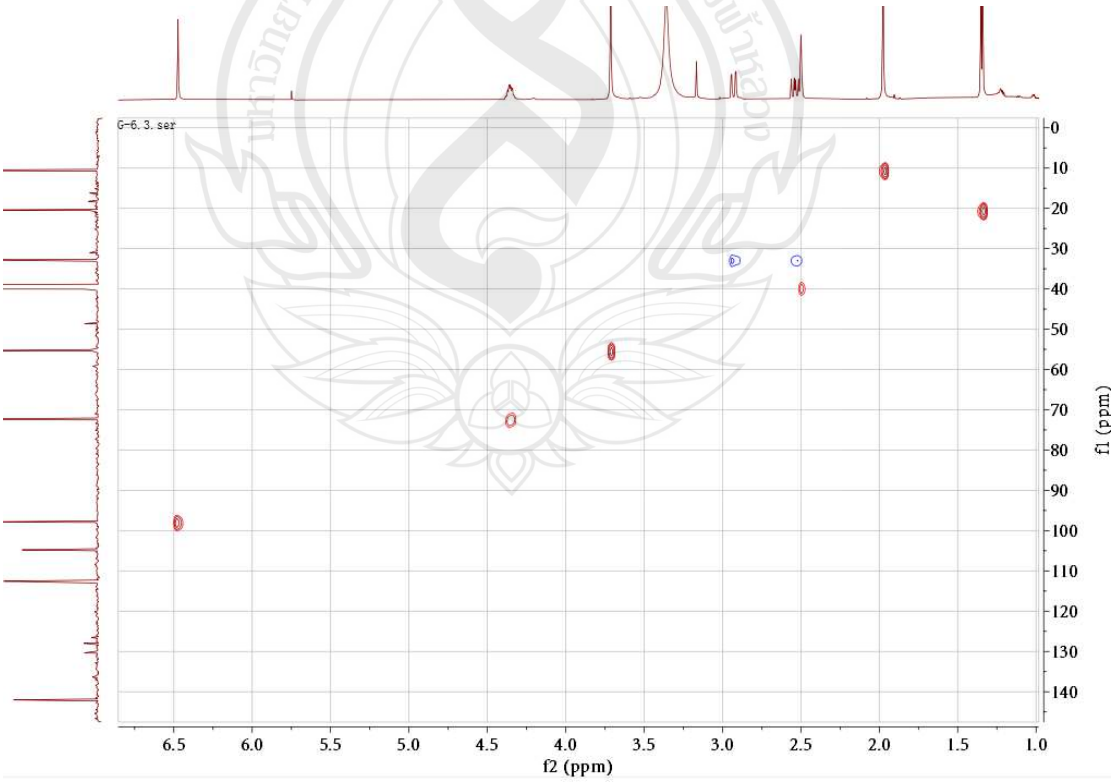

Figure A39 HSQC spectrum of compound **C7** (DMSO)

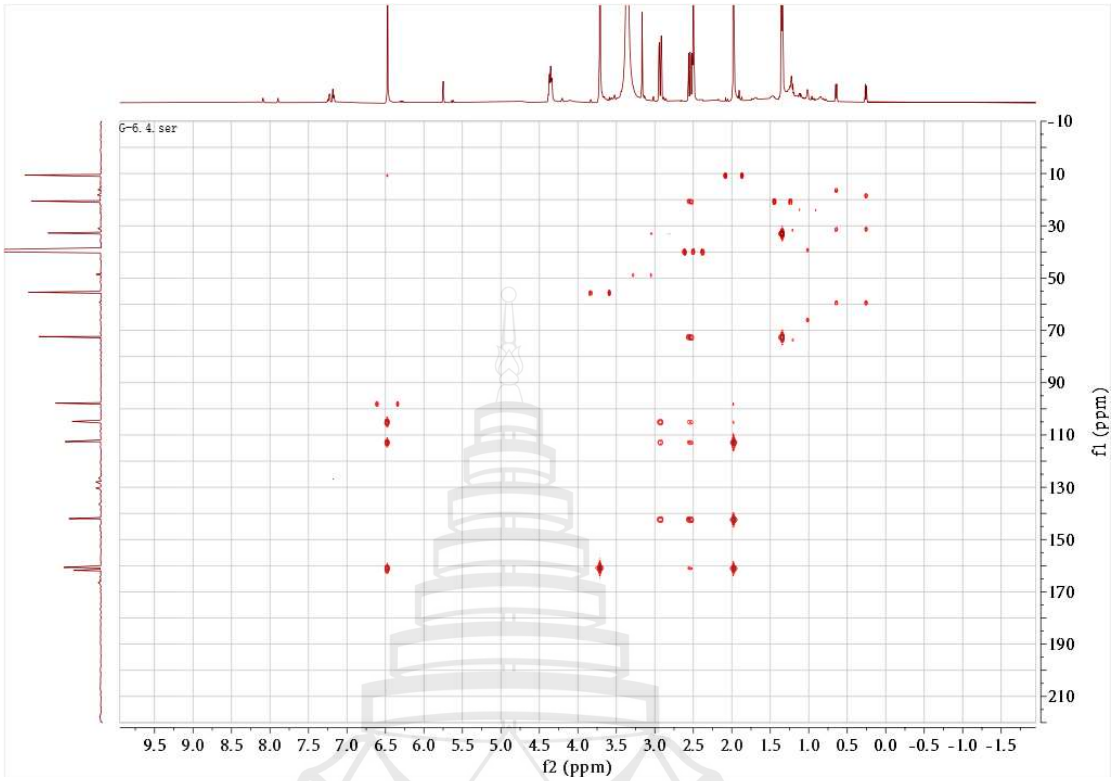

Figure A40 HMBC spectrum of compound **C7** (DMSO)

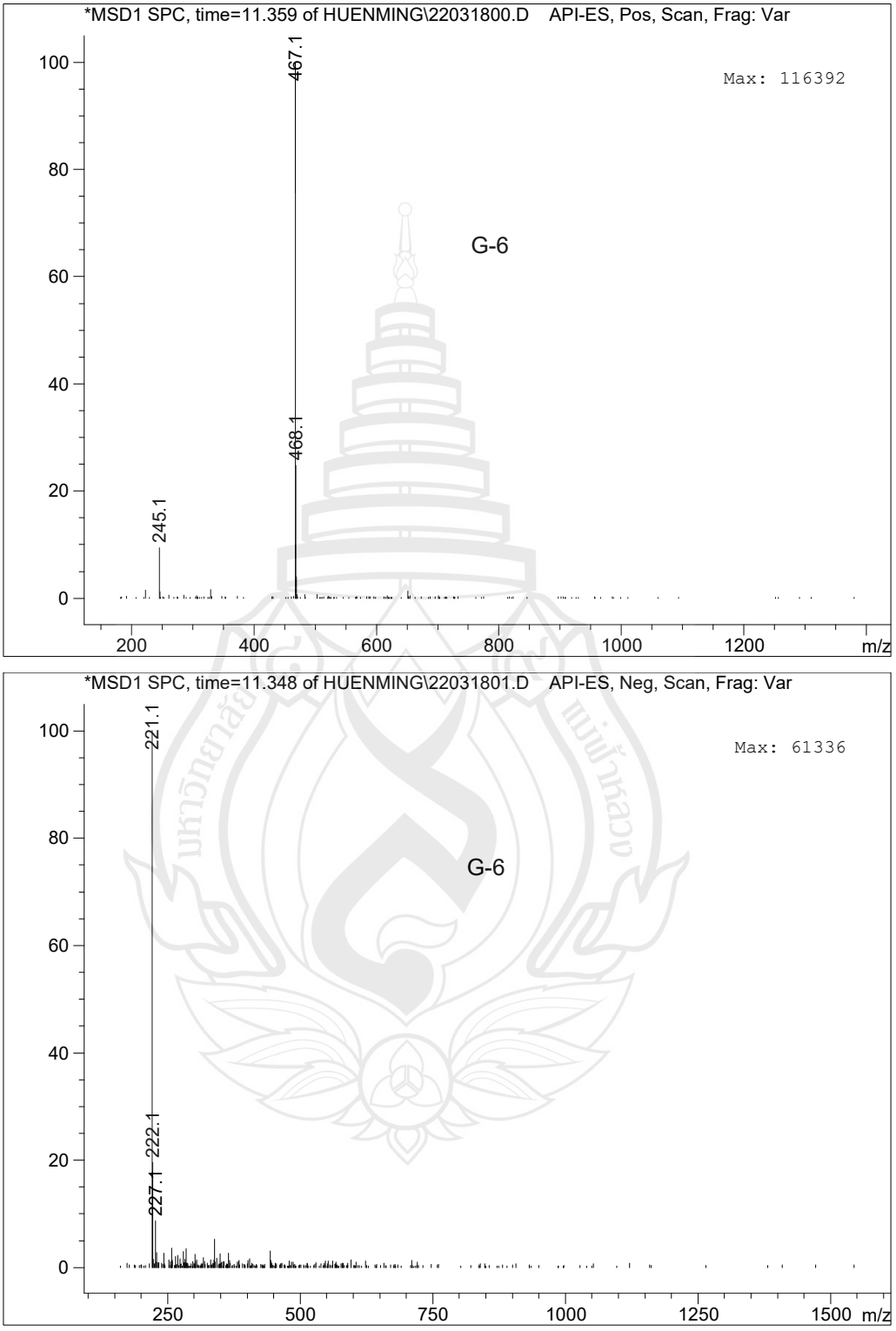

Figure A41 ESIMS of compound **C7**

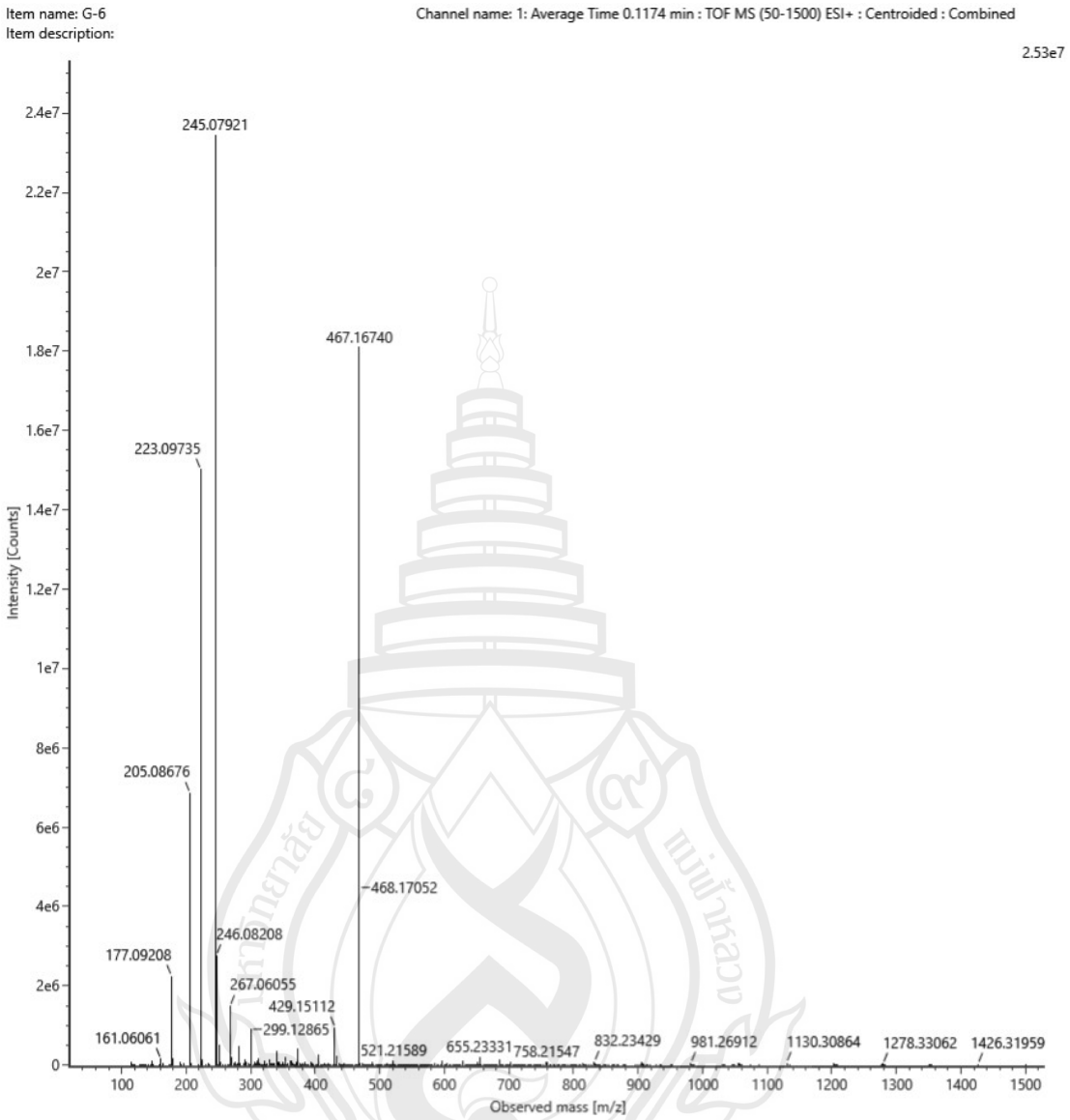

Note Add:Na+

Composition	$C_{12}H_{14}O_4Na$
i-FIT Confidence (%)	100.000000
Predicted m/z	245.078430
m/z error (PPM)	3.195714

Figure A42 HR-ESIMS of compound **C7**

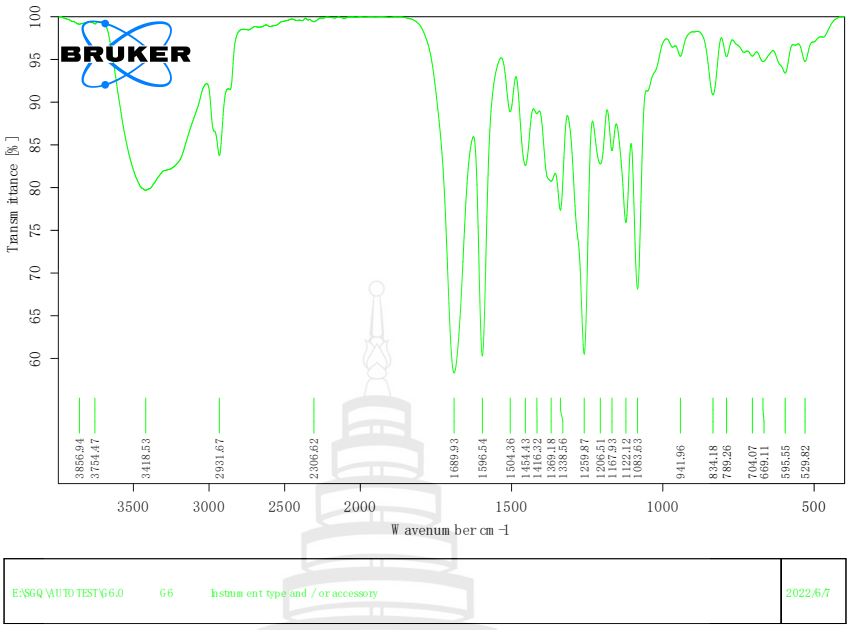

Figure A43 IR (KBr) spectrum of compound **C7**

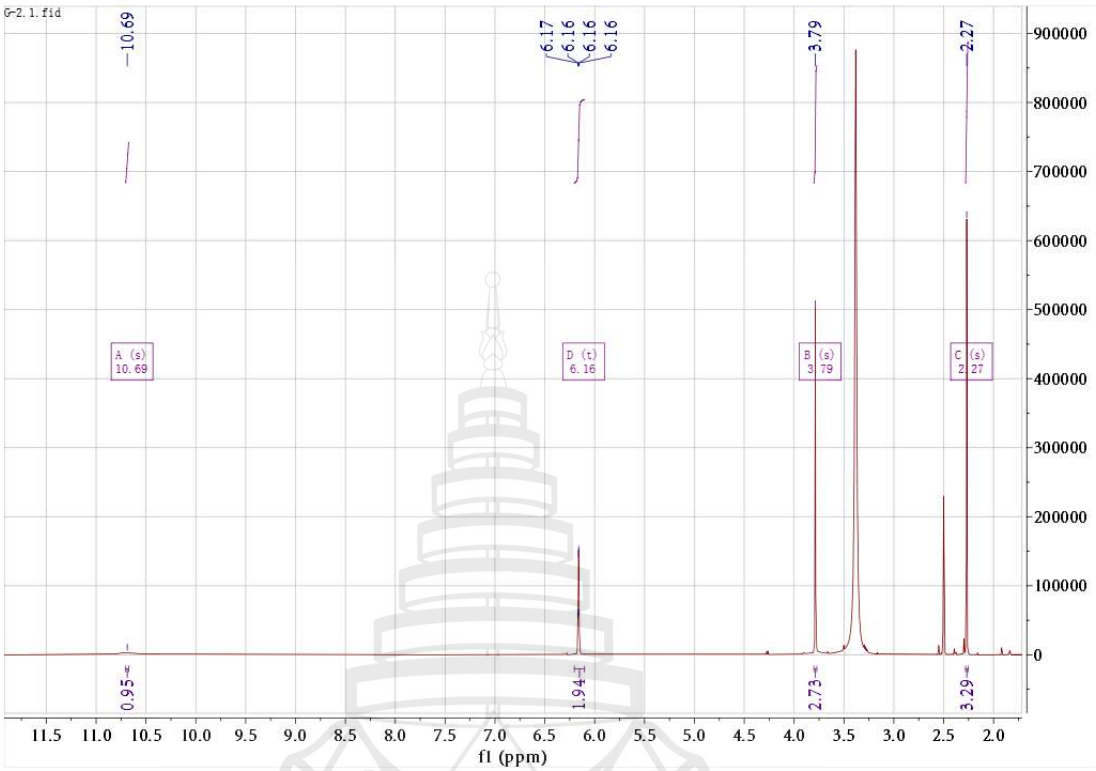

Figure A44 ^{1}H NMR spectrum of compound **C8** (600 MHz, DMSO)

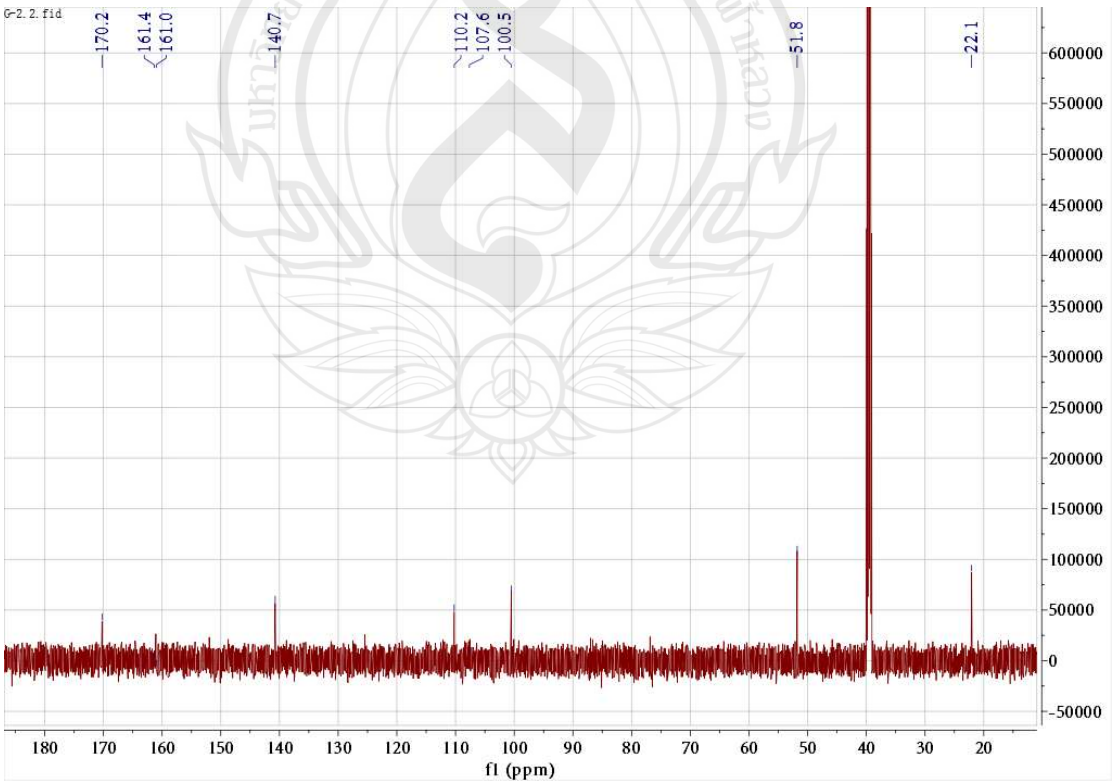

Figure A45 ^{13}C NMR spectrum of compound **C8** (150 MHz, DMSO)

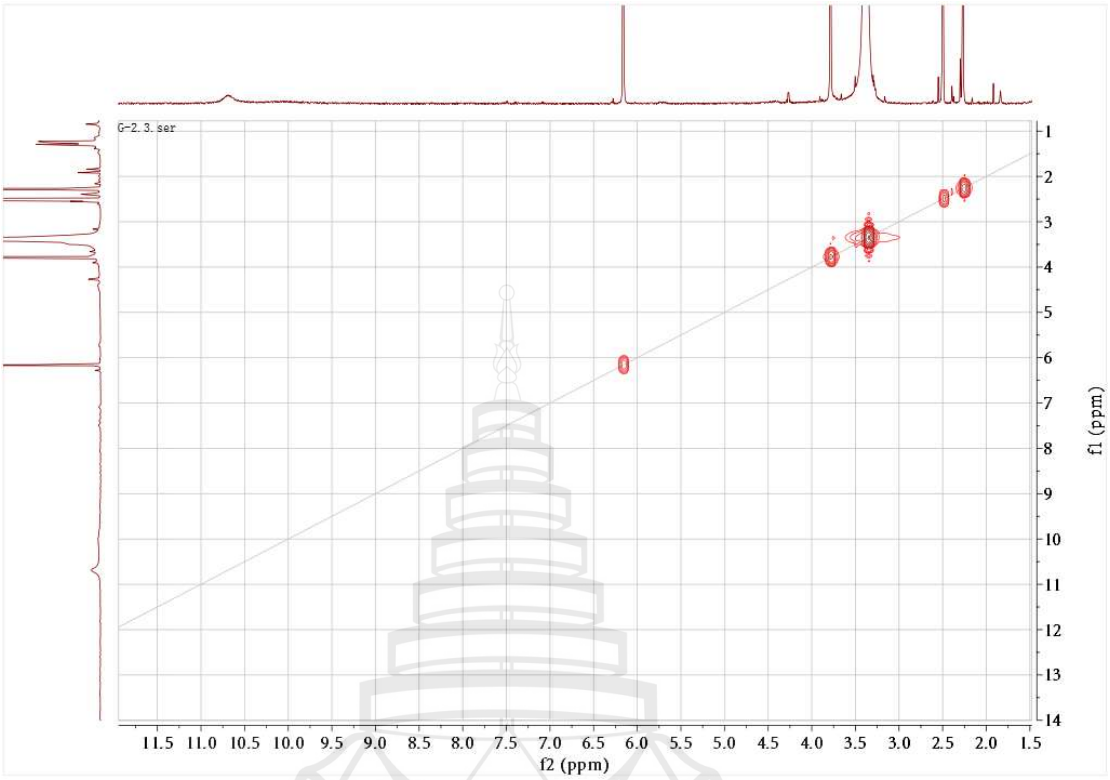

Figure A46 ^{1}H-^{1}H COSY spectrum of compound **C8** (DMSO)

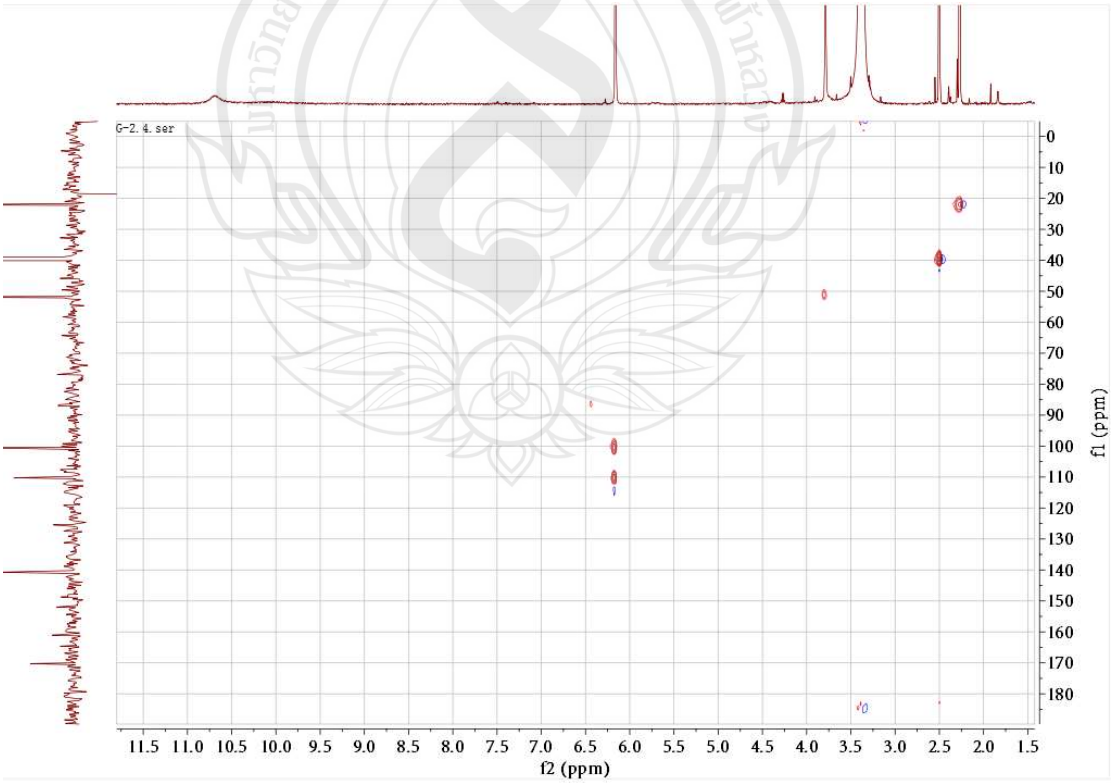

Figure A47 HSQC spectrum of compound **C8** (DMSO)

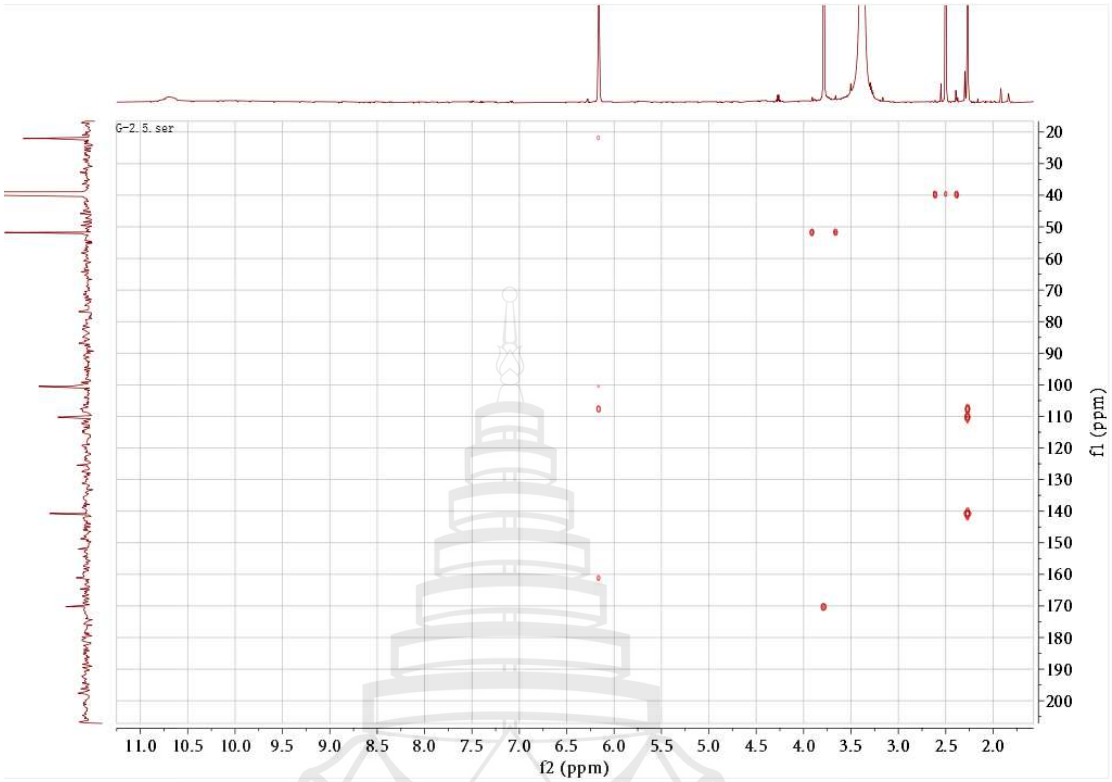

Figure A48 HMBC spectrum of compound **C8** (DMSO)

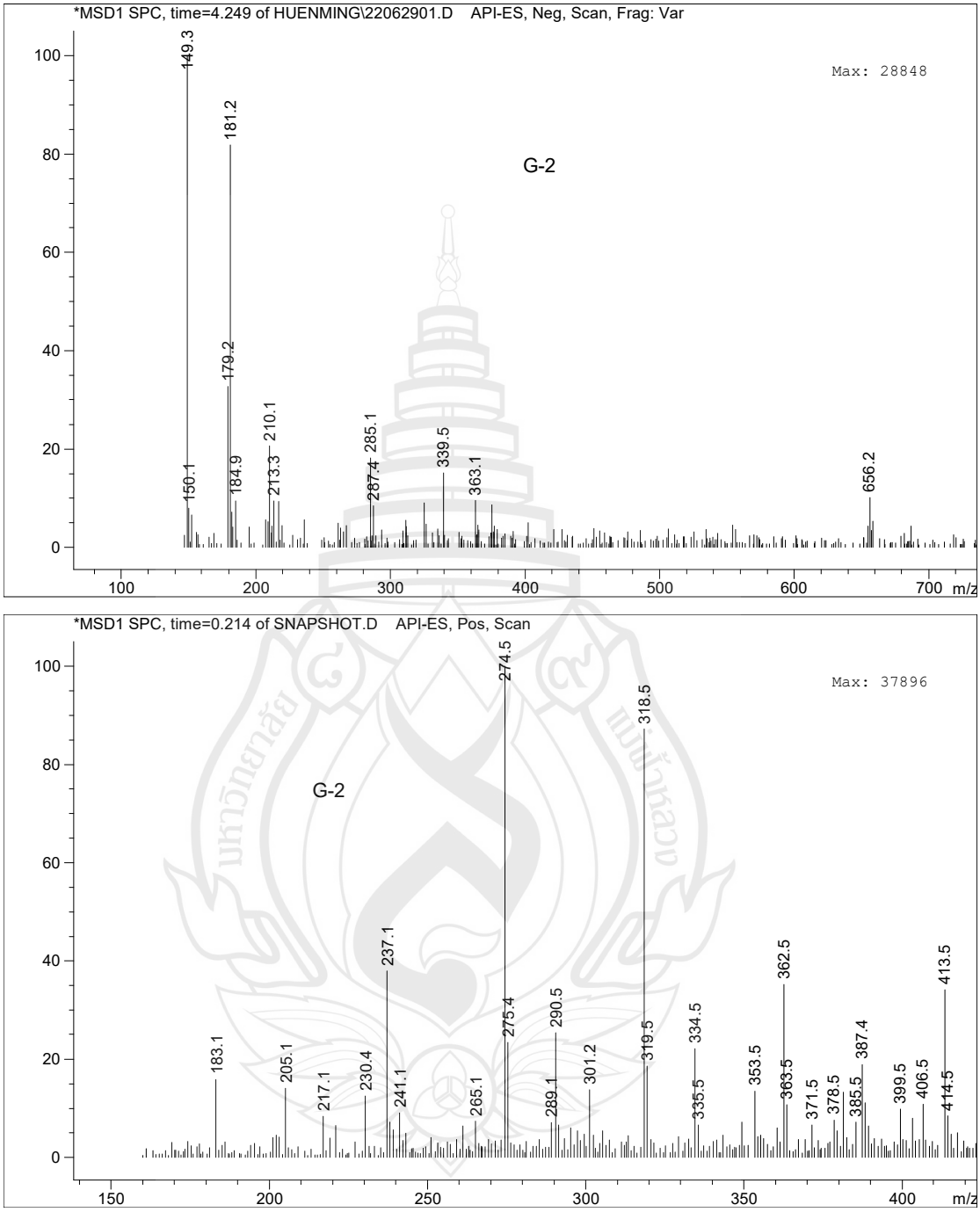

Figure A49 ESIMS of compound **C8**

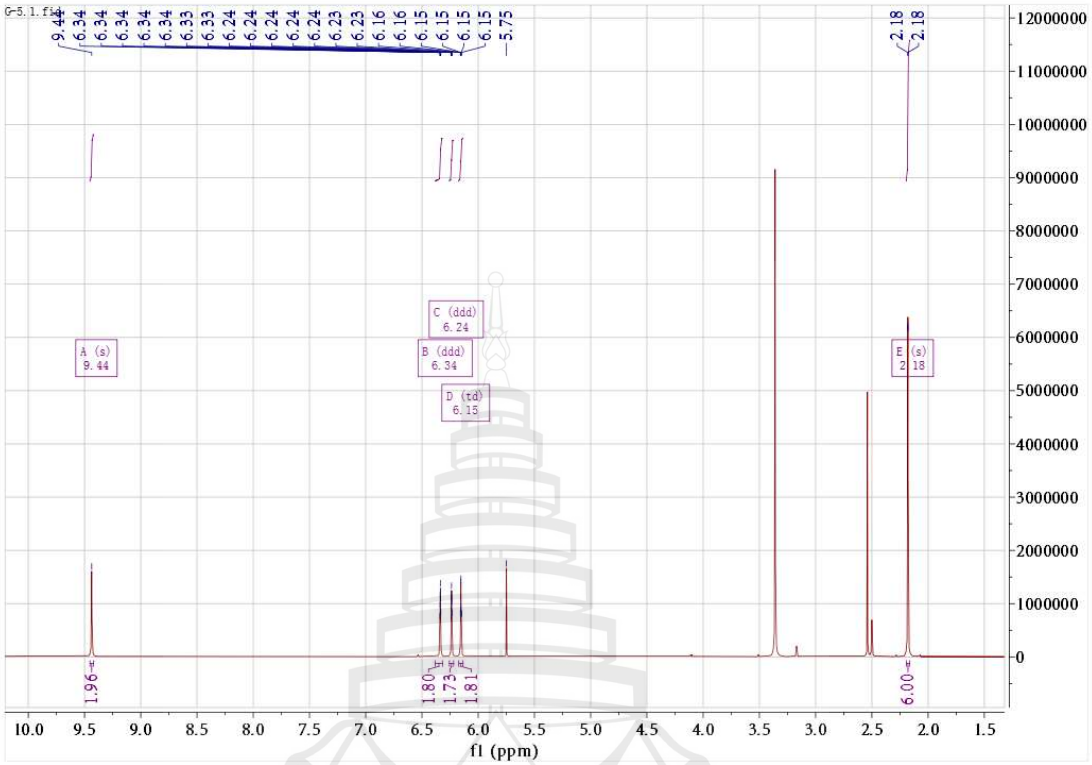

Figure A50 ^{1}H NMR spectrum of compound **C9** (600 MHz, DMSO)

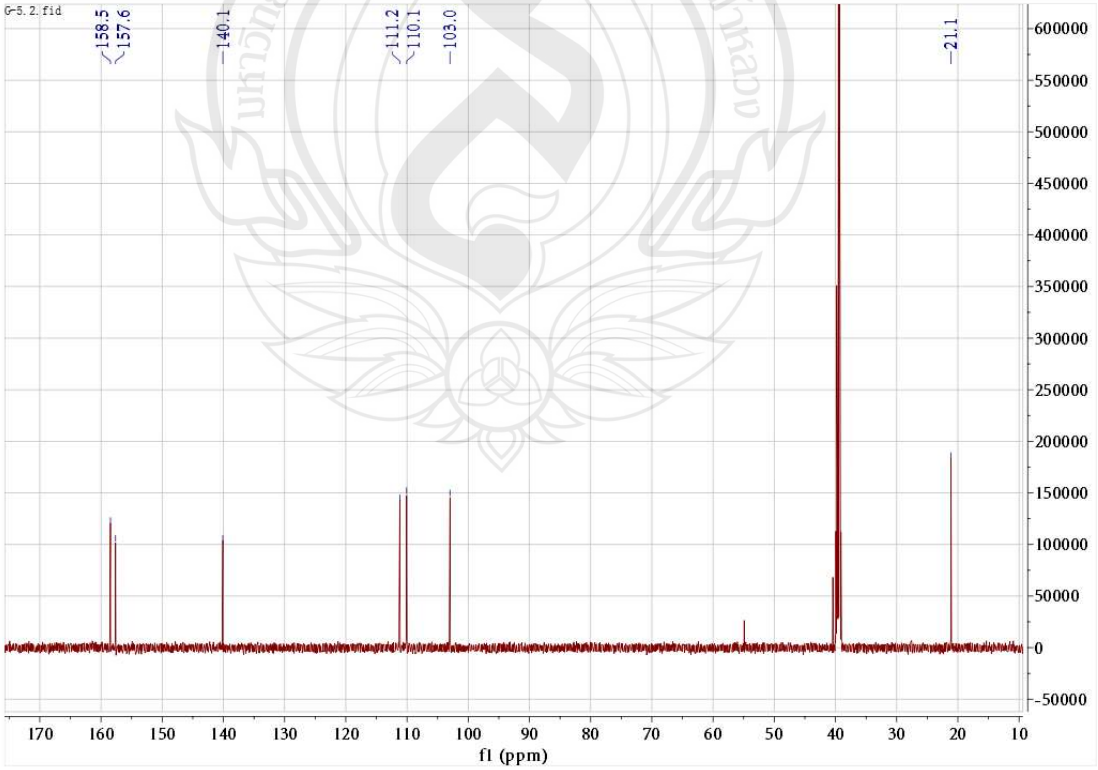

Figure A51 ^{13}C NMR spectrum of compound **C9** (150 MHz, DMSO)

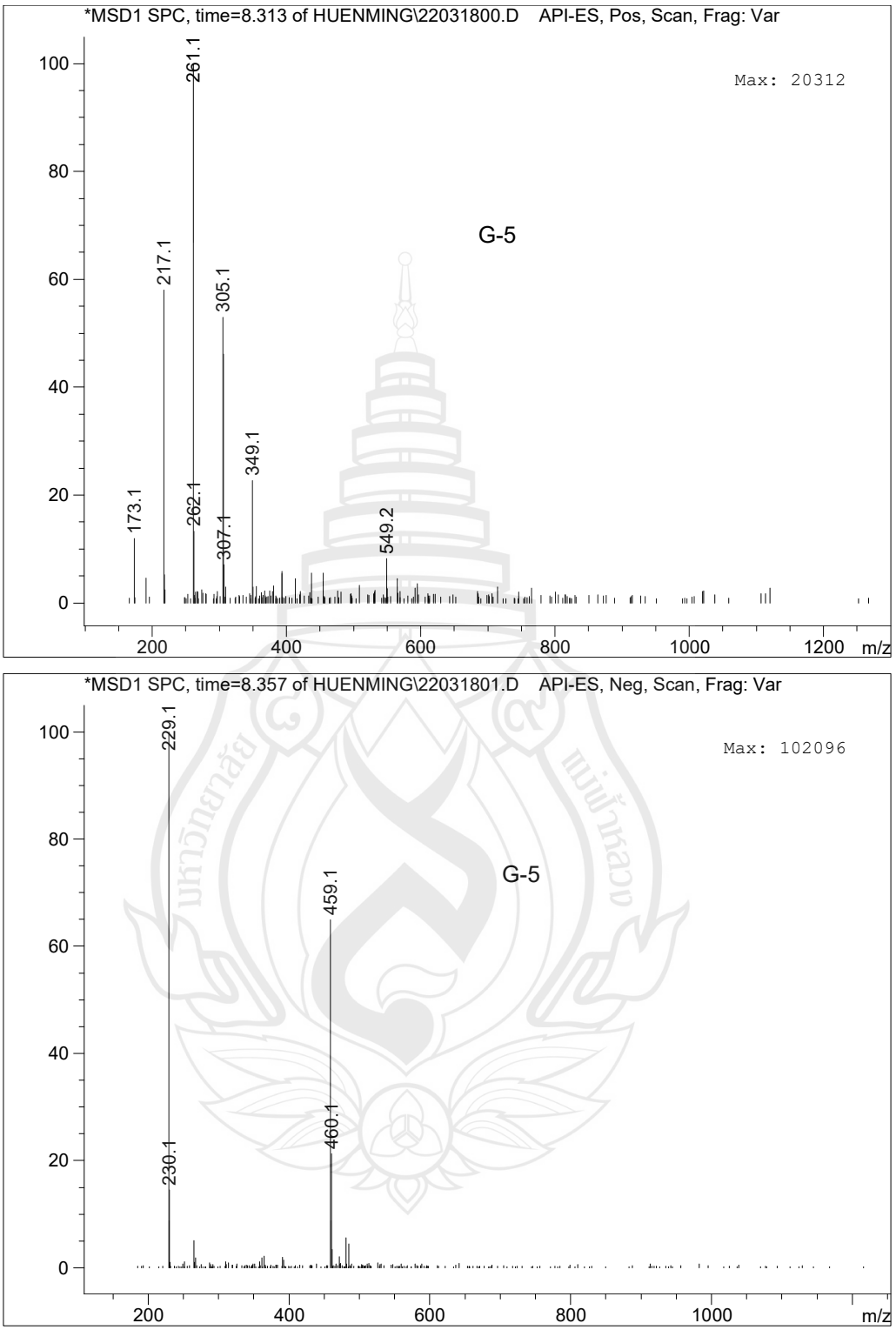

Figure A52 ESIMS of compound **C9**

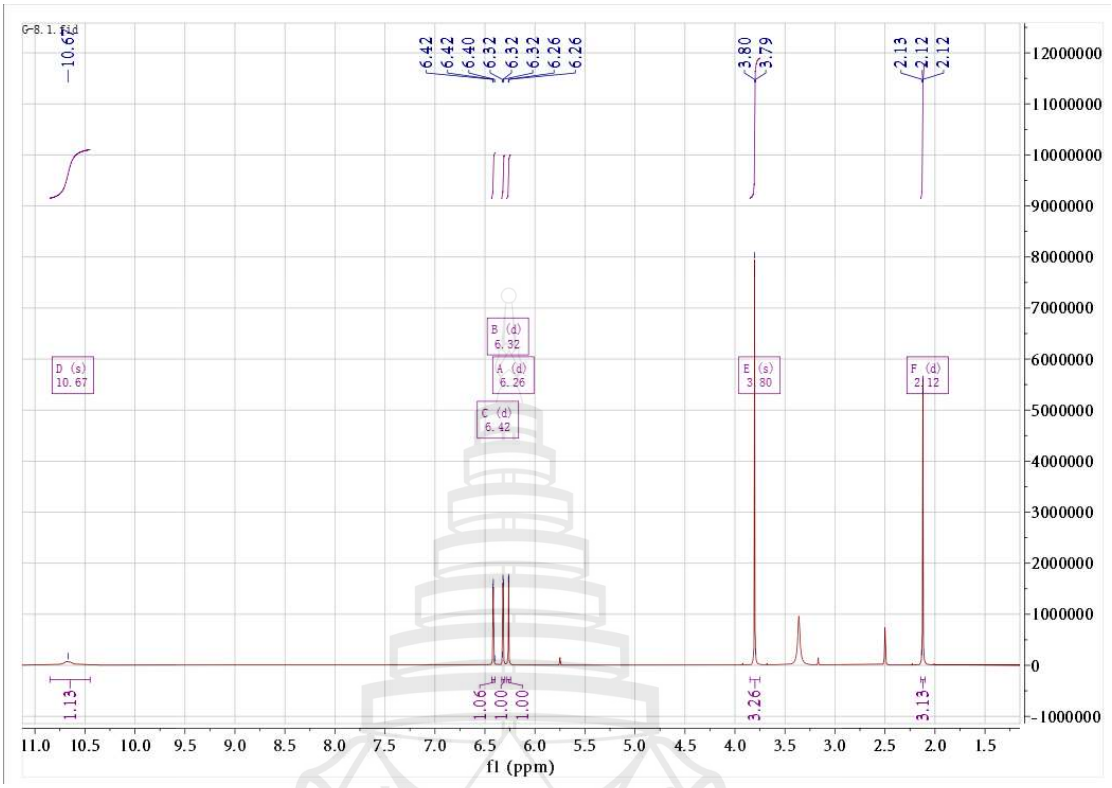

Figure A53 ^{1}H NMR spectrum of compound **C10** (600 MHz, DMSO)

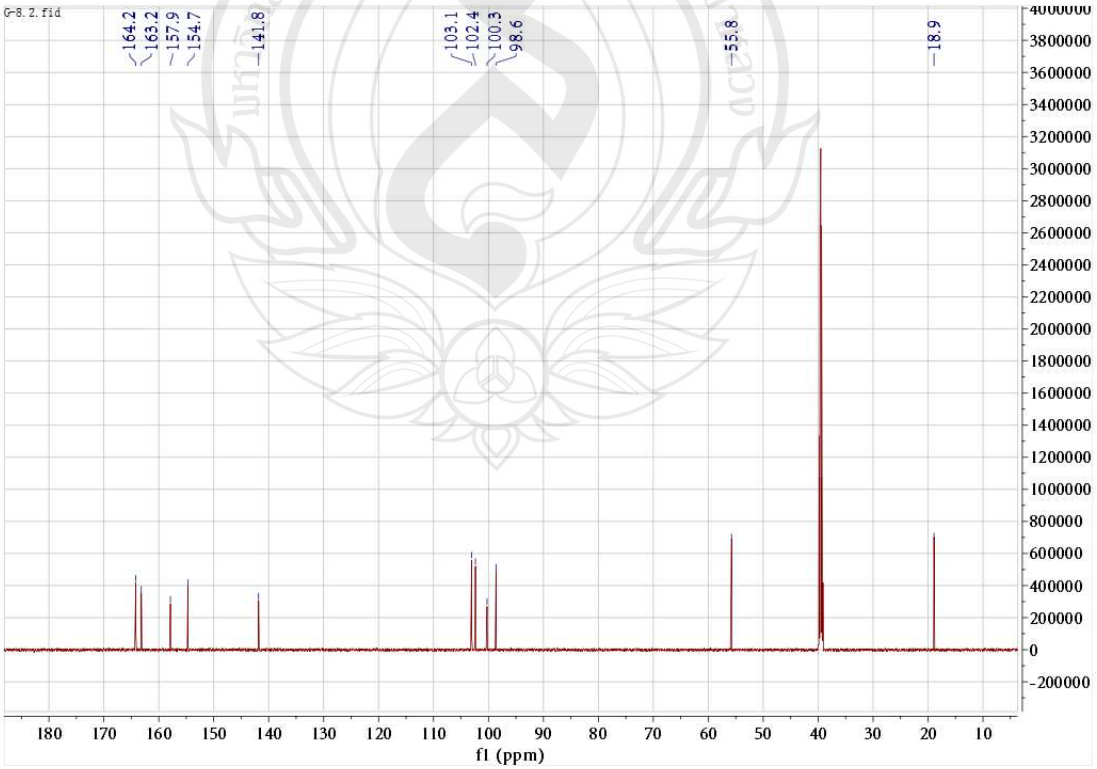

Figure A54 ^{13}C NMR spectrum of compound **C10** (150 MHz, DMSO)

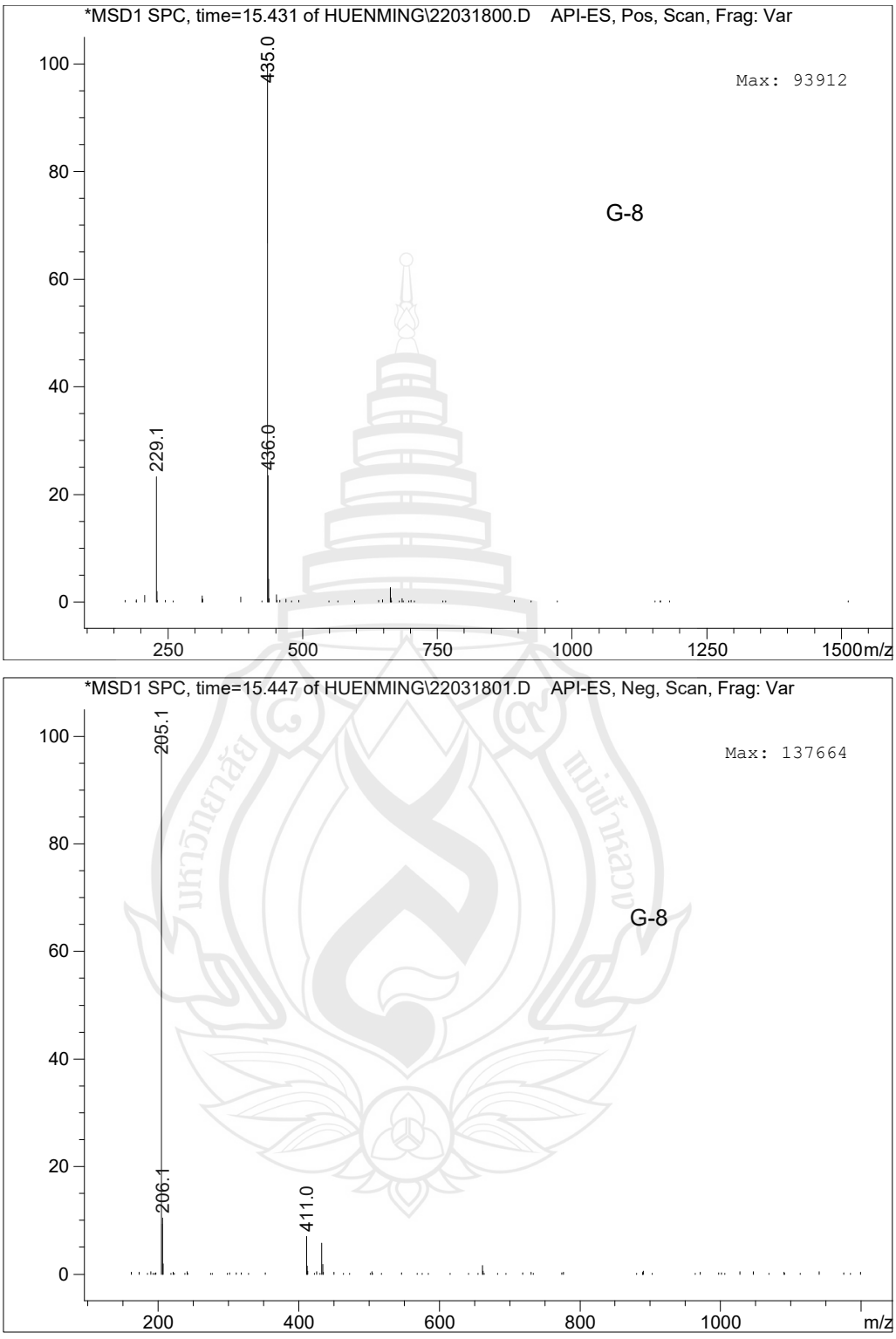

Figure A55 ESIMS of compound **C10**

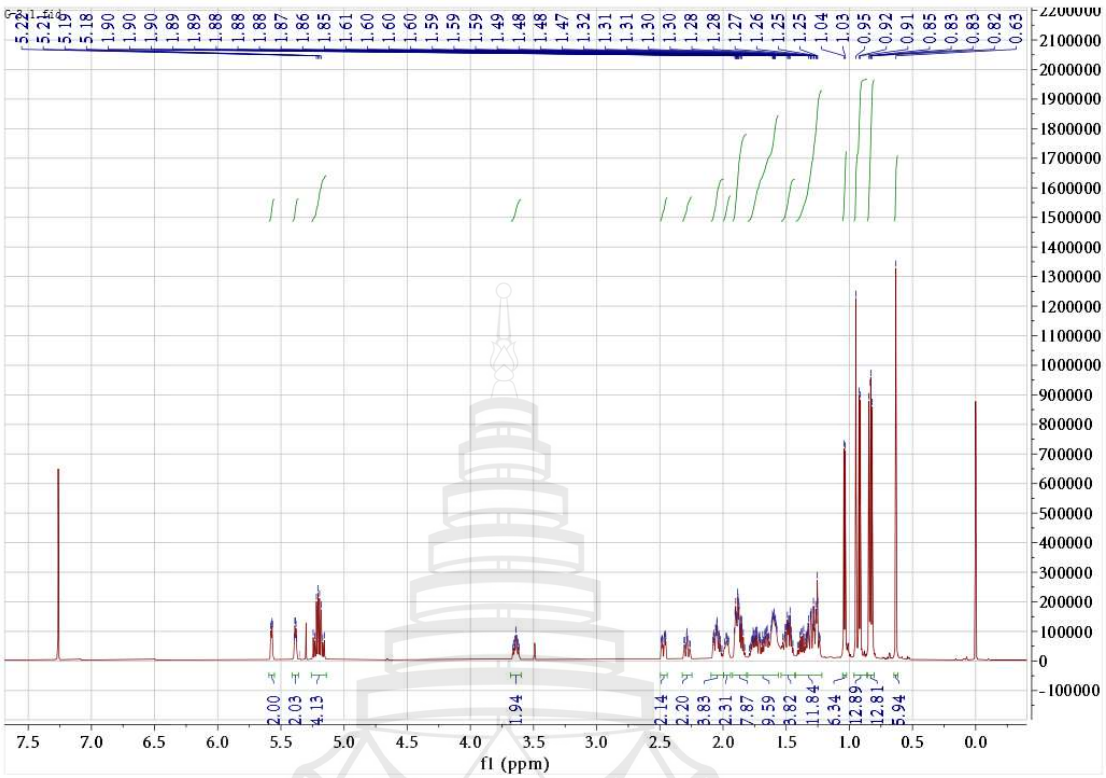

Figure A56 ^{1}H NMR spectrum of compound **C11** (600 MHz, $CDCl_3$)

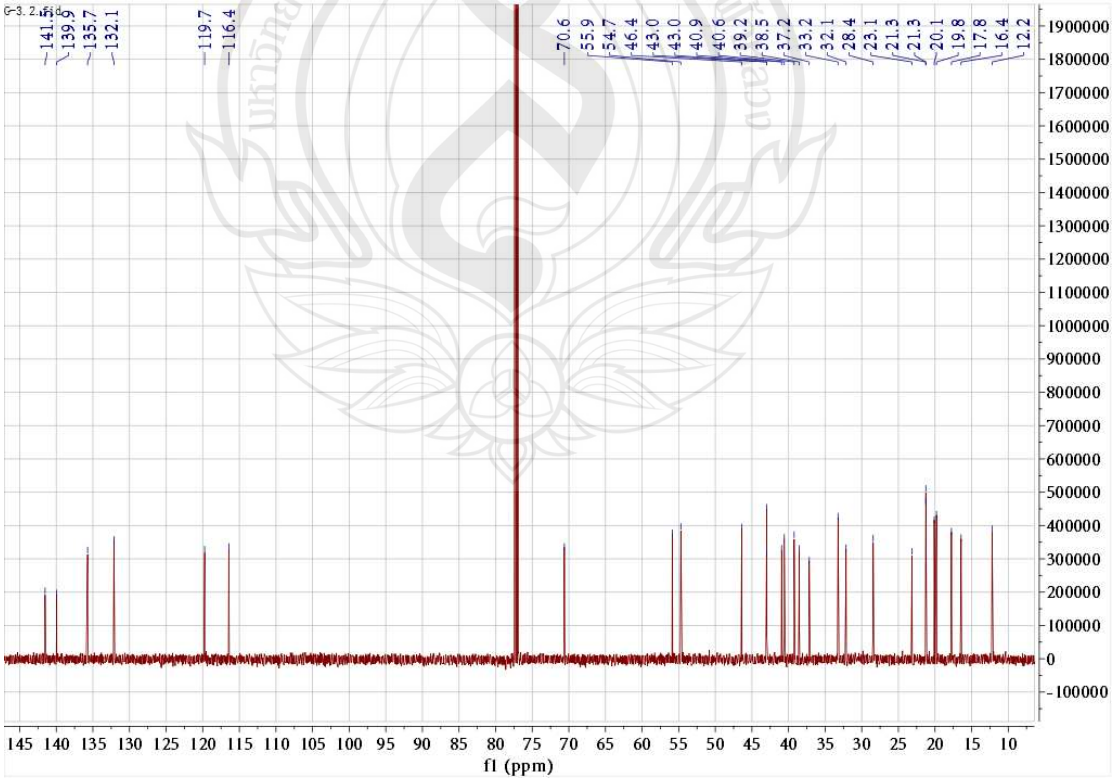

Figure A57 ^{13}C NMR spectrum of compound **C11** (150 MHz, $CDCl_3$)

The conformations of the isomers of compounds 4 and 9 were generated by MM+ method embedded in HypeChem. Density functional theory calculations were performed with the Gaussian 16 package (Frisch et al., 2019). The remaining conformers were optimized at the B3LYP/6-31G(d) level in gas phase and the conformers within an energy window of 2 kcal/mol were kept. NMR shielding tensors were calculated with the GIAO method at the mPW1PW91/6- 311G(d,p) level with the IEFPCM solvent model in DMSO. The shielding constants were converted into chemical shifts by referencing to TMS at 0 ppm according to the formula $\delta cal = \sigma TMS - \sigma cal$, where the σTMS (the shielding constant of TMS) was calculated at the same level. DP4+ probability analysis was performed using the calculated NMR shielding tensors with DP4+ excel file (Grimblat et al., 2015). ECD spectra were calculated by the TDDFT methodology at the B3LYP/def2TZVP utilizing IEFPCM in methanol.

References

Frisch, M. J., Trucks, G. W., Schlegel, H. B., Scuseria, G. E., Robb, M. A., Cheeseman, J. R., . . . Fox, D. J. (2019). *Gaussian 16, Revision C.01*. Gaussian, Inc.

Grimblat, N., Zanardi, M. M., & Sarotti, A. M. (2015). Beyond DP4: An improved probability for the stereochemical assignment of isomeric compounds using quantum chemical calculations of NMR shifts. *The Journal of Organic Chemistry, 80*, 12526–12534. https://doi.org/10.1021/acs.joc.5b02396

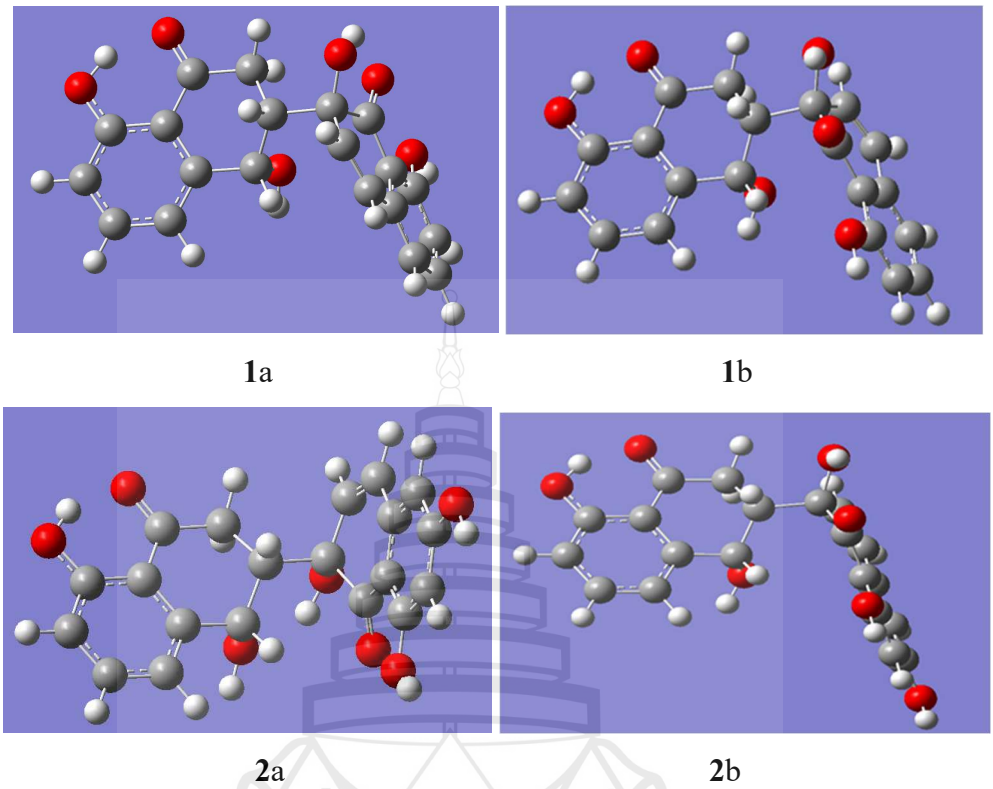

1a **1**b

2a **2**b

Figure A58 Optimized geometries of isomers of **C5** and **C6** at B3LYP/6-31G(d) level

Table A3 Optimized cartesian coordinates of conformers of **C5** at B3LYP/6-31G(d) level

		1a			**1b**	
C	-9.4233	-4.1044	2.0695	-9.8397	-3.7055	0.9459
C	-9.924	-2.8891	2.5292	-10.2549	-2.4946	1.4941
C	-9.2079	-1.7107	2.3109	-9.3453	-1.4459	1.6407
C	-7.9805	-1.7324	1.624	-8.0049	-1.5958	1.2396
C	-7.4808	-2.9615	1.167	-7.5911	-2.8221	0.6936
C	-8.2081	-4.1404	1.3925	-8.516	-3.8679	0.5472
C	-7.2095	-0.45	1.434	-7.0273	-0.4665	1.4689
C	-6.2959	-0.4854	0.189	-5.8441	-0.5158	0.4859
C	-5.3978	-1.7337	0.2753	-5.1837	-1.9025	0.5471
C	-6.1832	-3.0097	0.4517	-6.1729	-3.0167	0.2974
C	-5.4441	0.8146	0.0319	-4.8066	0.6332	0.6643
C	-4.6049	0.7964	-1.217	-4.007	0.6295	1.9302
C	-4.8617	1.5133	-2.3166	-4.0968	1.5679	2.8799
C	-6.0257	2.3935	-2.3705	-5.035	2.6809	2.7423
C	-6.7878	2.6688	-1.2234	-5.7463	2.901	1.5514
C	-6.3508	2.075	0.0746	-5.479	2.0002	0.3952
C	-6.3638	2.9996	-3.5888	-5.2104	3.5585	3.821
C	-7.4552	3.8642	-3.6705	-6.0874	4.639	3.7209
C	-8.2241	4.1239	-2.5383	-6.8054	4.8482	2.5455
C	-7.8941	3.525	-1.3204	-6.6382	3.9795	1.4656
O	-8.6968	3.7613	-0.2409	-7.3871	4.1822	0.3418
O	-6.705	2.5603	1.15	-5.727	2.3335	-0.7654
O	-6.4257	-0.2314	2.6038	-6.5731	-0.5492	2.8138
O	-5.7527	-4.0935	0.0561	-5.8239	-4.103	-0.1667
O	-7.7835	-5.3751	0.9792	-8.1895	-5.0925	0.0282
H	-6.9462	-0.5901	-0.6927	-6.2627	-0.4198	-0.5291
O	-4.4999	0.9102	1.1004	-3.8184	0.4838	-0.3786
H	-9.9747	-5.0255	2.2407	-10.5433	-4.5266	0.8329
H	-10.872	-2.8622	3.0615	-11.2882	-2.3714	1.8104
H	-9.616	-0.7715	2.6821	-9.6889	-0.5092	2.0773
H	-7.9273	0.372	1.3395	-7.5584	0.4848	1.3518
H	-4.8296	-1.8448	-0.655	-4.4116	-1.9795	-0.2271
H	-4.683	-1.6693	1.1034	-4.7147	-2.0923	1.5184
H	-3.7176	0.1668	-1.2021	-3.3041	-0.1884	2.0669
H	-4.2052	1.4544	-3.1799	-3.4867	1.5021	3.7755
H	-5.7769	2.8078	-4.4853	-4.6629	3.4093	4.7497
H	-7.7079	4.3311	-4.6199	-6.2134	5.3145	4.5639
H	-9.0818	4.7855	-2.6236	-7.4959	5.6853	2.4908
H	-9.2114	4.5714	-0.3887	-7.7493	5.0831	0.3448
H	-7.03	-0.2489	3.3684	-7.2649	-0.9657	3.3573
H	-6.9105	-5.2623	0.5382	-7.2319	-5.0784	-0.201
H	-5.035	0.9173	1.9238	-4.0714	1.1093	-1.0888

Functional	Solvent?	Basis Set	Type of Data
mPW1PW91	PCM	6-31+G(d,p)	Shielding Tensors

		DP4+	0.00%	100.00%	-	-	-
Nuclei	sp2?	xperimenta	Isomer 1	Isomer 2	Isomer 3	Isomer 4	Isomer 5
C		205.1	-7.8	-7.9			
C		32.8	159.0	160.2			
C		49.2	147.1	139.5			
C		65.9	123.4	125.5			
C	x	145.7	53.5	51.1			
C	x	119.7	81.2	80.7			
C	x	137.1	59.0	59.8			
C	x	117.1	79.7	79.9			
C	x	161.4	35.2	35.0			
C	x	114.7	82.3	82.7			
C	x	206.4	-7.5	-7.0			
C		73.5	111.6	117.1			
C	x	136.3	59.9	62.9			
C	x	125.7	69.7	68.3			
C	x	137.6	57.0	54.9			
C	x	118.9	78.1	78.2			
C	x	137.8	61.6	60.2			
C	x	117.1	82.1	82.4			
C	x	161.5	41.8	41.4			
C	x	113.2	79.5	82.3			

Figure A59 The results of the $DP4^+$ analysis of **C5**

Table A4 Optimized cartesian coordinates of conformers of **C6** at B3LYP/6-31G(d) level

		C6a			C6b	
C	-9.3964	-4.235	2.2546	-9.9012	-3.712	0.8603
C	-9.9058	-3.0171	2.6976	-10.2848	-2.5119	1.4533
C	-9.1999	-1.8363	2.4598	-9.3426	-1.5033	1.6617
C	-7.9743	-1.8585	1.7697	-8.0006	-1.6828	1.2783
C	-7.4657	-3.0901	1.3298	-7.6189	-2.8987	0.6873
C	-8.1827	-4.2713	1.5749	-8.5764	-3.9038	0.4788
C	-7.2143	-0.5729	1.558	-6.9899	-0.5985	1.5718
C	-6.3061	-0.6191	0.3095	-5.7876	-0.6494	0.612
C	-5.3966	-1.8582	0.4111	-5.1788	-2.0609	0.6273
C	-6.1695	-3.1383	0.6118	-6.201	-3.1264	0.3089
C	-5.4666	0.6859	0.1286	-4.7129	0.4519	0.8598
C	-4.6307	0.6544	-1.1222	-3.9381	0.3612	2.1377
C	-4.8929	1.3546	-2.2312	-4.0144	1.2557	3.1299
C	-6.0595	2.2305	-2.2951	-4.9137	2.4041	3.0313
C	-6.8239	2.515	-1.152	-5.5947	2.7059	1.8408
C	-6.3845	1.9388	0.1534	-5.3325	1.8547	0.646
C	-6.3977	2.8249	-3.5177	-5.0813	3.2333	4.1472
C	-7.4877	3.6848	-3.5987	-5.9187	4.3417	4.0759
C	-8.2653	3.9601	-2.4805	-6.609	4.6435	2.908
C	-7.933	3.3691	-1.2586	-6.4474	3.8199	1.7916
O	-8.7387	3.6071	-0.1808	-7.1666	4.0989	0.6639
O	-6.7447	2.4367	1.2211	-5.5368	2.261	-0.4994

Table A4 (continued)

	C6a			C6b		
O	-6.4274	-0.3291	2.7208	-6.5677	-0.7468	2.9213
O	-5.7298	-4.2247	0.2342	-5.8811	-4.2031	-0.1969
O	-7.7491	-5.5086	1.1791	-8.2822	-5.1157	-0.0873
H	-6.9591	-0.7431	-0.5677	-6.1806	-0.4955	-0.4061
O	-4.5208	0.8082	1.1928	-3.7093	0.3067	-0.1685
O	-7.7636	4.2377	-4.8138	-6.0385	5.1116	5.1945
H	-9.9399	-5.1579	2.4409	-10.6303	-4.5022	0.6989
H	-10.8526	-2.9901	3.232	-11.3192	-2.3661	1.7562
H	-9.6146	-0.8951	2.8181	-9.6621	-0.5747	2.1326
H	-7.9396	0.2413	1.4546	-7.4862	0.3743	1.4811
H	-4.8321	-1.9792	-0.5201	-4.3926	-2.1335	-0.133
H	-4.6784	-1.7741	1.2345	-4.7392	-2.3087	1.5993
H	-3.7405	0.0291	-1.1013	-3.2651	-0.4854	2.2471
H	-4.2385	1.2864	-3.0958	-3.4237	1.1273	4.0319
H	-5.8133	2.6299	-4.4144	-4.5603	3.0249	5.079
H	-9.1275	4.6136	-2.5583	-7.2739	5.4996	2.8685
H	-9.2182	4.4423	-0.3052	-7.4573	5.0253	0.6732
H	-7.0221	-0.3704	3.492	-7.2795	-1.1694	3.4334
H	-6.8781	-5.3956	0.7342	-7.3205	-5.1256	-0.2984
H	-5.0529	0.8186	2.0181	-3.8488	1.041	-0.8007
H	-8.5218	4.8397	-4.7323	-6.6322	5.8587	5.0126

	A	B	C	D	E	F	G	H
1	Functional		Solvent?		Basis Set		Type of Data	
2	■P▼1P▼91		PC■		6-31G(d)		Shielding Tensors	
3								
12			DP4+	3.13%	96.87%	-	-	-
14	Nuclei	sp2?	xperimenta	Isomer 1	Isomer 2	Isomer 3	Isomer 4	Isomer 5
15	C		205	-7.7	-8.0			
16	C		33.2	159.6	160.2			
17	C		48.8	147.2	139.7			
18	C		65.7	124.3	125.2			
19	C	x	146	53.3	51.2			
20	C	x	119.5	80.2	80.7			
21	C	x	137.2	58.4	59.8			
22	C	x	117	79.5	79.8			
23	C	x	161.4	35.4	34.7			
24	C	x	114.7	82.5	82.8			
25	C	x	203.4	-3.7	-3.5			
26	C		73.6	112.6	117.6			
27	C	x	136.8	59.7	61.3			
28	C	x	125.3	70.7	68.4			
29	C	x	139.6	55.6	52.8			
30	C	x	107.9	90.7	90.1			
31	C	x	166.2	36.4	35.5			
32	C	x	101.5	96.9	97.7			
33	C	x	164.8	40.1	38.8			
34	C	x	106.7	88.0	88.0			

Figure A60 The results of the $DP4^{+}$ analysis of **C6**

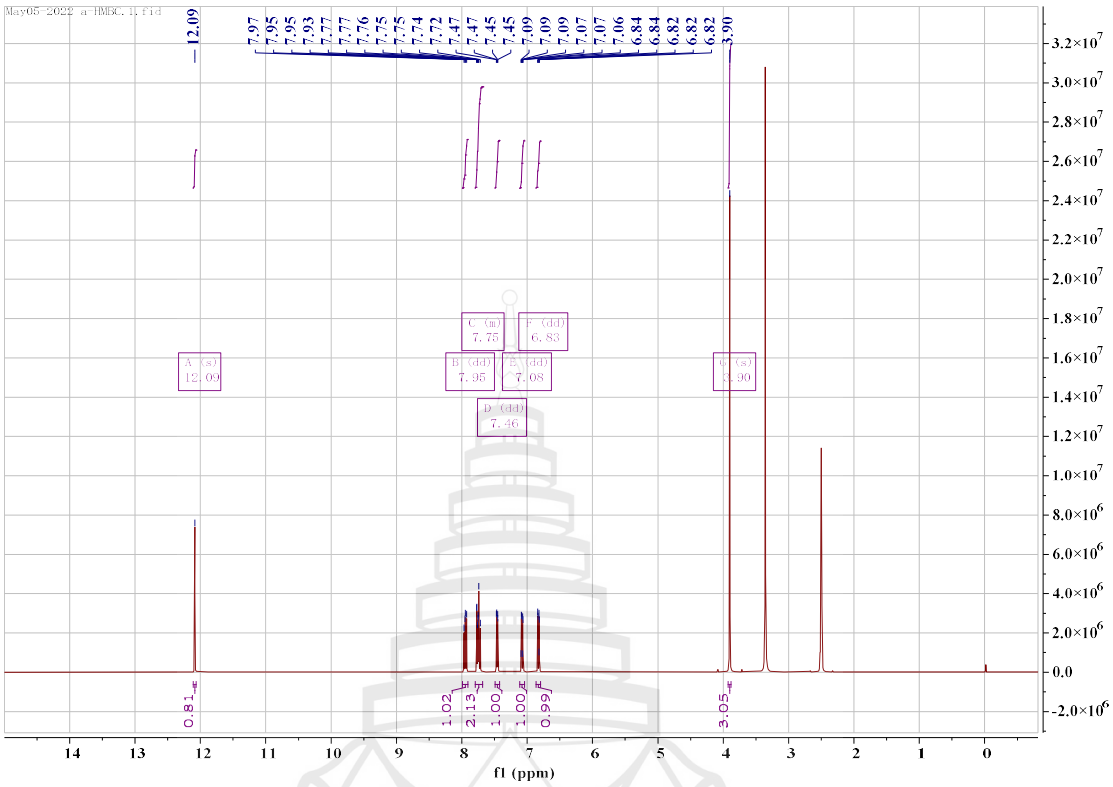

Figure A61 ^{1}H NMR spectrum of compound **C12** (400 MHz, DMSO)

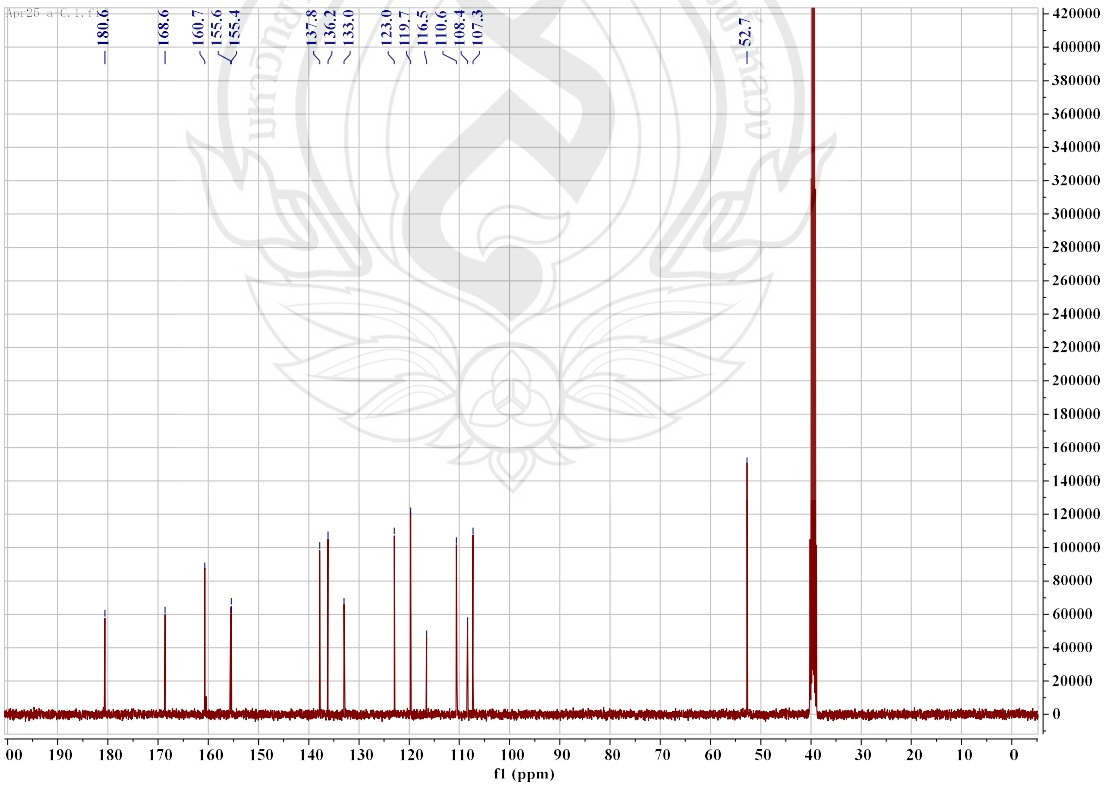

Figure A62 ^{13}C NMR spectrum of compound **C12** (100 MHz, DMSO)

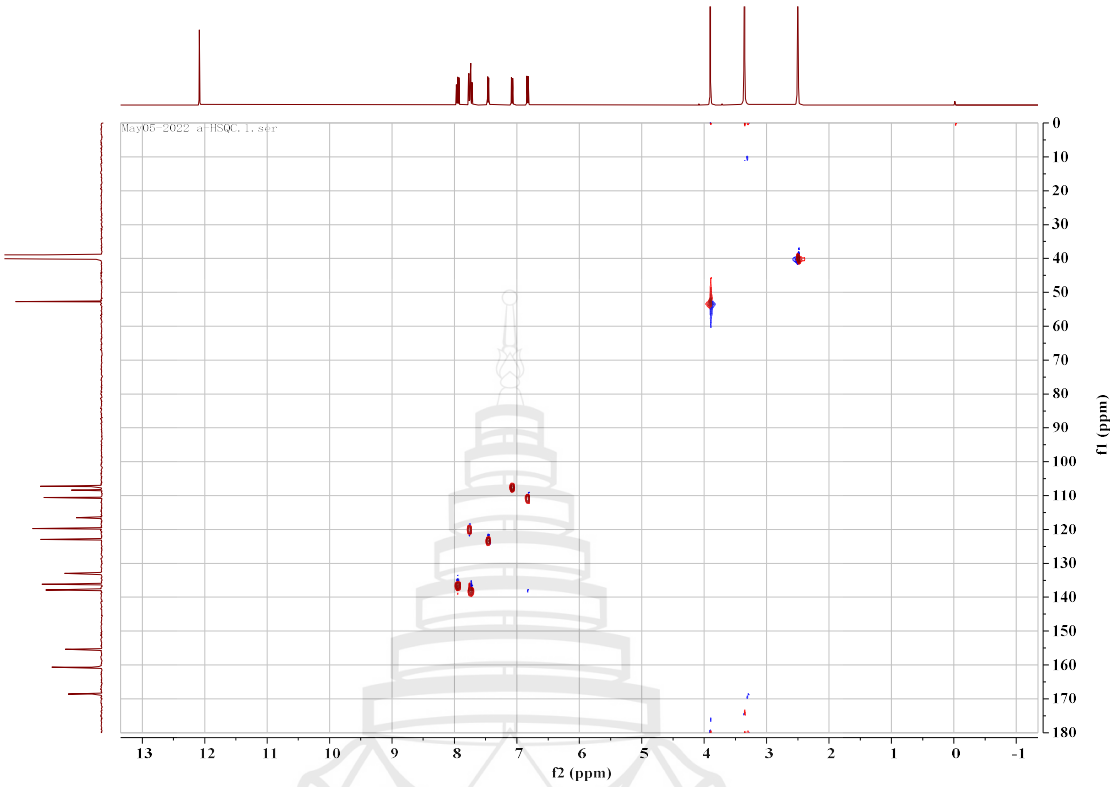

Figure A63 HSQC spectrum of compound **C12** (100 MHz, DMSO)

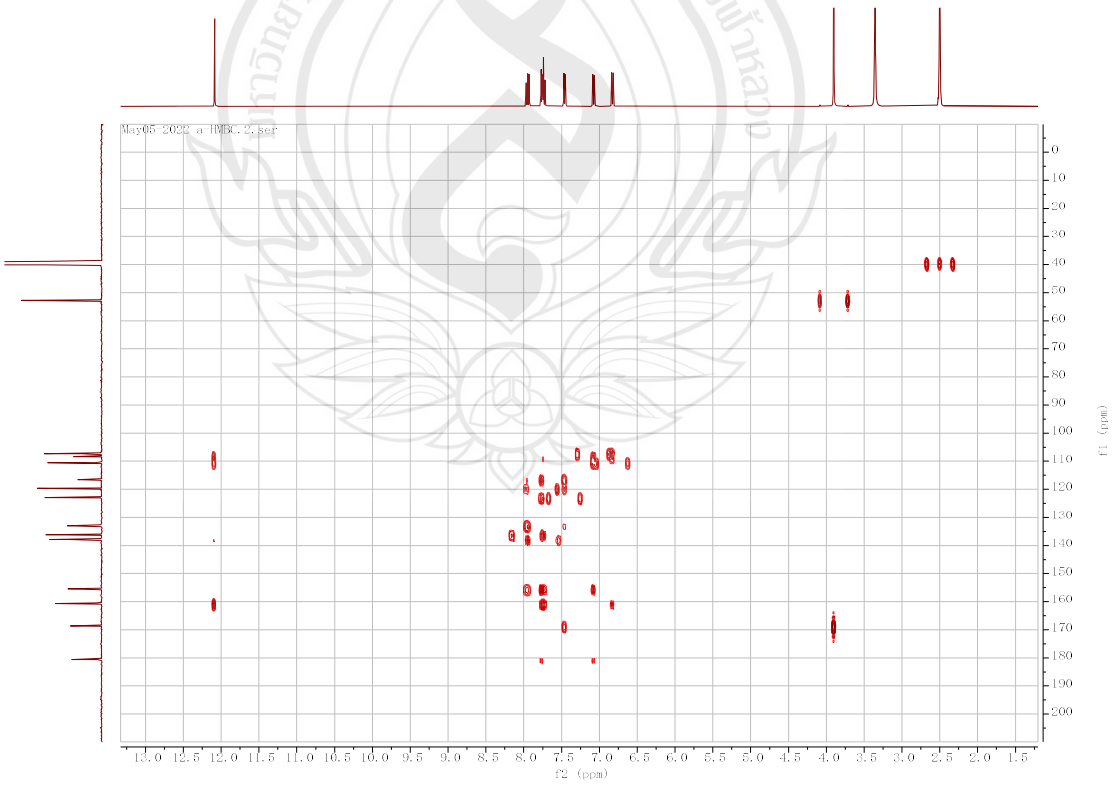

Figure A64 HMBC spectrum of compound **C12** (150 MHz, DMSO)

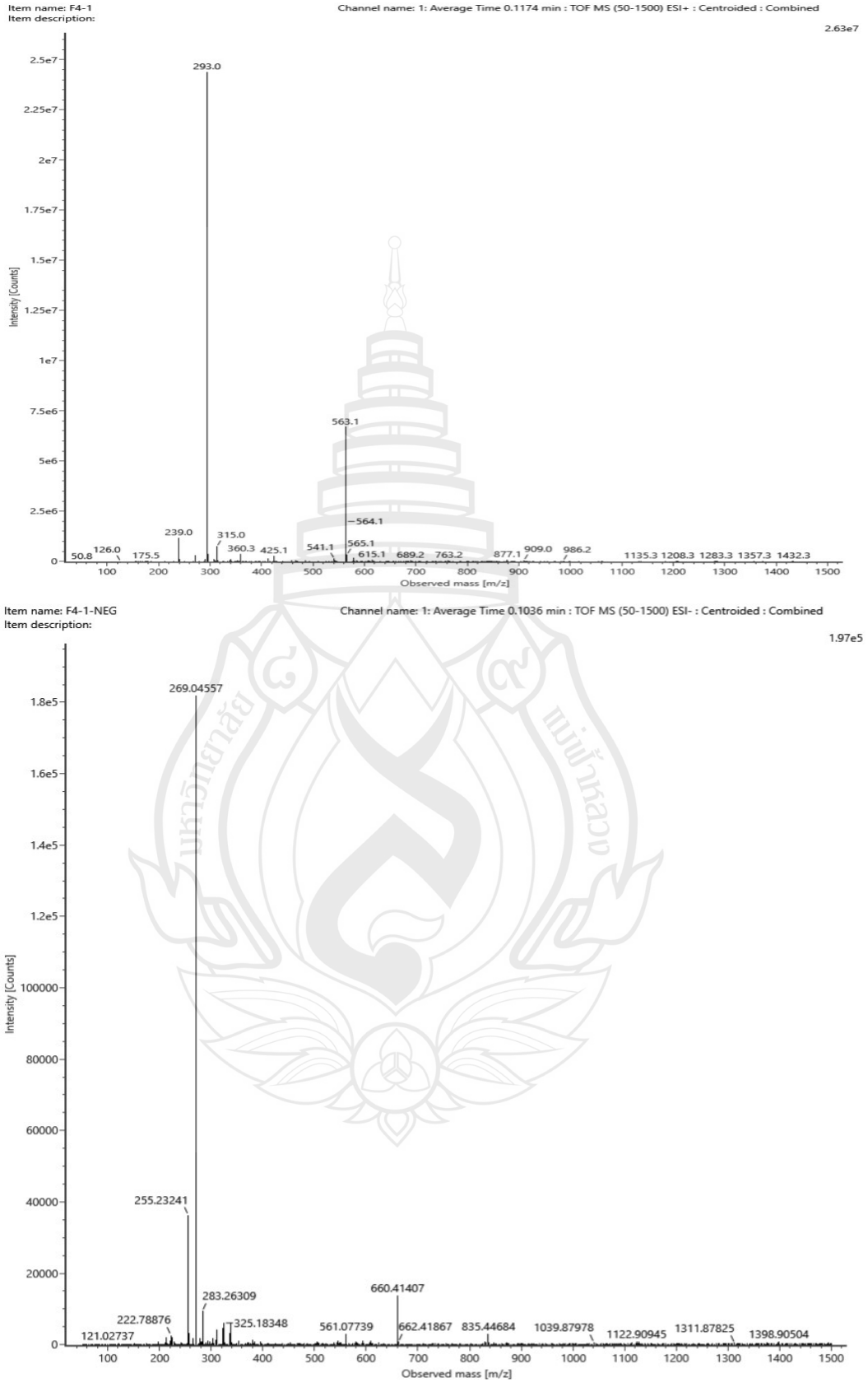

Figure A65 ESIMS of compound **C12**

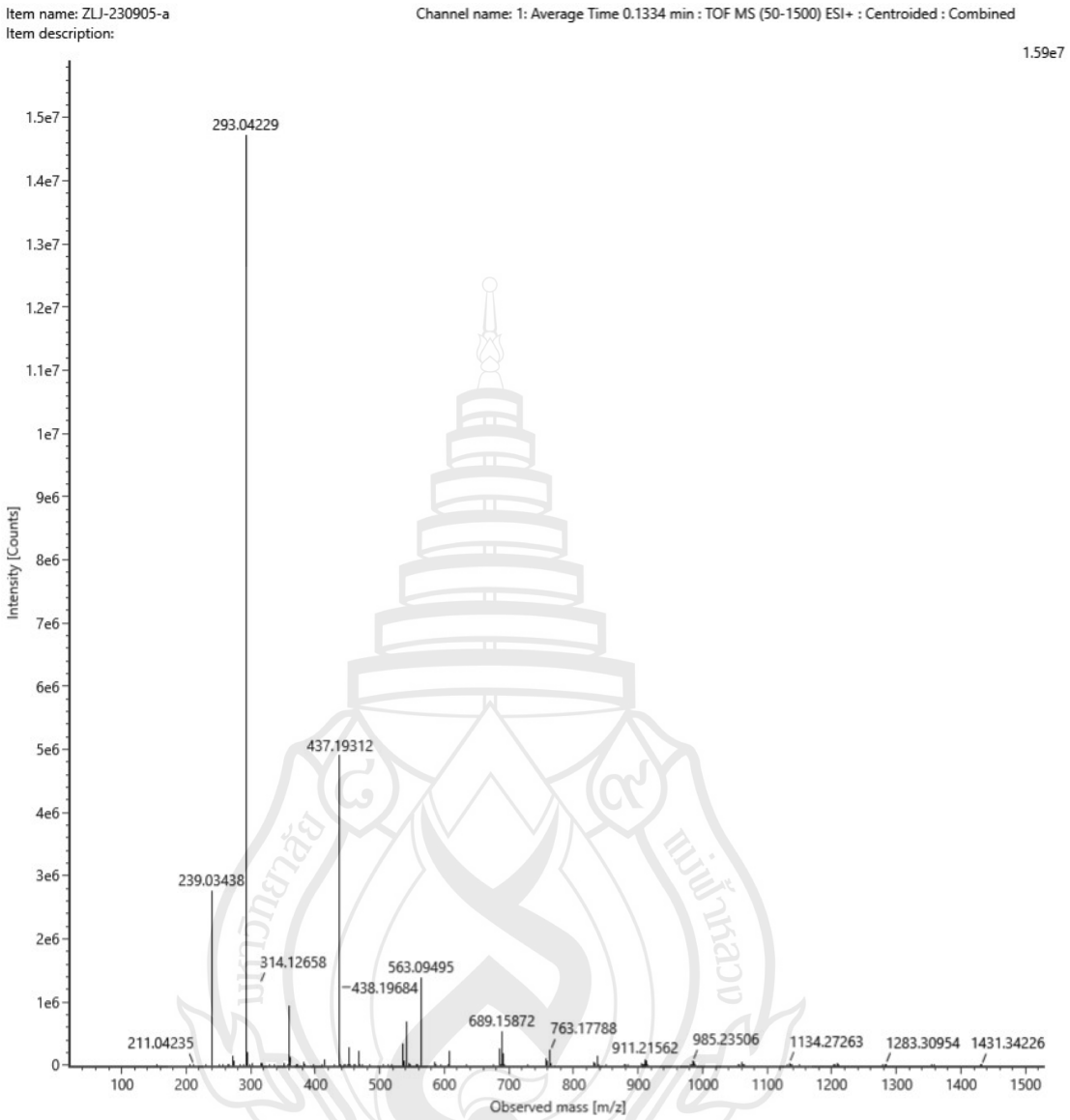

Note $[M+Na]^+$

Composition	$C_{15}H_{10}O_5Na$
i-FIT Confidence (%)	100.000000
Predicted m/z	293.042045
m/z error (PPM)	0.840616

Figure A66 HR-ESIMS of compound **C12** (ESI+)

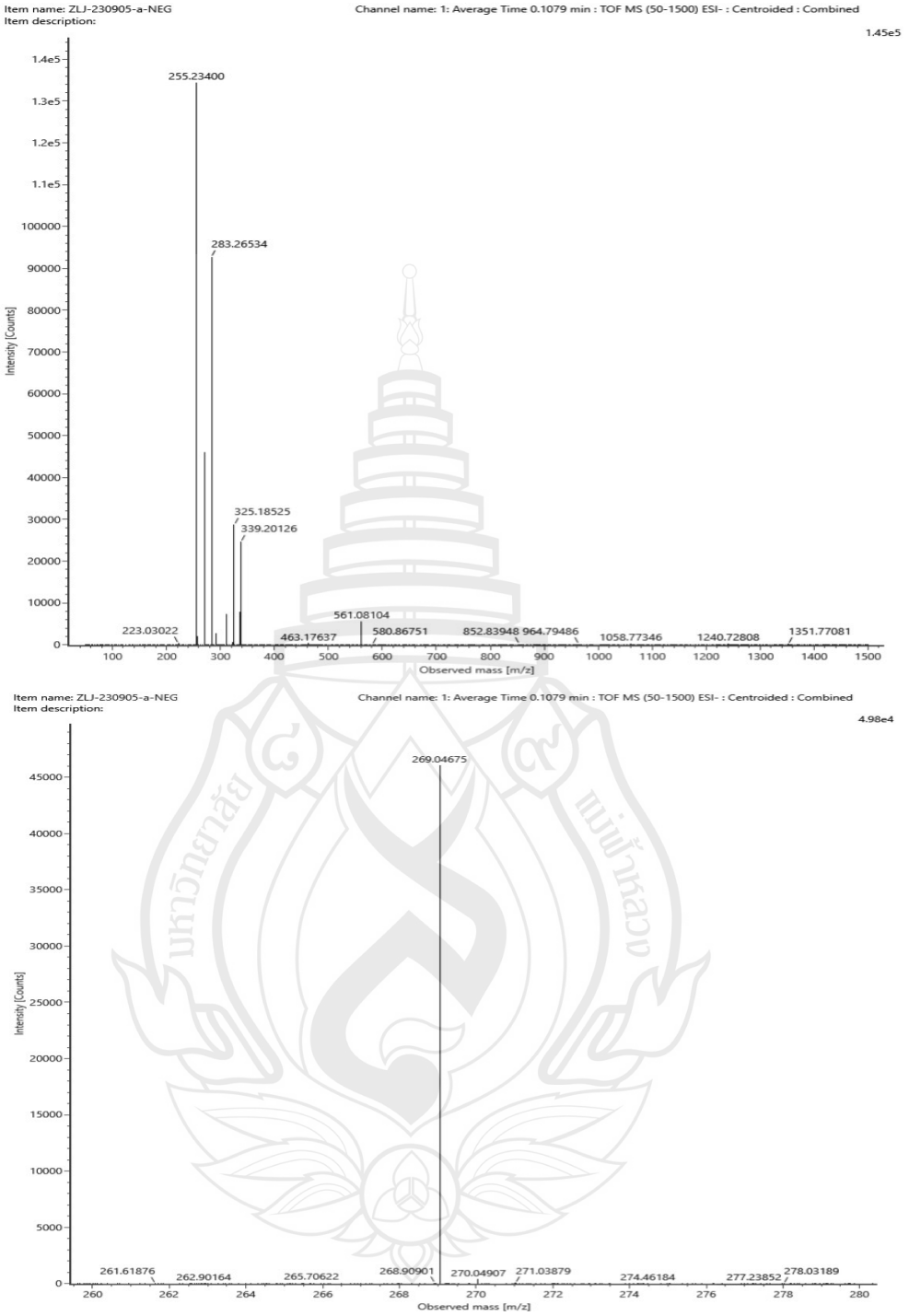

Note $[M-H]^-$

Composition	$C_{15}H_9O_5$
i-FIT Confidence (%)	100.000000
Predicted m/z	269.045547
m/z error (PPM)	4.454744

Figure A67 HRESIMS of compound **C12** (ESI-)

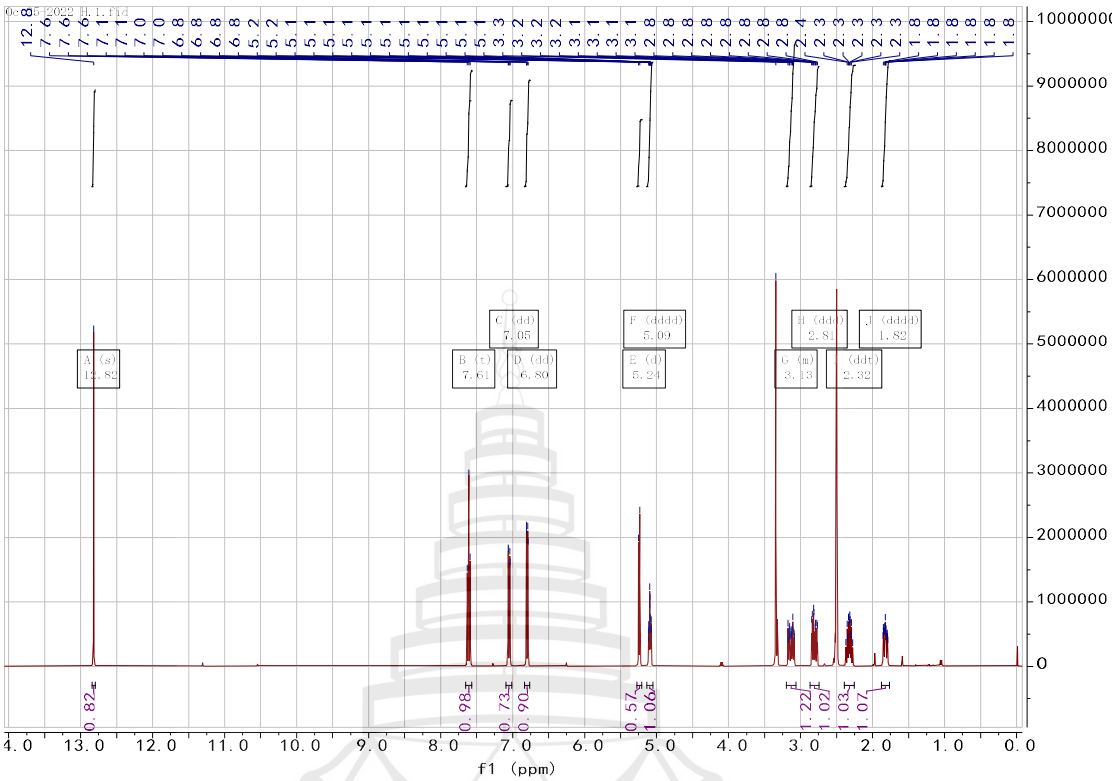

Figure A68 ^{1}H NMR spectrum of compound **C13** (400 MHz, DMSO)

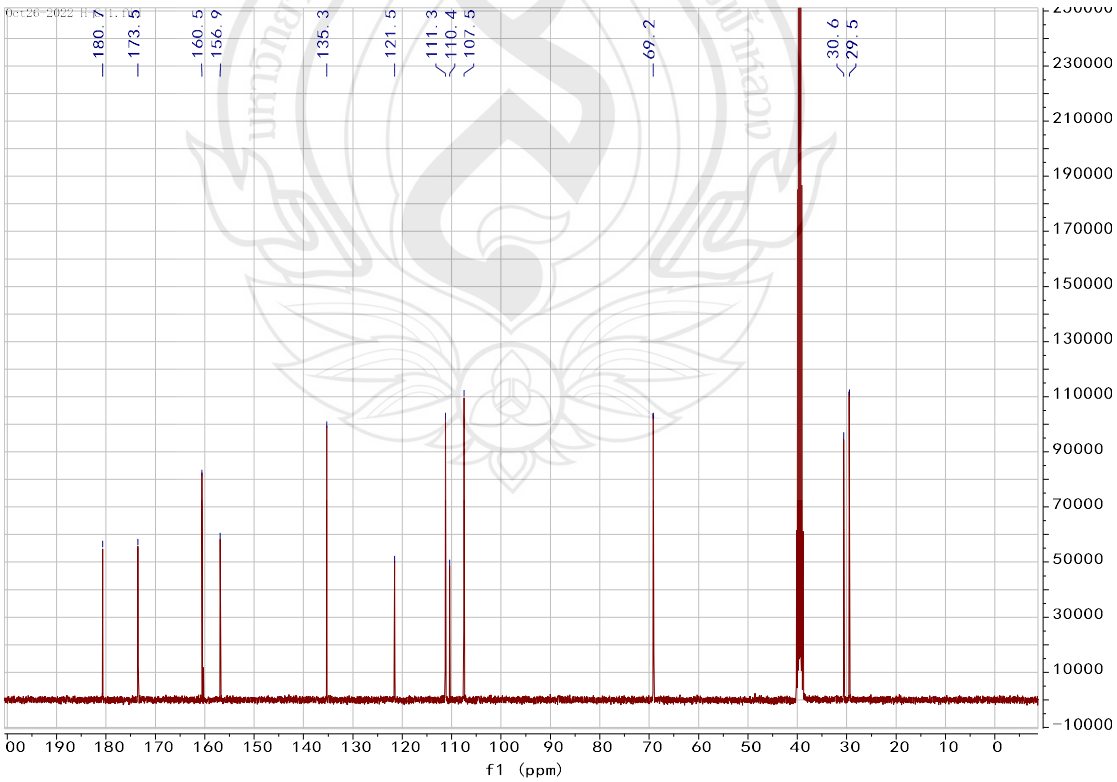

Figure A69 ^{13}C NMR spectrum of compound **C13** (100 MHz, DMSO)

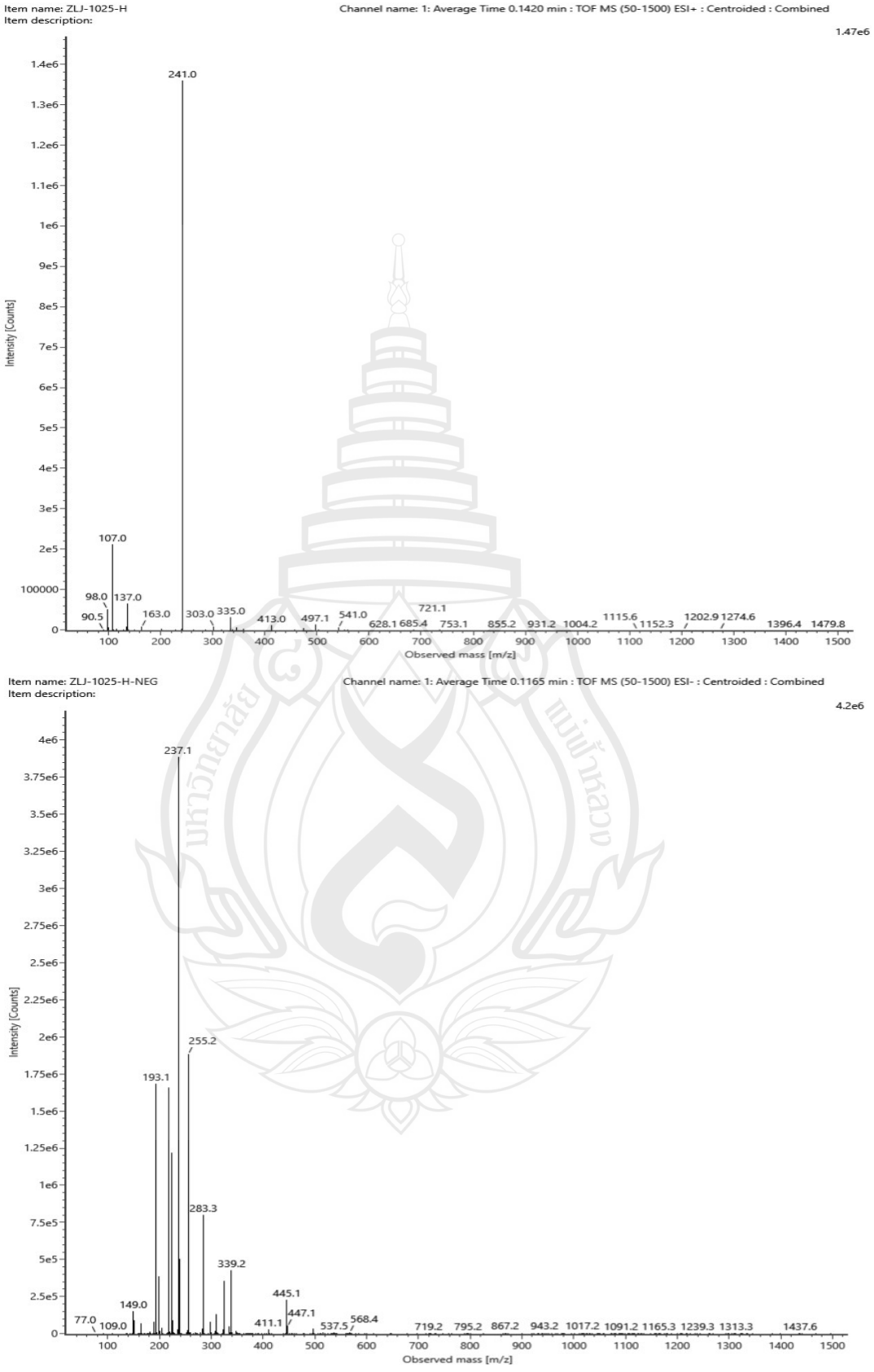

Figure A70 ESIMS of compound **C13**

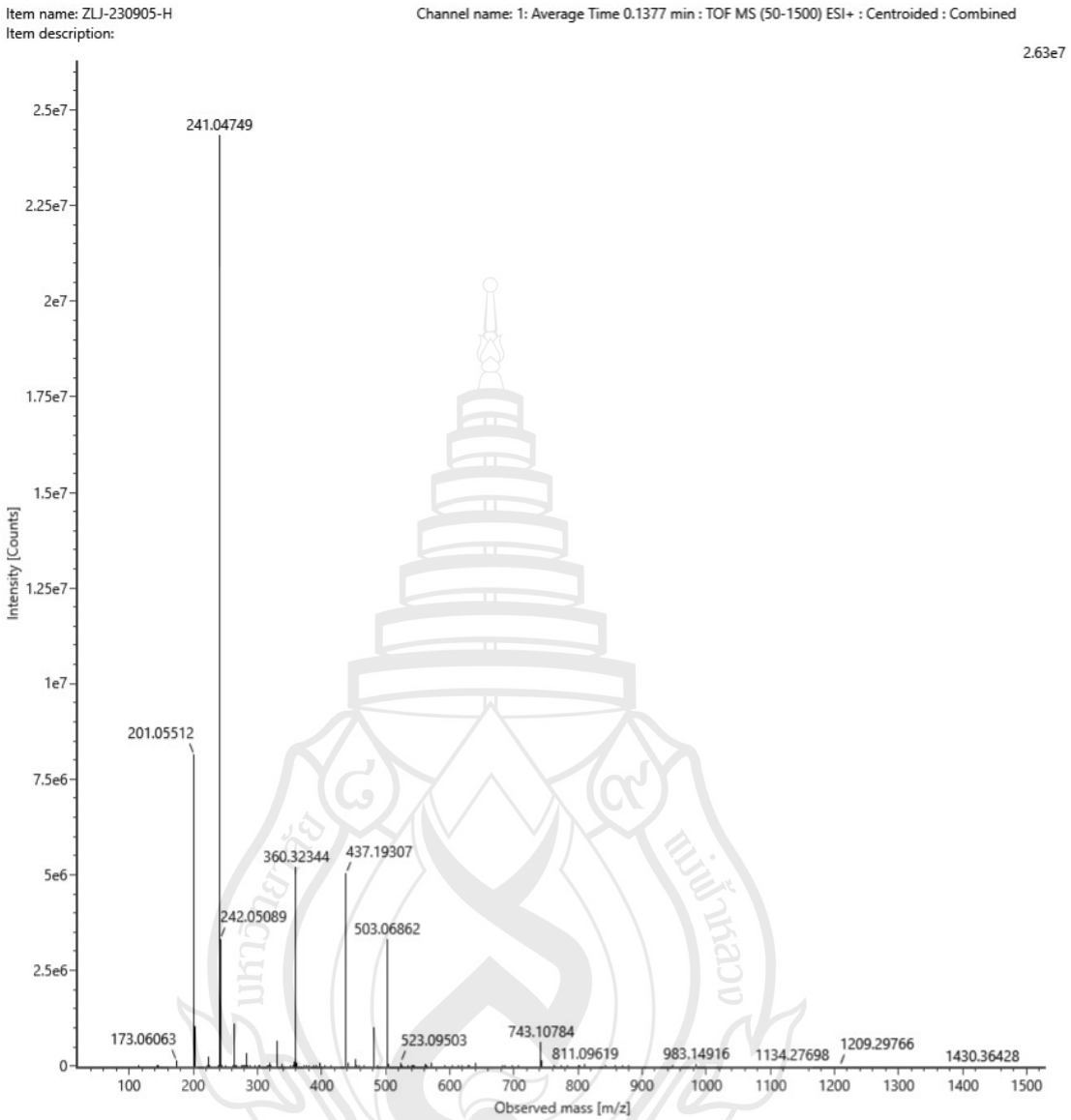

Note $[M+Na]^+$

Composition	$C_{12}H_{10}O_4Na$
i-FIT Confidence (%)	100.000000
Predicted m/z	241.047130
m/z error (PPM)	1.500214

Figure A71 HR-ESIMS of compound **C13** (ESI+)

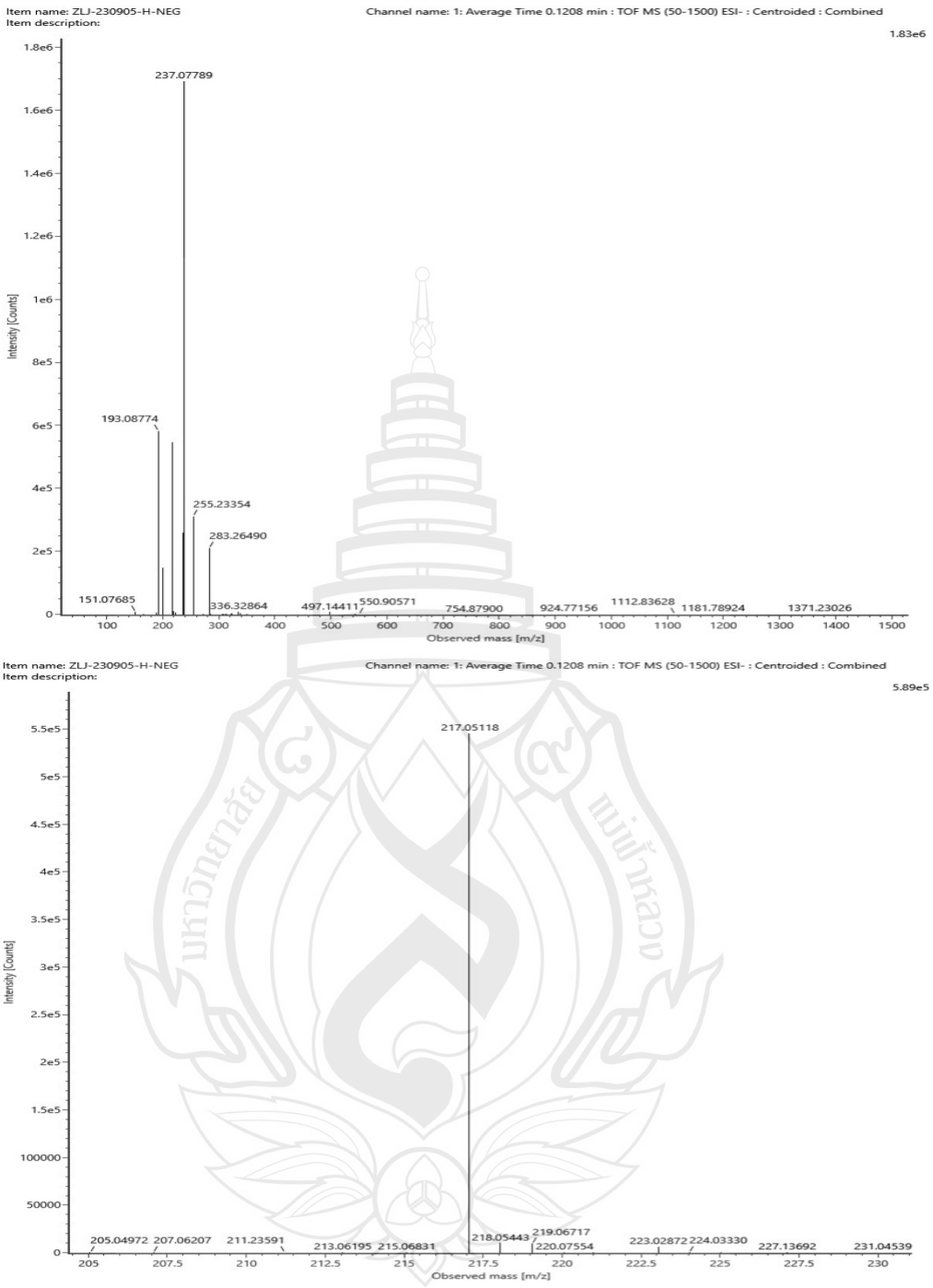

Note $[M-H]^-$

Composition	$C_{12}H_9O_4$
i-FIT Confidence (%)	100.000000
Predicted m/z	217.050632
m/z error (PPM)	2.511454

Figure A72 HR-ESIMS of compound **C13** (ESI-)

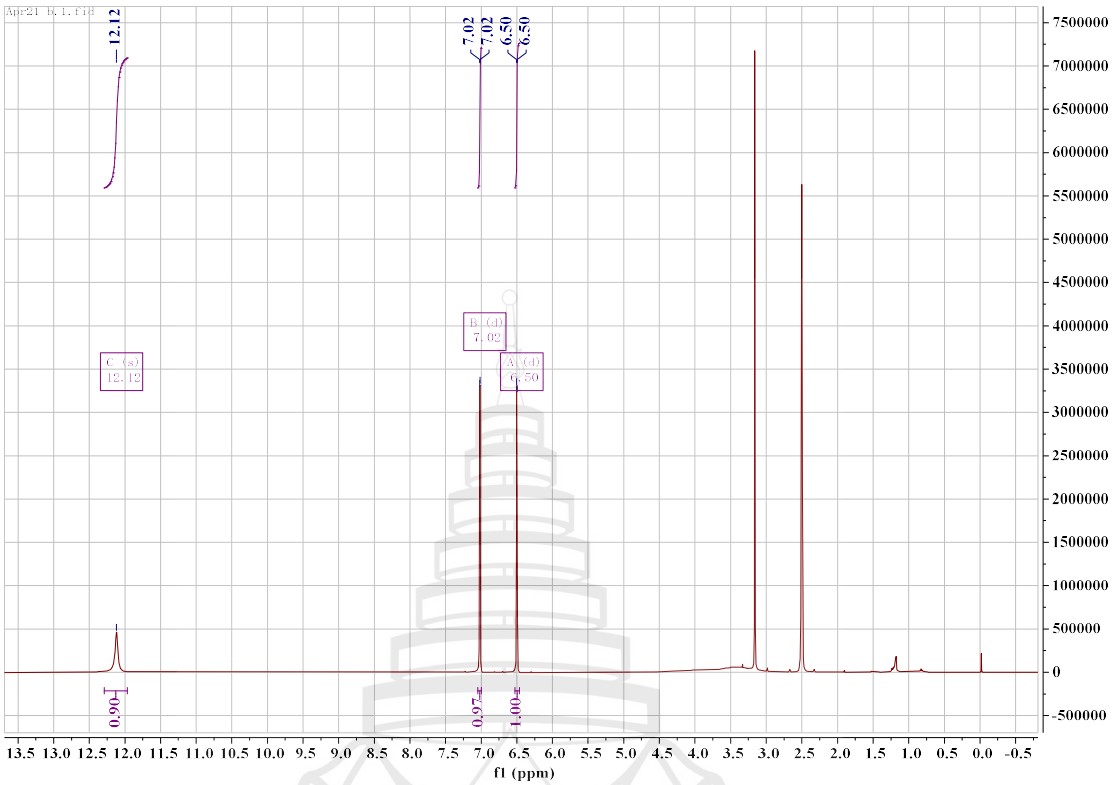

Figure A73 ^{1}H NMR spectrum of compound **C14** (400 MHz, DMSO)

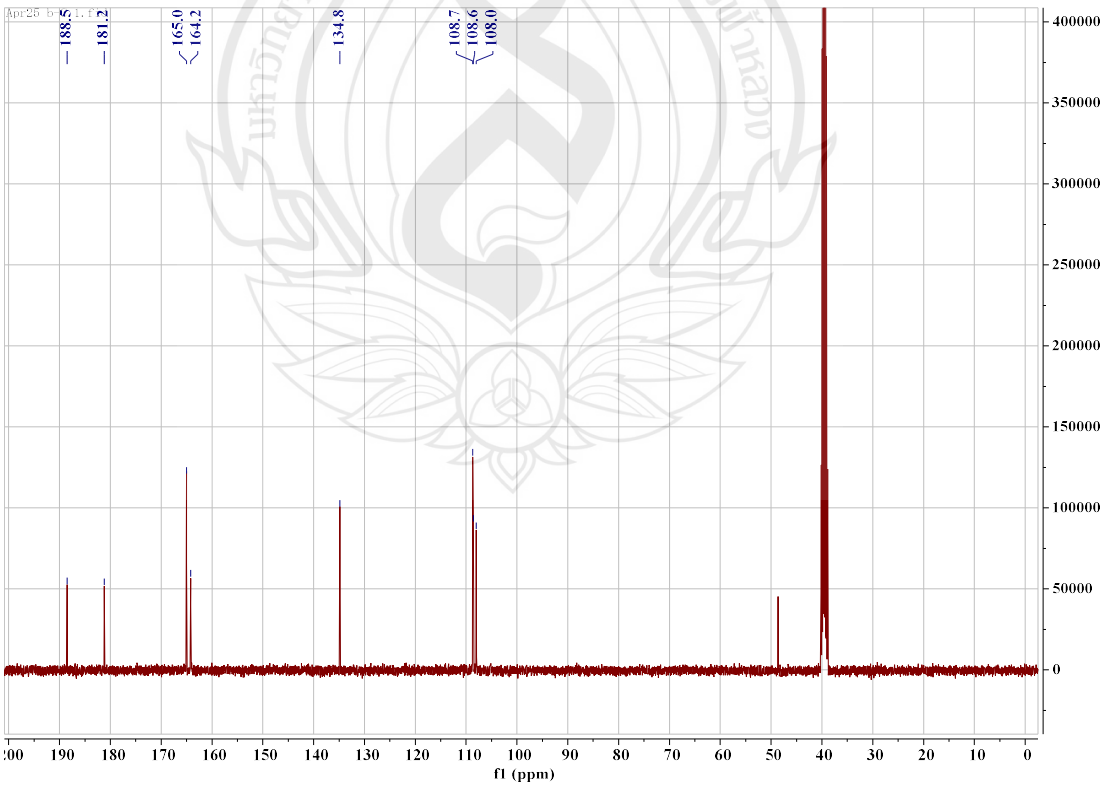

Figure A74 ^{13}C NMR spectrum of compound **C14** (100 MHz, DMSO)

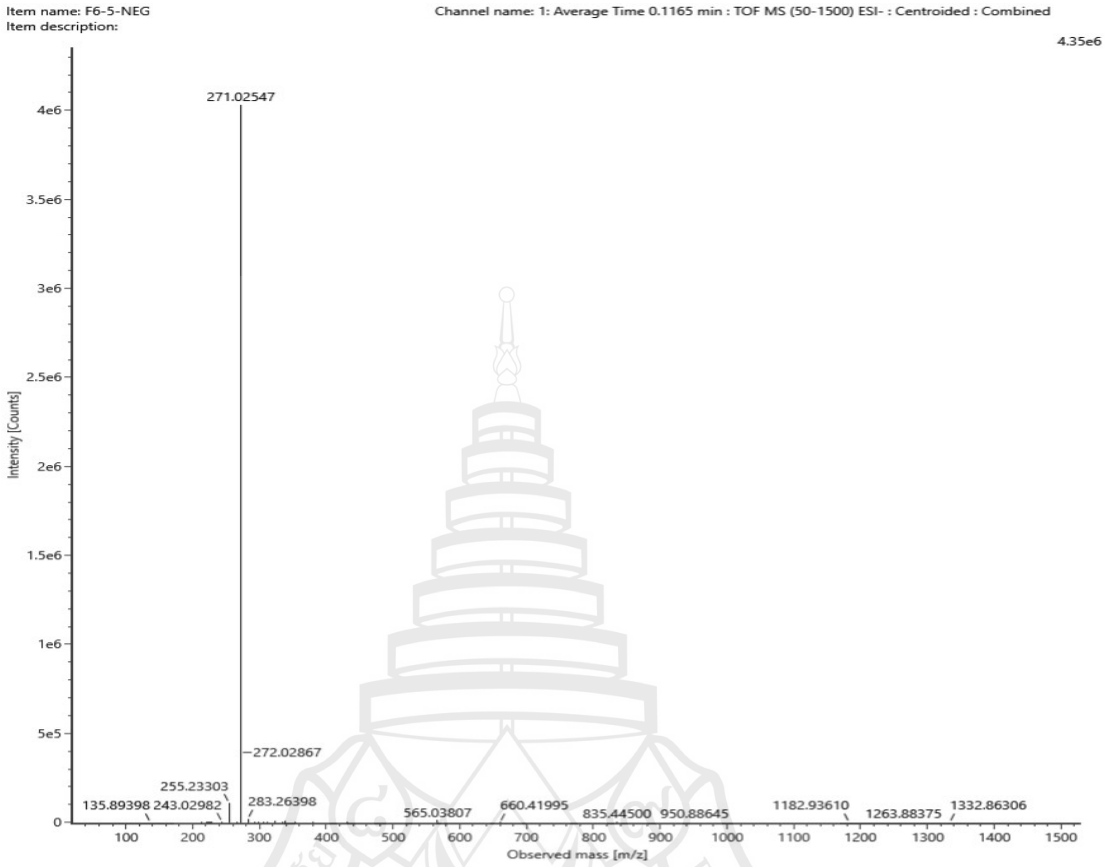

Figure A75 ESIMS of compound **C14**

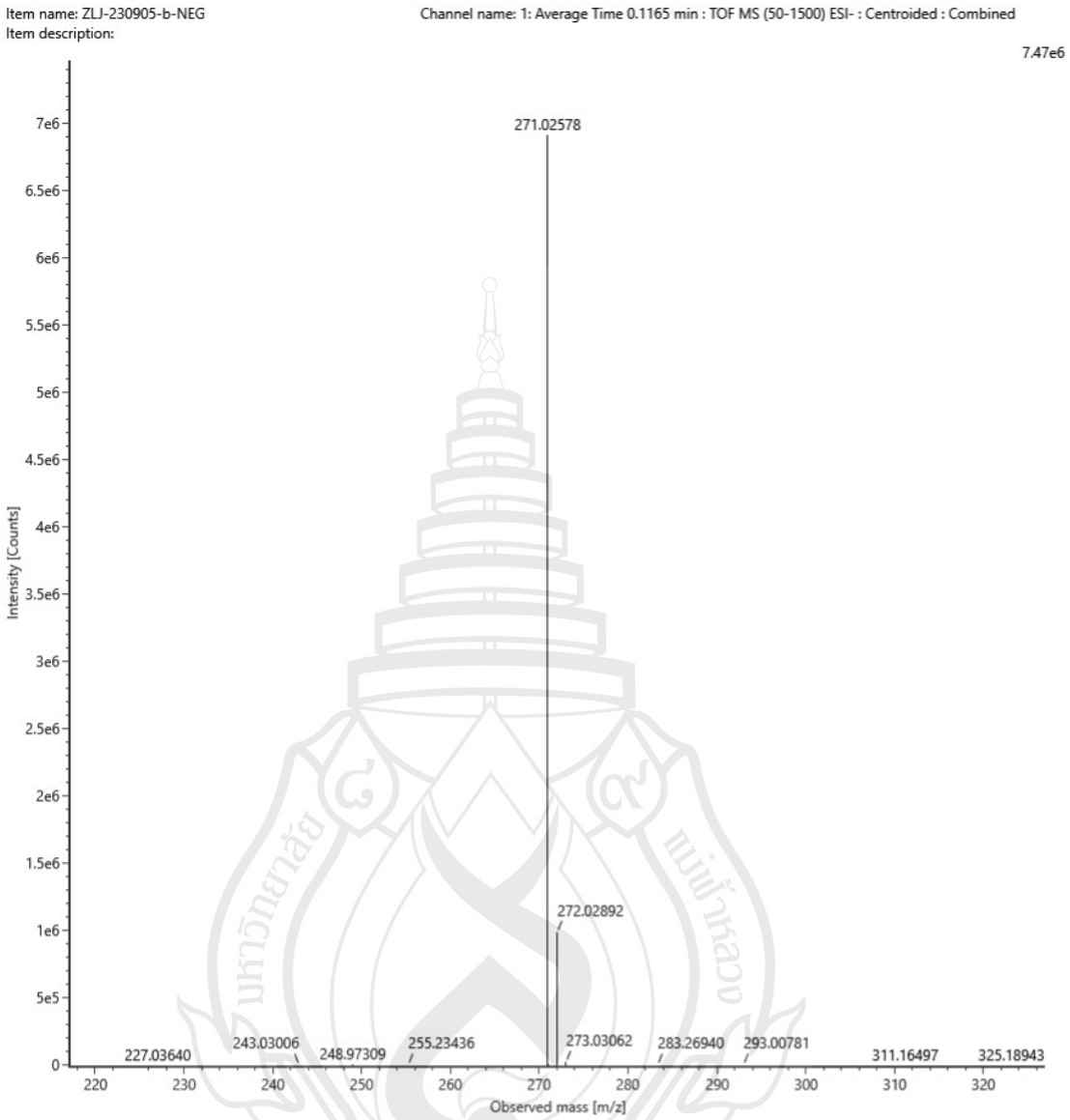

Note $[M-H]^-$

Composition	$C_{14}H_7O_6$
i-FIT Confidence (%)	100.000000
Predicted m/z	271.024812
m/z error (PPM)	3.560093

Figure A76 HR-ESIMS of compound **C14** (ESI-)

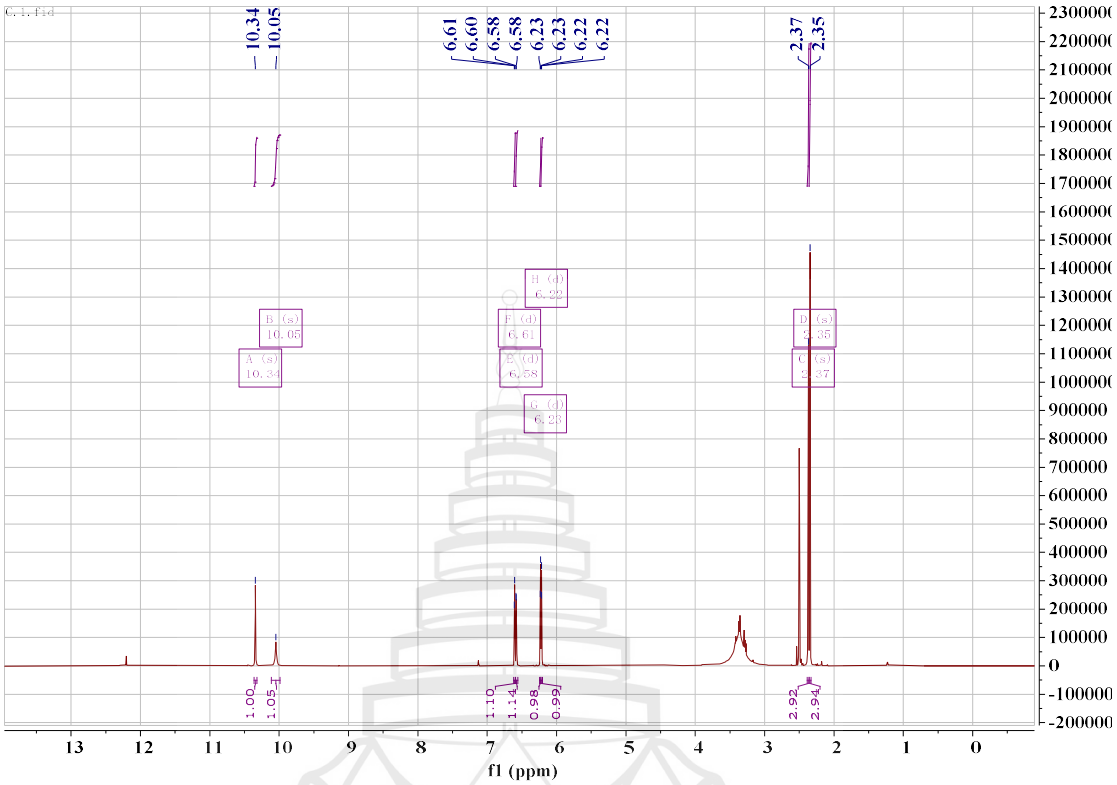

Figure A77 ^{1}H NMR spectrum of compound **C15** (600 MHz, DMSO)

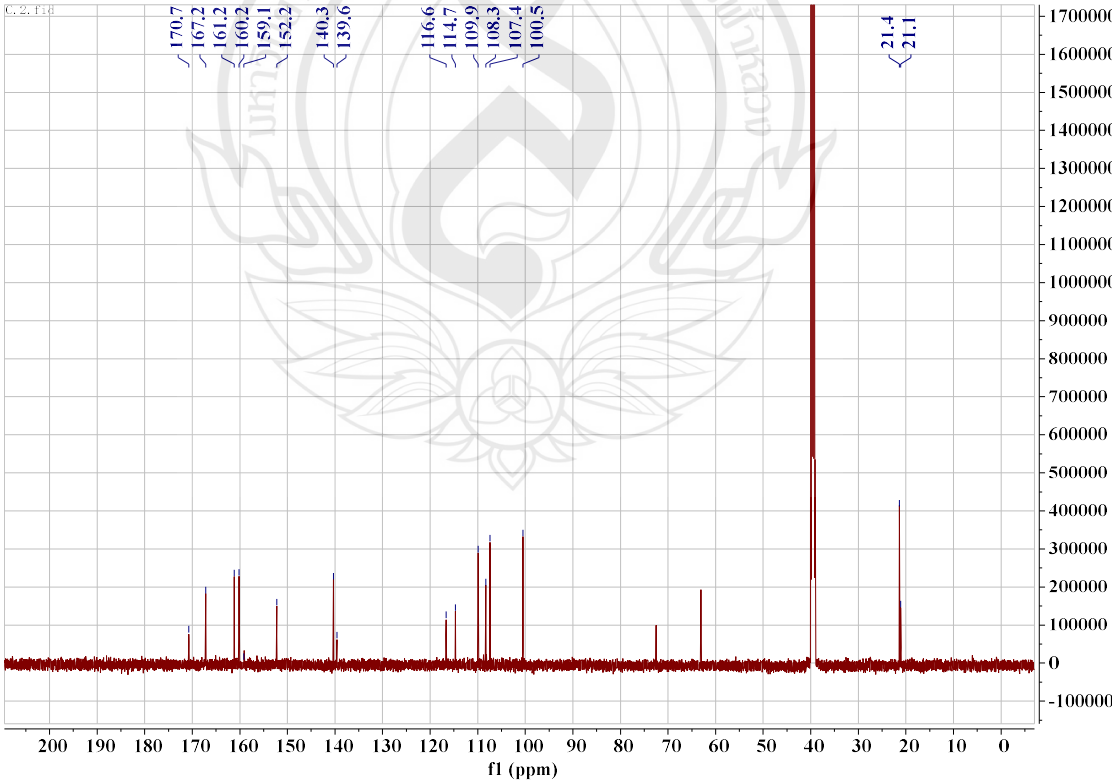

Figure A78 ^{13}C NMR spectrum of compound **C15** (150 MHz, DMSO)

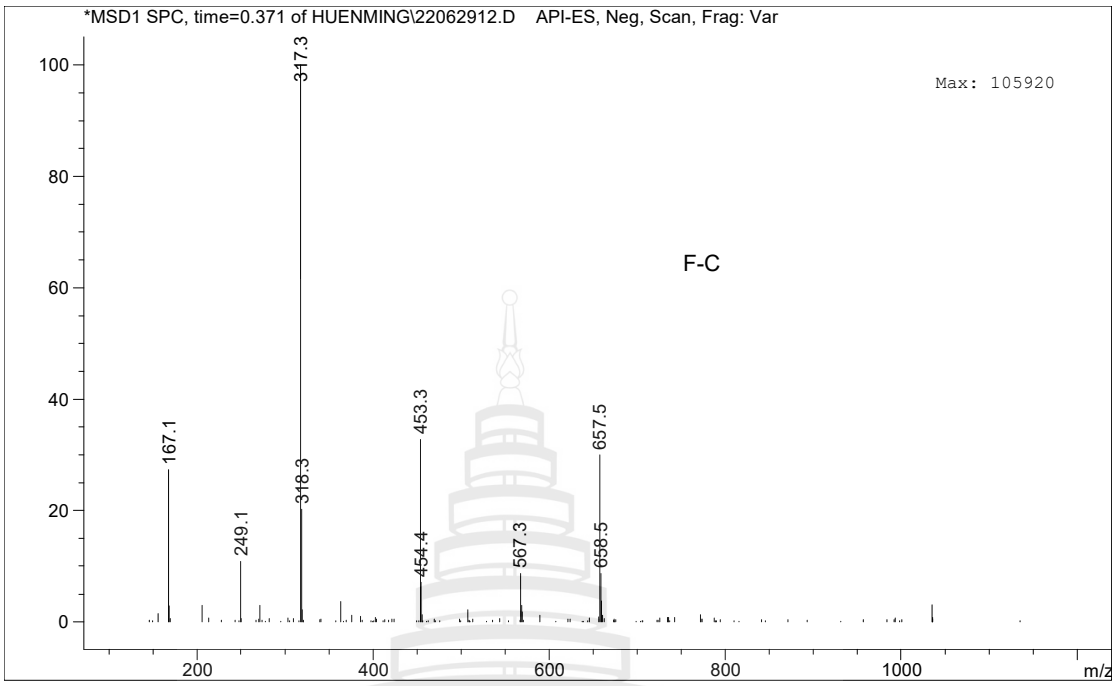

Figure A79 ESIMS of compound **C15**

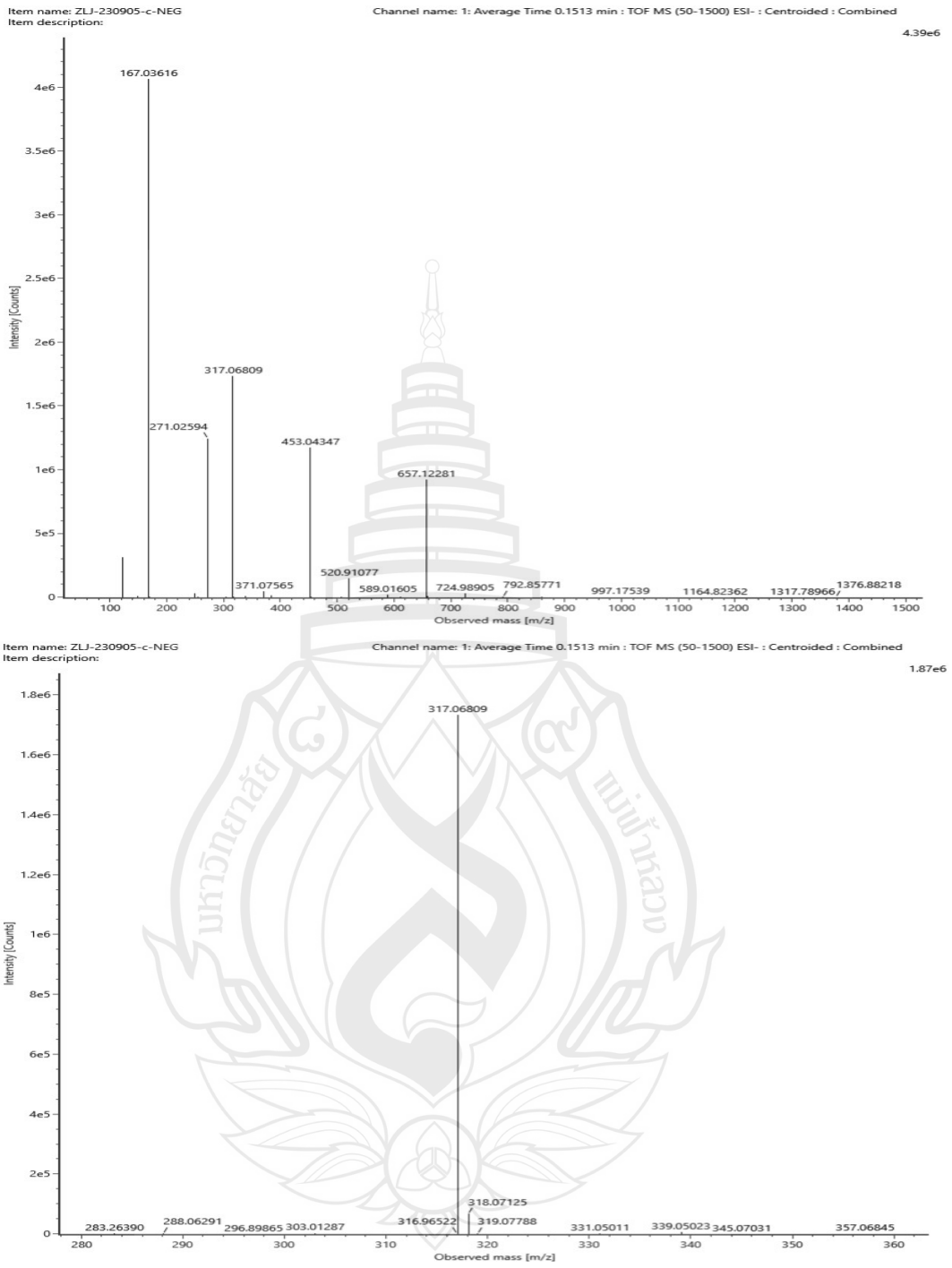

Note $[M-H]^-$

Composition	$C_{16}H_{13}O_7$
i-FIT Confidence (%)	100.000000
Predicted m/z	317.066676
m/z error (PPM)	4.444385

Figure A80 HR-ESIMS of compound **C15** (ESI-)

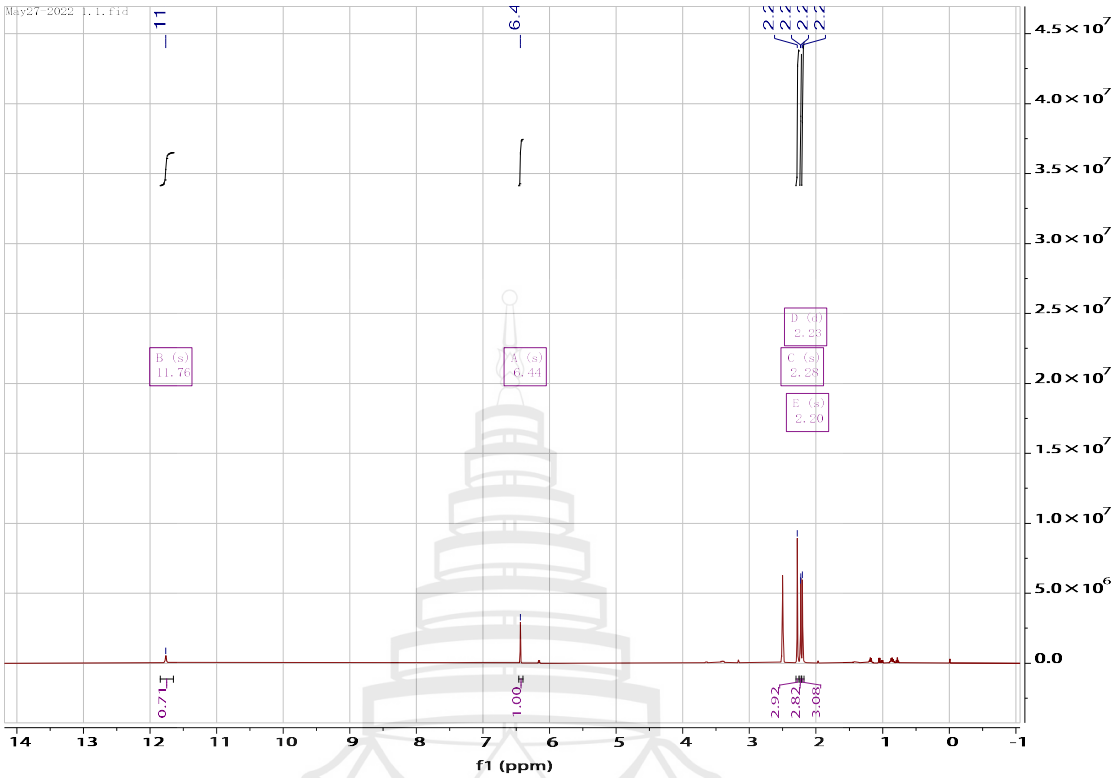

Figure A81 ^{1}H NMR spectrum of compound **C16** (400 MHz, DMSO)

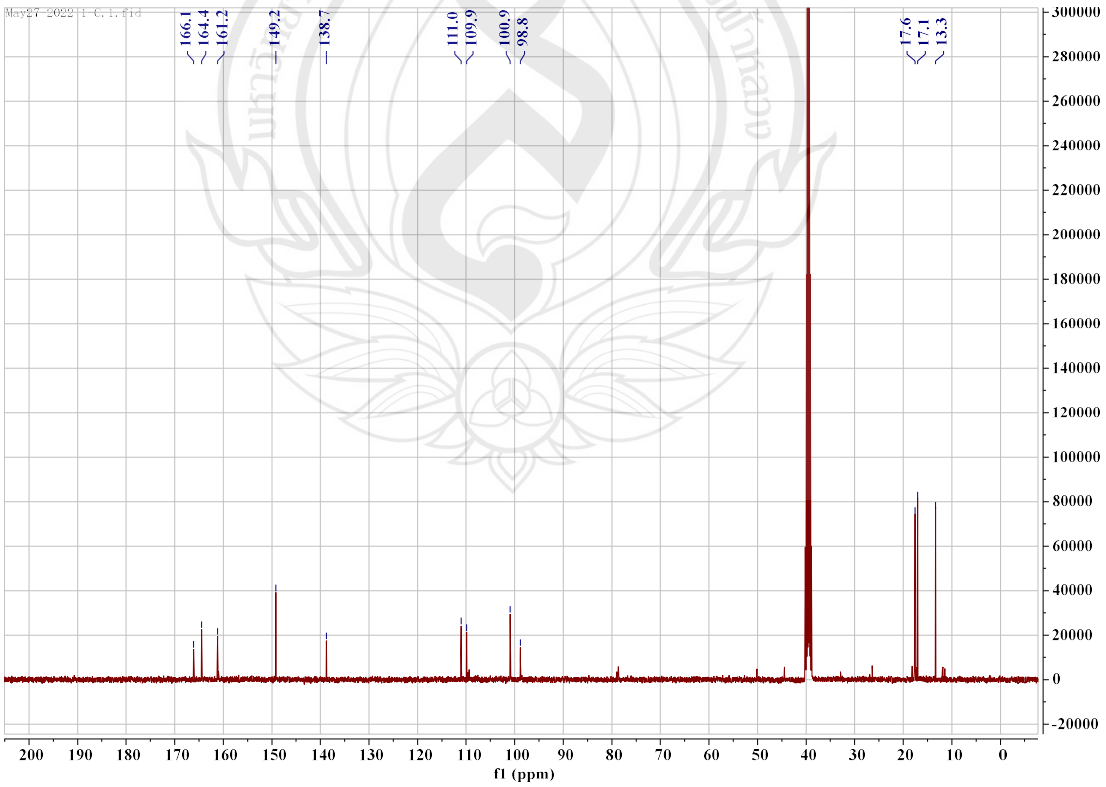

Figure A82 ^{13}C NMR spectrum of compound **C16** (100 MHz, DMSO)

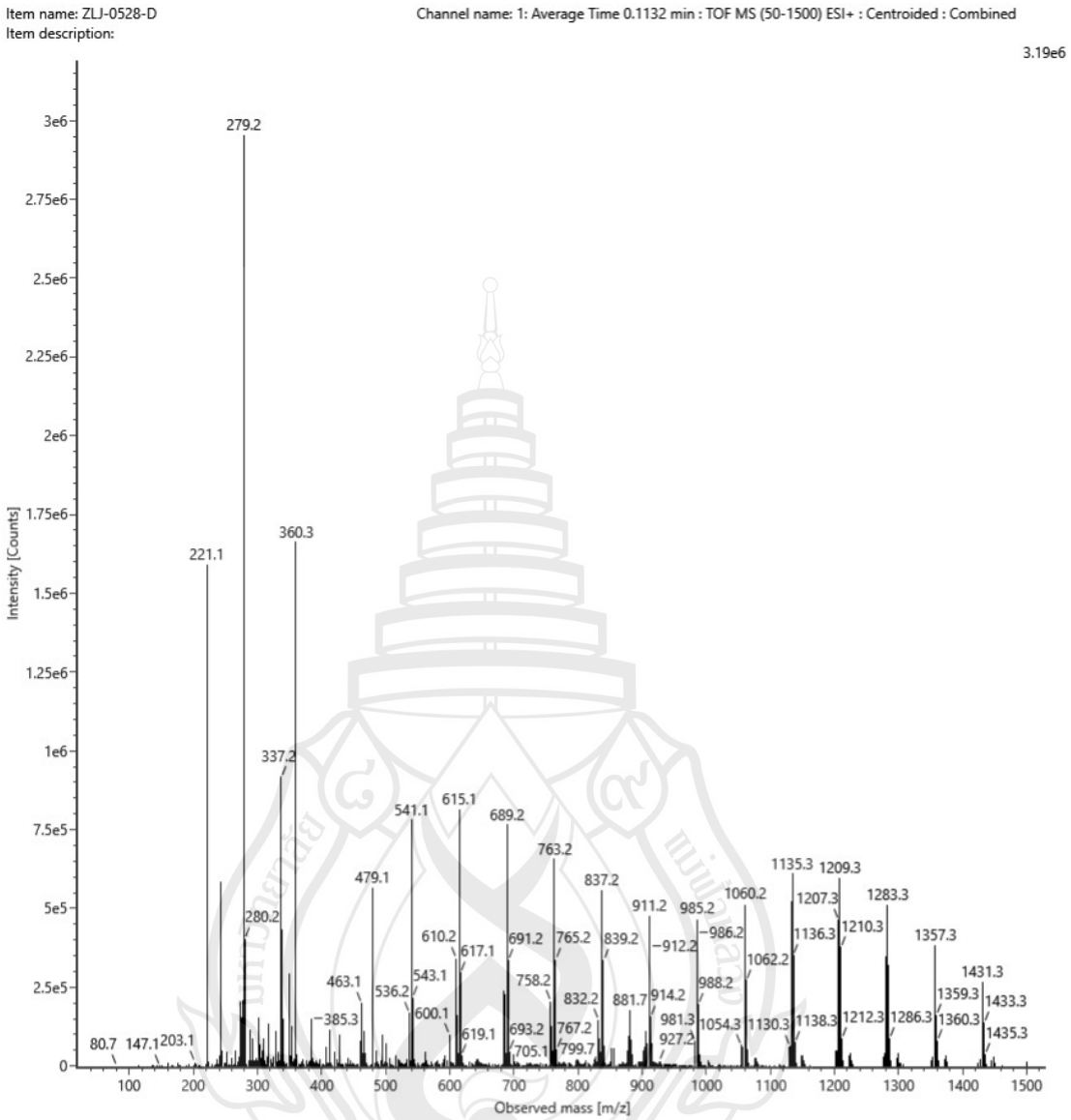

Figure A83 ESIMS of compound **C16**

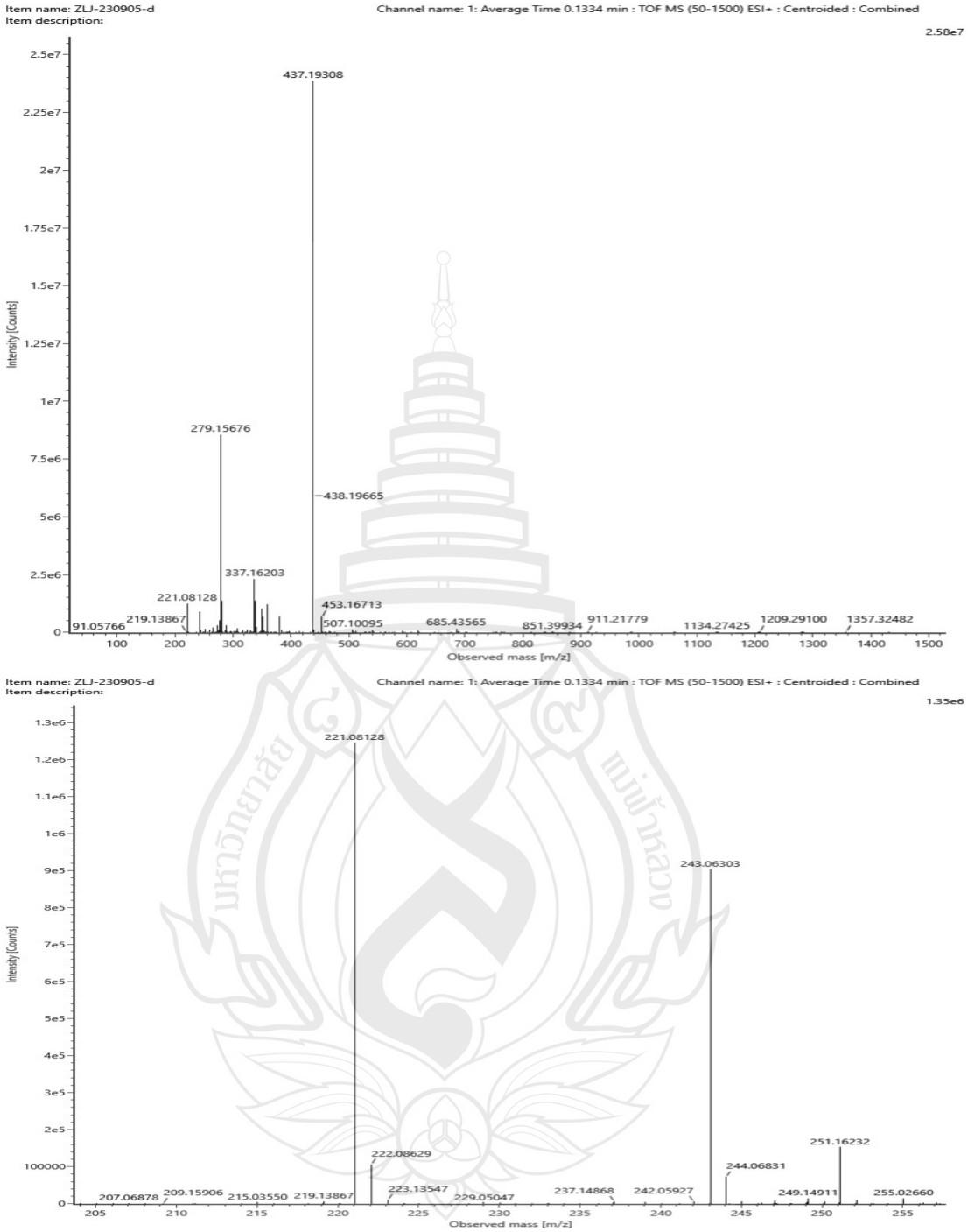

Note $[M+H]^+$

Composition	$C_{12}H_{13}O_4$
i-FIT Confidence (%)	100.000000
Predicted m/z	221.080835
m/z error (PPM)	2.020575

Figure A84 HR-ESIMS of compound **C16** (ESI+)

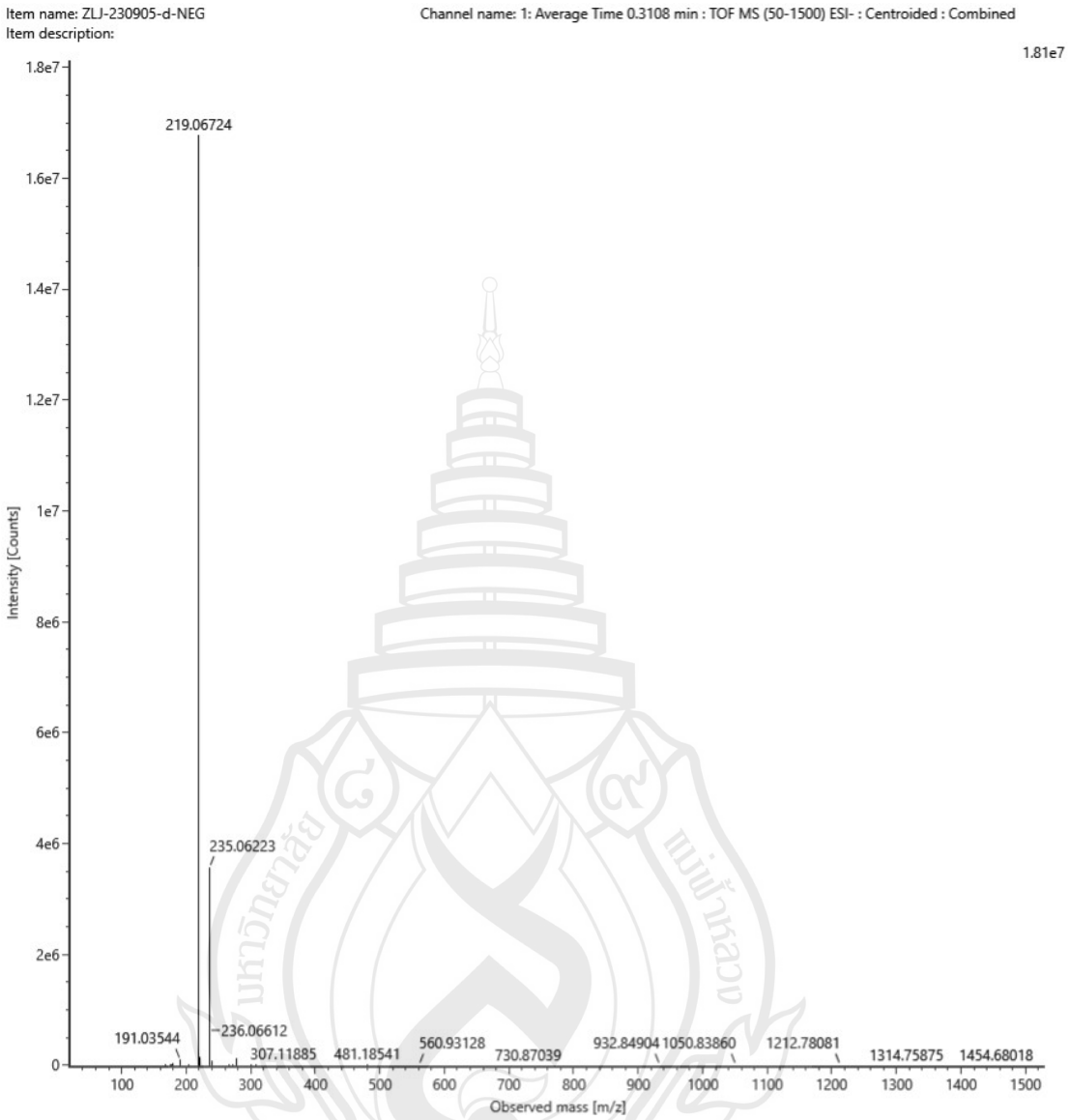

Note $[M-H]^-$

Composition	$C_{12}H_{11}O_4$
i-FIT Confidence (%)	100.000000
Predicted m/z	219.066282
m/z error (PPM)	4.351163

Figure A85 HR-ESIMS of compound **C16** (ESI-)

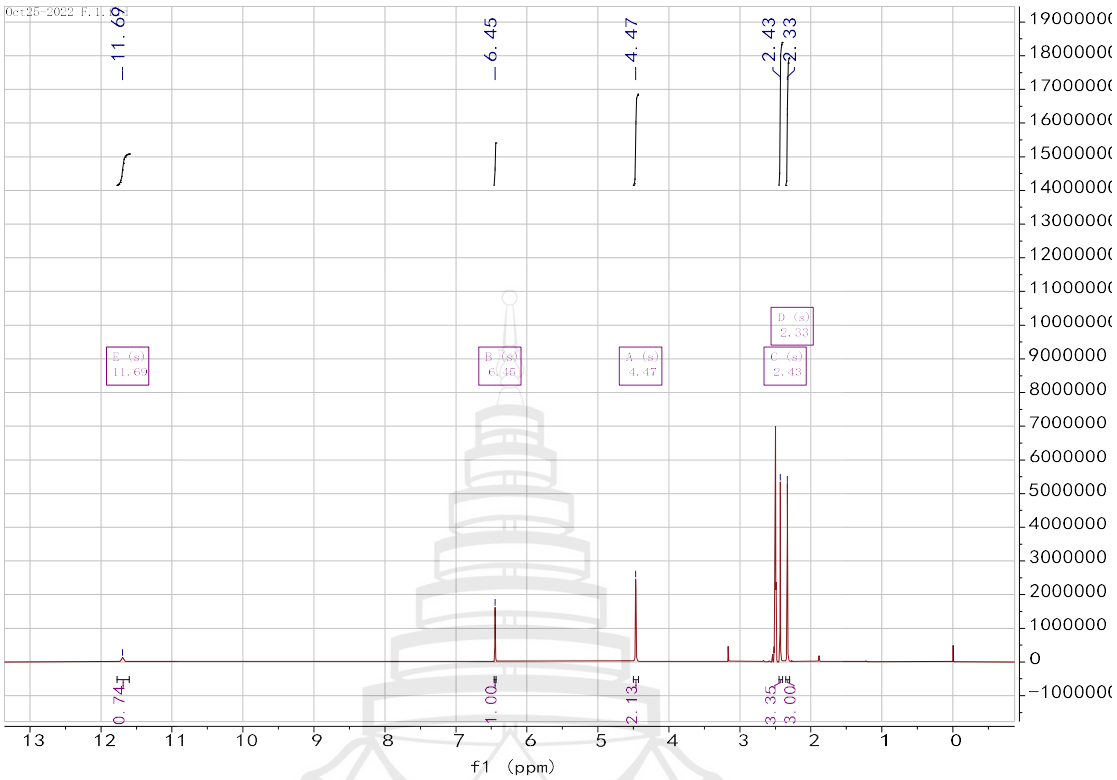

Figure A86 ^{1}H NMR spectrum of compound **C17** (400 MHz, DMSO)

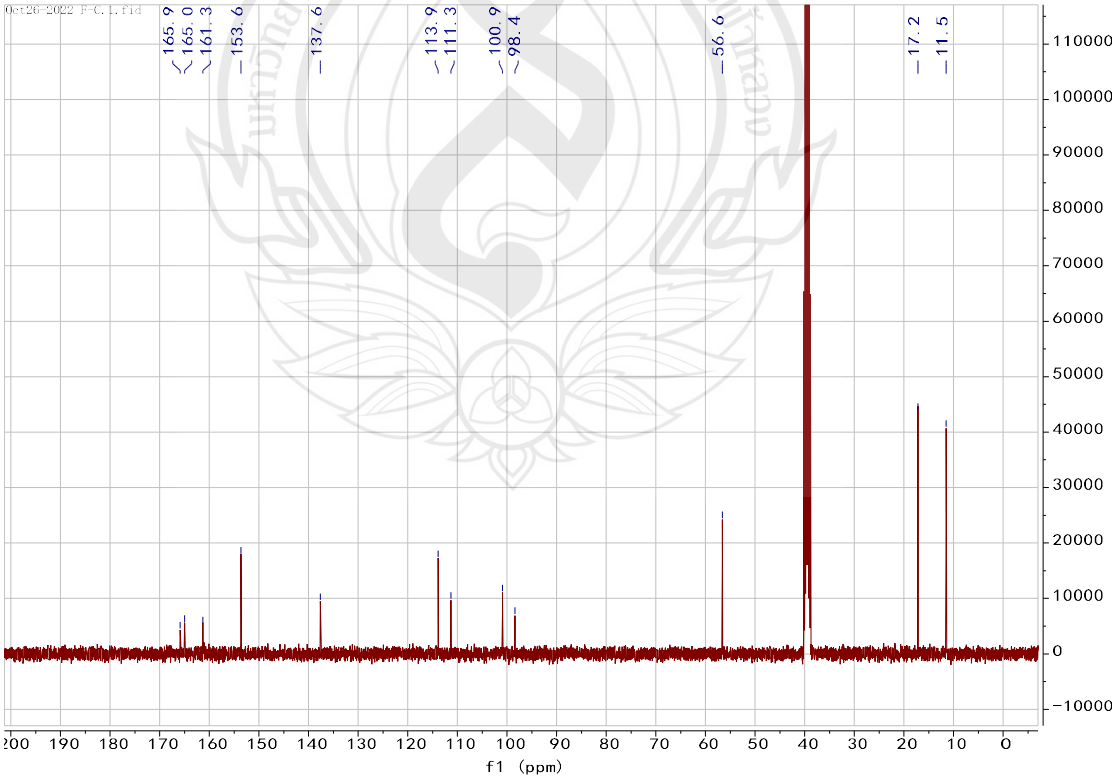

Figure A87 ^{13}C NMR spectrum of compound **C17** (100 MHz, DMSO)

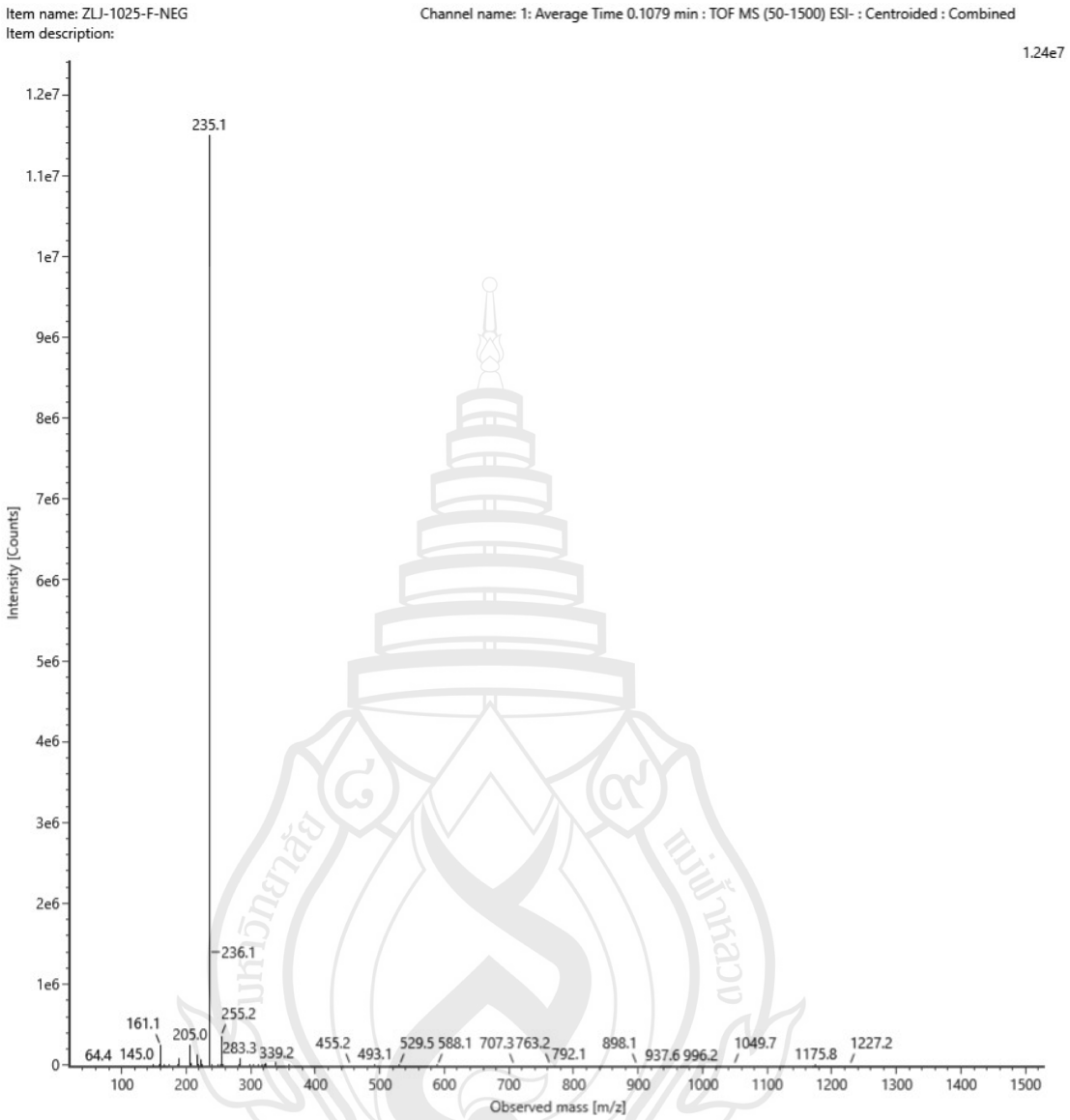

Figure A88 ESIMS of compound **C17**

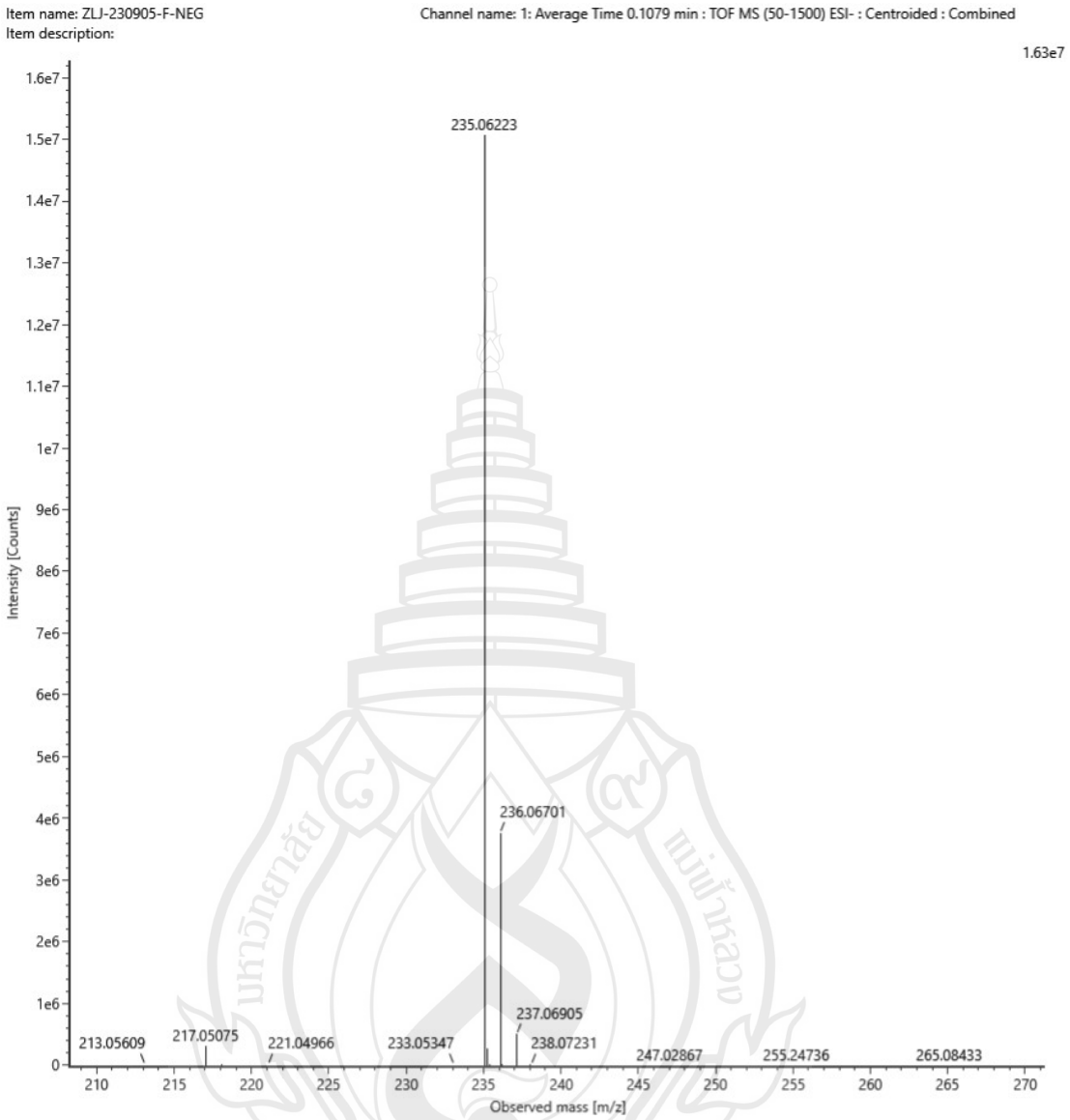

Note $[M-H]^-$

Composition	$C_{12}H_{11}O_5$
i-FIT Confidence (%)	100.000000
Predicted m/z	235.061197
m/z error (PPM)	4.375651

Figure A89 HR-ESIMS of compound **C17** (ESI-)

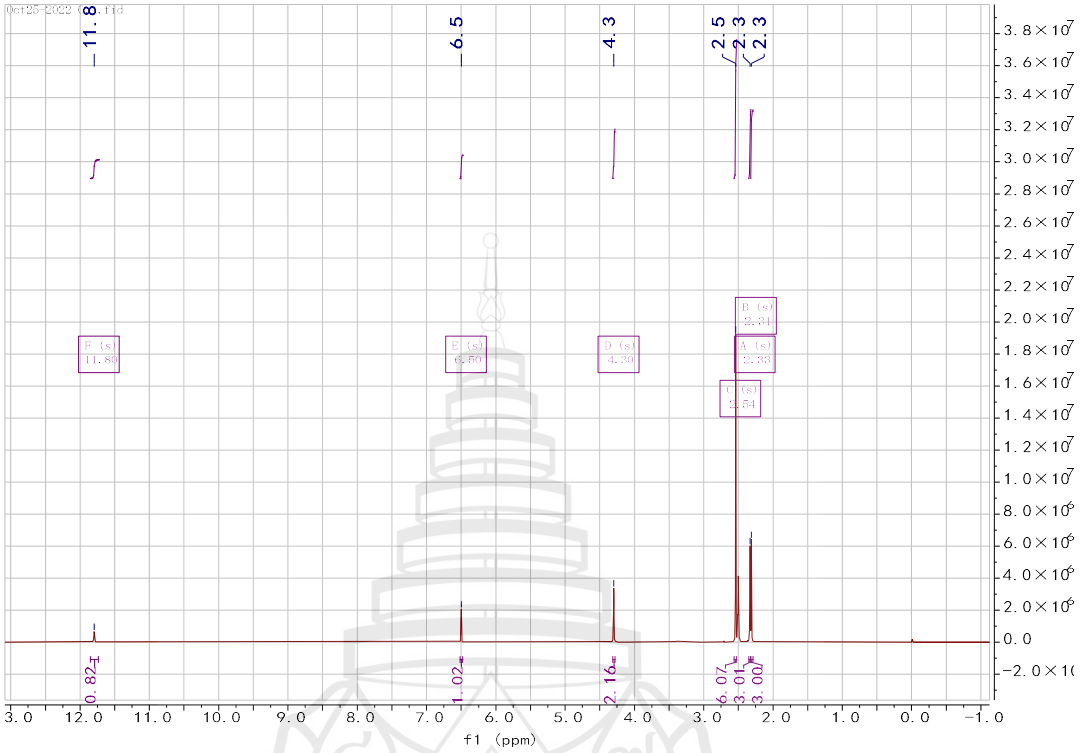

Figure A90 ^{1}H NMR spectrum of compound **C18** (400 MHz, DMSO)

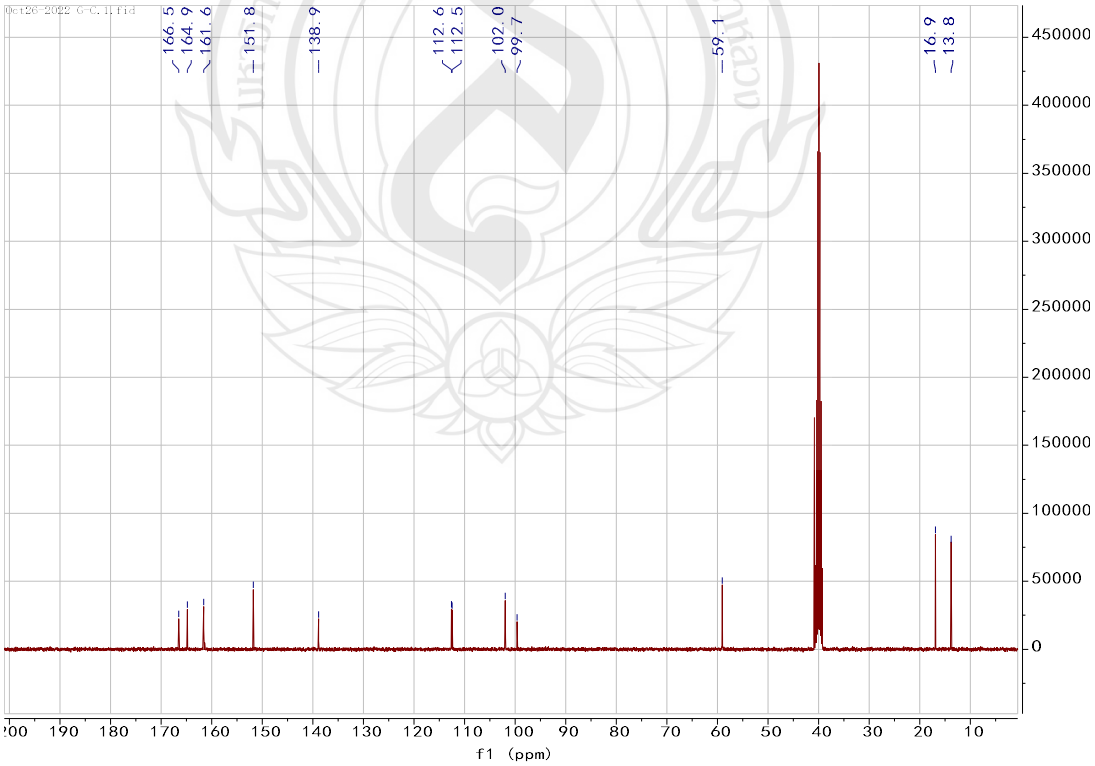

Figure A91 ^{13}C NMR spectrum of compound **C18** (100 MHz, DMSO)

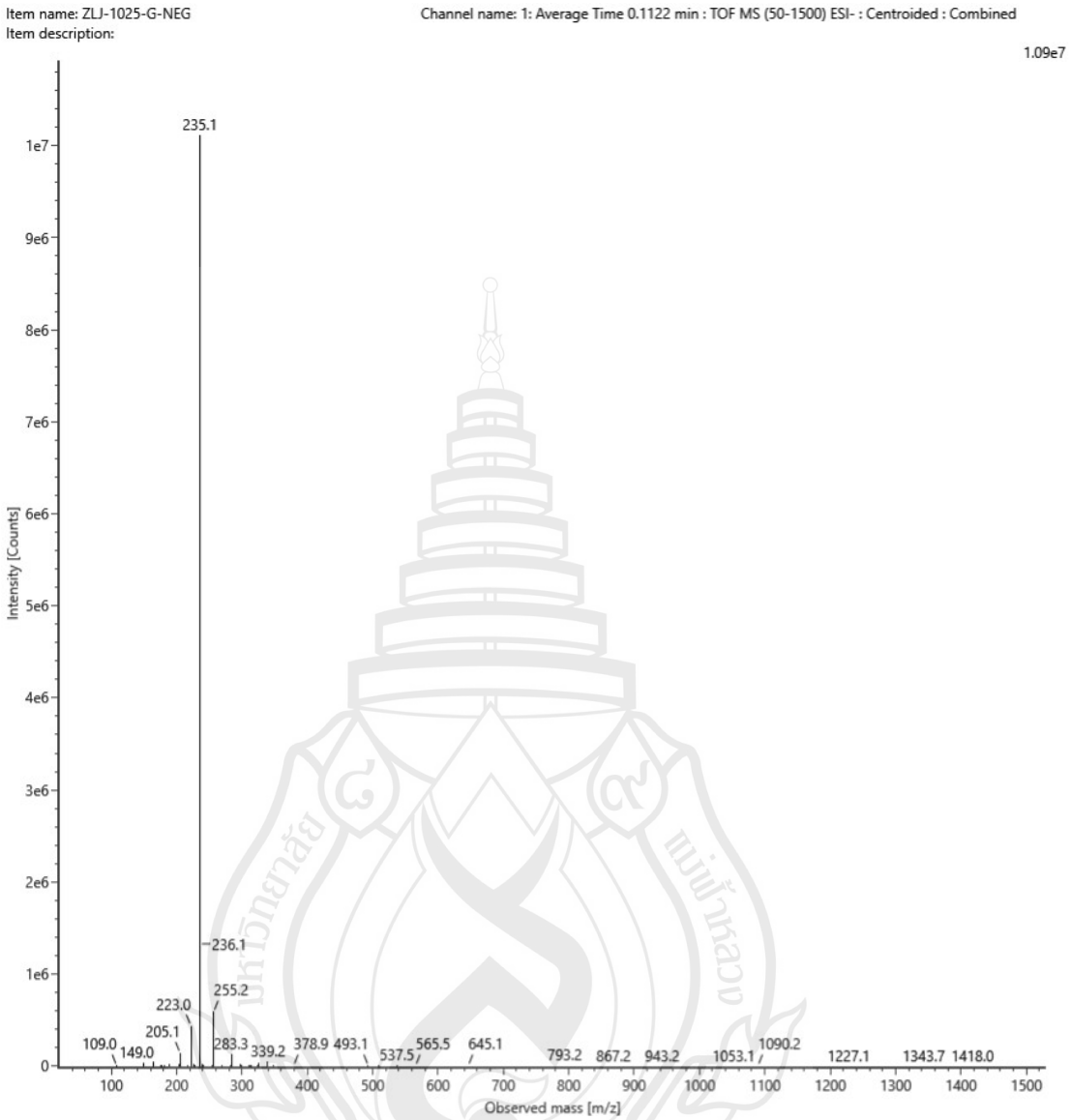

Figure A92 ESIMS of compound **C18**

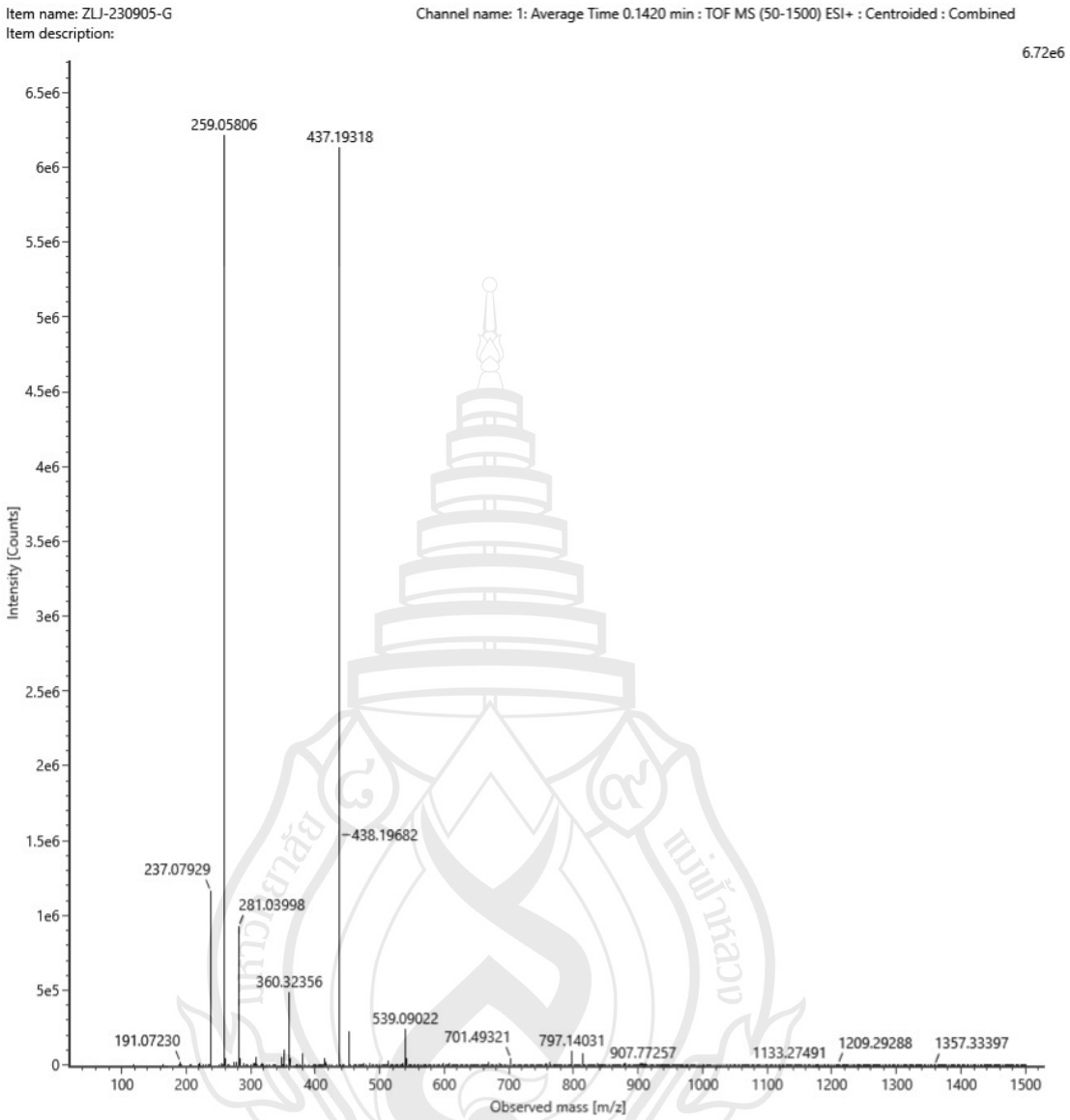

Note $[M+Na]^+$

Composition	$C_{12}H_{12}O_5Na$
i-FIT Confidence (%)	100.000000
Predicted m/z	259.057695
m/z error (PPM)	1.416100

Figure A93 HR-ESIMS of compound **C18** (ESI+)

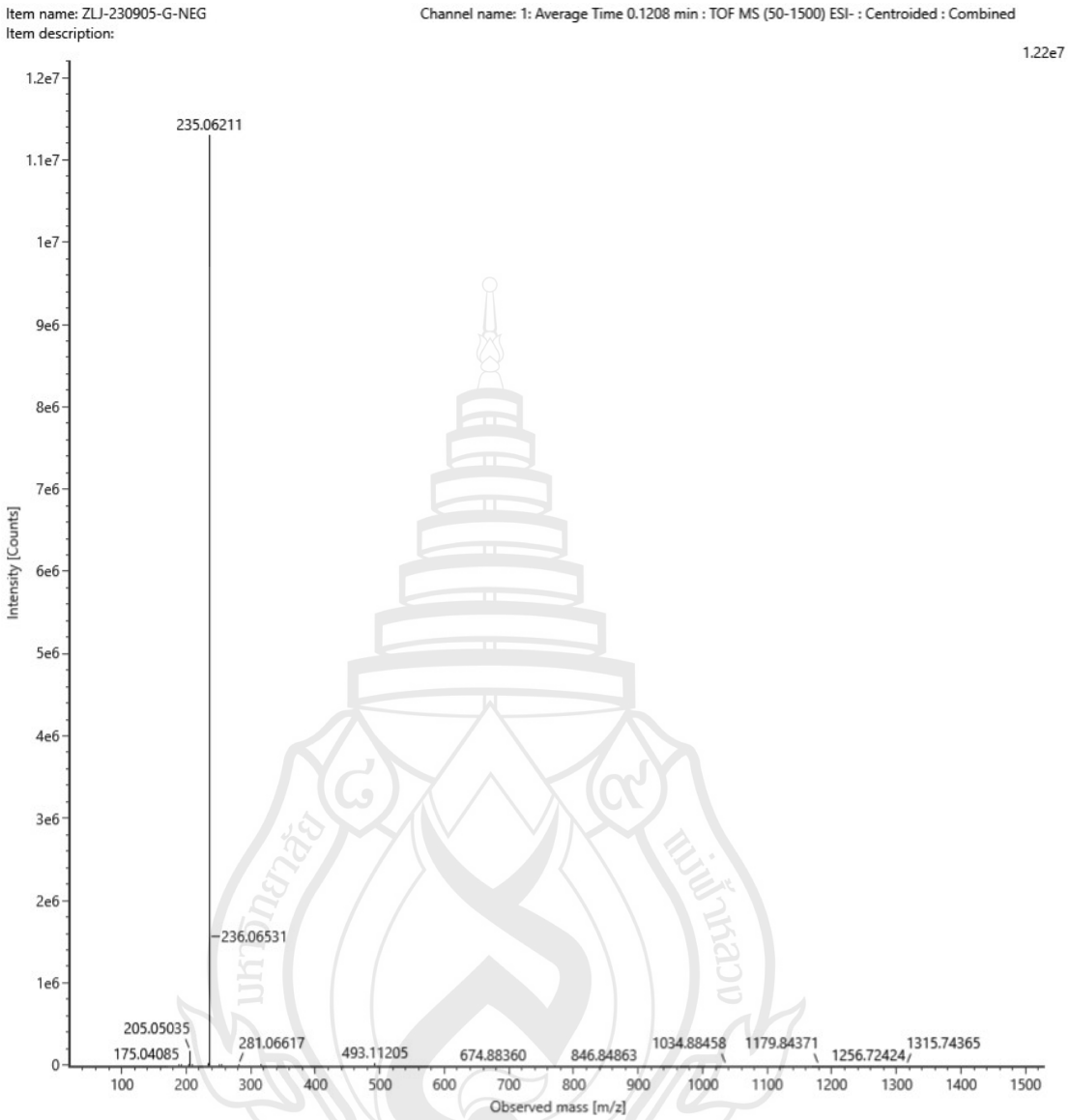

Note $[M-H]^-$

Composition	$C_{12}H_{11}O_5$
i-FIT Confidence (%)	100.000000
Predicted m/z	235.061197
m/z error (PPM)	3.867328

Figure A94 HR-ESIMS of compound **C18** (ESI-)

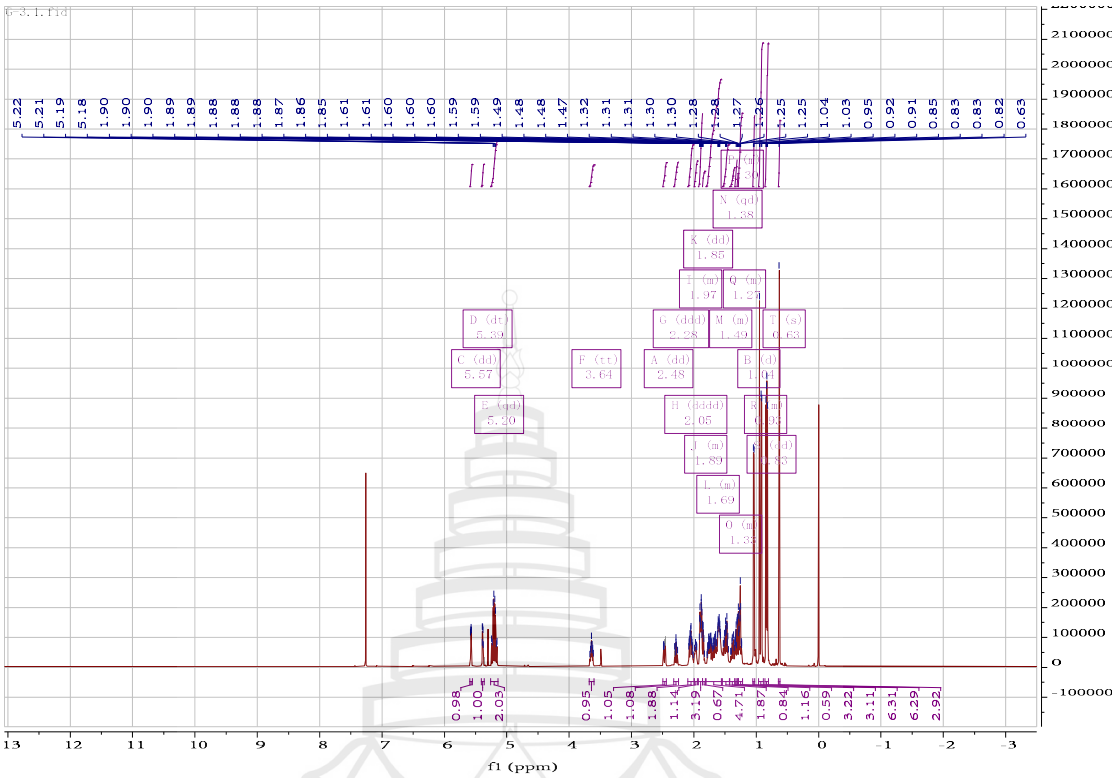

Figure A95 ^{1}H NMR spectrum of compound **C19** (600 MHz, DMSO)

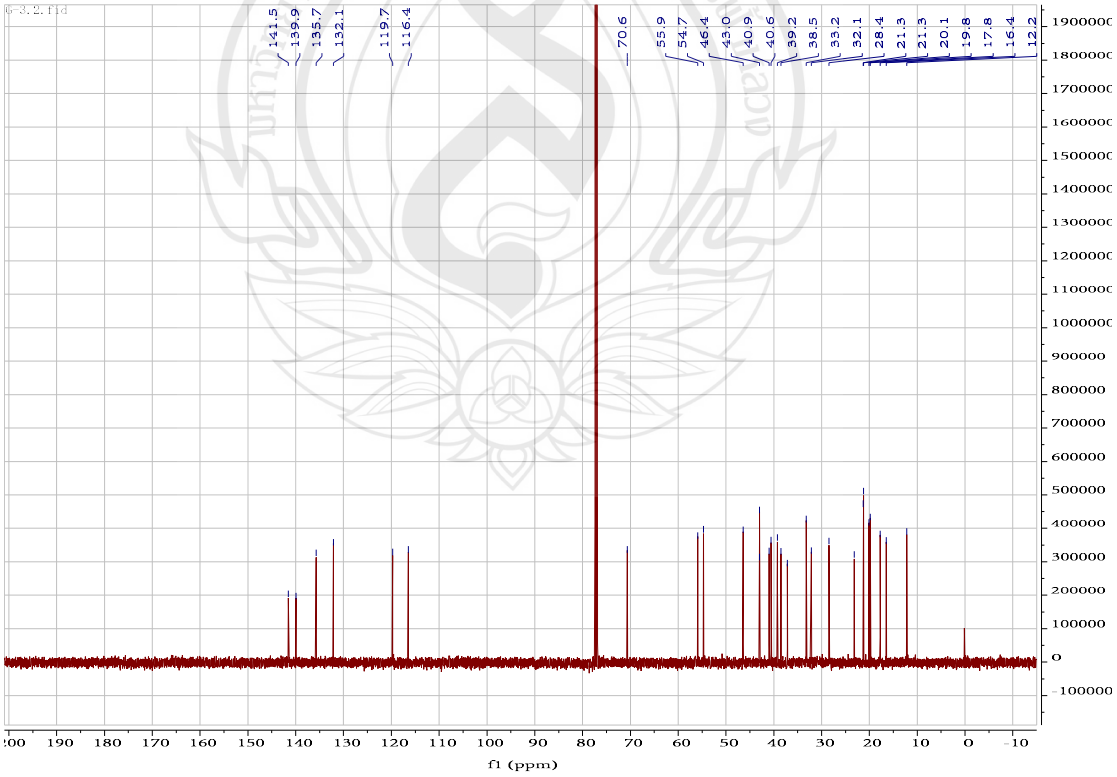

Figure A96 ^{13}C NMR spectrum of compound **C19** (150 MHz, DMSO)

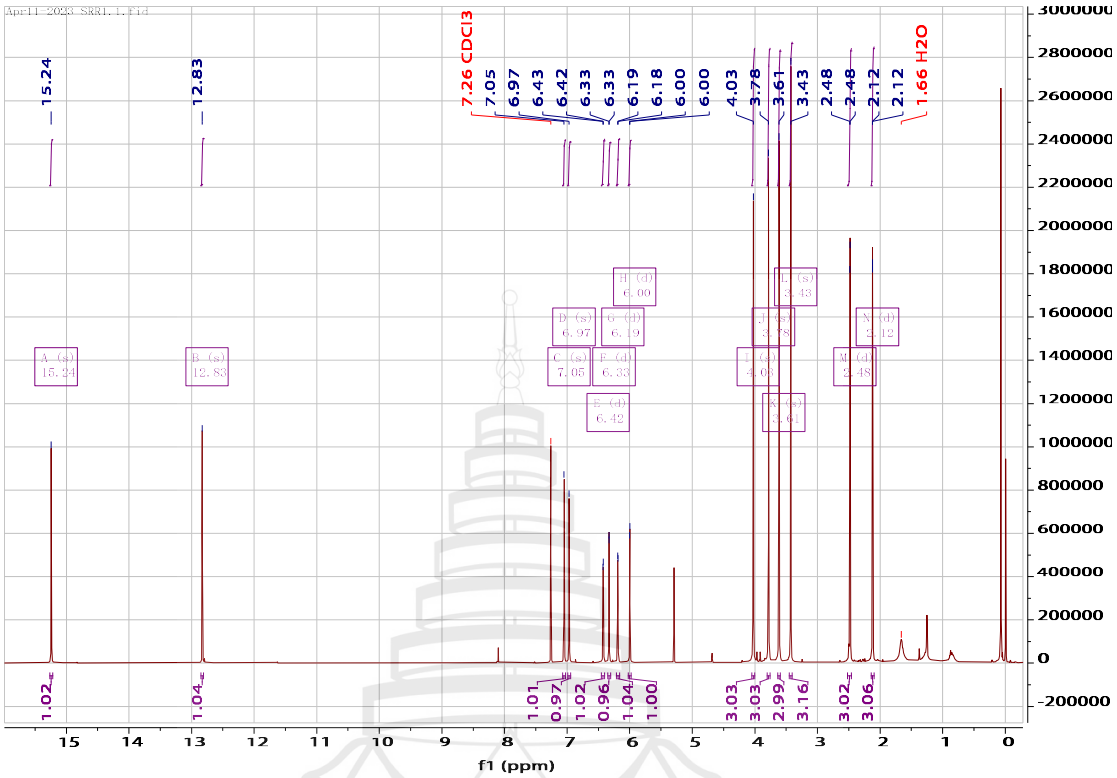

Figure A97 ^{1}H NMR spectrum of compound **C20**600 MHz, $CDCl_3$)

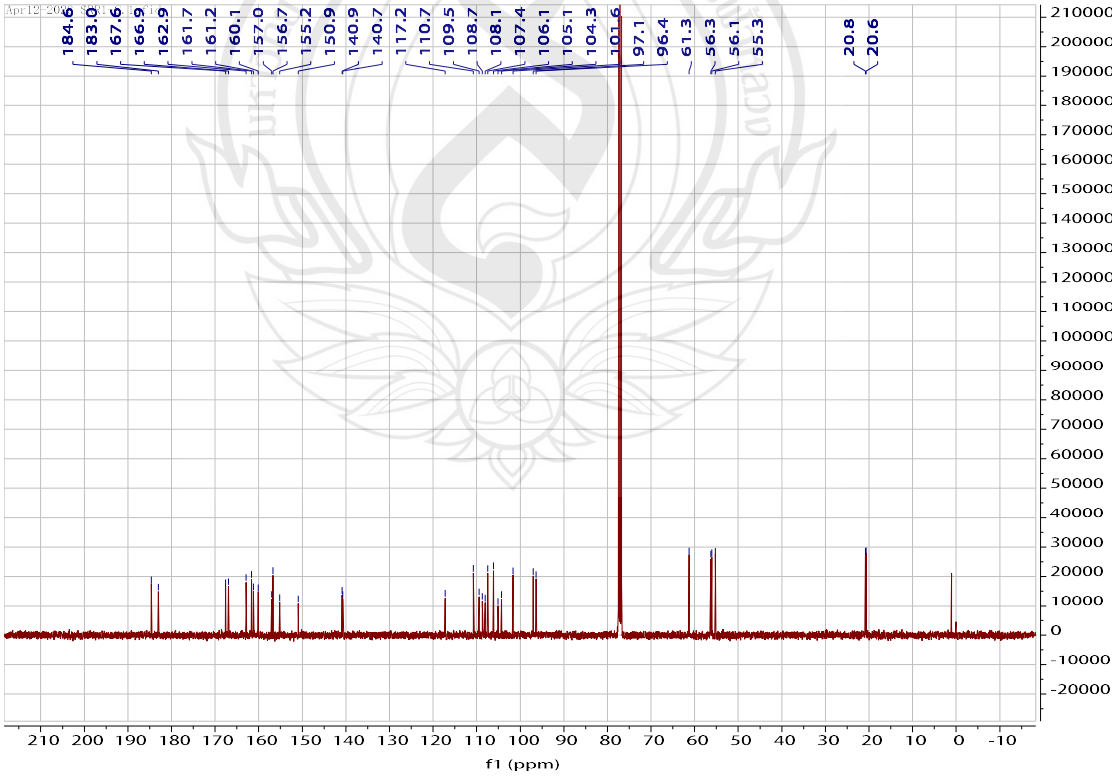

Figure A98 ^{13}C NMR spectrum of compound **C20**150 MHz, $CDCl_3$)

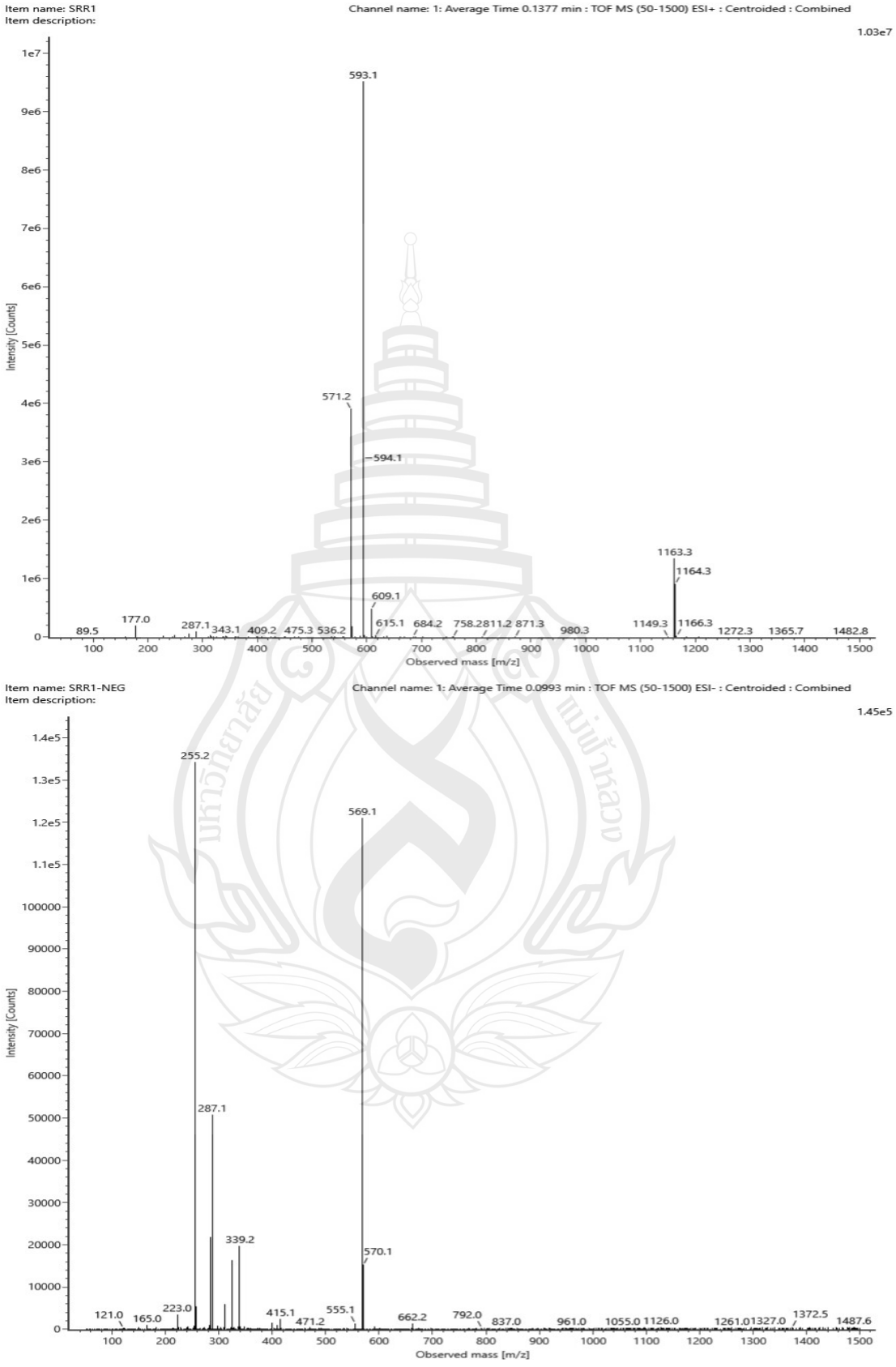

Figure A99 ESIMS of compound **C20**

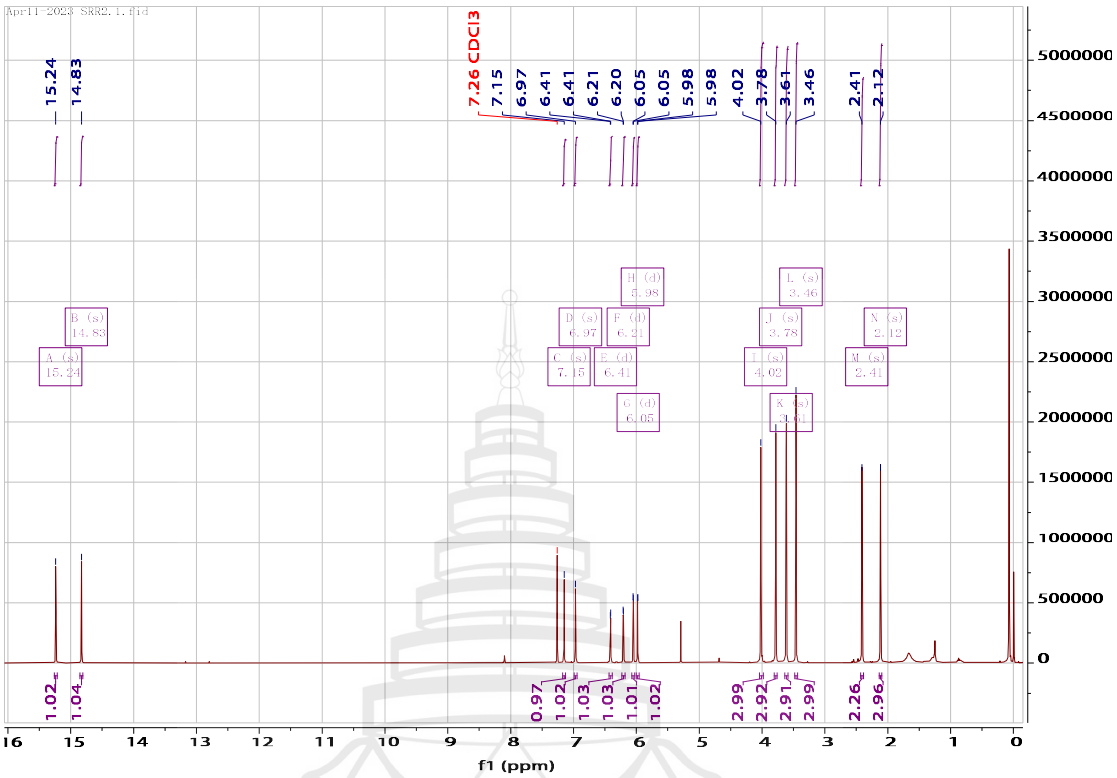

Figure A100 ^{1}H NMR spectrum of compound **C21**(400 MHz, $CDCl_3$)

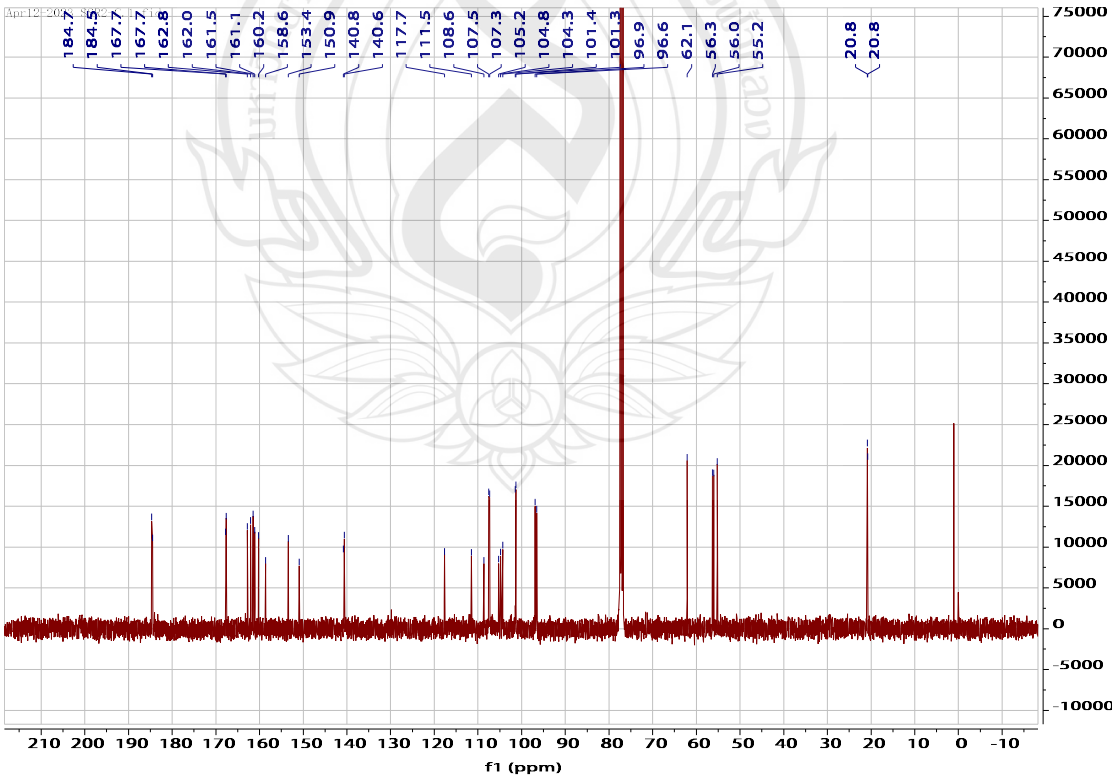

Figure A101 ^{13}C NMR spectrum of compound **C21**(100 MHz, $CDCl_3$)

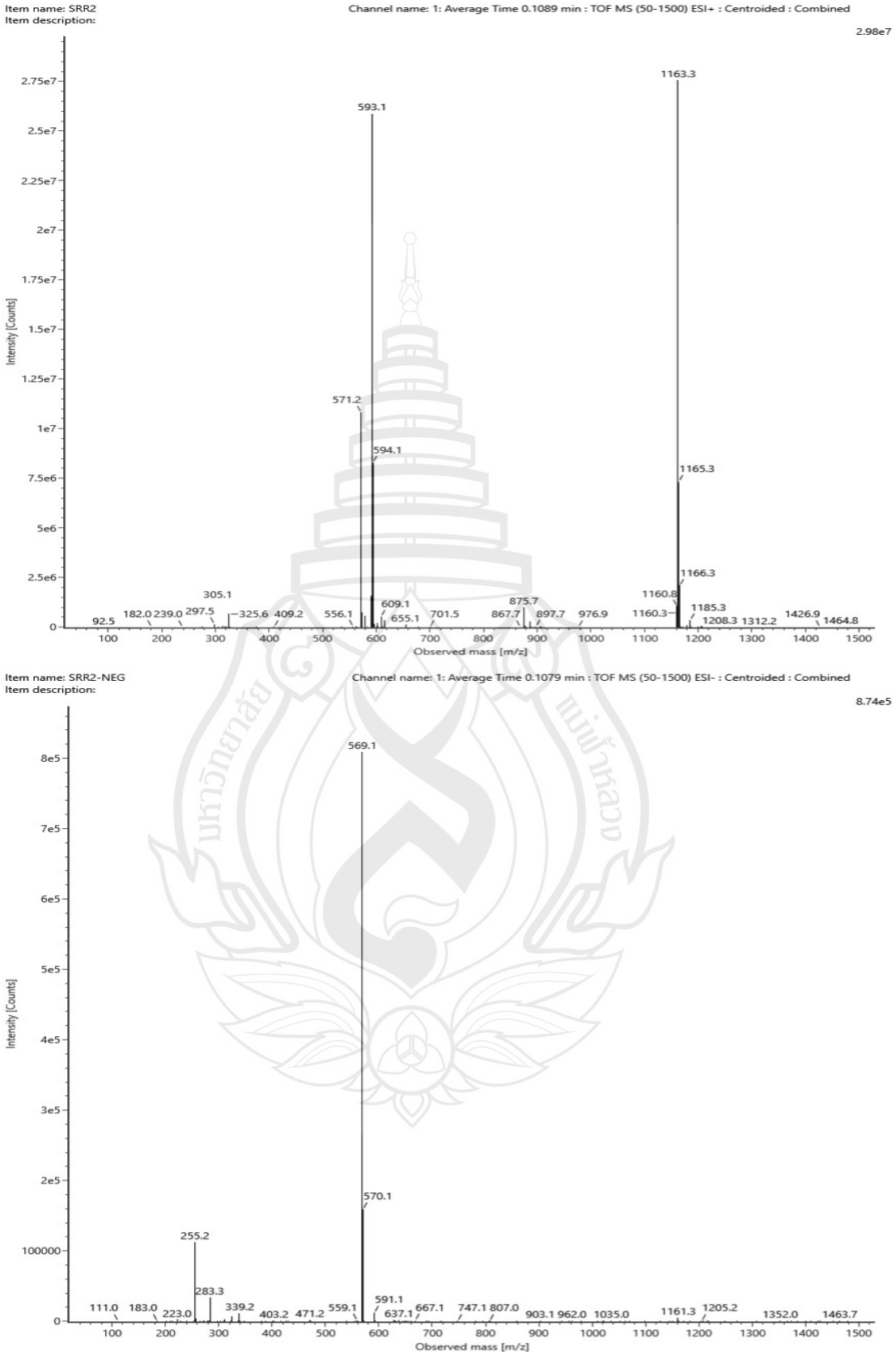

Figure A102 ESIMS of compound **C21**

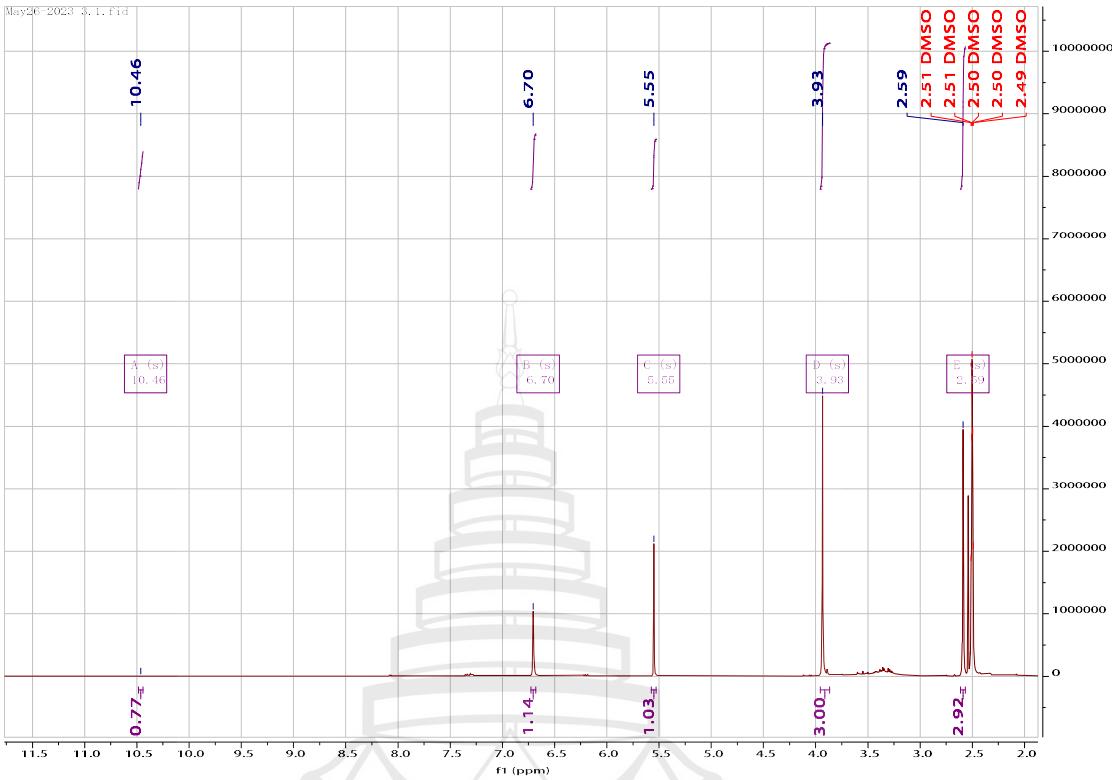

Figure A103 ^{1}H NMR spectrum of compound **C22**(400 MHz, DMSO)

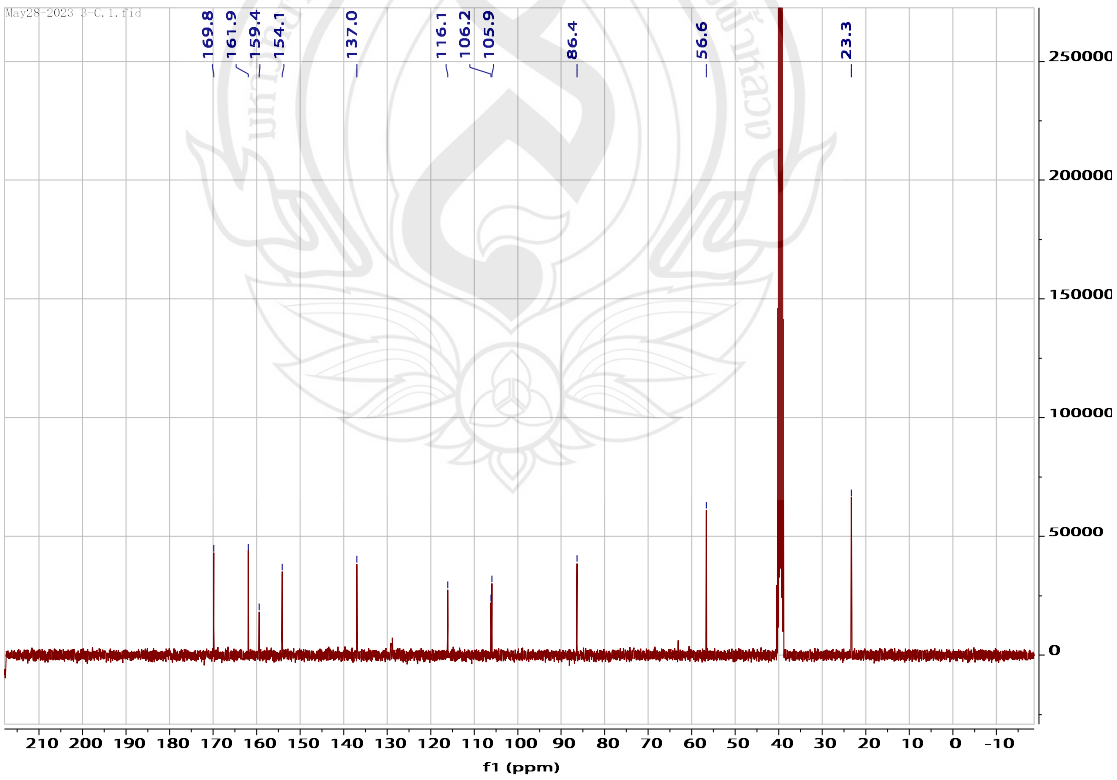

Figure A104 ^{13}C NMR spectrum of compound **C22**(100 MHz, DMSO)

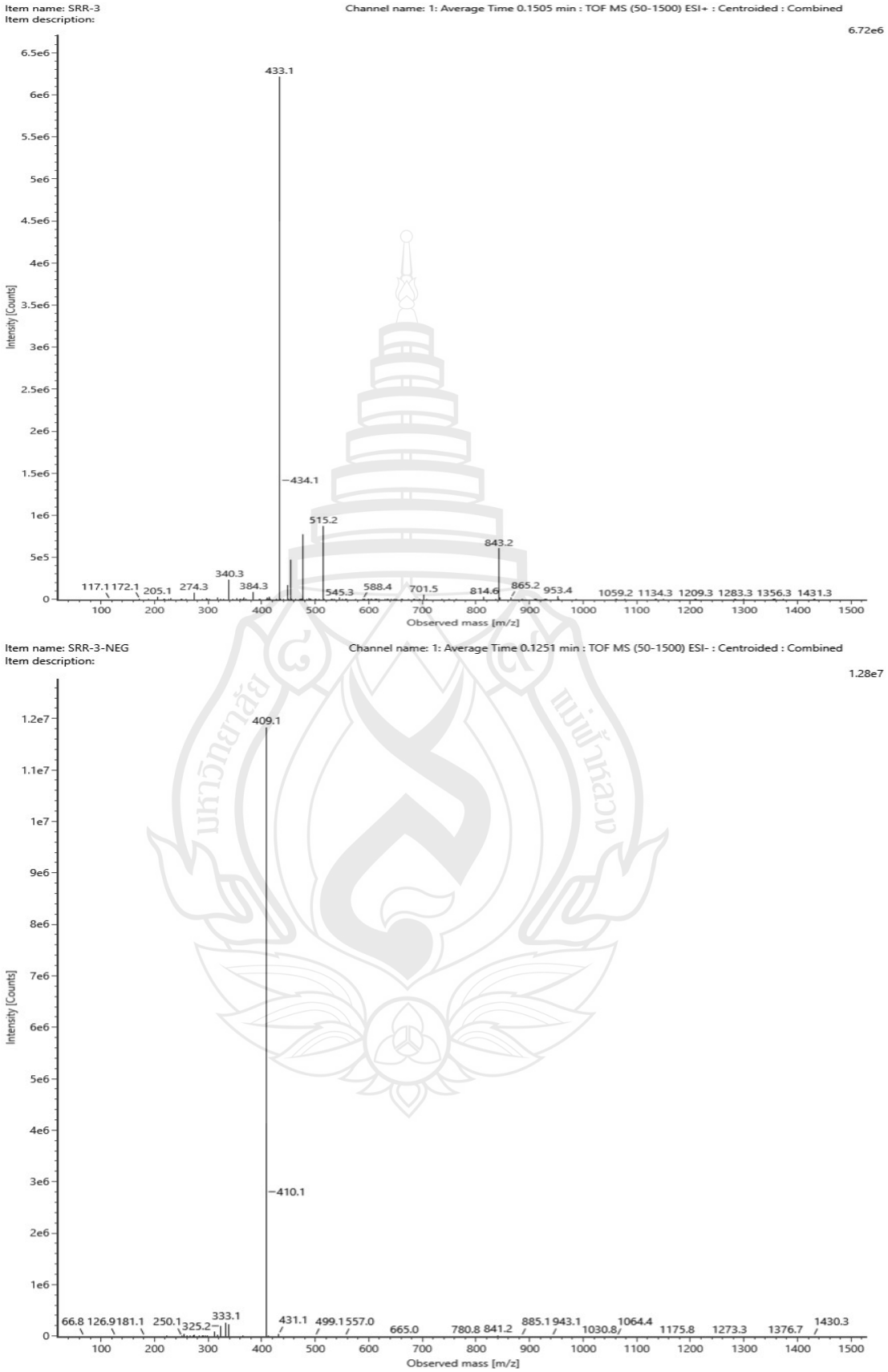

Figure A105 ESIMS of compound **C22**

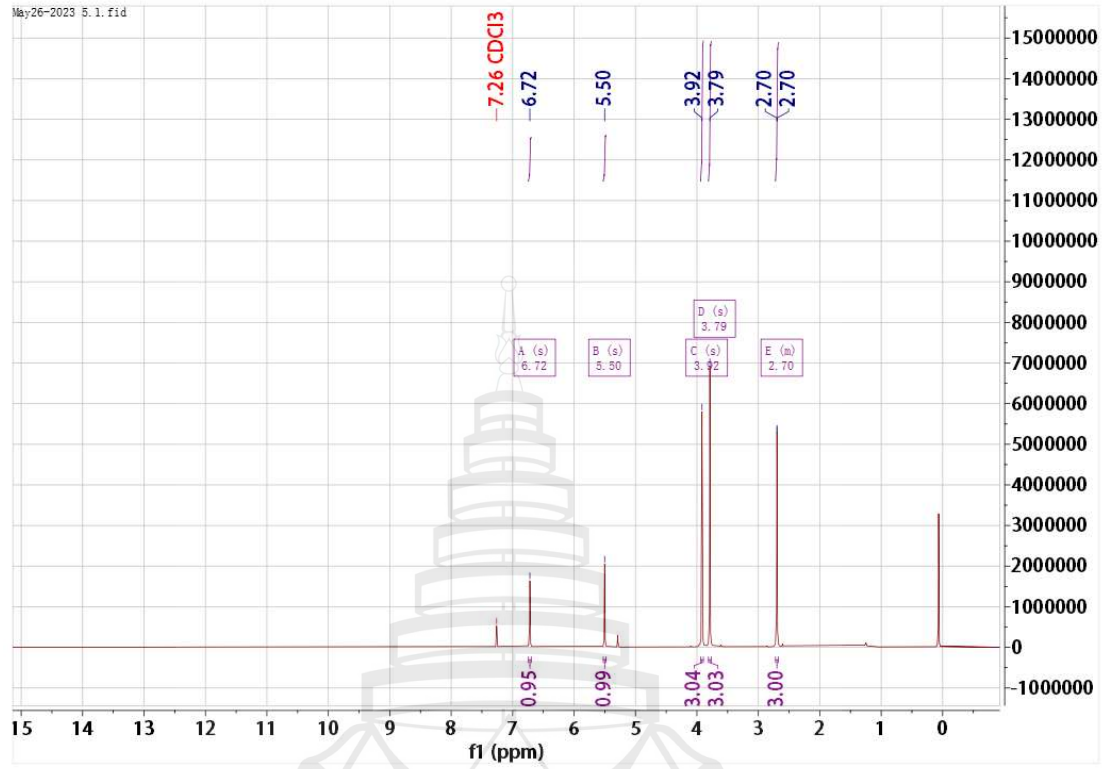

Figure A106 ^{1}H NMR spectrum of compound **C23**(400 MHz, $CDCl_3$)

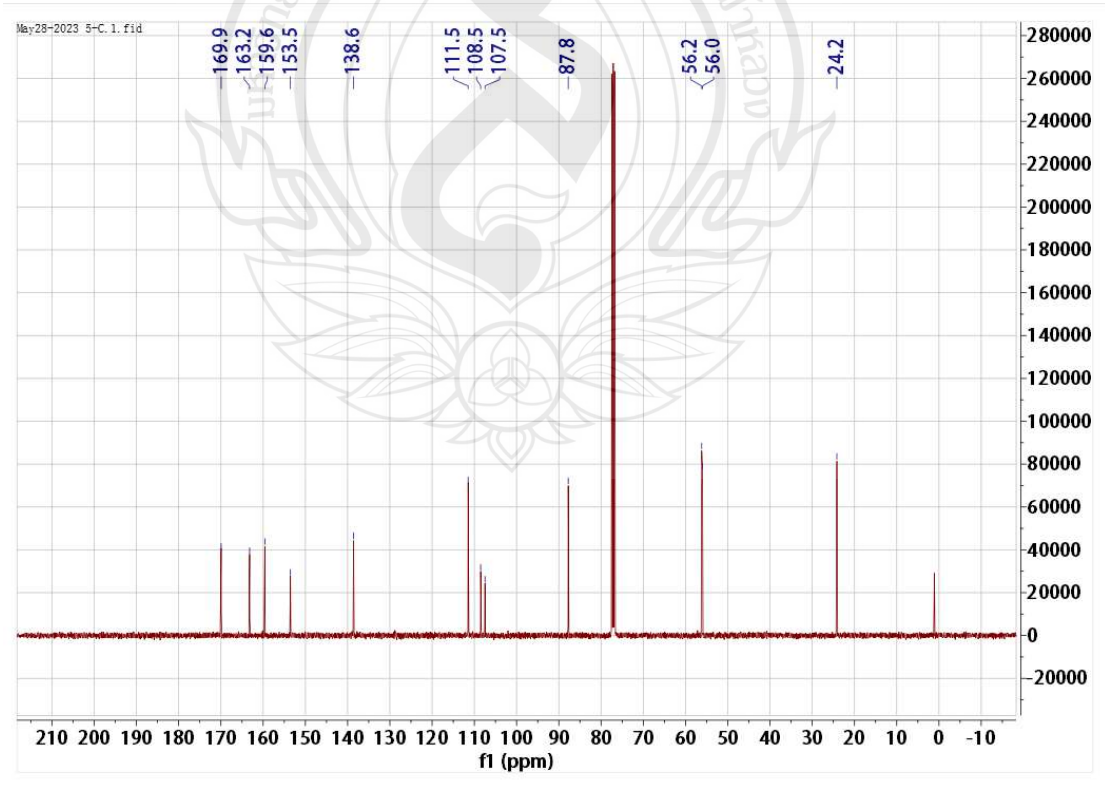

Figure A107 ^{13}C NMR spectrum of compound **C23**(100 MHz, $CDCl_3$)

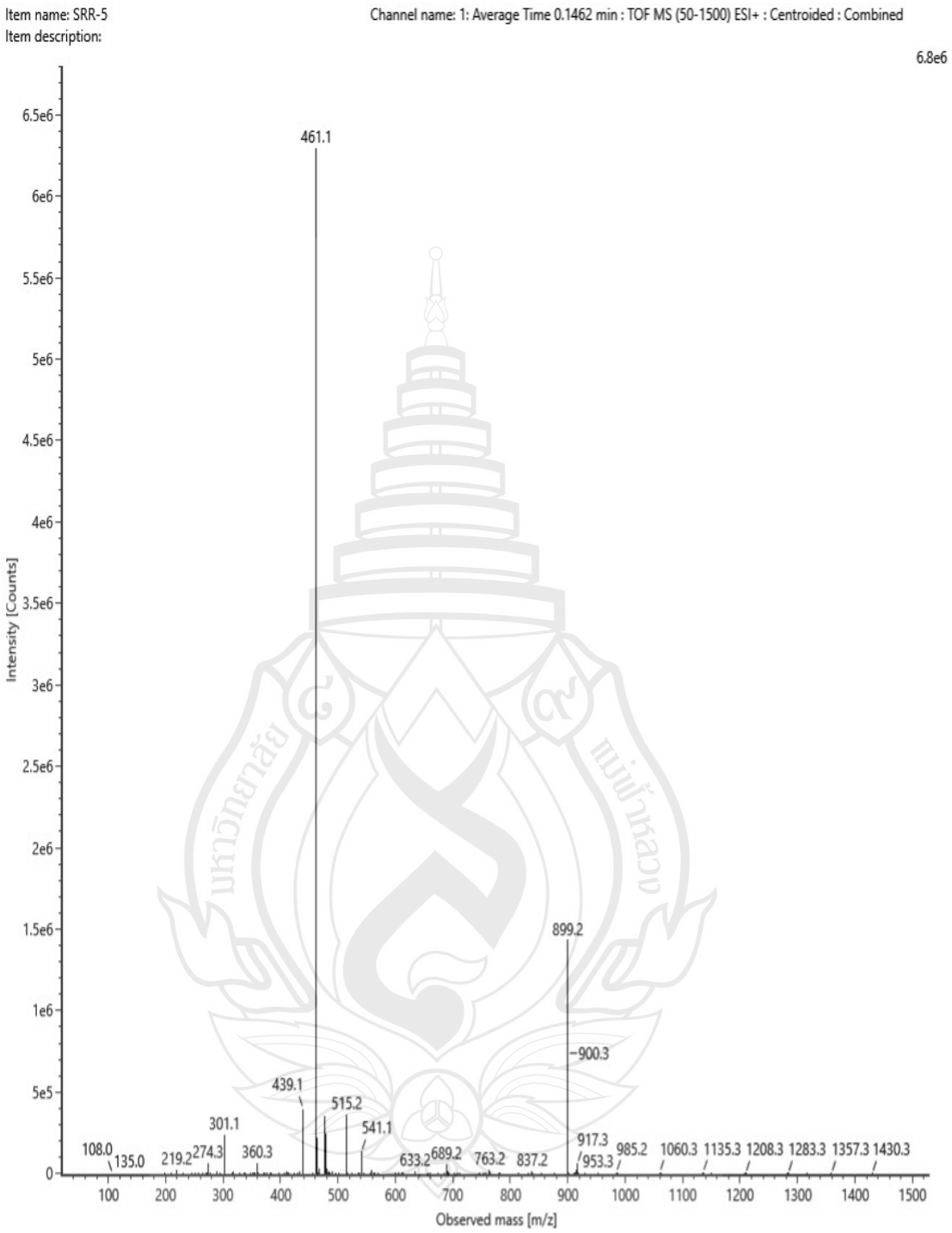

Figure A108 ESIMS of compound **C23**

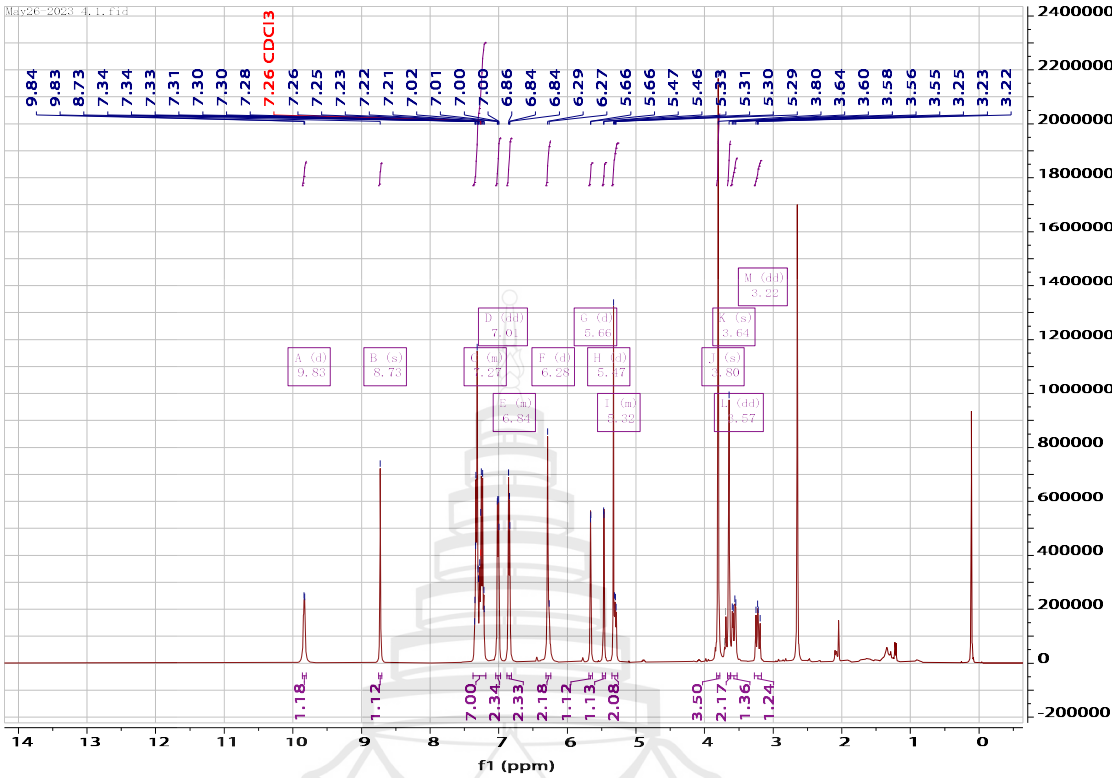

Figure A109 ^{1}H NMR spectrum of compound **C24**(400 MHz, $CDCl_3$)

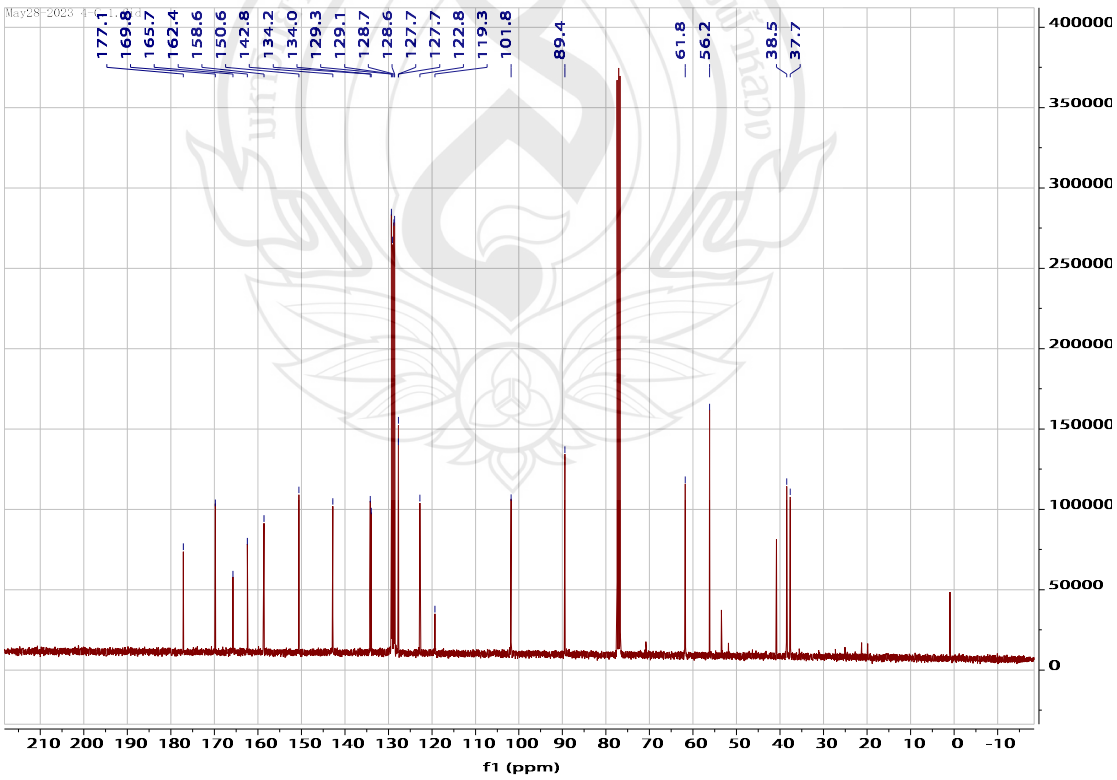

Figure A110 ^{13}C NMR spectrum of compound **C24**(100 MHz, $CDCl_3$)

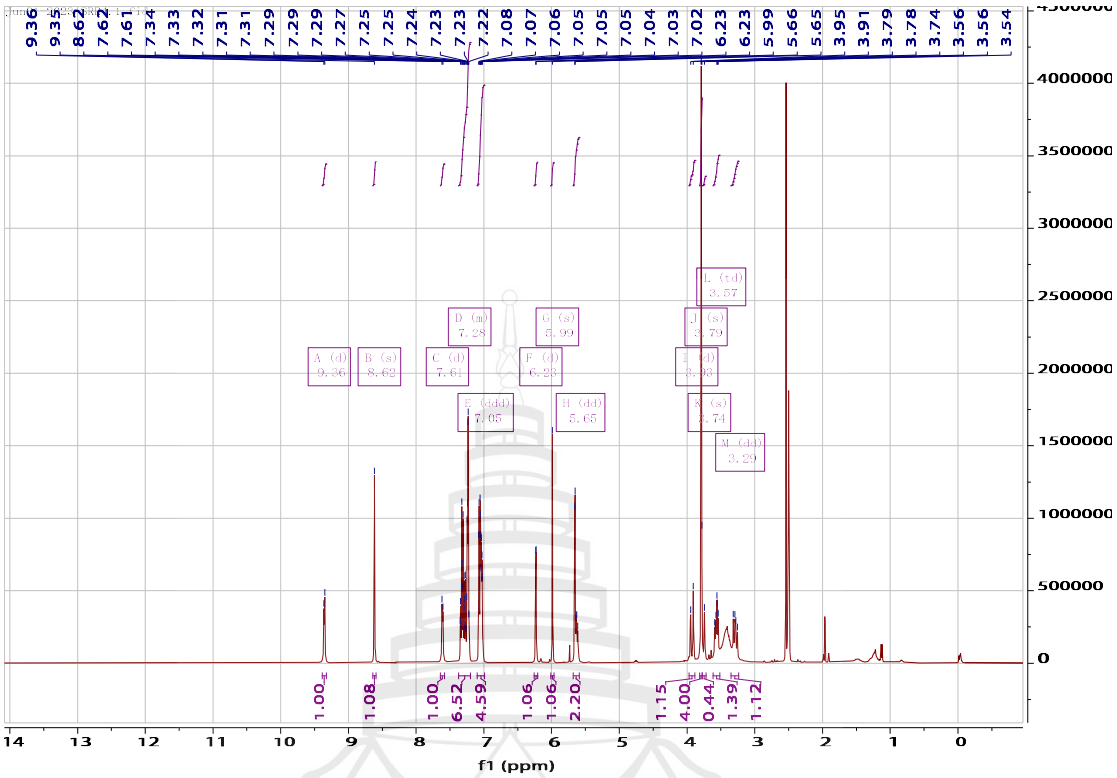

Figure A111 ^{1}H NMR spectrum of compound **C24** (400 MHz, DMSO)

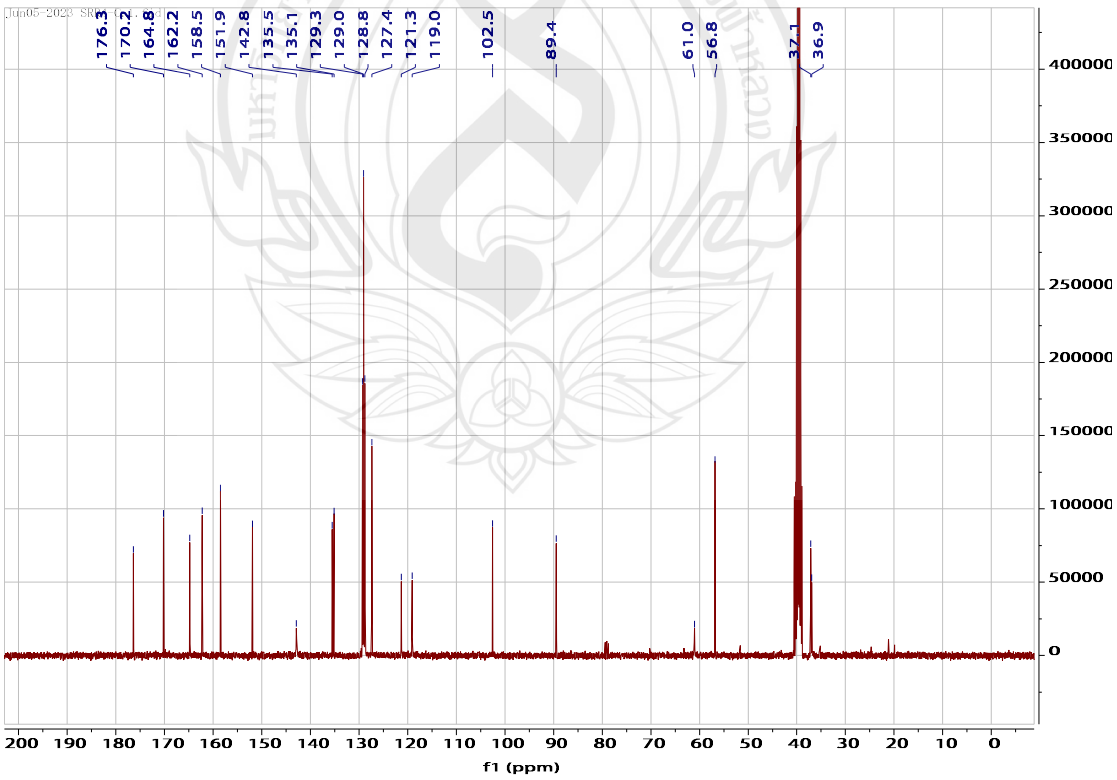

Figure A112 ^{13}C NMR spectrum of compound **C24** (100 MHz, DMSO)

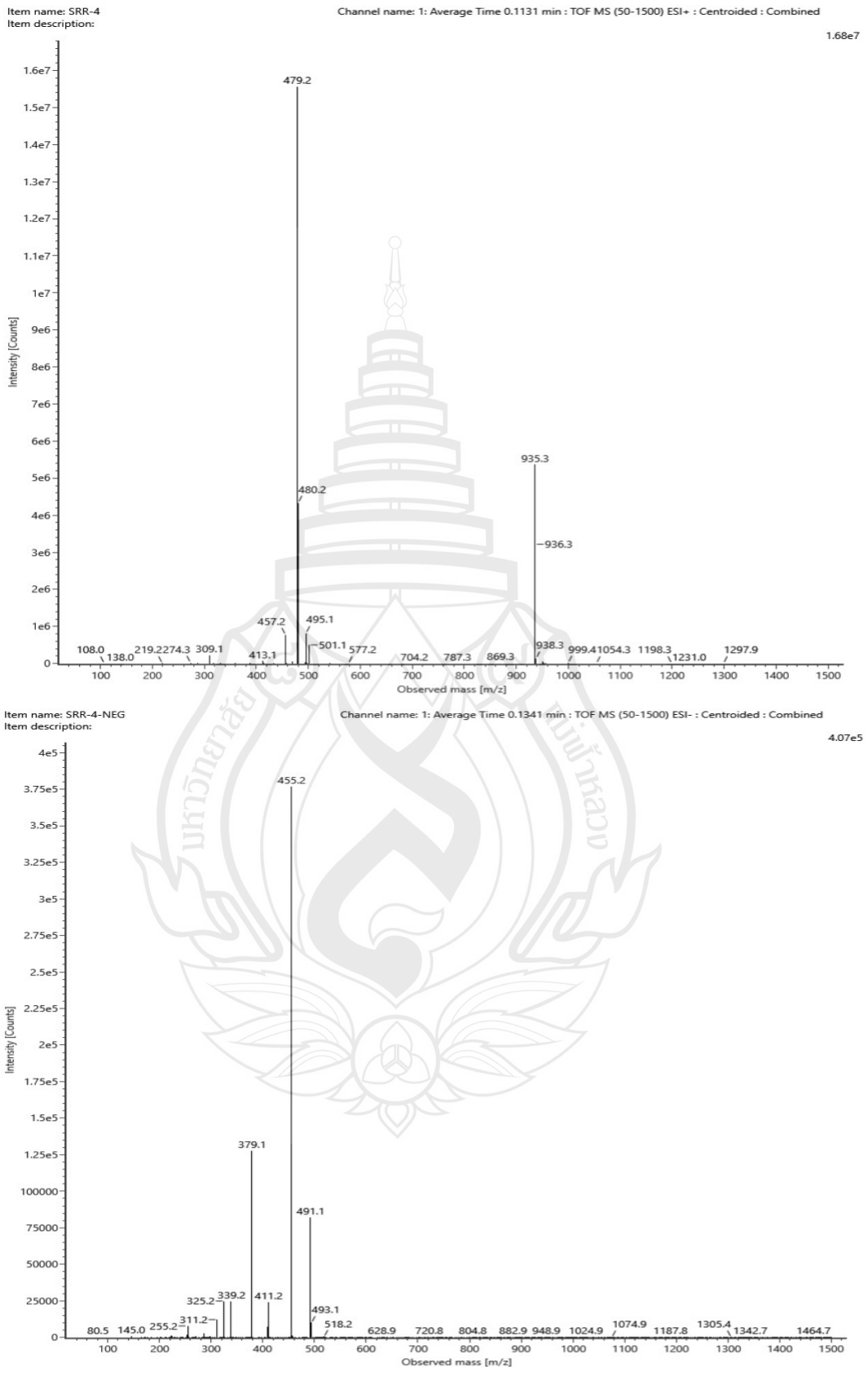

Figure A113 ESIMS of compound **C24**

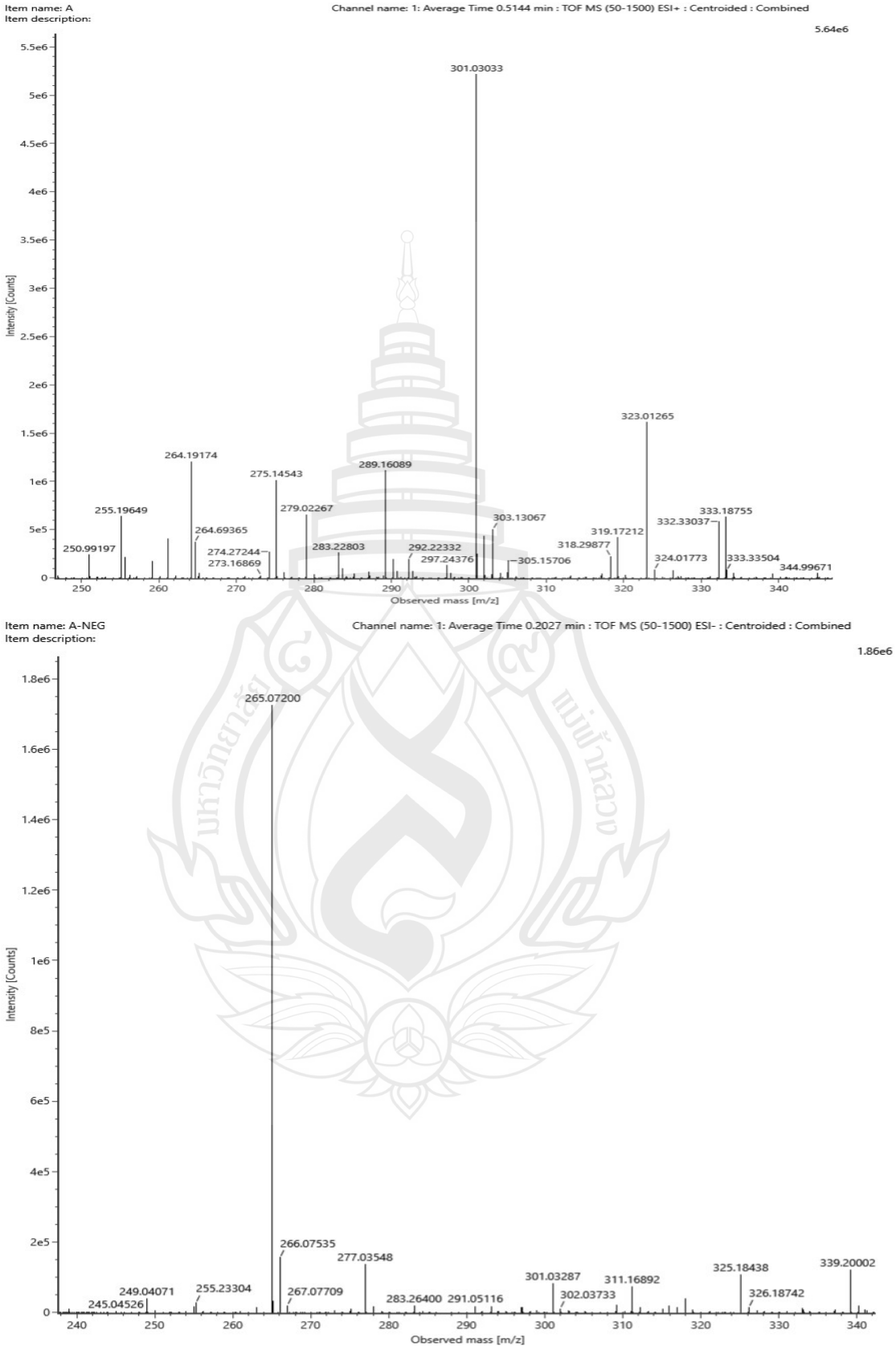

Figure A114 ESIMS of compound **C25**

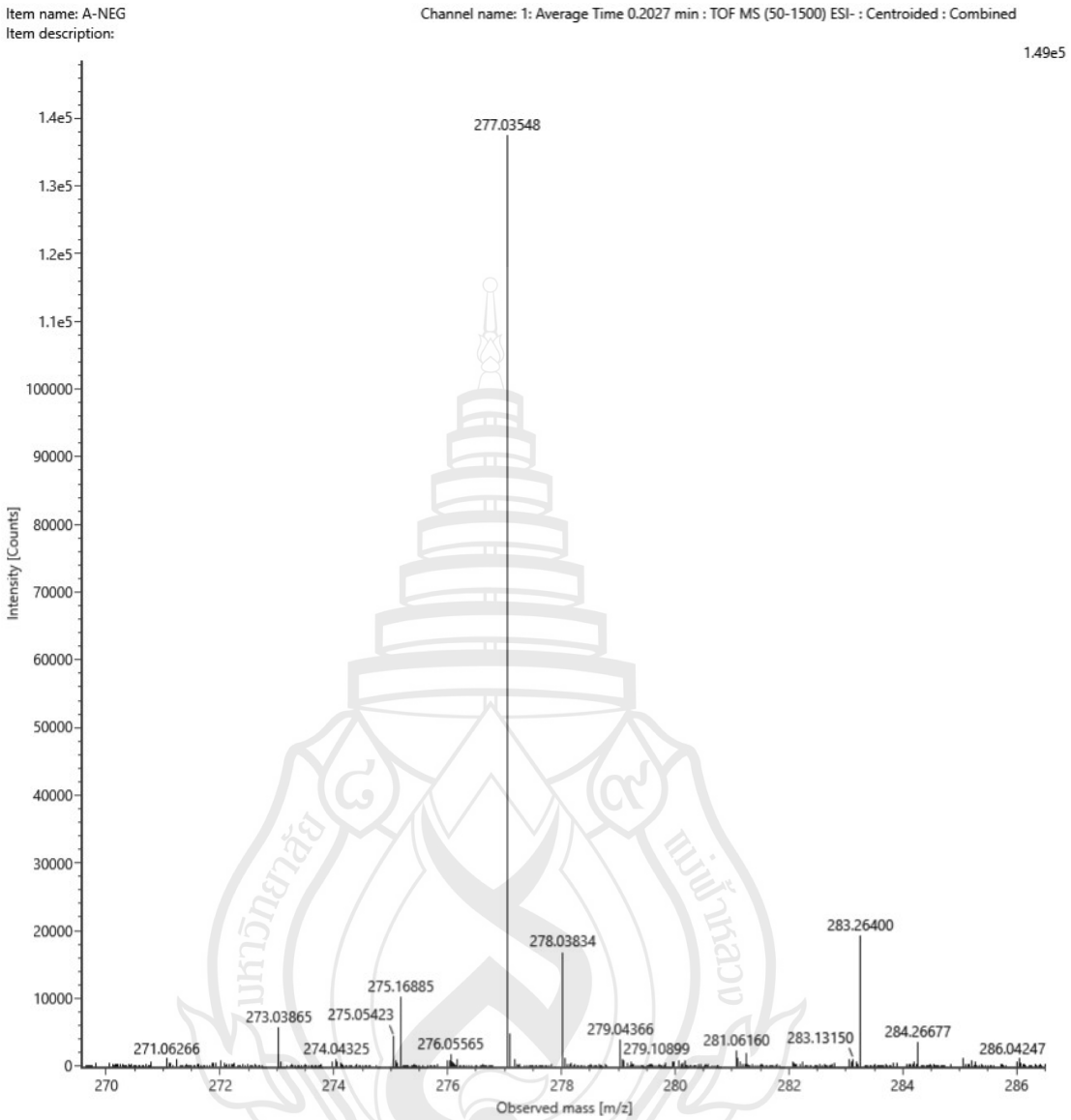

Note $[M-H]^-$

Composition	$C_{13}H_9O_7$
i-FIT Confidence (%)	100.000000
Predicted m/z	277.035376
m/z error (PPM)	0.373241

Figure A115 HR-ESIMS of compound **C25**

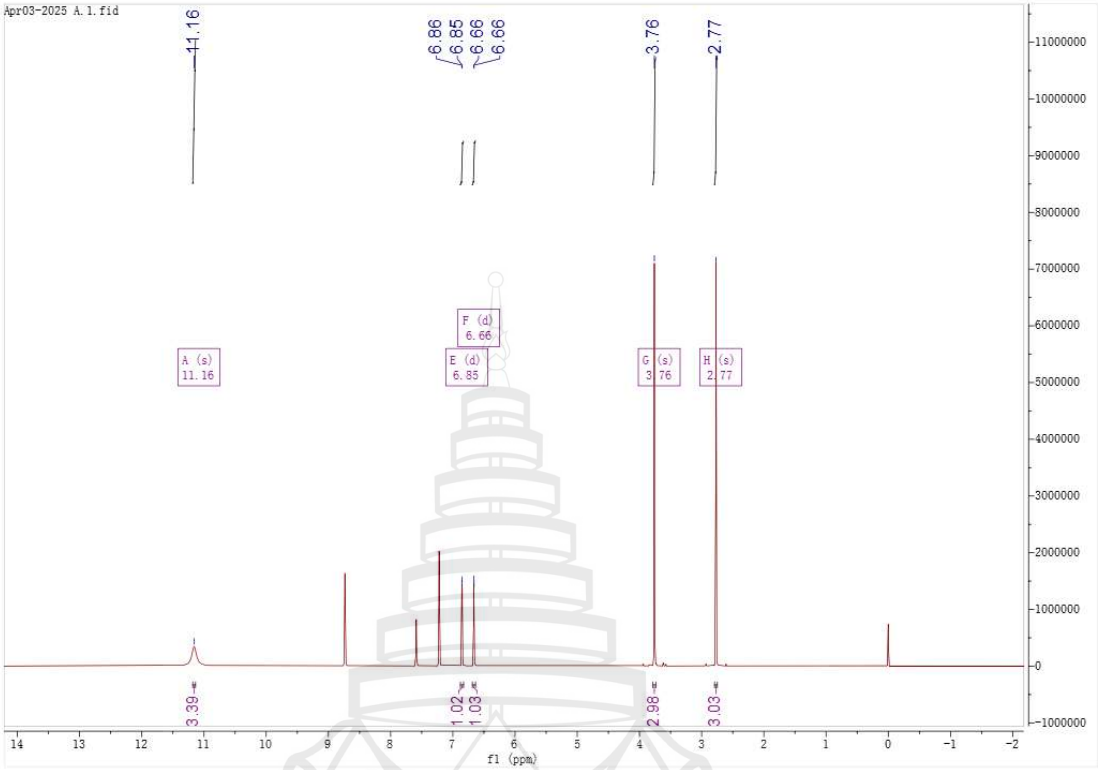

Figure A116 ^{1}H NMR spectrum of compound **C25** (400 MHz, C_5D_5N)

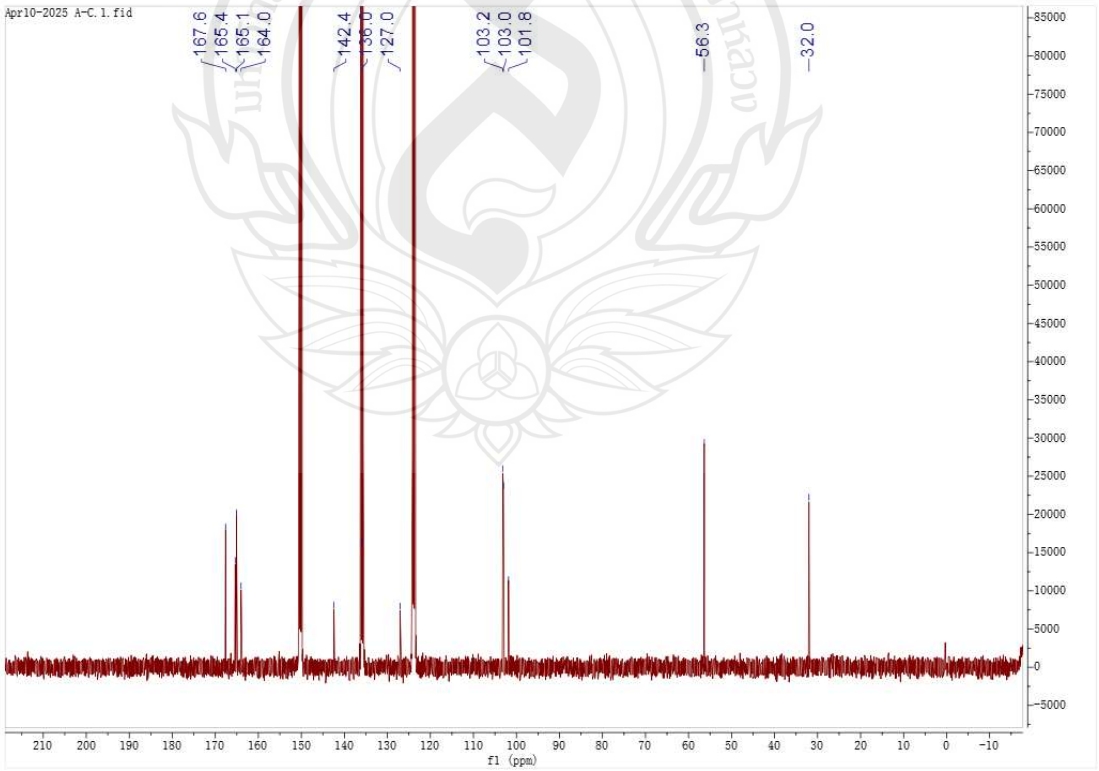

Figure A117 ^{13}C NMR spectrum of compound **C25** (100 MHz, C_5D_5N)

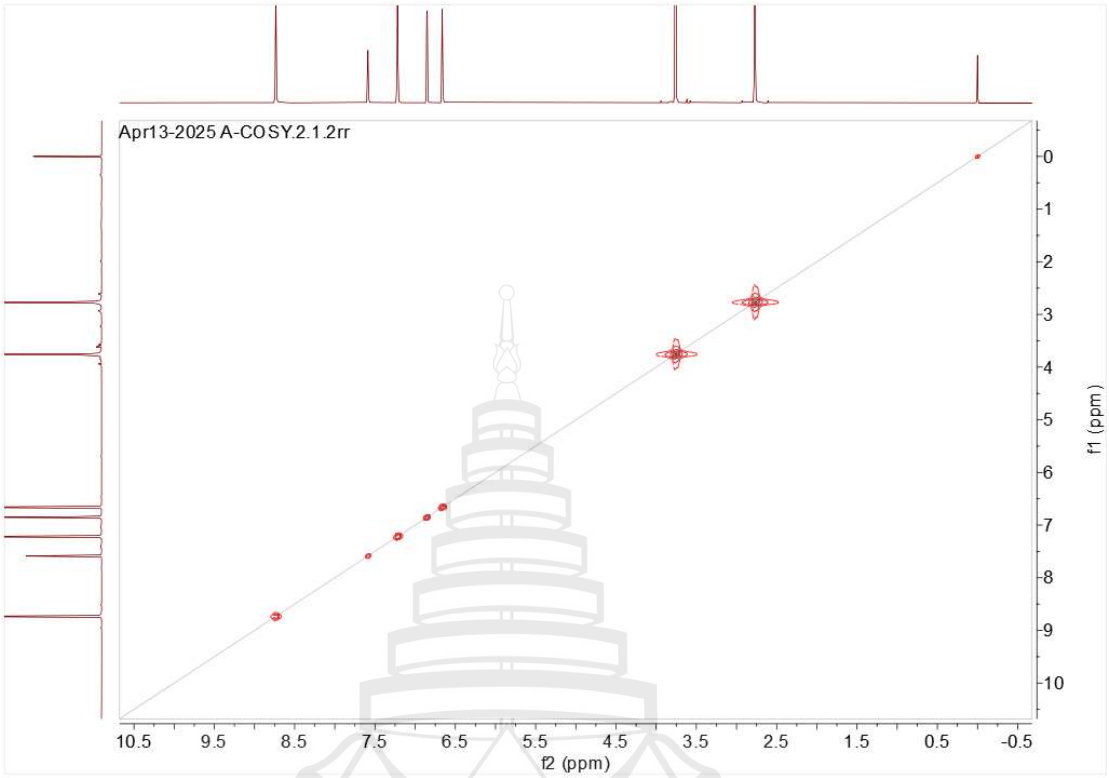

Figure A118 ^{1}H-^{1}H COSY spectrum of compound **C25** (C_5D_5N)

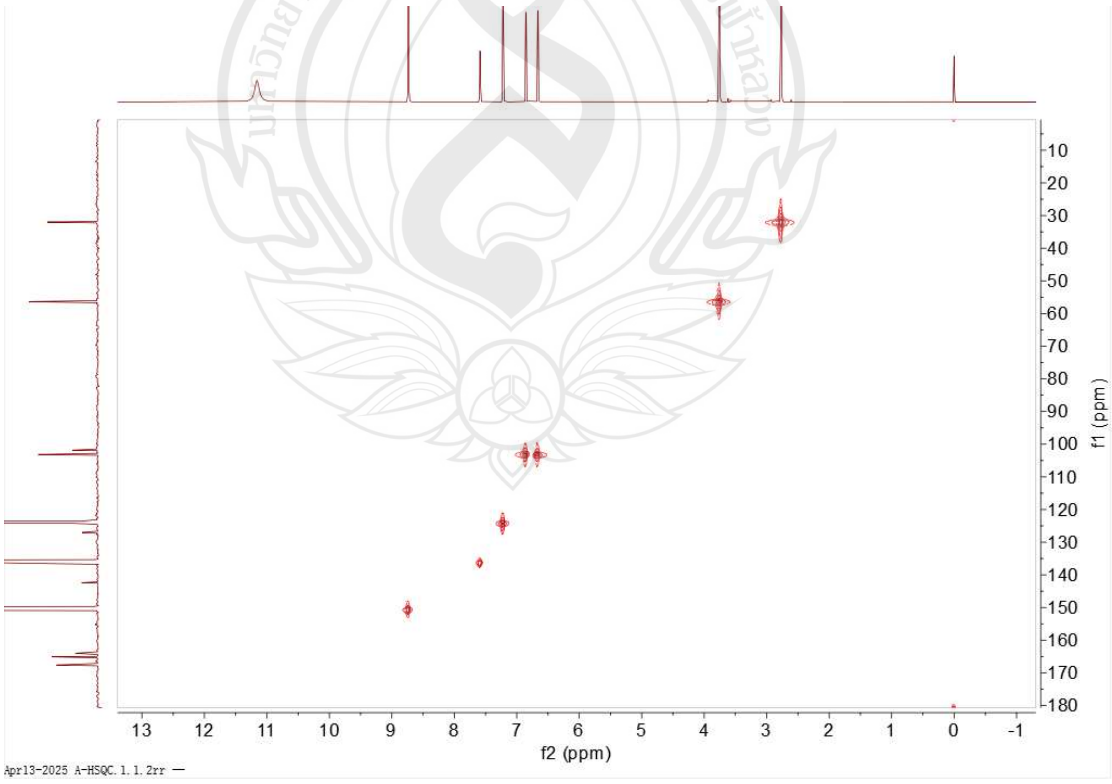

Figure A119 HSQC spectrum of compound **C25** (C_5D_5N)

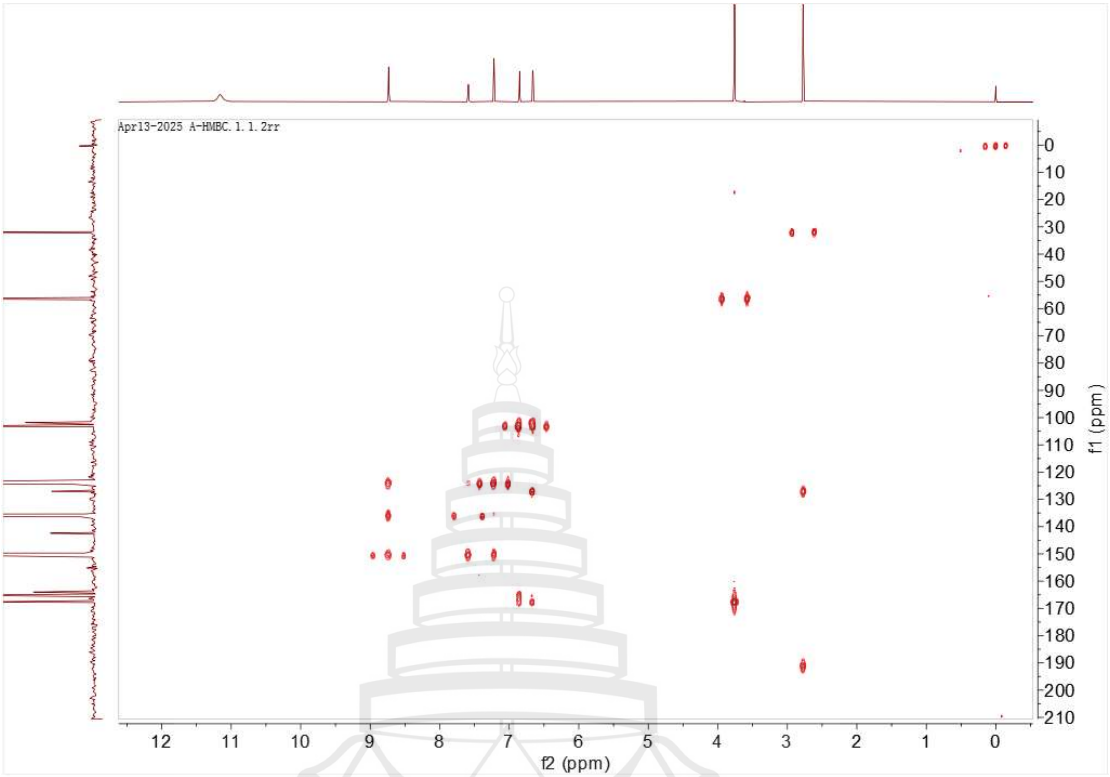

Figure A120 HMBC spectrum of compound **C25** (C_5D_5N)

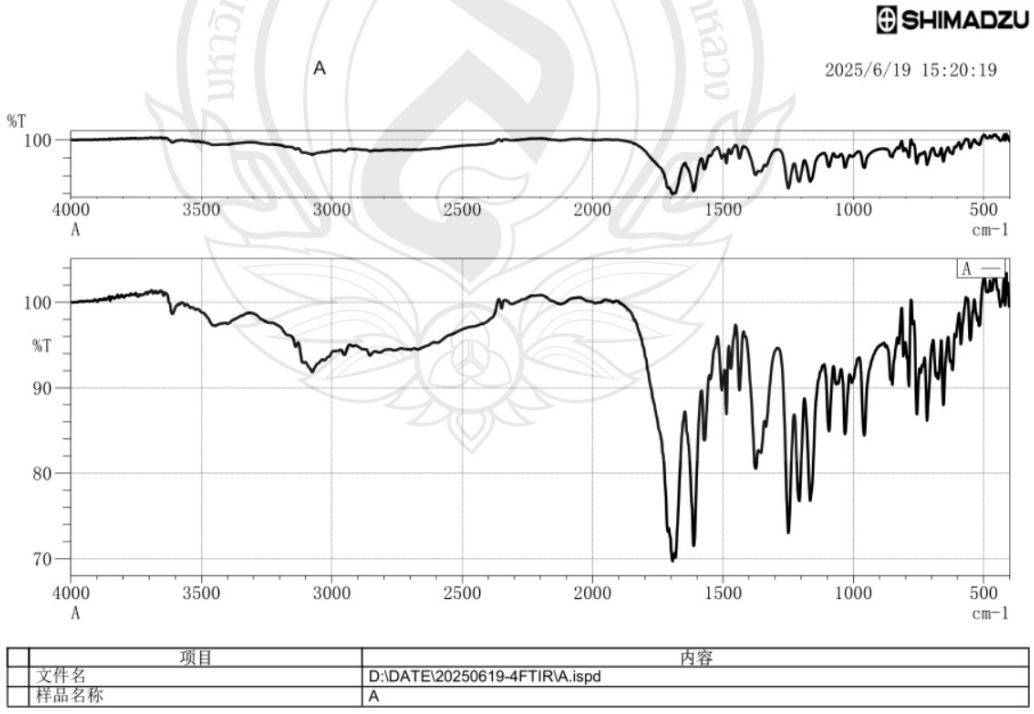

Figure A121 IR (KBr) spectrum of compound **C25**

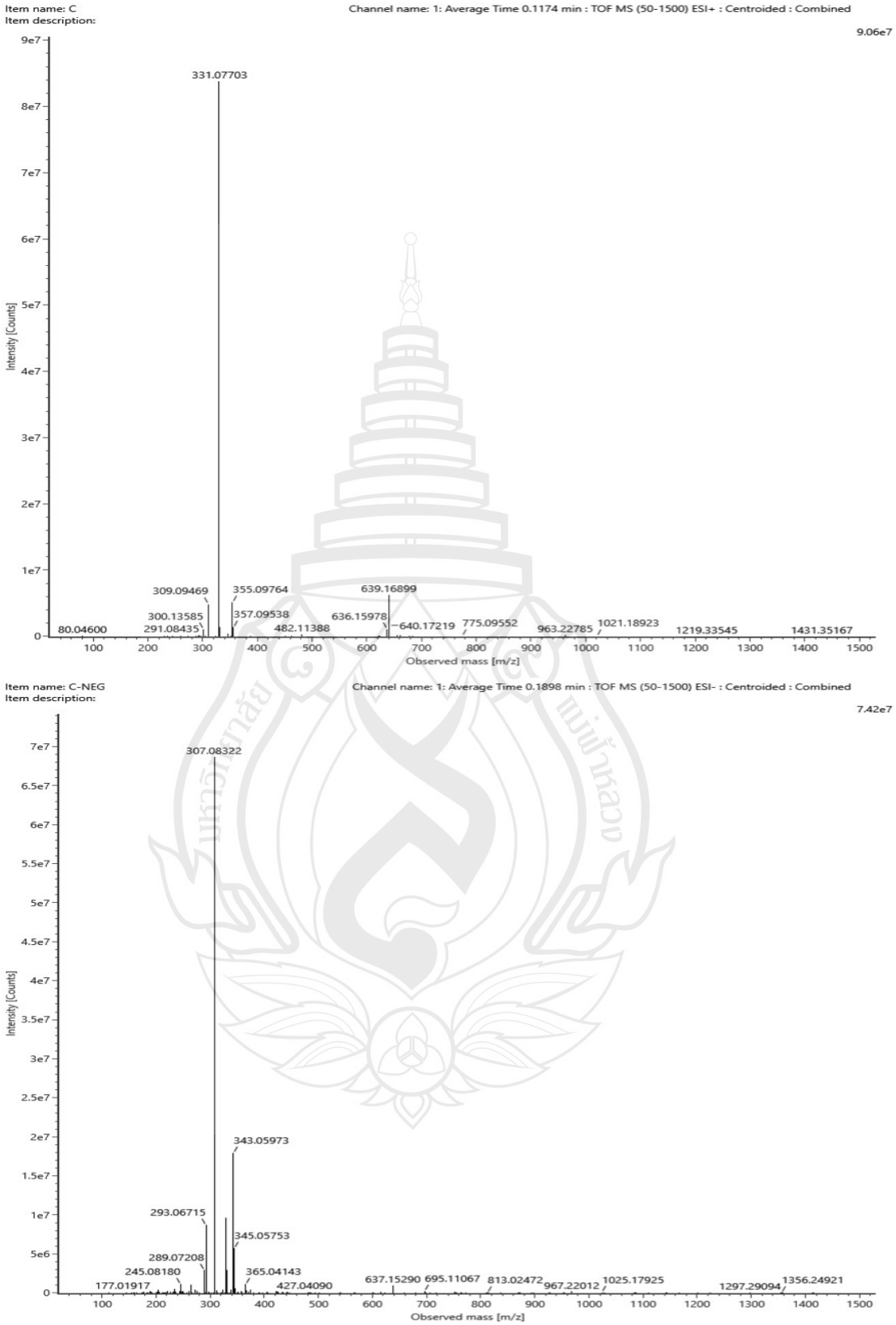

Figure A122 ESIMS of compound **C26**

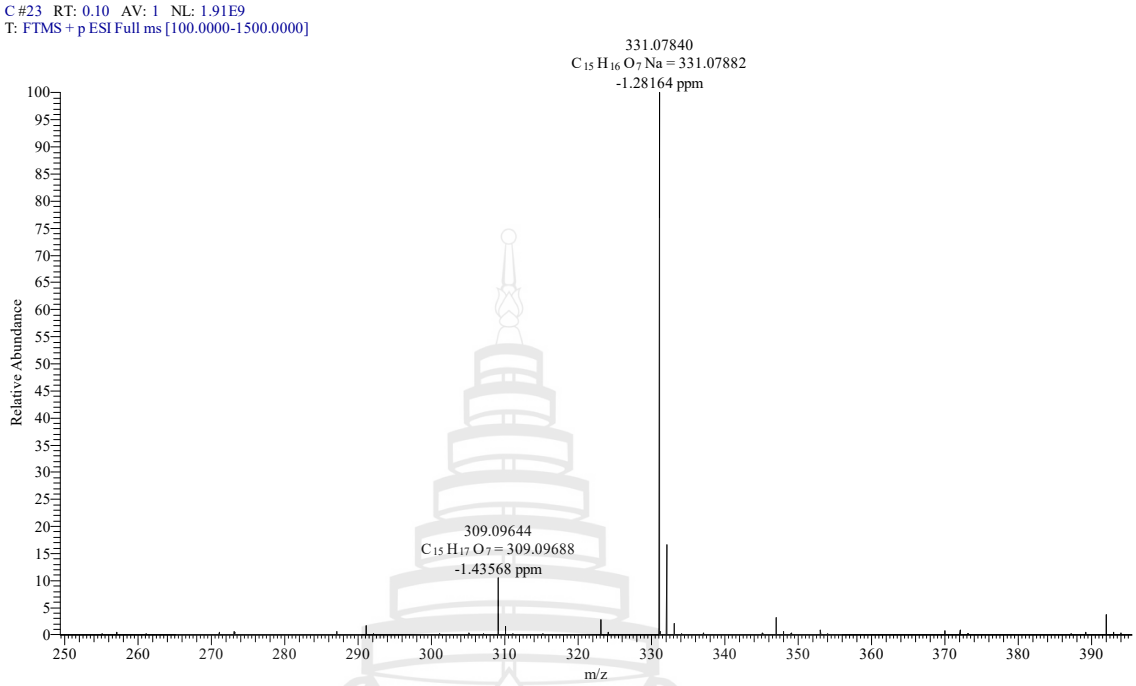

Figure A123 HR-ESIMS of compound **C26**

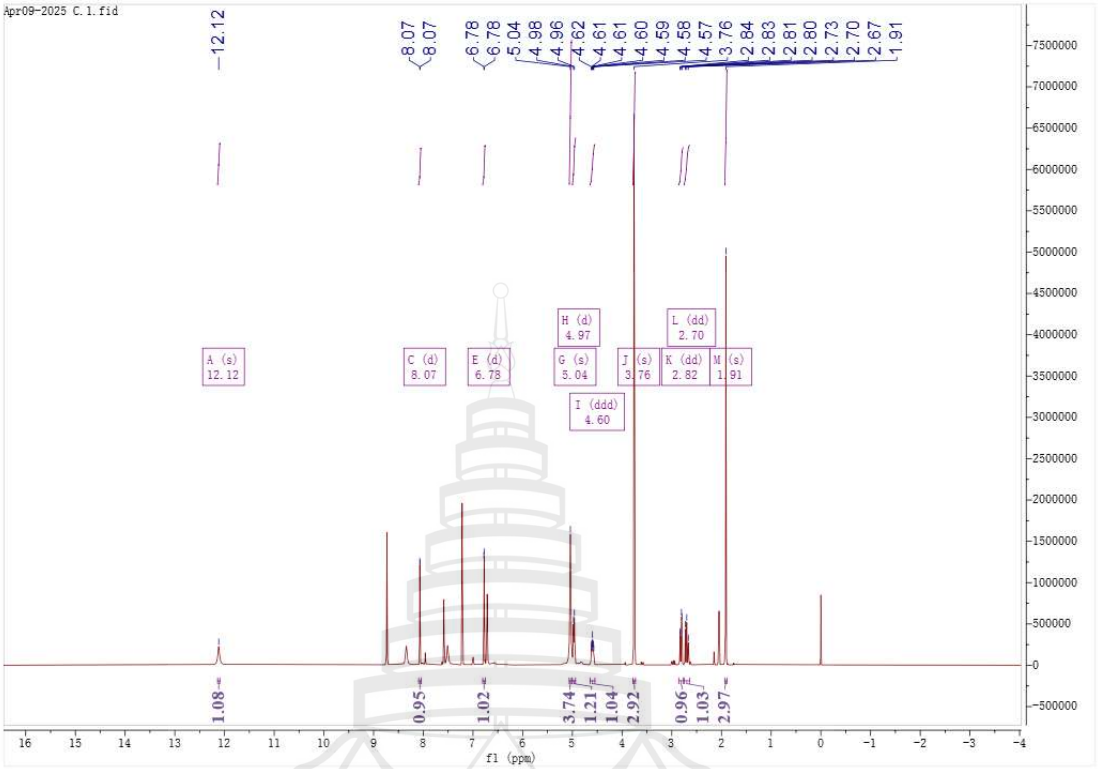

Figure A124 ^{1}H NMR spectrum of compound **C26** (400 MHz, C_5D_5N)

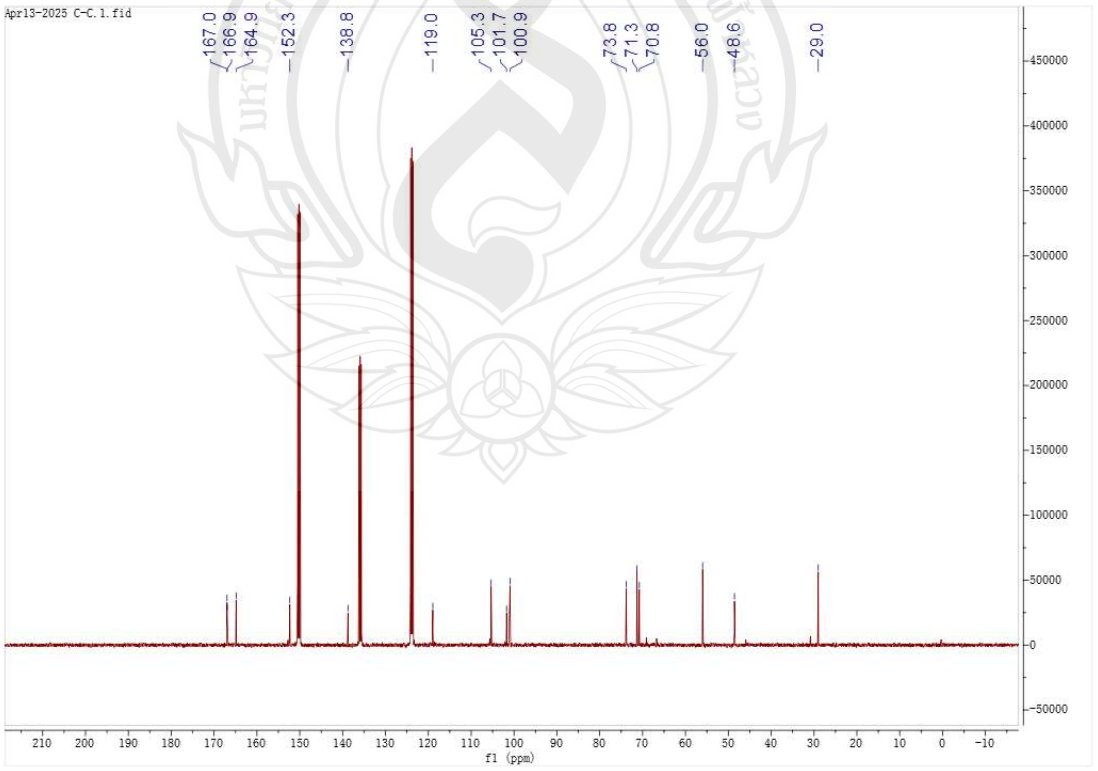

Figure A125 ^{13}C NMR spectrum of compound **C26** (100 MHz, C_5D_5N)

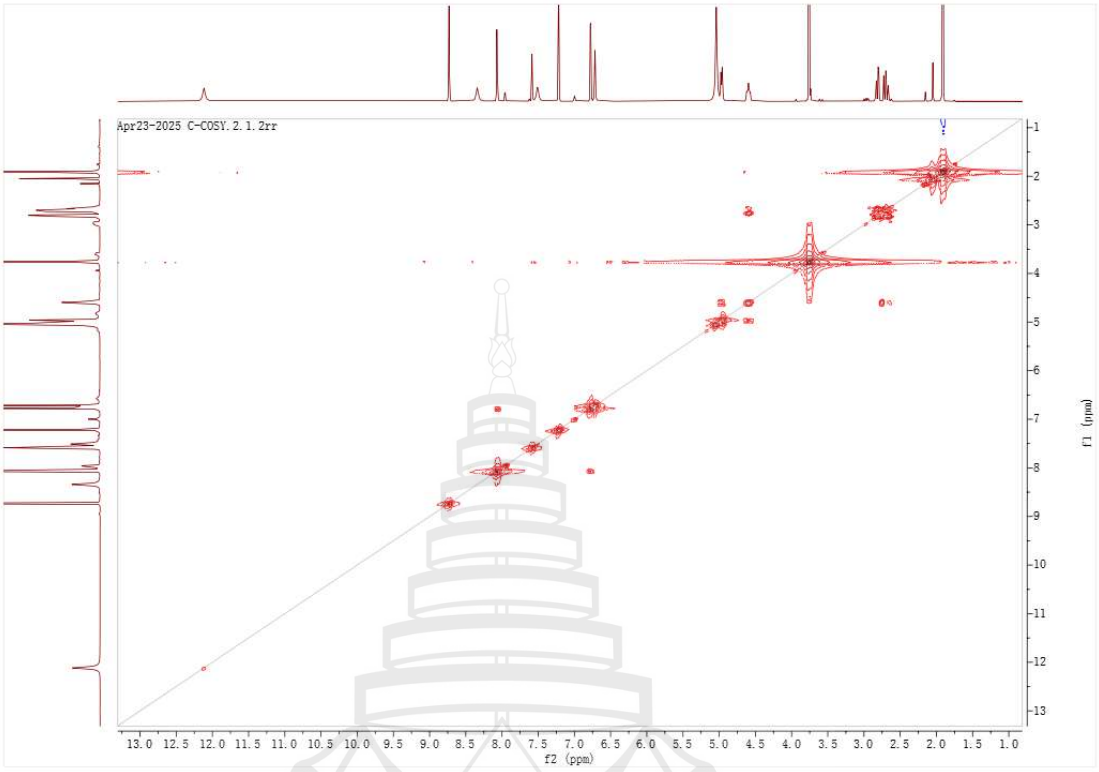

Figure A126 ^{1}H-^{1}H COSY spectrum of compound **C26** (C_5D_5N)

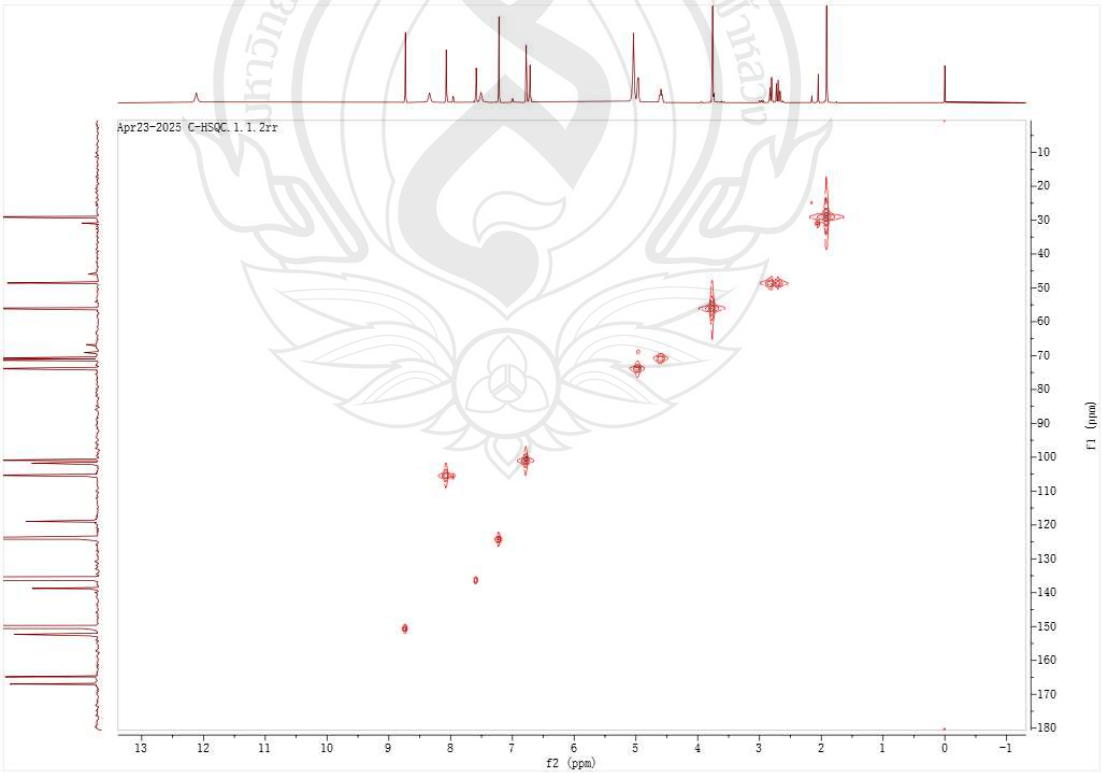

Figure A127 HSQC spectrum of compound **C26** (C_5D_5N)

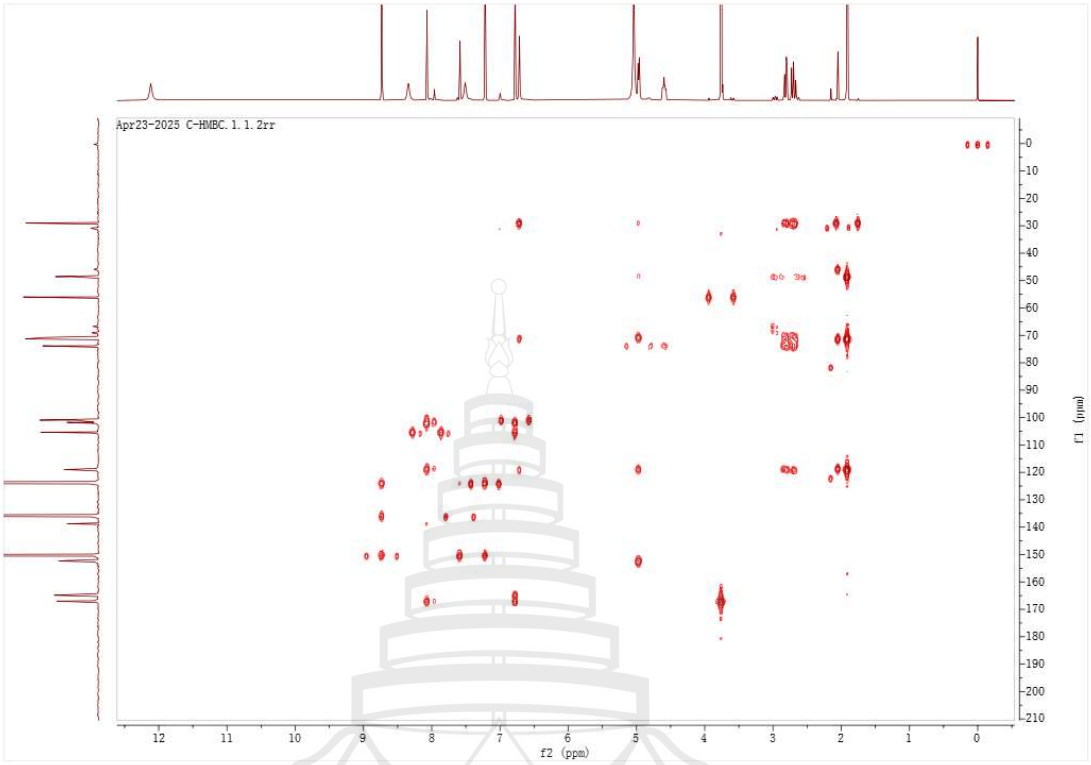

Figure A128 HMBC spectrum of compound **C26** (C_5D_5N)

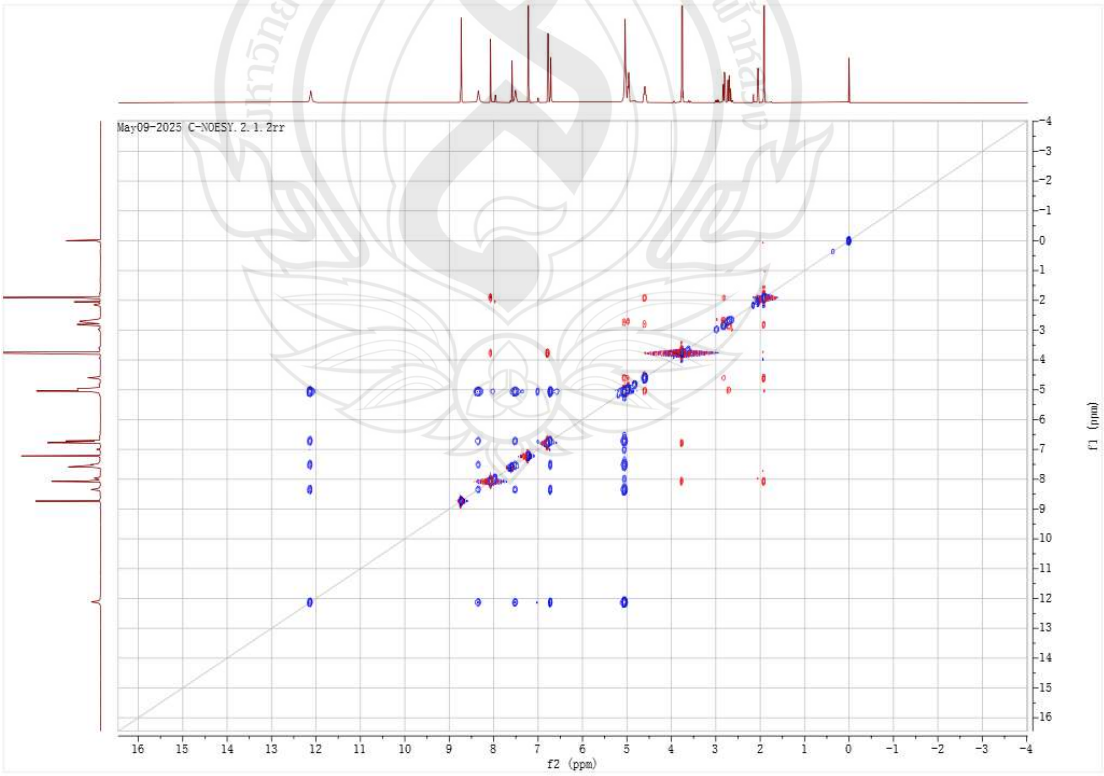

Figure A129 NOESY spectrum of compound **C26** (C_5D_5N)

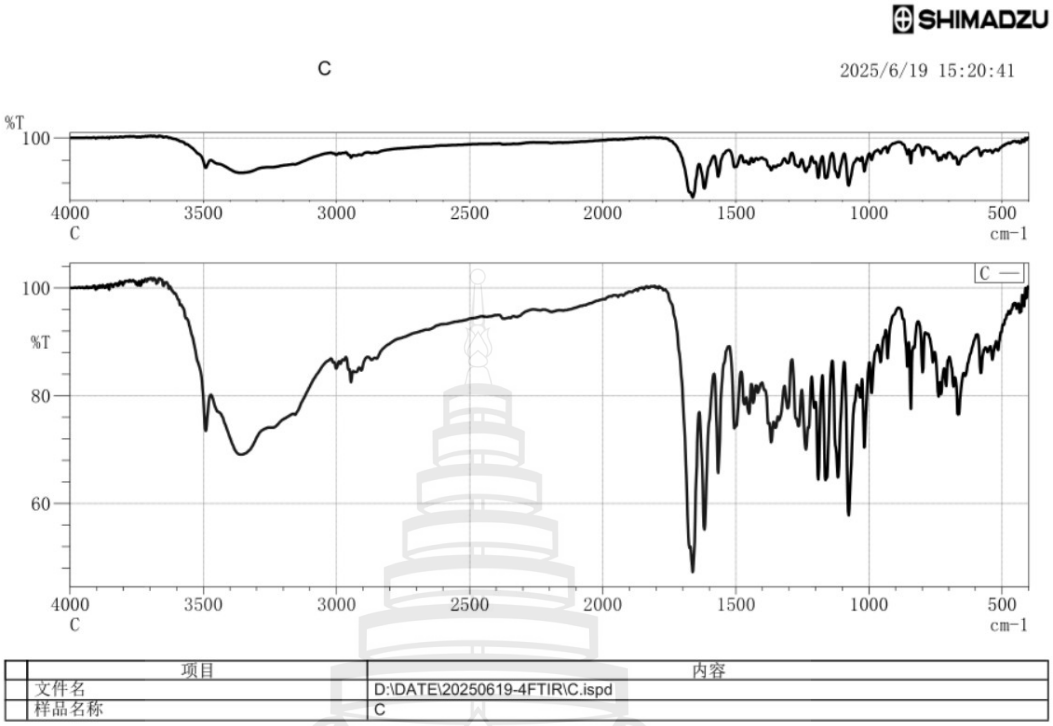

	项目	内容
	文件名	D:\DATE\20250619-4FTIR\C.ispd
	样品名称	C

Figure A130 IR (KBr) spectrum of compound **C26**

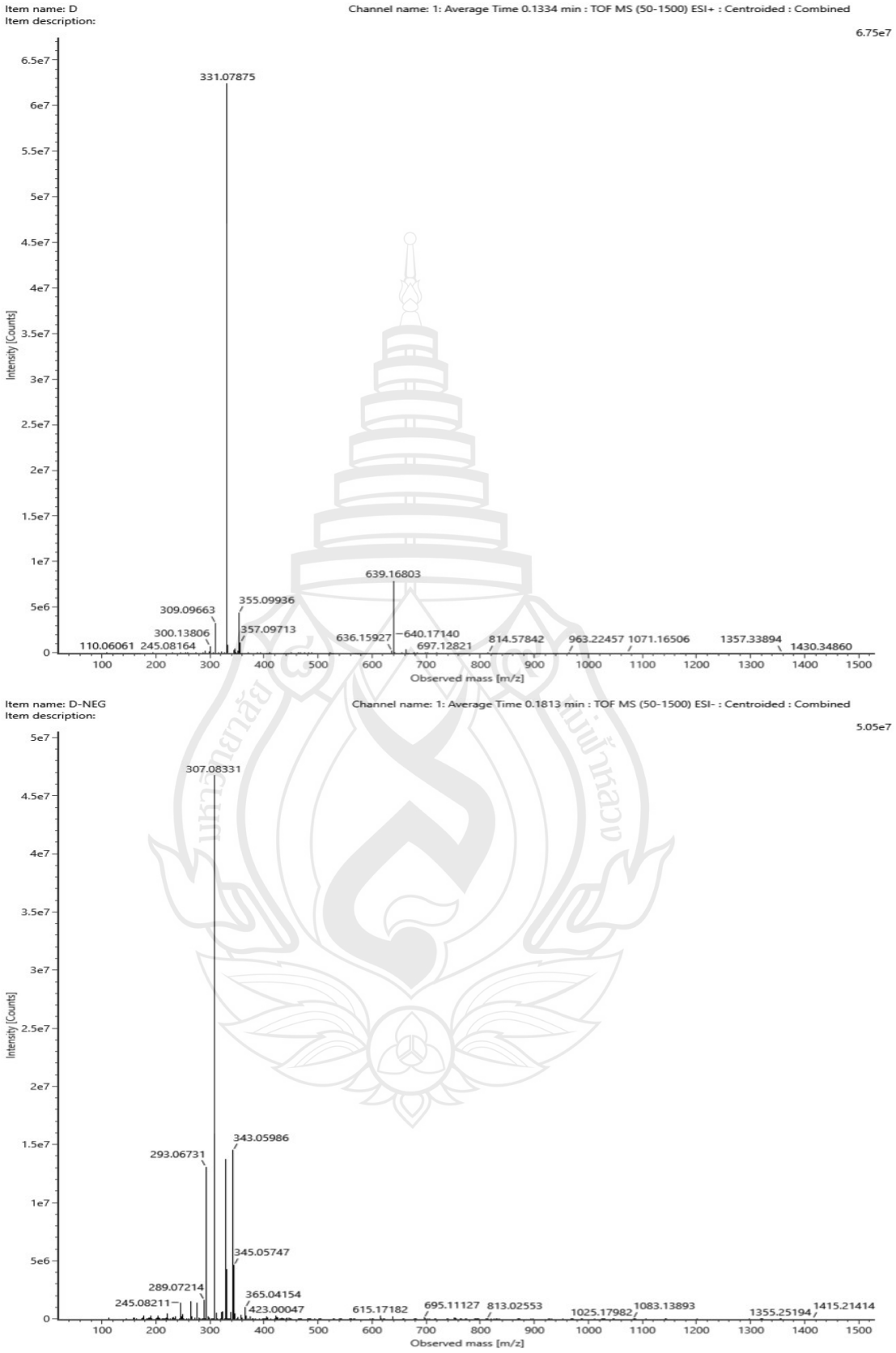

Figure A131 ESIMS of compound **C26**

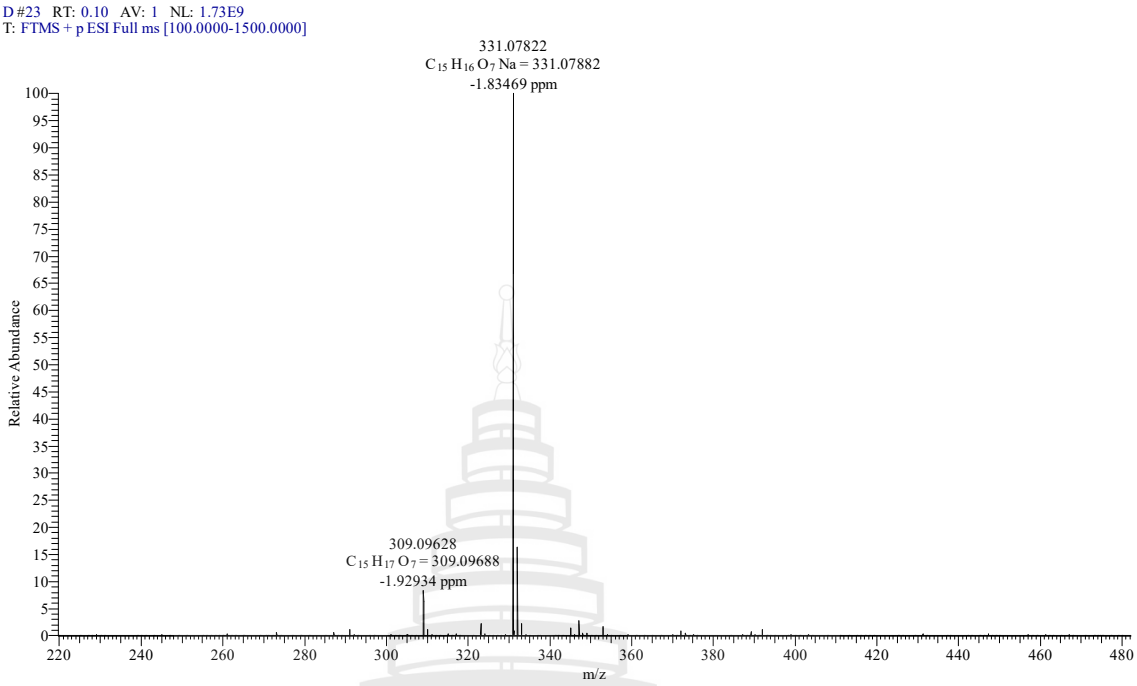

Figure A132 HR-ESIMS of compound **C26**

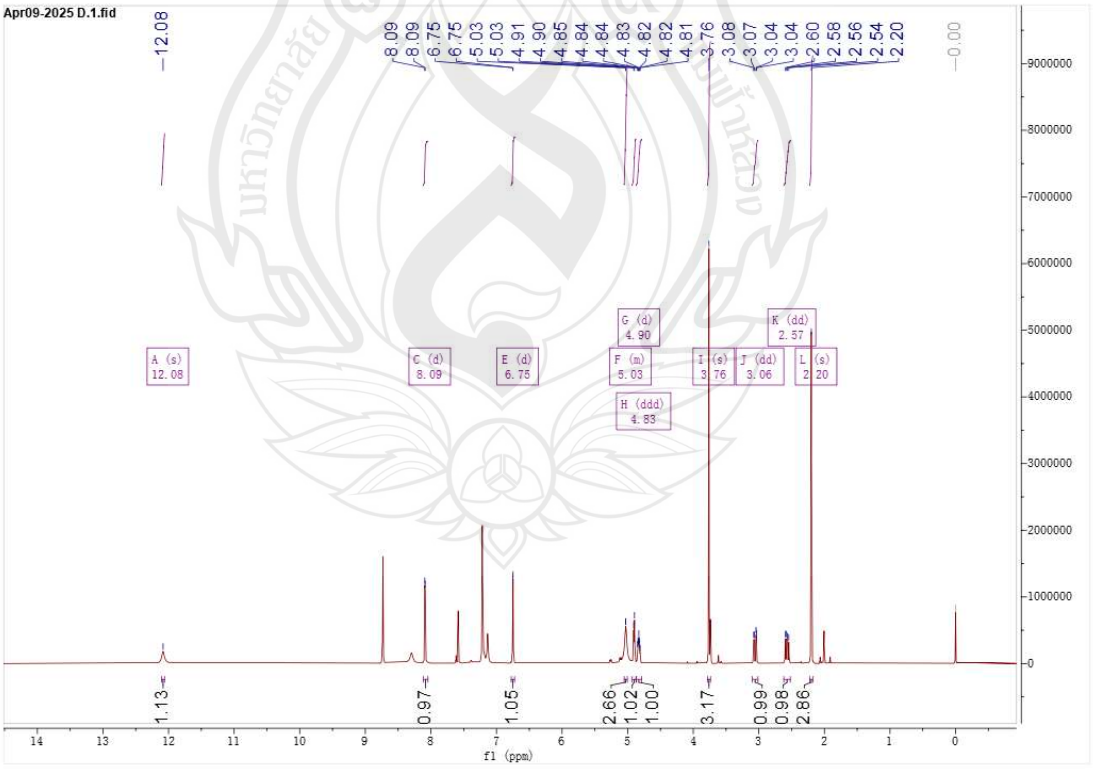

Figure A133 ^{1}H NMR spectrum of compound **C27** (400 MHz, C_5D_5N)

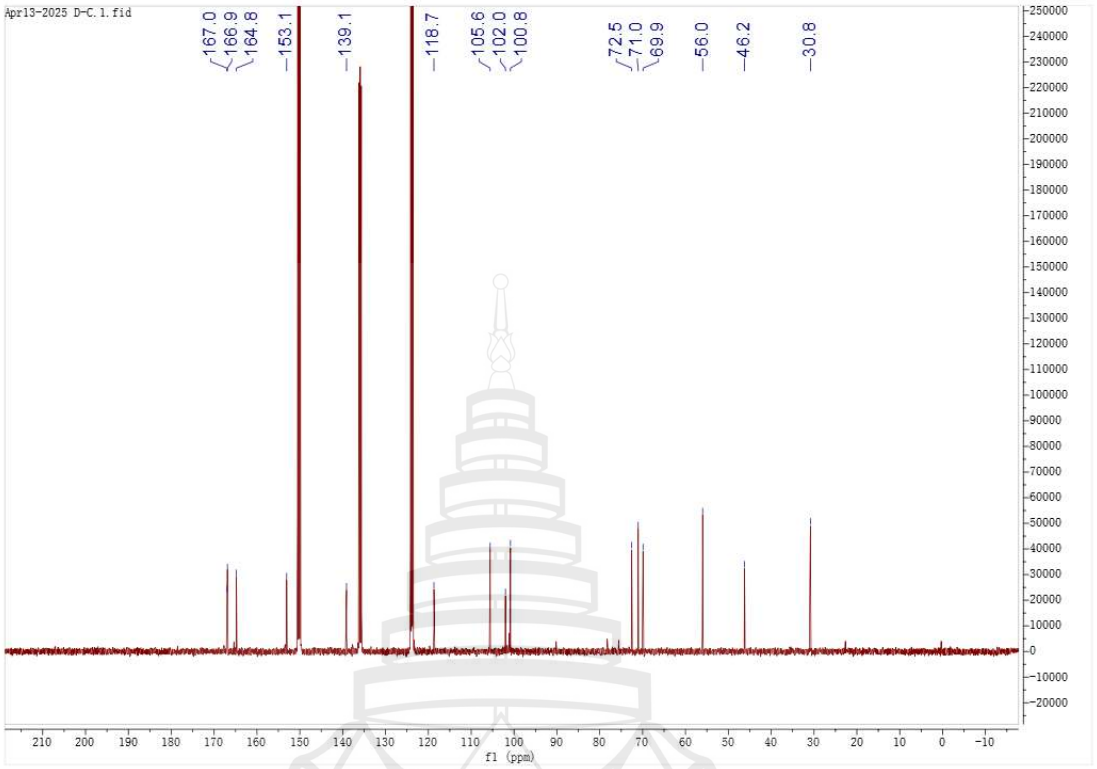

Figure A134 ^{13}C NMR spectrum of compound **C27** (100 MHz, C_5D_5N)

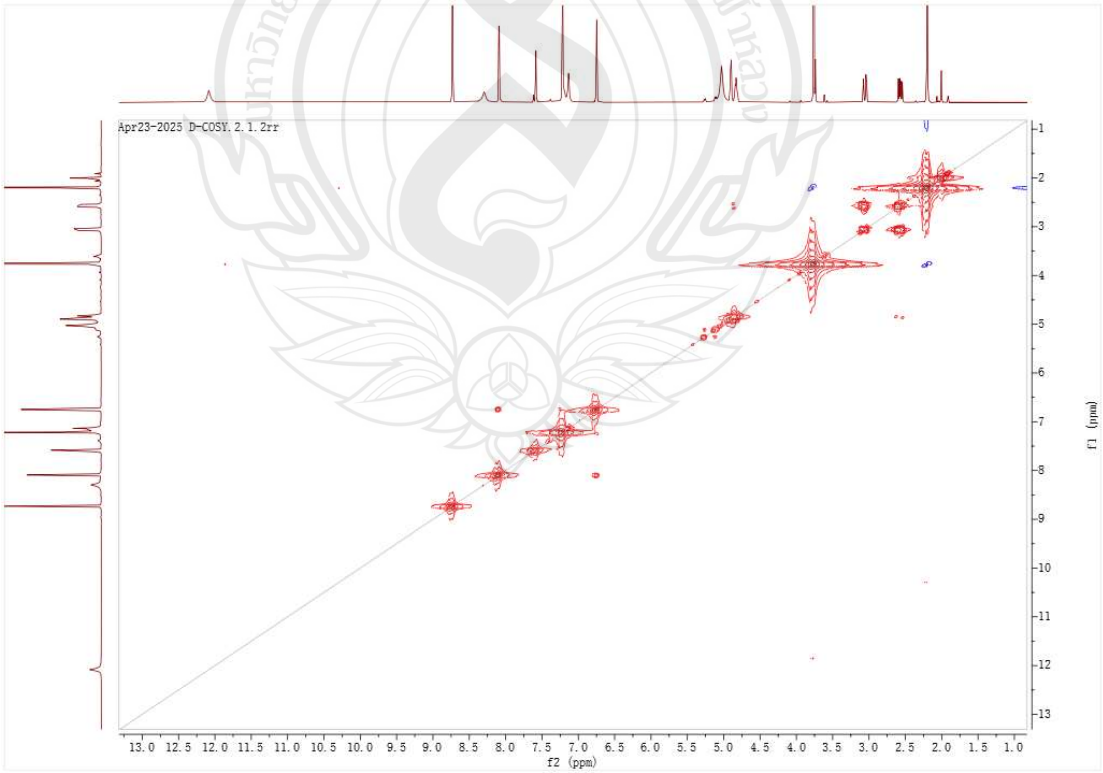

Figure A135 ^{1}H-^{1}H COSY spectrum of compound **C27** (C_5D_5N)

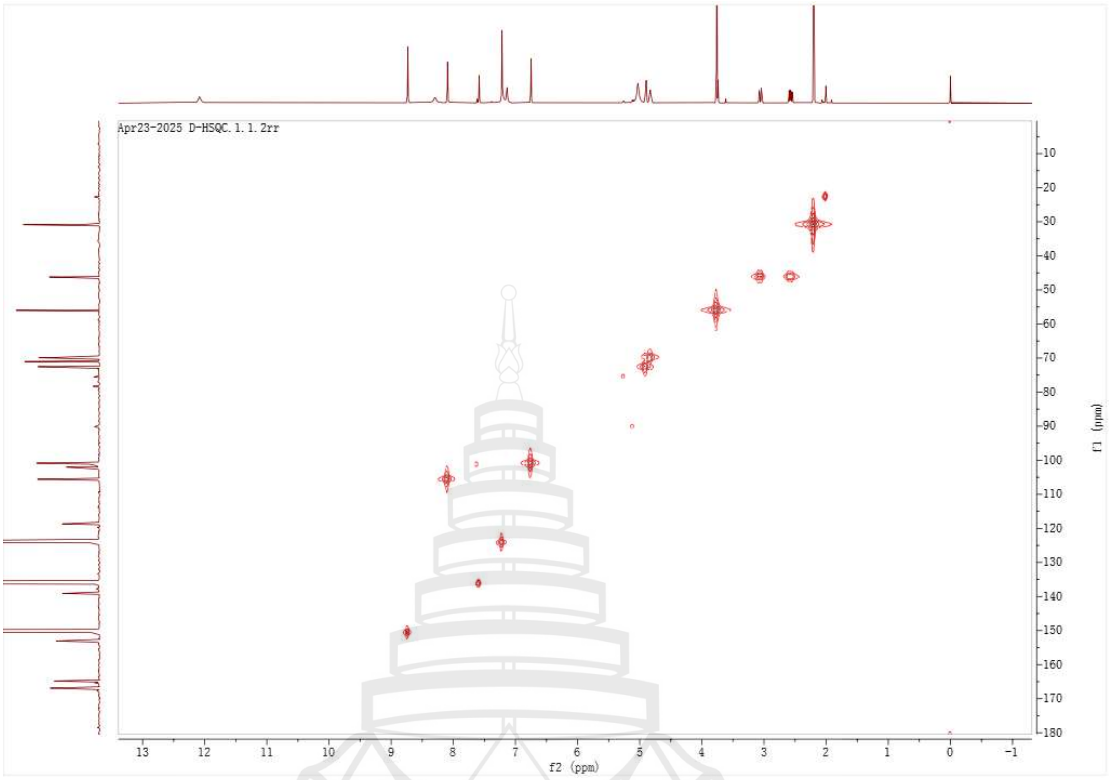

Figure A136 HSQC spectrum of compound **C27** (C_5D_5N)

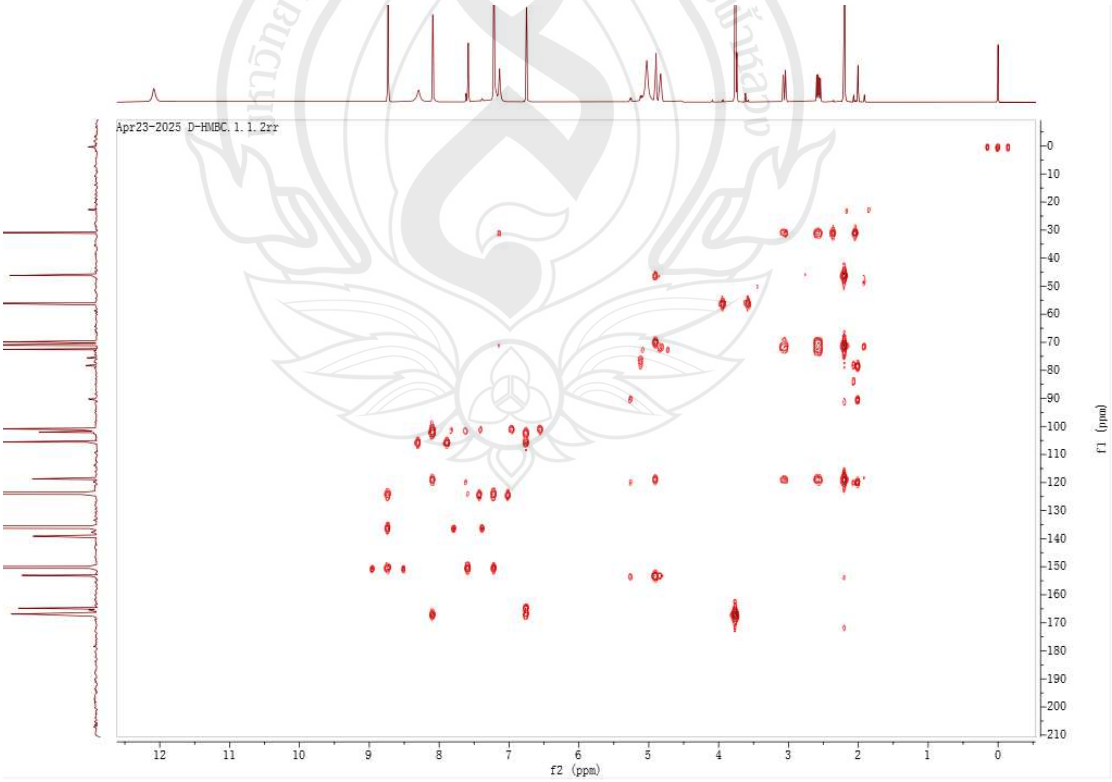

Figure A137 HMBC spectrum of compound **C27** (C_5D_5N)

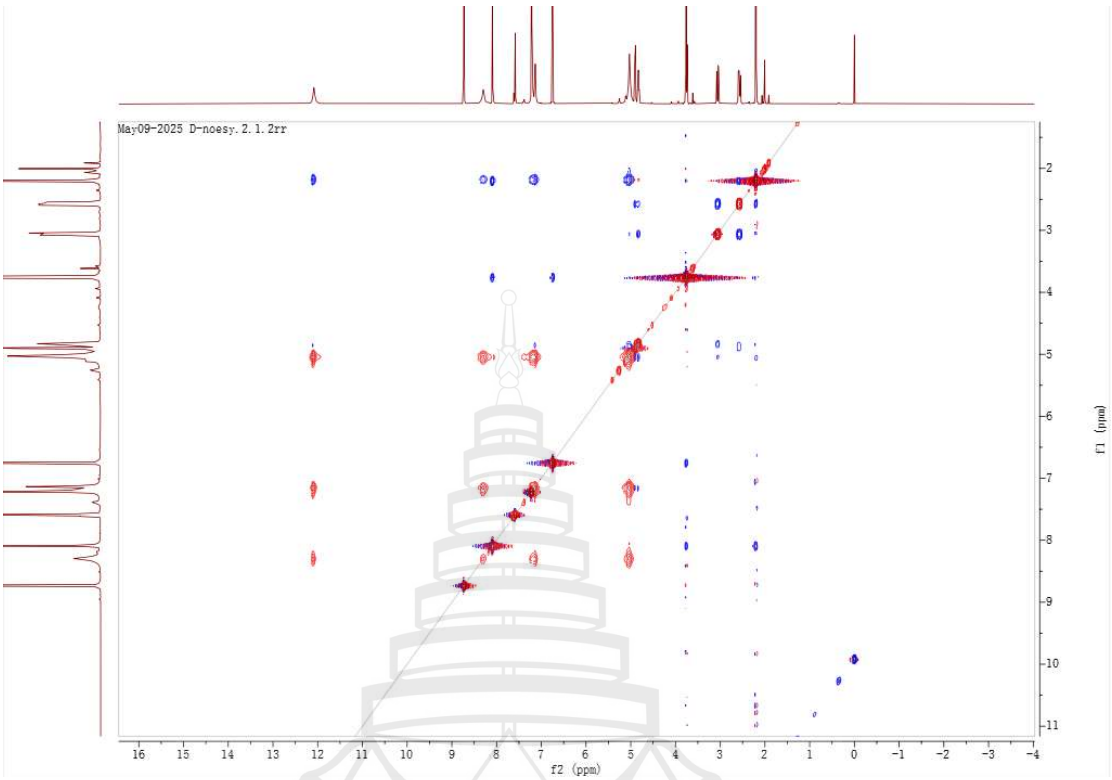

Figure A138 NOESY spectrum of compound **C27** (C_5D_5N)

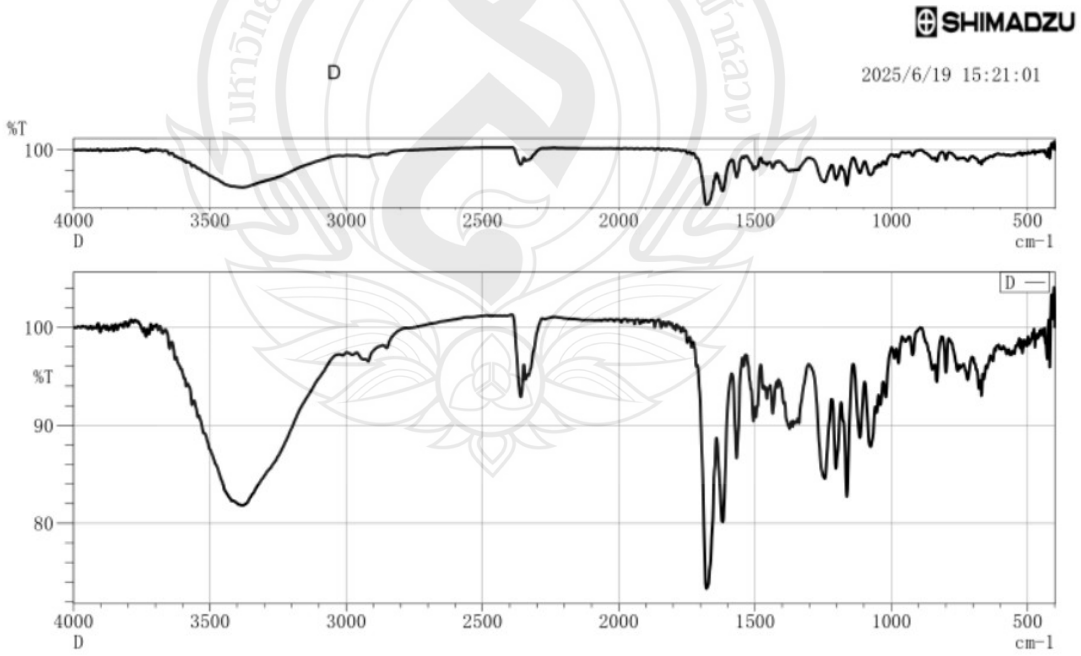

	项目	内容
	文件名	D:\DATE\20250619-4FTIR\D.ispd
	样品名称	D

Figure A139 IR (KBr) spectrum of compound **C27**

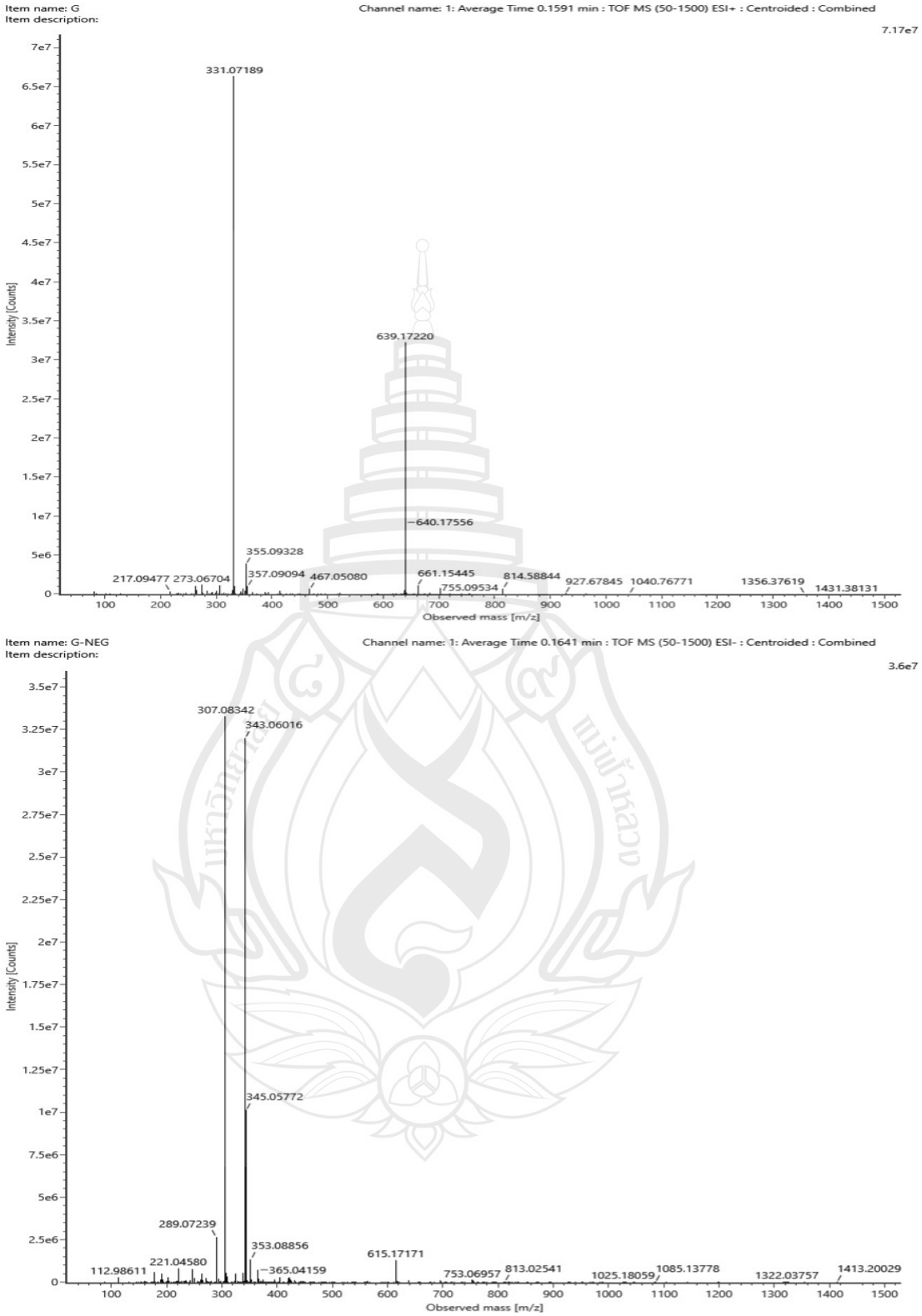

Figure A140 ESIMS of compound **C28**

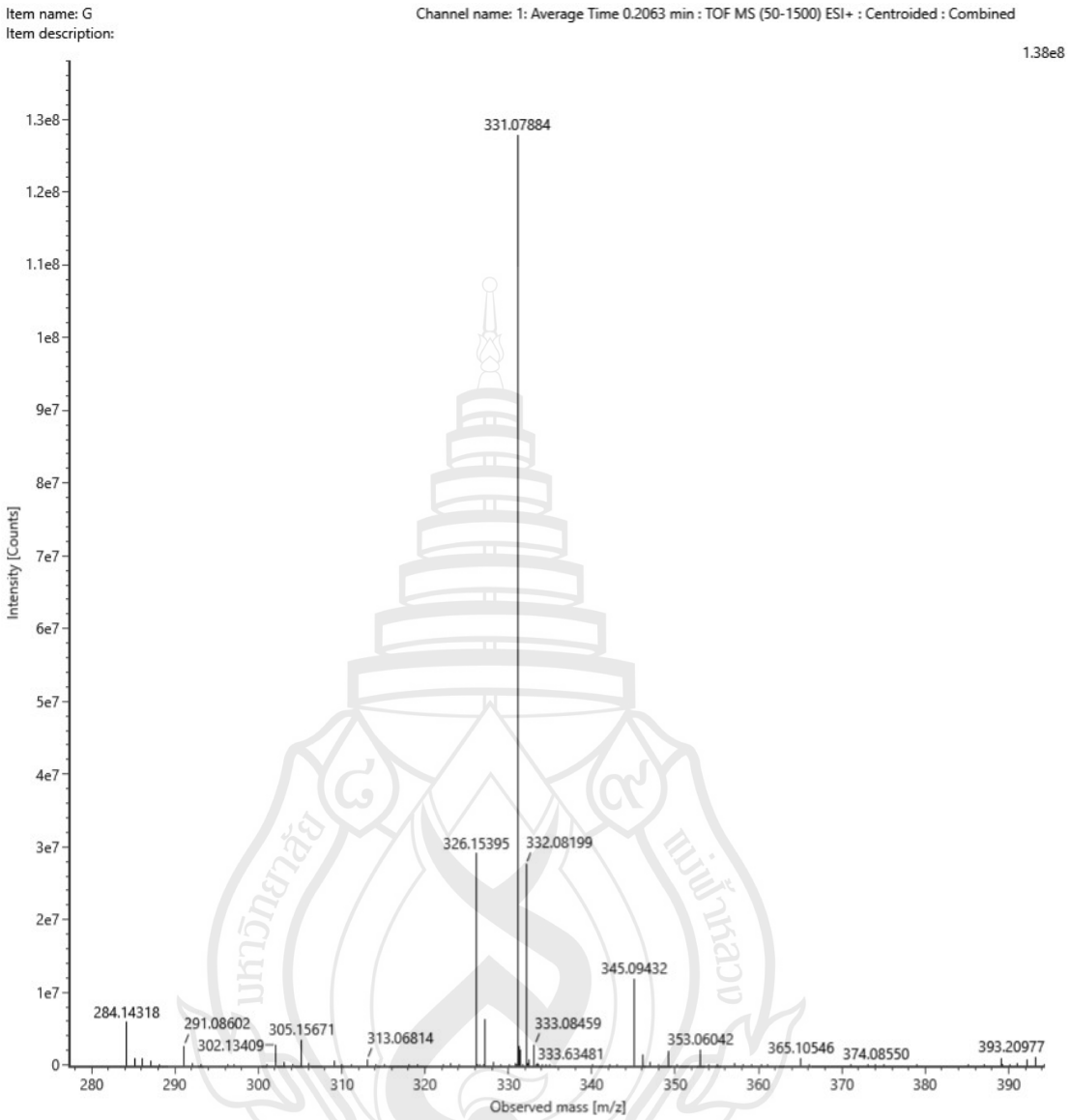

Note $[M + Na]^+$

Composition	$C_{15}H_{16}O_7N_a$
i-FIT Confidence (%)	100.000000
Predicted m/z	331.078824
m/z error (PPM)	0.048636

Figure A141 HR-ESIMS of compound **C28**

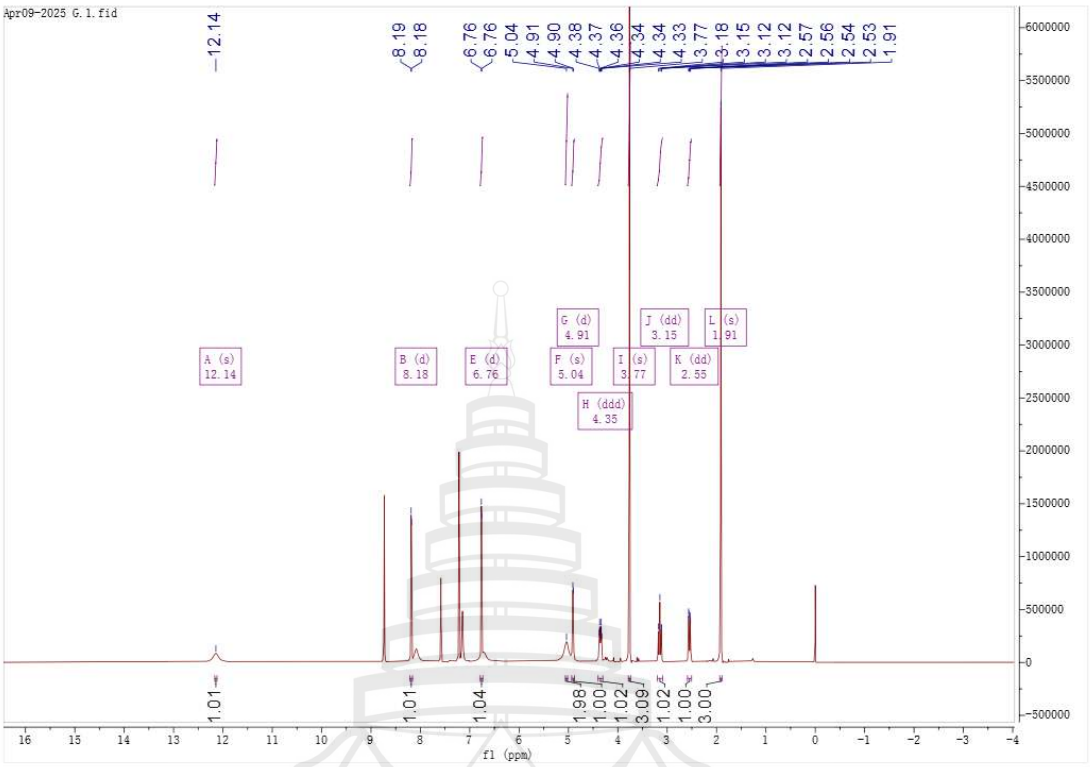

Figure A142 ^{1}H NMR spectrum of compound **C28** (400 MHz, C_5D_5N)

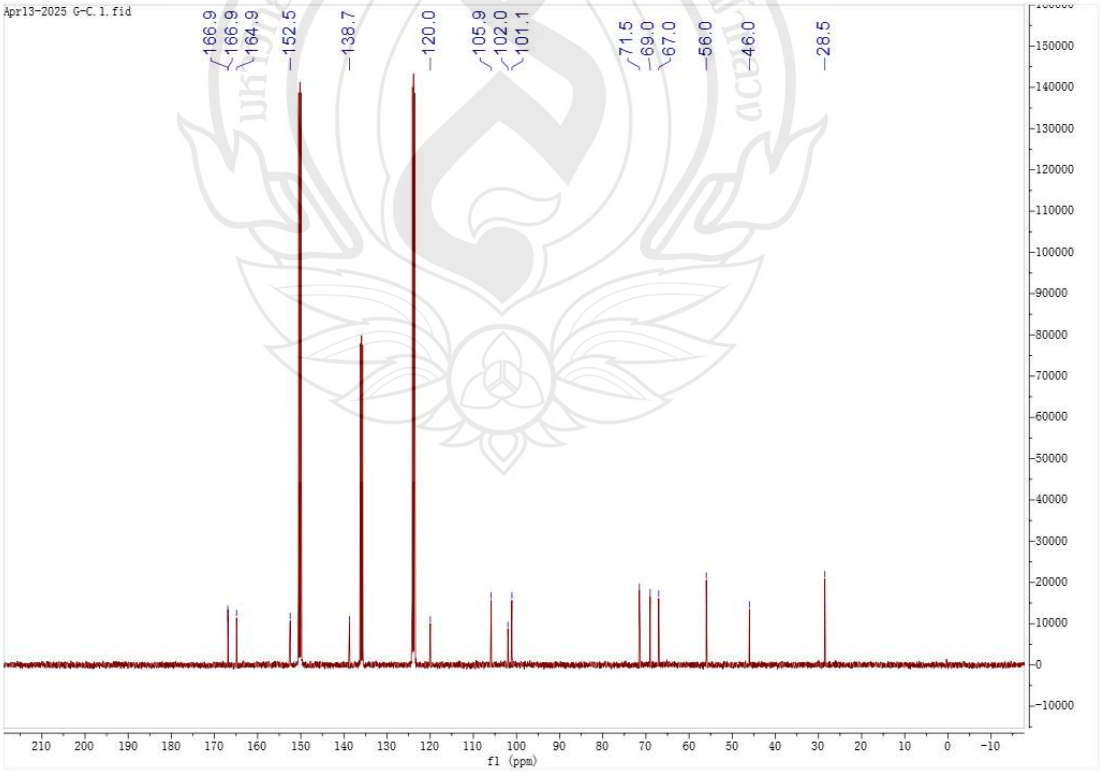

Figure A143 ^{13}C NMR spectrum of compound **C28** (100 MHz, C_5D_5N)

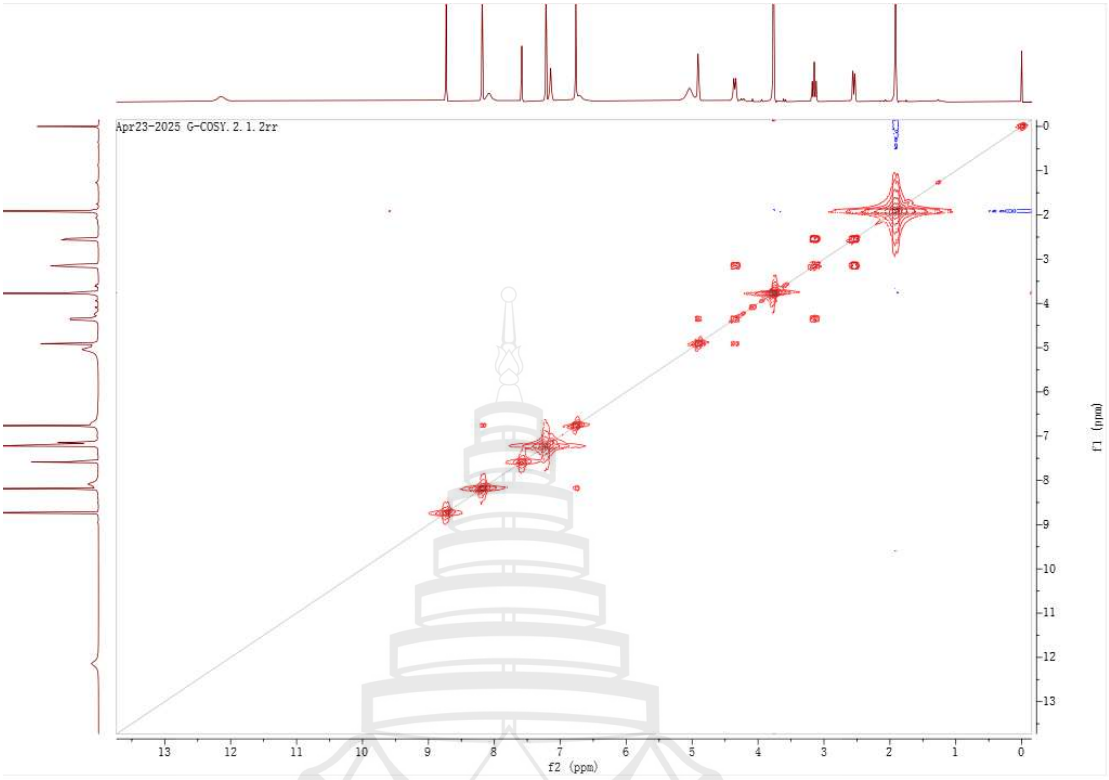

Figure A144 ^{1}H-^{1}H COSY spectrum of compound **C28** (C_5D_5N)

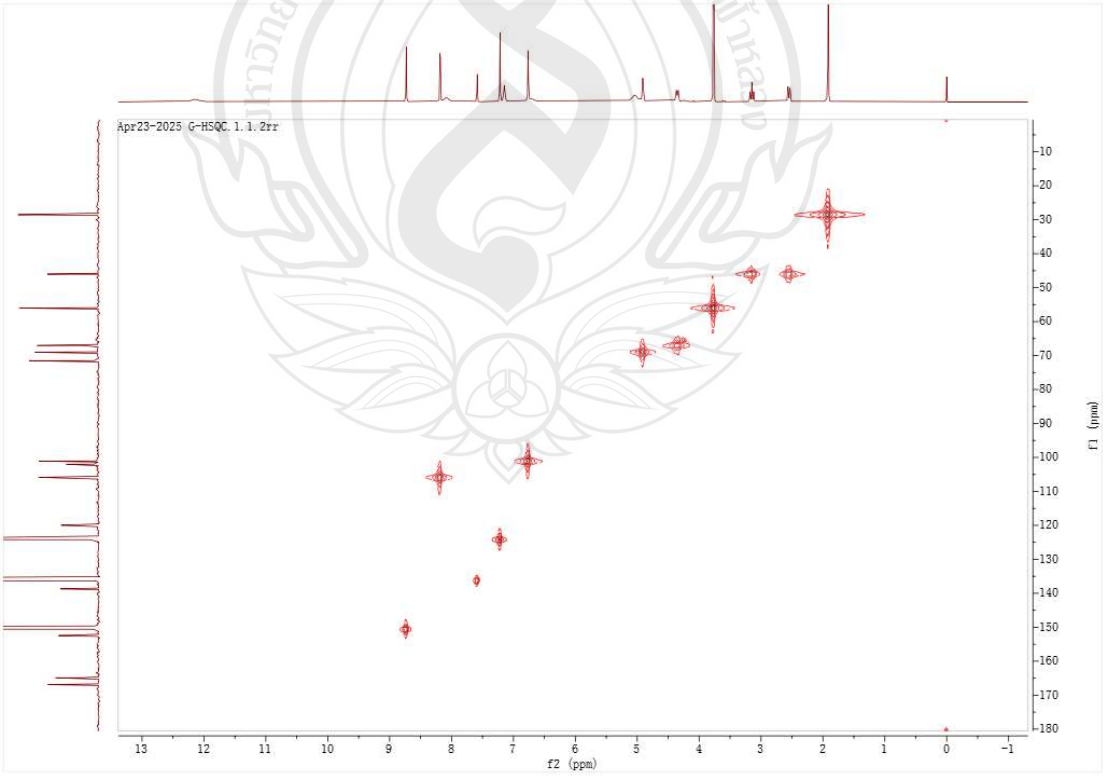

Figure A145 HSQC spectrum of compound **C28** (C_5D_5N)

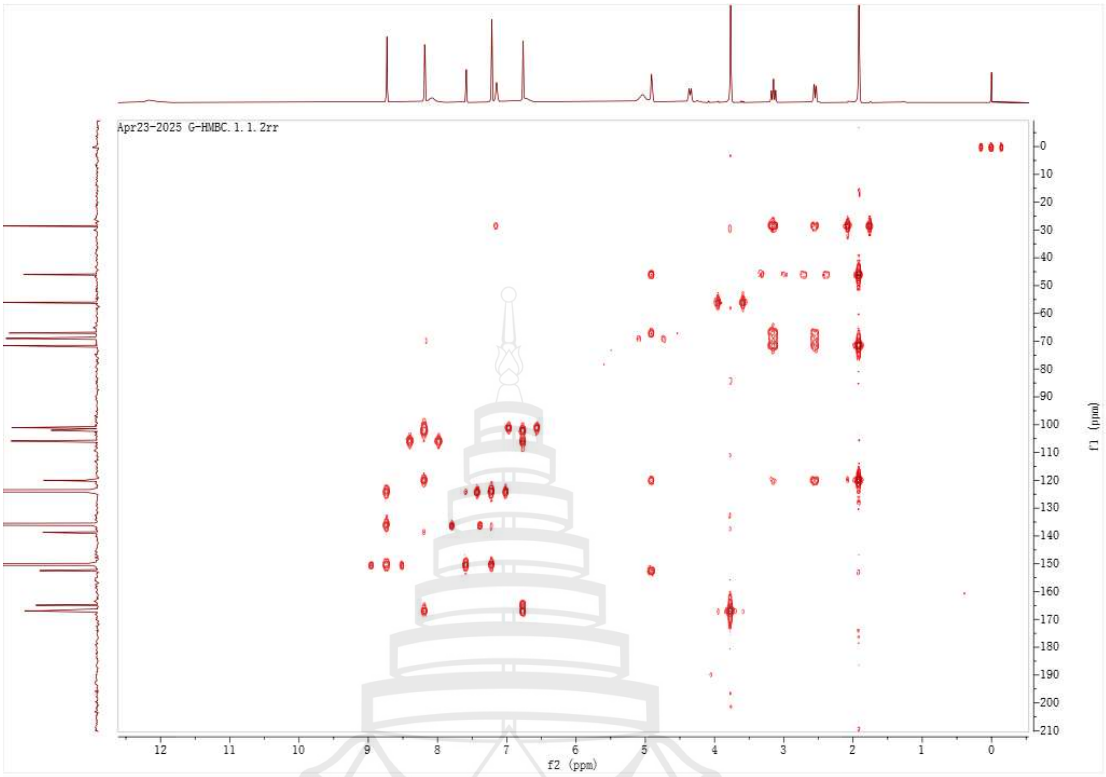

Figure A146 HMBC spectrum of compound **C28** (C_5D_5N)

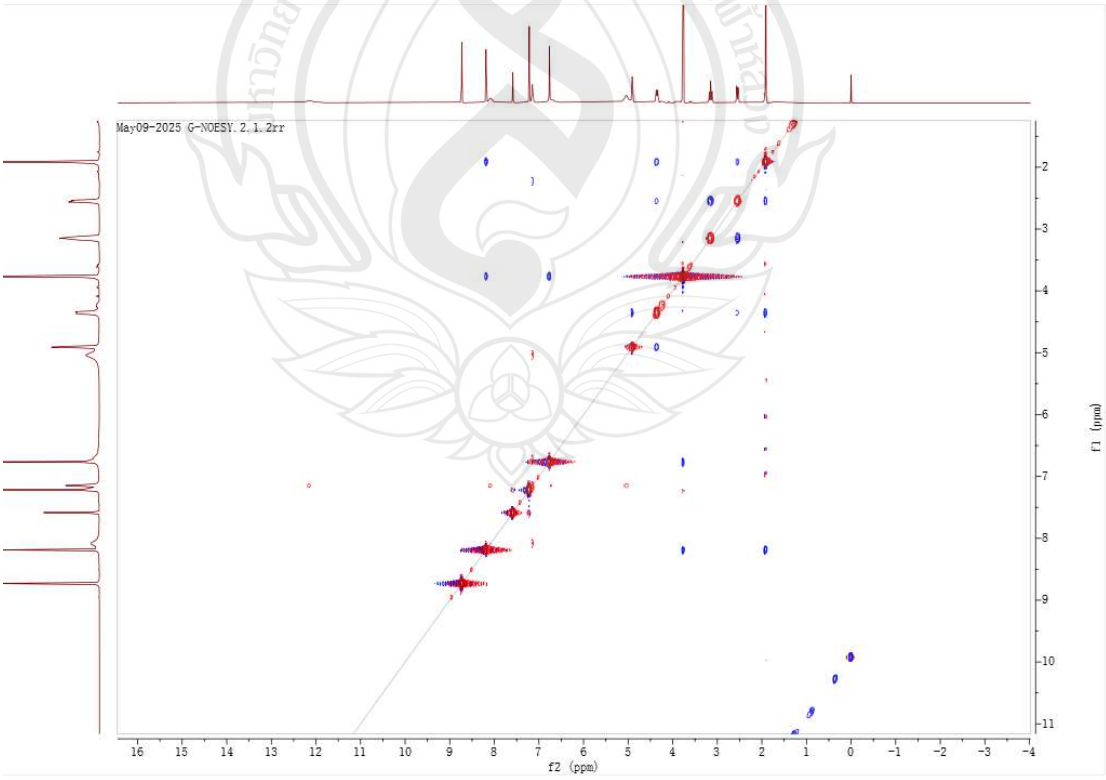

Figure A147 NOESY spectrum of compound **C28**

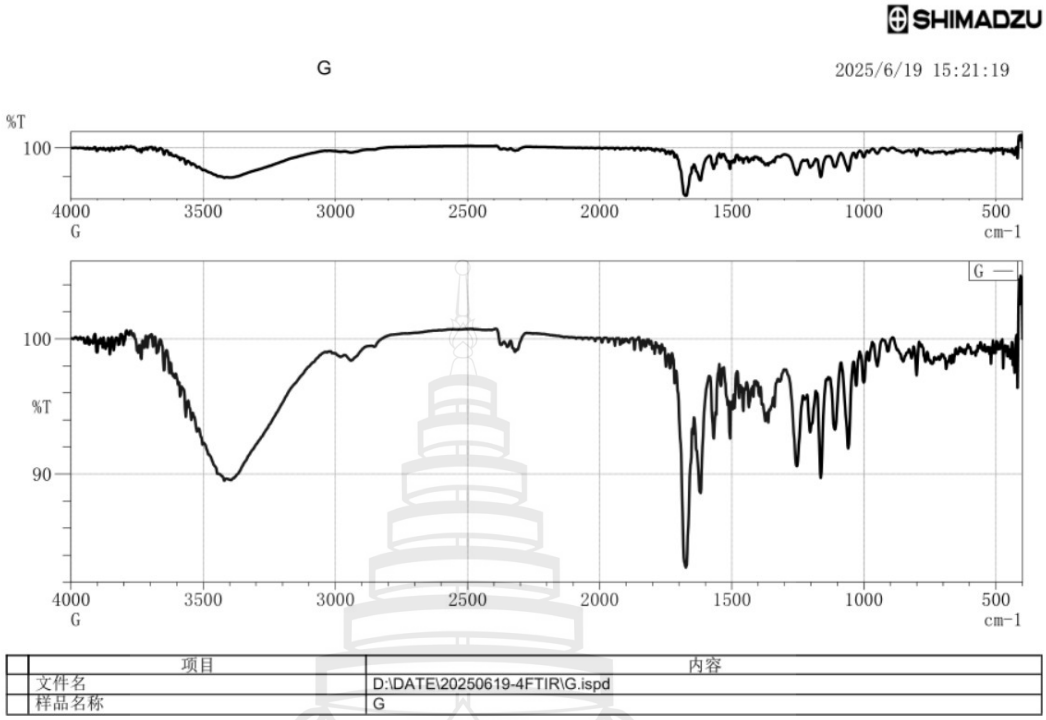

Figure A148 IR (KBr) spectrum of compound **C28**

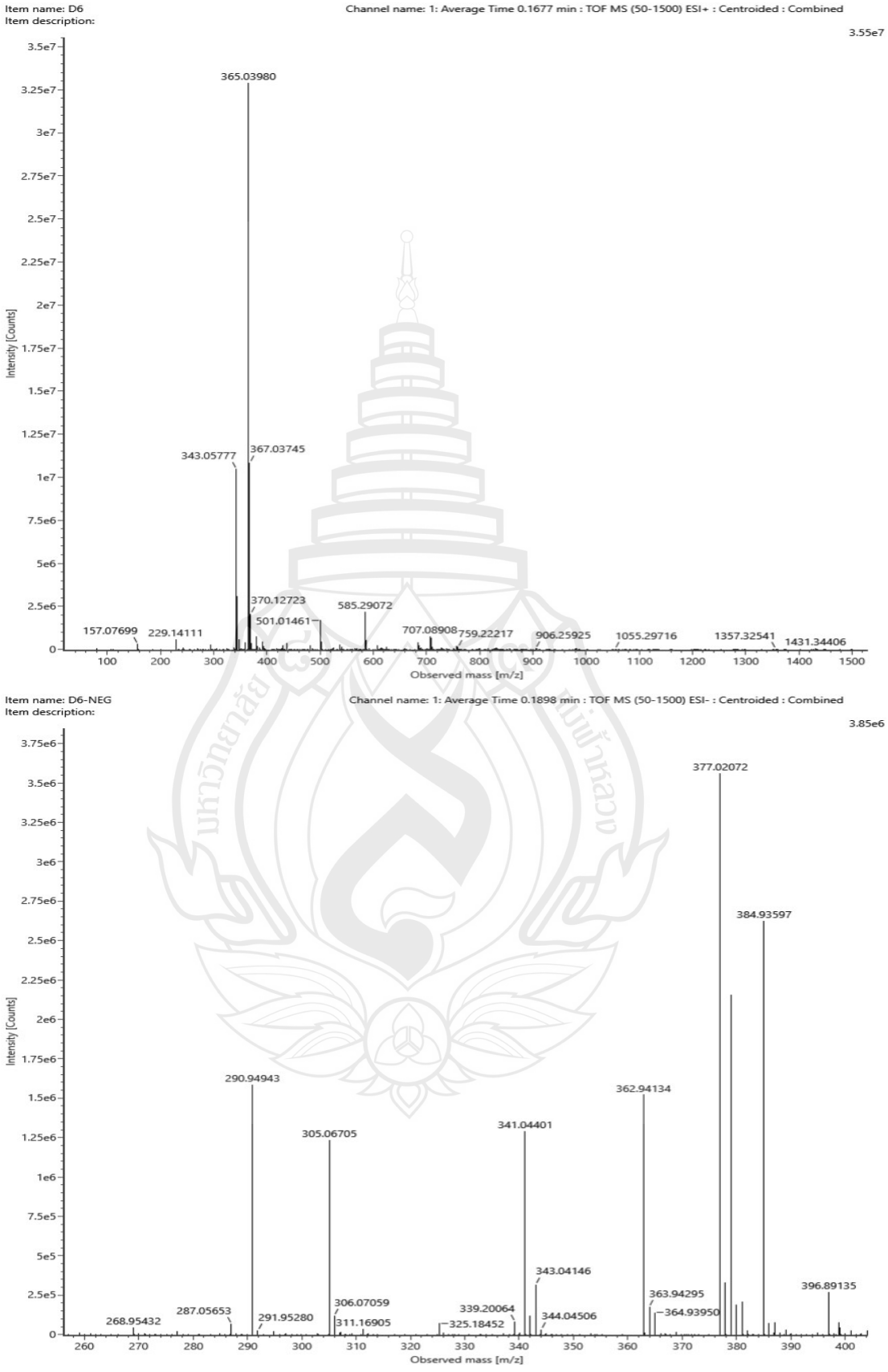

Figure A149 ESIMS of compound **C29**

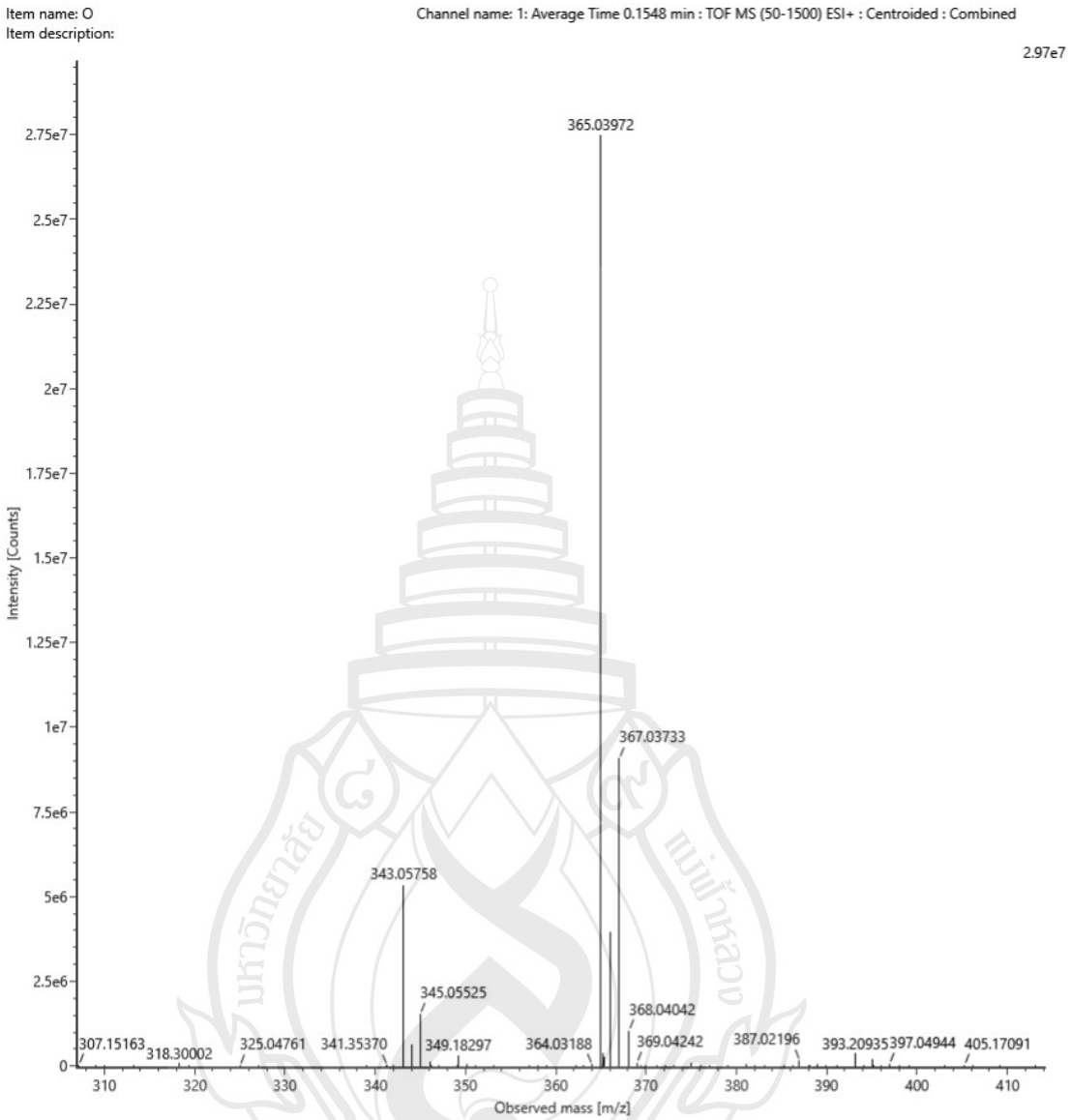

Note $[M+Na]^+$

Composition	$C_{15}H_{15}ClO_7N_a$
i-FIT Confidence (%)	100.000000
Predicted m/z	365.039852
m/z error (PPM)	-0.361574

Figure A150 HR-ESIMS of compound **C29**

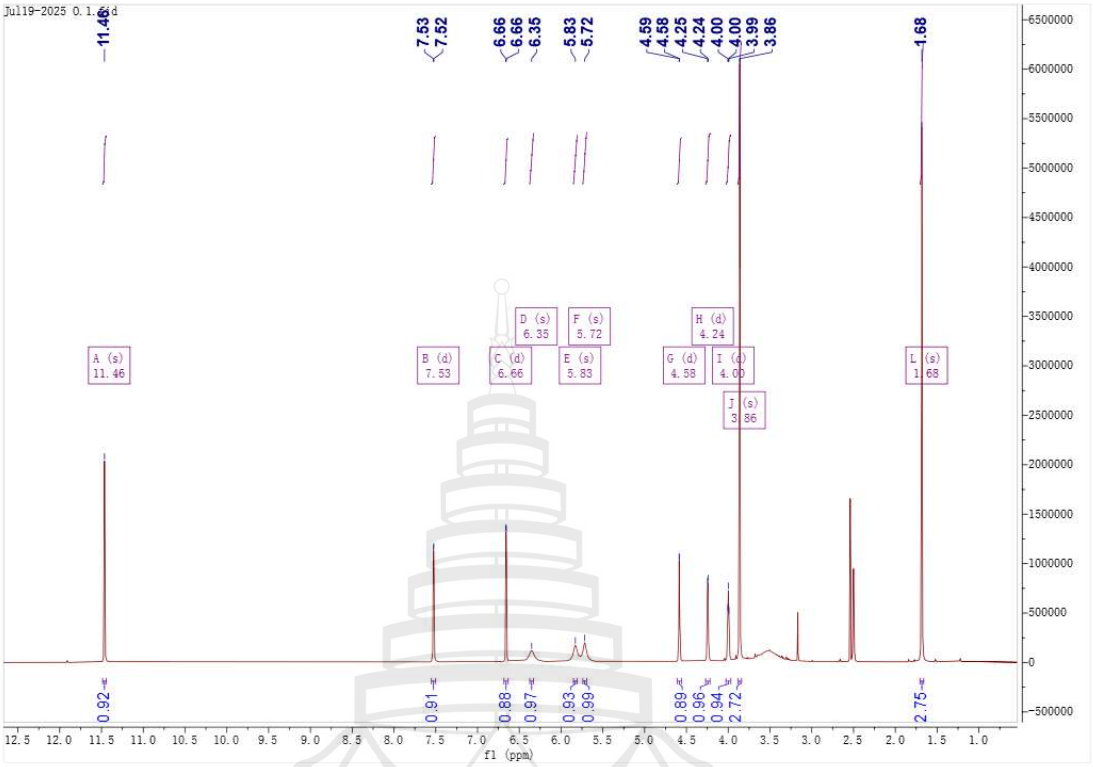

Figure A151 ^{1}H NMR spectrum of compound **C29** (400 MHz, DMSO)

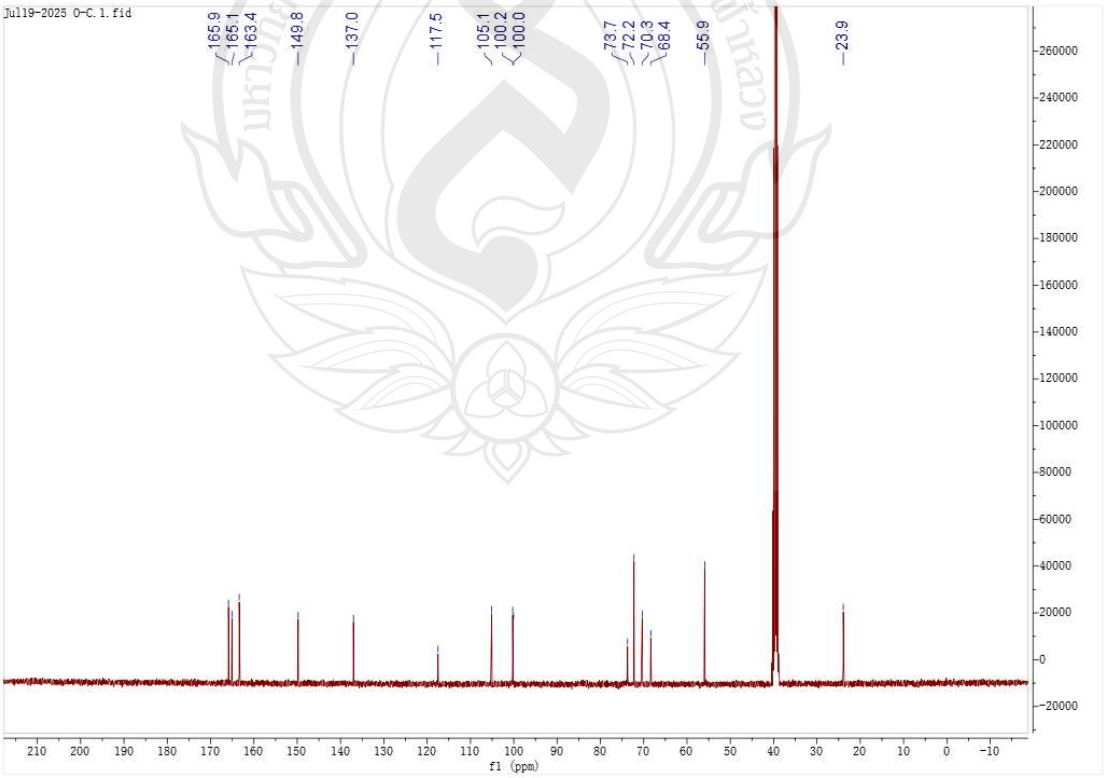

Figure A152 ^{13}C NMR spectrum of compound **C29** (100 MHz, DMSO)

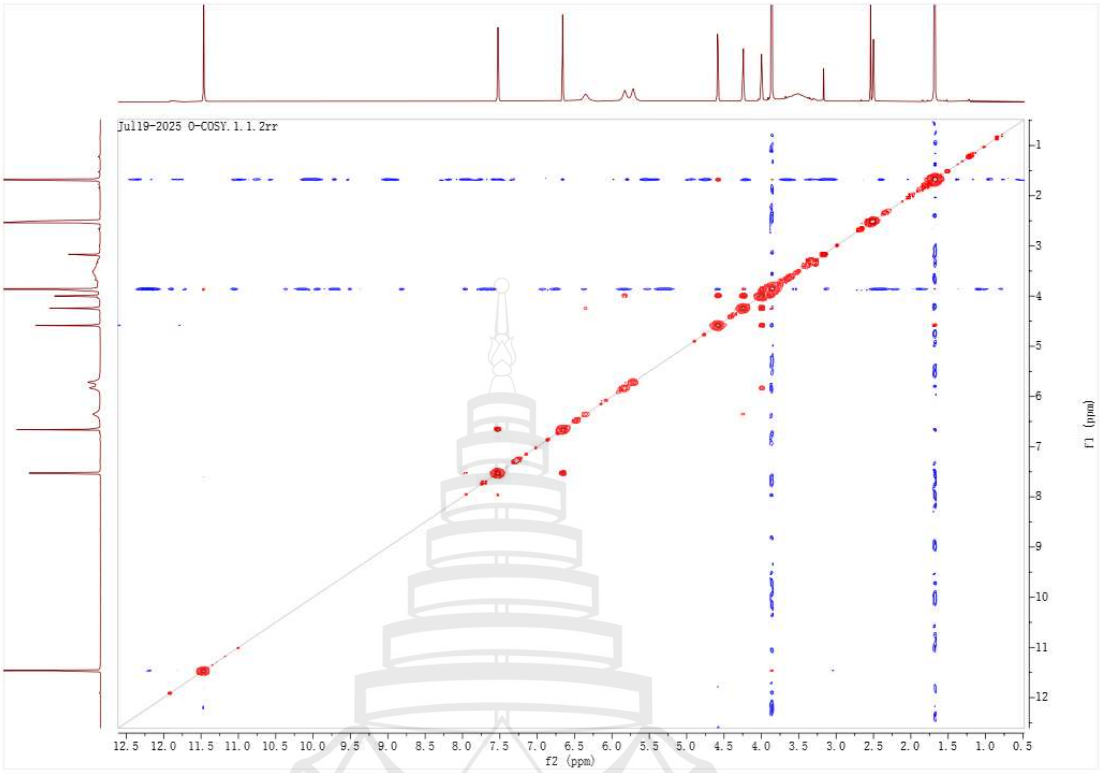

Figure A153 ^{1}H-^{1}H COSY spectrum of compound **C29** (DMSO)

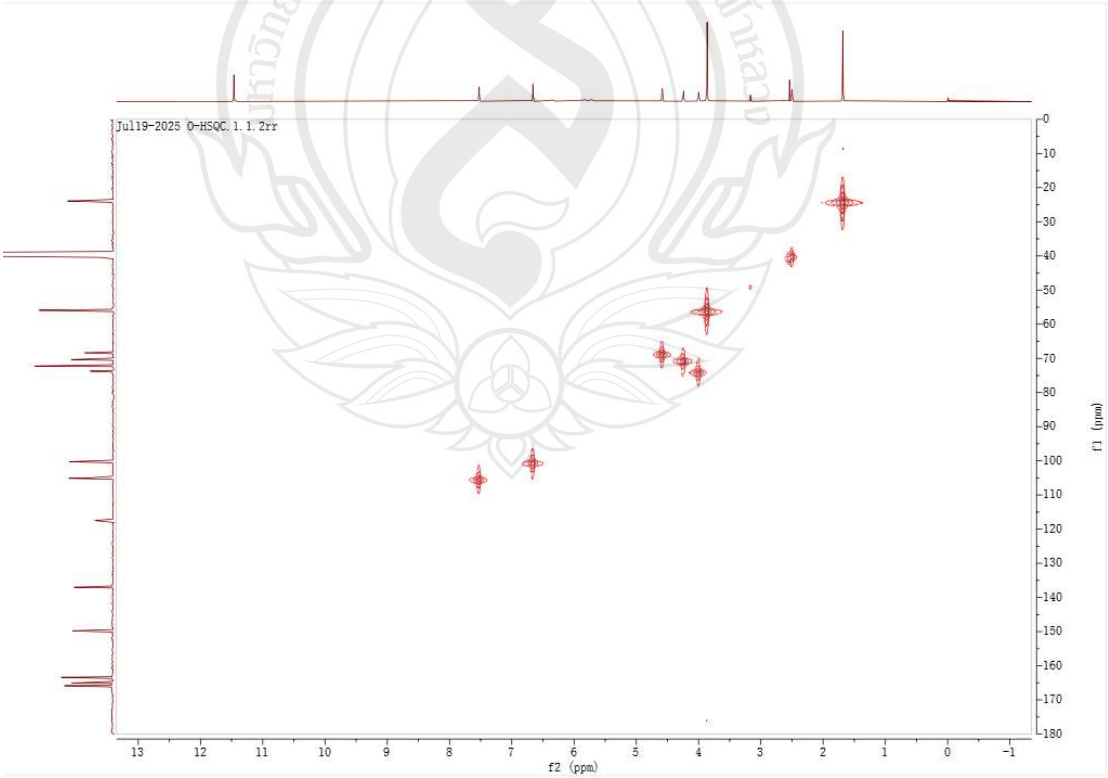

Figure A154 HSQC spectrum of compound **C29** (DMSO)

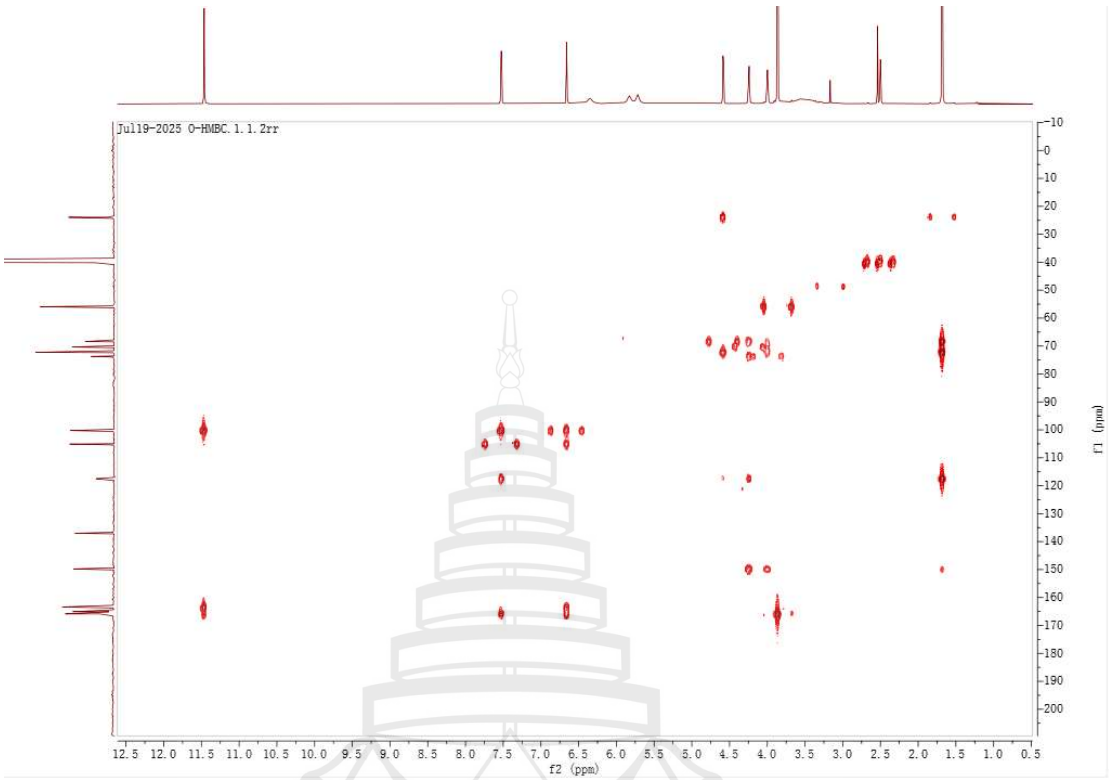

Figure A155 HMBC spectrum of compound **C29** (DMSO)

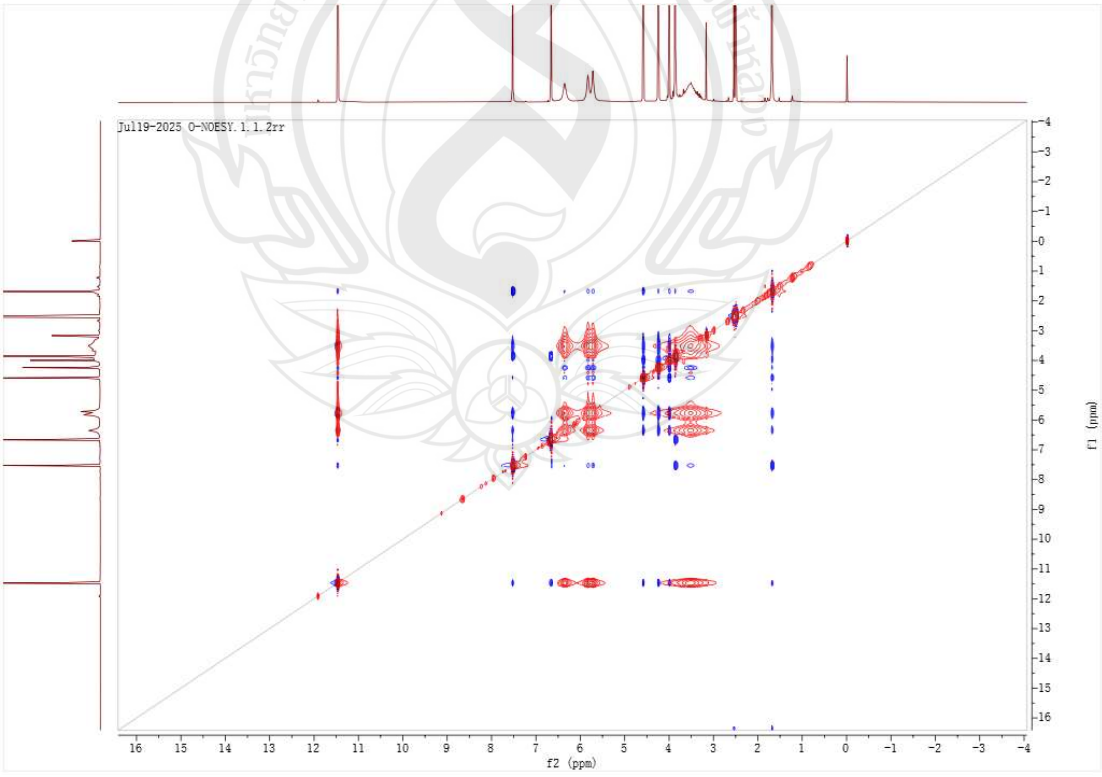

Figure A156 NOESY spectrum of compound **C29** (DMSO)

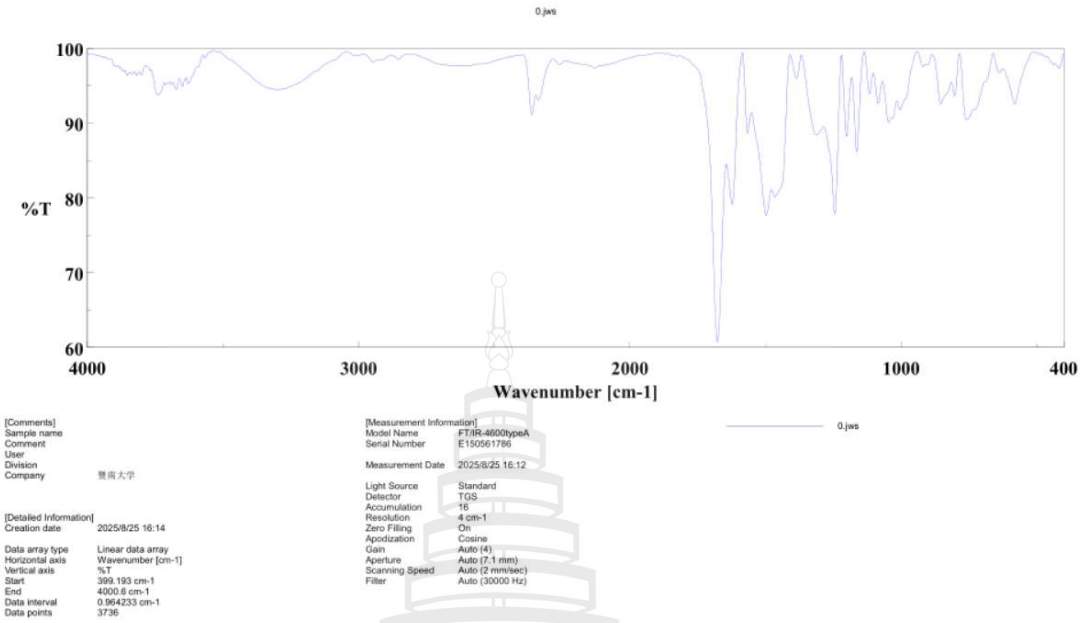

Figure A157 IR (KBr) spectrum of compound **C29**

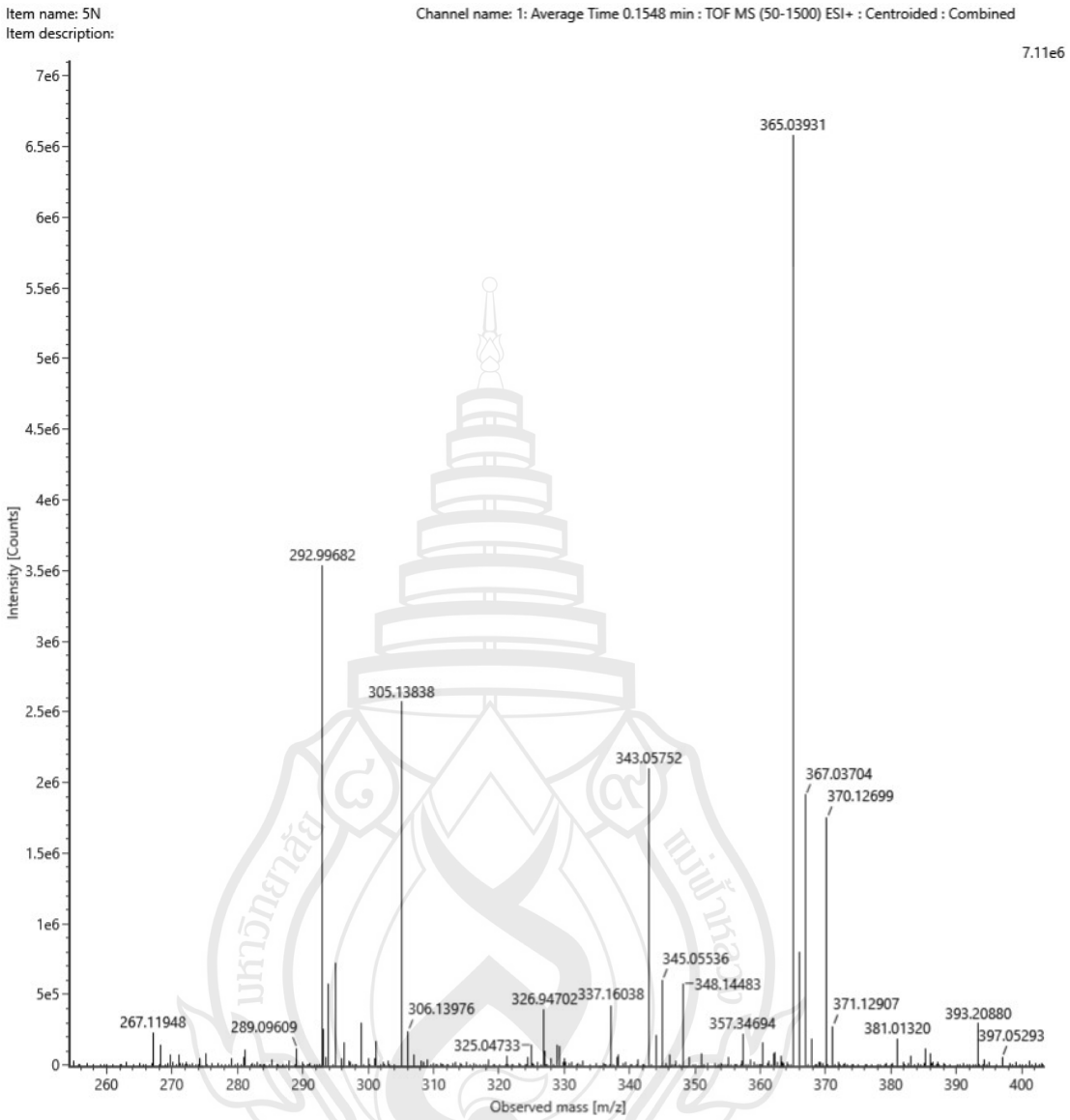

Figure A158 ESIMS of compound **C30**

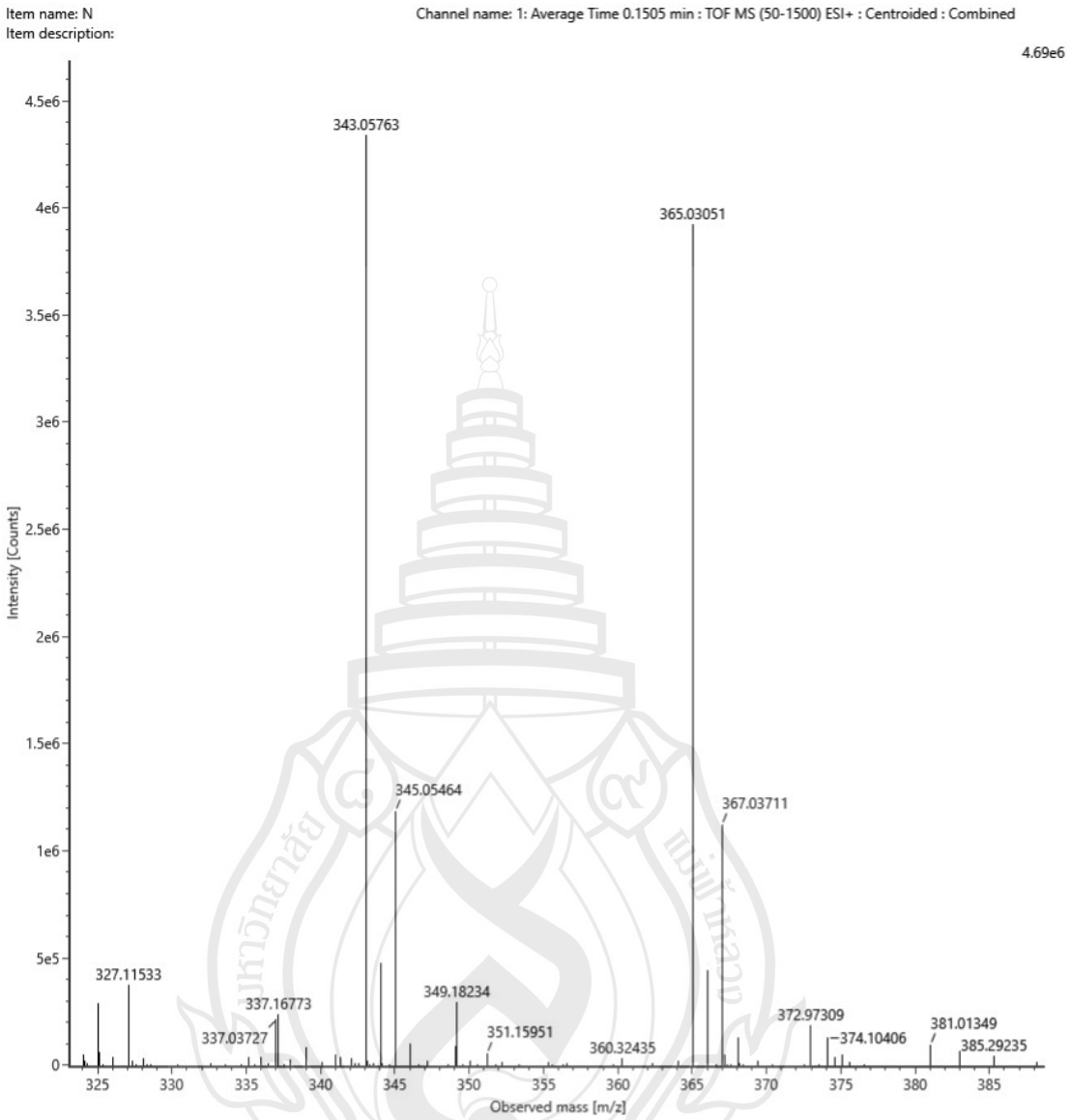

Note $[M+H]^+$

Composition	$C_{15}H_{16}ClO_7$
i-FIT Confidence (%)	100.000000
Predicted m/z	343.057907
m/z error (PPM)	-0.809812

Figure A159 HR-ESIMS of compound **C30**

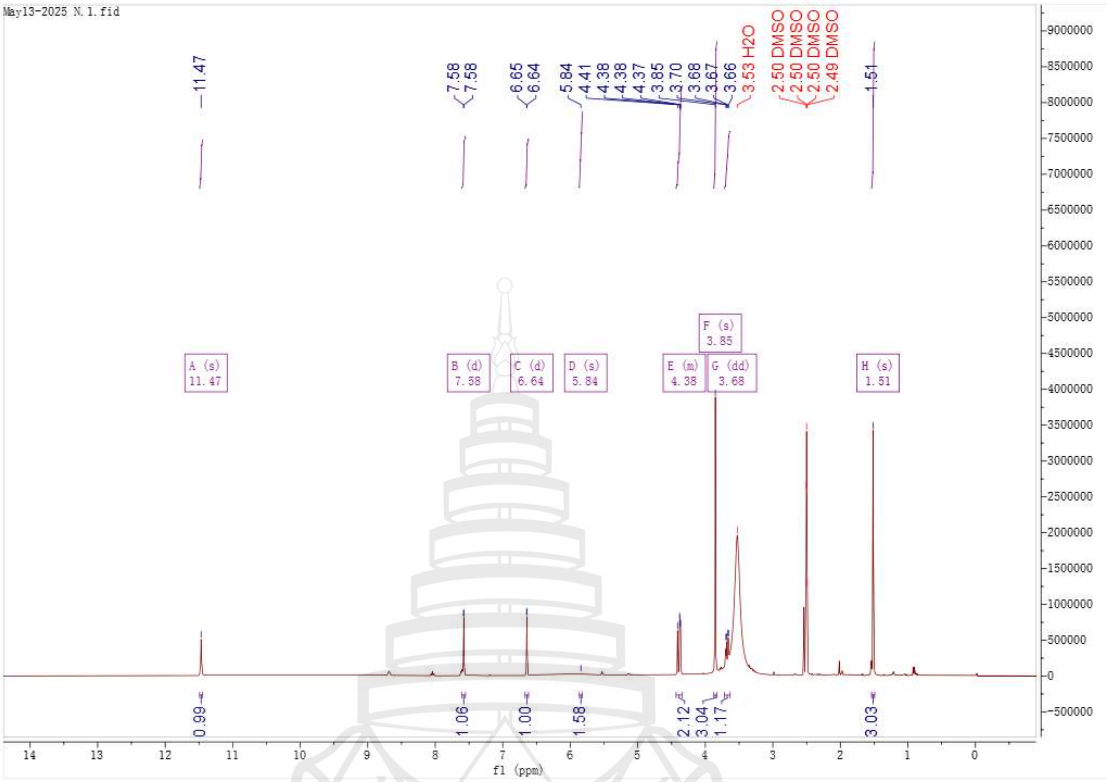

Figure A160 ^{1}H NMR spectrum of compound **C30** (400 MHz, DMSO)

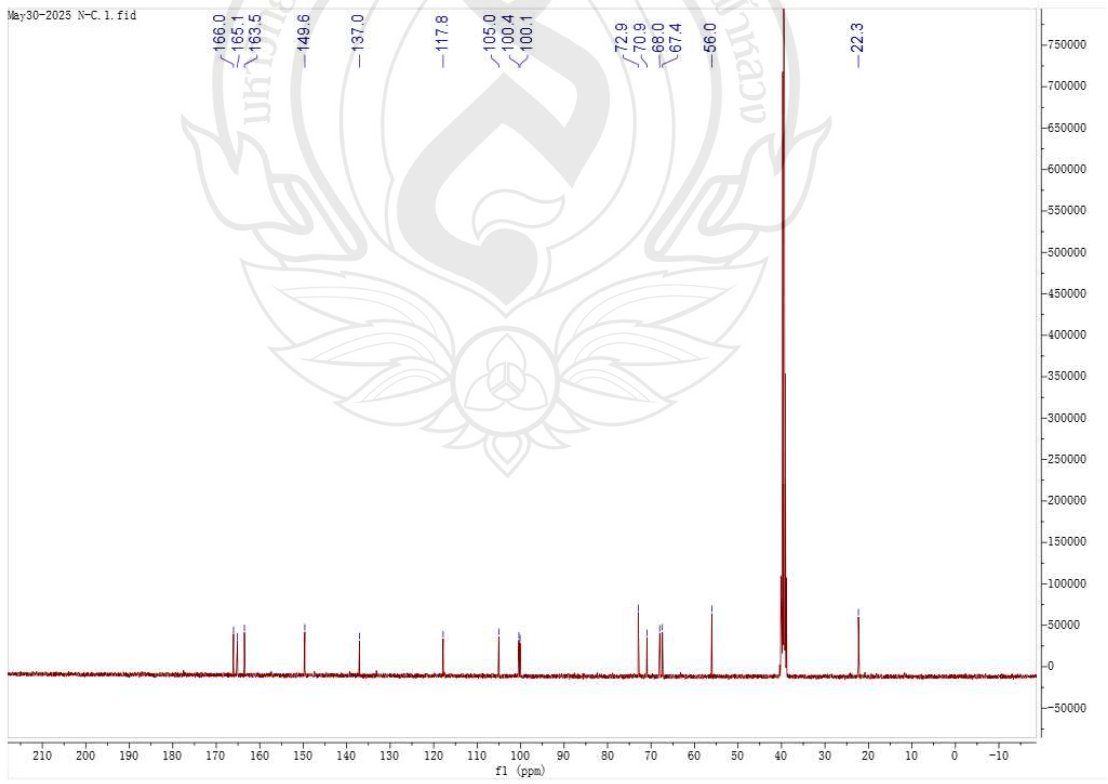

Figure A161 ^{13}C NMR spectrum of compound **C30** (100 MHz, DMSO)

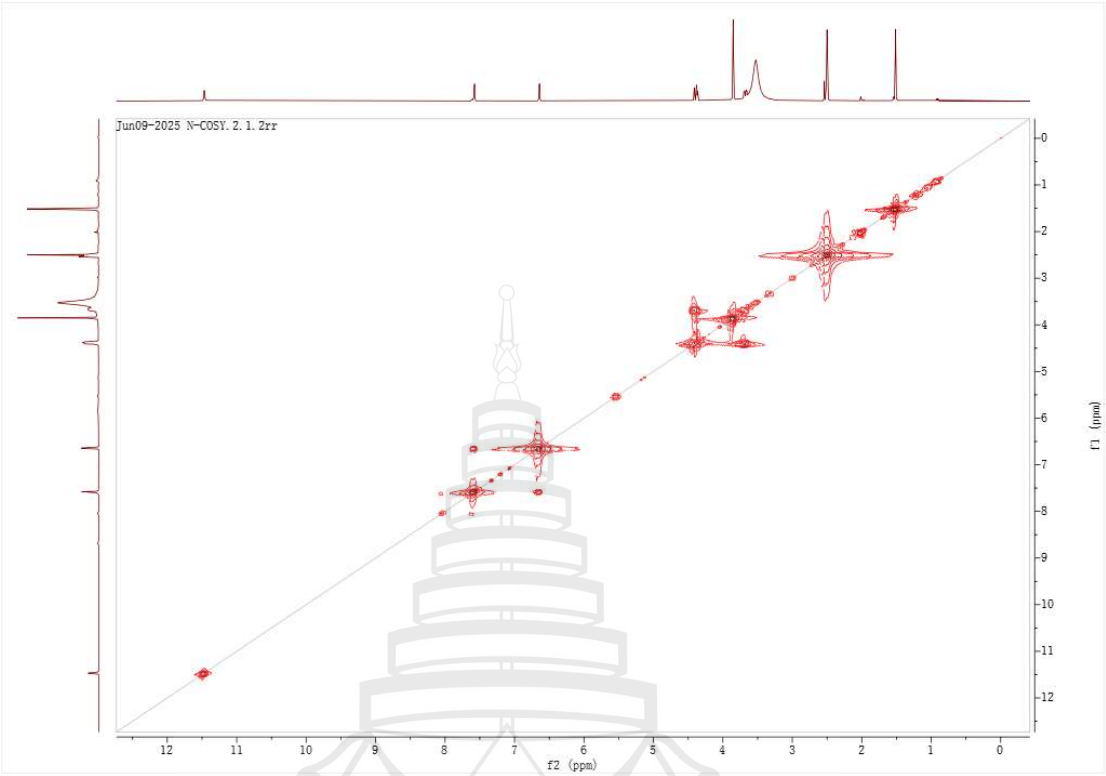

Figure A162 ^{1}H-^{1}H COSY spectrum of compound **C30** (DMSO)

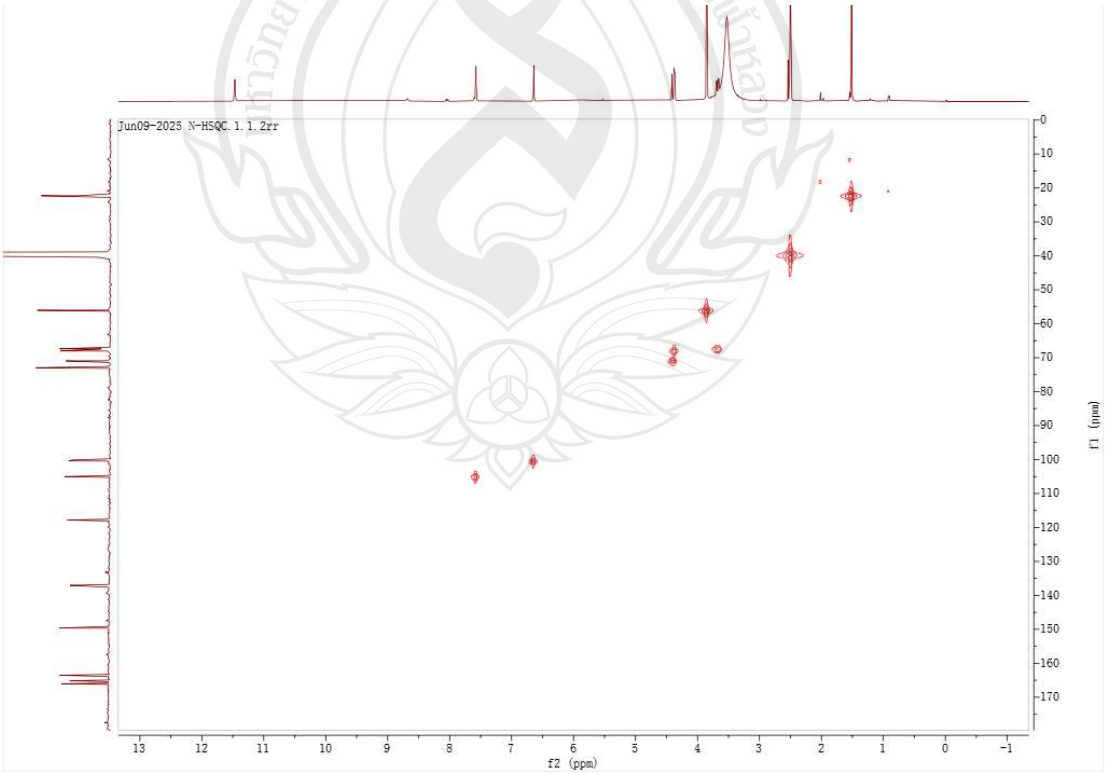

Figure A163 HSQC spectrum of compound **C30** (DMSO)

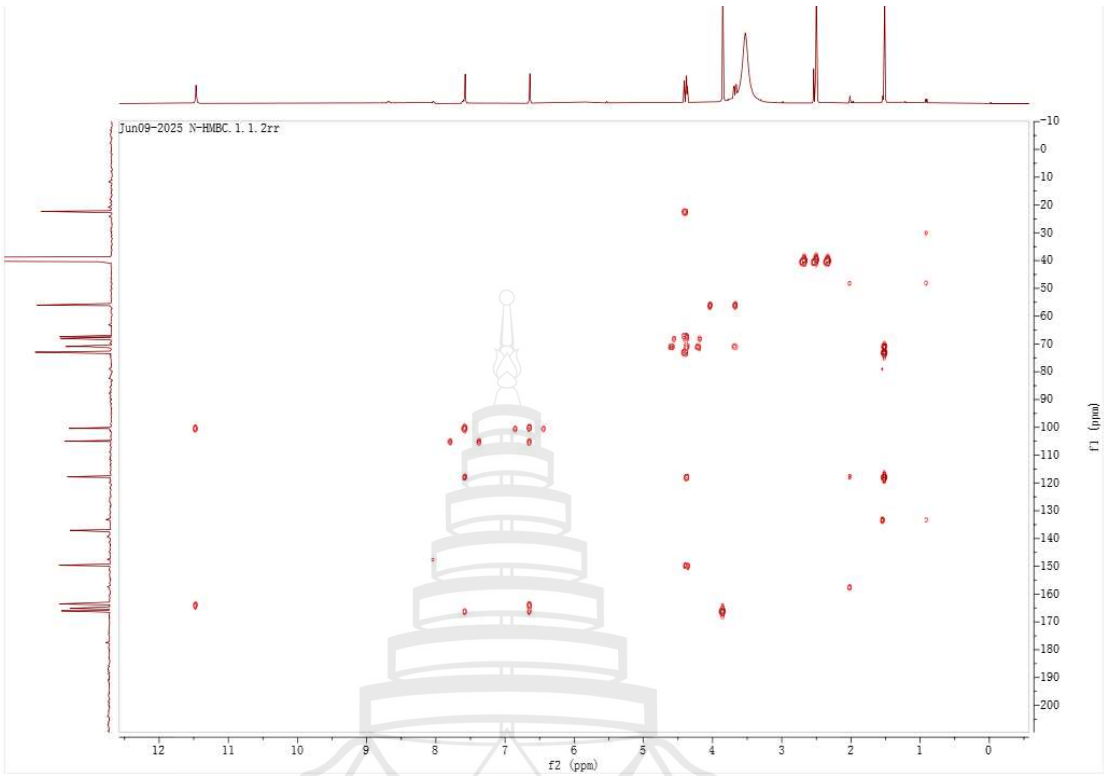

Figure A164 HMBC spectrum of compound **C30** (DMSO)

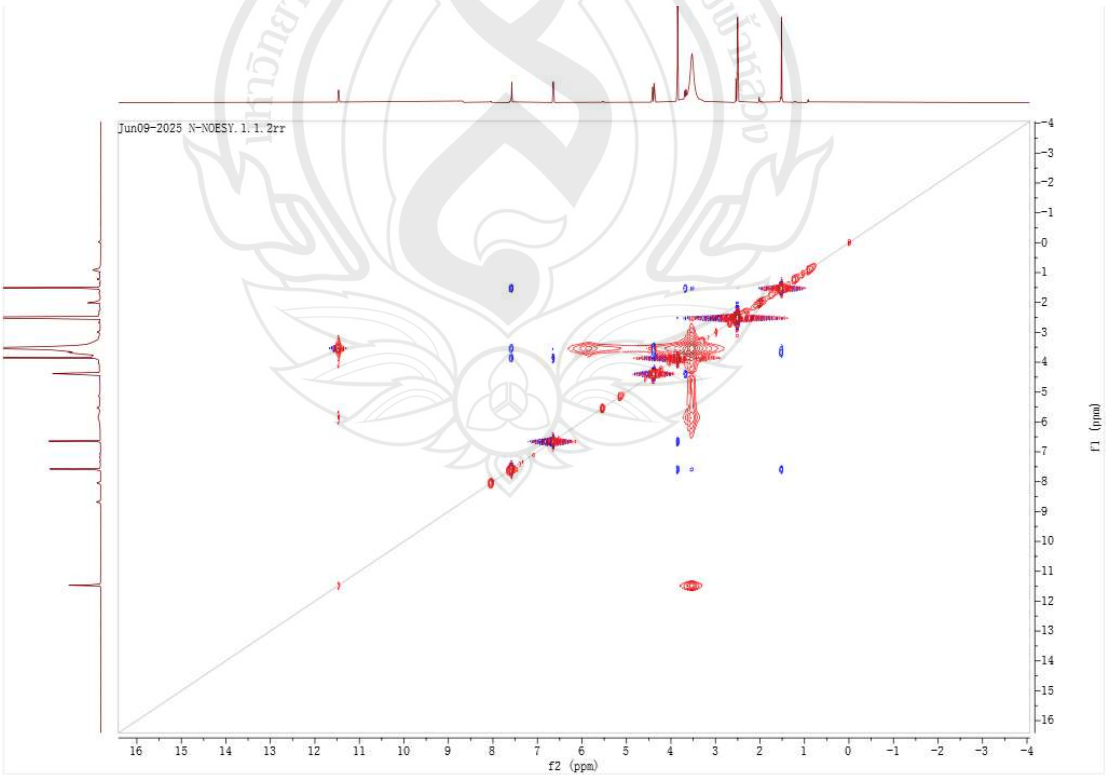

Figure A165 NOESY spectrum of compound **C30** (DMSO)

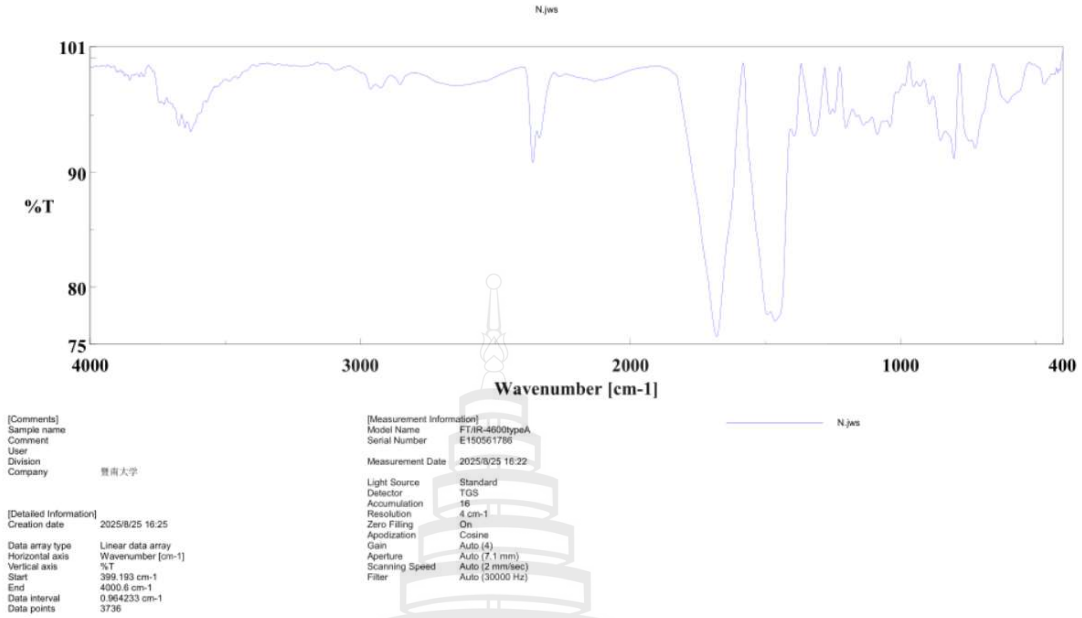

Figure A166 IR (KBr) spectrum of compound **C30**

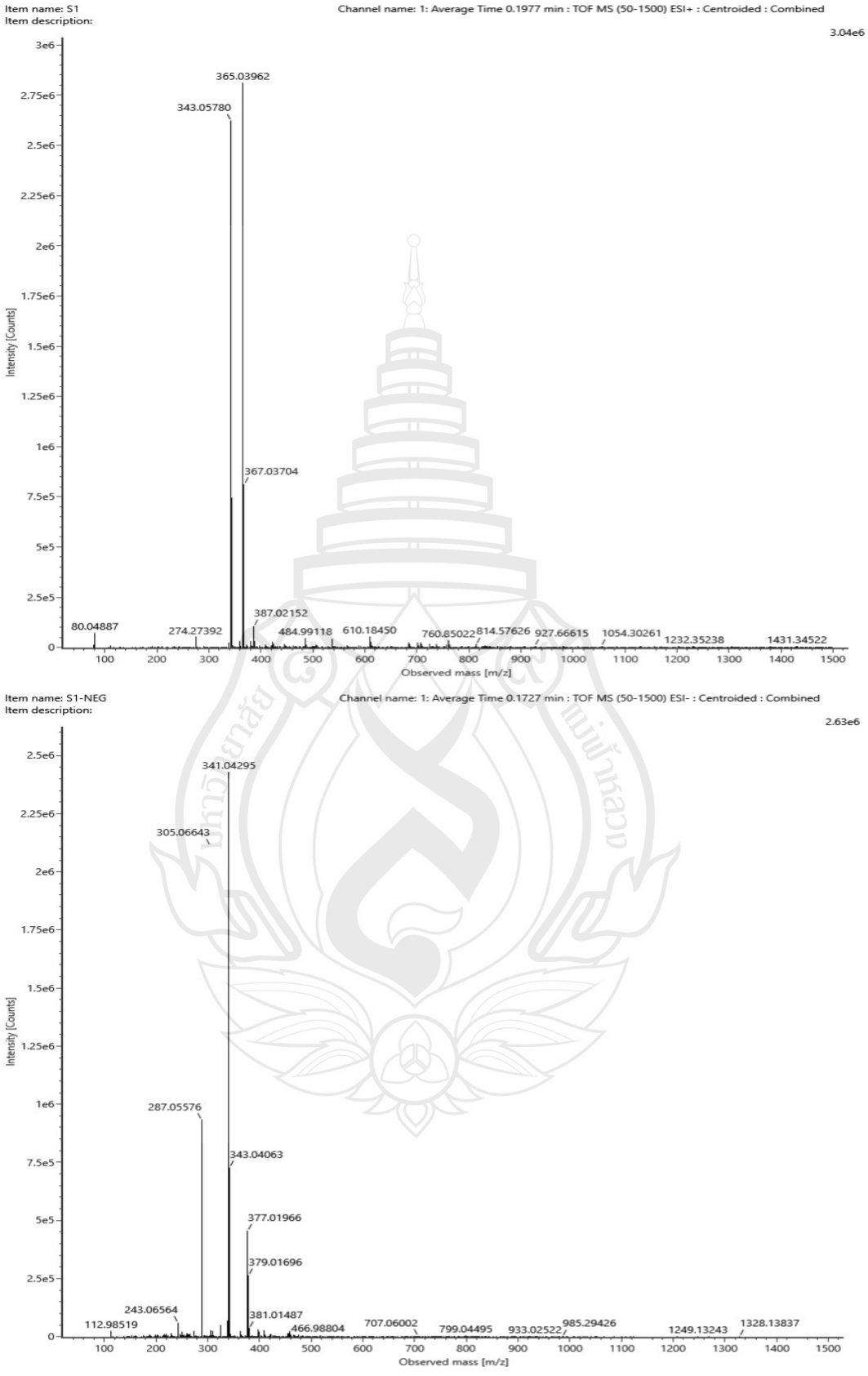

Figure A167 ESIMS of compound **C31**

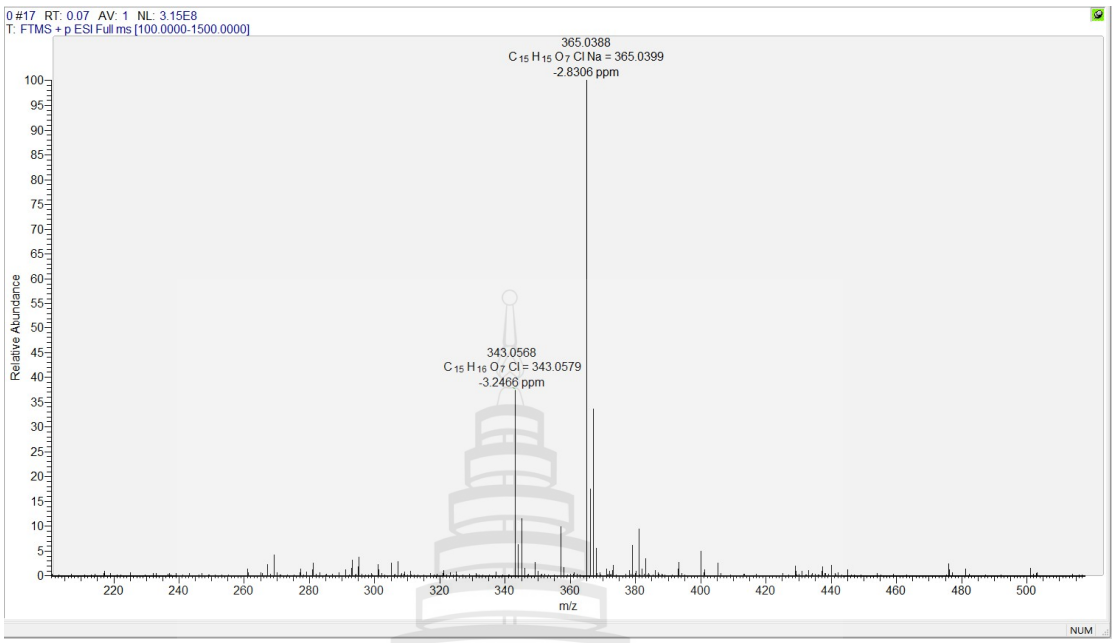

Figure A168 HR-ESIMS of compound **C31**

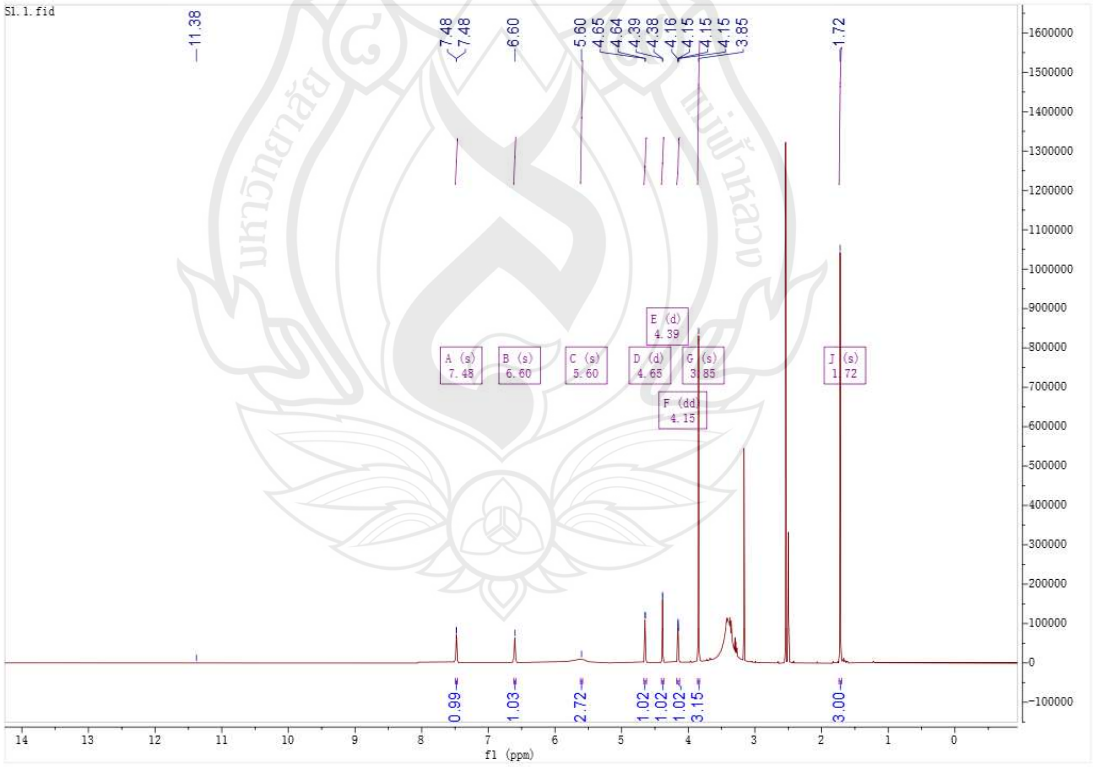

Figure A169 ^{1}H NMR spectrum of compound C31 (600 MHz, DMSO)

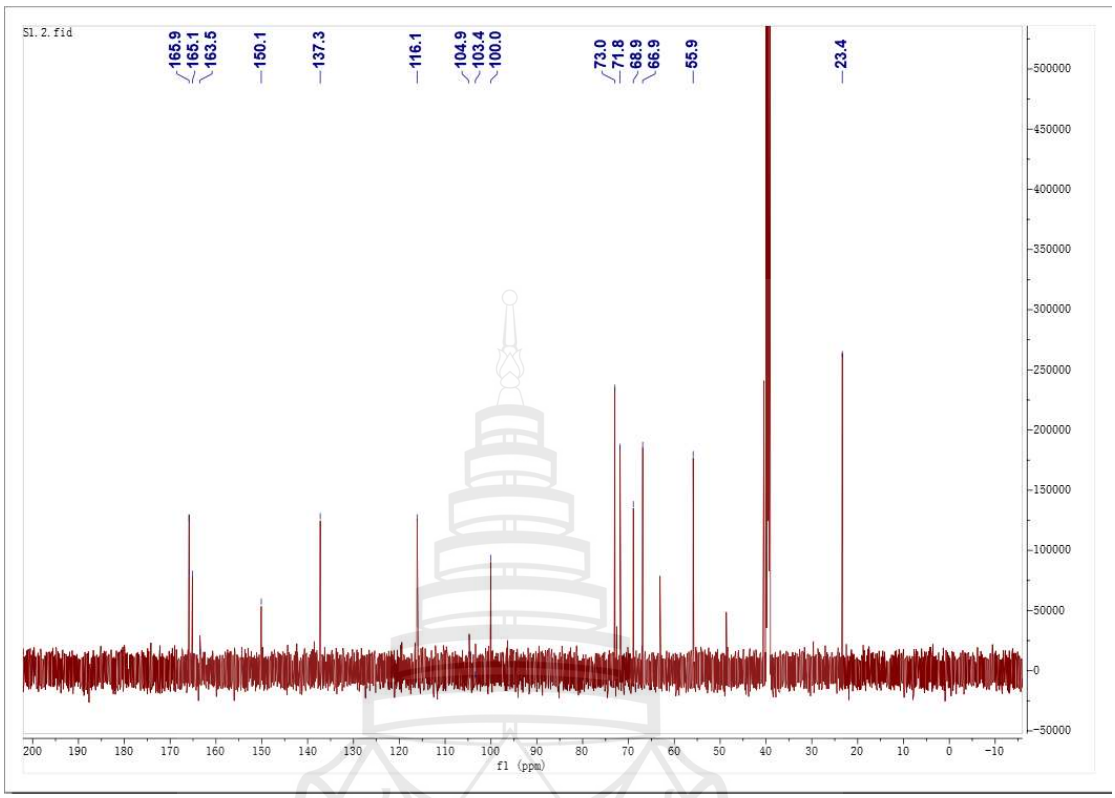

Figure A170 ^{13}C NMR spectrum of compound **C31** (150 MHz, DMSO)

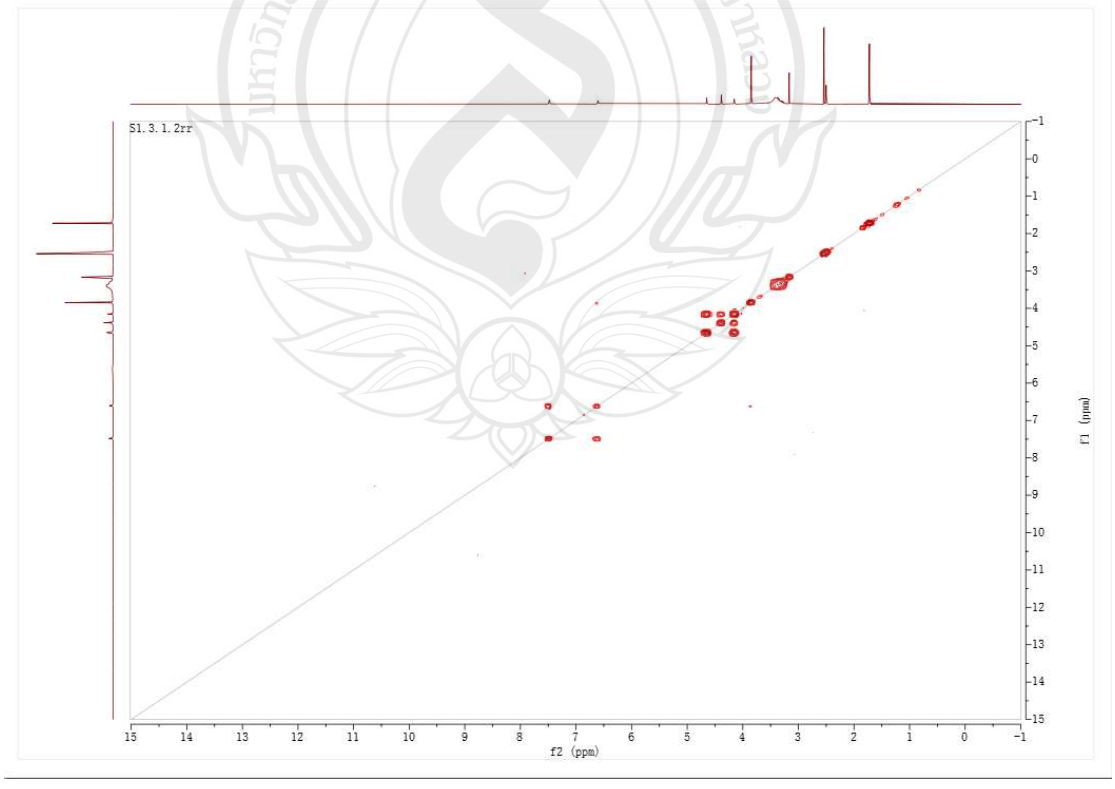

Figure A171 ^{1}H-^{1}H COSY spectrum of compound **C31** (DMSO)

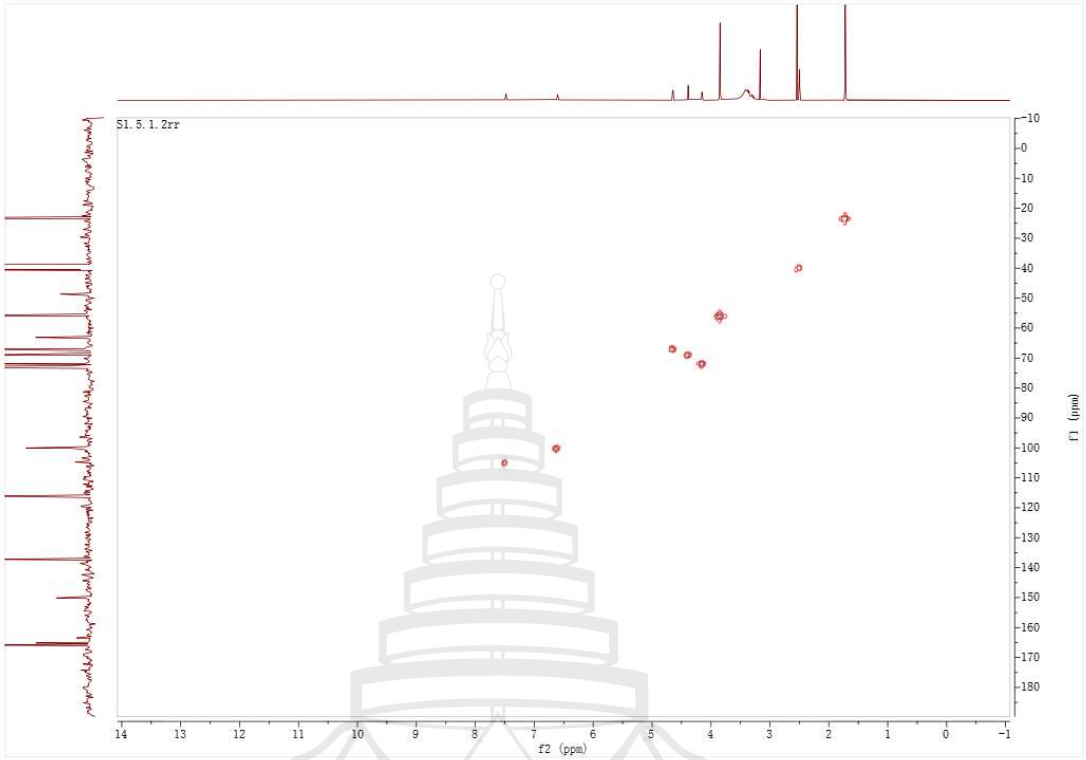

Figure A172 HSQC spectrum of compound **C31** (DMSO)

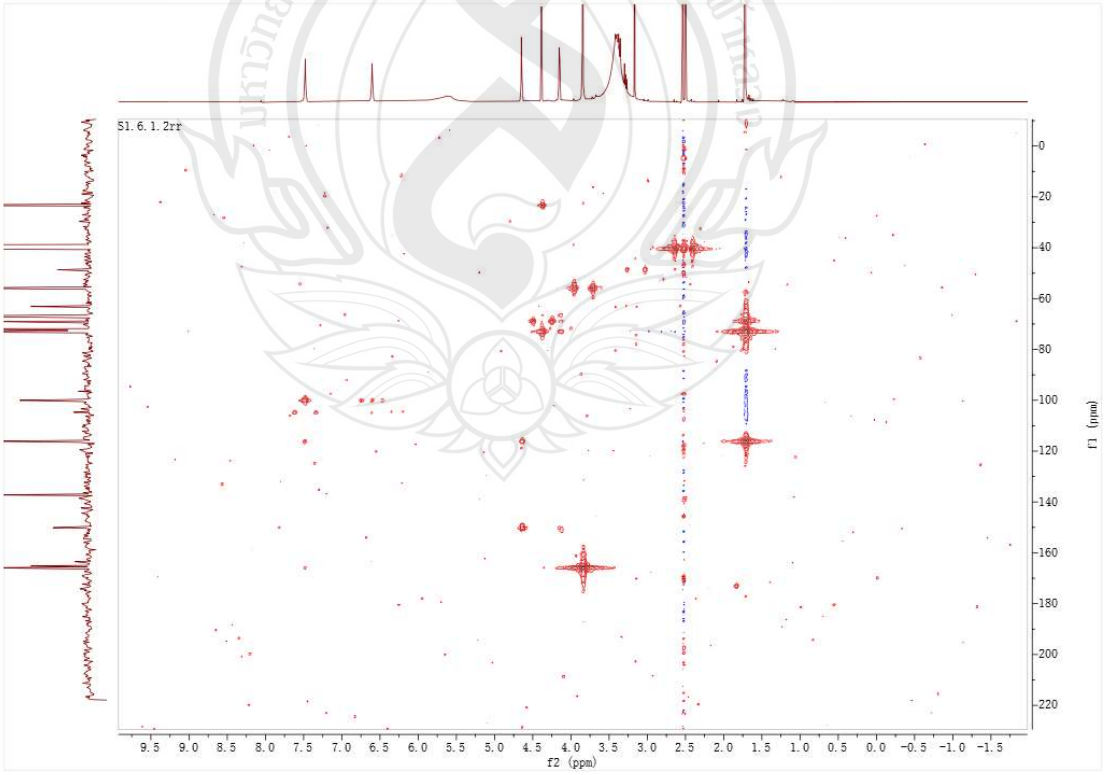

Figure A173 HMBC spectrum of compound **C31** (DMSO).

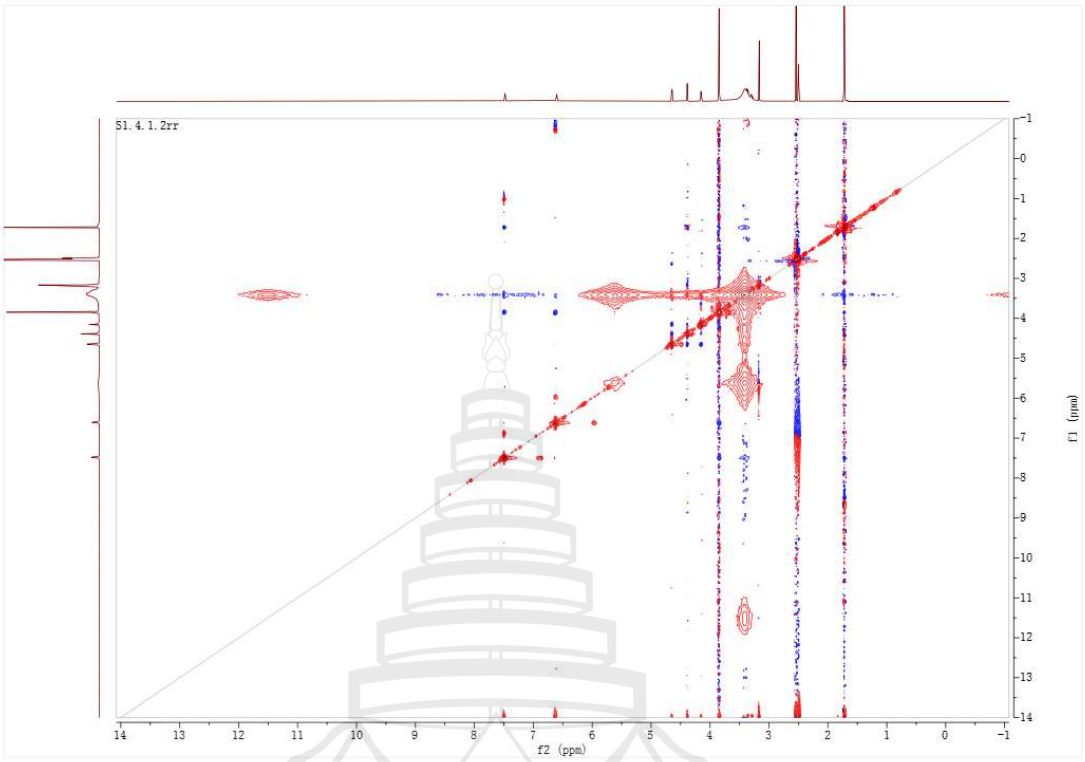

Figure A174 NOESY spectrum of compound **C31** (DMSO)

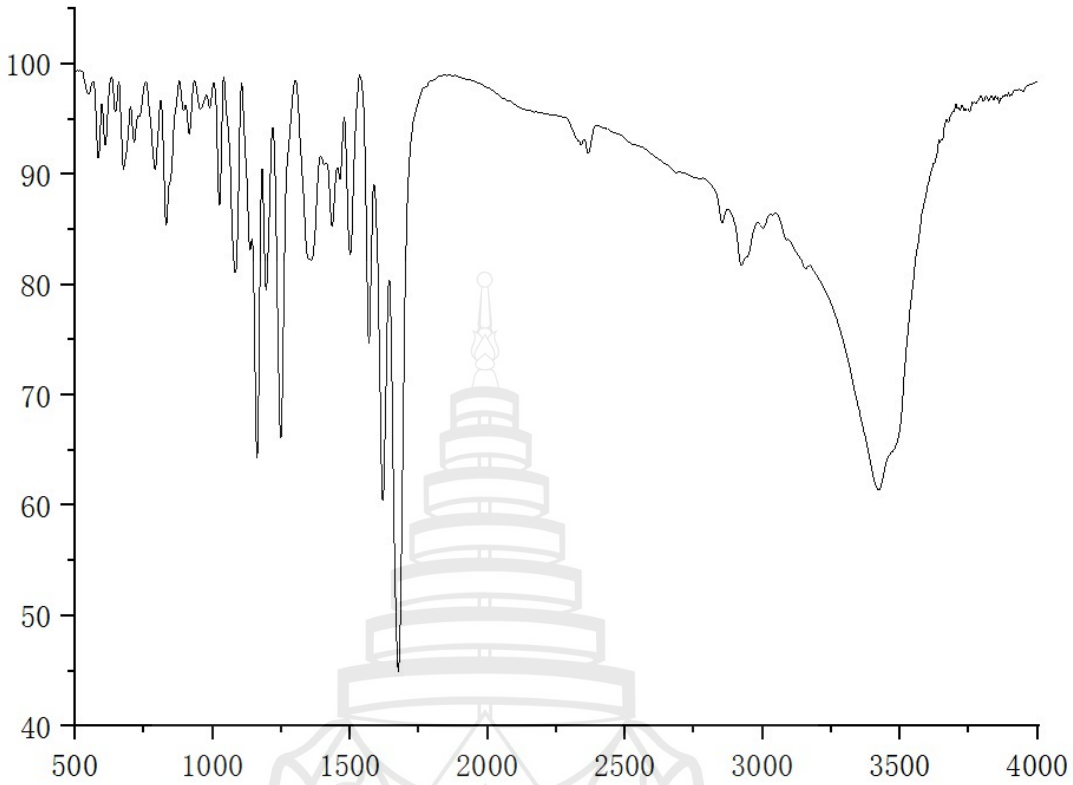

Figure A175 IR (KBr) spectrum of compound **C31**

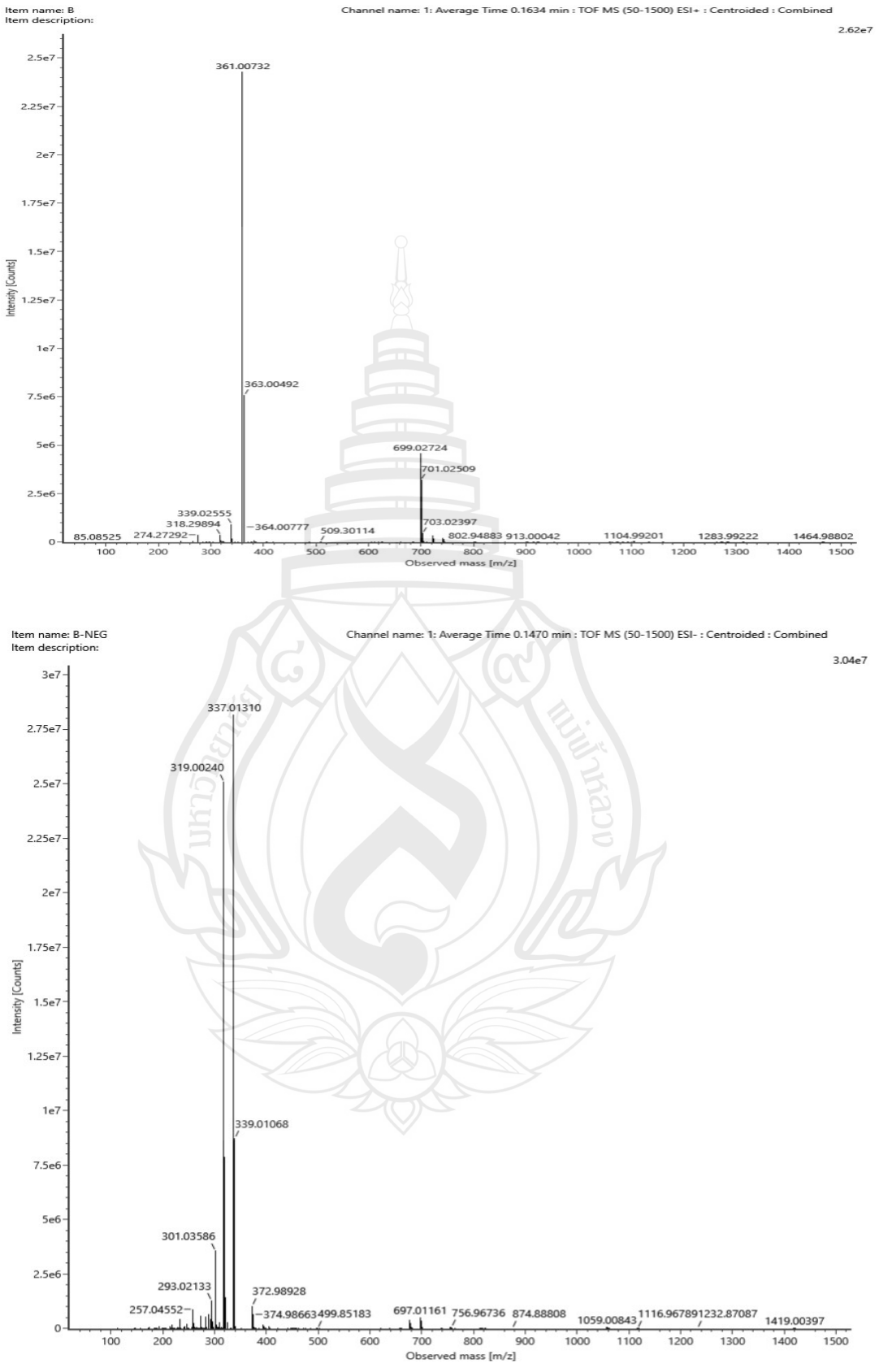

Figure A176 ESIMS of compound **C32**

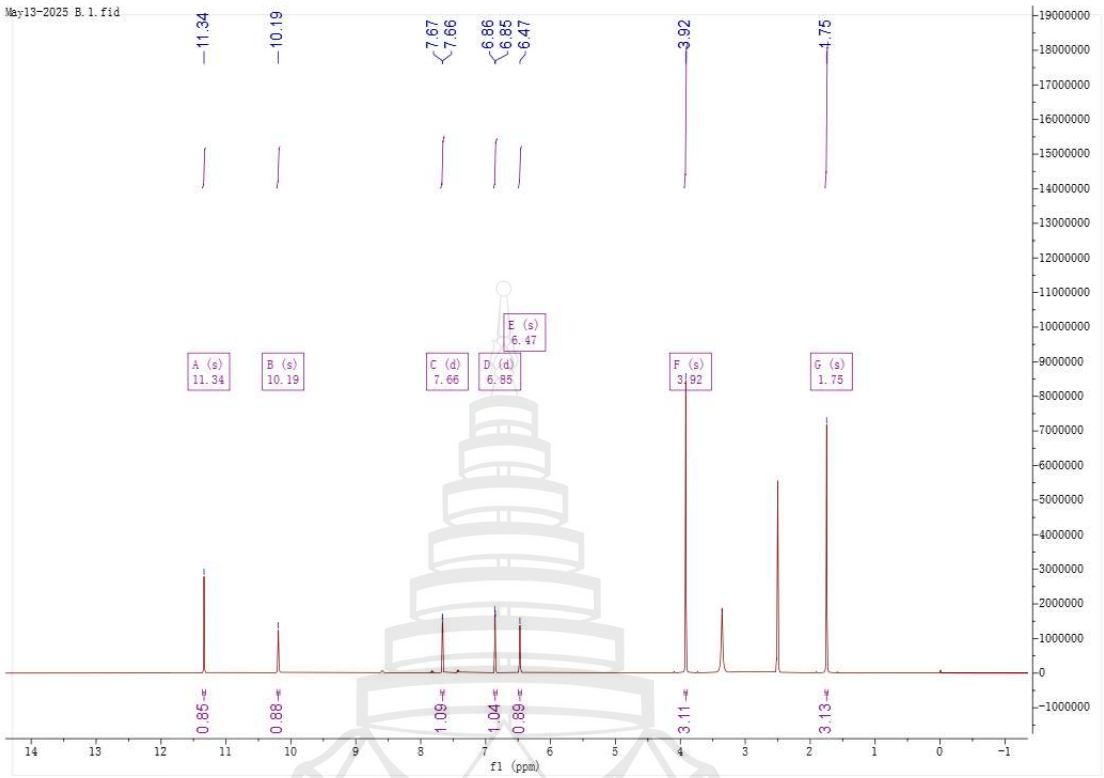

Figure A177 ^{1}H NMR spectrum of compound **C32** (400 MHz, DMSO)

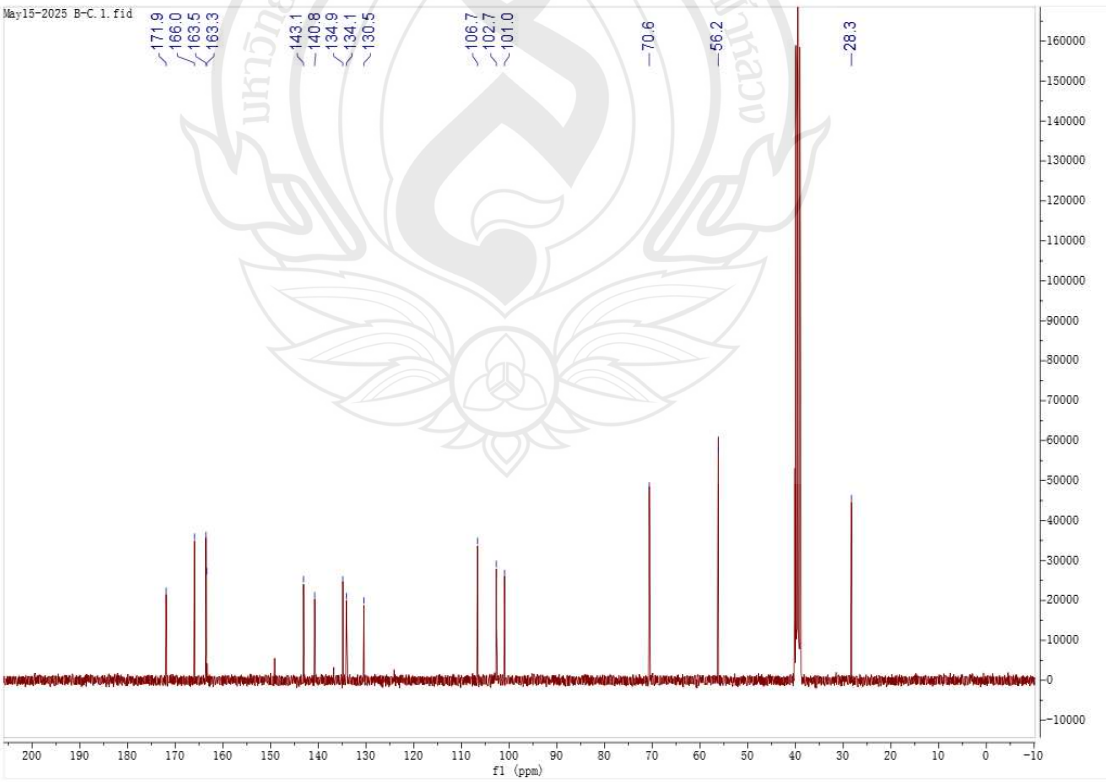

Figure A178 ^{13}C NMR spectrum of compound **C32** (100 MHz, DMSO)

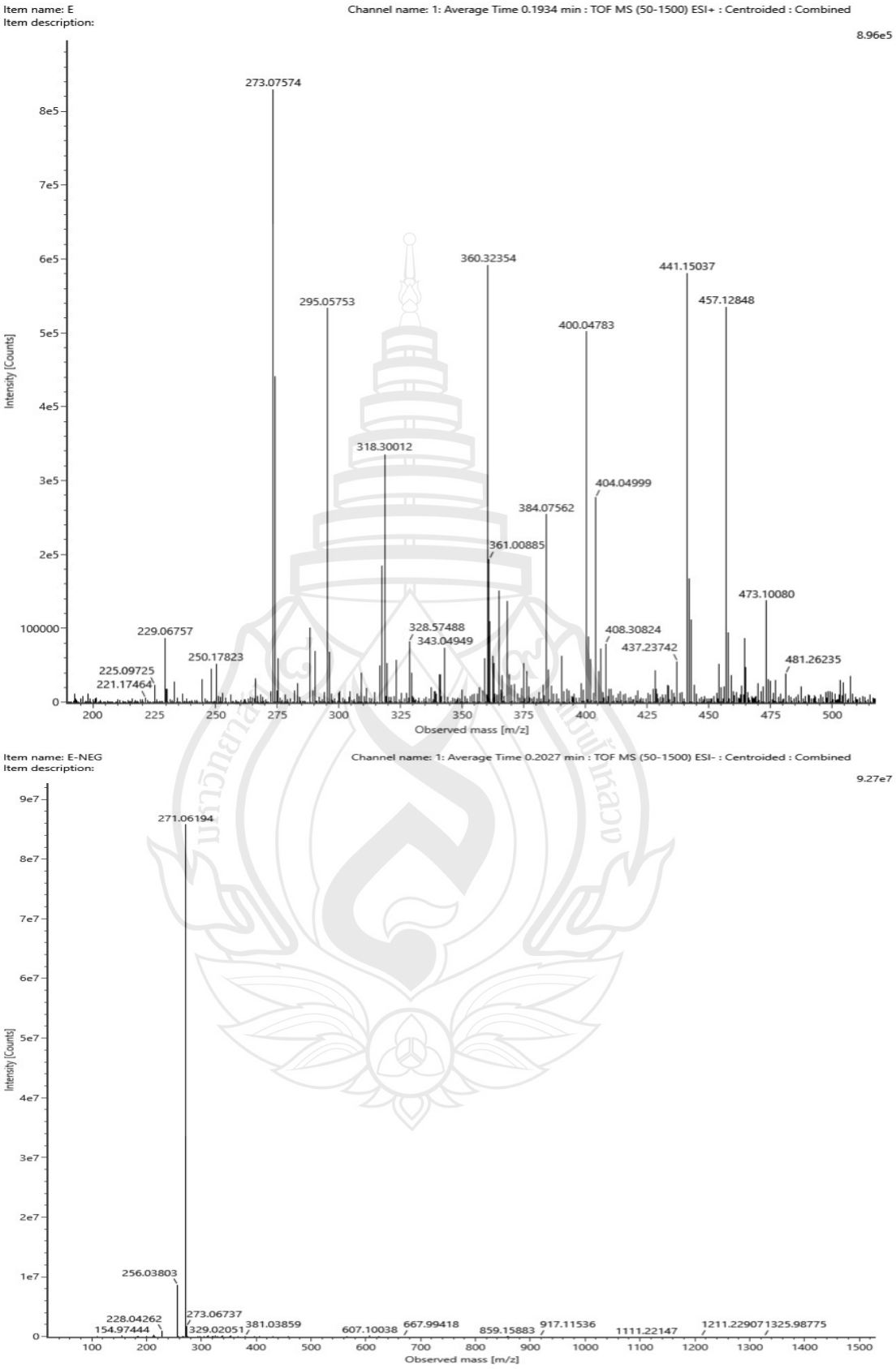

Figure A179 ESIMS of compound **C33**

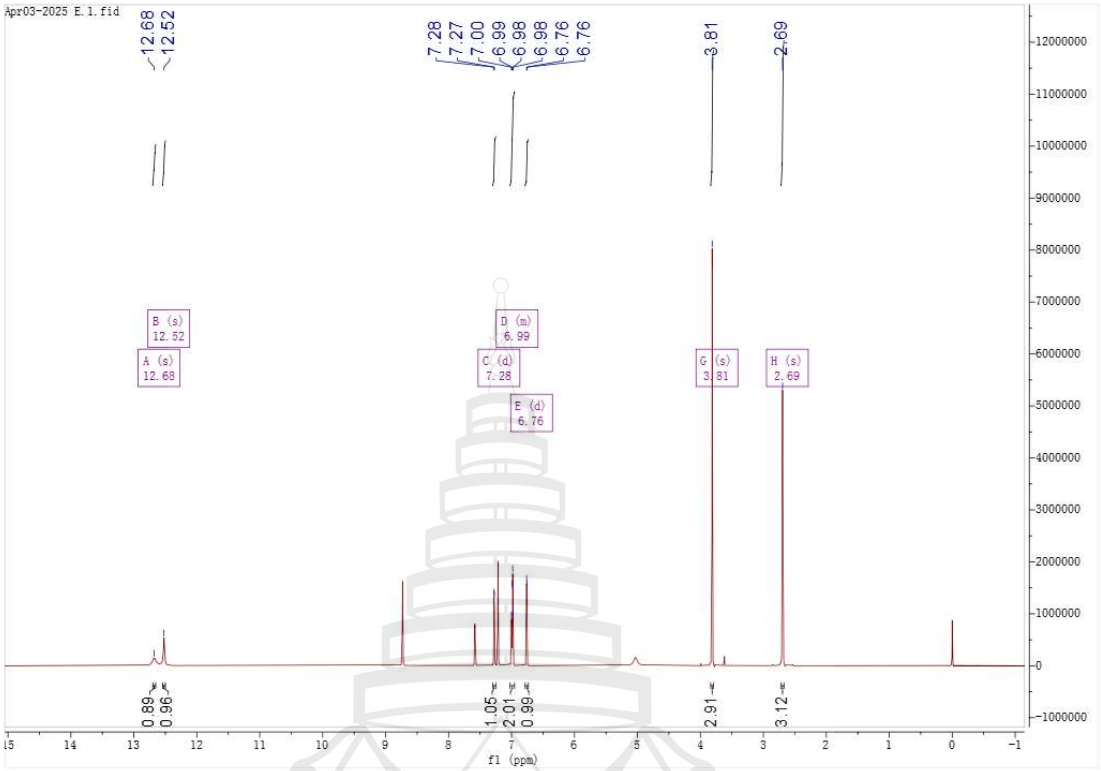

Figure A180 ^{1}H NMR spectrum of compound **C33** (400 MHz, C_5D_5N)

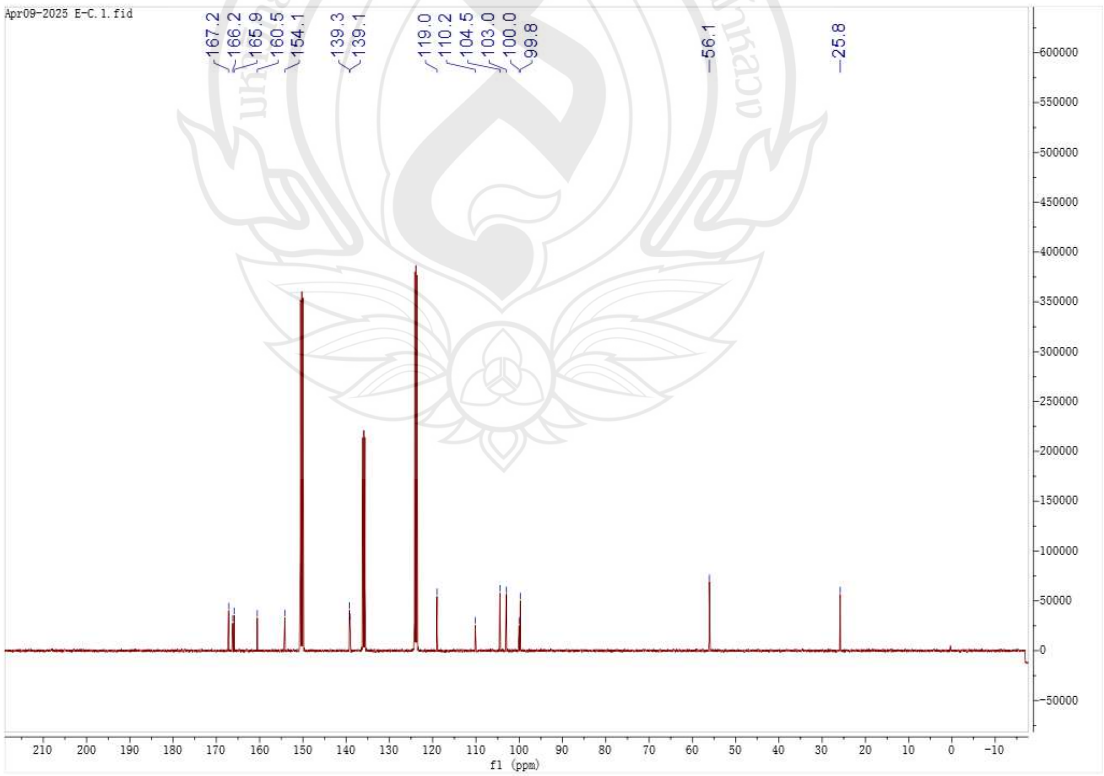

Figure A181 ^{13}C NMR spectrum of compound **C33** (100 MHz, DMSO)

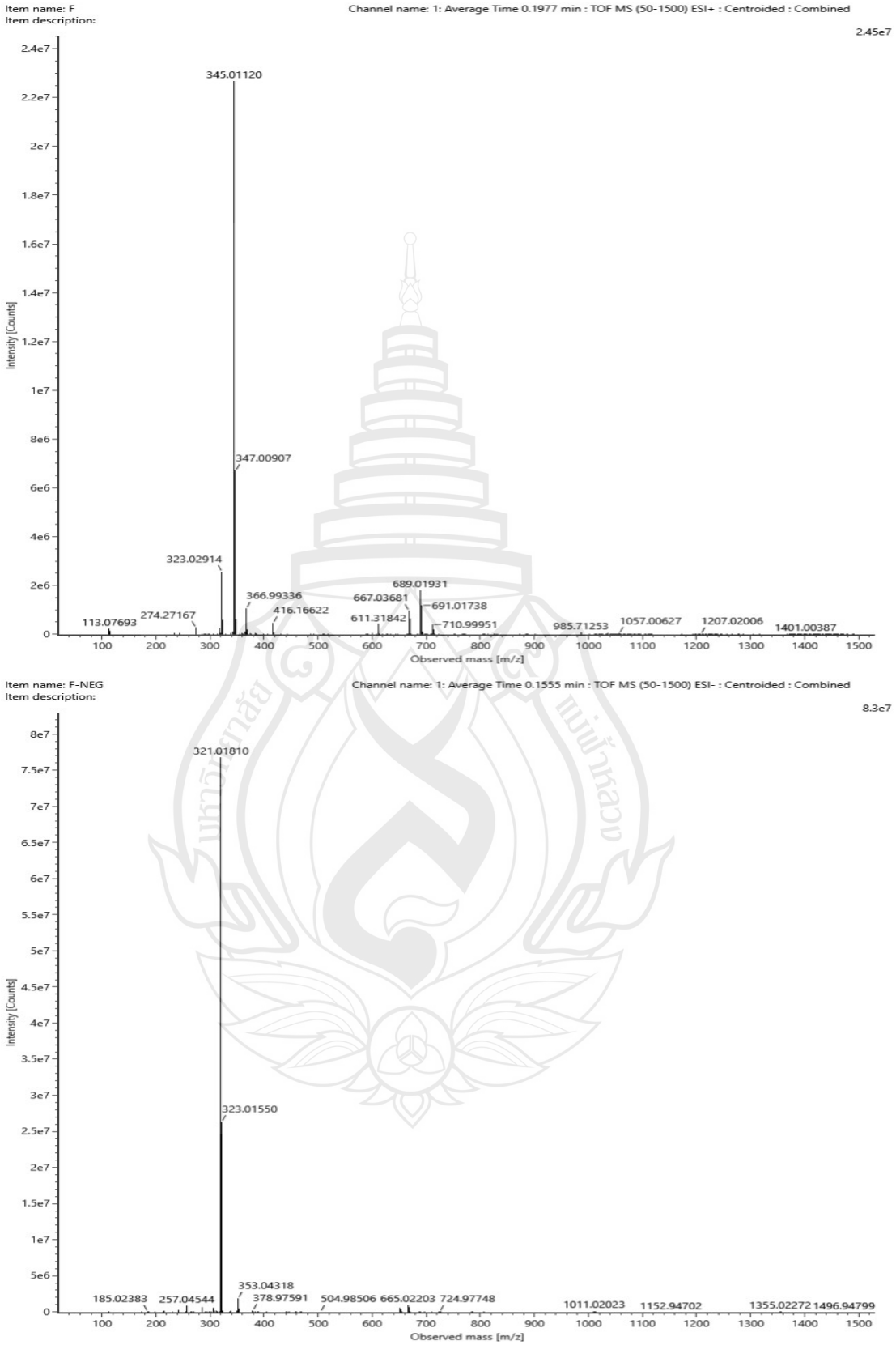

Figure A182 ESIMS of compound **C34**

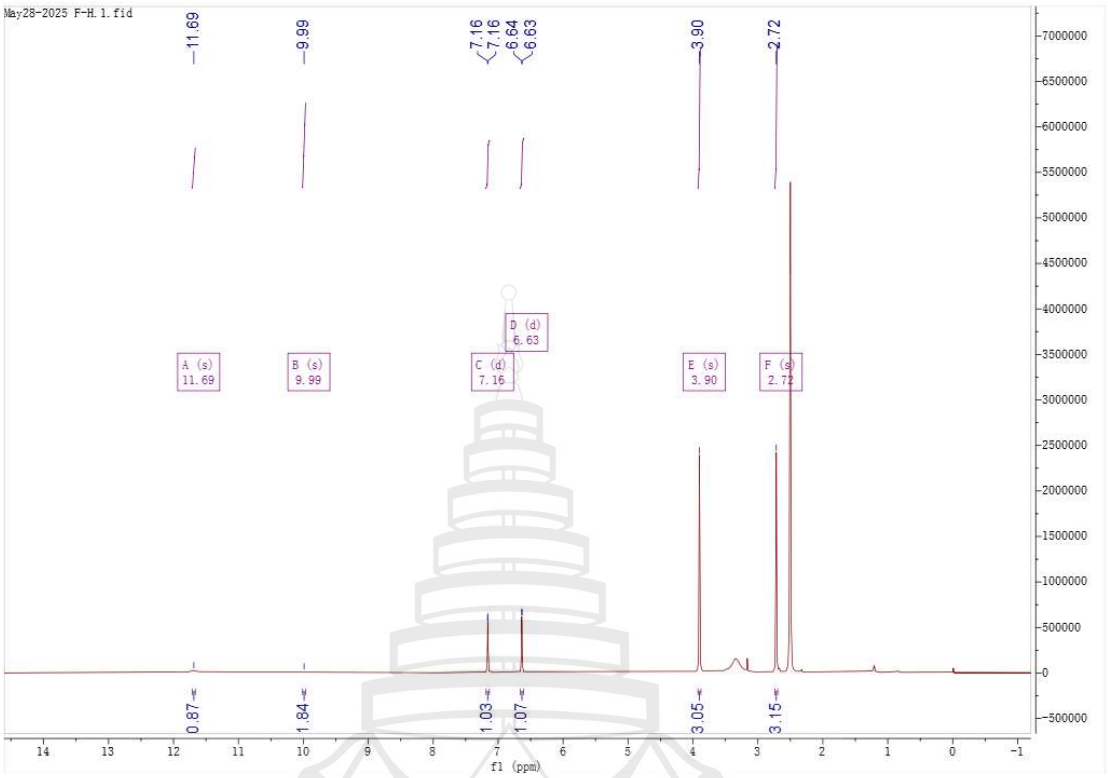

Figure A183 ^{1}H NMR spectrum of compound C34 (400 MHz, DMSO)

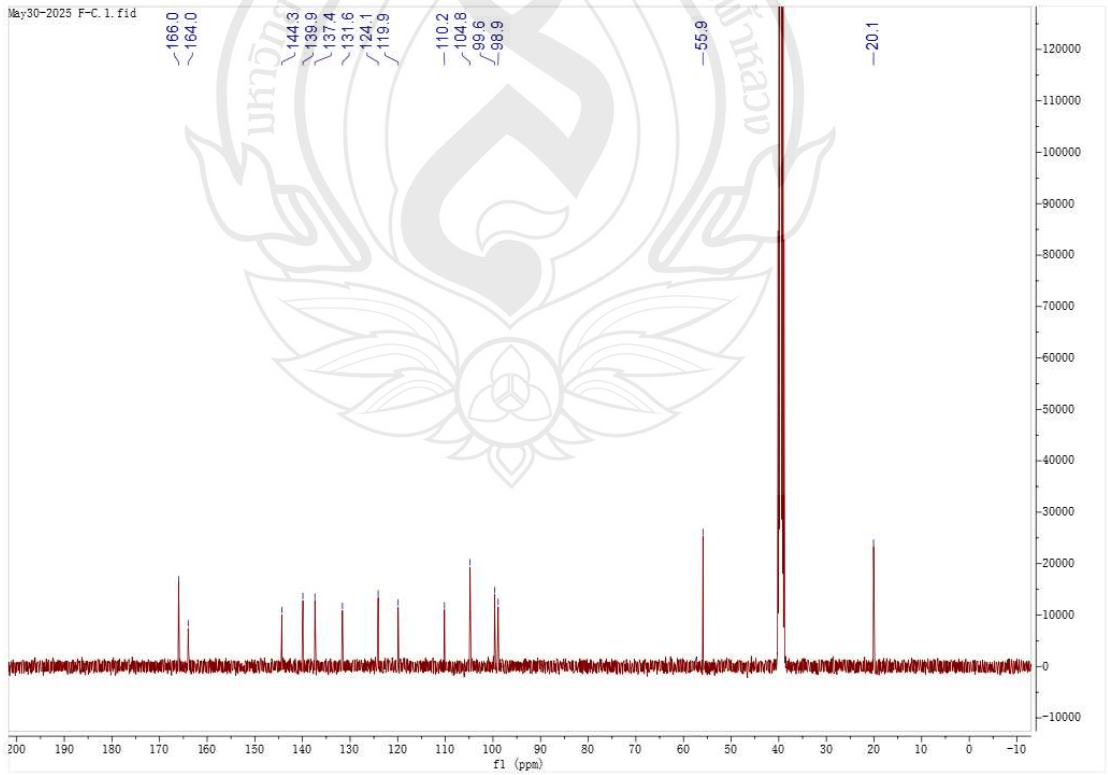

Figure A184 ^{13}C NMR spectrum of compound **C34** (100 MHz, DMSO)

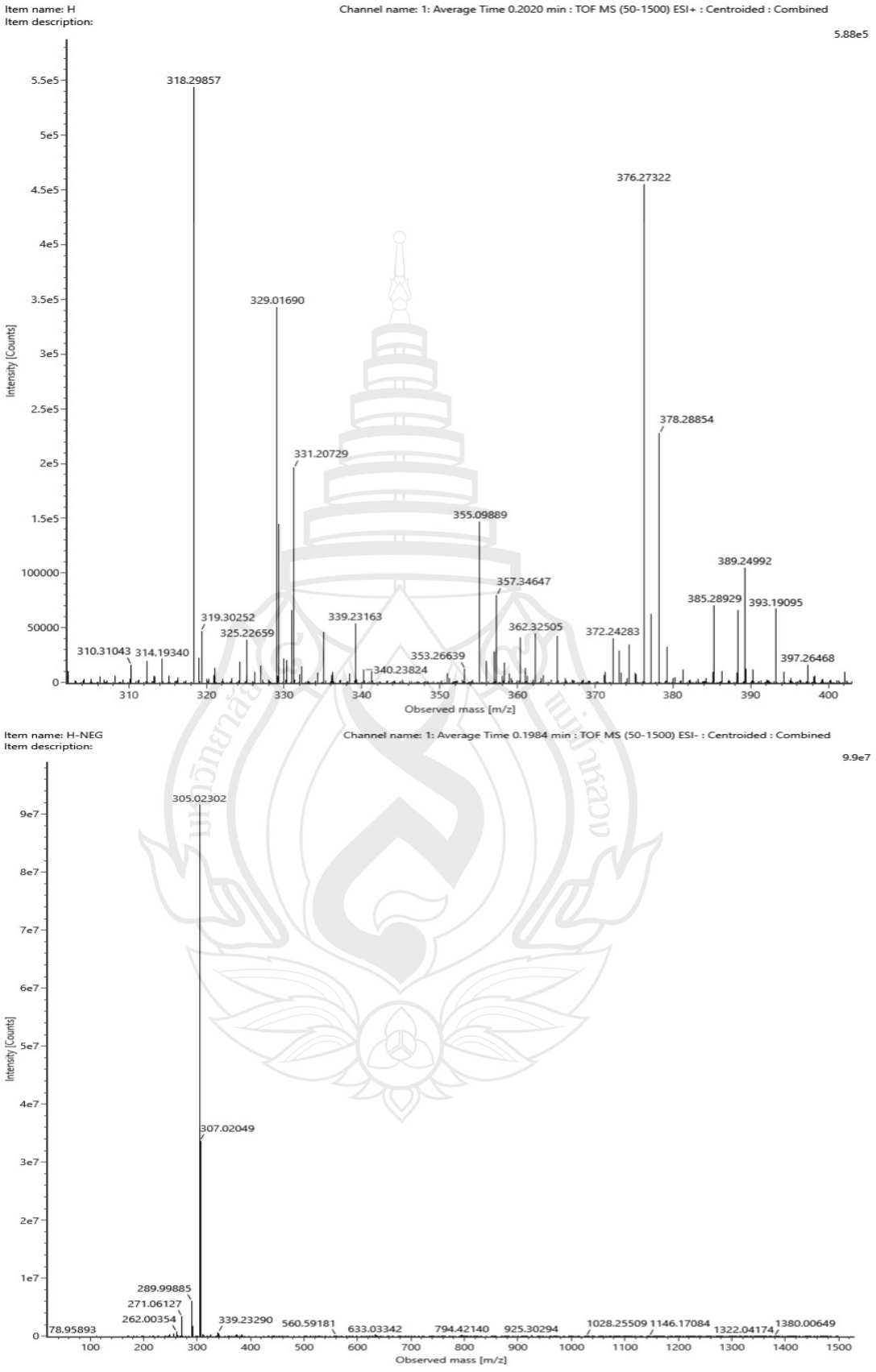

Figure A185 ESIMS of compound **C35**

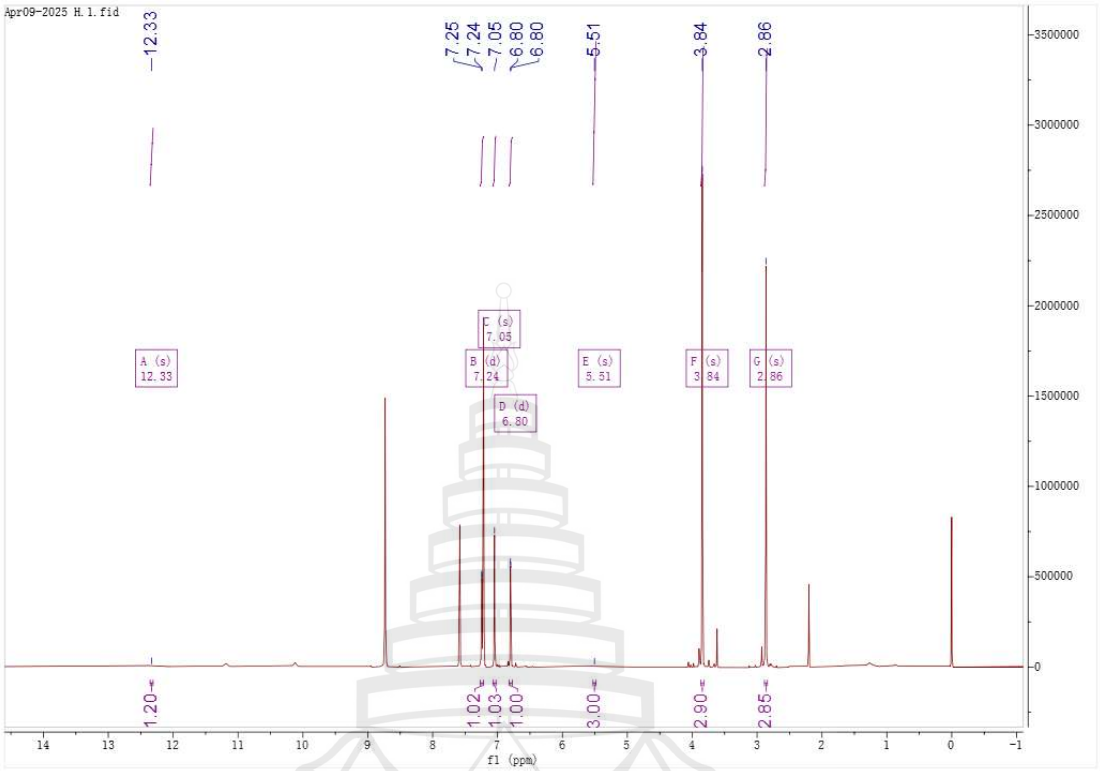

Figure A186 ^{1}H NMR spectrum of compound **C35** (400 MHz, C_5D_5N)

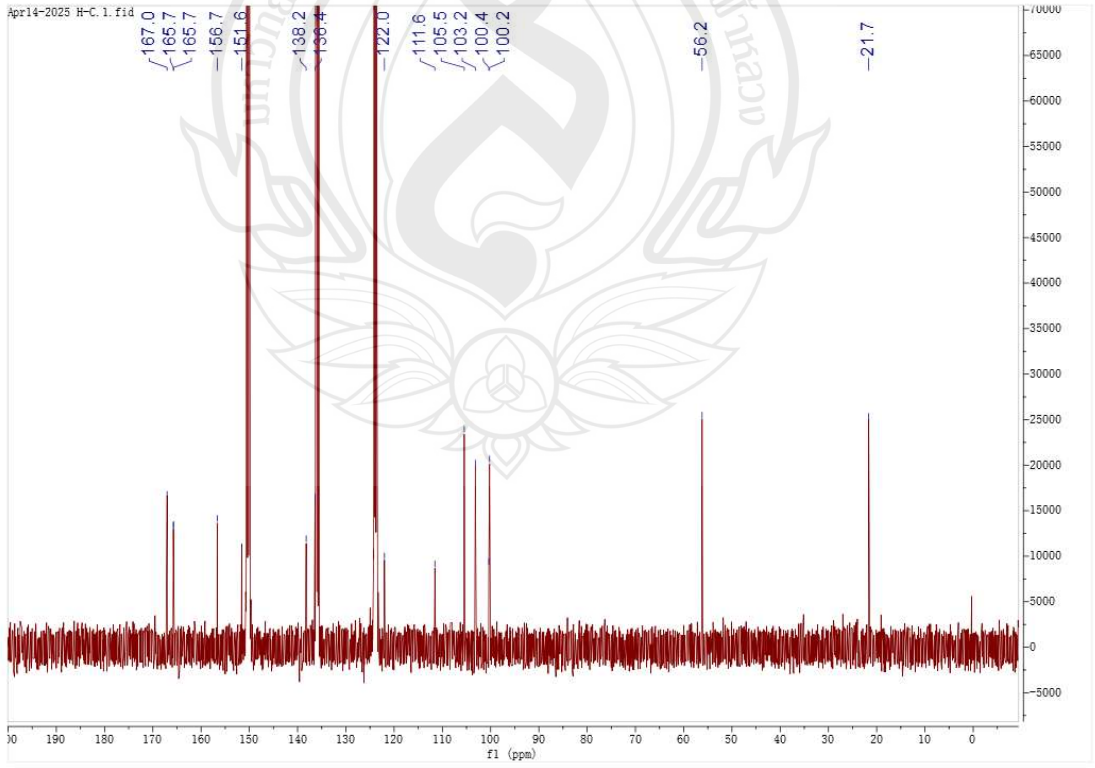

Figure A187 ^{1}H NMR spectrum of compound **C35** (400 MHz, C_5D_5N)

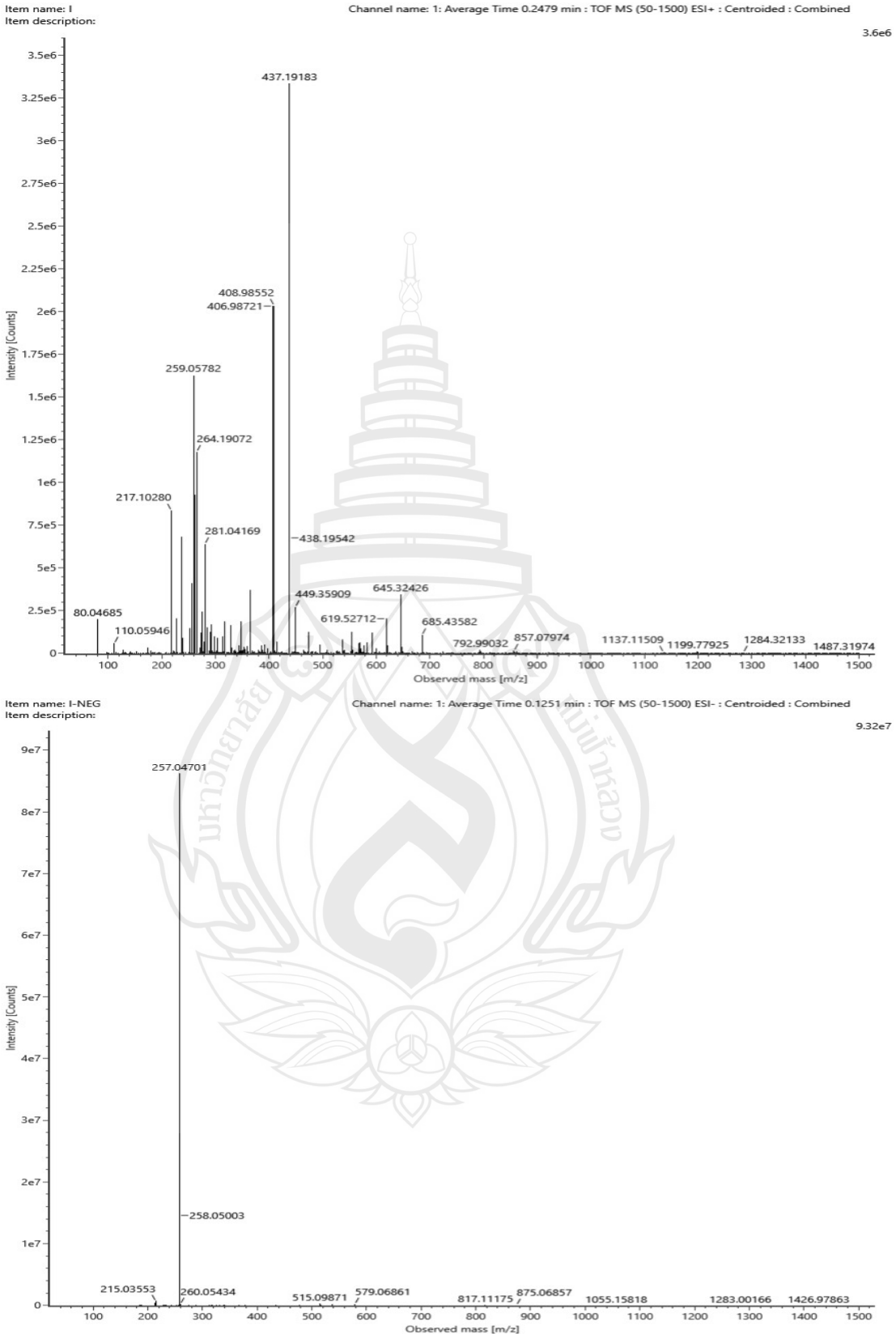

Figure A188 ESIMS of compound **C36**

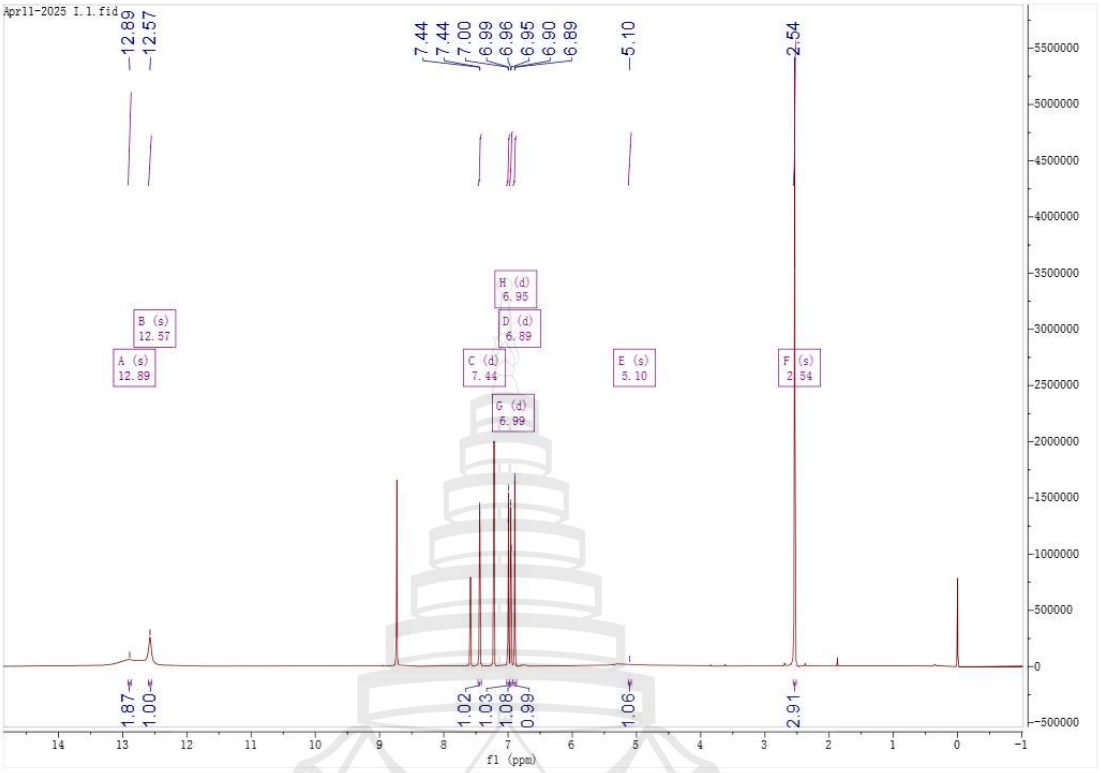

Figure A189 ^{1}H NMR spectrum of compound **C36** (400 MHz, C_5D_5N)

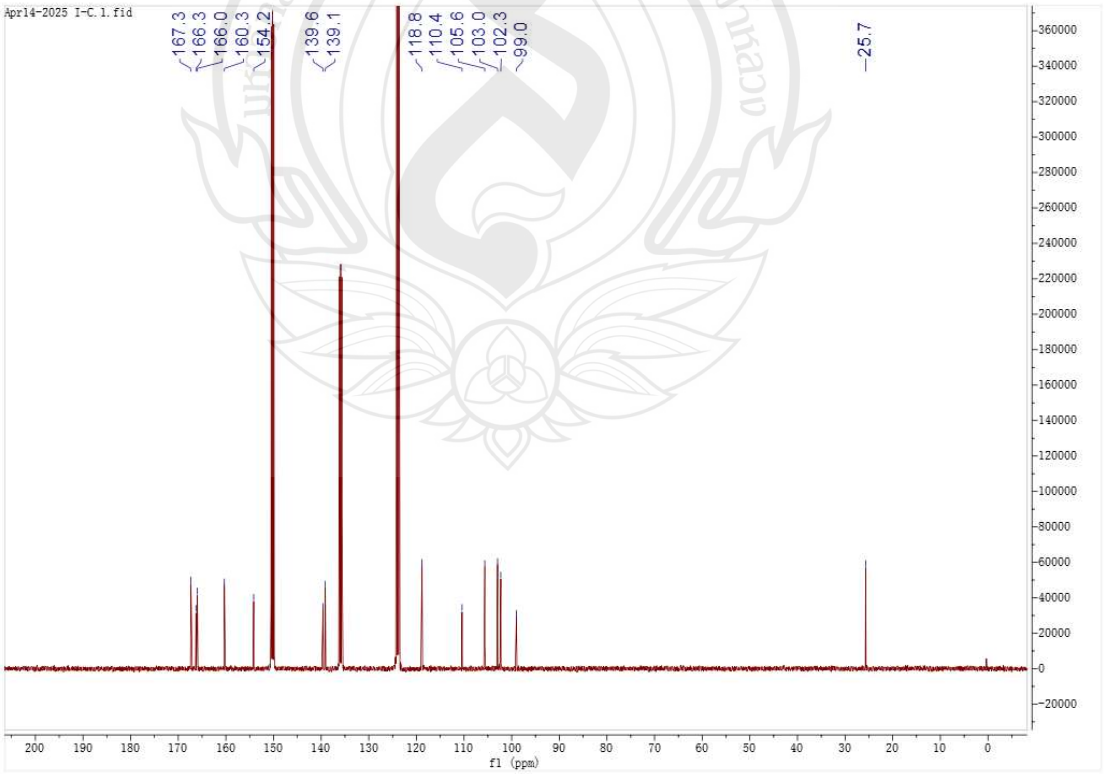

Figure A190 ^{13}C NMR spectrum of compound **C36** (100 MHz, C_5D_5N)

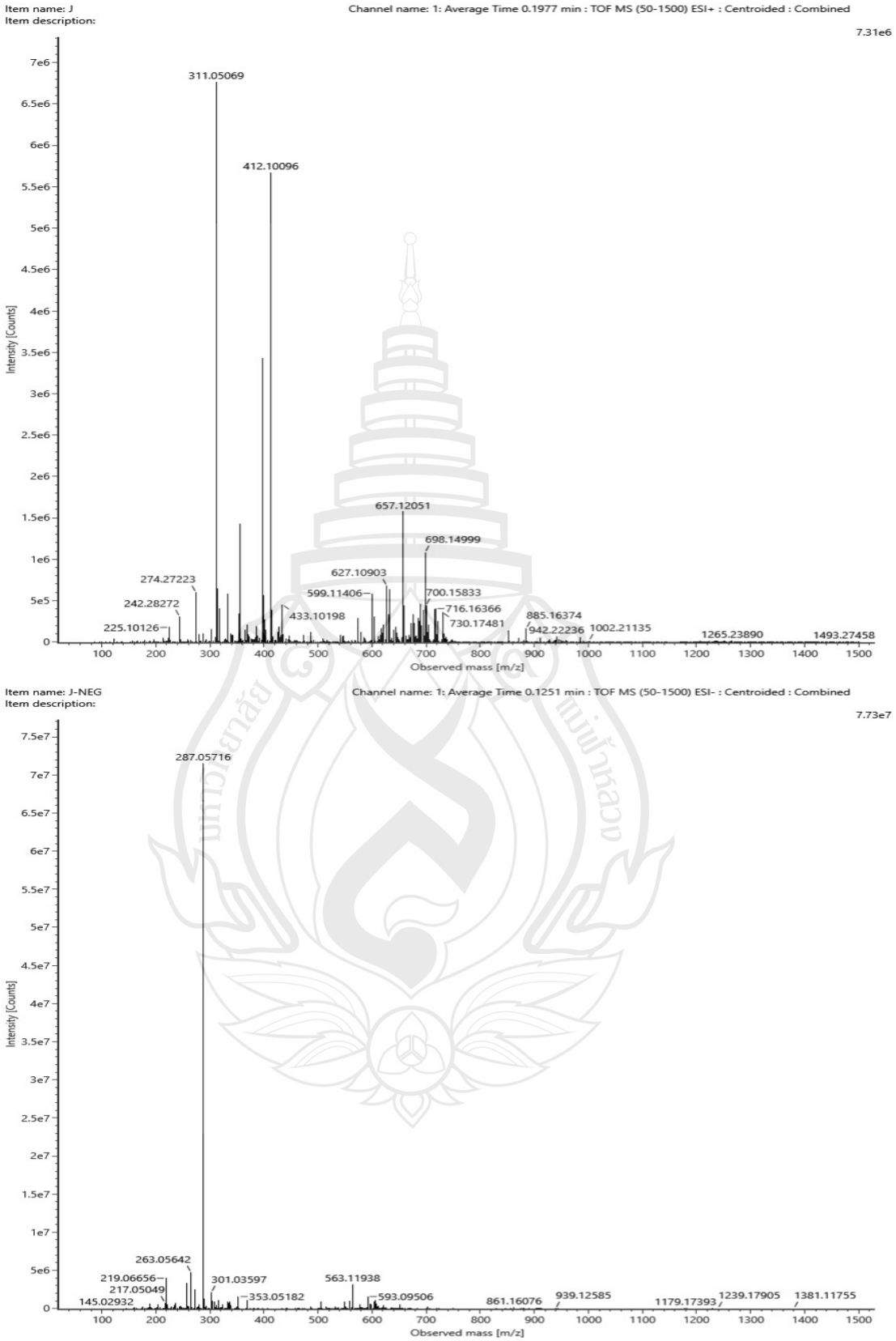

Figure A191 ESIMS of compound **C37**

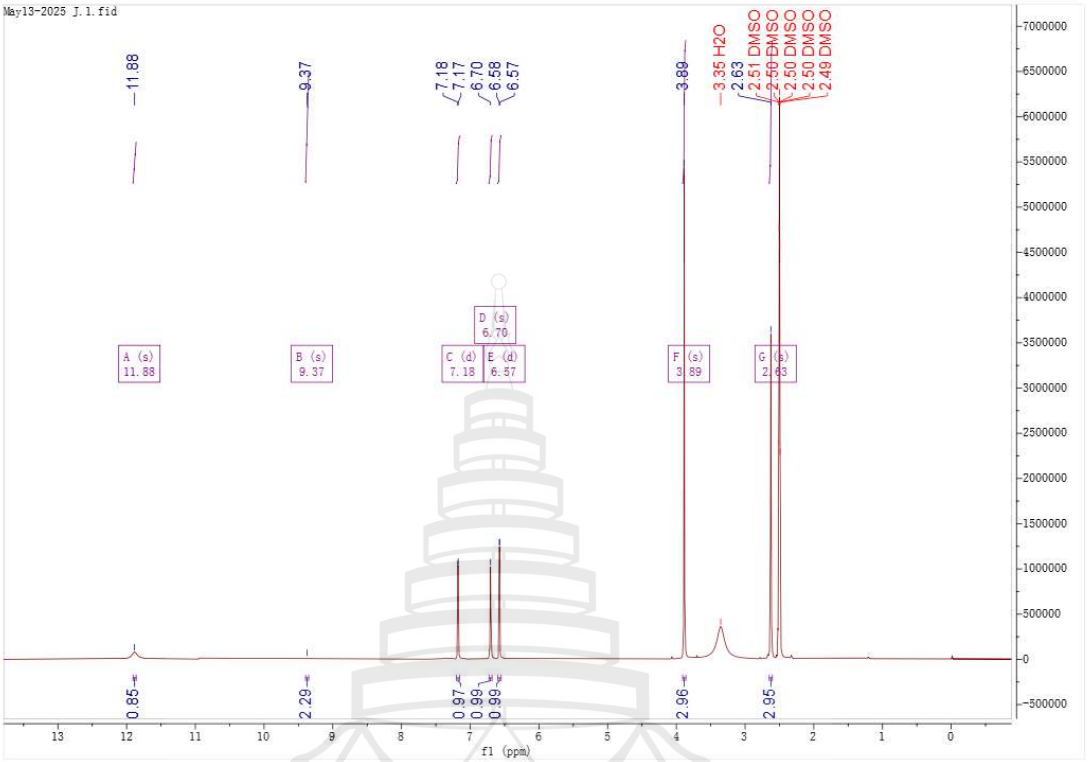

Figure A192 ^{1}H NMR spectrum of compound **C37** (400 MHz, DMSO)

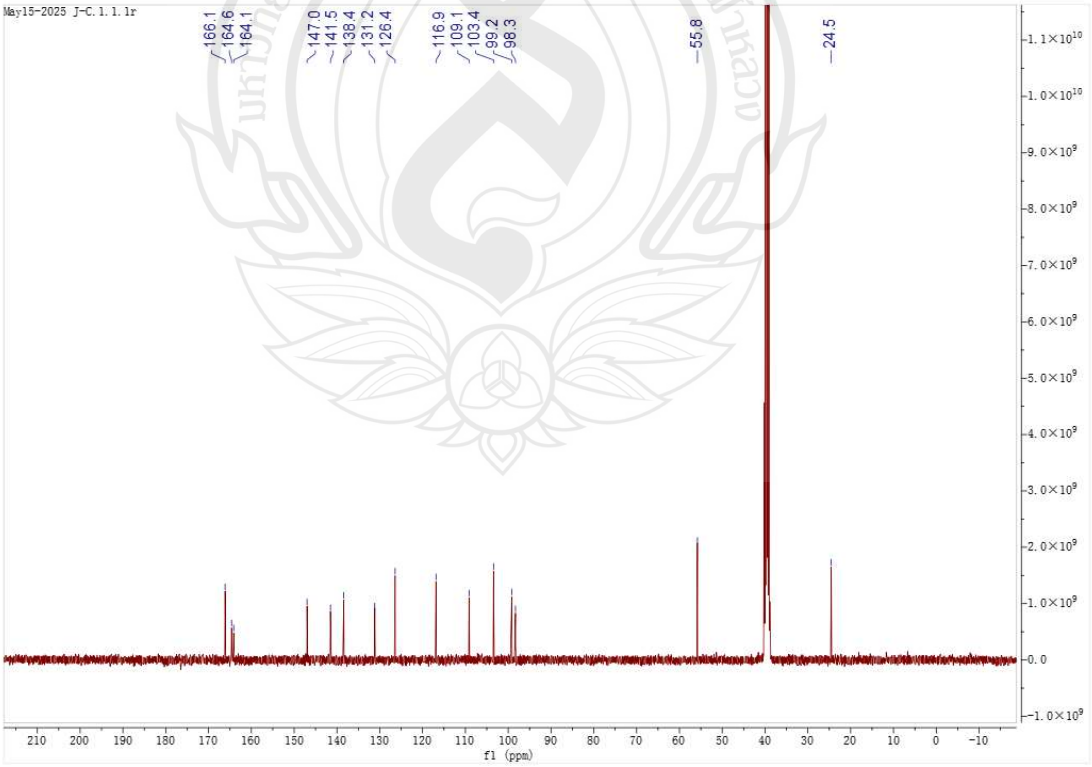

Figure A193 ^{13}C NMR spectrum of compound **C37** (100 MHz, DMSO)

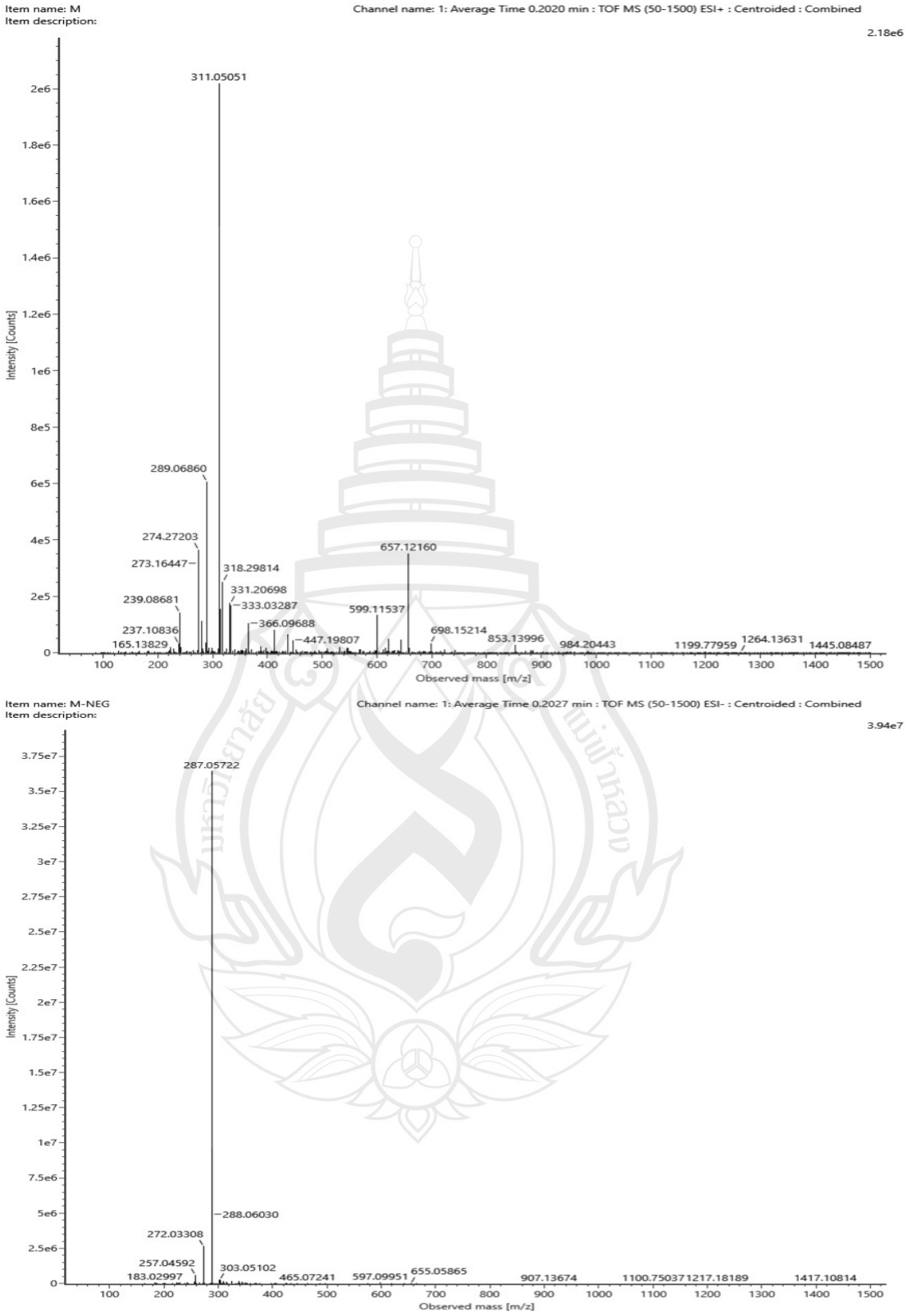

Figure A194 ESIMS of compound **C38**

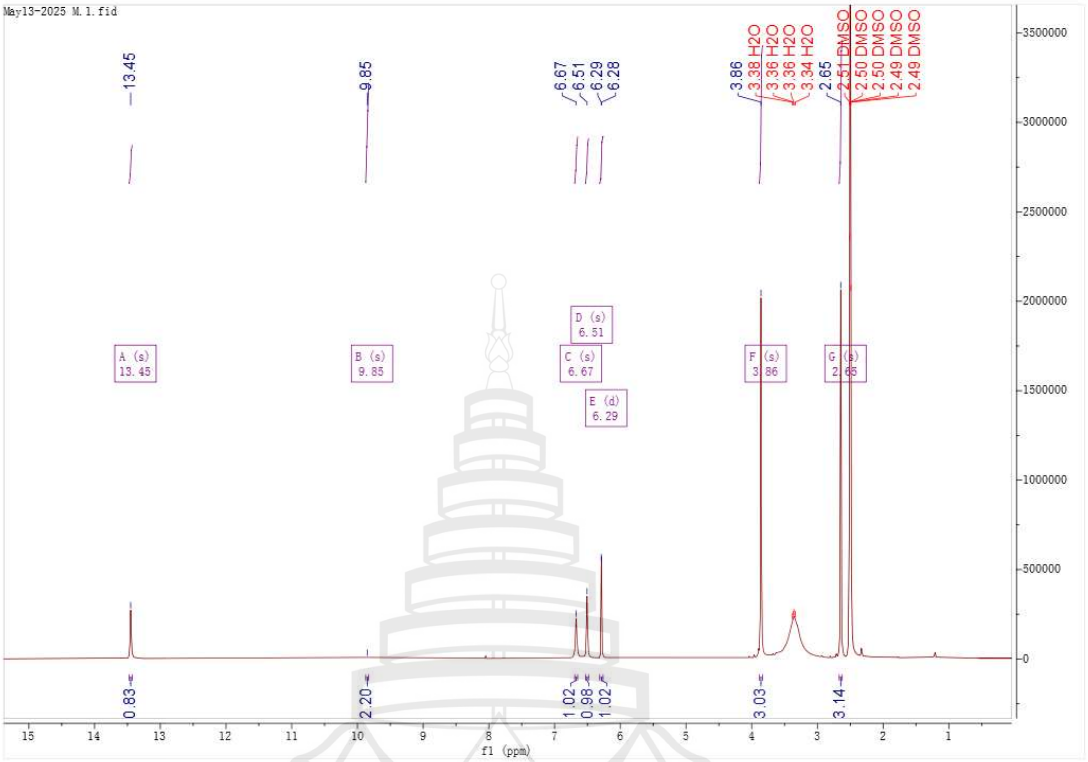

Figure A195 ^{1}H NMR spectrum of compound **C38** (400 MHz, DMSO)

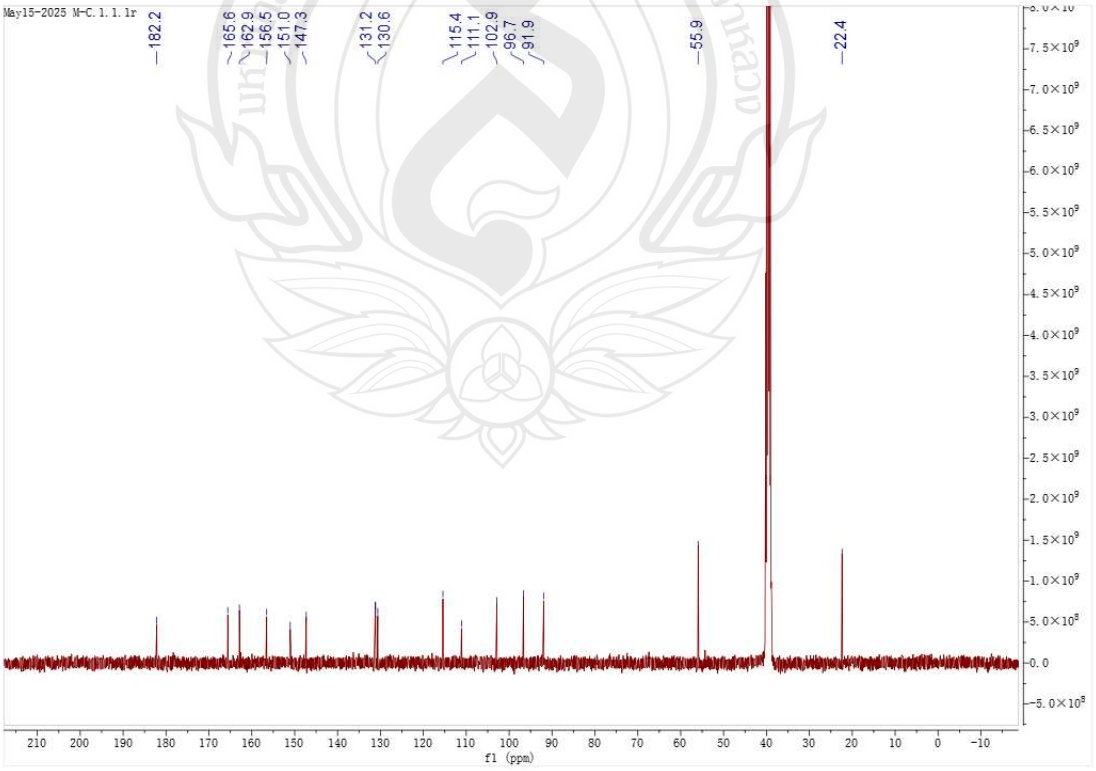

Figure A196 ^{13}C NMR spectrum of compound **C38** (100 MHz, DMSO)

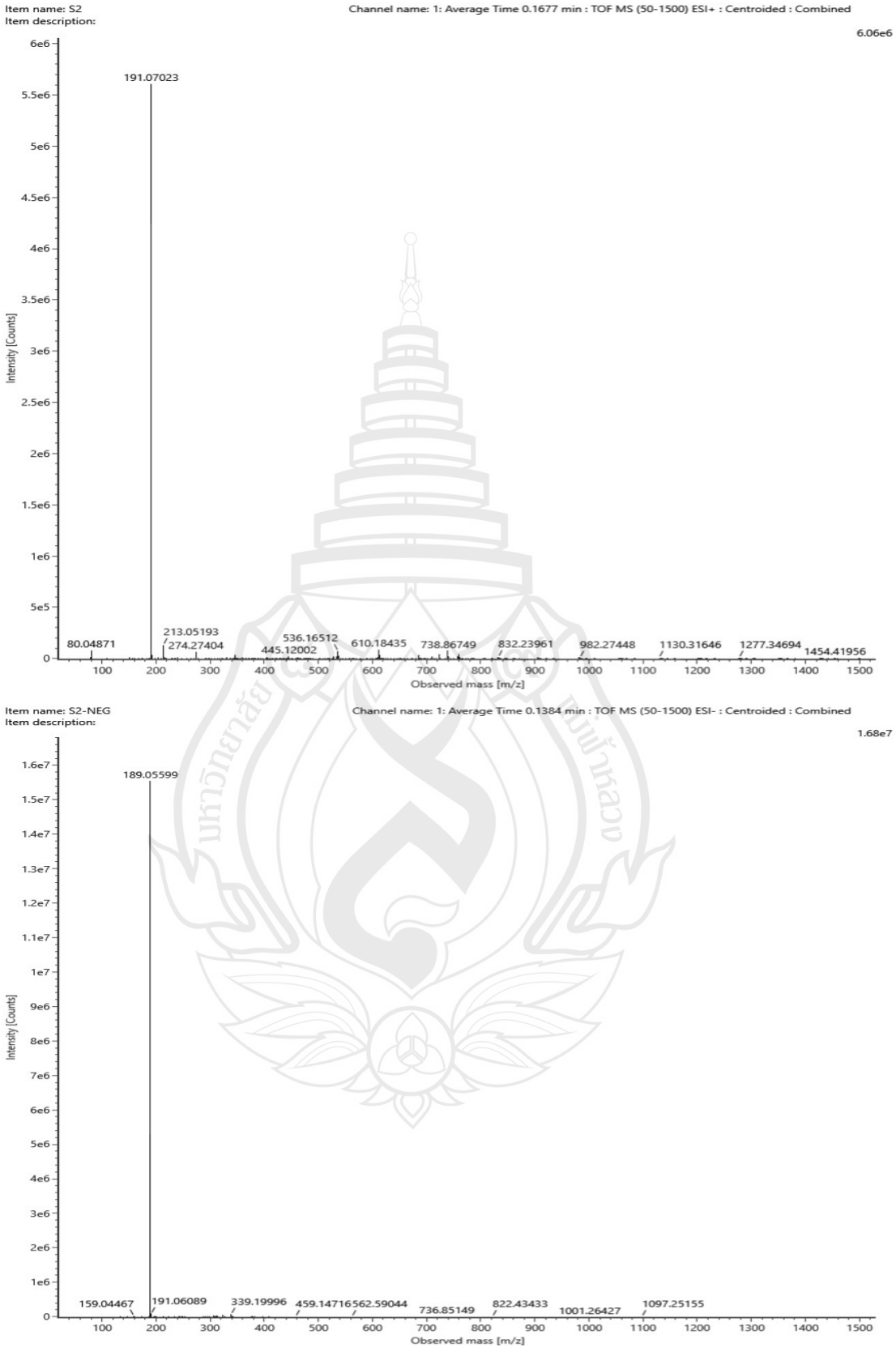

Figure A197 ESIMS of compound **C39**

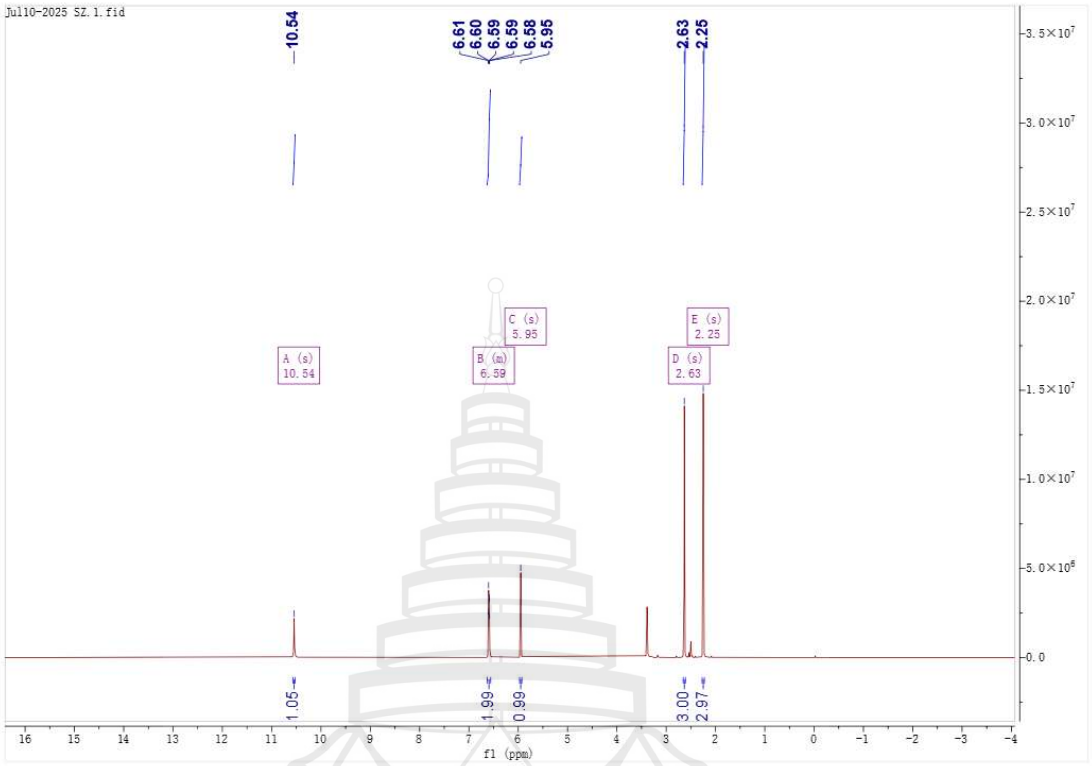

Figure A198 ^{1}H NMR spectrum of compound **C39** (400 MHz, DMSO)

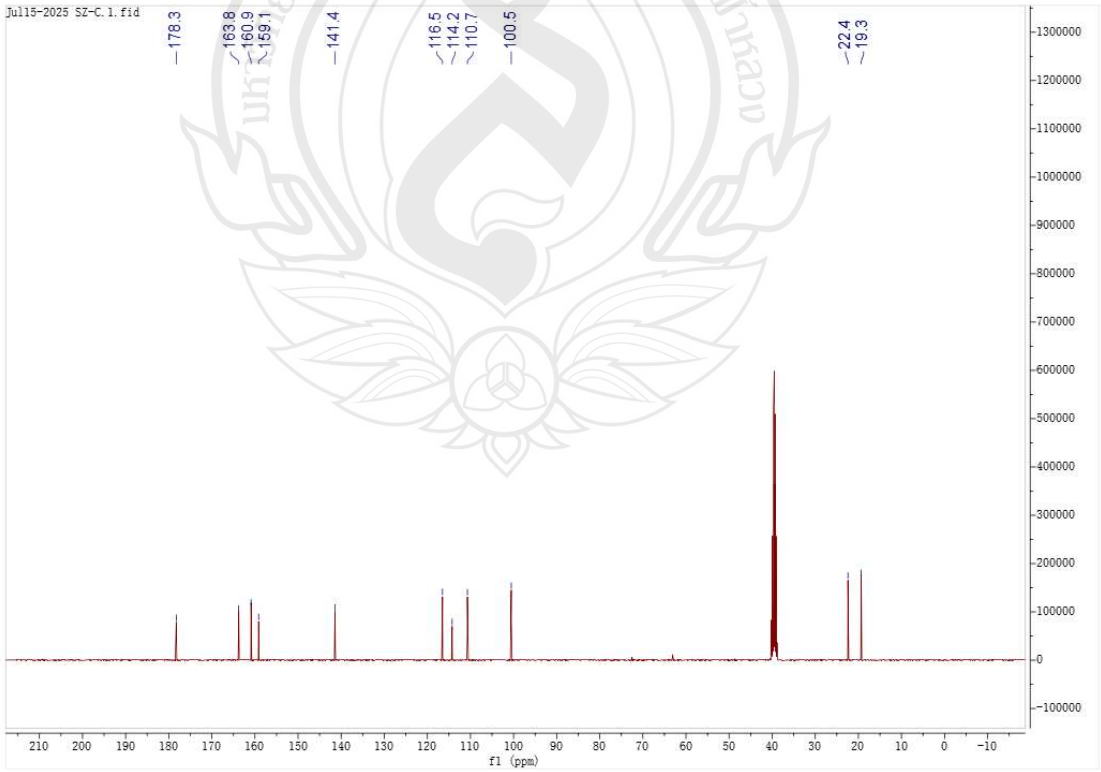

Figure A199 ^{13}C NMR spectrum of compound **C39** (100 MHz, DMSO)

The conformations of the isomers of compounds were generated by iMTD-GC method embedded in Crest program [1]. Two conformations with the root-mean-square (RMS) distance and energy deviation of 0.5 Å and 0.25 kcal/mol, respectively, were considered as duplicates and one of them was removed. Density functional theory calculations were performed with the Gaussian 09 package. ECD spectra were calculated by the TDDFT methodology at the B3LYP/def2TZVP utilizing IEFPCM in methanol. The final ECD spectra were simulated by averaging the spectra of lowest energy conformers according to the Boltzmann distribution theory and their relative Gibbs free energy (*ΔG*).

Reference

Pracht, P., Bohle, F., & Grimme, S. (2020). Automated exploration of the low-energy chemical space with fast quantum chemical methods. *Physical Chemistry Chemical Physics, 22*(14), 7169-7192.

Table A5 The energy and boltzmann distributions for the optimized geometries of **C27**

Optimized geometry	Energy(a.u.)	DE (kcal/mol)	Boltzmann distribution
C27-1	-1107.900731	0	57.04%
C27-2	-1107.900437	0.18	41.78%
C27-3	-1107.896895	2.41	0.98%
C27-4	-1107.895371	3.36	0.20%

C27-1			
C	-9.04052400	0.70343200	-1.58653800
C	-8.23312700	1.66287600	-0.97444400
C	-7.06912500	1.29997100	-0.28113500
C	-6.68727700	-0.03252200	-0.19518400
C	-7.51274500	-1.02612000	-0.80083300
C	-8.68797300	-0.63882400	-1.49526800
O	-9.49833200	-1.53553800	-2.08122000
O	-8.49859700	2.98543800	-0.99195900
C	-9.67014000	3.44489700	-1.67152300

Figure A200 Optimized cartesian coordinates of conformers of **C27** at B3LYP/6-311G(d) level

C	-5.47704100	-0.48619600	0.49374100
C	-5.23801200	-1.81287600	0.55431300
O	-6.06579900	-2.75669200	-0.00349500
C	-7.19426800	-2.42265700	-0.69869300
O	-7.84075000	-3.35160400	-1.17155900
C	-4.48089500	0.50306500	1.11676800
C	-3.44629500	-0.21531800	2.00388900
C	-2.93406800	-1.54536200	1.45920900
C	-4.10858700	-2.49937800	1.27460600
O	-5.17431300	1.46237200	1.93714800
C	-3.78225100	1.34498700	0.04204700
O	-2.17911000	-1.43728400	0.25070000
O	-4.53042000	-2.92881100	2.57140800
H	-9.94281100	0.95756300	-2.12392900
H	-6.50531700	2.07495700	0.21048800
H	-9.12717500	-2.43101800	-1.92248200
H	-9.62982500	3.19405600	-2.73404000
H	-10.57298800	3.02284100	-1.22399300
H	-9.67240400	4.52488200	-1.55073600
H	-3.91796000	-0.43338600	2.96633200
H	-2.61453200	0.46495700	2.19640400
H	-2.25054200	-1.99168500	2.18254700
H	-3.78382400	-3.35911300	0.67904900
H	-5.69638300	0.98256700	2.59265800
H	-4.48929000	1.78205300	-0.66071200
H	-3.23898500	2.15341100	0.53530300
H	-3.06129700	0.75007200	-0.51430800
H	-2.78058800	-1.31318200	-0.49389500
H	-5.20856300	-3.60600900	2.46057000
		C27-2	
C	-9.44359100	0.50055400	-1.39670600
C	-8.64801500	1.54788900	-0.91815700
C	-7.36489600	1.31211400	-0.41418300
C	-6.85728500	0.01173600	-0.38694900
C	-7.67272600	-1.06384300	-0.82938000
C	-8.97297800	-0.79912200	-1.34779800
O	-9.77516600	-1.78408200	-1.79007600

Figure A200 (continued)

O	-9.21155300	2.77219200	-0.98042900
C	-8.46046100	3.90164900	-0.52587800
C	-5.52159500	-0.31130700	0.11172800
C	-5.20912900	-1.61169100	0.28425400
O	-6.02720400	-2.63915200	-0.09614400
C	-7.23309000	-2.42589600	-0.70997200
O	-7.84387900	-3.42336100	-1.07622900
C	-4.47758900	0.76915800	0.41209400
C	-3.14294500	0.17001900	0.91137300
C	-3.31427500	-1.06292000	1.76943200
C	-3.95779500	-2.14993600	0.92735700
O	-4.99095200	1.69826600	1.38834300
C	-4.16804200	1.60652000	-0.83317300
O	-2.04304000	-1.47881700	2.24456900
O	-4.23935500	-3.23848800	1.79958700
H	-10.43236600	0.70583500	-1.78673100
H	-6.77686100	2.11265400	-0.00083000
H	-9.30327500	-2.63676000	-1.67673700
H	-9.10554400	4.76194400	-0.68360100
H	-8.22095600	3.81251600	0.53609100
H	-7.54185600	4.01957600	-1.10511400
H	-2.62324900	0.95114800	1.46776500
H	-2.51162500	-0.09716300	0.05856700
H	-3.98359900	-0.86341000	2.61860300
H	-3.24536200	-2.46338300	0.15201400
H	-5.31359300	1.20122200	2.15017400
H	-5.04210100	2.13592500	-1.20435800
H	-3.39924400	2.34197900	-0.58521800
H	-3.78930700	0.96643400	-1.63114400
H	-2.17390300	-2.32937700	2.68361200
H	-4.52731100	-3.99330000	1.27315500
	C27-3		
C	-9.33813900	0.67372400	-1.32434900
C	-8.49234700	1.67364600	-0.84047200
C	-7.21350600	1.37091700	-0.35085600
C	-6.75840900	0.05946200	-0.33912600
C	-7.62703900	-0.97760600	-0.78955100

Figure A200 (continued)

C	-8.91294400	-0.65002500	-1.29201300
O	-9.76356700	-1.58890600	-1.73917300
O	-8.82511100	2.98038800	-0.80117400
C	-10.11727000	3.37816500	-1.26741700
C	-5.43536900	-0.33273700	0.14560700
C	-5.18283200	-1.64747800	0.30074400
O	-6.05013200	-2.63435100	-0.08573200
C	-7.24903700	-2.35917200	-0.68771600
O	-7.90765000	-3.32358200	-1.06047500
C	-4.34274600	0.69517800	0.45469000
C	-3.03147200	0.02797200	0.92891900
C	-3.25178200	-1.20519600	1.77521100
C	-3.95398700	-2.25139800	0.92836500
O	-4.80618500	1.62598700	1.45316300
C	-4.00744400	1.54271500	-0.77687900
O	-1.99740400	-1.68589900	2.23403100
O	-4.28155800	-3.33355600	1.79286200
H	-10.32511600	0.88263700	-1.71124000
H	-6.61504600	2.17214100	0.05129700
H	-9.33123900	-2.46480200	-1.64010600
H	-10.90777200	2.90577500	-0.67967200
H	-10.15624700	4.45595100	-1.13369500
H	-10.24435300	3.13444600	-2.32473000
H	-2.46826200	0.77676200	1.48755400
H	-2.42455500	-0.25879900	0.06477800
H	-3.90327000	-0.98353900	2.63276500
H	-3.26365800	-2.59221300	0.14453800
H	-5.14422200	1.12814200	2.20758300
H	-4.85962000	2.12061200	-1.12566700
H	-3.20213000	2.23573700	-0.52256300
H	-3.66794900	0.90296100	-1.59263800
H	-2.16461700	-2.53375400	2.66587200
H	-4.61955100	-4.06427400	1.26216800
	C27-4		
C	-9.10991500	0.63043700	-1.54746300
C	-8.31353500	1.60319000	-0.94185200
C	-7.14344600	1.25891000	-0.25004000

Figure A200 (continued)

C	-6.74341700	-0.06759800	-0.15752700
C	-7.55595700	-1.07448400	-0.75931000
C	-8.73862700	-0.70626300	-1.45152000
O	-9.53789000	-1.61664800	-2.03205700
O	-8.59677500	2.92231600	-0.96458800
C	-9.77674200	3.36243400	-1.64210400
C	-5.52554700	-0.50261500	0.52939200
C	-5.26394000	-1.82450900	0.58761100
O	-6.07725700	-2.78061000	0.02946800
C	-7.21544200	-2.46557300	-0.65785400
O	-7.84956400	-3.40524200	-1.12664700
C	-4.53812600	0.49630600	1.13797000
C	-3.48997200	-0.20476300	2.02333800
C	-2.95917800	-1.52889800	1.48306100
C	-4.12200900	-2.49700300	1.30186800
O	-5.32104400	1.36239300	1.98430200
C	-3.85320200	1.33595500	0.04511900
O	-2.20431400	-1.41486800	0.27533200
O	-4.53115500	-2.93542700	2.59936000
H	-10.01716100	0.86997900	-2.08321900
H	-6.59049400	2.04276500	0.23905700
H	-9.15314200	-2.50608500	-1.87154400
H	-9.73674400	3.10731200	-2.70364800
H	-10.67222100	2.93009000	-1.18958400
H	-9.79360000	4.44286300	-1.52629800
H	-3.96860500	-0.41826500	2.98169200
H	-2.66019600	0.48144500	2.21104600
H	-2.27092400	-1.96352100	2.20900800
H	-3.78895200	-3.35098900	0.70249200
H	-4.72347700	2.02059000	2.36106600
H	-3.16948400	0.73411100	-0.55160500
H	-4.57527200	1.80369500	-0.62153000
H	-3.25852600	2.12408800	0.51579000
H	-2.80669200	-1.30467100	-0.47068200
H	-5.20936500	-3.61290600	2.49048100

Figure A200 (continued)

Table A6 The energy and boltzmann distributions for the optimized geometries of **C28**

Optimized geometry	Energy (a.u.)	DE (kcal/mol)	Boltzmann distribution
C28-1	-1107.902466	0.00	52.60%
C28-2	-1107.902158	0.19	37.96%
C28-3	-1107.900844	1.02	9.44%

	C28-1		
C	-9.63815800	0.11619500	-1.63072700
C	-9.10357100	1.12570500	-0.82911200
C	-7.87308800	0.96286500	-0.17645600
C	-7.15009800	-0.21458700	-0.32081500
C	-7.68703900	-1.25783100	-1.13263300
C	-8.93632000	-1.07520300	-1.77990800
O	-9.48559800	-2.02788400	-2.55165100
O	-9.71184300	2.31103100	-0.61444500
C	-10.97558900	2.56015600	-1.23539900
C	-5.85125700	-0.45103000	0.31066400
C	-5.24238300	-1.63463700	0.09401100
O	-5.78616000	-2.63576800	-0.67371100
C	-6.98994700	-2.50195000	-1.30398300
O	-7.37109900	-3.46172500	-1.96702900
C	-5.14285100	0.62080600	1.15144800
C	-4.00047100	0.00877700	1.97906300
C	-3.10023200	-0.91404900	1.16620300
C	-3.92596800	-2.09009300	0.65015200
O	-6.05554400	1.25639400	2.06189800
C	-4.62276600	1.74670200	0.25279400

Figure A201 Optimized cartesian coordinates of conformers of **C28** at B3LYP/6-311G(d) level

O	-1.99658700	-1.39471300	1.91758200
O	-4.13648200	-2.96333100	1.77470400
H	-10.58545700	0.21670200	-2.14064300
H	-7.52302500	1.75590000	0.46298300
H	-8.88080300	-2.80213800	-2.55543900
H	-10.89015200	2.52796800	-2.32408000
H	-11.72543800	1.83963700	-0.90027200
H	-11.26296600	3.55991800	-0.92083500
H	-3.41116400	0.81433000	2.42042500
H	-4.43426900	-0.57130700	2.80008400
H	-2.67856100	-0.37974100	0.31254200
H	-3.37466000	-2.62576000	-0.12757400
H	-6.43996200	0.57748600	2.63085100
H	-5.42449700	2.17954900	-0.34444500
H	-4.19040400	2.53327500	0.87435100
H	-3.85565600	1.37949600	-0.42972900
H	-2.34044300	-2.13181000	2.44398700
H	-4.24082900	-3.86575800	1.45487100
		4-2	
C	-9.67896300	-0.16120400	-1.46386600
C	-9.18178900	0.79012900	-0.56533000
C	-7.88421900	0.69503000	-0.05254400
C	-7.06240100	-0.36703500	-0.43594400
C	-7.57793000	-1.36852500	-1.29844100
C	-8.89493000	-1.24205800	-1.82470400
O	-9.41395300	-2.15770900	-2.66217100
O	-10.04110400	1.78015600	-0.24418600
C	-9.61134500	2.80088600	0.66069000
C	-5.69327100	-0.53224000	0.04461000
C	-5.09021500	-1.72456400	-0.14784300

Figure A201 (continued)

O	-5.63240500	-2.70963200	-0.92519500
C	-6.81658700	-2.55166000	-1.58881100
O	-7.14723100	-3.45802600	-2.34622200
C	-4.93492600	0.59043700	0.74491100
C	-3.47062900	0.20306400	1.03243300
C	-3.33476200	-1.21093200	1.55823800
C	-3.79940100	-2.20050100	0.48205400
O	-5.62523800	0.78874400	2.01216800
C	-4.92195200	1.88492000	-0.07708100
O	-4.09350900	-1.43255700	2.75317400
O	-3.97495200	-3.48493800	1.05658300
H	-10.68332800	-0.06294800	-1.85569300
H	-7.52963000	1.39989900	0.67844700
H	-8.74087800	-2.85836400	-2.80159200
H	-10.45604700	3.47789400	0.75702600
H	-9.36497400	2.38110500	1.63863400
H	-8.75078400	3.34215100	0.26077100
H	-2.88010200	0.29514400	0.11644800
H	-3.06095400	0.92090400	1.74779300
H	-2.29700800	-1.44017900	1.80769700
H	-3.03359800	-2.30218200	-0.29267300
H	-5.27987000	1.58860200	2.43101200
H	-4.32266700	2.63891700	0.44100600
H	-4.46326700	1.70506500	-1.05090900
H	-5.91549200	2.29201200	-0.24112200
H	-4.83160200	-0.79947400	2.76387500
H	-4.35075600	-3.31283800	1.93550400
	C28-3		
C	-9.63762900	0.13209800	-1.62281300
C	-9.09745600	1.11496200	-0.79303900
C	-7.86698300	0.92648300	-0.14638100

Figure A201 (continued)

C	-7.15134300	-0.25033000	-0.32517700
C	-7.69431500	-1.26673600	-1.16587200
C	-8.94233800	-1.05851300	-1.80725200
O	-9.49727100	-1.98471700	-2.60599400
O	-9.69856300	2.29669400	-0.54352500
C	-10.96207000	2.57031700	-1.15509000
C	-5.85249100	-0.51204500	0.29846900
C	-5.25507600	-1.69812100	0.05394500
O	-5.80623500	-2.67360600	-0.74018100
C	-7.00455100	-2.50990800	-1.37256200
O	-7.39001400	-3.44526300	-2.06669200
C	-5.12846800	0.54619100	1.14519400
C	-3.97721300	-0.07541100	1.95306800
C	-3.10009000	-1.00512700	1.12445000
C	-3.94367600	-2.16995700	0.60195700
O	-6.02496300	1.18117800	2.07050500
C	-4.61124300	1.67476900	0.24739000
O	-1.99834500	-1.50954600	1.86359400
O	-4.13460600	-3.14614500	1.64389500
H	-10.58447400	0.25238400	-2.12930500
H	-7.51125300	1.69971300	0.51380500
H	-8.89648600	-2.76158500	-2.63390900
H	-10.87809300	2.56948200	-2.24432200
H	-11.71490200	1.84399600	-0.83987100
H	-11.24377800	3.56187000	-0.81094000
H	-3.37452300	0.72481800	2.38541500
H	-4.40059100	-0.63953600	2.79252700
H	-2.67676600	-0.46643800	0.27385000
H	-3.39881900	-2.70571800	-0.17664200
H	-6.40675600	0.50327600	2.64231200

Figure A201 (continued)

H	-3.85503900	1.30708400	-0.44679700
H	-5.41743100	2.11717100	-0.33640300
H	-4.16622200	2.45331800	0.86986800
H	-2.33824100	-2.26809400	2.36163600
H	-4.85255900	-2.85704500	2.22163700

Figure A201 (continued)

Table A7 The energy and boltzmann distributions for the optimized geometries of **C29**

Optimized geometry	Energy(a.u.)	DE (kcal/mol)	Boltzmann distribution
C29-1	-1567.540018	0.00	65.88%
C29-2	-1567.538816	0.75	18.45%
C29-3	-1567.538662	0.85	15.67%

C29-1

C	-8.73093700	1.16577100	-2.60822800
C	-7.96068100	2.08694400	-1.89719600
C	-6.89724600	1.67141600	-1.08213000
C	-6.58463300	0.32383100	-0.96999700
C	-7.36566200	-0.63113200	-1.68702400
C	-8.43988100	-0.19020500	-2.50228400
C	-5.48119900	-0.18662900	-0.15836000
C	-5.26456500	-1.51533400	-0.13465000
O	-6.03654700	-2.42107800	-0.81497300
C	-7.09105500	-2.03778200	-1.59927300
C	-4.51088700	0.73606100	0.56881200
C	-3.72306300	-0.04029000	1.65130000
C	-3.11517300	-1.30522200	1.06677500
C	-4.22998200	-2.26212600	0.66966200

Figure A202 Optimized cartesian coordinates of conformers of **C29** at B3LYP/6-311G(d) level

O	-9.20733400	-1.04692100	-3.19542500
O	-7.70713600	-2.93579800	-2.16198000
O	-8.17033700	3.41878800	-1.92799800
C	-9.23990500	3.93091700	-2.72780400
O	-5.26022800	1.73178500	1.27433900
C	-3.56977300	1.41179500	-0.44308200
O	-2.77149000	0.87341300	2.16908100
O	-4.83239000	-2.79501900	1.84601400
Cl	-1.97849700	-2.09701000	2.25112600
H	-9.55646300	1.46076400	-3.23992100
H	-6.35506600	2.41702000	-0.52453800
H	-4.43950000	-0.32435900	2.42683800
H	-2.49316100	-1.08181600	0.20384500
H	-3.82487600	-3.06993400	0.05280900
H	-8.88424600	-1.95727800	-3.01877700
H	-10.20271200	3.54095700	-2.38957000
H	-9.21413400	5.00890800	-2.59298100
H	-9.09072400	3.68890300	-3.78267400
H	-4.61888800	2.19997100	1.82724900
H	-4.15102800	2.00260300	-1.14937100
H	-2.87426400	2.06985100	0.07701200
H	-2.99315600	0.68087900	-1.01281800
H	-2.47303100	0.55580600	3.02870800
H	-5.43415000	-3.50025200	1.57998400
	C29-2		
C	-8.65866300	1.27118300	-2.58528900
C	-7.83963400	2.15831700	-1.88621200
C	-6.78632300	1.69649000	-1.08203000
C	-6.53543300	0.33582600	-0.96959400
C	-7.36841300	-0.58390400	-1.67181600
C	-8.42859400	-0.09673800	-2.47856700

Figure A202 (continued)

C	-5.45056400	-0.22443000	-0.16397600
C	-5.30720000	-1.56356800	-0.12401100
O	-6.12541400	-2.43266600	-0.79224400
C	-7.15809500	-2.00200500	-1.57850900
C	-4.42303400	0.65519000	0.54417700
C	-3.64766800	-0.14703300	1.62940600
C	-3.11332700	-1.43068300	1.04023000
C	-4.28868500	-2.33850100	0.66422600
O	-9.24117300	-0.91908200	-3.16079900
O	-7.81765300	-2.87080800	-2.13785100
O	-7.98803600	3.49782900	-1.91907600
C	-9.04239800	4.05649800	-2.70829400
O	-5.02290100	1.75683300	1.24765400
C	-3.47683800	1.29252900	-0.47572600
O	-2.60580100	0.63566200	2.16726700
O	-4.97698500	-2.84836700	1.80033300
Cl	-2.02840600	-2.31858500	2.21087500
H	-9.47651800	1.60184300	-3.20923500
H	-6.20057200	2.42075100	-0.53983000
H	-4.36947600	-0.41279300	2.41178700
H	-2.48096500	-1.24550300	0.17528100
H	-3.92488000	-3.16100100	0.04116300
H	-8.95715800	-1.84276500	-2.98509800
H	-10.01788600	3.71174100	-2.35764900
H	-8.96562000	5.13245500	-2.57701300
H	-8.91644600	3.80508100	-3.76393500
H	-5.73846500	1.42239400	1.80448900
H	-2.74441400	1.91499600	0.03551400
H	-2.94749100	0.53168300	-1.04968200
H	-4.03765600	1.91051300	-1.17485400
H	-3.01143700	1.46442600	2.45637500

Figure A202 (continued)

H	-4.44007800	-3.55160700	2.18651400
	C29-3		
C	-8.65999400	1.22677800	-2.54928500
C	-7.84034800	2.12962600	-1.87110500
C	-6.77109200	1.68724000	-1.07709600
C	-6.50361900	0.33065800	-0.95455800
C	-7.33547800	-0.60542400	-1.63789500
C	-8.41341900	-0.13734600	-2.43281200
C	-5.40201800	-0.20911500	-0.15932300
C	-5.23161000	-1.54438800	-0.12151200
O	-6.04776500	-2.43079300	-0.77274400
C	-7.10748000	-2.01987400	-1.53782900
C	-4.38531800	0.68239500	0.54840400
C	-3.61080100	-0.11097000	1.64223500
C	-3.05582300	-1.39442500	1.06156500
C	-4.20825400	-2.31329200	0.67530400
O	-9.22691200	-0.97471800	-3.09552400
O	-7.76727800	-2.90241000	-2.07363000
O	-8.00346700	3.46694200	-1.91558000
C	-9.07390300	4.00661800	-2.69641900
O	-4.99782700	1.78174000	1.24488100
C	-3.44046400	1.32503700	-0.46892800
O	-2.57821000	0.68338500	2.18052100
O	-4.82013200	-2.82463900	1.85645700
Cl	-1.93555100	-2.24521200	2.21722100
H	-9.49036800	1.54241700	-3.16438100
H	-6.18568000	2.42308400	-0.55025600
H	-4.33526100	-0.37544300	2.42259700
H	-2.43871000	-1.19380700	0.18923100
H	-3.83117700	-3.13475400	0.05898300
H	-8.93173500	-1.89378300	-2.91568300

Figure A202 (continued)

H	-10.04108700	3.65607400	-2.32895200
H	-9.00610600	5.08461900	-2.57761200
H	-8.95953600	3.74506600	-3.75089800
H	-5.71447800	1.44368900	1.79813000
H	-2.71827900	1.95994100	0.04173500
H	-2.89899500	0.56761500	-1.03599000
H	-4.00569000	1.93176800	-1.17460200
H	-2.99182100	1.51270900	2.45658100
H	-5.42271200	-3.53210700	1.59846700

Figure A202 (continued)

Table A8 The energy and boltzmann distributions for the optimized geometries of **C30**

Optimized geometry	Energy(a.u.)	DE (kcal/mol)	Boltzmann distribution
C30-1	-1567.540625	0.00	39.68%
C30-2	-1567.540312	0.20	28.48%
C30-3	-1567.540134	0.31	23.59%
C30-4	-1567.539143	0.93	8.26%

C30-1			
C	-9.47989800	0.38928600	2.37134500
C	-8.63742500	1.19734900	1.60847800
C	-7.28005600	0.88228500	1.44110300
C	-6.74293200	-0.25313200	2.03354200
C	-7.59444100	-1.09116500	2.81385700
C	-8.96228900	-0.75187500	2.97533800
C	-5.34236300	-0.65939100	1.89779500
C	-4.94980100	-1.80964700	2.48466000
O	-5.78518200	-2.59927800	3.23160300
C	-7.09793500	-2.28533300	3.43786900

Figure A203 Optimized cartesian coordinates of conformers of **C30** at B3LYP/6-311G(d) level

C	-4.35050300	0.12701200	1.02779700
C	-2.89386000	-0.24901400	1.36918200
C	-2.66529700	-1.75376400	1.41693600
C	-3.59081900	-2.44385900	2.43394700
O	-9.80290400	-1.50451800	3.70269900
O	-7.74260800	-3.06151100	4.13469000
O	-9.04172100	2.32410000	0.98775800
C	-10.40706500	2.73086800	1.11755500
O	-4.50393300	1.53622800	1.15227300
C	-4.60678700	-0.16383600	-0.45821200
Cl	-2.41601600	0.51028900	2.98681100
O	-2.97928200	-2.51263100	3.72755300
O	-1.32248400	-2.10133200	1.65664700
H	-10.52699200	0.61193700	2.51809900
H	-6.66756900	1.55829300	0.86860200
H	-2.22002500	0.22506600	0.66084900
H	-2.91437200	-2.12809100	0.42085900
H	-3.71006700	-3.48838400	2.14105300
H	-9.29748400	-2.26687900	4.06103600
H	-10.65991200	2.92169800	2.16306600
H	-10.49227500	3.65147400	0.54653300
H	-11.08101900	1.97759100	0.70320000
H	-4.36159100	1.78655700	2.07483200
H	-5.61143500	0.16349100	-0.72271500
H	-3.89160600	0.38719400	-1.07117600
H	-4.52908600	-1.22611500	-0.68451400
H	-3.02997300	-1.64190300	4.14467400
H	-1.24475200	-2.25066400	2.61163200

Figure A203 (continued)

C30-2

C	-9.34138500	0.44933600	2.48964500
C	-8.39683000	1.30490600	1.92029600
C	-7.07300900	0.89025600	1.71009300
C	-6.67362300	-0.38963700	2.06806400
C	-7.61102500	-1.25232200	2.70482400
C	-8.94997600	-0.82317200	2.89204700
C	-5.31685000	-0.90390400	1.87913400
C	-4.96879100	-2.03590800	2.52459200
O	-5.86648400	-2.81509900	3.19659200
C	-7.20271800	-2.52151900	3.23806700
C	-4.31452900	-0.18886300	0.97333400
C	-3.01913800	-1.03807500	0.84741400
C	-2.53462400	-1.57529100	2.17470800
C	-3.57279900	-2.59604300	2.67234600
O	-9.87386600	-1.60752300	3.46993700
O	-7.92993000	-3.35338200	3.76806300
O	-8.66698100	2.56855400	1.53531200
C	-9.98853000	3.08152300	1.72830000
O	-4.01877300	1.05716900	1.63548800
C	-4.88526200	0.03076300	-0.43394100
Cl	-1.69799600	-0.05453000	0.04770600
O	-3.30000300	-2.91620800	4.02243300
O	-2.34241900	-0.57150600	3.16377800
H	-10.36857700	0.74193200	2.65334400
H	-6.37649500	1.60803200	1.30826200
H	-3.19213500	-1.86822000	0.16561400
H	-1.58067400	-2.09001100	2.05756800
H	-3.48873600	-3.52688200	2.10494000
H	-9.44530900	-2.45750100	3.71085400
H	-9.96176200	4.10219800	1.35633500

Figure A203 (continued)

H	-10.71973800	2.50238400	1.15986400
H	-10.25649000	3.08247000	2.78729100
H	-3.48639700	1.60854000	1.04529500
H	-4.14939600	0.53395000	-1.06268200
H	-5.12186800	-0.93108100	-0.89248900
H	-5.78974900	0.62950600	-0.41995800
H	-3.05011700	-2.07669800	4.44113900
H	-2.91616800	0.18700000	2.95945100
	C30-3		
C	-9.48276800	0.41014700	2.37800900
C	-8.66003300	1.19996900	1.57490400
C	-7.30285800	0.89213700	1.39583700
C	-6.74484200	-0.21775100	2.01738500
C	-7.57648200	-1.03834500	2.83726000
C	-8.94481300	-0.70600500	3.00978900
C	-5.34301700	-0.61443400	1.87472000
C	-4.93329600	-1.74599800	2.48165900
O	-5.75066100	-2.52327400	3.26120200
C	-7.06024700	-2.21027800	3.48702300
C	-4.35961600	0.15827700	0.98476100
C	-2.90003200	-0.17542600	1.35968800
C	-2.63144500	-1.67336900	1.44207100
C	-3.57426700	-2.38021400	2.42971600
O	-9.76681000	-1.44294300	3.77434600
O	-7.68591300	-2.96945100	4.21970200
O	-9.08584700	2.30190800	0.92397400
C	-10.45195100	2.70108500	1.06460300
O	-4.54016900	1.56853200	1.05818800
C	-4.59683700	-0.18830400	-0.49176400
Cl	-2.46157700	0.63441100	2.95350700
O	-2.96557200	-2.36144000	3.72744400

Figure A203 (continued)

O	-1.29005000	-1.97830000	1.73542800
H	-10.52938600	0.62833800	2.53449000
H	-6.70519300	1.55340500	0.79130500
H	-2.23092900	0.29029700	0.64073400
H	-2.82992200	-2.06946500	0.44336100
H	-3.69560200	-3.41853000	2.10887100
H	-9.24788100	-2.18865700	4.14830200
H	-11.12663500	1.92896300	0.68761200
H	-10.68842700	2.92438200	2.10758900
H	-10.55578200	3.60157700	0.46519000
H	-4.39082300	1.85252200	1.97003800
H	-5.60371600	0.11555300	-0.77652000
H	-3.88376900	0.35007400	-1.11849800
H	-4.50327000	-1.25704100	-0.67933100
H	-3.11472200	-3.21359800	4.15000200
H	-1.23798800	-2.03817400	2.70225100
		38	
		C30-4	
C	-9.56761300	0.30175200	2.50079600
C	-8.77724800	1.12060800	1.68844200
C	-7.41987300	0.84991700	1.48441400
C	-6.83160400	-0.26138000	2.09252200
C	-7.62778700	-1.10299300	2.91695600
C	-9.00561900	-0.80211600	3.11678800
C	-5.42535700	-0.62418500	1.91566900
C	-4.97742200	-1.75177100	2.50436100
O	-5.76111900	-2.54945300	3.29445200
C	-7.07310400	-2.26769200	3.54860900
C	-4.47904800	0.17313100	1.00659100
C	-3.00459000	-0.13237500	1.34450200
C	-2.70295000	-1.62488200	1.41102500

Figure A203 (continued)

C	-3.60687900	-2.35713300	2.41642500
O	-9.79472400	-1.56626300	3.89200700
O	-7.66649400	-3.04557500	4.28799500
O	-9.41587200	2.17199100	1.13473900
C	-8.67743300	3.06352500	0.29410100
O	-4.68463600	1.58011700	1.09150200
C	-4.74504400	-0.17090900	-0.46559900
Cl	-2.54545700	0.67740500	2.93237600
O	-2.96834400	-2.33297700	3.69942600
O	-1.34894400	-1.90281200	1.67044500
H	-10.61488600	0.53200000	2.64952800
H	-6.81271100	1.50668700	0.88847300
H	-2.36281600	0.35113500	0.61249000
H	-2.91697200	-2.01919200	0.41479700
H	-3.71444600	-3.39579100	2.09202000
H	-9.25070000	-2.30077400	4.25030700
H	-9.39252100	3.81424200	-0.03174000
H	-7.86719300	3.54351400	0.84758500
H	-8.27311700	2.53867500	-0.57444900
H	-4.51233500	1.86421800	1.99940500
H	-5.76545300	0.11038300	-0.72431000
H	-4.06026100	0.38696500	-1.10657500
H	-4.63163900	-1.23620300	-0.66138400
H	-3.08615300	-3.19174400	4.11849800
H	-1.27219600	-1.96665600	2.63536900

Figure A203 (continued)

Table A9 The energy and boltzmann distributions for the optimized geometries of **C31**

Optimized geometry	Energy(a.u.)	DE (kcal/mol)	Boltzmann distribution
C31-1	-1567.535532	0.00	63.95%
C31-2	-1567.534973	0.35	35.38%
C31-3	-1567.531210	2.71	0.66%
C31-4	-1567.527541	5.01	0.01%

	C31-1		
C	-6.19944500	-0.47442200	-3.83291700
C	-5.70945300	-0.18632400	-2.57257100
C	-5.34495800	-1.22479800	-1.69238200
C	-5.50992000	-2.55567900	-2.13351600
C	-6.01123900	-2.84009900	-3.41298200
C	-4.80190600	-0.99089700	-0.35965700
C	-4.49980600	-2.07176800	0.39488300
O	-4.67599100	-3.36104700	-0.02937700
C	-5.16876900	-3.68196100	-1.27648600
C	-4.44757100	0.42138600	0.13185500
C	-4.24623900	0.45503100	1.66415300
C	-3.38366800	-0.69117200	2.17690800
C	-3.95503400	-2.05562000	1.77334500
O	-5.27358100	-4.85595300	-1.54603800
O	-6.58140100	0.43649700	-4.75879000
C	-6.47108000	1.82769700	-4.44121100
O	-5.47783500	1.36332800	-0.16171700
C	-3.18576500	0.90958500	-0.58628900
O	-5.50737800	0.51971600	2.34240800
Cl	-5.31946600	-2.59155100	2.94852500
O	-3.12147100	-0.58584800	3.55692600

Figure A204 Optimized cartesian coordinates of conformers of **C31** at B3LYP/6-311G(d) level

O	-6.83507900	-2.07474900	-5.50428900
H	-5.63730100	0.83442600	-2.23814100
H	-6.12844700	-3.86872200	-3.72833300
H	-3.75835400	1.39662600	1.91702000
H	-2.40860000	-0.63010600	1.68706800
H	-3.21972400	-2.84265100	1.91316700
H	-6.82040100	2.35870600	-5.32213500
H	-7.09872900	2.07709800	-3.58316900
H	-5.43223500	2.09288400	-4.23377200
H	-6.10714600	1.31805600	0.57467800
H	-3.35373000	0.95398800	-1.66209500
H	-2.92929100	1.91150200	-0.23756600
H	-2.34049600	0.24352700	-0.41019100
H	-5.95059600	-0.34006000	2.31228700
H	-3.96050400	-0.41123100	4.00443100
H	-7.01844400	-1.23062700	-5.94274300
		7-2	
C	-6.31568200	-1.76189300	-4.21161400
C	-6.26997400	-0.45228400	-3.66776500
C	-5.75083700	-0.22599900	-2.40597500
C	-5.25444600	-1.29665400	-1.63738500
C	-5.35559800	-2.59897300	-2.16685400
C	-5.87057100	-2.82072800	-3.45476200
C	-4.69940100	-1.12325600	-0.30112600
C	-4.50758800	-2.23418800	0.44302900
O	-4.64186900	-3.49576500	-0.05507700
C	-4.97749800	-3.75642600	-1.37179700
C	-4.29237700	0.25002100	0.22406100
C	-3.60754600	0.15359900	1.61970500
C	-4.32317900	-0.85181700	2.51361400
C	-4.12698900	-2.23285100	1.89017900

Figure A204 (continued)

O	-4.96567000	-4.91225400	-1.72532700
O	-6.78157400	0.49061700	-4.49339000
C	-6.79646600	1.85365300	-4.05734500
O	-5.43926500	1.11330700	0.35372100
C	-3.30766200	0.95057400	-0.71558300
O	-3.54837600	1.43305700	2.21503100
Cl	-5.13918000	-3.45687800	2.82294700
O	-5.69084300	-0.46282600	2.57211000
O	-6.81816000	-1.95866500	-5.45487500
H	-5.77109100	0.76393000	-1.98038400
H	-5.93076500	-3.82840700	-3.84529500
H	-2.57592400	-0.18227500	1.49158400
H	-3.87938900	-0.83679300	3.51237300
H	-3.10461900	-2.57856000	2.04039900
H	-7.23670300	2.41854100	-4.87412500
H	-7.40690700	1.96356400	-3.15858600
H	-5.78096300	2.20662000	-3.86562500
H	-6.05910700	0.65204700	0.94164800
H	-2.94767700	1.85856300	-0.23115000
H	-2.45452900	0.29973400	-0.91377400
H	-3.75928900	1.22081900	-1.66604400
H	-4.37770000	1.87574200	1.97748600
H	-6.16840400	-1.05016200	3.17019200
H	-7.09019000	-1.10068100	-5.81264300
		C31-3	
C	-6.31409800	-1.83759600	-4.19268600
C	-6.33560800	-0.53418500	-3.63310900
C	-5.81265400	-0.29336000	-2.37550900
C	-5.24313800	-1.34140300	-1.62746500
C	-5.27642200	-2.64072600	-2.17242600
C	-5.79763000	-2.87738100	-3.45508800

Figure A204 (continued)

C	-4.67592500	-1.15436100	-0.29708100
C	-4.40841300	-2.26025300	0.43052400
O	-4.47815400	-3.51905700	-0.08294800
C	-4.81963400	-3.78349800	-1.39839500
C	-4.34925300	0.22836000	0.24485200
C	-3.63068100	0.17194900	1.62858600
C	-4.22027400	-0.90095600	2.53220800
C	-3.98654100	-2.25867100	1.86715100
O	-4.74637400	-4.93223600	-1.76573100
O	-6.91202600	0.38753200	-4.43944400
C	-6.99474100	1.74315500	-3.98815900
O	-5.61663600	0.89998200	0.41985800
C	-3.43292400	1.02086000	-0.69727600
O	-3.72612700	1.44775200	2.25118500
Cl	-4.87158100	-3.55991900	2.80334900
O	-5.57642300	-0.60023900	2.82205200
O	-6.82261000	-2.04865200	-5.43087600
H	-5.88674700	0.68849400	-1.93835100
H	-5.80580700	-3.88248300	-3.85654300
H	-2.56980800	-0.02941900	1.46649500
H	-3.70223400	-0.89799700	3.49244300
H	-2.93666700	-2.53784700	1.96225200
H	-5.99725900	2.14839900	-3.80542600
H	-7.47530500	2.29189200	-4.79309100
H	-7.59854600	1.81063900	-3.08080900
H	-5.41909600	1.78460500	0.76017300
H	-3.16170400	1.96381000	-0.21765400
H	-2.51567300	0.46025300	-0.88813600
H	-3.90138300	1.24222000	-1.65207000
H	-4.46997200	1.41066200	2.86916500
H	-6.00863300	-0.28745800	2.00992800

Figure A204 (continued)

H	-7.14913700	-1.20391300	-5.77425900
	C31-4		
C	-6.05185000	-1.52721400	-4.41757100
C	-5.87691300	-0.21414900	-3.91777300
C	-5.46771100	-0.01508800	-2.61118700
C	-5.21162400	-1.09208200	-1.74418600
C	-5.41633100	-2.39335300	-2.25139700
C	-5.83110600	-2.59944400	-3.57195800
C	-4.75771300	-0.93947800	-0.36729200
C	-4.56488900	-2.06294900	0.35896800
O	-4.77377900	-3.32521300	-0.13223400
C	-5.19392900	-3.57116000	-1.41984400
C	-4.37896800	0.43402200	0.20681900
C	-4.27976400	0.39753300	1.74971000
C	-3.51246400	-0.81190200	2.26916800
C	-4.12096400	-2.12870600	1.77139600
O	-5.34026800	-4.72468100	-1.74872700
O	-6.05165400	0.87856200	-4.71451600
C	-7.38907500	1.10400100	-5.19918000
O	-5.34813100	1.42850700	-0.11600500
C	-3.05098300	0.89348700	-0.40330600
O	-5.57857000	0.50240300	2.34713800
Cl	-5.59047900	-2.63640200	2.82450000
O	-3.34040000	-0.77510100	3.66658000
O	-6.41544700	-1.65877900	-5.71783400
H	-5.37377600	1.00172700	-2.26552500
H	-5.96190000	-3.61652600	-3.92431100
H	-3.76286100	1.30123400	2.07330700
H	-2.50479700	-0.78304400	1.84731300
H	-3.43679300	-2.95744200	1.92912500
H	-7.34855200	2.03919900	-5.75340400

Figure A204 (continued)

H	-7.71205400	0.29587700	-5.85404400
H	-8.08022700	1.20490800	-4.35828700
H	-6.02145000	1.38885500	0.58082100
H	-3.13783900	0.97680500	-1.48626800
H	-2.78532200	1.87388500	-0.00413200
H	-2.24472700	0.19109400	-0.18832900
H	-6.05907600	-0.33281600	2.25752000
H	-4.19739500	-0.56989800	4.06427900
H	-6.50995500	-2.59192300	-5.94692000

Figure A204 (continued)

APPENDIX B

ABSTRACT OF PUBLICATIONS

Chiang Mai J. Sci. 2023; 50(2): 1-12
https://doi.org/10.12982/CMJS.2023.010
Journal homepage : http://epg.science.cmu.ac.th/ejournal/

Research Article

A New Record of *Neohelicosporium guangxiense* and Its Secondary Metabolites

Lijuan Zhang [a,b,c], Jian Ma [b,c], Xiaoyan Ma [a], Xin Feng [a], Xuesong Bai [a], Yongtao Huang [a], Ruvishika S. Jayawardena [b,c], Ausana Mapook [c], Jichuan Kang [d] and Yongzhong Lu*[a,d]

[a] School of Food and Pharmaceutical Engineering, Guizhou Institute of Technology, Guiyang 550003, Guizhou, China
[b] School of Science, Mae Fah Luang University, Chiang Rai 57100, Thailand
[c] Center of Excellence in Fungal Research, Mae Fah Luang University, Chiang Rai 57100, Thailand
[d] Engineering and Research Center for Southwest Bio-Pharmaceutical Resources of National Education Ministry of China, Guizhou University, Guiyang 550025, Guizhou, China

*Author for correspondence; e-mail: yzlu@git.edu.cn

Received: 21 September 2022
Revised: 28 December 2022
Accepted: 31 December 2022

ABSTRACT

In a diversity study of helicosporous hyphomycetes, a new record *viz. Neohelicosporium guangxiense* was collected, isolated and identified based on multi-gene phylogenetic analyses and morphological evidence. In this study, secondary metabolites of *N. guangxiense* were also investigated, from which four compounds were isolated and identified, including three *a*-tetralon derivatives (**1-3**) and one isocoumarin derivative (**4**). This is the first time that these compounds were isolated from the fungal genus *Neohelicosporium*, and compound **1** was firstly isolated from natural resources. Their structures were assigned based on the extensive 1D/2D NMR spectroscopic analyses, ESI-MS, and HR-ESI-MS measurements, especially the 2D NMR spectra of compound **1** were described in detail, and the absolute configuration of compound **1** was also elucidated for the first time. Furthermore, the bioactivities of all compounds were inactive in our bioassays.

Keywords: Helicosporous hyphomycetes, saprophytic fungi, new record, secondary metabolites

1. INTRODUCTION

Helicosporous hyphomycetes as asexual fungi with their specific conidia coiled at least 180 in a two-dimensional plane or three-dimensional space are widely distributed in terrestrial and aquatic environments, especially in tropical and subtropical regions [1-4]. Researches on helicosporous hyphomycetes have been mainly focused on morphological and phylogenetic studies [1-8]. Until now only a few species were studied for their secondary metabolites with several novel structures, which had various biological activities including anti-tumor, anti-bacterial, anti-diabetes, etc [9-14]. All the above studies indicated that the metabolites of helicosporous hyphomycetes were abundant and had a potentially wide range of biological activities. These studies prompted us to study this kind of fungi to further discover novel active metabolites.

In this study, *Neohelicosporium guangxiense* as a new record from Guizhou province, China was collected, isolated, and identified based on multi-gene phylogenetic analyses and morphological

metabolites

MDPI

Article

Neogrisphenol A, a Potential Ovarian Cancer Inhibitor from a New Record Fungus *Neohelicosporium griseum*

Li-Juan Zhang [1,2,3,†], Ming-Fei Yang [4,5,6,†], Jian Ma [2,3], Xing-Juan Xiao [1], Xiao-Yan Ma [1], De-Ge Zheng [1], Mei-Yan Han [1], Ming-Lei Xia [1], Ruvishika S. Jayawardena [2,3], Ausana Mapook [2], Yuan-Pin Xiao [1], Ji-Chuan Kang [4,*] and Yong-Zhong Lu [1,4,*]

1 School of Food and Pharmaceutical Engineering, Guizhou Institute of Technology, Guiyang 550003, China; 6471105010@lamduan.mfu.ac.th (L.-J.Z.); xiaoxingjuanbenjuan@gmail.com (X.-J.X.); 20120065@git.edu.cn (X.-Y.M.); degezheng@gmail.com (D.-G.Z.); meiyanhan04@gmail.com (M.-Y.H.); xml0312xml@gmail.com (M.-L.X.); emaypx@gmail.com (Y.-P.X.)
2 Center of Excellence in Fungal Research, Mae Fah Luang University, Chiang Rai 57100, Thailand; 6371105007mj@gmail.com (J.M.); ruvishika.jay@mfu.ac.th (R.S.J.); phung.ausana@gmail.com (A.M.)
3 School of Science, Mae Fah Luang University, Chiang Rai 57100, Thailand
4 Engineering and Research Center for Southwest Bio-Pharmaceutical Resources of National Education Ministry of China, Guizhou University, Guiyang 550025, China; mf_yang@126.com
5 College of Life Sciences, Guizhou University, Guiyang 550025, China
6 Department of Health Management, Guiyang Healthcare Vocational University, Guiyang 550081, China
* Correspondence: jckang@gzu.edu.cn (J.-C.K.); yzlu@git.edu.cn (Y.-Z.L.); Tel.: +86-058188210723 (Y.-Z.L.)
† These authors equally contributed to this work.

Abstract: From the rice fermentation product of a new record fungus, *Neohelicosporium griseum*, two new polyketides, neogrisphenol A (**1**) and neogrisphenol B (**2**), one new isochroman-1-one, (*S*)-6-hydroxy-7-methoxy-3,5-dimethylisochroman-1-one (**3**), and four known compounds (**4**–**7**) were isolated. Their structures were determined using 1D- and 2D-NMR, mass spectrometry, and chemical calculations. The C-3–C-2′ polymerization mode between the two α-naphthalenone derivative moieties is uncommon in compounds **1** and **2**. Meanwhile, compounds **1**–**2** and **5** exhibited antibacterial activity against *Bacillus subtilis*, *Clostridium perfringens*, *Staphylococcus aureus*, and *Staphylococcus aureus*, with MIC values ranging between 16 and 31 μg/mL. In addition, compound **5** showed antifungal activity against *Sclerotinia sclerotiorum* and *Phytophthora nicotianae var. nicotianae*, with respective IC_{50} values of 88.14 ± 2.21 μg/mL and 52.36 ± 1.38 μg/mL. Compound **1** showed significant cytotoxicity against A2780, PC-3, and MBA-MD-231 cell lines with respective IC_{50} values of 3.20, 10.68, and 16.30 μM, and the cytotoxicity against A2780 cells was even higher than that of cisplatin (CDDP). With an IC_{50} value of 10.13 μM, compound **2** also exhibited cytotoxicity against A2780. The in vitro results showed that compound **1** inhibited A2780 cell proliferation, induced apoptosis, and arrested the cell cycle at the S-phase in a concentration-dependent manner.

Keywords: saprophytic fungi; helicosporous hyphomycetes; polyketide derivatives; antimicrobials; cytotoxicity

Citation: Zhang, L.-J.; Yang, M.-F.; Ma, J.; Xiao, X.-J.; Ma, X.-Y.; Zheng, D.-G.; Han, M.-Y.; Xia, M.-L.; Jayawardena, R.S.; Mapook, A.; et al. Neogrisphenol A, a Potential Ovarian Cancer Inhibitor from a New Record Fungus *Neohelicosporium griseum*. *Metabolites* **2023**, *13*, 435. https://doi.org/10.3390/metabo13030435

Academic Editor: Silvia Ravera

Received: 18 February 2023
Revised: 3 March 2023
Accepted: 13 March 2023
Published: 16 March 2023

1. Introduction

Secondary metabolites of fungi have enormous potential, particularly for drug discovery [1]. More than half of the compounds isolated from fungi were antibacterial, antifungal, or antitumor [1]. Research on secondary metabolites of fungi concentrated primarily on endophytic fungi of medicinal plants, whereas research on secondary metabolites of saprophytic fungi was relatively uncommon [2].

Helicosporous hyphomycetes, such as the species of *Helicosporium*, *Helicoma*, *Helicomyces*, and *Tubeufia*, are capable of producing a variety of bioactive compounds [3–9]. The vast majority of helicosporous hyphomycetes are members of the family *Tubeufiaceae*

Medicinal Chemistry Research
https://doi.org/10.1007/s00044-023-03172-1

MEDICINAL CHEMISTRY RESEARCH

ORIGINAL RESEARCH ARTICLE

Polyketides from *Neohelicosporium griseum*: structure assignment and bioactivity investigation

Lijuan Zhang[1,2,3] · Jian Ma[1,2,3] · Mingfei Yang[4] · Tianming Zhao[3] · Mei Yan Han[3] · Dege Zheng[3] · Ausana Mapook[2] · Yongzhong Lu[3] · Ruvishika S. Jayawardena[1,2,5]

Received: 12 September 2023 / Accepted: 8 November 2023

Abstract

In the pursuit of discovering new active metabolites from helicosporous hyphomycetes, rice fermentation products of *Neohelicosporium griseum* were examined. Eight compounds were isolated from this saprophytic fungus, namely vertixanthone (**1**), diaportheone A (**2**), 1,3,6,8-tetrahydroxyanthraquinone (**3**), lecanoric acid (**4**), decarboxycitrinone (**5**), 6,8-dihydroxy-4-hydroxymethyl-3,5-dimethyl-isochromen-1-one (**6**), decarboxyhydroxycitrinone (**7**), and ergosterin (**8**). The 1D and 2D NMR characteristics of compound **1** in DMSO-d_6 were detailed for the first time. Antimicrobial testing indicated that compounds **1**–**4** exhibited moderate activity against *Pseudomonas aeruginosa*, with compound **3** also showing weak activity against *Staphylococcus aureus*. In-vitro cytotoxicity assays revealed that compounds **1**, **3**, and **4** displayed cytotoxic activity against HELA cell lines, with respective IC_{50} values of 30.8, 13.7, and 14.1 μM. Compounds **1**, **3**, and **4** also showed significant cytotoxicity against A549 cell lines, with respective IC_{50} values of 24.7, 7.4, and 10.3 μM.

Keywords Helicosporous hyphomycetes · Natural product · Polyketones · Saprophytic fungi · Secondary metabolites

Introduction

Cancer incidence and mortality are rising worldwide. By 2020, roughly 19.3 million new cancer cases and nearly 10 million cancer-related deaths were documented, with an estimated 28.4 million new cancer cases projected for 2040 [1]. Concurrently, antimicrobial resistance (AMR) is emerging as a profound global public health challenge, with a predicted 10 million deaths annually worldwide by 2050 [2]. Given these trends, there is a pressing need to expedite the discovery of effective anti-tumor and new antimicrobial drugs. As science and technology advance, the approach to drug discovery has evolved from random screening to more rational design [3]. Nevertheless, natural products remain a vital source for discovering and developing drugs or lead compounds [3]. As the possibilities of obtaining natural products with novel structures and potent activity from traditional resources diminish, the exploration of micro-organisms, particularly underutilized fungal resources, has gained considerable attention from researchers [4].

Helicosporous hyphomycetes are a group of saprophytic fungi characterized by helicoid conidia. In the past, researchers have paid more attention to their morphology and phylogeny [5, 6]. However, these fungi can also produce secondary metabolites with novel structures and significant biological activity, especially in terms of anti-tumor activity [7, 8]. For instance, Neogrisphenol A, which is isolated from *Neohelicosporium griseum* (GZCC 23-0142), exhibits considerable inhibitory activity against the ovarian cancer cell line (A2780), and its effect is superior to that of cisplatin [7]. Rubracin D and E, isolated from *Tubeufia rubra*, have demonstrated the ability to reverse the multi-drug resistance of human breast cancer cells (MCF-7), showing superior effectiveness compared with verapamil

✉ Yongzhong Lu
yzlu@git.edu.cn

✉ Ruvishika S. Jayawardena
ruvishika.jay@mfu.ac.th

[1] School of Science, Mae Fah Luang University, Chiang Rai 57100, Thailand

[2] Center of Excellence in Fungal Research, Mae Fah Luang University, Chiang Rai 57100, Thailand

[3] School of Food and Pharmaceutical Engineering, Guizhou Institute of Technology, Guiyang 550025, China

[4] Department of Health Management, Guiyang Healthcare Vocational University, Guiyang 550081, China

[5] Kyung Hee University, 26 Kyungheedae-ro, Dongdaemun-gu, Seoul 02447, South Korea

Published online: 04 January 2024

Chiang Mai J. Sci. 2024; 51(4): e2024053
https://doi.org/10.12982/CMJS.2024.053
Journal homepage : http://epg.science.cmu.ac.th/ejournal/

Research Article

Antimicrobial Metabolites from the Freshwater Fungus *Tubeufia longihelicospora* Strain GZCC 23-0405

Lijuan Zhang [a,b,c], Jian Ma [a,b,c], Tianming Zhao [a], Meiyan Han [a], Dege Zheng [a], Ruvishika S. Jayawardena [b,c], Ausana Mapook [c] and Yongzhong Lu [a]*

[a] School of Food and Pharmaceutical Engineering, Guizhou Institute of Technology, Guiyang 550003, Guizhou, China

[b] School of Science, Mae Fah Luang University, Chiang Rai 57100, Thailand

[c] Center of Excellence in Fungal Research, Mae Fah Luang University, Chiang Rai 57100, Thailand

*Author for correspondence; e-mail: yzlu@git.edu.cn

Received: 8 November 2023
Revised: 20 April 2024
Accepted: 22 April 2024

ABSTRACT

In this study, five metabolites were successfully isolated from the culture medium of *Tubeufia longihelicospora* strain GZCC 23-0405, comprising two dimeric naphtha-*γ*-pyrones (**1**–**2**), two dimeric coumarins (**3**–**4**), and one alkaloid (**5**). The elucidation of their chemical structures relied on a combination of NMR, MS, and optical rotation methods. Interestingly, these compounds represent the first instances of such metabolites being isolated from helicosporous hyphomycetes. Additionally, compounds (**1**) and (**2**) exhibited significant antimicrobial potential, with MIC and MBC values of 62.0 μg mL^{-1} and 248 μg mL^{-1}, respectively, against *Pseudomonas aeruginosa*. This study provides a comprehensive account of the extraction, isolation, structural characterization, and antimicrobial properties of these compounds, shedding light on their potential significance in the field of natural product research.

Keywords: antimicrobial, freshwater fungi, secondary metabolites

1. INTRODUCTION

Since the advent of penicillin, fungal secondary metabolism has become a focal point in drug discovery [1–2]. Over the last 40 years, approximately 300 compounds have been isolated from freshwater fungi, including polyketones, quinones, alkaloids, and peptides [3]. These compounds have exhibited significant biological activities, such as inhibiting tumor cell proliferation, antibacterial, and insecticidal properties [3]. Many have been developed into anti-tumor drugs and antibiotics, with widespread applications in agriculture and the pharmaceutical industry [3–4].

Helicosporous Tubeufiaceae are found in both terrestrial and aquatic environments. However, research on their secondary metabolites remains sparse, with even fewer studies focusing on aquatic species [5]. It's worth noting that unexplored natural sources often yield novel active secondary metabolites [6]. Recent discoveries affirm this, with several unique active compounds identified from aquatic fungi [7–9]. Lu et al. discovered a novel fungal species, *Tubeufia rubra*, from decaying wood in freshwater [5]. Subsequent research by Qian et al. and Zeng et al. led to the isolation of four new and 22 known compounds from this species. Notably, Rubracin A, D, and E have shown potential in reducing Multi-Drug Resistance (MDR) in the MCF-7/ADM cancer cell line by

CURRICULUM VITAE

NAME Lijuan Zhang

EDUCATIONAL BACKGROUND

2005-2009 Bachelor of School of Pharmacy, Guizhou Medical University, China

2009-2012 Master of School of Pharmacy, Guizhou Medical University, China

PUBLICATIONS

First Author Publications

Zhang, L. J., Yang, M. F., Ma, J., Xiao, X. J., Ma, X. Y., Zheng, D. G., . . . Lu, Y. Z. (2023). Neogrisphenol A, a potential ovarian cancer inhibitor from a new record fungus *Neohelicosporium griseum*. *Metabolites*, 13(3), 435. https://doi.org/10.3390/metabo13030435

Zhang, L. J., Ma, J., Ma, X., Feng, X., Bai, X., Huang, Y., . . . Lu, Y. Z. (2023). A new record of *Neohelicosporium guangxiense* and its secondary metabolites. *Chiang Mai Journal of Science, 50*(2), 1–12. https://doi.org/10.12982/CMJS.2023.010

Zhang, L. J., Ma, J., Yang, M. F., Zhao, T. M., Han, M. Y., Zheng, D. G., . . . Lu, Y. Z. (2024). Polyketides from *Neohelicosporium griseum*: Structure assignment and bioactivity investigation. *Medicinal Chemistry Research, 33*(2), 308–313. https://doi.org/10.1007/s00044-023-03172-1

Zhang, L. J., Ma, J., Zhao, T. M., Han, M. Y., Zheng, D. G., Jayawardena, R. S., . . . Lu, Y. Z. (2024). Antimicrobial metabolites from the freshwater fungus *Tubeufia longihelicospora* strain GZCC 23-0405. *Chiang Mai Journal of Science, 51*(4), e2024053. https://doi.org/10.12982/CMJS.2024.053

Zhang, L.J., Jayawardena, R. S., Ausana, M., Liu, N.G., Ma, J., Xiao, X.J., . . . Sun, J. Z. (2025). Strategies for mining new secondary metabolites from fungi: From classical approaches to genomics-based mining. *Fungal Biology Reviews*. (in press)

Zhang, L. J., Ma, X., Han, M. Y., Zheng, D. G., Ma, J., Xiao, X. J., . . . Lu, Y. Z. (2025). Novel polyhydroxy-chlorinated dibenzo-α-pyrones derivatives with fused six-membered rings from the saprophytic fungus Helicosporium sexuale LZ15. *Phytochemistry*. (in press)

Co-author

Lu, Y. Z., Ma, J., Xiao, X. J., Zhang, L. J., Xiao, Y. P., & Kang, J. C. (2022). Four new species and three new records of helicosporous hyphomycetes from China and their multi-gene phylogenies. *Frontiers in Microbiology, 13*, 1053849. https://doi.org/10.3389/fmicb.2022.1053849

Wang, X. J., Wanasinghe, D. N., Zhang, J., Ma, J., Zhou, P., Zhang, L. J., . . . Zhang, Z. (2023). Insights from the endophytic fungi in Amphisphaeria (Sordariomycetes): A. orixae sp. nov. from Orixa japonica and its secondary metabolites. *Microorganisms, 11*(5), 1268. https://doi.org/10.3390/microorganisms11051268

Xiao, X. J., Ma, J., Zhang, L. J., Liu, N. G., Xiao, Y. P., Tian, X. G., . . . Lu, Y. Z. (2023). Additions to the genus Helicosporium (Tubeufiaceae, Tubeufiales) from China with an identification key for Helicosporium taxa. *Journal of Fungi, 9*(7), 775. https://doi.org/10.3390/jof9070775

Ma, J., Zhang, L. J., Boonmee, S., Xiao, X. J., Liu, N. G., Xiao, Y. P., . . . Lu, Y. Z. (2023). Morphological and phylogenetic analyses reveal three new species and one new record of Tubeufia (Tubeufiales, Tubeufiaceae) from southern China. *MycoKeys, 99*, 87–116. https://doi.org/10.3897/mycokeys.99.107606

Ma, J., Gomdola, D., Boonmee, S., Shen, H. W., Tang, X., Zhang, L. J., . . . Lu, Y. Z. (2024). Three new species of Neohelicomyces (Tubeufiales, Tubeufiaceae) from freshwater and terrestrial habitats in China. *MycoKeys, 105*, 317–340. https://doi.org/10.3897/mycokeys.105.124129

Zhang, J. Y., Hyde, K. D., Zhang, L. J., Bai, S., Bao, D. F., Al-Otibi, F., . . . Lu, Y. Z. (2025). Two novel hyphomycetes associated with ferns from China. *MycoKeys, 113*, 101–122. https://doi.org/10.3897/mycokeys.113.137678

Zhang, J. Y., Hyde, K. D., Ma, J., Wu, N., Al-Otibi, F., Zhang, L. J., . . . Lu, Y. Z. (2025). Morpho-phylogenetic evidence reveals Pseudolomaanthathailandica gen. et sp. nov. and Submultiguttulisporamultiseptata gen. et sp. nov. in Chaetosphaeriaceae. *MycoKeys, 113*, 123–146. https://doi.org/10.3897/mycokeys.113.142643

Xiao, X. J., Liu, N. G., Ma, J., Zhang, L. J., Bao, D. F., Bai, S., . . . Lu, Y. Z. (2025). Three new asexual Kirschsteiniothelia species from Guizhou Province, China. *MycoKeys, 113*, 147–170. https://doi.org/10.3897/mycokeys.113.139427

Han, M. Y., Karunarathna, S. C., Lu, L., Zheng, D. G., Suwannarach, N., Elgorban, A. M., . . . Tibpromma, S. (2025). Three new species of Camporesiomyces (Tubeufiaceae, Tubeufiales, Dothideomycetes) associated with coffee in Yunnan, China. *MycoKeys, 117*, 315–348. https://doi.org/10.3897/mycokeys.117.154573

Zheng, D., Lu, W., Han, M., Dai, D. Q., Zhang, L. J., Elgorban, A. M., . . . Karunarathna, S. C. (2025). Volvopluteus yunnanensis (Pluteaceae, Agaricales), a novel species from Yunnan Province, China. *Phytotaxa, 706*(3), 269–280. https://doi.org/10.11646/phytotaxa.706.3.5

Han, M., Karunarathna, S. C., Lu, L., Zheng, D., Dai, D., Suwannarach, N., . . . Hyde, K. D. (2025). Pseudodictyosporium yunnanensis sp. nov. (Dictyosporiaceae, Pleosporales) from dead twigs of Coffea arabica in China. *Phytotaxa, 711*(1), 28–42. https://doi.org/10.11646/phytotaxa.711.1.2

Zheng, D., Voto, P., Tibpromma, S., Lu, W., Han, M., Kumla, J., . . . Karunarathna, S. C. (2025). Candolleomyces yunnanensis (Psathyrellaceae, Agaricales), a novel species from Yunnan Province, China. *Phytotaxa, 711*(3), 281–292. https://doi.org/10.11646/phytotaxa.711.3.3